

CIVIL ENGINEERING STUDIES

STRUCTURAL RESEARCH SERIES NO. 460

PB 301091



EXPERIMENTAL STUDY OF FRAME-WALL INTERACTION IN REINFORCED CONCRETE STRUCTURES SUBJECTED TO STRONG EARTHQUAKE MOTIONS

by
DANIEL P. ABRAMS
and
METE A. SOZEN

A Report on a Research Project
Sponsored by
THE NATIONAL SCIENCE FOUNDATION
Research Grant PFR 78-16318

ASRA INFORMATION RESOURCES
NATIONAL SCIENCE FOUNDATION

UNIVERSITY OF ILLINOIS
OF URBANA-CHAMPAIGN
URBANA, ILLINOIS

MAY 1979

REPRODUCED BY
**NATIONAL TECHNICAL
INFORMATION SERVICE**
U.S. GOVERNMENT PRINTING OFFICE

1
2
3
4
5
6
7
8
9
10
11
12
13
14
15
16
17
18
19
20
21
22
23
24
25
26
27
28
29
30
31
32
33
34
35
36
37
38
39
40
41
42
43
44
45
46
47
48
49
50
51
52
53
54
55
56
57
58
59
60
61
62
63
64
65
66
67
68
69
70
71
72
73
74
75
76
77
78
79
80
81
82
83
84
85
86
87
88
89
90
91
92
93
94
95
96
97
98
99
100

UIIU-ENG-79-2002

EXPERIMENTAL STUDY OF FRAME-WALL INTERACTION
IN REINFORCED CONCRETE STRUCTURES
SUBJECTED TO STRONG EARTHQUAKE MOTIONS

by

Daniel P. Abrams
and
Metec A. Sozen

A Report to the
NATIONAL SCIENCE FOUNDATION
Research Grant PFR 78-16318

University of Illinois
at Urbana-Champaign
Urbana, Illinois
May, 1979



ACKNOWLEDGMENT

The experimental study described in this report was part of a continuing study of reinforced concrete structures subjected to earthquake motions. Work was performed in the Structural Research Laboratory of the Civil Engineering Department of the University of Illinois in Urbana. Research was funded by the Division of Problem-Focused Research Applications (PFRA) of the Applied Science and Research Applications Directorate (ABRA) of the National Science Foundation under grant PFR-78-16318.

The writers wish to express their appreciation to the kind and patient people who were involved with the project.

Mr. O. H. Ray and Professor V. J. McDonald and their staffs are thanked for assistance with fabrication and testing of the models and recording of data. Grateful recognition is extended to Mr. G. Lafenhagen for his conscientious and reliable operation of testing equipment.

Gratitude is due to Professors Schnobrich, Foutch, and Pecknold and to members of the NSF advisory panel for their piercing criticism. Members of the panel were M. H. Eligator of Weiskopf and Pickworth, A. E. Fiorato of the Portland Cement Association, W. D. Holmes of Rutherford and Chekene, W. P. Moore Jr. of Walter P. Moore and Associates, and A. Walser of Sargent and Lundy Engineers.

Special attention is due to J. D. Aristizabal and J. Lybas whose advice and direction in the early stages of the project were essential. D. Reed, D. Schipper and M. Kreger are thanked for their artful testing of wall and frame elements. B. Volkert is thanked for his systematic manner

in reducing portions of the data. J. Moehle, D. Morrison and M. Saïdi are thanked for their valuable discussions.

Mrs. Mary Ann Speck, Mrs. Patricia Lane, Mrs. Sara Cheely and Mrs. Laura Goode are thanked for their patience in typing the report.

The IBM-360/75 and CDC-Cyber 175 computing systems of the Department of Computer Science were used for data reduction and analysis of the structures.

This report was prepared as a doctoral dissertation by D. P. Abrams under the direction of Professor M. A. Sozen.

TABLE OF CONTENTS

CHAPTER	Page
1. INTRODUCTION.	1
1.1 Object and Scope	1
1.2 Previous Research.	2
2. OUTLINE OF EXPERIMENTAL PROGRAM	5
3. DESIGN OF EXPERIMENT.	8
3.1 Conceptual Design.	8
3.2 Design of Test Structures.	10
4. MEASURED HYSTERESIS RELATIONSHIPS OF MEMBERS.	16
4.1 Object of Tests.	16
4.2 Experimental Program	17
4.3 Observed Behavior.	18
4.4 Comparison of Measured and Calculated Behavior	20
4.5 Comparison of Small- and Full-Scale Behavior	22
5. OBSERVED RESPONSE TO SIMULATED EARTHQUAKE MOTION.	24
5.1 Introductory Remarks	24
5.2 General Comments	24
5.3 Observed Response of Structures During Initial Test Runs	28
5.4 Observed Response of Structures During Subsequent Test Runs.	37
6. INTERPRETATIONS OF OBSERVED DYNAMIC RESPONSE.	45
6.1 Introductory Remarks	45
6.2 Base Motions.	45
6.3 Measured Dynamic Characteristics of Test Structures.	51
6.4 Frequency Content of Measured Response	61
6.5 Interpretation of Measured Response Using a Linear SDOF Oscillator.	67
7. DISCUSSION OF TEST RESULTS.	71
7.1 Introductory Remarks	71
7.2 Strength of Test Structures.	71
7.3 Calculation of Dynamic Characteristics Using a Linear Model.	76
7.4 Reliability of Measurement of Force Resisted by Wall	79
7.5 Identification of Reductions in Stiffness Using a Linear Model.	84
7.6 Evaluation of Design Method.	91

	Page
8. SUMMARY AND CONCLUSIONS	98
REFERENCES	103
APPENDIX	351

LIST OF TABLES

Table	Page
3.1 Stiffnesses Used for Design	106
3.2 Calculated Mode Shapes and Frequencies for Design	107
3.3 Smeared Damping Values.	108
3.4 Column Net Axial Tensions for Design, kN.	109
5.1 Key to Figures and Tables Presenting Observed Response.	110
5.2 Measured Widths of Cracks at Beam Ends, mm.	111
5.3 Measured Response at Time of Maximum Displacement	112
6.1 Spectrum Intensities, mm.	120
6.2 First-Mode Shapes Measured During Earthquake Simulations.	121
6.3 First-Mode Shapes Measured During Steady-State Tests.	123
6.4 Damping Factors Calculated from Free-Vibration Response	124
6.5 Damping Factors Calculated from Steady-State Response	125
6.6 Influence of Lateral Loads on Wall Forces	126
7.1 Measured Shear and Moment Maxima.	128
7.2 Relative Interstory Displacements for Initial Simulations	128
7.3 Column and Wall Stiffnesses of Linear Model	129
7.4 Calculated Frequencies and Mode Shapes.	130
7.5 Rotation at Base of Wall Calculated from Measured Forces and Displacements	131
7.6 Influence of Permanent Rotations on Residual Wall Forces.	132
7.7 Comparison of Measured Wall Base Moment Maxima and Capacities, kN-m.	134
7.8 Normalized Wall Response Maxima	135
7.9 Measured and Calculated Stiffness Reductions.	136
7.10 Comparison of Shape Factors Determined from Design Calculations and Measurements	137

Table	Page
A.1 Summary of Measured Gross Cross-Sectional Member Dimensions.	363
A.2 Measured Story Masses.	368
A.3 Measured Properties of Concrete.	369
A.4 Measured Properties of Reinforcement	370

LIST OF FIGURES

Figure	Page
2.1 Test Structure Description.	138
2.2 Experimental Arrangement.	139
2.3 Schematic Description of One Cycle of Loading Program	140
3.1 Shear Diagrams using Eight-Inch Wall.	141
3.2 Determination of Time Scale	142
3.3 Description of Analytical Model Used for Design	143
3.4 Spectral-Response Curve Used for Design	144
3.5 Interpretation of Damage Ratio.	145
3.6 Comparison of Design Requirements with Different Methods	146
3.7 Calculated Mode Shapes for Design	148
3.8 Calculated Displacements for Design	149
3.9 Calculated First-Mode Moments for Design.	150
3.10 Design Moments.	152
3.11 Interaction Diagram for Columns	154
3.12 Description of Reinforcement.	156
4.1 Description of Frame and Wall Specimens	160
4.2 Test Apparatus for Cyclic-Load Tests.	161
4.3 Loading Programs for Cyclic-Load Tests.	162
4.4 Measurements for Cyclic-Load Tests.	163
4.5 Measured Hysteresis Relationships	164
4.6 Observed Damage at Maximum Displacement	168
4.7 Measured and Calculated Beam Response	170
4.8 Comparison of Displacement and Rotation Measurements for Frame Specimens.	172

Figure	Page
4.9 Measured and Calculated Column Stiffnesses	173
4.10 Measured and Calculated Wall Response	174
4.11 Measured Behavior of Large-Scale Members	175
5.1 Description of Recorded Waveforms	177
5.2 Observed Crack Patterns before Initial El Centro Simulations	178
5.3 Measured Motions of Initial El Centro Simulations	180
5.4 Measured Response to Initial El Centro Simulations	181
5.5 Shear and Moment Response to Initial El Centro Simulations	192
5.6 Distributions of Response to Initial El Centro Simulations	196
5.7 Observed Crack Patterns following Initial El Centro Simulations	202
5.8 Measured Motions of Second El Centro Simulations	204
5.9 Measured Response to Second El Centro Simulations	205
5.10 Shear and Moment Response to Second El Centro Simulations	212
5.11 Distributions of Response to Second El Centro Simulations	216
5.12 Observed Crack Patterns following Second El Centro Simulations	218
5.13 Distributions of Response to Third El Centro Simulations	220
5.14 Observed Crack Patterns before Initial Taft Simulations	222

Figure	Page
5.15 Measured Motions of Initial Taft Simulations	224
5.16 Measured Response to Initial Taft Simulations	225
5.17 Shear and Moment Response to Initial Taft Simulations.	236
5.18 Distributions of Response to Initial Taft Simulations.	240
5.19 Observed Crack Patterns following Initial Taft Simulations.	246
5.20 Measured Motions of Second Taft Simulations	248
5.21 Measured Response to Second Taft Simulations	249
5.22 Shear and Moment Response to Second Taft Simulations.	256
5.23 Distributions of Response to Second Taft Simulations.	260
5.24 Observed Crack Patterns following Second Taft Simulations	262
5.25 Distributions of Response to Third Taft Simulations	264
6.1 Fourier-Amplitude Spectra of Base Motions	266
6.2 Spectral-Response Curves of El Centro Simulations	268
6.3 Spectral-Response Curves of Taft Simulations	276
6.4 Variation of Maximum Base Acceleration with Spectral Acceleration.	284
6.5 Variation of Maximum Base Acceleration with Spectrum Intensity	284
6.6 Variation of Spectrum Intensity with Damping Factor.	285

Figure	Page
6.7 Comparison of Displacement Spectral Response for Initial Simulations.	286
6.8 Comparison of Acceleration Spectral Response for Initial Simulations.	288
6.9 Spectral-Response Curves for Partial Durations	290
6.10 Measured Apparent Fundamental Frequencies	292
6.11 Apparent Frequencies Measured During Free-Vibration Tests.	293
6.12 Variation of Displacement with Spectrum Intensity	293
6.13 Fourier-Amplitude Spectra of Tenth-Level Displacements Measured During Earthquake Simulations	294
6.14 Accelerations and Corresponding Fourier-Amplitude Spectra Measured During Free-Vibration Tests.	296
6.15 Calculated Natural Frequencies.	300
6.16 Fourier-Amplitude Spectra of Minor Direction Acceleration.	302
6.17 Equivalent-Viscous Damping Factors Calculated from Measured Response.	303
6.18 Frequency-Response Curves of Response to Steady-State Base Motions	304
6.19 Frequency Content of Measured Response.	306
6.20 Comparison of Measured and Calculated Response Maxima	326
6.21 Measured and Calculated Variations in Base Moment with Tenth-Level Displacement.	328
7.1 Possible Collapse Mechanisms.	332
7.2 Measured Inertial Forces.	333

Figure	Page
7.3 Description of Analytical Model	334
7.4 Calculation of Spring Flexibility at Base of Columns	335
7.5 Calculated Fundamental Frequencies.	336
7.6 Calculated First-Mode Response.	338
7.7 Calculated Force Distributions on Wall.	342
7.8 Increase in Moment Capacity of Wall with Axial Load.	343
7.9 Comparison of Measurements with Calculated Displacements	344
7.10 Comparison of Measurements with Design Shears and Moments Resisted by Entire Structure.	346
7.11 Comparison of Measurements with Design Shears and Moments Resisted by Wall.	348
7.12 Representative Load-Deflection Relationship for Beams	350
A.1 Test Apparatus.	371
A.2 Free-Vibration Test	372
A.3 Test-Structure Components	373
A.4 Instrumentation	377
A.5 Fabrication of Specimens.	381
A.6 Erection of Test Structures	383
A.7 Measured Stress-Strain Diagrams	385

CHAPTER 1

INTRODUCTION

1.1 Object and Scope

The overall objective of the experimental study was to develop a better understanding of the response of reinforced concrete frame-wall structures subjected to earthquake motions. An incidental objective of the research was to investigate improved methods of analysis for design of structures behaving in linear and nonlinear ranges of response.

To accomplish these objectives four model frame-wall structures were constructed and subjected to strong base motions generated by an earthquake simulator. The multistory structures were not models of any particular prototype but physical representations of an engineer's concept of lateral-load resistance in a building. Each small-scale structure consisted of planar elements resisting inertial loads resulting from a single direction of motion. Story weights, coupling frames and walls at each of ten levels, were ridiculously stiff and attached so that the mass would be effectively lumped at the centroid of each story level. Observed response of the structures was interpreted to investigate behavior as one would with results of a numerical analysis of a similar idealized model.

Comparing response of a physical model with that of a mathematical model is a useful technique for investigating mechanisms of behavior. However, an understanding of response, which may result in improved methods of analysis for design, may be inferred directly from response of the

physical model. The experimental analysis presented in this study consisted of proportioning structures according to a proposed design method, testing the structures, and interpreting observed response to evaluate the applicability of procedures used with the design method. Distributions of reinforcement were established from results of a conventional linear modal analysis. Stiffnesses of selected members of the design model were arbitrarily reduced to localize nonlinear behavior and to obtain an economical pattern of reinforcement. Measured response of the test structures (accelerations and displacements) were examined in terms of apparent modal properties to evaluate the correctness of the design method in estimating lateral loads applied to the nonlinearly behaving structures. Internal-force measurements were also examined to investigate frame-wall interaction in the nonlinear range of response and to check the reliability of the design method for proportioning individual elements.

1.2 Previous Research

Several approaches to the development of improved analytical methods for earthquake-resistant design of reinforced concrete structures have been attempted. Because costs of testing full-scale multistory buildings in the nonlinear range of response are generally prohibitive, research has consisted primarily of studies using either numerical or small-scale physical models. Hidalgo and Clough [11] subjected a large-scale (approximately two-thirds) frame structure to strong simulated base motions. Examination of measured response of the two-story structure was mainly concerned with detailing of members and joints rather than overall response.

Mahin and Bertero [17] evaluated the use of linear and nonlinear analytical techniques to identify response of three buildings that were damaged significantly during earthquakes. Results of their research emphasized the need for explicit considerations of the effects of inelastic behavior in estimating response parameters such as drifts, internal forces and ductility requirements.

Tansirikongo and Pecknold [24] investigated approximate modal analysis methods for bilinear multi-degree-of-freedom systems using elastic and inelastic response spectra. Story displacements calculated using approximate methods were from 5 to 40 percent different than values calculated using a more refined nonlinear dynamic analysis.

Pique [21] investigated the use of simple analytical models to estimate inelastic dynamic response of frames. His research demonstrated that shear-beam and equivalent single-degree-of-freedom models could provide reasonable approximations of response to that calculated using a more elaborate point-hinge model.

The primary objective of previous experimental studies of small-scale structures has been to match test results with calculated response. An understanding of behavior was inferred from assumed concepts included with the analytical model if a good correlation between measured and calculated results was observed. One of the few model structures of this category not tested on the University of Illinois Earthquake Simulator was a one-fifth scale six-story, single-bay frame investigated by Wilby [26]. Several small-scale structures have been tested at the University of Illinois as part of a continuing series of research projects involved with effects of earthquake motions on reinforced concrete buildings. Gulkan [7] tested

the applicability of a linear-model approach with a one-story single-bay frame. Investigation of multistory structures [1, 9, 15, 18, 20] began with Otani testing a three-story frame, followed by Lybas and Aristizabal examining energy dissipation capabilities of six- and ten-story coupled-wall structures. Cecen, Healey and Moehle tested ten-story, three-bay frames similar to the frames described in this report.

CHAPTER 2

OUTLINE OF EXPERIMENTAL PROGRAM

The experimental study consisted of tests of reinforced-concrete model structures subjected to a program of base motions generated by an earthquake simulator. Each ten-story structure comprised two frames resisting lateral inertial loads in parallel with one slender structural wall. Geometry of each structure was the same (Fig. 2.1). However, patterns of reinforcement were varied according to a design concept as discussed in the next chapter.

Experimental parameters of the four-structure series were the base motions and strength of structures.

A photograph of the experimental arrangement is presented in Fig. 2.2. The frames and wall were coupled at each level by a 465 kg mass so that lateral displacements of each element would be equal. A system of steel channels was provided to transfer lateral and vertical forces from the mass to the centroid of each frame joint without eccentricities. Lateral forces were transferred to the wall from the mass by a connection with negligible resistances to rotations about each principal axis of the wall. Construction of the test structures was planned so that no dead load was supported by the wall. Both frames and wall were secured to the simulator platform with prestressed steel angles which assured a fixed-base condition for all motions.

Base motions consisted of scaled earthquake simulations of progressively increasing intensities, and low-amplitude steady-state excitations. Earthquake motions modeled were the north-south component of the ground motion measured at El Centro, California in the 1940 Imperial Valley Earthquake, and the N21E component of the motion measured at Taft, California in the 1952 Tehachapi Earthquake. The time axis of these recorded accelerograms was compressed by a factor of 2.5 so that frequency contents of each base motion would be in similar ranges as natural frequencies of the test structures. A typical sequence of loading is depicted in Fig. 2.3. Intensities of initial earthquake simulations were representative of design-bases motions. Subsequent test runs were approximately two and three times as intense as initial test runs. Following earthquake simulations, the last two structures in the series were subjected to sinusoidal base excitations at frequencies within ranges of expected natural fundamental frequencies. Before and after each base motion structures were subjected to low-amplitude impulses so that free-vibration response could be examined.

Response of each structure was recorded continuously on forty-eight channels. Measurements at each level included displacement, acceleration, and strain in the bolts of the connecting system which indicated force resisted by the wall. Accelerations were measured in transverse and vertical directions also for detection of torsional and axial response. Data was converted to digital form, calibrated, and stored on magnetic tape for further processing and plotting.

Detailed descriptions of the testing apparatus and procedures for fabricating, erecting and testing the structures and recording and reducing data are presented in the Appendix.

The experimental study also included two series of cyclic-load tests to determine hysteresis properties of the small-scale members. Four wall specimens were fixed at base and loaded laterally with a single concentrated force. Four interior and four exterior beam-column units were loaded with representative story shears at idealized locations of contraflexure. Descriptions and results of static tests are presented in Chapter 4.

CHAPTER 3

DESIGN OF EXPERIMENT

Conceptual design of the test structures and base motions is discussed in the first section of this chapter. Reasons for selecting frame and wall geometries, size of story weights, and intensity and frequency content of base motions are presented. The method of analysis used for proportioning reinforcement is discussed in the second section of this chapter followed by description of the reinforcing schemes and anticipated maximum displacements.

3.1 Conceptual Design

(a) Geometry of Test Structures

Locations and sizes of structural elements in most buildings are seldom chosen with optimization of the structure in mind. Walls may be included in the structural configuration because of architectural demands. For example, slender walls for an elevator shaft serve a vital building function but may not influence appreciably displacement response of a high-rise building subject to strong ground motion. However, the wall will resist a fraction of the lateral load redundantly with other structural elements which provides the engineer with options for proportioning strength throughout the structural system economically.

Previous tests of model frame structures without walls [9, 18] revealed serviceable behavior during design earthquake simulations. Selections of wall dimensions for this experimental study were, therefore, not intended to necessarily stiffen the frames, but to result in a structural system where wall-frame interaction could be examined. The ideal geometry of wall and frames was considered to be one where variations in force distributions for each component could be perceptible with cracking of concrete and yielding of reinforcement.

Frame geometries were not varied from the previous series of tests so that comparisons of observed behavior could be made. Ten stories were originally selected so that higher-mode response could be examined. Aspect ratios of story heights to bay widths were selected to be comparable to ratios of actual buildings. Overall dimensions of the frames were limited by the size of the simulator platform. Frames with three bays were tested so that response would include behavior of interior and exterior joints. Beam and column depths were established so that reasonable reinforcing ratios would result and shear deformations would be minimal.

Wall depths were established so that total story shears would be resisted mainly by wall at base and by frames at upper storys. To demonstrate why an eight-inch (203mm) wall was selected, calculated shear at each story resisted by frames and wall are presented in Fig. 3.1. Shear diagrams have been generated using the analytical model described in the next section with a triangularly shaped lateral-load distribution. Diagrams are shown for stiffnesses based on uncracked and post-yield behavior.

(b) Size of Story Weights

Story weights were made as large as space limitations would permit so that minimum intensities of base motion would result in yield of reinforcing bars of a reasonable diameter. Story weights were also made as stiff as possible in the horizontal plane so that lateral displacements of wall and frame would be equal.

(c) Base Motions

Preliminary natural frequencies were used to establish a factor for compressing the time axis of the base motion. As depicted in Fig. 3.2, a time scale factor of 2.5 was chosen so that the fundamental frequency of the test structures would be in the range of decreasing spectral acceleration. This range was selected so that the structures would resist less load with increasing damage. A smoothed spectral-response curved representing response to recorded ground motions of El Centro and Taft earthquakes was used.

Maximum base accelerations were established for initial earthquake simulations so that the small diameter reinforcing bars would be stressed to yield.

3.2 Design of Test Structures

(a) Description of Analytical Model

Linear analyses were made for design using the model described in Fig. 3.3. The model consisted of a single frame coupled in the same plane with a wall so that lateral displacements would be equal at each level. Calculation of response considered flexural and shear deformations of beams, columns and

wall. Axial deformations of columns was considered, but axial deformations of beams was neglected. Further idealizations included rigid joint cores, fixed bases, and lumped masses at each level. To parallel current design-office practice a commercial dynamic analysis program, ETABS [27], was used for computing response. Displacement and force maxima were calculated for the first three modes of vibration using the smoothed spectral-response curve shown in Fig. 3.4.

(b) Stiffness Assumptions

Stiffnesses of frame members and lightly reinforced wall were selected arbitrarily in the design process to obtain an economical distribution of strength. Stiffnesses of the heavily reinforced wall were selected formally to conform with conventional calculations of cracked-section stiffness. A "deterministic" stiffness was felt to be a precarious value because of uncertainties associated with calculation of stiffness of a reinforced-concrete member: quantitative estimate of modulus of elasticity of concrete, extent of cracking, shear deformations and slip of reinforcement. To illustrate inaccuracies of cracked-section stiffnesses, calculated values are compared with measured values (Fig. 4.7) in the next chapter. Implicit in a design method that models stiffnesses arbitrarily or incorrectly is the possible occurrence of nonlinear behavior in members that respond stiffer in the elastic range than assumed for design. If members are detailed properly and provided strengths are equal to required strengths, nonlinear behavior will result in an average stiffness that will correspond to the assumed softened stiffness. Reduced stiffnesses of beams and lightly reinforced wall were

chosen so that nonlinear behavior would occur in these members. Beam and wall stiffnesses were calculated by dividing cracked-section stiffnesses by six and three. Stiffnesses used for design are summarized in Table 3.1.

The design procedure followed the Substitute-Structure Method [22] explicitly. The principal feature of the method is that advantages of nonlinear behavior may be modeled using a linear modal analysis. Stiffnesses are reduced arbitrarily by a "damage ratio", defined in Fig. 3.5, which establishes limits of tolerable response in selected members. Strength requirements vary with the arbitrary selection of damage ratios which reduces design criterion to one of acceptable displacements.

Increases in energy dissipation with increased nonlinear behavior are represented by the formula below.

$$\beta_s = 0.2 (1 - 1/(\mu)^{1/2}) + 0.02$$

where β_s = substitute (equivalent viscous) damping factor
and μ = damage ratio.

Damping factors for each mode are determined by "smearing" damping factors for individual members in the same proportion as distributions of strain energies.

To illustrate the economy of the method, design forces and first-mode displacements calculated for the substitute structure (lightly reinforced wall structure) are compared with values obtained from conventional methods using gross-section and cracked-section stiffnesses (Fig. 3.6). Design requirements for beams, columns and wall were reduced substantially for the

substitute structure. Displacements for the softened structure were larger but within acceptable limits for serviceability (one percent of height). Apart from changes in distribution of moments within the redundant structure, the total force resisted by the combined frame-wall system was reduced because of lower natural frequencies (1.9 versus 3.5 and 4.3 Hz) and higher damping factors (12 versus assumed values of 10 percent).

(c) Anticipated Response

Natural frequencies and mode shapes calculated for design are presented in Table 3.2 and Fig. 3.7. Smeared damping factors calculated from strain-energy distributions of the first three modes are summarized in Table 3.3. Anticipated maximum displacements for each structure type (Fig. 3.8) suggested a reduced lateral inertial load for the structure with the lightly reinforced wall. First- and second-mode displacements were only slightly larger for the softened-wall structure because natural frequencies (1.9 versus 2.4) and damping factors (12 versus 8.5) reduced spectral accelerations to 62 percent of accelerations of the stiffer structure.

First-mode beam, column and wall moments calculated for design (Fig. 3.9) demonstrated anticipated wall-frame interaction. Single curvature of lower-story columns suggested the dominance of the stiff wall at base. Smaller beam and column moments at lower stories and larger moments at base of wall signified the larger stiffness selected for design of the heavily reinforced wall. Reversal in direction of force resisted by wall, indicated by a point of contraflexure, suggested that wall and frame stiffnesses were matched for a revealing force interaction.

(d) Longitudinal Reinforcement Requirements

Design forces were obtained by multiplying the square root of the sum of the squares (RSS) of the first three modal components by the factor below.

$$\alpha = \frac{V_{abs} + V_{rss}}{2 \cdot V_{rss}}$$

where V_{abs} = sum of absolute values of first- and second-mode base shear

V_{rss} = RSS of first three modes of base shear

Furthermore, column moments were increased by a factor of 1.2 to lessen the likelihood of nonlinear behavior of members carrying vertical axial loads.

Design moments are presented in Fig. 3.10. Net axial tensions for columns are listed in Table 3.4 for use with column interaction diagrams (Fig. 3.11). Reinforcement for beams and wall was selected directly from design moments. Provided yield strengths which are plotted in Fig. 3.10 were calculated using the following relationship [6] commonly used for ultimate flexural capacities of reinforced concrete members.

$$M_u = A_s f_y d \left(1 - 0.59 \frac{A_s}{bd} \frac{f_y}{f'_c} \right)$$

where M_u = moment at yield of tensile reinforcement

A_s = area of tensile reinforcement

f_y = yield strength of reinforcement

d = effective depth of section

f'_c = compressive strength of concrete

Increase in strength because of compression reinforcement was also included for heavily reinforced walls. Measured strength parameters are tabulated in the Appendix. As demonstrated in Fig. 3.10, flexural strengths provided for beams and wall were in many cases much larger than required. Excessive strengths were a result of (1) a minimum of four bars per section necessary for confinement, and (2) a uniform pattern of reinforcing bars of the same diameter. Column strengths provided also exceeded requirements because of these two reasons. As demonstrated with interaction diagrams (Fig. 3.11) calculated using conventional methods [6], two bars per face in columns was sufficient for most of the column members. Descriptions of frame and wall reinforcement are presented in Fig. 3.12.

(e) Details for Shear and Anchorage

Shear reinforcement was provided in columns and beams so that ultimate flexural moments could be developed at each end of the member. Shear reinforcement for the wall was provided based on shear forces from the analysis which were increased conservatively by a safety factor of three.

Anchorage of longitudinal reinforcement was provided conservatively also by assuming a bond strength of 1.4 MPa. Bars were hooked at the top of columns and walls, and at the ends of beams (Fig. 3.12) for additional development length. At column and wall bases, bars were welded to embedded plates capable of resisting the full tensile strength of the section.

Static tests of frame and wall elements, discussed in the next chapter, indicated no loss of specimen strength resulting from shear or bond distress.

CHAPTER 4

MEASURED HYSTERESIS RELATIONSHIPS OF MEMBERS

Results of cyclic-load tests of frame and wall members are presented and discussed in this chapter. Measured stiffnesses and strengths are compared with calculated values and behavior of full-scale reinforced concrete members.

4.1 Object of Tests

Samples of frame and wall elements were subjected to slowly applied load reversals to examine behavior of the small-scale members in the non-linear range. Incidental objectives of the tests are noted below.

(1) Strength, stiffness, and energy dissipation characteristics were examined to justify correlations with behavior of full-scale reinforced concrete structures subjected to loading reversals.

(2) Frame specimens were subjected to similar displacement histories as the ten-story structures to view internal response. Average stiffnesses of measured hysteresis loops were used to evaluate the correctness of using a linear model to calculate response maxima (See 7.4). Measured stiffnesses and strengths were also compared with values assumed for design to reconcile differences between anticipated and measured response (Sec. 7.5).

(3) Measured hysteresis relationships provided a reference to K. Emori [5] for investigating the accuracy of a nonlinear analytical model.

(4) Measured strengths of wall and beam members were used to calculate collapse loads for comparison with measured response maxima (Sec. 7.2).

4.2 Experimental Program

Test specimens and experimental procedures were established so that local behavior of ten-story structures could be visualized from response of static-test specimens. Geometries of specimens (Fig. 4.1) were chosen to simulate flexural behavior of the test structures. Beam and column lengths were selected to model idealized locations of points of contraflexure: center of bays and mid-heights of stories. Exterior-and interior-joints specimens were tested to investigate behavior of longitudinal beam reinforcement with respect to bonding with concrete. Heights of wall specimens were selected to represent equivalent moment-shear ratios at base of ten-story walls. Cross section dimensions, materials and fabrication procedures were the same as described in the Appendix for the ten-story structures.

Equivalent story displacements could be measured with the testing apparatus used for frame specimens (Fig. 4.2a). Pseudo story shears were transferred across column members that were restrained against rotation by flexural stiffness of beam members. Loading programs (Fig. 4.3a) were representative of measured histories of fifth-story displacements of structures subjected to design-basis earthquake simulations. Large amplitude displacements of structure FW1 resulting from an El Centro simulation and of structure FW4 resulting from a Taft simulation composed loading patterns "A" and "B". Measurements (Fig. 4.4a) consisted of displacement

at point of load application, and displacement and rotation of joint. Experimental procedures and a complete set of measured data for frame specimens are presented in detail in Reference 14.

The testing apparatus used to test wall specimens (Fig. 4.2b) transferred a lateral load across the cantilever specimens to a fixed-base foundation. Because of uncertainties of curvature distribution along the height of dynamically tested walls, no attempt was made to simulate recorded displacement histories. Instead, the performance of walls was tested by subjecting wall specimens to loading programs (Fig. 4.3b) of progressively increasing displacements within the nonlinear range. Measurements (Fig. 4.4b) consisted of displacements at each level and rotation near the base. Descriptions of the test apparatus and experimental procedures for the wall tests are presented in the Appendix.

4.3 Observed Behavior

(a) Frame Specimens

A palpable observation from measured hysteresis relationships of frame specimens (Fig. 4.5a and 4.5b) was that extensive nonlinear behavior had occurred in the frames. Shapes of hysteresis curves plotted from displacement or joint rotation measurements were nearly identical (Fig. 4.7) which demonstrated that nonlinear behavior had occurred in beams and not columns.

Perceptible reductions in stiffness in load-reversal regions of interior-joint specimens (Fig. 4.5b) coupled with observations of excessive crack widths suggested deterioration of bond between longitudinal beam

reinforcement and concrete within the joint. Beams framing into exterior joints (Fig. 4.5a) did not reveal this tendency as corroborated by better energy dissipation capabilities.

Average stiffnesses for loading cycles with progressively increasing rotations decreased for interior-and exterior-joint specimens. Softening of beams to a limit corresponding to a damage ratio of six as assumed for design was not attained partially because strengths were larger than assumed. Further discussion of measured and design stiffnesses is presented in Sec. 7.5.

When displaced to limits of the testing apparatus (approximately ten times the maximum displacement of the loading pattern), frame specimens resisted maximum loads with no loss of strength. Damage was concentrated at beam ends (Fig. 4.6a and 4.6b). No distress in shear, or anchorage strength, or excessive cracking within the joint core was observed.

(b) Wall Specimens

Behavior of wall specimens was represented by stable hysteresis loops (Fig. 4.5c and 4.5d) indicating energy dissipation capability superior to that of frames. Similarly shaped curves plotted from displacement and rotation near base indicated that nonlinear behavior was concentrated near base of wall. Rotational stiffnesses of the first-quarter cycle and the absence of a sudden increase in rotation upon reversal of the load suggested that extension of anchored reinforcement had occurred elastically, and that nonlinear behavior was attributable to yield of longitudinal reinforcement.

Average stiffnesses of cycles of progressively increasing displacements reduced. Final loading cycles, particularly of lightly reinforced walls, revealed appreciable stiffness reductions. However, maximum displacements of these cycles were well beyond the range observed for ten-story walls.

Failure of wall specimens occurred at extremely large displacements as a result of fracture of reinforcement. Extensive formations of shear cracks and severe crushing of concrete was observed for heavily reinforced walls (Fig. 4.6c). Limited propagation of shear cracks and nominal crushing of concrete was observed for lightly reinforced walls (Fig. 4.6d). Accumulation of plastic deformation of reinforcement was much more perceptible for lightly reinforced walls.

4.4 Comparison of Measured and Calculated Behavior

Although design of reinforcement was based on stiffnesses that were chosen arbitrarily, correct assumptions of strength and stiffness in the linear range of response were necessary for members to soften to assigned limits. In this section, calculated values of strength and stiffness based on cracked sections are compared to measured behavior of frame and wall specimens.

(a) Frame Behavior

Envelopes of load-rotation measurements for the first quarter of all loading cycles (Fig. 4.7a) provided a definable indication of beam behavior. Before initial cracking of concrete, measured behavior could be represented

satisfactorily with calculated stiffnesses based on gross sections. After cracking, calculated stiffnesses based on cracked sections could not represent the softening of the curve attributable to slip of beam reinforcement.

Measured beam strengths were larger than values calculated for design (Fig. 4.7b). Design strengths included tensile resistance of a single layer of reinforcing bars whereas large curvatures at maximum loads may have resulted in tension of the bars near the compression fibers. Calculated flexural strengths considering tensile strengths of both layers of bars were coincident with measured strengths.

Similarly shaped hysteresis loops of displacement and rotation (Fig. 4.8) suggested linear column behavior. Deflection of the column may be interpreted from displacement and rotation measurements using the relationship below.

$$\delta_{\text{column}} = \Delta - \theta_{\text{joint}} h$$

where

δ_{column}	=	deflection of half-story column
Δ	=	measured displacement at level of beam
θ_{joint}	=	measured joint rotation
h	=	half story height (119 mm)

As demonstrated in Fig. 4.9, column behavior could be represented satisfactorily with calculated stiffness based on cracked section.

(b) Wall Behavior

Moment-displacement relationships for the first-quarter cycle of loading (Fig. 4.10) indicated that wall specimens were softer in the linear

range than calculated considering only curvatures. Rotation at base of wall, attributable to pullout of anchored reinforcement, was the primary source of discrepancy between measured and calculated behavior. Eliminating rotation components from displacement measurements revealed that behavior above base could be represented closely using cracked-section stiffnesses.

Flexural strengths of wall specimens were approximated reasonably well with values calculated for design (Fig. 4.10).

4.5 Comparison of Small- and Full-Scale Behavior

The primary goal of selecting materials for the model structures was to simulate characteristics of full-scale reinforced concrete structures subjected to loading reversals. Consequent load-deflection relationships for members of the models and actual buildings were essential for valid extrapolation of conclusions made from the test results.

Numerous investigators [2, 3, 8, 10, 16, 25] have reported tests of large-scale reinforced concrete structural elements subjected to cyclic loads. Measured hysteresis curves from four tests are presented in Fig. 4.11 for qualitative comparison with measured curves for the small-scale frame and wall elements. Similar tendencies are noted below.

- (1) Slope of the curve in the loading portion of the first quarter cycle was appreciably larger than in loading portions of subsequent cycles.
- (2) Slope of the curve near maximum loads reduced substantially.
- (3) Slope of the curve in unloading portions of a cycle was larger than the slope in the previous loading portion.

(4) Slope of the curve reduced suddenly in load-reversal portions of a cycle, particularly for interior-joint specimens.

(5) Slope of the curve in low-load portions of a cycle increased with loading.

(6) Maximum loads attained in early cycles could also be attained in later cycles.

(7) Average slope of the curve for a loading cycle reduced following a cycle of larger maximum deflection.

These similarities suggest that the mechanisms of energy dissipation in full-scale reinforced concrete structures were modeled correctly with the materials used to fabricate the test structures.

CHAPTER 5

OBSERVED RESPONSE TO SIMULATED EARTHQUAKE MOTION

5.1 Introductory Remarks

Observed dynamic response of the test structures subjected to simulated earthquake motion is presented in this chapter. Observations are viewed through the window of recorded signals and observed patterns of concrete damage.

5.2 General Comments(a) Response Histories

Measurements from the recorded signals comprised absolute acceleration, displacement relative to base, and strain in the bolts connecting the wall with the remainder of the structural system. The measured bolt strain indicated force resisted by the wall at each level.

Confirmation of the reliability of the reduced acceleration waveforms was provided by comparison of nearly identical accelerations for north and south frames. Displacements were not measured for individual frames except at the top level where agreement was observed. Checks at various times during each test run showed the deflected shape to be smooth indicating individual measurements to be consistent. A discussion of the reliability of the force measurements is presented in Sec. 7.4.

Shear and moment response histories are presented with the observed response because the calculation of shear and moment was no more than the summation of observed accelerations using masses and story heights as additional calibration factors. Shears and moments were calculated from accelerations measured on the north side of each structure. The secondary effect of gravity load acting through lateral displacements was included with the moments.

Representative acceleration and displacement records are depicted in Fig. 5.1 to serve as an introduction to the presentation of the observed waveforms. Amplitude is plotted on the vertical axis versus time in seconds on the horizontal axis. Units of response are given in the title above each waveform. The duration of each simulation was initialized at an arbitrary point in time common with all of the measured response histories. Response was recorded for an additional three seconds following the forced base excitation to observe free-vibration response. Residual amplitude resulting from nonlinear behavior during a test run has been reported also at the start of the record for a subsequent test run.

Forty-eight channels of recorded signals were observed for each test run. Including shear and moment response a total of 816 waveforms were examined. Not all of these response histories are presented in this report. Acceleration records are reported only for the north frame because of observed symmetry of response. Acceleration and force resisted by wall are presented for all levels for initial test runs and at alternate levels for second test runs. Displacement, shear and moment response histories are presented for alternate levels for all test runs because of the similarity of waveform shape between adjacent levels.

Measured response histories for all test runs are not reported. Response to initial test runs is reported for all test structures. Response histories for higher intensity simulations are presented only for second test runs because of small differences in observed earthquake intensities and behavior with third test runs.

(b) Sign Conventions

The convention for the positive sense of displacement, acceleration or force applied to the wall was arbitrary but mutual consistency of signs between each form of response was necessary to avoid confusion for later interpretation. Displacement was assigned a positive sense as the structure swayed east. Acceleration was established kinematically consistent with displacement so that, for harmonic motion, acceleration would be negative for a positive displacement. Lateral inertial force was considered to resist acceleration according to D'Alembert's principle so that a positive force would result from a negative acceleration. Positive displacement occurred with a positive force which was consistent with elementary structural principles. Lateral forces resisted by wall were sensed with the same sign as lateral inertial loads. Shear and moment were calculated so that a positive lateral force would increase shear and moment.

(c) Terminology

The term "mode" is used in this report with the terms "frequencies" and "shapes". For ideally linear behavior these terms may be defined using classical descriptions found in dynamics textbooks. For nonlinear behavior there cannot be a particular frequency or shape pertaining to a mode. However, apparent first- and higher-mode frequencies and shapes were

observed. In this report "first mode" shall refer to the condition when the response of all ten levels is in phase. "Second mode" and "third mode" shall refer to the conditions when there is one and two stationary points along the height of structure.

Double-amplitude response refers to the sum of maximum positive and negative displacements within a particular half cycle.

(d) Organization of Chapter

The measurements are organized so that response to the same earthquake simulation type may be compared for structures with heavily and lightly reinforced walls. The initial condition of each structure is reported first. Damage observed prior to initial test runs due to shrinkage, lifting, transport and erection is presented with figures of crack patterns for the frames and wall of a structure. Response histories of base motions, displacements, accelerations, forces resisted by wall, shears and moments are then presented followed by distributions of the same response along the height of structure at selected instants. Shear and moment for the wall are shown with a solid line. Shear and moment for the entire structure are shown with a broken line. Response at times of maximum displacement are also shown in tabular form. Crack patterns and widths observed after a test run are reported. A key to figure and table designations is provided in Table 5.1.

5.3 Observed Response of Structures During Initial Test Runs

(a) Initial Condition of Test Structures

The initial condition of each test structure subjected to the initial or "design earthquake" simulation of El Centro (FW1, FW2) or Taft (FW3, FW4) is depicted in Fig. 5.2 and Fig. 5.14. Cracks were marked immediately prior to the first test run on each side of the wall for test structures FW1 and FW2, and on the formed side of each frame for test structures FW3 and FW4. The largest crack width was smaller than 0.02 mm.

(b) Base Motions

Base accelerations measured on the north and south frames for each test structure subjected to the El Centro simulation are presented in Fig. 5.3. Amplitude and frequency characteristics of the base accelerations for the north and south frames were nearly identical with maximum base accelerations of 0.50 g and 0.52 g for test structure FW1 and 0.48 g and 0.48 g for test structure FW2. High-frequency components were dominant in the records for the structure with the lightly reinforced wall (FW2). Direct comparison of the response of each structure is still acceptable because the high frequencies are out of the range of the natural frequencies of the first and second modes.

Base accelerations were measured on the north and south frames of the structures subjected to the Taft simulations and were found to be similar. Maximum base accelerations of 0.47 g were measured for both the north and south frames of test structure FW4. Test structure FW3 was subjected to maximum base accelerations of 0.42 g and 0.41 g for the north and south frames. Response histories of the base accelerations measured on the north

frame (Fig. 5.15) for each structure (FW3, FW4) were of nearly identical frequency content. Measured base displacements were similar for each structure with maximum amplitudes of 12.2 mm and 11.8 mm for test structures FW4 and FW3.

A more detailed interpretation of the base motion is presented in the next chapter with the use of spectral-response curves.

(c) Vertical and Transverse Accelerations

Response histories of vertical acceleration measured at the top of the north-east column for each structure (FW1, FW2, FW3 and FW4) contained similar frequencies (28, 27, 28, and 24 hz) and similar maximum amplitudes (0.17, 0.18, 0.18, and 0.23 g). Vertical accelerations measured at the top of the south-west column were not of equal amplitude with those measured at the top of north-east column suggesting a vertical translation of the tenth level mass as well as a small rotation. The dominant frequency remained constant throughout the duration.

Accelerations in the transverse (minor) direction were small for each structure (maximums of 0.11, 0.09, 0.09 and 0.07 g for structures FW1, FW2, FW3 and FW4). Because of the small amplitudes, electronic noise in the recording process had a significant influence on the measured response histories. The accelerations presented in Fig. 5.4 and 5.16 are from measurements at the east end of the tenth level mass. Transverse accelerations were also measured at the west end for structures FW1 and FW2 where similar response was observed of the opposite sign indicating a more prevalent torsional rather than translational motion in the minor direction.

(d) Displacements

Displacement response histories for each structure (Fig. 5.4 and 5.16) were of similar shape at all levels indicating the dominance of the apparent fundamental mode on the displacement response. Each structure responded at an apparent first-mode frequency which decreased throughout the duration of the test run. Small vibrations of each structure at a higher frequency were observed at the lower levels during low-amplitude motions.

Structures with heavily reinforced walls (FW1, FW4) deflected more "regularly" than the structures with lightly reinforced walls (FW2, FW3). Structures FW1 and FW4 responded at a more consistent fundamental frequency than structures FW2 and FW3. Amplitudes of displacement were of similar magnitude in each direction for structures FW1 and FW4, and not for structures FW2 and FW3. The structures with heavily reinforced walls oscillated through more cycles of large-amplitude displacement than did the structures with lightly reinforced walls. Residual displacements at the end of the test run were essentially zero for structures FW1 and FW4, and measurable for structures FW2 and FW3. Deflected shapes (Fig. 5.6 and 5.18) at times of maximum response indicated the stiffening effect of the heavily reinforced walls at the base. At the lower stories, structures FW1 and FW4 deflected similarly to a cantilever beam in flexure, and at the upper stories similarly to a frame or "shear beam." Structures FW2 and FW3 deflected more as a frame for the full height with a rotation at base larger than that of structures FW1 and FW4. Maximum interstory displacements were observed between the fifth and seventh stories for all

structures and were similar for structures of the same base motion type (1.7 and 1.5 percent of story height for FW1 and FW2, and 1.2 and 1.1 percent for FW3 and FW4).

A series of large-amplitude displacements were observed during the initial three seconds of El Centro simulations. During this period structure FW1 responded with seven cycles of high amplitude displacement. Structure FW2 responded at a frequency similar to that of structure FW1 during the first four cycles of large amplitude motion before being limited to smaller amplitudes at a lower frequency. At nearly the same instant, a shift in the displacement record was introduced which was present for the rest of the duration and remained as a permanent displacement once the motion had ceased. Maximum displacements at the tenth level were essentially equal for each structure subjected to El Centro simulations, and occurred at nearly the same instant (28.2 mm at 1.96 seconds for structure FW1, and 27.7 mm at 1.98 seconds for structure FW2).

Large-amplitude displacements were more uniformly distributed over the full duration for structures subjected to Taft simulations than structures subjected to El Centro simulations. Structure FW4 vibrated at a higher apparent fundamental frequency than did structure FW3. Maximum displacements at the tenth level for each structure type were similar but did not occur at similar times (16.9 mm at 2.09 seconds for structure FW3, and 18.2 mm at 5.96 seconds for structure FW4). Residual displacement for structure FW3 was introduced during the first cycle of large amplitude displacement, and was smaller than the residual for the structure with the lighter reinforced wall subjected to an El Centro simulation.

(e) Accelerations

Accelerations were observed to be synchronized with and had the same periodicity as measured displacements and forces resisted by wall. Frequencies larger than the apparent fundamental frequency were prevalent in the measured acceleration records. Lateral force distributions along the height (Fig. 5.6 and 5.10) determined from measured accelerations were sensitive to changes in time because of the controlling influence of the high frequencies.

Response histories of acceleration at lower levels were similar in form to that of accelerations measured at the base. Frequency content of the base motion was prominent in acceleration records of the lower six levels of each structure. Maximum base accelerations were amplified at the first, second, fifth and tenth levels by factors of

	<u>FW1</u>	<u>FW2</u>	<u>FW3</u>	<u>FW4</u>
Tenth level	2.1	1.9	1.7	1.1
Fifth level	1.2	0.7	1.3	0.6
Second level	1.3	0.8	1.2	1.0
First level	1.3	0.7	1.2	0.9

The acceleration amplification, at the instant of maximum base acceleration, for structure FW4 was low and the acceleration at the top was in a direction opposite to that of the base acceleration.

Frequency characteristics of the measured accelerations, particularly at upper levels, indicated strong participation of the second and third modes on the total acceleration response. Accelerations at the eighth level

for each structure were devoid of frequencies in the range of calculated second-mode frequencies. Third-mode frequencies which were visible in response histories at seventh, eighth and tenth levels were not observed at ninth level.

(f) Forces Resisted by Wall

Response histories of force resisted by wall at lower levels were synchronized with and contained similar frequencies as accelerations at those levels. Force response histories at upper levels were dominated by the apparent fundamental-mode frequency observed with displacements. Forces measured at the tenth level were opposite in sign to forces measured below the ninth level. Ninth level forces were small in amplitude and contained high frequencies not observed at other upper levels.

Residual forces acting between the wall and frames at the end of a test run were measured at nearly all levels for all test structures. Shifts in all force records occurred during the first cycle of large-amplitude displacement. Residual forces were larger for the structures subjected to El Centro simulations than Taft simulations. Larger residuals were observed at first level for the structures with lightly reinforced walls than for the structures with heavily reinforced walls.

Because of different hysteresis properties and loading histories of wall and frames (Sec. 4.3) the distribution of lateral inertial force between wall and frames did not remain constant for different amplitudes within a particular cycle, nor were they constant for similar amplitudes at different times during the test run. Distributions for initial test runs are presented (Fig. 5.6 and 5.18) at three times during the cycle of maximum

displacement, and at times of maximum positive and negative displacement for two cycles occurring at different portions of the test duration.

Comparison of force distributions at similar amplitudes of response for each test structure was difficult because of the confusion introduced by residuals which resulted in erratically appearing force distributions. One example is the large residual forces measured at the first level of lightly reinforced walls. Additionally, measured accelerations containing high frequencies did not provide a standard lateral inertial load distribution for comparing force distributions of different walls. Despite these limitations the following general trends were observed.

(1) Force distributions of each structure type were similar for low-amplitude motion, and dissimilar for high-amplitude motion.

(2) At lower levels the wall resisted most of the total lateral load. At the tenth level the frames resisted all of the total load in addition to restraining the wall from deflecting as it would if it were not connected to the frames.

(3) At larger amplitudes, heavily reinforced walls resisted a larger percentage of the total lateral load than lightly reinforced walls, especially at upper stories.

(g) Shears and Moments

Shear and moment response histories (Fig. 5.5 and 5.17) calculated from measured acceleration and force responses had similar characteristics as recorded response histories. Shear and moments were synchronized with displacements at apparent fundamental-mode frequencies. Maxima of shear and moment responses occurred at nearly the same instant as did the maxima of

displacement and acceleration. Response histories of shear and moment at upper levels resembled acceleration and force response histories at the same levels. At lower levels, the shape of response histories of moment resisted by the entire structure were nearly identical to the shape of displacement response histories. Shear and moment for entire structure response were slightly higher for structures with heavily reinforced walls.

Cycles of large-amplitude shear and moment were observed during the first three seconds of El Centro simulations (Fig. 5.5). Cycles of large-amplitude shear and moment were distributed over the total duration of Taft simulations (Fig. 5.17). Residual shears and moments at the end of a test run were larger for structures subjected to El Centro than Taft simulations.

Shears and moments for the wall (shown by a solid curve in the figures) were in phase with shears and moments for the entire structure at lower levels. At upper levels, shears and moments for the wall opposed those for the entire structure.

Moments at lower levels of heavily reinforced walls and shears at lower levels of both wall types were resisted almost exclusively by the wall at small amplitudes of motion.

The wall resisted a large portion of the total first-story shear for each structure type (approximately eighty and sixty percent for heavily and lightly reinforced walls). Heavily reinforced walls were more effective in resisting shears at higher stories than lightly reinforced walls. A larger participation of the apparent second mode on the shear response was observed at lower levels for lightly reinforced walls.

The fraction of the total base moment resisted by the wall was consistently lower than the fraction of the total first-story shear resisted

by the wall. Maximum amplitudes of moment at the base of each wall were close to the maximum moment capacities observed from cyclic-load tests. Walls with heavier reinforcement resisted approximately 45 percent of the total base moment occurring at the peak displacement of each half-cycle. Walls with light reinforcement resisted approximately 20 percent of the total base moment for the first few cycles of large-amplitude motion. For the rest of the test run, the base moment resisted by the lightly reinforced walls was negligible.

Moment diagrams at particular instants (Fig. 5.6 and 5.10) indicated a lower point of contraflexure for lightly reinforced walls than for heavily reinforced walls. For most instants, the point of contraflexure for each wall type became higher as the amplitude of the total moment increased. The increase in height was more sensitive to changes in amplitude for the heavily than lightly reinforced walls.

Yield of tensile reinforcement appears to have occurred at the base of the wall of test structure FW1 as observed by the plateaus in the moment response histories when the structure swayed in the negative direction. The moment measured at the plateaus (approximately 7.0 kN-m) was less than the moment at which the tensile reinforcement yielded during the cyclic-load tests (14.4 kN-m) indicating a possible initial moment from unrecorded forces applied to the wall during the construction process.

(h) Condition of Test Structures Following Test Run

Cracks were marked following the initial test run for structures subjected to both El Centro simulations (Fig. 5.7) and Taft simulations (Fig. 5.19). Crack widths were measured at the ends of each beam of each

frame following the test run. The mean crack width for any particular level is presented in Table 5.2.

5.4 Observed Response of Structures During Subsequent Test Runs

(a) Base Motions

Base accelerations measured on north and south frames for each test structure subjected to El Centro simulations are presented in Fig. 5.8. Maximum base accelerations for the second test run were measured to be 1.58 g and 1.82 g for the north and south frames of test structure FW1, and 0.92 g and 0.92 g for test structure FW2. The acceleration maxima for structure FW1 are measured from "spikes," or amplitudes of very short duration, and should not be used as an index of the simulated earthquake intensity. To provide a clearer comparison of base-motion intensity, the amplitudes at an arbitrary instant (0.88 seconds) were measured to be 0.60 g for both the north and the south frames of structure FW1. At the same instant, accelerations of 0.55 g were measured at the base of both the north and the south frames of structure FW2.

Measured response histories of base motions for structures subjected to Taft simulations (Fig. 5.20) had similar frequency characteristics and amplitudes. Acceleration maxima measured at the base of the north and the south frames were 0.93 g and 0.94 g for structure FW4, and 0.97 g and 0.94 g for structure FW3. Base displacement maxima were 27.5 mm and 25.5 mm for structures FW4 and FW3.

(b) Vertical and Transverse Accelerations

Response histories of vertical acceleration (Fig. 5.9 and 5.21) measured at the top of the north-east column for each structure (FW1, FW2, FW3 and FW4) contained similar frequencies (23, 23, 22 and 19 Hz) which remained constant throughout the duration. Similar maximum amplitudes were measured for structures subjected to the same earthquake simulation type (0.34 and 0.38 g for FW1 and FW2, and 0.54 and 0.51 g for FW3 and FW4).

Accelerations measured in the vertical direction at the top of the south-west column were not of equal amplitude with those measured at the top of the north-east column indicating vertical translation as well as rotation of the mass. The increase in amplitude with higher intensity base motion was not observed in previous tests of frames without walls [9,18].

Transverse accelerations measured at the east and west ends of the tenth level mass had similar amplitudes but were opposite in sign indicating a small torsional motion. Maximum amplitudes were 0.23, 0.12, 0.17 and 0.10 g for structures FW1, FW2, FW3 and FW4.

(c) Displacements

Features observed in the displacement response for the initial test run were observed also for the second test run. Response histories (Fig. 5.9 and 5.21) at each level were similar in shape indicating the prominence of an apparent fundamental mode in displacement response. The apparent first-mode frequency decreased throughout the duration of the test run, but with a smaller change than that observed for the initial test run. Components of displacement response at the second-mode frequency were more prevalent in the second test run than in the first test run.

The shape of displacement response histories for structures with heavily reinforced walls (FW1, FW4) subjected to the second test run resembled the shape of response histories for structures with lightly reinforced walls (FW2, FW3) subjected to the first test run. Residual displacements for structures FW1 and FW4 were larger following the second test run than following the initial test run. During the second test run, structures with lightly reinforced walls responded with more irregular amplitudes and more inconsistent frequencies than did structures with heavily reinforced walls. Residual displacements for structures FW2 and FW3 were smaller following the second test run than following the first test run.

Deflected shapes at times of maximum positive and negative displacement for the second test run (Fig. 5.11 and 5.23) were similar to deflected shapes observed for the first test run. Maximum interstory displacements were observed between the fifth and seventh stories for all structures, and were similar for structures subjected to the same base motion (2.5 and 2.3 percent of story height for structures FW1 and FW2, and 2.9 and 2.8 percent for structures FW3 and FW4).

Structures subjected to El Centro simulations responded with large-amplitude displacements which were distributed over the full duration rather than being concentrated over the first three seconds as observed for initial test runs. Structures subjected to Taft simulations responded similarly as observed for the first test run with large-amplitude displacements being distributed over the full duration. Maximum displacements at the tenth

level were similar for structures subject to the same base motion (38 and 43 mm for FW1 and FW2, and 48 and 46 mm for FW3 and FW4).

(d) Accelerations

Characteristics observed in measured acceleration response histories of the initial test run were also apparent for the second test run (Fig. 5.9 and 5.21). Accelerations were in phase with displacements at the apparent fundamental-mode frequency. High frequencies were dominant in the records at nearly all levels. Response histories at lower levels resembled measured base accelerations. Frequencies observed in the base accelerations were noticed in acceleration records for the lower six levels of each structure. The spike in the base acceleration record of structure FW1 was observed in acceleration response histories up to the fourth level. Maximum base accelerations were amplified at the first, second, fifth and tenth levels by factors of:

	<u>FW1</u>	<u>FW2</u>	<u>FW3</u>	<u>FW4</u>
Tenth Level	0.7	0.9	1.3	1.1
Fifth Level	0.8	0.6	0.5	0.5
Second Level	1.0	1.0	1.6	1.0
First Level	1.1	0.9	1.3	1.1

Maximum accelerations below the fourth level occurred at the same instant as maximum base accelerations. Above the fourth level maximum accelerations occurred at instants which varied from level to level.

Acceleration records at upper levels revealed similar influences of higher modes as observed for the initial run. Eighth-level acceleration

response histories contained nearly no components at the apparent second mode frequency. Third-mode frequencies which were present at other upper levels were not visible at ninth level.

(e) Forces Resisted by Wall

Characteristics of response histories of forces resisted by wall for the first test run were evident in response histories of the second test run (Fig. 5.9 and 5.21). Response histories at all levels were synchronized with displacements and accelerations at the apparent fundamental-mode frequency. At lower levels, force response histories contained similar frequencies as acceleration response histories at the same levels. Spikes in the acceleration records of structure FW1 were observed in the force records up to the fourth level. Forces measured at tenth level were opposite in sign to the forces measured below ninth level. Amplitudes of force resisted by wall were similar to amplitudes measured for the first test run.

Subsequent test runs revealed characteristics not observed in force response of initial test runs. Response histories at upper levels contained more high-frequency components than observed in first test runs. The distribution of cycles of large-amplitude force was more uniform over the duration of subsequent test runs than over the duration of the initial run for El Centro simulations.

Amplitudes of force resisted by wall measured at the end of the first test run were nearly identical with measurements at the beginning of the second test run indicating little relaxation of the structures and

little drift in strain gages during the intermission between test runs. Net residual forces measured over the duration of subsequent test runs were considerably smaller than for the initial test run. Net residual forces of structures subjected to El Centro simulations were similar to those of structures subjected to Taft simulations.

Force distributions at times of maximum displacement (Fig. 5.11 and 5.23) appeared to be more erratically shaped than those of the first test run because of the strong influence of shifts in the force response histories. Inelastic deformations, particularly at the base of the wall, controlled the shape of force distributions more than inertial loads.

(f) Shears and Moments

Although amplitudes of shear and moment were larger for higher intensity base motions, many characteristics observed in the response histories of the initial test run were visible in response histories of subsequent test runs (Fig. 5.10 and 5.22).

Maxima of shear and moment occurred at nearly the same instant as did maxima of acceleration and displacement. Shapes of moment response histories at lower levels were nearly identical to displacement histories at the same levels. At upper levels, shear and moment response histories contained several components at high frequencies. Shears and moments for the wall at upper levels opposed those for the total structure.

Shears and moments for the total structure were slightly larger for structures with heavily reinforced walls. The participation of the second mode on the first-story shear response was greater for structures

with lightly reinforced walls than for structures with heavily reinforced walls.

Moment diagrams for each structure (Fig. 5.11 and 5.23) at times of maximum displacement indicated little change in the point of contraflexure from the first test run.

Differences were observed in shear and moment response between initial and subsequent runs. The portion of the total first-story shear resisted by the wall varied with each test structure. Shear resisted by the wall at the first story of structure FW1 (approximately 60 percent of the total shear) was less than the percentage observed for the same structure subjected to the first test run. The other heavily reinforced wall (FW4) resisted a similar percentage of the total shear at the first story during the second run (approximately eighty percent) as it did during the first run. Structures with lightly reinforced walls (FW2, FW3) resisted shears unsymmetrically as the structures deflected in positive and negative directions. The wall of each structure resisted nearly all of the shear at the first story in the positive direction, but only a small fraction in the negative direction.

Each wall resisted similar percentages of total moment at lower levels during subsequent test runs as it did during initial test runs. Wall moments at upper levels of structure FW3 for the second test run were observed to be in phase with the total-structure moment at small amplitudes, and of opposite sense at large amplitudes.

Structures subjected to El Centro simulations responded with large-amplitude shears and moments which were distributed more uniformly over

the full duration of the second run than the first run. The distribution of cycles of large-amplitude shears and moments over the full duration of subsequent Taft simulations was similar to the distribution for the initial test run.

(g) Condition of Test Structures Following Test Run

Cracks marked after the second run (Fig. 5.12 for structures subjected to El Centro simulations and Fig. 5.24 for structures subjected to Taft simulations) indicated an increase in damage to each structure during the second test run. Crack widths measured at the beam ends (Table 5.2) were larger than those measured previously.

CHAPTER 6

INTERPRETATIONS OF OBSERVED DYNAMIC RESPONSE

6.1 Introductory Remarks

The previous chapter presented the observed response with a minimum amount of interpretation. In this chapter, measured base motions are interpreted using Fourier-amplitude spectra and spectral-response curves. Dynamic characteristics of each test structure are examined through interpretation of measured response histories using Fourier transform techniques, and through interpretation of measurements obtained during free and steady-state vibration tests.

6.2 Base Motions

To aid in the evaluation of the response of test structures to simulated earthquake motions, Fourier-amplitude spectra and spectral-response curves have been calculated from measured base accelerations. These curves serve as the basis for interpreting the frequency content of each base motion, and the impact of each base motion on resulting structural response.

(a) Frequency Content of Measured Base Motions

Fourier-amplitude spectra calculated from accelerations measured at the base of north frames, which were essentially the same as those

calculated from south accelerations, are presented in Fig. 6.1. Comparing spectra of the same simulation type revealed nearly identical frequency contents of base motions for all test runs of both structures subjected to Taft simulations. Frequency contents of El Centro base motions differed for simulations occurring on different test dates. High-frequency accelerations measured at the base of structure FW1 during the first test run (Fig. 5.3) which are visible on the plot at 37 Hz were not observed during the testing of structure FW2. Frequencies in the range of 10 to 25 Hz were more prevalent for El Centro accelerations measured at the base of structure FW1 than accelerations measured at the base of structure FW2.

(b) Spectral-Response Curves

Maximum responses to measured base accelerations of several linear single-degree-of-freedom oscillators with varying natural frequencies were calculated for a full range of oscillator frequencies (from 1.0 to 50.0 Hz) and damping factors (0, 2, 5, 10 and 20 percent). The calculation involved a numerical process for solving the convolution integral whose derivation may be found in most books on dynamics [4, 13, 19] for calculating the response of an oscillator to a general impulsive load. Spectral-response curves are presented so that comparisons may be made between simulations of the same earthquake type. Curves calculated from observed acceleration records of El Centro and Taft simulations are presented in Fig. 6.2 and 6.3. Spectral-response curves of displacement, velocity and acceleration are plotted in tripartite format for the first two test runs of each

structure. Individual curves of acceleration and displacement are presented in arithmetic format for all three test runs of each structure so that loads and displacements may be more easily read.

Spectral-response curves calculated from accelerations measured at the base of the north frame were nearly identical with those calculated using south accelerations. Spectral-response curves presented in this report are calculated from north accelerations.

Spectral-response curves of displacement were similar in shape for all test runs of each base-motion type. Spectral-response curves of acceleration were similar in shape for all test runs of Taft simulations. For El Centro simulations, spectral-response curves of acceleration were similar in shape for frequencies less than 5.0 Hz.

To examine differences in acceleration spectral response at higher frequencies, spectral accelerations at a high frequency and damping factor (50 Hz and 0.20) have been plotted versus the maximum measured base acceleration (Fig. 6.4). For an oscillator whose natural frequency is much higher than the frequencies of the base acceleration, the maximum acceleration of the oscillator should approach that of the base motion. This trend was generally observed for the measured base motions because the frequency of 50 Hz is beyond the range of the dominant frequencies of the undistorted base accelerations. Maximum base accelerations for the second and third test runs of structure FW1 (Fig. 5.8) occurred as "spikes," or at a relatively high frequency resulting in a larger spectral than maximum base acceleration. Spectral acceleration at 50 Hz was also higher than the maximum base acceleration for the base motion of the first test

run of structure FW2 because of high frequency accelerations observed in the base motion response history (Fig. 5.3). The high frequency was approximately 37 Hz as measured from Fourier-amplitude spectra of the base motion (Fig. 6.1) which was close to the frequency (50 Hz) at which the spectral acceleration was compared.

(c) Spectrum Intensities

Because of distortions of maxima observed in measured base-acceleration records of higher intensity simulations, maximum base acceleration should not be used as a measure of base motion intensity. Spectrum intensity is defined in this report as the area under the spectral-response curve of velocity calculated for a given damping factor between natural periods of an oscillator of 0.04 and 1.00 seconds. This definition is derived from Housner's (1952) concept of spectrum intensity as a measure of earthquake intensity. Alterations have been made in the bounding periods defined by Housner [12] to account for compressing the duration of the actual earthquake by a factor of 2.5.

Spectrum intensities have been calculated for each of the base motions measured for each test structure. The relationship between maximum base acceleration and spectrum intensity (Fig. 6.5) confirms that maximum base accelerations are an inaccurate index of intensity for stronger simulations.

To simplify comparisons of spectrum intensity with structural response, spectrum intensities based on damping factors of 0.00, 0.02, 0.05, and 0.20 are compared with spectrum intensities based on a damping factor of 0.10 (Fig. 6.6). The linear relationship indicates that, for the measured

base motions, spectrum intensity calculated using any one of the damping factors would serve as an equally good measure of base motion intensity. Spectrum intensities calculated from measured base motions using a damping factor of 0.10 are presented in Table 6.1.

Spectrum intensities for the first test run of all structures were similar (a coefficient of variation of 4.8 percent). Spectrum intensities for the second and third test runs were not similar for each test structure (coefficients of variation of 11 and 14 percent for runs two and three) making comparison of response of different structures for a particular higher intensity test run difficult.

For the same simulation type, structures with more heavily reinforced walls were subjected to base motions of larger spectrum intensity than for structures with lightly reinforced walls. Except for the initial test run of structures FW3, spectrum intensities of Taft simulations were larger than those of El Centro simulations.

(d) Comparison of Spectral-Response Curves
for the First Test Run

Displacement spectral-response curves for initial test runs of El Centro simulations (Fig. 6.7) were nearly identical. For Taft simulations spectral curves of displacement were similar in shape for each base motion of both test structures but differed in magnitude by approximately the same factor as did spectrum intensities. Spectral displacements for both El Centro and Taft simulations increased with decreasing frequency to a frequency of approximately 2.0 Hz. Spectral displacements

for El Centro simulations continued to increase for frequencies less than 2.0 Hz but remained nearly constant for Taft simulations.

Acceleration spectral-response curves were essentially the same curve for initial test runs of El Centro simulations for frequencies below 5.0 Hz (Fig. 6.8). For Taft simulations spectral-response curves of acceleration followed the same pattern as for displacement. Curves were similar in shape for each base motion of both structures but varied in amplitude. Spectral accelerations for both El Centro and Taft simulations decreased similarly for frequencies below 4.0 Hz. No comparisons can be made between spectral accelerations of El Centro and Taft simulations for frequencies larger than 4.0 Hz.

Spectral-response curves used to estimate lateral loads in the design process (Sec. 3.3) are plotted in Fig. 6.8 for comparison with spectra calculated from measured base accelerations. Design spectra were based on maximum base accelerations of 0.40 g as compared with measured values of 0.55, 0.48, 0.42 and 0.47 g for test structures FW1, FW2, FW3 and FW4. First-mode forces were approximated more accurately in the design process than higher-mode forces as seen by larger deviations between the design spectra and spectra based on measured base motions for frequencies larger than 5.0 Hz.

(e) Study of Partial Durations

To investigate the influence of selected portions of the duration on response, spectral-response curves have been calculated for the first three, six and nine seconds of both El Centro and Taft simulations (Fig. 6.9).

Maximum response resulting from acceleration impulses during the first three seconds of El Centro simulations were the same maxima as calculated for the full duration. Maximum response resulting from the first six seconds of Taft simulations were equal to maxima resulting from accelerations of the full duration except for oscillators with natural periods between 0.31 and 0.72 seconds.

6.3 Measured Dynamic Characteristics of Test Structures

Natural frequencies, mode shapes, and an estimate of the energy dissipation of each test structure are interpreted in this section using measurements obtained during free-vibration and steady-state tests, and earthquake-simulation test runs. Because of probable nonlinear behavior of the test structures, a particular natural frequency, deflected shape, or damping factor for a particular mode may not exist. Unique values discussed in this section are attributed to measured vibrations with characteristics similar to those of a structure behaving linearly.

(a) Natural Frequencies

Free-vibration tests were performed before all earthquake simulations and all steady-state tests. Steady-state tests were performed following each earthquake simulation for test structures FW3 and FW4. Apparent fundamental-mode frequencies measured during each type of vibration are summarized in Fig. 6.10. The maximum tenth-level displacement measured during the previous earthquake simulation has been plotted to serve as an index of the current stiffness of each structure.

Fundamental frequencies obtained from free-vibration tests were determined from Fourier-amplitude spectra of measured tenth-level accelerations (Fig. 6.14). Frequencies obtained from steady-state tests were measured during apparent resonant conditions (Fig. 6.18). Fourier spectra of tenth-level displacement response (Fig. 6.13) were used to establish dominant fundamental-mode frequencies measured during each earthquake simulation. Because of variations in stiffness and base motion occurring over the duration of a simulation, apparent fundamental frequencies varied over a range as wide as 3.0 Hz. The single frequency used for comparison with frequencies of other test runs was the frequency at which the spectral amplitude was the largest.

Vibration of a structure that softens with increasing displacement would be expected to decrease in frequency as amplitude of the motion increases. This tendency was observed from vibration tests that deflected test structures varying amounts. Maximum tenth-level displacements during free-vibration and steady-state tests were approximately 0.5 and 5.0 mm. During earthquake simulations, maximum tenth-level displacement (one-half of double-amplitude) varied from 18 mm to 56 mm. Frequencies measured during free-vibration tests were consistently larger than those measured with other types of vibration tests. Steady-state frequencies were in most cases larger than those measured during earthquake-simulation test runs.

Frequencies of structures containing walls that were lightly reinforced (FW2, FW3) decreased more significantly during third test runs than

for structures with heavily reinforced walls (FW1, FW4). This trend was observed only for response during earthquake simulations, and not from low-amplitude vibration tests.

Apparent frequencies of structures with generally decreasing stiffness would be expected to decrease. Second-mode translational frequencies obtained from Fourier-amplitude spectra of measured free-vibration response did reduce appreciably during the initial earthquake simulation (Fig. 6.11). First-mode frequencies, however, remained essentially constant.

To examine the relative decrease between first- and second-mode frequencies with cracking of concrete, frequencies have been calculated for test structures with varying distributions of cracking (Fig. 6.15). Cracking was considered to occur progressively from the base to the top level of each test-structure type. Symmetrical patterns of cracking consisted of both frames cracked, both frames with the wall cracked, and the wall cracked alone. The unsymmetrical case of only one frame cracked with the wall was also examined. Test structures were modeled with linear-elastic elements using the ETABS computer program. Stiffnesses were based on transformed sections for members which were considered to be uncracked, and cracked sections for members which were considered to be cracked.

Salient conclusions of the study are

- (1) For any amount of cracking (stiffness reduction), decrease in frequency was greater for the second mode than for the first mode.
- (2) First- and second-mode frequencies were more sensitive to cracking of the frames than the wall. First-mode frequencies were nearly insensitive to cracking of the wall.

- (3) First-mode frequencies were more sensitive to cracking at lower levels of the frames and wall than at upper levels.
- (4) Second-mode frequencies were more sensitive to cracking at upper levels of the frames and lower levels of the wall than at other portions of the structure.
- (5) Cracking of only one frame reduced the first-mode frequency nearly equally as cracking of both frames.
- (6) Cracking of only one frame reduced the second-mode frequency much less than cracking of both frames.

Another dominant frequency of approximately 7 Hz was observed in Fourier-amplitude spectra of the free-vibration response (Fig. 6.14) measured before initial test runs. The same frequency was observed in Fourier-amplitude spectra of tenth-level transverse accelerations measured during initial free-vibration tests (Fig. 6.16) suggesting the existence of the 7 Hz frequency as a fundamental torsional frequency. This frequency was not observed during subsequent free-vibration tests, except for one test which followed test run three of structure FW1. Excitation of the presumed torsional mode may be attributed to unsymmetrical cracking of the frames before being subjected to large-amplitude motions of initial test runs. Free-vibration tests following initial test runs resulted in measured frequencies which agree with calculated values for a fully cracked, but symmetrical, structure. Prominent vibrations in the torsional mode may have reappeared following the third test run of structure FW1 because of unsymmetrical spalling of concrete in frames, or a possible eccentricity

of the load applied to the tenth-level mass which was used to excite the structure in free vibration.

The small change in measured first-mode translational frequency before and after initial test runs may be attributed to unsymmetrical, partially cracked frames prior to the run and symmetrical, cracked frames following the run. This is consistent with the small change in the calculated first-mode frequencies as one frame of the unsymmetrical idealized structure cracked (conclusion 5 from calculation of frequencies). The larger decrease in measured second-mode translational frequencies occurring during initial test runs is also consistent with the presumed pattern of cracking and the trend of the calculated second-mode frequencies (conclusion 6 from calculation of frequencies).

(b) Mode Shapes

A unique deflected shape for a particular mode of response may not be an ambiguous concept for the nonlinearly behaving test structures because measured deflected shapes (Fig. 5.6, 5.11, 5.18 and 5.23) appeared to represent response of structures behaving linearly. Deflected shapes of the test structures vibrating at the apparent fundamental-mode frequency were inferred from displacement records measured during earthquake simulations. Response histories at all ten levels were filtered to exclude components at frequencies larger than the apparent fundamental-mode frequency. Mode shapes, tabulated in Table 6.2, were representative of response at varying displacement amplitudes within a particular cycle, and at maximum amplitudes of successive cycles.

Mode shapes were inferred also from displacements measured during resonant conditions of steady-state vibration tests of structures FW3 and FW4 and are presented in Table 6.3.

The variation in shape for different amplitudes of vibration, test structure, and type of vibration (earthquake-simulation or steady-state) was small. To examine the measured shapes further, the following shape characteristics were calculated which were useful for interpretation of measured response of the test structures as single-degree-of-freedom (SDOF) systems.

- (1) Modal participation factor, c_n , defines participation of an individual mode of a structure subject to a motion at base:

$$c_n = \frac{[\phi_n]^T [m] [1]}{[\phi_n]^T [m] [\phi_n]}$$

where $[\phi_n]$ = mode shape

$[m]$ = mass matrix

or, for equal masses at all ten levels:

$$c_n = \left(\frac{\sum_{i=1}^{10} \phi_i}{\sum_{i=1}^{10} \phi_i^2} \right)$$

Displacements and accelerations for a particular mode may be related to those of a SDOF system using the modal participation factor and the coordinate of the mode shape at a particular level as follows.

$$d_{n_i} = c_n \phi_{n_i} D_n$$

$$a_{n_i} = c_n \phi_{n_i} A_n$$

where d_{n_i} , a_{n_i} = displacement and acceleration for mode n
and level i

D_n , A_n = displacement and acceleration for mode n
of SDOF system

- (2) Effective weight coefficient, γ_n , relates the total weight of the structure, W (45.8kN), and the SDOF acceleration (in terms of gravity acceleration) to the base shear for a particular mode n :

$$V_{bn} = \gamma_n W A_n$$

The derivation of γ_n follows from the summation of inertial forces at each level which are related to a SDOF acceleration:

$$\gamma_n = \frac{(\sum \phi_{n_i})^2}{10(\sum \phi_{n_i}^2)}$$

for equal masses at all ten levels.

- (3) Effective height of resultant lateral load, H_n , is the height above the base at which the total lateral load acts for mode n :

$$H_n = h \left(\frac{\sum (i) (\phi_{n_i})}{\sum \phi_{n_i}^2} \right) \quad i = 1, 10$$

for equal masses and uniform story heights, h , throughout structure.

The modal participation factor, base shear coefficient and effective height of resultant lateral load were calculated for measured mode shapes and are

tabulated with each shape in Tables 6.2 and 6.3. Shape characteristics were similar for all test structures and were insensitive to changes in amplitude of vibration. This conclusion indicates that the measured response may be interpreted in terms of the response of a series of SDOF oscillators each vibrating at a particular modal frequency.

(c) Energy Dissipation

Estimates of energy dissipated by each structure responding at the apparent fundamental-mode frequency were derived from data measured during free-vibration and steady-state vibration tests. Accelerations measured at the tenth level during free-vibration tests were used with the logarithmic decrement method [4, 13] to calculate estimates of the equivalent-viscous damping factor for each test structure. Acceleration response histories (Fig. 6.14) were first filtered to exclude components at frequencies larger than four Hz so that amplitudes of the apparent first-mode motion would be more clearly visible for interpretation. Filtered records are represented in the figure with a solid line which is superimposed over a broken line which represents the total measured response. Calculated damping factors inferred from free-vibration test data are presented in Table 6.4.

Apart from calculated estimates of energy dissipation, filtered free-vibration response histories revealed two tendencies which were observed for all test structures.

(1) Response measured during free-vibration tests attenuated much more rapidly after the test structure had been subjected to an initial

earthquake simulation. The apparent increase in energy dissipation may be attributable to cracking of the concrete during initial earthquake simulations.

(2) Response at higher frequencies attenuated more rapidly than response at the apparent first-mode frequency indicating a greater amount of energy dissipation for higher modes.

Energy dissipation at a higher amplitude (5.0 mm tenth-level displacement versus 0.5 mm for free-vibration tests) was inferred from response amplification measured during steady-state tests. Frequency-response curves (Fig. 6.18) were constructed by plotting the magnification of base displacement versus the input frequency. Magnification of base displacement was defined as the ratio of the maximum equivalent single-degree-of-freedom displacement of the structure relative to the base and the maximum base displacement. An equivalent single-degree-of-freedom displacement was calculated by dividing the measured tenth-level displacement by the ordinate of the mode shape at the tenth level and the modal participation factor, both of which were determined from displaced shapes measured at apparent resonant frequencies. According to a similar formulation by Jacobsen and Ayre [13] the equivalent-viscous damping factor may be approximated as one-half of the inverse of the magnification factor at resonance. Alternatively, the damping factor may be approximated by the width of the frequency-response curve,

$$\beta = \frac{\omega_2 - \omega_1}{2\omega_R}$$

where β = equivalent-viscous damping factor
 ω_1, ω_2 = input frequencies at a magnification equal to
the maximum magnification $1/\sqrt{2}$
 ω_R = resonant frequency.

Damping factors have been approximated using both of these derivations with data from steady-state vibration tests of structures FW3 and FW4 (Table 6.5). It should be noted that response of test structures subjected to sinusoidal base motions may not have been completely linear. Damping factors have been calculated using a method which is based on linear behavior, and should therefore be viewed only as approximations of actual energy dissipation. Despite this limitation, three tendencies were observed from the frequency-response curves (Fig. 6.18) with progressive softening of each test structure.

(1) Magnification of base displacement decreased as the natural frequency decreased indicating an increase in energy dissipation with softening of the structure.

(2) The test structure containing the lightly-reinforced wall (FW3) had smaller magnifications of base displacement than did the structure containing the heavily-reinforced wall (FW4). This tendency may be attributable to a greater amount of energy dissipation for the structure with a greater extent of nonlinear behavior.

(3) As the natural frequency of a test structure decreased, the shape of the frequency-response curve became less symmetrical. The slope of the low-frequency side of each curve became steeper, and the slope of the high-frequency side became flatter suggesting a greater extent of nonlinear behavior.

Damping factors calculated from data measured during free- and steady-state vibration tests are plotted versus the maximum tenth-level displacement observed during the previous earthquake simulation (Fig. 6.17). As for the comparison of natural frequencies with changes in stiffness, maximum tenth-level displacement has been plotted to serve as an index of the current stiffness of each structure. The trend of the increase in energy dissipation with event was similar for each type of vibration test. A smaller increase in energy dissipation was observed following higher-intensity earthquake simulations than following lower-intensity simulations. Additionally, damping factors calculated from data measured at larger amplitudes (steady-state tests) were larger than those calculated from data measured at smaller amplitudes (free-vibration tests).

6.4 Frequency Content of Measured Response

When a structure is subjected to a strong motion at the base, resulting response is a complex interaction of the changing dynamic characteristics of the structure and the frequency content, sequence, and intensity of the base motion. The frequency content of any type of response (acceleration, displacement, shear, etc.) may not directly reflect the stiffness properties of a building. Interpretation of the relative amplitude of the components of the observed response is necessary to identify ranges of natural frequencies, and to suggest relative participations of each mode.

Measured response histories of the test structures are interpreted in this section with respect to frequency content. Records have been

transferred to the frequency domain by an analysis which decomposed each record into a series of sinusoidal components at frequencies ranging from 0.0 to 40.0 Hz. Normalized amplitudes of each component have been plotted versus the frequency of each component as Fourier-amplitude spectra. A further step reassembled components within a particular frequency range resulting in time-domain response which was filtered to exclude components at frequencies outside the particular range. In this manner measured response histories were filtered to exclude all components at frequencies larger than apparent fundamental frequencies.

Representative Fourier-amplitude spectra and corresponding filtered waveforms for each form of measured response are presented in Fig. 6.19. Filtered records are shown as solid lines which are superimposed over measured records which have been represented as broken lines. Displacement, acceleration, force-on-wall, shear, and moment response were measured during the initial test run of structure FW4. To show variations in frequency content of response of walls with appreciable differences in reinforcing ratios, Fourier-amplitude spectra and filtered waveforms of response of a lightly reinforced wall (initial test run of structure FW3) are presented also in Fig. 6.18.

(a) Displacement Response

The frequency content of measured displacement records (Fig. 6.19a) consisted primarily of frequencies that were apparent fundamental mode. Filtered waveforms were essentially the same curves as measured waveforms, and nearly no frequencies were observed on Fourier-amplitude spectra outside of the range of fundamental-mode frequencies. The same shape of

measured waveforms at each level supports the observation that the displacement response of the test structures may be represented by a single-degree-of-freedom system.

(b) Acceleration Response

Unlike displacement response the frequency content of measured acceleration response (Fig. 6.19b) consisted of many high-frequency components. At lower levels (below third level) frequency contents of accelerations resembled that of base accelerations (Fig. 6.1) suggesting behavior of a rigid structure. At upper levels, accelerations did not include base-acceleration frequencies but did contain high frequencies attributable to higher-mode effects.

Despite changes in natural frequencies with damage and amplitude of motion, apparent first-, second-, and third-mode components of acceleration at each level were observed to be distributed along the height with essentially the same shape as the mode shape. For example, amplitudes of filtered acceleration waveforms at each level were distributed similarly to displacements. Zero ordinates of second-mode shapes could be inferred from frequency contents of measured accelerations. Though the range in second-mode frequencies was generally wide on Fourier-amplitude spectra (approximately from 10 to 20 Hz) nearly no components were visible at the eighth level. Furthermore, filtered waveforms at the eighth level were essentially the same curve as measured acceleration response histories at that level signifying a constant node point and shape of an apparent second mode for all amplitudes and instants throughout the duration. A

similar but less revealing trend may be observed for apparent third-mode frequencies by examining frequency contents of acceleration records at the fifth and ninth levels. The consistent pattern of high-frequency accelerations along the height of structure implies that the distribution of lateral forces applied to the nonlinearly behaving test structures may be represented using a modal analysis.

(c) Shear and Moment Response

The large participation of high-frequency components in lateral-force response was not observed in shear or moment response. Amplitudes on Fourier-amplitude spectra of shear and moment response (Fig. 6.19c and 6.19d) at frequencies larger than apparent fundamental-mode frequencies were small. Filtered waveforms of shear and moment response presented in the same figure indicated a large participation of the apparent fundamental-mode. High-frequency lateral forces at upper levels did influence shear and moment response at upper levels but appeared to have cancelled for shear and moment response at lower levels. Increases in shear or moment at lower levels resulting from high-frequency accelerations at lower levels were negligible.

Filtered shears and moments at all levels varied with time similarly as did measured displacements indicating an apparent linear response of the test structures.

(d) Wall Response

Frequency contents of wall response (Fig. 6.19e and 6.19f) were unlike frequency contents of acceleration response at the same level sug-

gesting the presence of forces resisted by wall that were not simply some fraction of the lateral inertial load applied to the structure. Internal forces resulting from frame-wall interaction must have also been present.

High-frequency components of the base motion observed in acceleration response at lower levels were not prevalent in wall response. At the tenth level, lateral inertial forces (accelerations) contained apparent second- and third-mode frequencies yet force was applied to the wall at frequencies which were predominately in the range of fundamental-mode frequencies.

To gain insight into the relationship between force applied to the wall at a particular level and lateral force applied to the structure at all levels, a set of influence coefficients was calculated and is presented in Table 6.6. The force applied to the wall at a particular level may be calculated by summing the products of lateral force applied to the structure and the corresponding influence coefficient. Coefficients have been determined using the Mueller-Breslau principle with the linear model of the softened structure described in Sec. 7.3 with beam and wall stiffnesses inferred from cyclic-load tests. Influence coefficients are the lateral deflections at each level resulting from an imposed unit axial distortion of a particular link member connecting the wall and frames of the analytical model.

According to Table 6.6, the wall resisted most of the total lateral load at the first level (100 and 93 percent for heavily and lightly reinforced walls). However, forces resisted by wall at the first level were

dependent also on loads applied to the structure at upper levels. Because the sum of upper level lateral loads was much larger than the lateral load at the first level, force resisted by wall at first level would be expected to be influenced predominantly by loads applied to the structure at upper levels. Frequency contents of wall response (Fig. 6.19e) at lower levels were observed to be similar to frequency contents of acceleration, or lateral load, response (Fig. 6.19b) at upper levels.

The small high-frequency components in the tenth-level wall response may be explained also with the set of influence coefficients. Forces applied to the wall at the tenth level, according to Table 6.6, were dependent largely on lateral forces applied to the test structure at the seventh, eighth and ninth levels. Because of the large accelerations measured at these levels which were predominantly at a fundamental frequency, the force resisted by wall at tenth level would be expected to be acting predominantly at a fundamental frequency.

Frequency contents observed in response of force resisted by wall were reflected in the response of wall shears and moments. Shear and moment response of structure FW4 (Fig. 6.19g and 6.19i) contained few frequencies other than apparent fundamental-mode frequencies. An exception to this tendency was observed for the moment response at the sixth level which was near a point of contraflexure for the first-mode loading. Shear and moment response for structure FW3 (Fig. 6.18h and 6.18j) contained a large participation of second-mode frequencies as did the force response. The conspicuous appearance of second-mode frequencies

in the wall response of structure FW3, and the predominantly first-mode wall response of structure FW4 suggested the sensitivity to characteristics of the base motion and a small change in second-mode frequency.

6.5 Interpretation of Measured Response Using a Linear SDOF Oscillator

Measured hysteresis relationships for frame elements (Fig. 4.5) subjected to loading programs which simulated recorded displacement histories indicated that the test structures had incurred substantial nonlinear deformations during earthquake simulations. However, nearly identical measured displacement shapes for all amplitudes of motion (Sec. 6.3b) suggested that response of the nonlinearly behaving multi-degree-of-freedom (MDOF) structures may be represented by a series of single-degree-of-freedom (SDOF) oscillators each with a natural frequency equal to that of a particular mode of the MDOF structures. Furthermore, observations of apparent modal frequencies (Sec. 6.3a) implied the possibility of modeling nonlinear behavior of a particular cycle using a linear stiffness.

Maxima of displacement and acceleration response of linear SDOF oscillators subjected to measured base motions were determined using spectral-response curves (Fig. 6.2 and 6.3). Frequencies of the oscillators were set equal to measured natural frequencies of the test structures for cycles of maximum response. Damping factors were estimated with values obtained from data obtained during steady-state vibration tests (Fig. 6.17). Calculated SDOF response was extended to estimate MDOF response using

characteristics of measured mode shapes from Table 6.2. Comparisons of measured with calculated first-mode maximum response are shown for displacement at level ten (Fig. 6.20a), acceleration at level eight (Fig. 6.20b), shear at first story (Fig. 6.20c), and moment at base (Fig. 6.20d). The choice of level at which a particular comparison was made was based on small participations of higher modes (as indicated by frequency contents of measured response histories) so that the response of a single apparent mode could be investigated.

The calculation procedure did estimate measured displacements, accelerations, shears and moments reliably for each of the four test structures subjected to design-basis earthquake simulations. For subsequent simulations calculated response, excluding displacement response, was progressively smaller than measured response as the intensity of the base motion increased. Increases in second-mode participation were observed in frequency contents of measured eighth-level acceleration and first-story shear response. However, the increases were not substantial enough to reconcile differences between calculated first-mode and measured response. Error in the calculation procedure was largest for accelerations but was not reflected as greatly in shear or moment response. Calculated estimates of displacements of test structures subjected to higher intensity base motions agreed reasonably well with measured values, and would have served as an adequate criterion of structural behavior for design.

Maxima of each cycle of measured base moment and tenth-level displacement have been plotted (Fig. 6.21) to compare force-displacement relation-

ships measured at various times throughout the test run with calculated relationships using a linear SDOF oscillator. Base moment has been chosen as a measure of total lateral load resisted by a structure because of small participations of higher modes.

It should be noted that calculated stiffnesses have been based on softened structures whose frequencies were measured during the cycle of maximum displacement. Calculated moment-displacement relationships should represent lower bounds of all moment-displacement data points and not necessarily envelope curves. Structures subjected to motions resulting in cycles of successively increasing displacement responded with a gradual deterioration of stiffness characterized by a round-shaped curve circumscribing the moment-displacement data points. This tendency was prevalent for structures with heavily reinforced walls (FW1, FW4) subjected to initial test runs. Cycles of maximum displacements for other test structures and test runs occurred early into durations resulting in more linearly shaped envelopes of moment-displacement maxima.

Comparison of calculated slopes with measured data demonstrated further the acceptability of using a model based on linear behavior to represent the measured nonlinear response. Calculated stiffnesses agreed well with measured moment-displacement data for design-basis earthquake simulations. For subsequent test runs calculated stiffnesses were in the range of measured data but did not always represent a lower bound to apparent measured stiffnesses (the third test runs of structures FW1 and FW4). The reason may be in part because observed frequencies during subsequent test runs were difficult to identify because of erratically

shaped displacement response histories (Fig. 5.9 and 5.21). Also, permanent displacements which were measured during many subsequent test runs were not included in the linear-model interpretation. The general tendencies of the test results, however, suggested that a linear model may be used to represent adequately for design purposes the nonlinear response measured during initial earthquake simulations. More specifically, the test structures may have been proportioned at the base to resist a moment which was a direct function of the anticipated displacement of the softened structure.

CHAPTER 7

DISCUSSION OF TEST RESULTS

7.1 Introductory Remarks

Interpretations of observed dynamic response presented in the preceding chapter consisted primarily of comparisons of measured data. An identification of deformational characteristics of the members was not necessary. In this chapter observed response is interpreted more extensively with the use of member stiffnesses and strengths inferred from results of cyclic-load tests of wall and frame elements. Ultimate strengths of the test structures are calculated and compared with maxima of measured lateral loads. Dynamic characteristics of the structures are calculated using a linear analytical model and are compared with measured characteristics. Using the same model, reductions in stiffness of beams and wall are identified from measured wall response to demonstrate the adequacy of representing nonlinear wall-frame interaction with linear principles. Before investigating wall forces in detail, however, the reliability of force measurements is discussed in terms of consistency with other measurements.

7.2 Strength of Test Structures

Collapse of the test structures did not occur. However, an evaluation of the strength of the structures is presented in this section

to serve as a check on acceleration measurements, and to provide insight into the dynamic behavior of the structures. Maximum measured moments at base and shears at first story (Table 7.1) were used to represent the total lateral load resisted by the structures.

(a) Collapse Mechanism

Ideally, for a frame structure collapse will occur when applied loads exceed the strength of the structure. An unstable mechanism will be developed resulting from inelastic rotations at ends of critical members. Several patterns of inelastic-hinge formation may be geometrically admissible for a mechanism to occur, however, the pattern requiring the minimum amount of work from the applied loads will be the mechanism at which collapse will occur. Three categories of mechanisms were considered for the calculation of test-structure strength.

The first category comprised all combinations of hinge formation in the columns and wall above the base and is depicted in Fig. 7.1 (a). Because work of the external loads was dependent on distribution of inertia loads along the height of structure for this category of mechanisms, the most severe distribution of a single load applied at the tenth level was considered.

The second category consisted of a mechanism with hinges at the base of columns and wall, and at the ends of beams at all levels. (Fig. 7.1 b). Because of the triangular deflected shape, the limiting base moment for this mechanism was independent of loading distribution.

The third category considered overturning of the entire test structure resulting from an assumed uplift of the columns (Fig. 7.1 c).

This mechanism was eliminated from the selection of a governing mechanism however, because maximum axial tensions developed in the exterior columns from limiting beam shears and dead load did not exceed tensile capacities of the columns.

Collapse loads were calculated for each mechanism using the principle of virtual displacements with wall and beam strengths measured from cyclic-load test data (Fig. 4.5 and 4.7), and column strengths estimated from calculated interaction diagrams (Fig. 3.11). Because of the large amount of internal work required to develop yielding in the wall above the base, mechanisms of the first category were not found critical. For the governing mechanism (Fig. 7.1 (b)) limiting moments at base, M_{bmax} , and shears at first story, V_{bmax} , were calculated using the following relationships.

$$M_{bmax} = 0.229 W_{int} ; V_{bmax} = \frac{10 \sum_{i=1}^{10} \alpha_i}{\sum_{i=1}^{10} (i)(\alpha_i)} (W_{int})$$

where W_{int} = total internal work,
 = 119 KN for structures with lightly reinforced walls
 = 165 KN for structures with heavily reinforced walls
 α_i = ordinate of shape of loading distribution at level i

(b) Factors of Safety Against Collapse

Factors of safety against collapse have been calculated by dividing the calculated limiting base moment or first-story shear by the measured moment or shear. Calculations based on first-story shear and base moment should result in the same factor of safety, however, both have been used so that calculation procedures may be confirmed. Additionally, higher frequency shear response may suggest the influence of strain rate on strength increase when compared with moment response.

Because the calculation of limiting first-story shear was dependent on the distribution of inertial loads, the minimum factor of safety against collapse should not have occurred necessarily at the same time as the maximum shear. Measured load distributions at 0.01 second intervals are compared in Fig. 7.2 for a structure subjected to a representative high-intensity base motion (structure FW1, test run 3). Instants near the times of maximum first-story shear and base moment are represented. As demonstrated by appreciable differences in load distribution, the calculation of limiting first-story shear demanded consideration of distributions at several instants. Loading distributions were calculated from measured acceleration response histories at 0.004 second intervals. The minimum factor of safety based on first-story shear calculated using this approach, however, was found to occur at the same instant as the maximum base moment. This was expected because the limiting base moment was independent of loading distribution and time for the governing collapse mechanism. The factor of safety based on base moment would then be expected to occur at

the time of maximum base moment. Factors of safety against collapse are summarized below.

<u>Test Structure</u>	<u>Based on Base Moment</u>	<u>Based on First-Story Shear</u>
FW1	0.92	0.94
FW2	0.85	0.87
FW3	0.83	0.86
FW4	0.88	0.88

Factors of safety were nearly the same whether calculated using base moment or first-story shear as the criterion. The implications of the close agreements were that the calculation procedures were correct, and that strength increases resulting from higher frequency shear response were not greater than those resulting from lower frequency moment response.

The fact that all factors of safety were less than one was contrary to observations that collapse did not occur. The minimum factor of safety represents a maximum 20 percent increase in strength than calculated. Two effects not considered in the calculations may be attributable to presumed strength increases as discussed in Sec. 7.4 (c). Strain-rate effects may have increased yield stress of reinforcement. Additionally, compressive axial forces may have been acting on wall during high-intensity simulations which would increase the flexural capacity of wall from that calculated. If factors of safety are calculated using measured wall moments at base instead of maximum moments observed from cyclic-load tests, the minimum factor of safety becomes 0.97.

In summary, the critical collapse mechanism for all test structures included yielding of the reinforcement at base of wall and columns, and at beam ends which agreed with observed crack patterns (Fig. 5.12 and 5.24). Minimum factors of safety against collapse occurred at times of maximum moment. Calculated values of factor of safety were as low as 0.83 suggesting neglected strength increases because of strain rate effects and compressive axial force on wall.

7.3 Calculation of Dynamic Characteristics Using a Linear Model

Despite nonlinear response at the member level, as indicated by measured hysteresis relationships of frame and wall members, overall measured response of the test structures contained characteristics indicative of structures behaving linearly: frequency contents of observed waveforms revealed dominant components at particular frequencies (Fig. 6.13), displaced shapes were nearly constant for all amplitudes of motion (Sec. 6.3 (b)), response maxima of the composite wall-frame system could be estimated reliably for all four structures subjected to design-basis earthquake simulations using measured shapes and SDOF oscillators behaving linearly (Sec. 6.5). Because of these observations of apparent linear behavior, an attempt is presented in this section to calculate dynamic characteristics using a linear analytical model. Stiffnesses of the model for members with nonlinear deformations have been approximated with average slopes of measured hysteresis relationships for cycles of maximum displacement. Natural frequencies and mode shapes were calculated using the model and are compared with dynamic characteristics interpreted from measurements.

(a) Description of Linear Model

Features of the analytical model (Fig. 7.3) that were different or not included in the design model (Sec. 3.2) were (1) beam flexural stiffnesses, (2) wall flexural stiffnesses, and (3) consideration of lack of fixity at column and wall bases. Because approximations of stiffnesses of members with nonlinear deformations could not be accurately established, a range of stiffness for these members was considered. Relative reductions in beam stiffness resulting from nonlinear behavior were assumed to be directly proportional with measured interstory displacements. Beam stiffnesses have been normalized with respect to values at the fifth level so that correlations may be made with measurements of static-test specimens which were subjected to loading programs representative of interstory displacements at the fifth story. Distributions of beam stiffnesses relative to the beam stiffness at fifth level are tabulated in Table 7.2. Flexibility at base of wall was modeled with a rotational spring of which stiffness was varied over a range determined from measured displacements of wall specimens subjected to cyclic loads.

Rotational springs were used also to model pullout of anchored reinforcement at base of columns. Referring to Fig. 7.4, flexibility of these springs was calculated considering a uniform bond stress distribution along the length of the developed portion of the bar. It should be noted that by using the same calculation procedure, pullout of reinforcement at base of wall which was implicit in cyclic-load test measurements would result in values of 2.5 and 0.8×10^{-7} radian/kN-mm for lightly and heavily reinforced walls.

Stiffnesses of wall members where measured moments exceeded measured moduli of rupture were calculated considering fully cracked sections. Column and wall stiffnesses inferred from measurements obtained during cyclic-load tests of frame and wall components were in close agreement with values calculated using cracked-section stiffnesses (Sec. 4.4). Column and wall stiffnesses used in the analytical model are tabulated in Table 7.3. A nominal value for the modulus of elasticity of 20,000 MPa, based on data from test cylinders, was assumed.

(b) Calculated Frequencies and Mode Shapes

Fundamental frequencies calculated using the analytical model have been plotted versus the fifth-level beam stiffness used in each calculation (Fig. 7.5). Beam stiffness has been expressed in terms of a damage ratio (as defined in Fig. 3.5) so that effects of beam damage on frequency may be more clearly stated. Calculated frequencies are presented also for a range of possible flexibilities of wall at base. Tendencies associated with variations in these stiffnesses are noted.

(1) Reduction in frequency resulting from softening in beams was much greater than that resulting from softening at base of wall.

(2) Reduction in frequency resulting from softening in beams and wall decreased with increase of softening.

(3) Reduction in frequency resulting from softening in beams decreased at essentially the same rate for all levels of softening of wall.

Ranges of calculated second-mode frequencies are presented in Table 7.4. Calculated mode shapes were insensitive to variations in

assumed stiffnesses as demonstrated in Table 7.4 by small differences in shapes for extreme stiffness considerations.

Frequencies calculated considering beams to be cracked (damage ratio of 1.0) coincided with frequencies measured during free-vibration tests following initial test runs (Fig. 6.14). Comparisons of calculated frequencies with frequencies observed during earthquake simulations will be presented in Sec. 7.5 following examination of stiffness reductions in beams and wall.

7.4 Reliability of Measurement of Force Resisted by Wall

Because the measurement of forces, through measurement of strain, resisted by wall was attempted for the first time in this study, checks for consistency with other measurements was felt appropriate. Frequency characteristics of the measured forces were discussed in Sec. 6.4 (d) and were found to be consistent with frequency contents of measured displacements and accelerations. Other comparisons supporting the reliability of the force measurements were:

- (1) measured displacements with displacements calculated from measured forces,
- (2) patterns of measured residual forces with patterns calculated from distributions of permanent rotations,
- (3) measured moments at base of wall with estimated flexural strength of wall.

(a) Displacements Calculated from Forces

At particular instants, tenth-level displacement was calculated from measured wall forces. A simple model was used which considered

linear behavior along the full height of wall, and a linear rotational spring at base. Cracked and uncracked stiffnesses were assumed depending on the magnitude of the measured moments at each level. Because of the dependence of the spring stiffness on loading history, deflection was calculated for a fixed base and set equal to the measured displacement to determine the necessary base rotation. Base moment from the measured forces and calculated base rotation are listed in Table 7.5. Comparison of these values with the experimental curve of moment-rotation (Fig. 4.5 (c) and (d)) suggested that the measured forces resulted in credible displacements.

(b) Pattern of Residual Forces

A salient feature of the measured force response was residuals measured at the end of a test run. The residual measurement was not electronic drift in the gage because of nearly identical readings at the end of a test run and at the beginning of a subsequent test run more than an hour later. Forces were prevalent between wall and frames for the unloaded structure after a dynamic test because of different inelastic deformations of wall and frames.

Measured residual forces were smaller for structures subjected to Taft simulations than those subjected to El Centro simulations because of more balanced loading reversals throughout the duration.

The influence of permanent rotations, resulting from inelastic action, on residual force resisted by wall at a particular level was examined using the Mueller-Breslau principle. Using the mathematical

model described in Sec. 7.3 (a) with beam and wall stiffnesses inferred from cyclic-load tests, a unit axial distortion was imposed between wall and frames at a particular level. Moments generated at beam ends and at base of wall by the distortion were coefficients that indicated the influence of permanent rotation on residual force at that particular level.

As demonstrated by the influence coefficients (Table 7.6), permanent rotation at the base of wall had a significant effect on residual force at first and second levels. Using the calculated influence coefficient for the lightly reinforced wall at the first level (528 kN/radian) with the measured residual force (3.2 kN for FW2-Run 1) indicated a rotation at the base of wall equal to 0.006 radians. The experimentally obtained relationship between moment and rotation at the base of the wall (Fig. 4.5 (d)) confirmed that 0.006 radians was a credible permanent rotation for the loading history of the El Centro simulation. Using the same base rotation with the influence coefficient for the force at the second level (-64 kN/radian) resulted in a calculated force of -0.4 kN which was consistent with the -0.7 kN measured force.

Permanent rotations at the end of the beams were the primary influence on residual forces at upper levels. By examination of the influence coefficients, the largest residual should occur at the level where the difference between permanent rotations at adjacent levels was a maximum. A large residual force was measured at the sixth level for the heavily reinforced wall subjected to an El Centro simulation (Fig. 5.4). This

suggested the maximum difference in permanent rotations at ends of beams to be between levels seven and five which seemed credible because the maximum difference in frame story shears was between stories seven and five (Fig. 5.5). A similar argument can be made for the lightly reinforced wall subjected to the El Centro simulation where a large residual was measured at the seventh level.

(c) Wall Base Moments

Moment at base of wall determined from measured forces were used as a check on the reliability of strain gage readings by comparing them with flexural capacities of walls. Response maxima of the moment histories (Fig. 5.5, 5.10, 5.17, 5.22) are listed in Table 7.7 with strengths observed under static conditions (Fig. 4.5(c) and (c)). Moments calculated from measured forces were larger than observed static-loading strengths for most test runs. However this did not discount the reliability of individual force measurements because of possible increases in strength resulting from compressive axial load on wall, and increases in yield stress of reinforcement due to strain rate effects.

Tension tests performed by Staffier [23] on knurled specimens of No. 8 gage black annealed wire indicated that a twenty percent increase in upper yield stress was possible at a strain rate of 0.04 per second which was the approximate maximum rate measured from the response histories of base moment.

Ideally, no axial force should have been present on the wall at the start of the test sequence. Unequal vertical displacement of the wall

relative to the frames, especially from rotation at the base of the wall, could have resulted in compressive axial forces on the wall. Vertical accelerations as high as 0.8g (Fig. 5.9 and 5.21) were measured during subsequent test runs corroborating the exchange of vertical force between frames and wall. A simple model (Fig. 7.8 (a)) was used to estimate the magnitude of the axial force for a rotation of 0.01 radian at base of wall. Axial stiffnesses of the columns were based on the cross-sectional area of the reinforcement, and a modulus of elasticity of 200,000 MPa. Axial stiffness of the wall and flexural stiffness of the floor levels were considered to be infinite so that a maximum axial force on wall would result. A maximum axial force on wall was calculated to be approximately twenty-five percent of the total dead load. The increase in flexural strength of the wall for this axial load was approximately twenty percent as determined from the moment-axial load interaction diagram (Fig. 7.8(b)).

Increases in strength of wall during earthquake simulations over static strengths was also suggested in Sec. 7.2 where maximum shears and moments resisted by the combined frame-wall system were investigated.

It should be noted that the base moments for the first and second test runs of test structure FW3 were based on a force at the ninth level equal to zero because of a malfunctioning tape recorder channel. The ninth-level force was small for the initial test run of the other test structures justifying the approximation of zero force. The zero force assumption may not have been justified for the second test run because of a possible residual force at the ninth level. A -1.5 kN residual force was observed

at the start of the third test run which may have been present for the second run. The sense of this residual would decrease the maximum observed moment, and the difference between negative and positive maxima.

(d) Summary

The discussion of the reliability of the measurement of forces resisted by wall revealed that

- (1) the force measurement was synchronized with displacement and acceleration measurements,
- (2) measured forces resulted in calculated deflections similar to measured displacements,
- (3) residual forces acting between the wall and frames were consistent with patterns of permanent rotations,
- (4) moment at base of wall determined from measured forces were larger than static flexural strengths which may be attributable to strain-rate effects and axial load on the wall.

7.5 Identification of Reductions in Stiffness Using a Linear Model

Quantitative estimates of reductions in stiffness resulting from nonlinear behavior may be inferred from experimental tests of frame and wall members subjected to cyclic loads. In this section reductions in stiffness are estimated using an alternate approach. Reductions are identified from response measurements using a linear model which is assumed to represent nonlinear response accurately. Correctness of the

assumption is then examined by comparing reductions in stiffness based on the linear model with average slopes of measured hysteresis loops.

(a) Description of Linear Analysis

The analytical model used in this study was the same model used to calculate dynamic characteristics in Sec. 7.3 (a). Softening of the wall was represented by increasing flexibilities of the rotational spring at base. Softening of the beams was represented by increasing damage ratios. Lateral loads were distributed according to fundamental-mode shapes which were calculated for each combination of frame and wall stiffness. A unit spectral acceleration for all first-mode frequencies was used so that the calculation would be applicable for structures with different base motions.

(b) Identification Parameters

Using displacements or accelerations of the overall structure as identification parameters of member stiffness would be erroneous. Response of the frame-wall system, like a set of parallel springs, would depend not on stiffness of individual components, but on the sum of their stiffnesses. In this respect, identical response of the composite structure may result from an infinite number of combinations of frame and wall stiffnesses. Admissible parameters, however, would be internal-response measurements such as frame or wall response.

Measurement of force resisted by the wall at a particular level would be expected to be sensitive to wall and frame stiffnesses, and would

therefore serve as an appropriate identifier. However, measurements of shear and moment at base of wall were preferred because

- (1) shear and moment response comprised a population of ten measurements, thus diminishing the error resulting from individual gages,
- (2) shear and moment response contained smaller residual components than individual force measurements which simplified interpretation using a linear analysis,
- (3) shear and moment response contained fewer high-frequency components than individual force measurements, which facilitated comparisons with results of first-mode calculations.

Results of linear analyses are presented in Fig. 7.6. Shear at base of wall (Fig. 7.6a) was plotted versus flexibility of wall at base so that stiffness reductions of wall at base could be identified from measurements of wall base shear. Moment at base of wall (Fig. 7.6b) was plotted versus damage of fifth-level beams so that stiffness reductions of beams could be identified from measurements of wall base moment. Base-moment curves include a discontinuity because of different distributions of beam damage. Stiffnesses representing cracked and rigid beams were calculated using a uniform damage ratio for all beams. Stiffnesses representing beams behaving in the nonlinear range were calculated using a distribution of damage ratios identical with the distribution of measured interstory displacements (Table 7.2).

Shear resisted by wall at base would be expected to be insensitive to stiffness properties of frames because observed shears at base were

resisted primarily by wall. This expectation is confirmed with the calculation results (Fig. 7.6a) for walls with small base flexibilities (less than 5.0 radian/KN-mm). However, for larger base flexibilities, which would be expected for the lightly reinforced walls during initial test runs and for all walls during higher intensity runs, shear resisted by wall at base was sensitive to frame stiffness. In this range of wall flexibility, wall base shear decreased with increased softening of beams. The reversed tendency may be explained by examining force distributions on wall (Fig. 7.7). For walls fixed at base no force reversal at level one was present and wall base shear did not vary appreciably. For walls with a large base flexibility (10×10^{-7} radian/KN-mm) reductions in beam stiffness resulted in increased reversals at level one and reduced shears resisted by wall at base. Reversals in force on wall were attributable to interactive forces between wall and frames resulting from constrained displacements at each level.

Ideally, no interactive forces would develop between frames and walls with, when separated, identical deflected shapes. Conversely, large interactive forces would develop between frames and walls with dissimilar deflected shapes. A frame with rigid beams (shear beam) loaded at top, or a rigid wall pinned at base would deflect in a triangular shape. A frame with no beams would deflect in the same shape as would a wall fixed at base (flexure beam). Therefore, larger interactive forces and smaller shears at base of wall would result from combinations of (1) light beam damage (shear beam) and light damages of wall at base (flexure beam), and (2) heavy beam damage (flexure beam) and heavy damage of wall at base (wall pinned at base).

For the range of relative wall-frame stiffnesses of the test structures, shear at base of wall was insensitive to combinations of damage of the first category. For heavy damage or large flexibilities of wall at base, shear at base of wall was sensitive to softening of beams. For this reason, identification of stiffness reductions at base of wall may be inconclusive for structures with excessive nonlinear behavior of wall at base.

(c) Amplitude of Total Lateral Load

Calculated results of moment and shear at base of wall (Fig. 7.6) were based on a modal analysis using a unit spectral acceleration response for all frequencies. For comparison with calculated values, measured maxima of shear and moment response were normalized with respect to the intensity of the particular earthquake simulation as described below.

Spectral-response curves were not used to determine index values of base motion intensity because inaccurate estimates of damping factor would have resulted in a wide range of plausible spectral accelerations. Amplitude of the total lateral load was inferred from measured first-mode shapes, and measured base moments resisted by the combined wall-frame system. First-mode SDOF accelerations, A_1 , were related directly to base moment, M_b , by the relationship (Sec. 6.3b)

$$A_1 = \frac{M_b}{\gamma_1 W H_1}$$

where γ_1 and H_1 were established as functions of the first-mode shape and

were found to be nearly constant for all amplitudes of motion. It should be noted that accelerations determined in this manner were equal to values read from spectral-response curves (Fig. 6.2 and 6.3) in ranges of damping factors from eight to twelve percent.

Maxima of measured shear and moment response at base of wall, and corresponding base-moment response of entire structure were read from records which were filtered to exclude components at frequencies larger than four Hz so that comparison could be made with calculated first-mode values. Measured wall-response maxima and normalized values are tabulated in Table 7.8.

(d) Comparison of Calculated and Measured Stiffnesses

Reduced stiffnesses, identified from measured wall response using a linear model, are summarized in Table 7.9. Stiffnesses based on average slopes of measured hysteresis loops are presented for comparison with calculated values so that the correctness of using a linear model to represent nonlinear response may be investigated.

Flexibility of wall at base and damage ratio of beams were determined from normalized moments and shears (Table 7.8) using calculated curves (Fig. 7.6). Reductions in wall stiffness were identified from measured shears using beam stiffnesses inferred from cyclic-load tests. Reductions in beam stiffness were identified from measured moments using wall stiffnesses inferred from cyclic-load tests.

Beam stiffnesses based on measured hysteresis relationships were determined from load and joint-rotation measurements. Stiffness was

established as the slope of a line connecting points on the curve representing maximum rotations in each direction of loading. Values of stiffness for interior and exterior-joint specimens were averaged.

Flexibilities at base of wall refer to load-rotation measurements of cyclic-load tests. Because loading programs for wall specimens were not patterned to represent measured displacement histories of the test structures, moment-rotation stiffnesses were inferred using limiting rotations corresponding to first-level displacements of the test structures measured during initial earthquake simulations.

Comparison of measured and calculated stiffness reductions (Table 7.9), with qualification, revealed satisfactory correlations. Differences between measured and calculated values may be attributable to uncertainties in the measured values of shear and moment at base of wall. Measurements, particularly shears, were subject to interpretation because of the filtering process used to view first-mode components. Furthermore, wall response measurements of structures FW1 and FW3 were distorted. As discussed in Sec. 5.2 (g), forces may have been acting on the wall of structure FW1 before the initial earthquake simulation. Shear and moment records for structure FW3 did not include ninth-level forces: damage ratio of 2.9, instead of 1.4, would result from a wall base moment of 14 kN-m which would require a 0.8 kN force on wall at the ninth level which was credible considering measurements at ninth level of other structures.

Using stiffnesses identified in this study or measured with cyclic-load tests resulted in calculated fundamental frequencies (Fig. 7.5)

which agreed with measured frequencies (Fig. 6.13). The major implication of the correspondence between measured and calculated stiffness reductions is that a linear model may be used with reduced stiffnesses to approximate response maxima of structures behaving in nonlinear ranges of response. However, the small population of experimental data (test structures FW2 and FW4) was insufficient to support a strong argument in favor of this implication. A larger population of data may be generated analytically using a nonlinear dynamic response computer program developed by K. Emori [5]. The usefulness of a linear-model representation may then be examined further with varying reinforcing ratios and base motions.

An incidental result of this identification study was an explanation of the sensitivity of wall-frame interaction to varying combinations of stiffness deterioration of wall and frames. In the next section, an understanding of these sensitivities will help explain why the simplified analytical model used for design was successful.

7.6 Evaluation of Design Method

Test structures subjected to initial earthquake simulations responded with no loss of possible building function. Displacements were within acceptable ranges for serviceability, and no cracking or crushing of concrete requiring repair was observed. The design method used to proportion reinforcement was successful. However, interpretations of measured response suggested that member stiffnesses were not the same as assumed for design.

- (1) A damage ratio for the beams of six was assumed for design whereas values of approximately three were inferred from cyclic-

load test measurements, and four from the identification study presented in the preceding section.

- (2) Fixity at column and wall bases was assumed for design whereas rotations resulting from pullout of anchored reinforcement were observed during wall static tests.
- (3) Uniform softening along the height of lightly reinforced walls was assumed for design whereas nonlinear behavior was observed only locally at base during cyclic-load tests.

To demonstrate why the design method was successful despite differences in structural characterization, estimates of response used for design are compared with measurements in Fig. 7.9 through 7.11. Design values were adjusted by spectral accelerations calculated from measured intensities of motion so that comparisons between measured response and response based on assumed behavior could be made independently of predictions of base-motion intensity. Spectral accelerations for first-mode response were determined as described in Sec. 7.5 (c). Second-mode response was calculated using spectral accelerations determined from measured base motions, and an estimated damping factor of ten percent.

(a) Inaccuracies of Assumed Behavior

Measured displacements were smaller than values calculated for design (Fig. 7.9) which may be attributable to stiffer beams than assumed. Using beam stiffnesses inferred from cyclic-load tests (where specimens were subjected to loading programs representative of measured dynamic-test displacements), calculated displacements corresponded with measure-

ments. Further corroboration that beam stiffnesses were approximately one half of design assumptions (damage ratios of three rather than six) was close agreement of calculated first-mode frequencies (Fig. 7.5) with measured values (Fig. 6.13).

To suggest why the beams did not soften as assumed for design, a representative load-deflection relationship measured during cyclic-load tests is compared in Fig. 7.12 with an idealized relationship used for design. Beams may not have softened as much as assumed because of larger flexural strengths provided than required. Higher strengths would have hindered the onset of yield and retarded anticipated softening. Higher strengths were primarily a result of the following two factors.

- (1) More reinforcement was provided than required by the design method. Beam reinforcement was proportioned so that a simple pattern of bars of the same size would result. Additionally, a minimum of four bars per section was provided for confinement of concrete.
- (2) Beam flexural strengths were higher than calculated for design because of neglected tensile resistance of reinforcement near the extreme compression fiber. Strengths measured during cyclic-load tests correlated with values calculated assuming both layers of reinforcement to yield in tension. Light reinforcing ratios and a probable loss of bond of longitudinal beam reinforcement across column widths would support this implication.

Ratios of provided strengths, as measured during static tests, and design moments for beams are listed below.

<u>Level</u>	<u>Structures with Heavily Reinforced Walls</u>	<u>Structures with Lightly Reinforced Walls</u>
10	1.8	2.3
9	1.6	1.8
8	1.6	1.2
7	1.6	2.0
6	1.6	1.7
5	1.7	1.6
4	2.0	1.6
3	2.4	1.9
2	3.4	1.5
1	5.9	3.4

It should be noted that other behavior characteristics may have influenced reductions in beam stiffness. Uniform damage of beams at every level, as assumed for design, could not have occurred unless displacements of all stories were equal. More intense earthquake simulations than predicted for design may have utilized portions of underestimated strengths. Quantitative estimates of stiffness reductions resulting from increases in strength and other characteristics would require an analytical investigation beyond the scope of this experimental study. However, beam stiffnesses of approximately twice those assumed for design appear credible considering the higher strengths provided.

(b) Comparison of Measurements with Design Requirements

Design estimates of shears and moments resisted by the entire structure and the wall are compared with measured values in Fig. 7.10 and 7.11. Because response of individual beams and columns was not measured, accuracy of the design method for calculating frame response must be inferred from correlations of measured and estimated responses for both the entire structure and the wall.

As mentioned in Sec. 3.2 (d) design values were estimated by the square root of the sum of the squares (RSS) of the first three modal components, multiplied by the following ratio of base shears.

$$\alpha = \frac{V_{\text{rss}} + V_{\text{abs}}}{2 V_{\text{rss}}},$$

where V_{abs} = sum of absolute values of first- and second-mode base shear

V_{rss} = RSS of first three modes of base shear

Investigation of methods to combine modal components is not the object of this study, however comparisons of calculated with measured values may vary depending on the method of combination. For example, three commonly used methods resulted in a wide range of calculated-to-measured ratios of wall base shear as noted below.

<u>Test Structure</u>	<u>Sum of Absolute Values of First and Second Modes</u>	<u>RSS of First, Second and Third Modes</u>	<u>α (RSS)</u>
FW1	1.6	1.2	1.4
FW2	1.7	1.3	1.5
FW3	1.6	1.3	1.4
FW4	1.1	0.9	1.0

Quantitative comparisons of calculated and measured response including high-frequency components should be made with attention to these deviations.

Measured shear and moment diagrams for the entire structure correlated closely with design values (Fig. 7.10). Similarities of measured and calculated values would be expected if measured and calculated shapes were similar. As discussed in Sec. 6.3 (b), shears and moments for a mode may be expressed in terms of an effective weight and an effective height, each a function of the mode shape. Factors determined from first-mode shapes calculated for design are compared in Table 7.10 with factors determined from measured shapes.

Differences between calculated and measured first-story shears were larger than differences for base moments as suggested by similar trends between effective weights and products of effective weights and heights. Shear and moment response of the combined frame-wall system was insensitive to variations in stiffness assumptions because mode shapes were relatively insensitive to stiffness considerations.

Measured shears and moments for the wall were generally smaller than design estimates (Fig. 7.11). Shears at upper stories revealed

inconsistent trends with calculated values suggesting sensitive force distributions on wall. At lower stories, measured values appear to have been smaller than estimated which was primarily a result of adjusting design values for this comparison by measured base-motion intensities. Design moments presented in Fig. 7.11 may exceed flexural strengths because the design moments actually used were based on a lower intensity base motion. Because differences between measured and estimated response of the combined frame-wall system (Fig. 7.10) were small, apparent differences in wall response would suggest actual differences in frame response.

An understanding of the implications of inaccurate stiffness assumptions on wall response (Fig. 7.6) will qualify trends between measured and estimated response. Referring to Fig. 7.6b, beam damage ratios of three rather than six as assumed for design would reduce wall base moments by as much as twenty percent. Flexibilities at base of wall not considered for design would also reduce wall base moments. However, referring to Fig. 7.6a, flexibility at base of wall would reduce wall base shears substantially with nearly no effect from inaccurate beam stiffnesses.

In summary, inappropriate stiffness assumptions for design resulted in only slightly different distributions of forces between wall and frames than calculated for design. Stiffer beams than assumed attracted more of the total shear and moment to the frames which was resisted by higher beam strengths than assumed. More intense base motions than assumed for design, however, utilized full flexural capacities of wall which resulted in an economical design despite inaccurate stiffness assumptions.

CHAPTER 8

SUMMARY AND CONCLUSIONS

The object of this experimental study was to investigate behavior of reinforced concrete frame-wall structures subjected to strong earthquake motions. Each small-scale structure (total height of 2.29 meters) consisted of two three-bay frames and one wall resisting lateral loads in parallel (Fig. 2.1 and 2.2). Measurements at each of ten levels included accelerations, displacements and forces resisted by the wall. Experimental parameters of the four-structure series were the simulated earthquake motion (El Centro, NS component or Taft, N21E component), and the strength of structure.

Strength of members was established according to a design method that recognized energy dissipation capabilities of reinforced concrete structures in the nonlinear range of response. A linear analytical model with arbitrarily softened members was used with spectral-response curves representing scaled base motions to obtain estimates of maximum response. Beam stiffnesses, calculated using conventional methods for cracked sections, were divided by six to save reinforcement and localize nonlinear behavior of frames at ends of beams. Two conceptions of response at base of wall resulted in structure types with radically different wall reinforcement. Walls intended to respond nonlinearly were reinforced with one-fourth as much reinforcement as walls intended to respond linearly. Reinforcing requirements were obtained by assuming cracked-section stiffness for the

"linear" walls and one-third of cracked-section stiffness for the "nonlinear" walls. Frame reinforcement was approximately the same for both structure types.

Each structure was subjected to three earthquake simulations of progressively increasing intensity. Spectral-response curves computed from measured base motions of initial simulations were similar for each day of testing, but revealed slightly more intense motions than considered for design of the structures. Intensities of subsequent test runs were approximately 2.0 and 2.5 times intensities of initial simulations. Complementary dynamic testing included excitation of the structures at low amplitudes in free and steady-state vibration.

To support the investigation of response to earthquake motions, replicas of portions of the frame and wall were subjected to slowly applied cyclic loads. Measured load-deflection relationships were used to substantiate modeling of hysteretic response of reinforced concrete structures, and to interpret internal response of test structures subjected to earthquake motions.

In addition to providing data for testing a numerical model of the structures [5], observed response of the test structures suggested tendencies from which the following conclusions were made.

(1) Structures behaved in the nonlinear range. Response of the combined frame-wall system over the duration of an earthquake simulation revealed:

- (a) a decrease in apparent natural frequencies
- (b) an increase in energy dissipation

- (c) permanent displacements
- (d) residual forces resisted by wall
- (e) a softened relationship between base moment and displacement

Nonlinear behavior occurred at regions selected in the design process as indicated by

- (a) cracks at ends of beams and base of wall
- (b) measured hysteresis relationships of frame and wall specimens
- (c) amplitudes of moment measured at base of wall
- (d) pattern of residual forces resisted by wall

(2) Arbitrary softening of wall in the design process resulted in a more economical structure with no loss of serviceability. Decreased frequencies and increased energy dissipation capabilities of structures with a softened wall resulted in smaller lateral loads which compensated for the increased flexibility of structure. Measured displacements of structures with lightly and heavily reinforced walls were nearly equal.

(3) Strength of the test structures could be calculated conservatively using conventional procedures of limit design with static strengths of members.

(4) Displaced shapes measured at variable amplitudes of motion were nearly equal which suggested that response at any level of the nonlinearly behaving structures could be represented with a single-degree-of-freedom system.

(5) Response of the combined frame-wall system contained characteristics indicative of structures behaving linearly.

- (a) Frequency contents of measured response revealed dominant components at particular frequencies.

- (b) Measurements of acceleration at eighth level did not contain apparent second-mode frequencies suggesting an invariable second-mode shape for all amplitudes of motion.
- (c) Response maxima could be estimated reliably using a linear oscillator to represent the structure.

(6) Apparent natural frequencies and mode shapes for first and second modes coincided with those of a linear analytical model with member stiffnesses equal to average slopes of measured hysteresis loops.

The major implication of conclusions (4), (5) and (6) is that a linear modal analysis using softened member stiffnesses was acceptable for calculating response maxima of the combined frame-wall system.

(7) Force resisted by individual frames or wall could not be calculated reliably using a linear model because of the following reasons.

- (a) Force residuals which were a result of variable extents of nonlinear behavior of frames and wall could not be calculated with a linear analysis.
- (b) Maximum force response did not necessarily occur at same time as maximum displacement because internal forces between frames and wall were sensitive to relative softening of beams and wall at base.
- (c) Unlike displacement or acceleration response, force response was sensitive to participation of second-mode components which were highly dependent on the natural frequency of the oscillator and characteristics of the base motion.

(8) Effects of frame-wall interaction along the vertical axis was indicated by high-frequency accelerations measured in the vertical direction. Increases in amplitude of accelerations with base-motion intensity suggested a transfer of axial load between wall and frames as a result of a suppressed tendency for the wall to lift at base.

(9) The redundant system of frames and wall behaved in accordance with the strengths provided. Individual strengths and stiffnesses were different from those assumed for design, yet response of the combined frame-wall system was estimated reliably for each structure. Forces resisted by individual frames or wall were not estimated correctly for reasons mentioned in conclusions (7) and (8). However measured moments at base of wall had to be limited by strengths provided.

(10) The design method was successful for each of the four test structures: displacements were within acceptable ranges for serviceability and no cracking or crushing of concrete requiring repair was observed for base motions corresponding to the design level.

REFERENCES

1. Aristizabal-Ochoa, J. D., and M. A. Sozen, "Behavior of Ten-Story Reinforced Concrete Walls Subjected to Earthquake Motions," Civil Engineering Studies, Structural Research Series No. 431, University of Illinois, Urbana, October 1976.
2. Bertero, V. V., and E. P. Popov, "Hysteretic Behavior of Ductile Moment-Resisting Reinforced Concrete Frame Components," Earthquake Engineering Research Center, University of California, Berkeley, Report No. EERC 75-16, April 1975.
3. Blakeley, R. W. G., L. M. Megget, and M. J. N. Priestly, "Seismic Performance of Two Full Size Reinforced Concrete Beam-Column Joint Units," Bulletin, New Zealand National Society for Earthquake Engineering, V. 8, No. 1, March 1975, pp. 38-69.
4. Clough, R. W., and J. Penzien, Dynamics of Structures, McGraw-Hill Inc., 1975.
5. Emori, K., and W. C. Schnobrich, "Analysis of Reinforced Concrete Frame-Wall Structures for Strong Motion Earthquakes," Civil Engineering Studies, Structural Research Series No. 457, University of Illinois, Urbana, December 1978.
6. Ferguson, P. M., Reinforced Concrete Fundamentals, John Wiley and Sons, Inc., 1958.
7. Gulkan, P. and M. A. Sozen, "Response and Energy Dissipation of Reinforced Concrete Frames Subjected to Strong Base Motions," Civil Engineering Studies, Structural Research Series No. 377, University of Illinois, Urbana, May 1971.
8. Hanson, N. W., and H. W. Conner, "Seismic Resistance of Reinforced Concrete Beam-Column Joints," Journal of the Structural Division, ASCE, Vol. 93, ST5, October 1967, pp. 533-560.
9. Healey, T. J., and M. A. Sozen, "Experimental Study of the Dynamic Response of a Ten-Story Reinforced Concrete Frame with a Tall First Story," Civil Engineering Studies, Structural Research Series No. 450, University of Illinois, Urbana, August 1978.
10. Higashi, Y., and Y. Ohwada, "Experimental Studies on Reinforced Concrete Beam-Column Connections Subjected to Lateral Loads," Transactions of the Architectural Institute of Japan, No. 157, March 1969.
11. Hildalgo, P., and R. W. Clough, "Earthquake Simulator Study of a Reinforced Concrete Frame," Earthquake Engineering Research Center, University of California, Berkeley, Report No. EERC 74-13, December 1974.

12. Housner, G. W., "Behavior of Structures During Earthquakes," Journal of the Engineering Mechanics Division, ASCE, Vol. 85, No. EM4, October 1959.
13. Jacobsen, L. S., and R. S. Ayre, Engineering Vibrations, McGraw-Hill Inc., 1958.
14. Kreger, M. E., and D. P. Abrams, "Measured Hysteresis Relationships for Small-Scale Beam-Column Joints," Civil Engineering Studies, Structural Research Series, No. 453, University of Illinois, Urbana, August 1978.
15. Lybas, J. M., and M. A. Sozen, "Effect of Beam Strength and Stiffness on Dynamic Behavior of Reinforced Concrete Coupled Walls," Civil Engineering Studies, Structural Research Series, No. 444, University of Illinois, Urbana, July 1977.
16. Ma, S. M., V. V. Bertero, and E. P. Popov, "Experimental and Analytical Studies of the Hysteretic Behavior of Reinforced Concrete Rectangular and T-Beams," Earthquake Engineering Research Center, University of California, Berkeley, Report No. EERC 76-2, May 1976.
17. Mahin, S. A. and V. V. Bertero, "An Evaluation of Some Methods for Predicting Seismic Behavior of Reinforced Concrete Buildings," Earthquake Engineering Research Center, University of California, Berkeley, Report No. EERC 75-5, May 1975.
18. Moehle, J. P., and M. A. Sozen, "Earthquake-Simulation Tests of a Ten-Story Reinforced Concrete Frame with a Discontinued First-Level Beam," Civil Engineering Studies, Structural Research Series No. 451, University of Illinois, Urbana, August 1978.
19. Newmark, N. W. and E. Rosenblueth, Fundamentals of Earthquake Engineering, Prentice-Hall, Inc. 1971.
20. Otani, S., and M. A. Sozen, "Behavior of Multistory Reinforced Concrete Frames During Earthquakes," Civil Engineering Studies, Structural Research Series No. 408, University of Illinois, Urbana, July 1974.
21. Pique, J. R., "On the Use of Simple Models in Nonlinear Dynamic Analysis," Research Report R76-43, Department of Civil Engineering, Massachusetts Institute of Technology, September 1976.
22. Shibata, A., and M. A. Sozen, "The Substitute-Structure Method for Earthquake-Resistant Design of Reinforced Concrete Frames," Civil Engineering Studies, Structural Research Series No. 412, University of Illinois, Urbana, October 1974.
23. Staffier, S. R. and M. A. Sozen, "Effect of Strain Rate on Yield Stress of Model Reinforcement," Civil Engineering Studies, Structural Research Series No. 415, University of Illinois, Urbana, February 1975.

24. Tansirikongkol, V. and D. A. Pecknold, "Approximate Modal Analysis of Bilinear MDF Systems Subjected to Earthquake Motions," Civil Engineering Studies, Structural Research Series No. 449, University of Illinois, Urbana, August 1978.
25. Uzumeri, S. M., and M. Seckin, "Behavior of Reinforced Concrete Beam-Column Joints Subjected to Slow Load Reversals," Report 74-05, Department of Civil Engineering, University of Toronto, March 1974.
26. Wilby, G. K., "Response of Concrete Structures to Seismic Motions," Ph.D. Thesis, Department of Civil Engineering, University of Canterbury, Christchurch, New Zealand, July 1975.
27. Wilson, E. L., J. P. Hollings, and H. H. Dovey, "Three Dimensional Analysis of Building Systems (Extended Version)," Earthquake Engineering Research Center, University of California, Berkeley, Report No. EERC 75-13, April 1975.

Table 3.1 Stiffnesses Used for Design

Level/ Story	Moments of Inertia, $\times 10^4 \text{ mm}^4$							
	Structure with Heavily Reinforced Wall				Structure with Lightly Reinforced Wall			
	Beams*	Ext. Col.	Int. Col.	Wall	Beams	Ext. Col.	Int. Col.	Wall
10	0.80	10.6	14.7	1660	0.80	10.6	10.6	553
9	1.08	10.6	14.7	1660	0.80	10.6	10.6	553
8	1.08	10.6	10.6	1660	0.80	10.6	10.6	553
7	1.08	10.6	10.6	1660	1.08	10.6	10.6	553
6	1.08	10.6	10.6	2400	1.08	10.6	10.6	553
5	1.08	10.6	10.6	2400	1.08	10.6	10.6	553
4	0.80	10.6	10.6	2470	1.08	10.6	10.6	553
3	0.80	10.6	10.6	2470	1.08	14.7	10.6	553
2	0.80	10.6	10.6	2470	0.80	14.7	10.6	553
1	0.80	10.6	10.6	2470	0.80	14.7	10.6	553

*Frame Values for Single Frame

Modulus of Elasticity = 25 MP a

Table 3.2 Calculated Mode Shapes and Frequencies for Design

	Structure with Heavily Reinforced Wall			Structure with Lightly Reinforced Wall		
	First Mode	Second Mode	Third Mode	First Mode	Second Mode	Third Mode
Frequency, Hz.	2.40	9.35	22.7	1.86	6.80	15.8
Mode Shape Level						
10	1.00	1.00	-1.00	1.00	1.00	-1.00
9	0.88	0.45	0.10	0.91	0.51	0.00
8	0.76	-0.08	0.87	0.80	0.03	0.76
7	0.63	-0.52	0.98	0.69	-0.39	0.98
6	0.50	-0.80	0.44	0.58	-0.67	0.62
5	0.36	-0.88	-0.39	0.45	-0.84	-0.11
4	0.24	-0.77	-0.97	0.33	-0.81	-0.81
3	0.14	-0.54	-1.05	0.21	-0.64	-1.09
2	0.07	-0.29	-0.73	0.11	-0.37	-0.86
1	0.02	-0.09	-0.27	0.03	-0.12	-0.33

Table 3.3 Smeared Damping Values

	Structure with Heavily Reinforced Wall			Structure with Lightly Reinforced Wall		
	Beams	Columns	Wall	Beams	Columns	Wall
Damage Ratio	6	1	1	6	1	3
Damping Factor	0.14	0.02	0.02	0.14	0.02	0.10
Strain Energy Participation Factor						
Mode 1	0.55	0.05	0.40	0.70	0.11	0.19
Mode 2	0.31	0.07	0.62	0.45	0.14	0.41
Mode 3	0.14	0.09	0.77	0.22	0.19	0.59
Smeared Damping Factor, β_s						
Mode 1		0.085			0.12	
Mode 2		0.057			0.11	
Mode 3		0.036			0.096	

Table 3.4 Column Net Axial Tensions for Design, kN*

Story	Structure with Heavily Reinforced Wall		Structure with Lightly Reinforced Wall	
	Exterior Columns	Interior Columns	Exterior Columns	Interior Columns
10	-0.1	-0.5	-0.1	-0.6
9	0.1	-1.1	-0.2	-1.1
8	0.3	-1.6	-0.3	-1.7
7	0.4	-2.2	-0.2	-2.2
6	0.6	-2.7	0.0	-2.8
5	0.7	-3.3	0.1	-3.3
4	0.5	-3.9	0.2	-3.9
3	0.3	-4.4	0.3	-4.4
2	-0.1	-4.9	0.2	-5.0
1	-0.5	-5.5	-0.1	-5.6

$$*RSS \left(\frac{V_{ABS} + V_{RSS}}{2V_{RSS}} \right) - \text{Dead Load}$$

Table 5.1 Key to Figures and Tables Presenting Observed Response

Figure or Table	Structures Subjected to E1 Centro Simulations (FW1, FW2)		Structures Subjected to Taft Simulations (FW3, FW4)	
	Run 1	Run 2	Run 1	Run 2
Response Histories				
Base Motions	5.3	5.8	5.15	5.20
Measured Response	5.4	5.9	5.16	5.21
Shear and Moment Response	5.5	5.10	5.17	5.22
Distribution of Response Along Structure Height				
	5.6	5.11	5.18	5.23
Crack Patterns Following Test Run				
	5.7	5.12	5.19	5.24
Table of Measured Response at Time of Maximum Displacement				
Structure with Heavily Reinforced Wall	5.3a	5.3c	5.3e	5.3g
Structure with Lightly Reinforced Wall	5.3b	5.3d	5.3f	5.3h

Table 5.2 Measured Widths of Cracks at Beam Ends,* mm

Level	Test Structure											
	FW1			FW2			FW3			FW4		
	Run 1**	Run 2	Run 3	Run 1	Run 2	Run 3	Run 1	Run 2	Run 3	Run 1	Run 2	Run 3
10	0.06	0.08	0.11	0.05	0.09	0.11	0.08	0.12	0.17	0.06	0.13	0.20
9	0.06	0.08	0.11	0.05	0.09	0.13	0.08	0.11	0.17	0.05	0.15	0.20
8	0.06	0.10	0.11	0.06	0.10	0.14	0.10	0.14	0.24	0.07	0.15	0.20
7	0.06	0.10	0.11	0.06	0.10	0.13	0.08	0.11	0.18	0.06	0.16	0.21
6	0.06	0.10	0.11	0.08	0.10	0.15	0.06	0.12	0.19	0.07	0.15	0.22
5	0.06	0.09	0.11	0.07	0.10	0.12	0.07	0.10	0.18	0.08	0.21	0.23
4	0.07	0.11	0.13	0.07	0.11	0.14	0.07	0.11	0.20	0.07	0.18	0.20
3	0.07	0.10	0.11	0.06	0.10	0.14	0.06	0.11	0.20	0.06	0.12	0.17
2	0.06	0.08	0.11	0.06	0.10	0.13	0.06	0.13	0.20	0.06	0.14	0.18
1	0.06	0.08	0.10	0.06	0.10	0.13	0.06	0.10	0.20	0.06	0.14	0.17

* Mean of crack widths at ends of all beams per level

** Measured following test run

Table 5.3 Measured Response at Time of Maximum Displacement
(a)
Response at 1.96 Seconds
Test Structure FW1
Test Run 1

Level	Displacement (mm.)	Acceleration (g.)	Force on Wall (kN.)	Shear (kN.)		Moment (kN.-m.)	
				Total	Wall	Total	Wall
10	28.2	-0.62	-2.62	2.8	-2.6	0.7	-0.6
9	26.5	-0.62	1.30	5.6	-1.3	2.0	-0.9
8	23.8	-0.64	2.91	8.6	1.6	4.0	-0.5
7	20.5	-0.71	2.12	11.8	3.7	6.7	0.3
6	17.0	-0.69	1.85	14.9	5.6	10.2	1.6
5	13.5	-0.58	3.05	17.6	8.6	14.4	3.5
4	9.5	-0.45	2.72	19.6	11.3	18.9	6.1
3	7.1	-0.29	1.75	20.9	13.1	23.8	9.1
2	4.1	-0.10	2.87	21.4	15.9	28.8	12.8
1	2.0	0.07	-1.27	21.0	14.7	33.7	16.2

Table 5.3 (contd.) Measured Response at Time of Maximum Displacement
 (b)
 Response at 1.98 Seconds
 Test Structure FW2
 Test Run 1

Level	Displacement (mm.)	Acceleration (g.)	Force on Wall (kN.)	Shear (kN.)		Moment (kN.-m.)	
				Total	Wall	Total	Wall
10	27.7	-0.66	-3.93	3.0	-3.9	0.7	-0.9
9	25.0	-0.65	-0.57	5.9	-4.5	2.1	-1.9
8	22.9	-0.61	2.44	8.7	-2.1	4.1	-2.4
7	20.2	-0.57	0.24	11.3	-1.8	6.8	-2.8
6	16.9	-0.43	1.20	13.3	-0.6	9.9	-3.0
5	13.9	-0.28	1.75	14.6	1.1	13.3	-2.7
4	10.4	-0.21	1.62	15.5	2.8	16.9	-2.1
3	8.1	-0.15	0.39	16.2	3.2	20.7	-1.3
2	4.9	-0.10	0.96	16.6	4.1	24.7	-0.4
1	2.2	0.01	5.49	16.6	9.6	28.6	1.8

Table 5.3 (contd.) Measured Response at Time of Maximum Displacement
(c)
Response at 1.42 Seconds
Test Structure FW1
Test Run 2

Level	Displacement (mm.)	Acceleration (g.)	Force on Wall (kN.)	Shear (kN.)		Moment (kN.-m.)	
				Total	Wall	Total	Wall
10	-38.4	1.06	2.93	-4.8	2.9	-1.1	0.7
9	-40.1	0.98	-0.09	-9.3	2.8	-3.3	1.3
8	-32.9	0.81	-2.11	-13.0	0.7	-6.3	1.5
7	-30.2	0.62	-1.93	-15.8	-1.2	-10.0	1.2
6	-25.4	0.42	-4.35	-17.7	-5.5	-14.2	-0.1
5	-19.6	0.32	-0.92	-19.1	-6.5	-18.7	-1.5
4	-15.1	0.32	-0.66	-20.6	-7.1	-23.5	-3.2
3	-10.8	0.35	-3.90	-22.2	-11.0	-28.8	-5.7
2	-6.6	0.42	-0.76	-24.1	-11.8	-34.4	-8.4
1	-3.3	0.47	-1.67	-26.3	-13.5	-40.6	-11.5

Table 5.3 (contd.) Measured Response at Time of Maximum Displacement
 (d)
 Response at 2.46 Seconds
 Test Structure FW2
 Test Run 2

Level	Displacement (mm.)	Acceleration (g.)	Force on Wall (kN.)	Shear (kN.)		Moment (kN.-m.)	
				Total	Wall	Total	Wall
10	-42.8	0.51	2.59	-2.3	2.6	-0.5	0.6
9	-39.2	0.54	-0.32	-4.7	2.3	-1.7	1.1
8	-32.7	0.60	-0.95	-7.5	1.3	-3.4	1.4
7	-32.0	0.59	-3.40	-10.2	-2.1	-5.8	0.9
6	-27.5	0.63	-1.56	-13.0	-3.6	-8.9	0.1
5	-23.4	0.56	-2.01	-15.6	-5.6	-12.6	-1.2
4	-18.2	0.48	0.63	-17.7	-5.0	-16.8	-2.3
3	-14.6	0.39	-3.14	-19.5	-8.2	-21.5	-4.2
2	-8.9	0.28	-1.26	-20.8	-9.4	-26.4	-6.4
1	-4.7	0.19	9.01	-21.7	-0.4	-31.6	-6.4

Table 5.3 (contd.) Measured Response at Time of Maximum Displacement
(e)
Response at 5.96 Seconds
Test Structure FW4
Test Run 1

Level	Displacement (mm.)	Acceleration (g.)	Force on Wall (kN.)	Shear (kN.)		Moment (kN.-m.)	
				Total	Wall	Total	Wall
10	18.2	-0.64	-3.22	2.9	-3.2	0.7	-0.7
9	16.5	-0.59	-0.93	5.6	-4.1	2.0	-1.7
8	14.6	-0.54	4.37	8.0	0.2	3.8	-1.6
7	12.5	-0.46	2.81	10.1	3.0	6.2	-0.9
6	10.4	-0.36	2.97	11.7	6.0	8.9	0.4
5	8.3	-0.27	1.56	13.0	7.6	12.0	2.2
4	6.1	-0.21	1.41	14.0	9.0	15.2	4.2
3	4.2	-0.15	1.70	14.6	10.7	18.6	6.7
2	2.6	-0.07	1.20	15.0	11.9	22.1	9.4
1	1.0	0.02	1.56	14.9	13.4	25.6	12.5

Table 5.3 (contd.) Measured Response at Time of Maximum Displacement
 (f)
 Response at 2.09 Seconds
 Test Structure FW3
 Test Run 1

Level	Displacement (mm.)	Acceleration (g.)	Force on Wall (kN.)	Shear (kN.)		Moment (kN.-m.)	
				Total	Wall	Total	Wall
10	16.9	-0.53	-3.37	2.4	-3.4	0.6	-0.8
9	16.1	-0.52	0.00	4.8	-3.4	1.7	-1.5
8	14.1	-0.48	2.96	6.9	-0.4	3.3	-1.6
7	12.4	-0.42	1.29	8.9	0.9	5.3	-1.4
6	10.4	-0.34	0.76	10.4	1.6	7.8	-1.1
5	8.5	-0.26	-0.03	11.5	1.6	10.5	-0.7
4	6.6	-0.20	1.05	12.4	2.7	13.4	-0.1
3	4.7	-0.14	1.23	13.1	3.9	16.4	0.8
2	3.0	-0.08	1.10	13.5	5.0	19.6	2.0
1	1.4	-0.00	2.29	13.5	7.3	22.7	3.6

Table 5.3 (contd.) Measured Response at Time of Maximum Displacement
 (g)
 Response at 4.28 Seconds
 Test Structure FW4
 Test Run 2

Level	Displacement (mm.)	Acceleration (g.)	Force on Wall (kN.)	Shear (kN.)		Moment (kN.-m.)	
				Total	Wall	Total	Wall
10	45.5	-1.63	-4.91	7.4	-4.9	1.7	-1.1
9	40.7	-1.33	-1.59	13.4	-6.5	4.8	-2.6
8	36.1	-0.95	9.91	17.7	3.4	9.0	-1.8
7	30.0	-0.56	5.31	20.3	8.7	13.7	0.2
6	23.6	-0.15	5.46	21.0	14.2	18.7	3.4
5	17.7	0.19	-0.06	20.1	14.1	23.4	6.6
4	13.0	0.41	-1.99	18.3	12.1	27.7	9.4
3	8.2	0.65	-0.51	15.3	11.6	31.4	12.1
2	4.7	0.90	-3.20	11.2	8.4	34.1	14.0
1	1.9	1.10	0.19	6.1	8.6	35.5	16.0

Table 5.3 (contd.) Measured Response at Time of Maximum Displacement
(h)
Response at 2.15 Seconds
Test Structure FW3
Test Run 2

Level	Displacement (mm.)	Acceleration (g.)	Force on Wall (kN.)	Shear (kN.)		Moment (kN.-m)	
				Total	Wall	Total	Wall
10	48.0	-0.73	-4.11	3.3	-4.1	0.8	-0.9
9	45.8	-0.66	0.00	6.3	-4.1	2.3	-1.9
8	40.5	-0.61	3.19	9.1	-0.9	4.4	-2.1
7	37.2	-0.52	2.42	11.4	1.5	7.1	-1.8
6	30.8	-0.48	2.84	13.6	4.3	10.4	-0.8
5	25.8	-0.43	2.38	15.6	6.7	14.1	0.8
4	20.6	-0.40	2.63	17.4	9.3	18.2	2.9
3	15.0	-0.30	1.48	18.7	10.8	22.7	5.4
2	9.3	-0.16	-0.39	19.5	10.4	27.4	7.8
1	4.6	0.05	6.55	19.2	17.0	32.0	11.7

Table 6.1 Spectrum Intensities, mm

Damping Factor = 0.10

Test Run	Test Structure			
	FW1	FW2	FW3	FW4
1	232	229	219	246
2	429	404	484	514
3	505	398	520	561

Table 6.2 First-Mode Shapes Measured During Earthquake Simulations

Maximum Tenth-Level Displacement, mm	Test Structure FW1					Test Structure FW2				
	Run 1			Run 2	Run 3	Run 1			Run 2	Run 3
	7	17	28	38	69	10	22	28	43	62
Level										
10	1.00	1.00	1.00	1.00	1.00	1.00	1.00	1.00	1.00	1.00
9	0.97	0.95	0.95	0.93	0.92	0.93	0.91	0.91	0.90	0.88
8	0.85	0.84	0.83	0.79	0.77	0.83	0.83	0.83	0.77	0.77
7	0.76	0.73	0.72	0.71	0.69	0.75	0.73	0.73	0.70	0.72
6	0.63	0.60	0.59	0.57	0.57	0.63	0.61	0.61	0.62	0.58
5	0.52	0.48	0.47	0.45	0.45	0.52	0.50	0.50	0.51	0.51
4	0.37	0.35	0.34	0.31	0.32	0.40	0.38	0.38	0.38	0.38
3	0.27	0.25	0.25	0.23	0.22	0.31	0.29	0.29	0.30	0.30
2	0.16	0.15	0.15	0.14	0.13	0.19	0.18	0.18	0.20	0.17
1	0.08	0.07	0.07	0.07	0.05	0.09	0.08	0.08	0.08	0.09
c_1	1.35	1.37	1.38	1.41	1.42	1.38	1.40	1.40	1.43	1.44
γ_1	0.757	0.743	0.741	0.733	0.727	0.780	0.771	0.771	0.781	0.778
H_1 , meter	1.63	1.64	1.65	1.66	1.66	1.61	1.62	1.62	1.61	1.61

Table 6.2 (contd.) First-Mode Shapes Measured During Earthquake Simulations

Tenth Level Displacement, mm.	Test Structure FW3					Test Structure FW4				
	Run 1			Run 2	Run 3	Run 1			Run 2	Run 3
	4	14	17	48	59	11	17	18	46	66
Level										
10	1.00	1.00	1.00	1.00	1.00	1.00	1.00	1.00	1.00	1.00
9	0.95	0.94	0.93	0.94	0.92	0.92	0.91	0.91	0.91	0.92
8	0.82	0.81	0.80	0.83	0.83	0.80	0.80	0.80	0.81	0.82
7	0.72	0.70	0.69	0.75	0.74	0.68	0.68	0.67	0.69	0.71
6	0.60	0.58	0.57	0.62	0.59	0.56	0.56	0.56	0.55	0.57
5	0.49	0.46	0.45	0.52	0.50	0.45	0.43	0.43	0.43	0.47
4	0.37	0.35	0.34	0.42	0.41	0.33	0.32	0.32	0.32	0.36
3	0.26	0.25	0.23	0.29	0.29	0.22	0.22	0.22	0.21	0.26
2	0.17	0.15	0.14	0.19	0.19	0.13	0.13	0.13	0.13	0.18
1	0.08	0.06	0.06	0.09	0.10	0.06	0.05	0.05	0.06	0.08
c_1	1.39	1.40	1.41	1.38	1.40	1.41	1.42	1.43	1.41	1.41
γ_1	0.759	0.742	0.735	0.771	0.780	0.726	0.724	0.728	0.721	0.757
H_1 , meter	1.63	1.65	1.66	1.61	1.61	1.66	1.67	1.67	1.67	1.63

Table 6.3 First-Mode Shapes Measured During Steady-State Tests

Level	Test Structure FW3			Test Structure FW4		
	Run 1*	Run 2	Run 3	Run 1	Run 2	Run 3
10	1.00	1.00	1.00	1.00	1.00	1.00
9	0.93	0.92	0.91	0.88	0.88	0.89
8	0.81	0.80	0.78	0.78	0.79	0.79
7	0.71	0.73	0.70	0.67	0.67	0.65
6	0.57	0.58	0.58	0.55	0.53	0.53
5	0.45	0.43	0.45	0.43	0.41	0.42
4	0.34	0.36	0.36	0.32	0.31	0.32
3	0.24	0.25	0.23	0.22	0.21	0.24
2	0.13	0.15	0.15	0.12	0.13	0.15
1	0.06	0.08	0.07	0.05	0.06	0.07
c_1	1.40	1.41	1.42	1.44	1.44	1.45
γ_1	0.733	0.747	0.744	0.723	0.720	0.735
H_1 , meter	1.66	1.64	1.64	1.67	1.67	1.65

* Following Run 1

Table 6.4 Damping Factors Calculated from Free-Vibration Response

Test Structure	Free-Vibration Test			
	Before Run 1	Before Run 2	Before Run 3	Following Run 3
FW1				
a_n	0.0120	0.0200	0.0200	0.0140
a_{n+m}	0.0060	0.0038	0.0036	0.0035
m	5	5	5	4
β^*	0.022	0.053	0.055	0.055
FW2				
a_n	0.0070	0.0160	0.0160	--
a_{n+m}	0.0025	0.0045	0.0037	--
m	11	3	3	--
β	0.015	0.067	0.078	--
FW3				
a_n	0.0070	0.0170	0.0207	0.0195
a_{n+m}	0.0035	0.0037	0.0040	0.0046
m	10	4	4	3
β	0.011	0.061	0.065	0.077
FW4				
a_n	0.0070	0.0160	0.0180	0.0170
a_{n+m}	0.0040	0.0052	0.0045	0.0032
m	14	3	3	3
β	0.0060	0.060	0.074	0.089

124

$$*\beta = \frac{\delta_m}{2\pi m} \quad ; \quad \delta_m = \ln\left(\frac{a_n}{a_{n+m}}\right)$$

$$a_n = \text{Acceleration at } n \text{ cycles (g's)}$$

$$a_{n+m} = \text{Acceleration at } m+n \text{ cycles}$$

Table 6.5 Damping Factors Calculated from Steady-State Response

Steady-State Test	FW3		Test Structure		FW4	
	Resonance*	Half-Power*	Resonance	Half-Power	Resonance	Half-Power
Following Run 1	0.089	0.090	0.070	0.078	0.070	0.078
Following Run 2	0.110	0.082	0.093	0.103	0.093	0.103
Following Run 3	0.110	0.097	0.094	0.112	0.094	0.112
High Amplitude Following Run 3	0.120	0.140	0.081	0.079	0.081	0.079

* See Sec. 6.3 for explanation of calculation methods.

Table 6.6 Influence of Lateral Loads on Wall Forces

(a) Structure with Heavily Reinforced Wall

Force Acting on Wall at Level	Level of Unit Lateral Load Applied to Structure									
	10	9	8	7	6	5	4	3	2	1
10	-0.311	-0.985	-0.740	-0.544	-0.382	-0.255	-0.160	-0.091	-0.044	-0.014
9	0.384	1.225	0.180	0.135	0.095	0.063	0.040	0.023	0.011	0.004
8	0.133	0.078	1.001	0.011	0.008	0.005	0.003	0.002	0.001	0.000
7	0.055	0.033	0.007	0.960	0.008	0.002	0.002	0.001	0.001	0.000
6	0.031	0.009	-0.015	-0.044	0.906	-0.046	-0.027	-0.016	-0.008	-0.002
5	0.086	0.062	0.036	0.008	-0.029	0.910	-0.038	-0.020	-0.010	-0.003
4	0.061	0.049	0.035	0.020	0.001	-0.028	0.911	-0.036	-0.016	-0.006
3	0.024	0.018	0.011	0.003	-0.007	-0.017	-0.036	0.912	-0.029	-0.007
2	0.036	0.030	0.023	0.016	0.007	-0.005	-0.019	-0.042	0.907	-0.028
1	0.347	0.332	0.317	0.298	0.277	0.250	0.214	0.168	0.104	0.999

Table 6.6 Influence of Lateral Loads on Wall Forces

(b) Structure with Lightly Reinforced Wall

Force Acting on Wall at Level	Level of Unit Lateral Load Applied to Structure									
	10	9	8	7	6	5	4	3	2	1
10	-0.297	-0.965	-0.703	-0.489	-0.334	-0.222	-0.141	-0.083	-0.043	-0.016
9	0.657	1.463	0.378	0.262	0.179	0.119	0.076	0.045	0.023	0.009
8	-0.210	-0.204	0.769	-0.122	-0.085	-0.056	-0.036	-0.021	-0.011	-0.004
7	-0.069	-0.110	-0.151	0.774	-0.116	-0.077	-0.049	-0.029	-0.015	-0.006
6	0.034	0.008	-0.021	-0.062	0.834	-0.075	-0.049	-0.029	-0.015	-0.006
5	0.096	0.071	0.045	0.016	-0.019	0.875	-0.041	-0.026	-0.013	-0.005
4	0.012	-0.001	-0.014	-0.030	-0.051	-0.077	0.832	-0.065	-0.036	-0.013
3	0.048	0.039	0.029	0.018	0.004	-0.015	-0.039	0.868	-0.029	-0.012
2	0.167	0.154	0.140	0.124	0.104	0.077	0.040	-0.006	0.877	-0.022
1	0.189	0.183	0.175	0.167	0.156	0.142	0.123	0.096	0.058	0.929

Table 7.1 Measured Shear and Moment Maxima

Test Structure	Run 1		Run 2		Run 3	
	V (kN)	M (kN-m)	V	M	V	M
FW1	21	34	28	41	42	41
FW2	18	28	25	32	25	31
FW3	16	23	26	33	20	33
FW4	21	34	31	41	35	43

Table 7.2 Relative Interstory Displacements for Initial Simulations

Level	Structures with Heavily Reinforced Walls	Structures with Lightly Reinforced Walls
10	0.5	0.8
9	0.7	0.8
8	0.8	1.0
7	0.9	1.0
6	1.0	1.0
5	1.0	1.0
4	0.9	1.1
3	0.7	0.9
2	0.7	0.8
1	0.5	0.7

Table 7.3 Column and Wall Stiffnesses of Linear Model

Story	Moments of Inertia, x 10 ⁴ mm ⁴					
	Structure with Heavily Reinforced Wall			Structure with Lightly Reinforced Wall		
	Exterior Column*	Interior Column	Wall	Exterior Column	Interior Column	Wall
10	10.6	14.7	3790	10.6	10.6	3790
9	10.6	14.7	3790	10.6	10.6	3790
8	10.6	10.6	3790	10.6	10.6	1660
7	10.6	10.6	3790	10.6	10.6	1660
6	10.6	10.6	2400	10.6	10.6	1660
5	10.6	10.6	2400	10.6	10.6	1660
4	10.6	10.6	2470	10.6	10.6	1660
3	10.6	10.6	2470	14.7	10.6	1660
2	10.6	10.6	2470	14.7	10.6	1660
1	10.6	10.6	2470	14.7	10.6	1660
Flexibility of Spring at Base (x10 ⁻⁵ radian/ kN-mm)	1.4	1.4	Variable	1.4	1.0	Variable

*For single frame

Table 7.4 Calculated Frequencies and Mode Shapes

	Structure with Heavily Reinforced Wall				Structure with Lightly Reinforced Wall			
	First Mode		Second Mode		First Mode		Second Mode	
	Case 1*	Case 2**	Case 1	Case 2	Case 1	Case 2	Case 1	Case 2
Frequencies, Hz.	3.63	1.72	13.7	8.85	3.49	1.57	12.1	7.49
Mode Shapes Level								
10	1.00	1.00	-1.00	-1.00	1.00	1.00	-1.00	-1.00
9	0.91	0.90	-0.55	-0.56	0.91	0.90	-0.55	-0.54
8	0.83	0.80	-0.10	-0.12	0.83	0.79	-0.09	-0.08
7	0.72	0.69	0.32	0.28	0.72	0.68	0.34	0.34
6	0.61	0.58	0.67	0.62	0.61	0.57	0.66	0.65
5	0.49	0.47	0.87	0.84	0.49	0.46	0.83	0.83
4	0.36	0.36	0.88	0.90	0.37	0.35	0.83	0.86
3	0.23	0.26	0.71	0.80	0.24	0.24	0.67	0.74
2	0.12	0.16	0.44	0.58	0.13	0.15	0.41	0.52
1	0.04	0.07	0.15	0.29	0.04	0.06	0.14	0.25

130

*Case 1: $\mu_{beams} = 1$, Fixed base of wall

**Case 2: $\mu_{beams} = 10$, Flexibility at base of wall = 20×10^{-7} rad/KN-mm

Table 7.5 Rotation at Base of Wall Calculated from Measured Forces and Displacements

Test Structure	Time	Measured Moment (kN-m)	Calculated Rotation at Base of Wall (x 1000, Radians)
FW1	0.87	9.3	- 1.3
	0.98	- 3.8	- 6.0
	1.96	16.2	- 0.1
FW2	0.87	3.8	6.4
	1.00	- 1.9	- 6.7
	1.99	1.5	17.0
FW3	2.12	3.6	5.9
	2.28	- 3.4	- 5.2
	4.28	1.1	5.5
FW4	2.02	8.2	- 1.8
	2.32	10.1	- 2.3
	3.09	11.0	- 0.9

Table 7.6 Influence of Permanent Rotations on Residual Wall Forces

(a) Structure with Heavily Reinforced Wall

Force Acting on Wall at Level	Permanent Rotation at Base of Wall	Level of Beams with Permanent End Rotations									
		10	9	8	7	6	5	4	3	2	1
10	136	241	94	-105	-57	-40	-31	-21	-16	-12	-8
9	-34	329	58	259	-14	10	7	5	4	3	2
8	-3	49	233	-18	210	-24	1	1	0	0	0
7	2	3	39	-200	-3	183	-27	4	0	0	0
6	23	6	10	37	-193	-2	179	-26	-2	-1	-1
5	31	7	10	8	38	-174	-1	157	-31	-2	-2
4	47	3	6	5	4	32	-175	1	178	-32	-2
3	95	2	3	3	2	2	31	-159	1	188	-36
2	124	2	3	3	3	3	2	18	-178	3	223
1	392	4	6	6	6	6	8	9	40	-176	-7

Table 7.6 Influence of Permanent Rotations on Residual Wall Forces

(b) Structure with Lightly Reinforced Wall

Force Acting on Wall at Level	Permanent Rotation at Base of Wall	Level of Beams with Permanent End Rotations									
		10	9	8	7	6	5	4	3	2	1
10	58	214	54	-87	-40	-41	-26	-18	-15	-9	-6
9	-31	-326	75	197	-33	36	9	10	7	5	3
8	15	101	-216	-6	201	-69	10	-9	-3	-3	-2
7	20	-20	72	-167	-3	201	-69	8	-10	-2	-2
6	19	14	-9	55	-202	2	206	-61	12	-9	-1
5	20	3	11	-7	69	-203	3	192	-65	11	-6
4	36	3	3	7	-11	66	-206	2	208	-57	12
3	82	2	3	1	8	-12	67	-194	16	183	-68
2	-64	3	3	3	3	11	-8	68	-226	0	220
1	528	2	2	2	3	3	10	-9	75	-169	-39

Table 7.7 Comparison of Measured Wall Base Moment Maxima and Capacities, kN-m

Test Structure	Capacity*	Run 1	Run 2	Run 3
FW1	15.0	16.2 -9.0	13.8 -14.5	11.8 -20.6
FW2	4.6	5.1 - 6.9	5.2 - 7.9	8.6 - 4.2
FW3	4.6	(5.0)** (-5.2)	(12.8) (-7.3)	9.9 - 6.0
FW4	15.0	14.0 -13.6	22.3 -17.1	21.0 -16.0

*Capacity measured during cyclic load tests.

** Values in parenthesis based on zero force at level 9 where measurements were not obtained because of a malfunction in the tape recorder.

Table 7.8 Normalized Wall Response Maxima

(Initial Test Run)

	Time	Displacement	M_b^* (kN-m)	γ_1	H_1 (meter)	A_1^{**} (g)	Measured		Normalized	
							M_{bw} (kN-m)	V_{bw} (kN)	M_{bw}^{****} (kN-m)	V_{bw}^{****} (kN)
FW1	1.96	28.2	29	0.74	1.6	0.54	12	11	22	20
FW2	1.38	20.0	21	0.77	1.6	0.37	5.3	5.6	14	15
FW3	2.12	18.7	20	0.74	1.7	0.35	3.3	7.4	9.4	21
FW4	3.21	21.7	27	0.73	1.7	0.48	11.2	12.3	23	26

*Refer to Sec. 7.5(c) for explanation of notation.

**At time of maximum wall response

*** M_{bw}^i = Normalized moment at base of wall = M_{bw}/A_1

V_{bw}^i = Normalized shear at base of wall = V_{bw}/A_1

Table 7.9 Measured and Calculated Stiffness Reductions

Test Structure	Flexibility of Wall at Base ($\times 10^{-7}$ radian/kN-mm)		Damage Ratio of Fifth-Level Beams	
	Measured	Calculated	Measured	Calculated
FW1	3.8 (SW2)*	4.3	3.4 (EJ2)*	4.5
	2.4 (SW4)		3.0 (IJ1)	
FW2	10.5 (SW3)	8.2	3.4 (EJ2)	3.8
			3.0 (IJ1)	
FW3	7.0 (SW3)	4.2	2.9 (EJ5)	1.4
			2.9 (IJ3)	
FW4	1.6 (SW2)	1.5	2.9 (EJ5)	4.0
	1.2 (SW4)		2.9 (IJ3)	

*() Frame- or Wall-Specimen Designation

Table 7.10 Comparison of Shape Factors Determined from Design Calculations and Measurements

	Structures with Heavily Reinforced Walls			Structures with Lightly Reinforced Walls		
	Design	Measured		Design	Measured	
		FW1	FW4		FW2	FW3
Eff. Weight, $\gamma_1 W,$	31.2	34.0	33.4	32.9	35.3	33.7
Eff. Height, $h,$ (meter)	1.71	1.65	1.67	1.67	1.62	1.66
$h \gamma_1 W$ (kN-m)	53.4	56.1	55.8	54.9	57.2	55.9

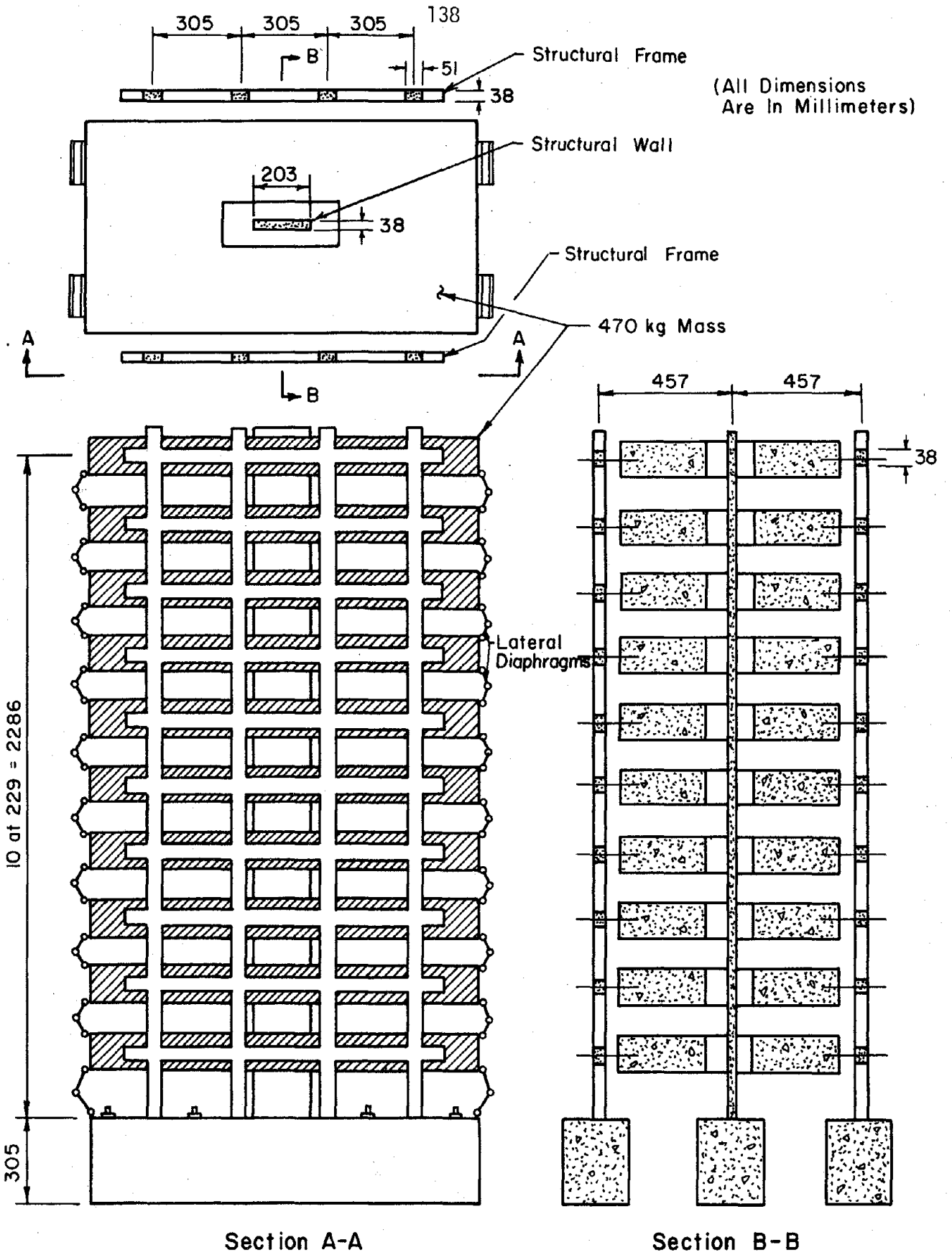


Fig. 2.1 Test Structure Description

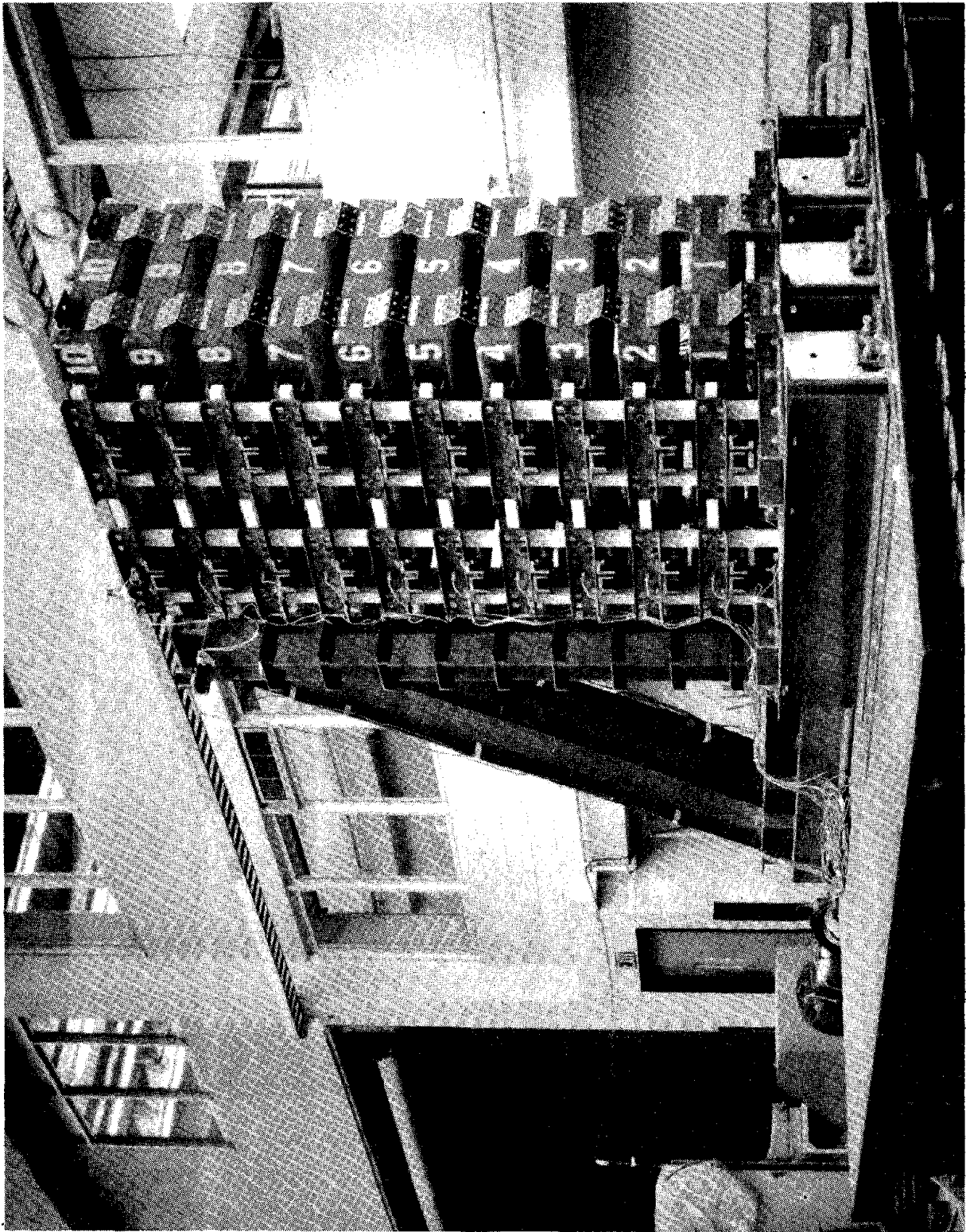


Fig. 2.2 Experimental Arrangement

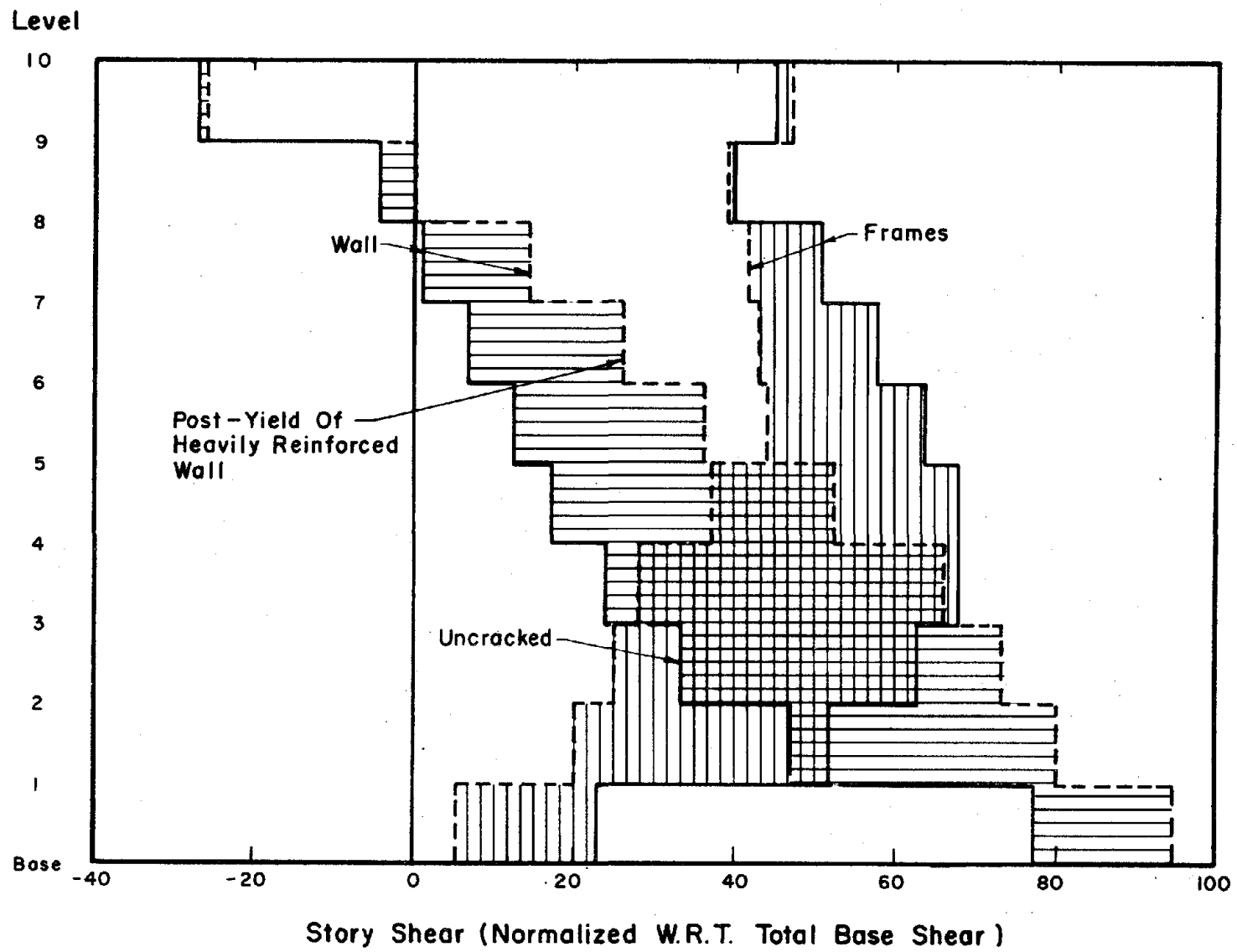


Fig. 3.1 Shear Diagrams using Eight-Inch Wall

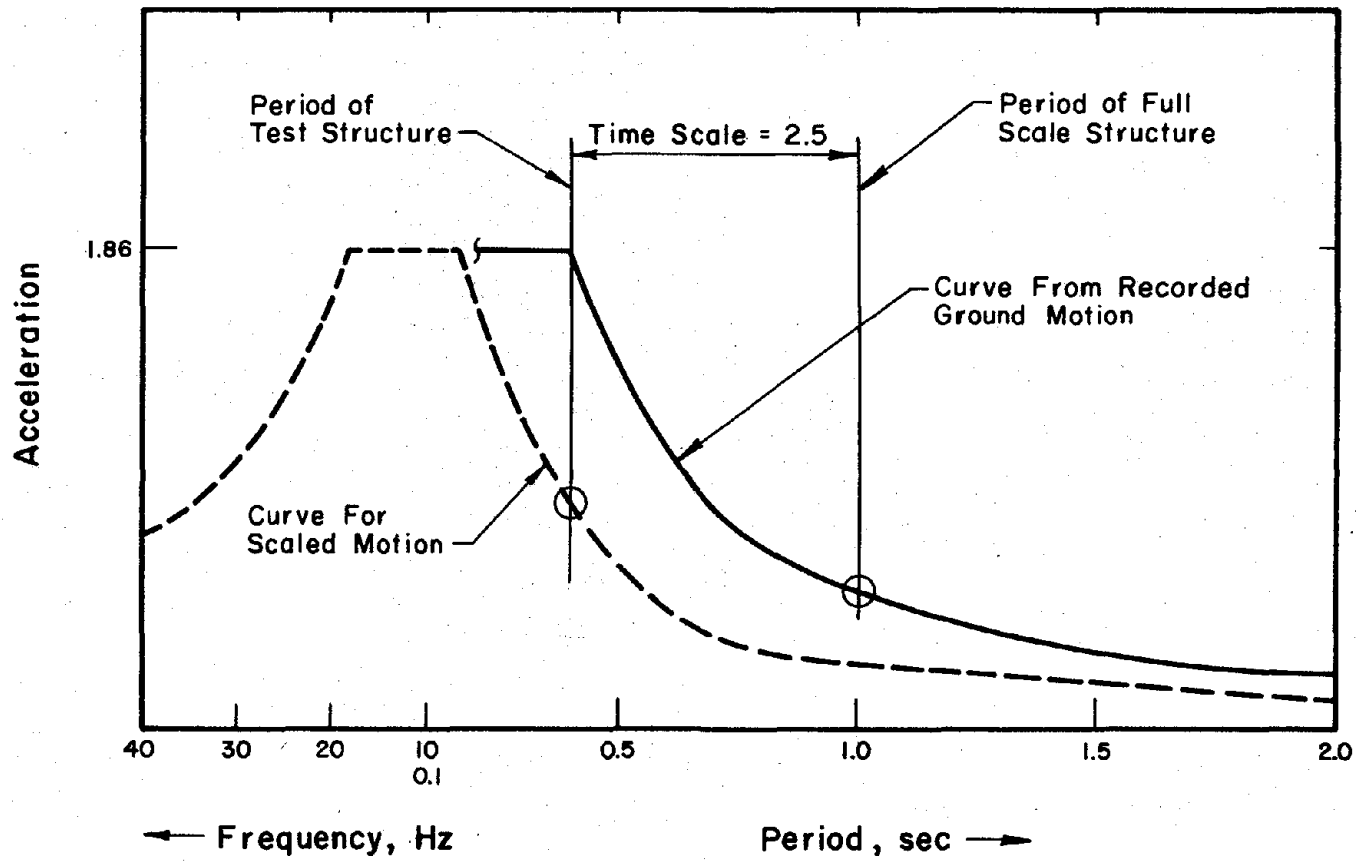


Fig. 3.2 Determination of Time Scale

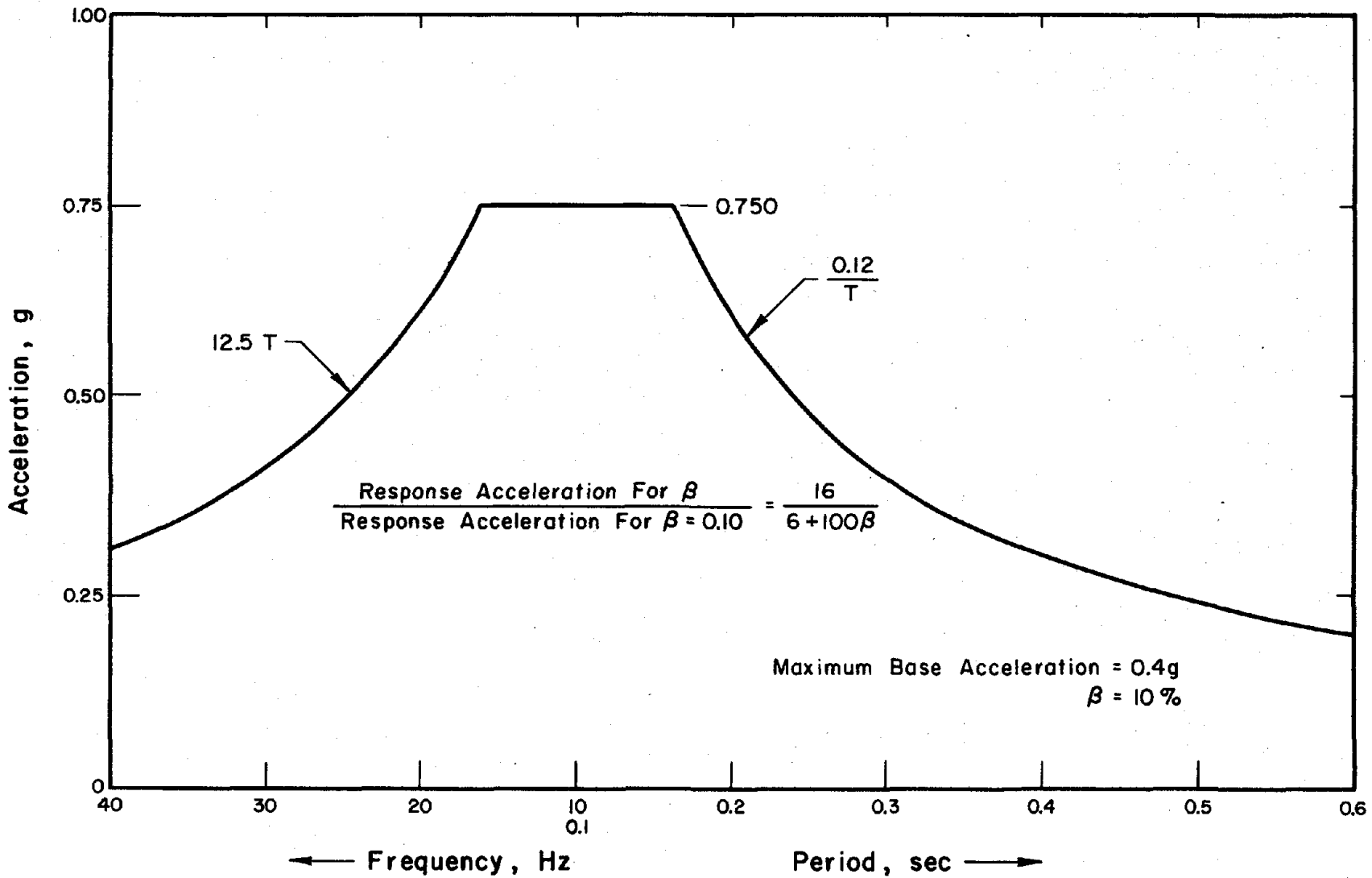


Fig. 3.4 Spectral-Response Curve Used for Design

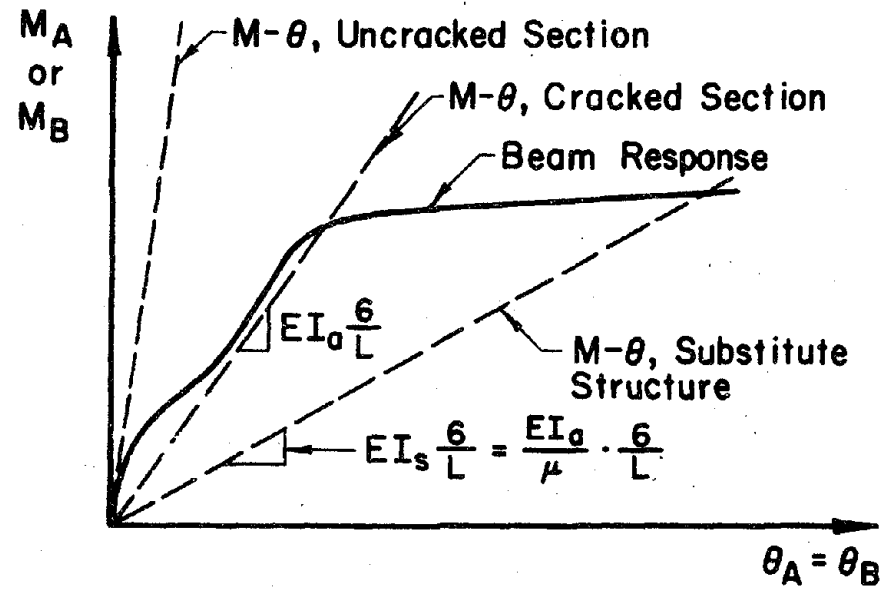
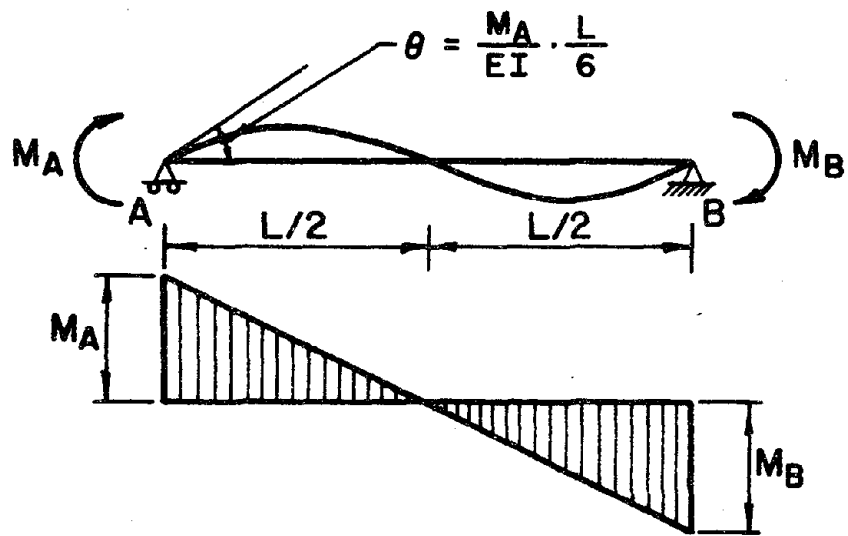


Fig. 3.5 Interpretation of Damage Ratio

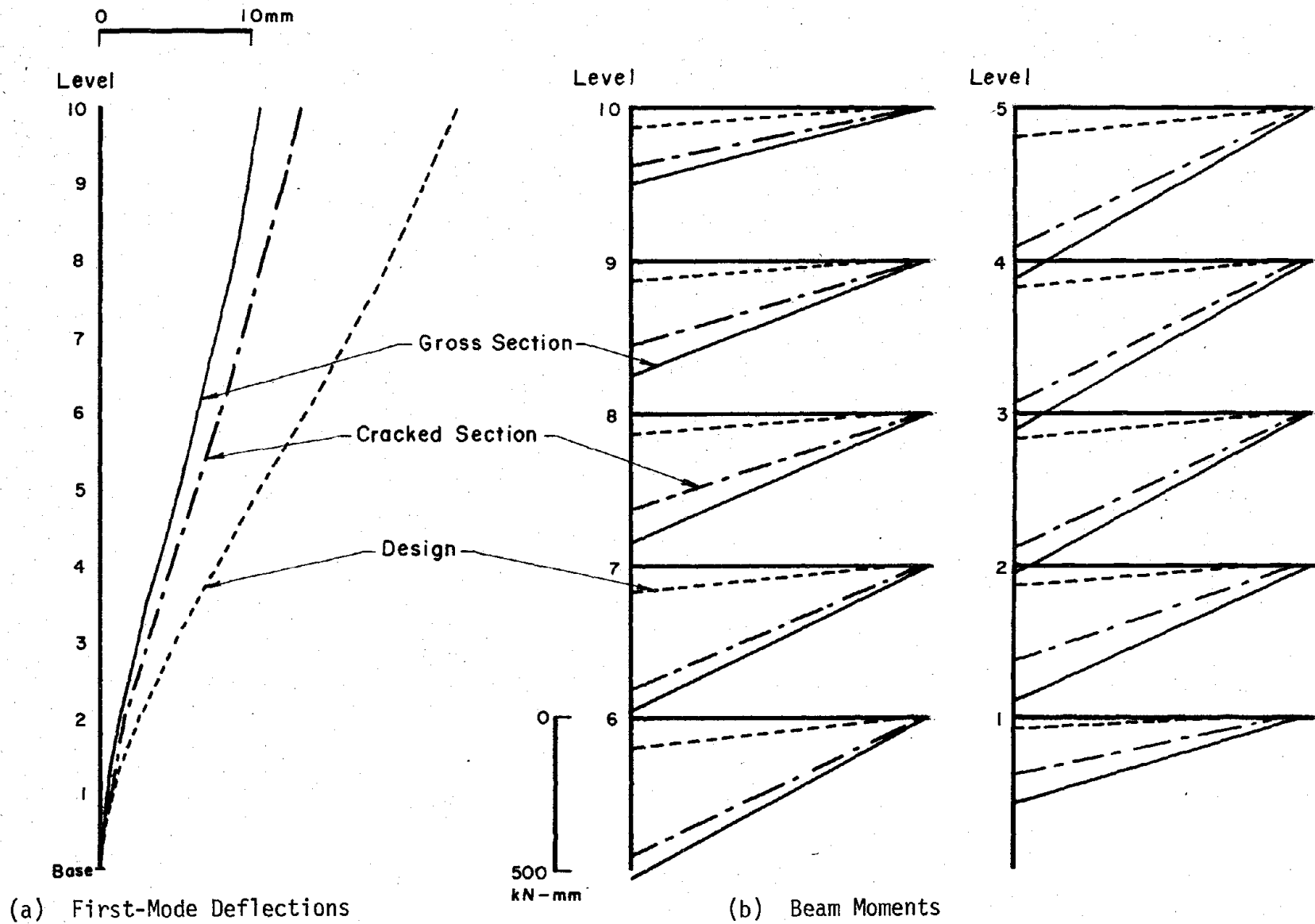
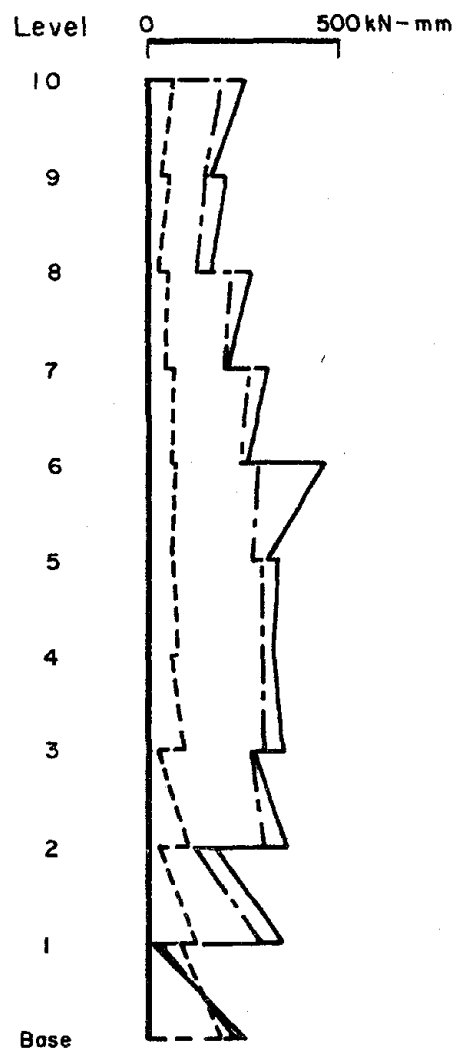
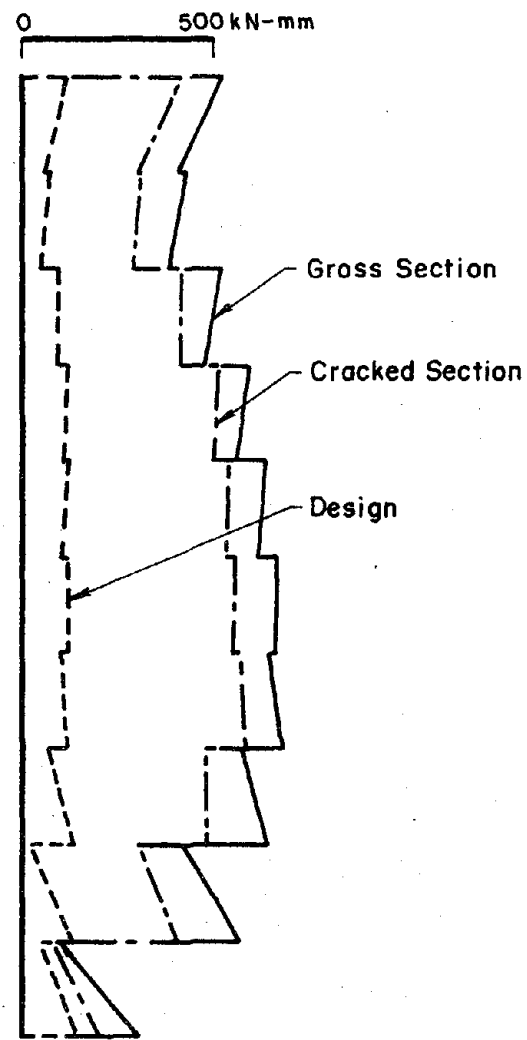


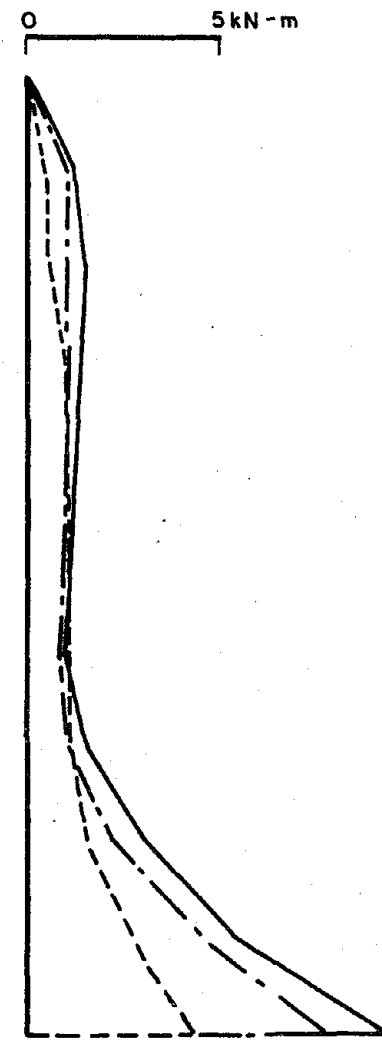
Fig. 3.6 Comparison of Design Requirements with Different Methods



(c) Exterior-Column Moments



(d) Interior-Column Moments



(e) Wall Moments

Fig. 3.6 (contd.) Comparison of Design Requirements with Different Methods

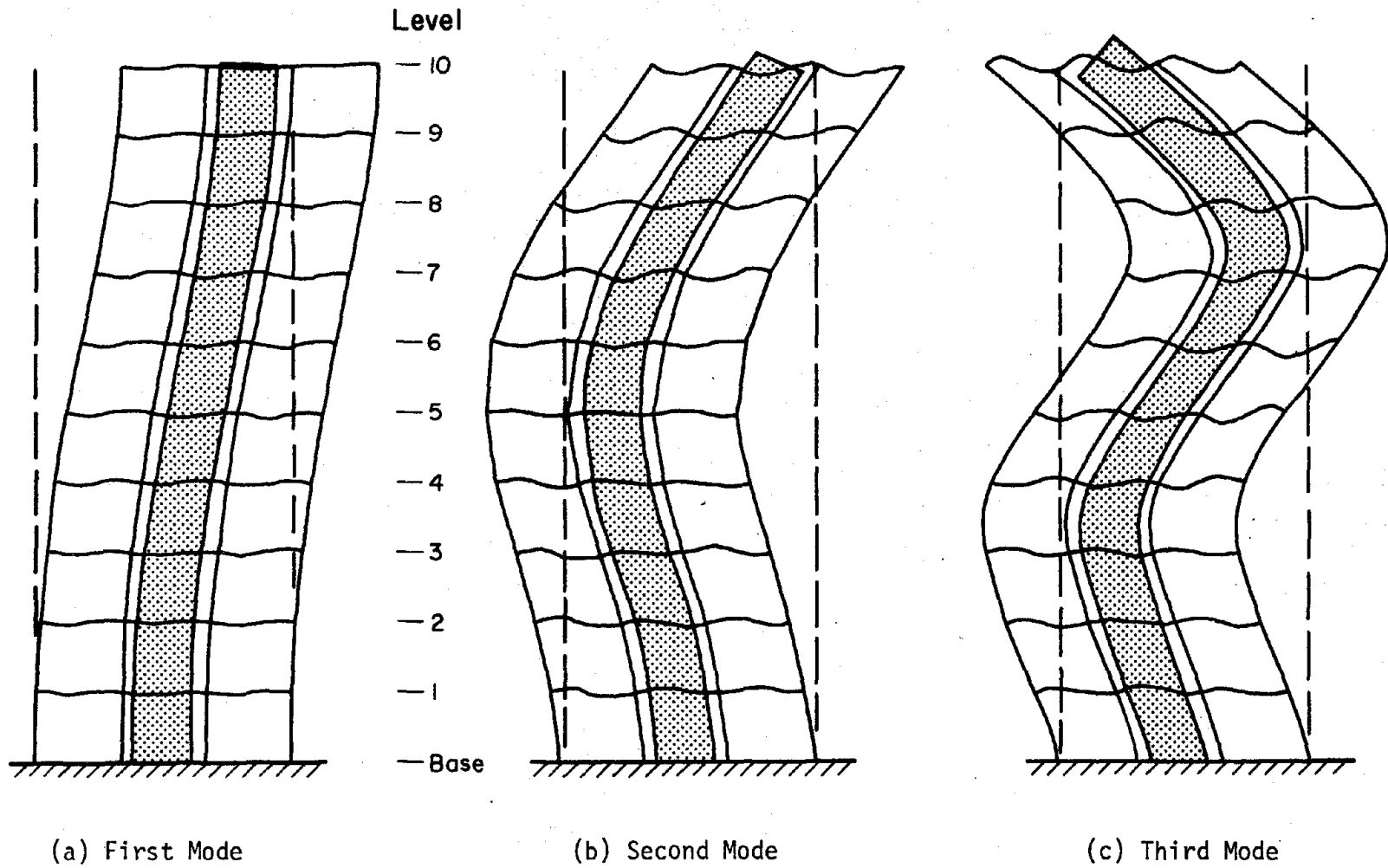


Fig. 3.7 Calculated Mode Shapes for Design

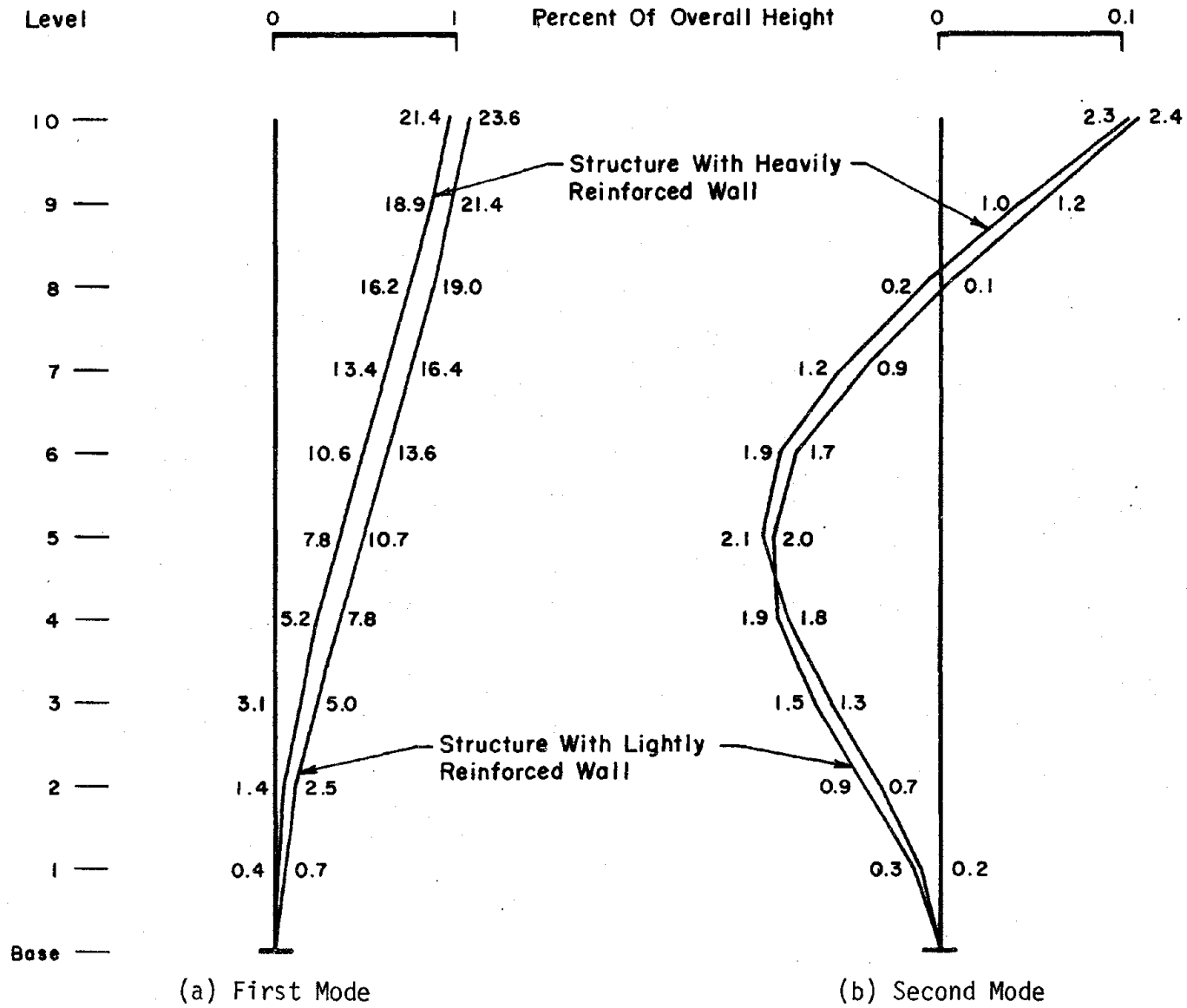
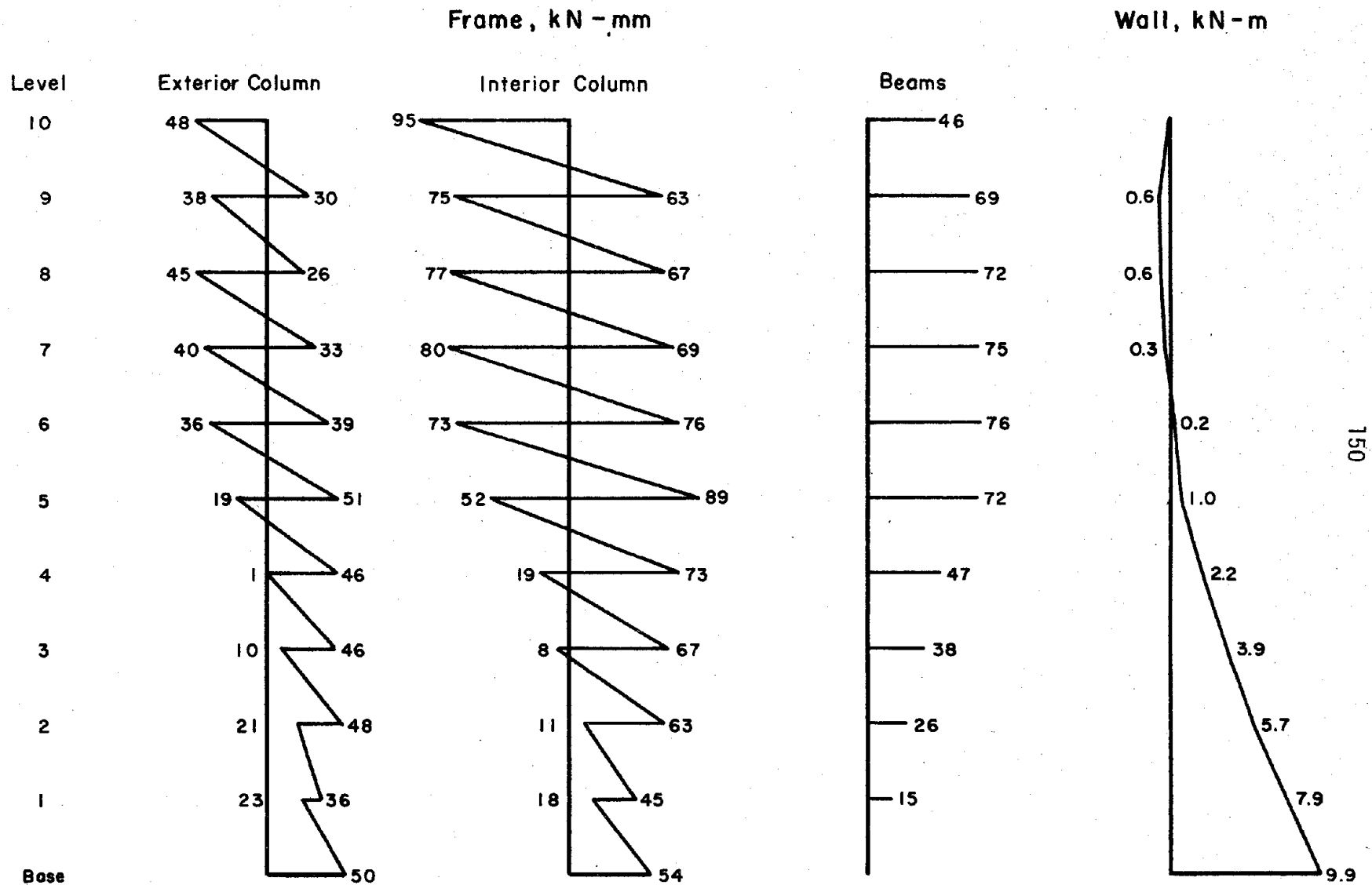
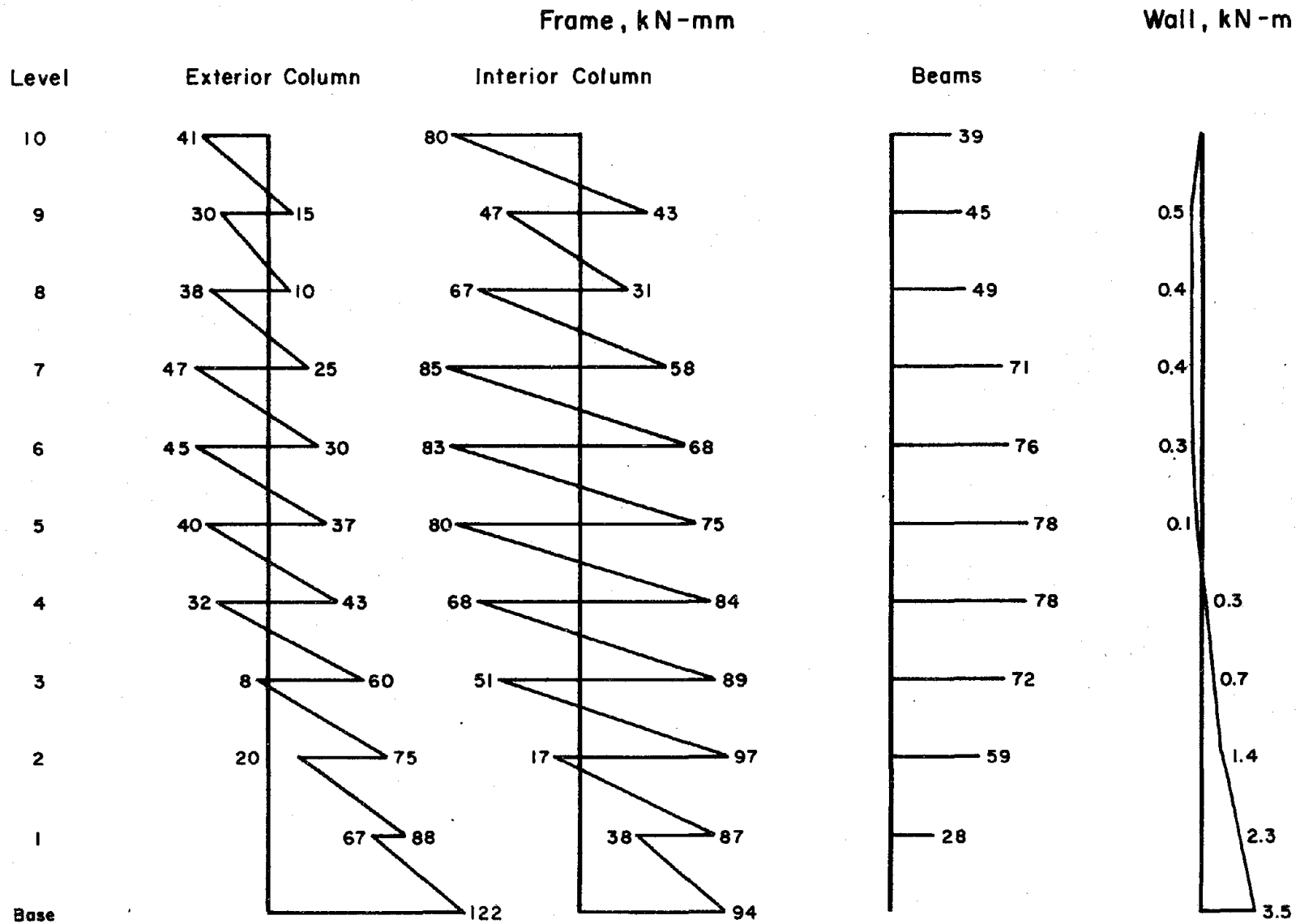


Fig. 3.8 Calculated Displacements for Design



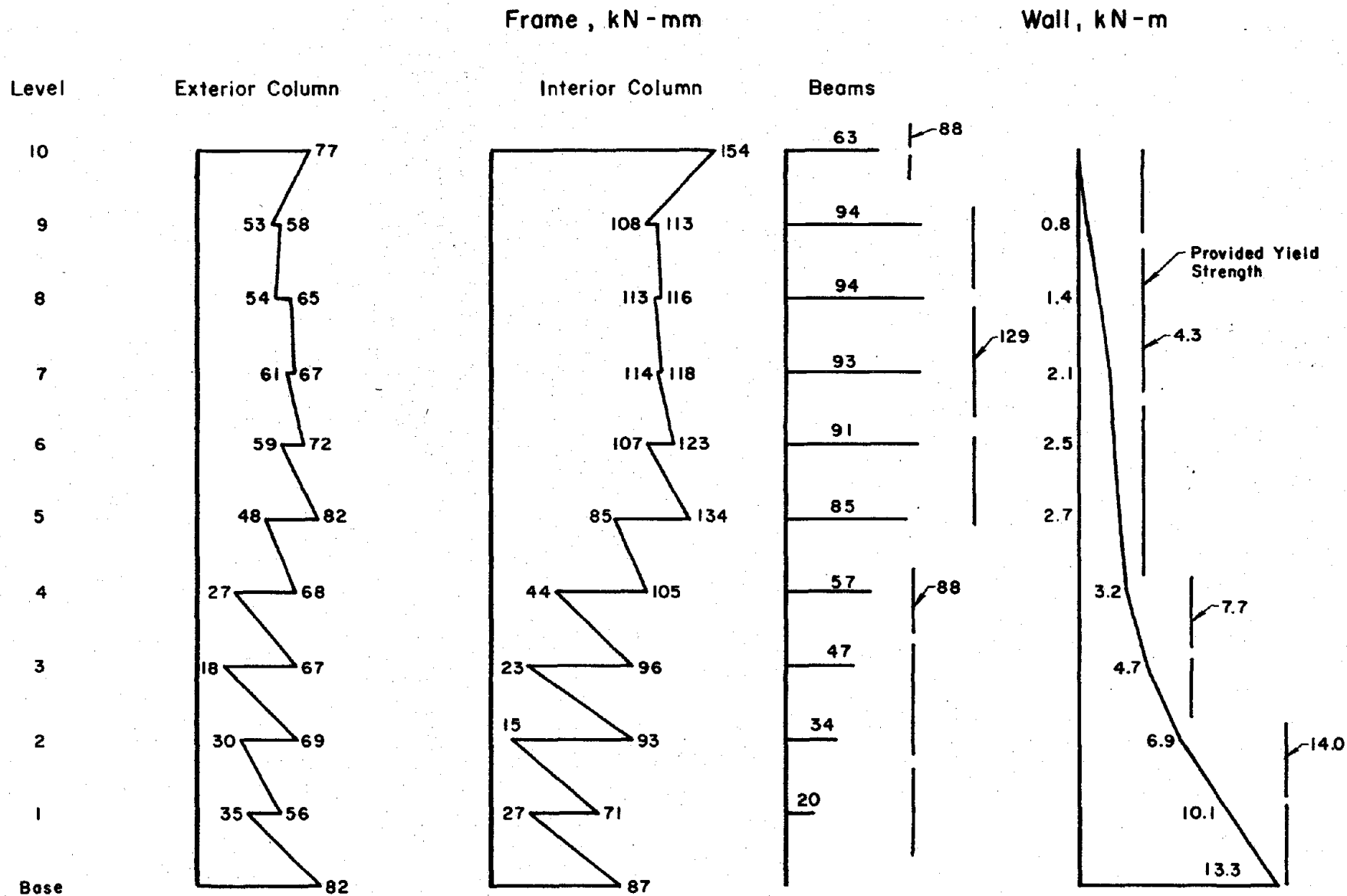
(a) Structure with Heavily Reinforced Wall

Fig. 3.9 Calculated First-Mode Moments for Design

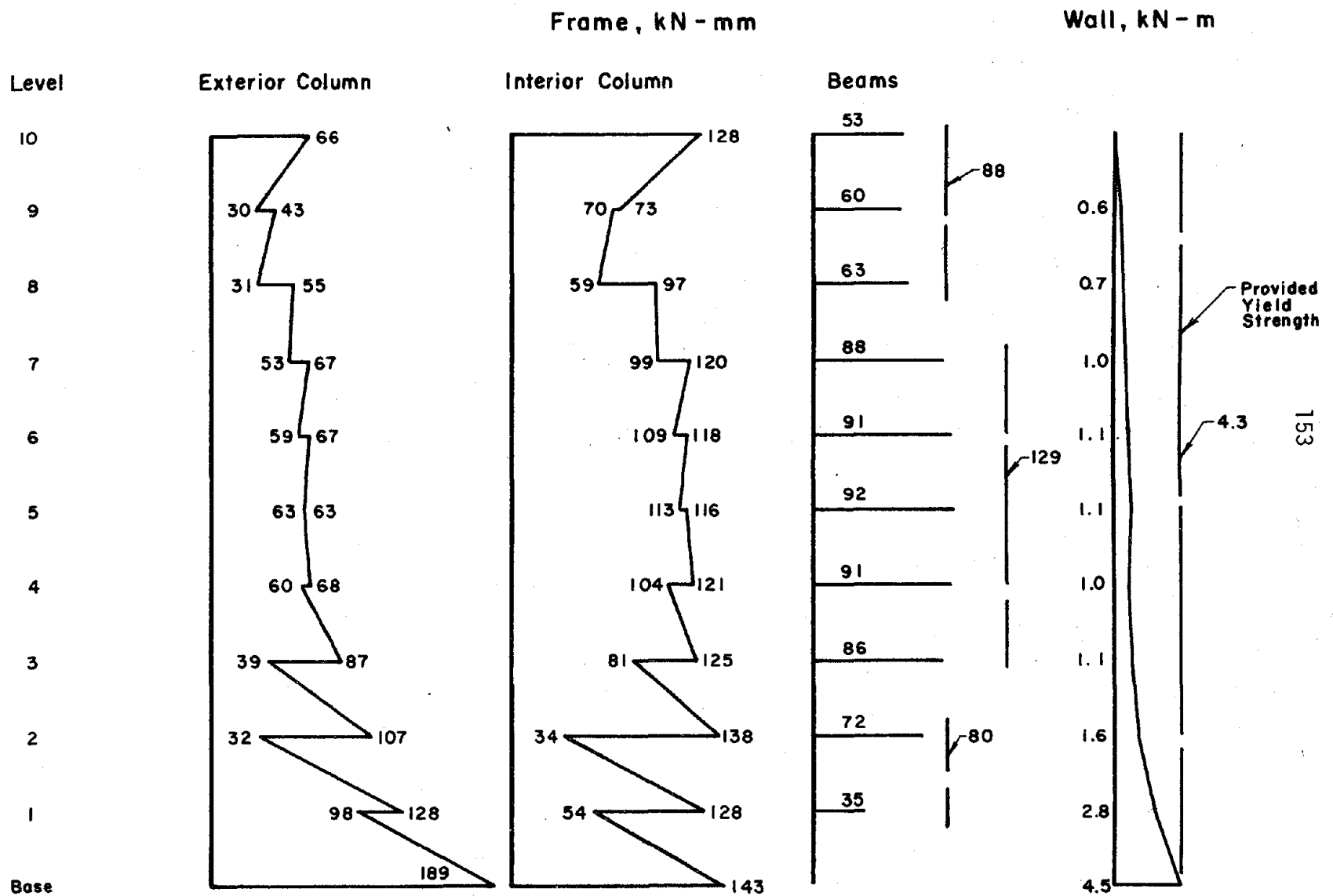


(b) Structure with Lightly Reinforced Wall

Fig. 3.9 (contd.) Calculated First-Mode Moments for Design



(a) Structure with Heavily Reinforced Wall
 Fig. 3.10 Design Moments



(b) Structure with Lightly Reinforced Wall

Fig. 3.10 (contd.) Design Moments

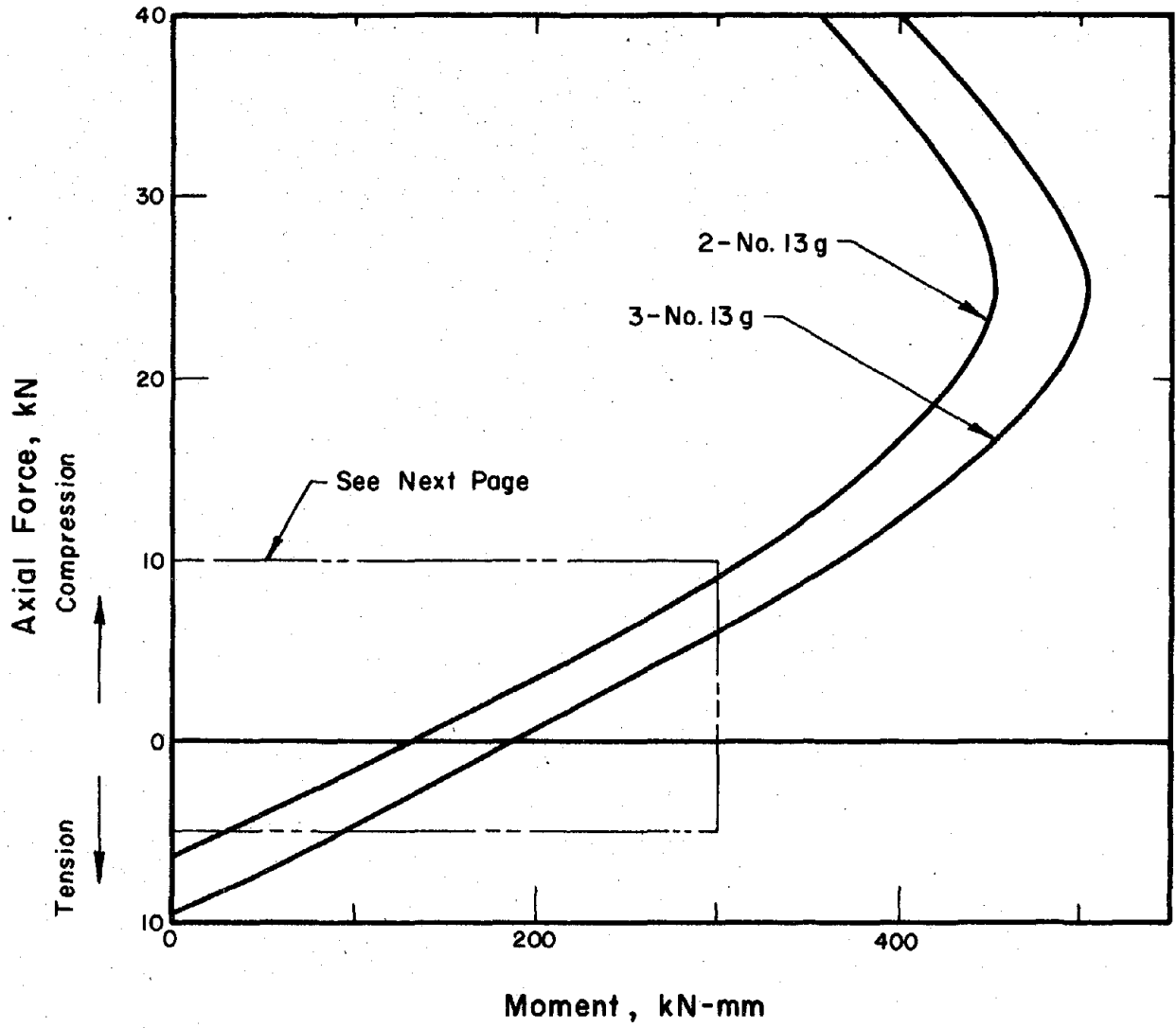
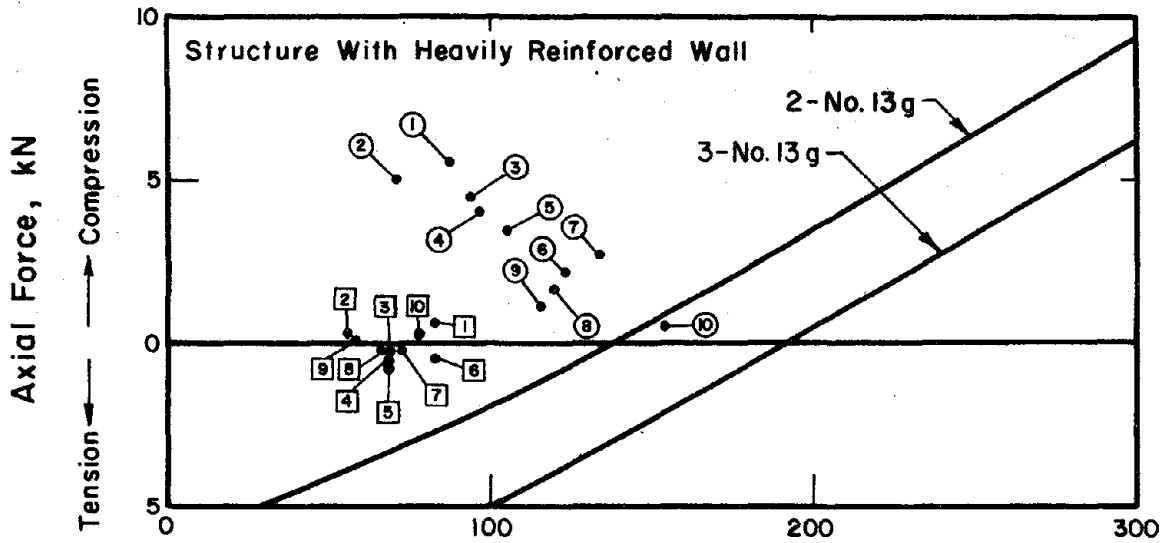


Fig. 3.11 Interaction Diagram for Columns



Key : □ Exterior Column, Story i
 ○ Interior Column

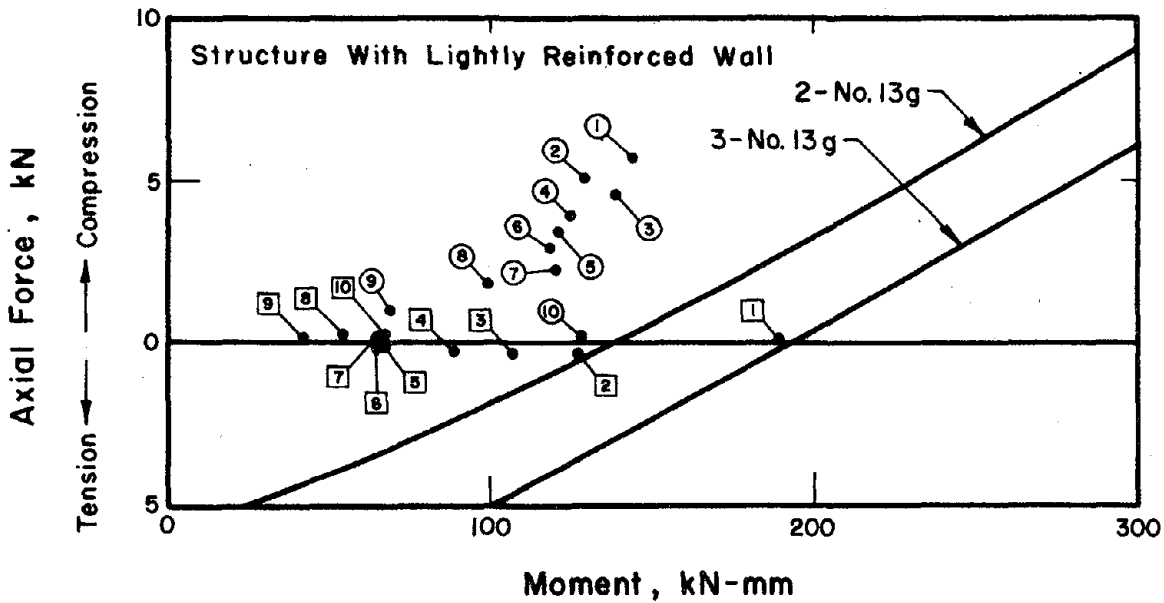


Fig. 3.11 (contd.) Interaction Diagram for Columns

FRAME REINFORCING SCHEDULE

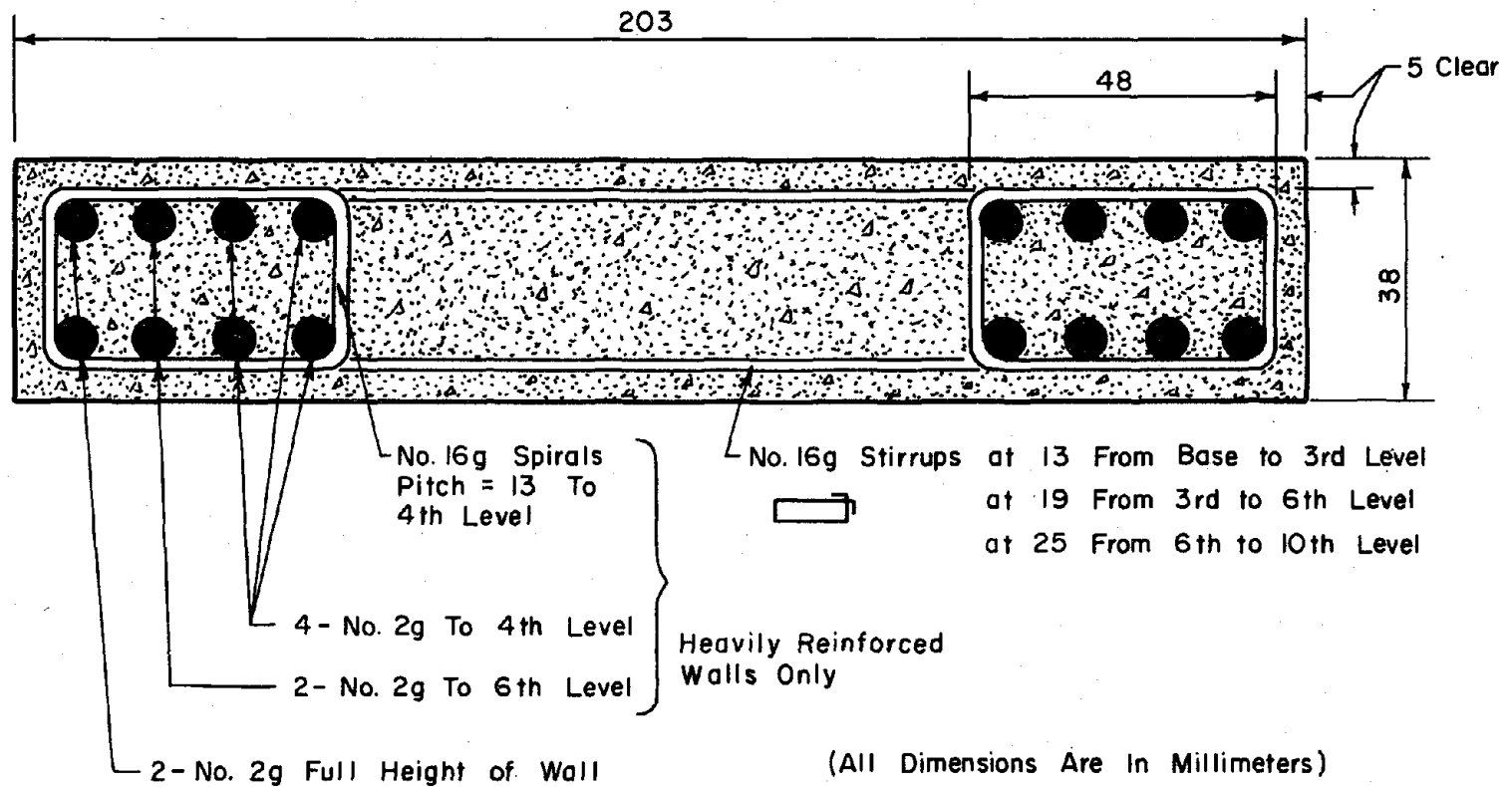
Number Of No.13 g Wires Per Face

Story Or Level	Structure With Heavily Reinforced Wall			Structure With Lightly Reinforced Wall		
	Beams	Exterior Columns	Interior Columns	Beams	Exterior Columns	Interior Columns
10	2	2	3	2	2	2
9	3	↑	3	2	↑	↑
8	3		2	2		
7	3	↑	↑	3		
6	3			3		
5	3			3		
4	2	↓	↓	3	2	↓
3	2			3		
2	2	↓	↓	2	3	
1	2			2	2	3

157

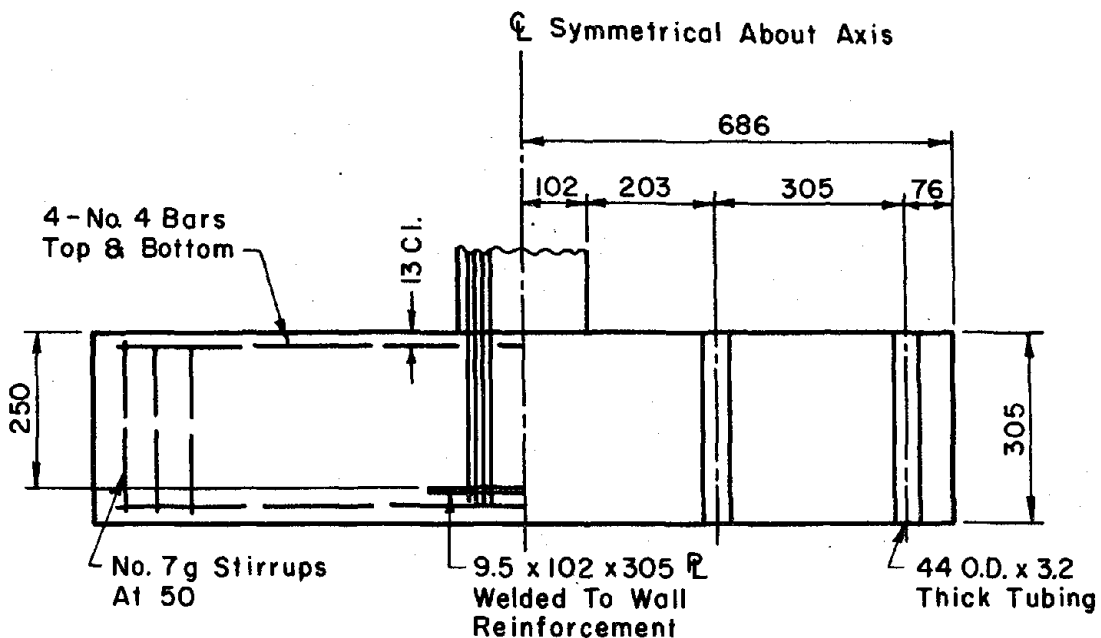
(a) (contd.) Frame Reinforcement

Fig. 3.12 (contd.) Description of Reinforcement

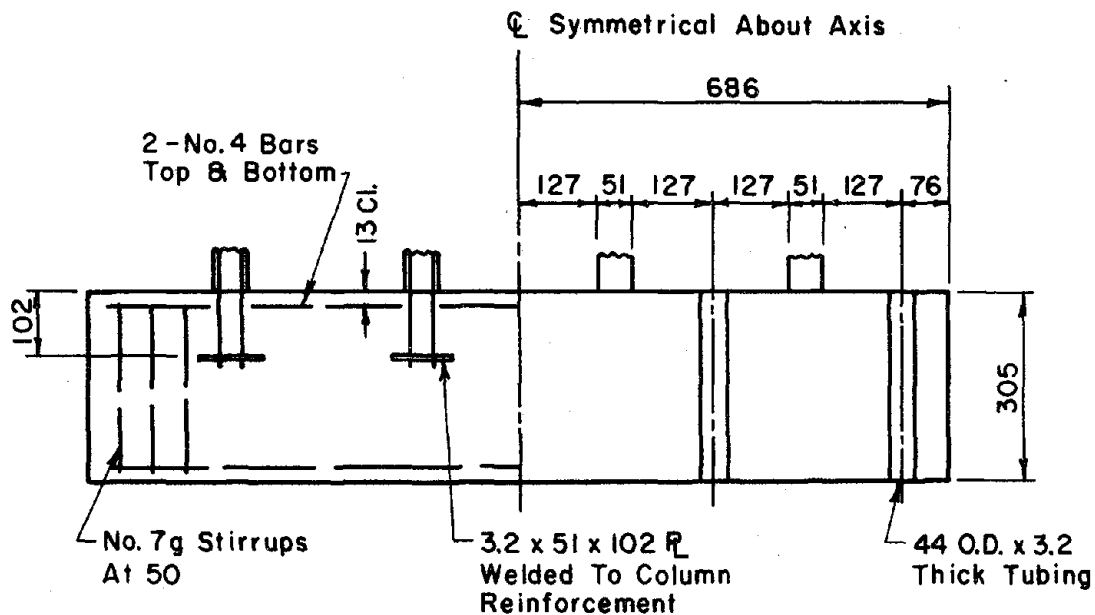


(b) Wall Reinforcement

Fig. 3.12 (contd.) Description of Reinforcement



Typical Wall Base Anchorage



Typical Frame Base Anchorage

(All Dimensions In Millimeters)

(c) Base Anchorage

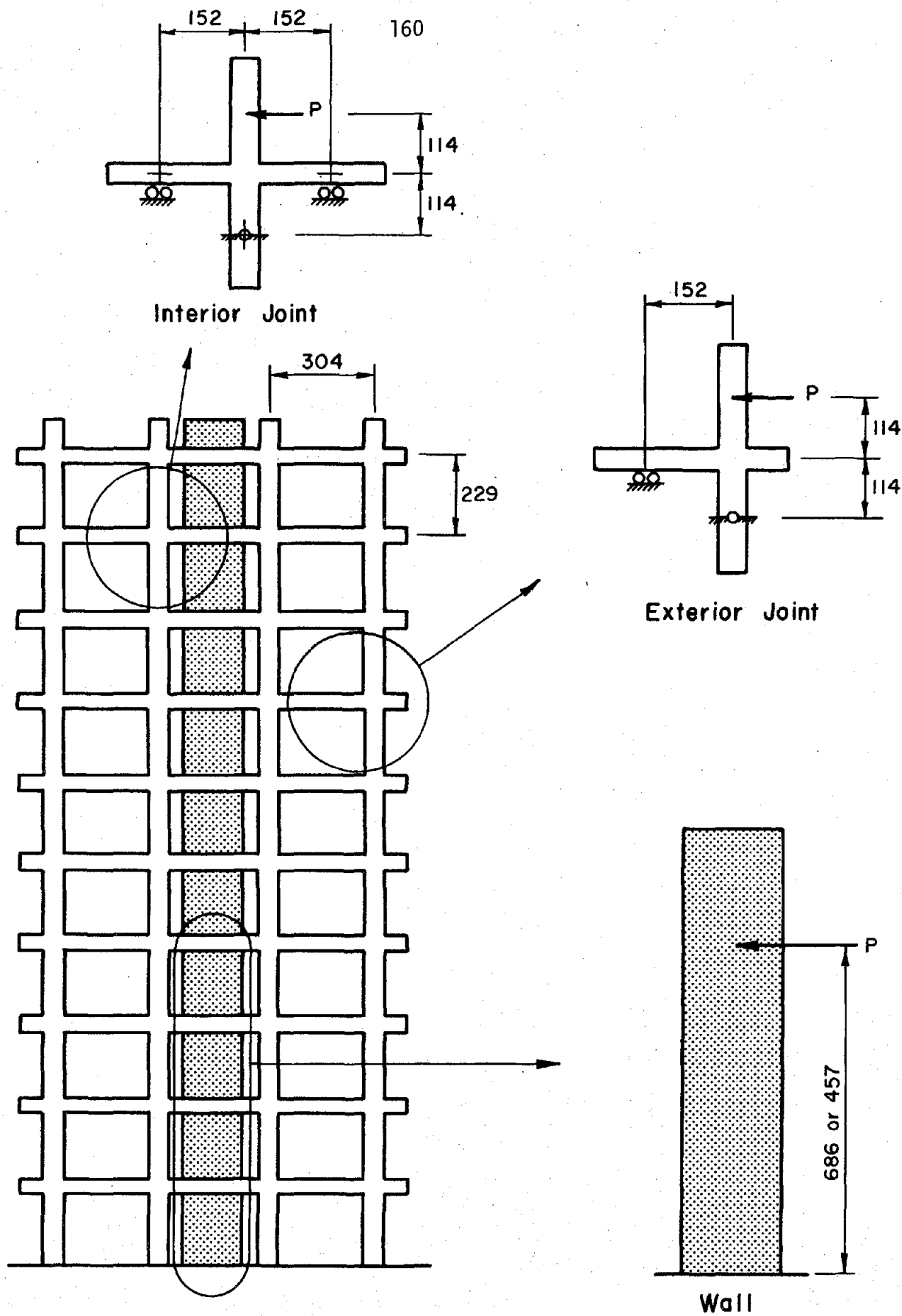
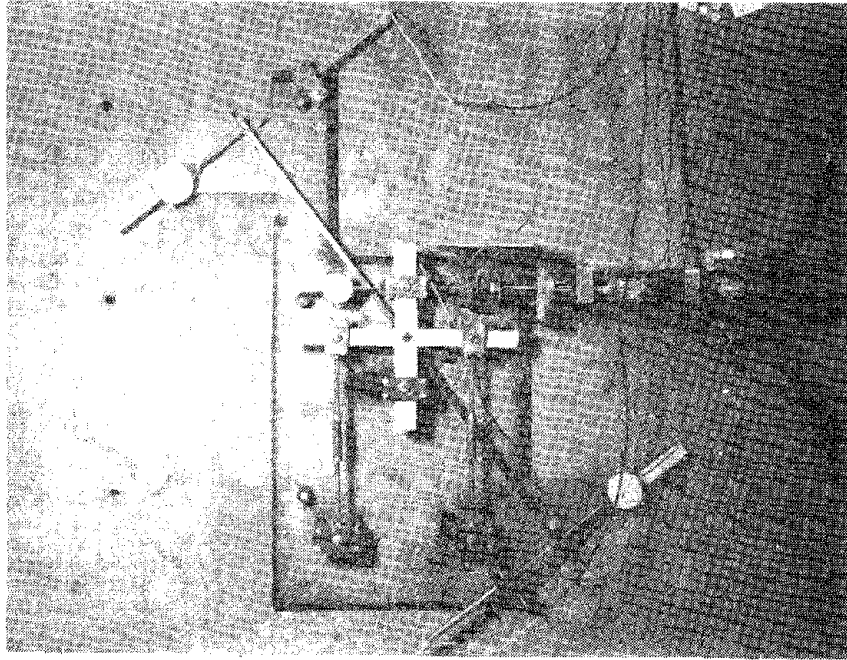
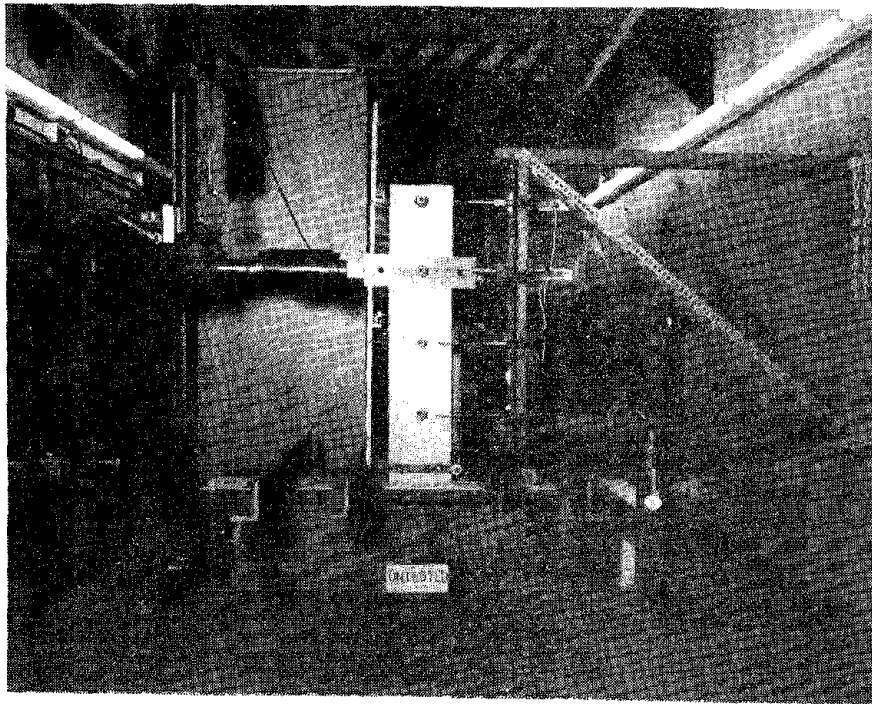


Fig. 4.1 Description of Frame and Wall Specimens

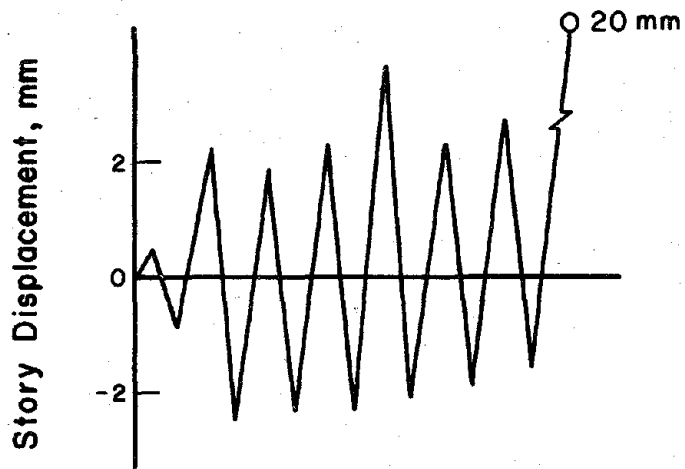


(a) Frame Specimen

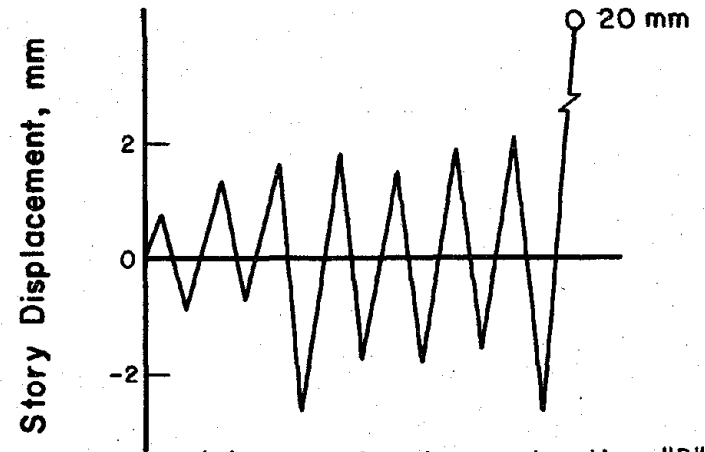


(b) Wall Specimen

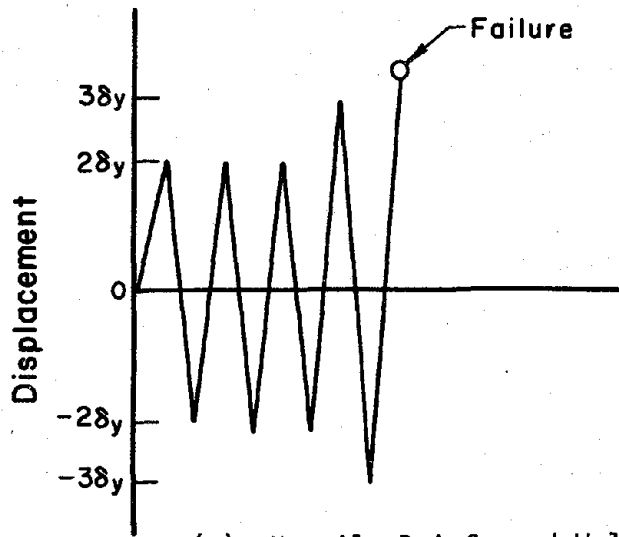
Fig. 4.2 Test Apparatus for Cyclic-Load Tests



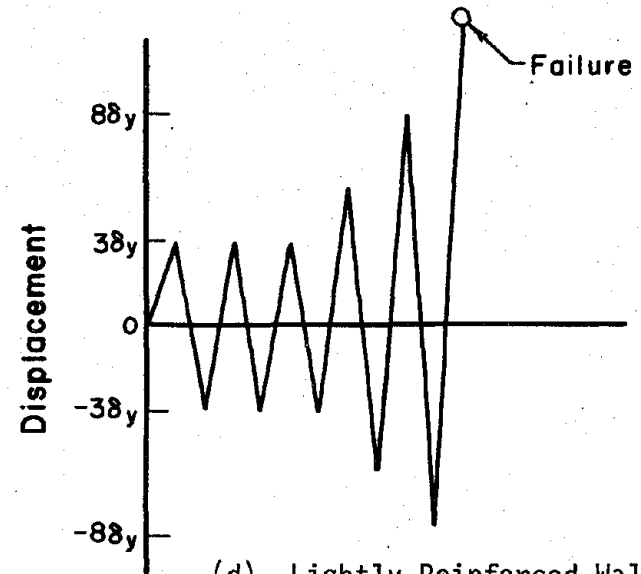
(a) Frame Specimen - Loading "A".



(b) Frame Specimen - Loading "B".

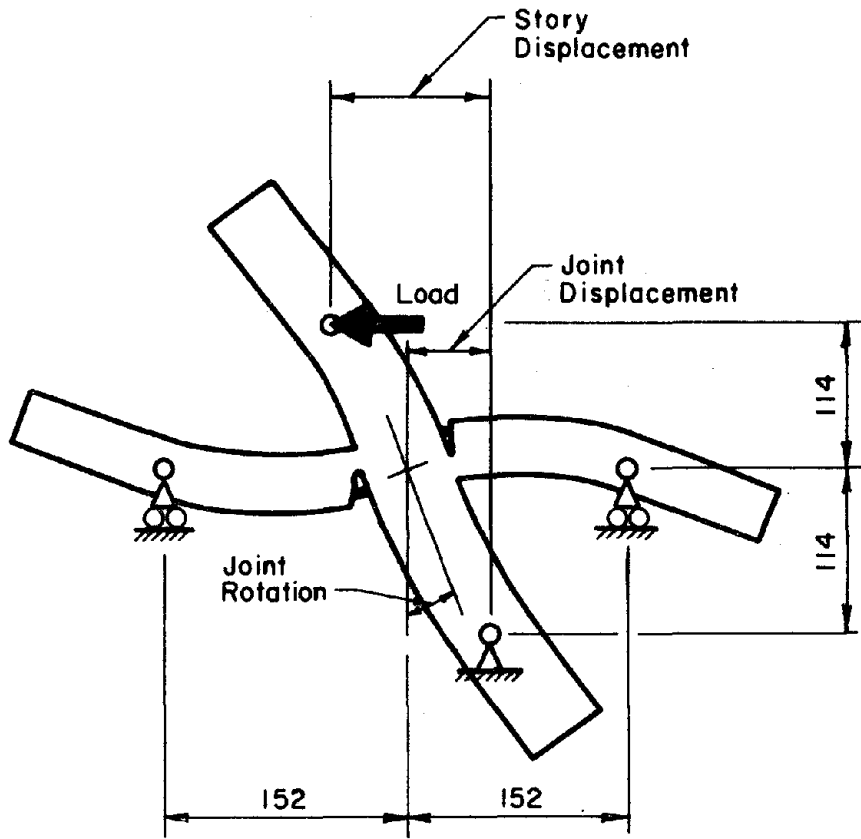


(c) Heavily Reinforced Wall Specimen

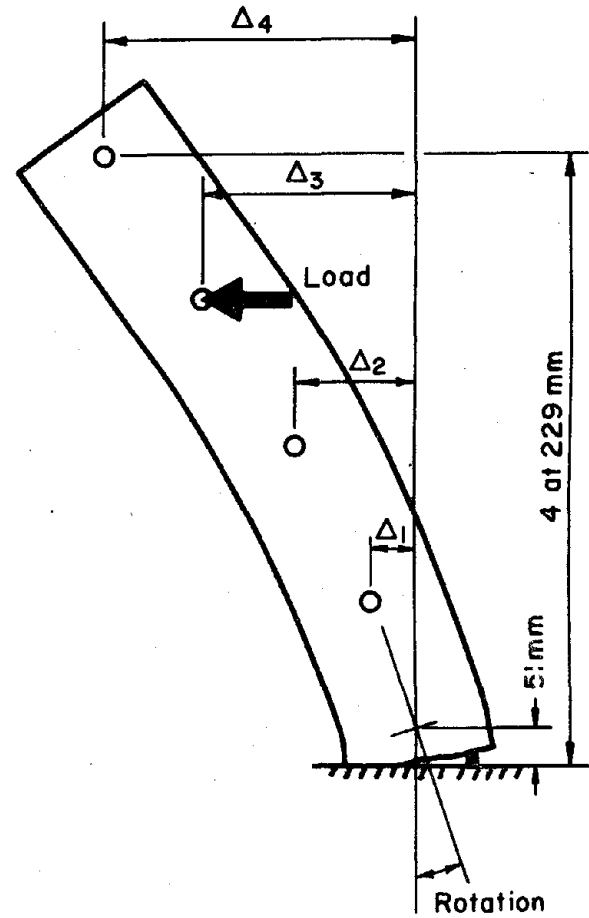


(d) Lightly Reinforced Wall Specimen

Fig. 4.3 Loading Programs for Cyclic-Load Tests



(a) Frame Specimens



(b) Wall Specimens

Fig. 4.4 Measurements for Cyclic-Load Tests

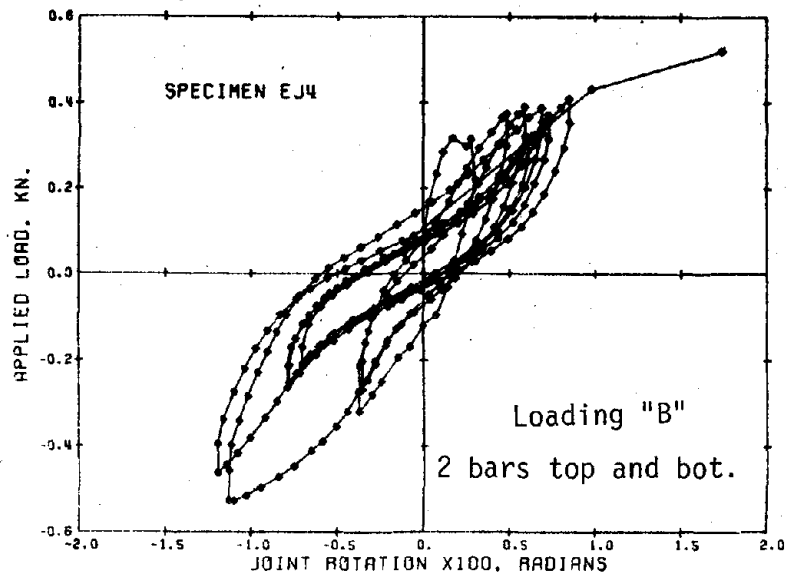
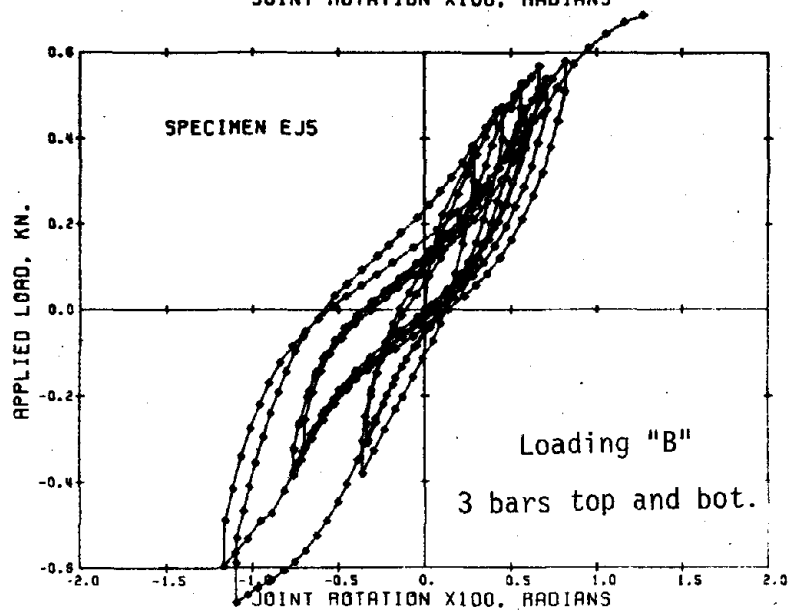
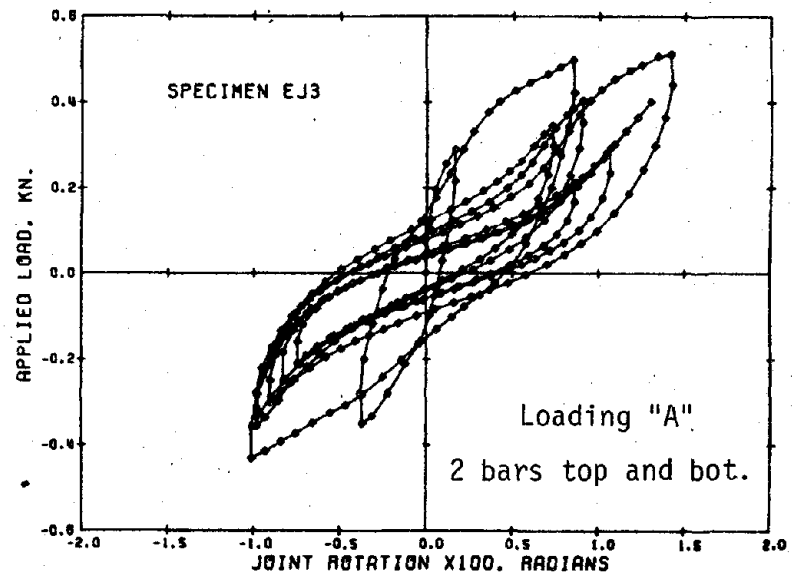
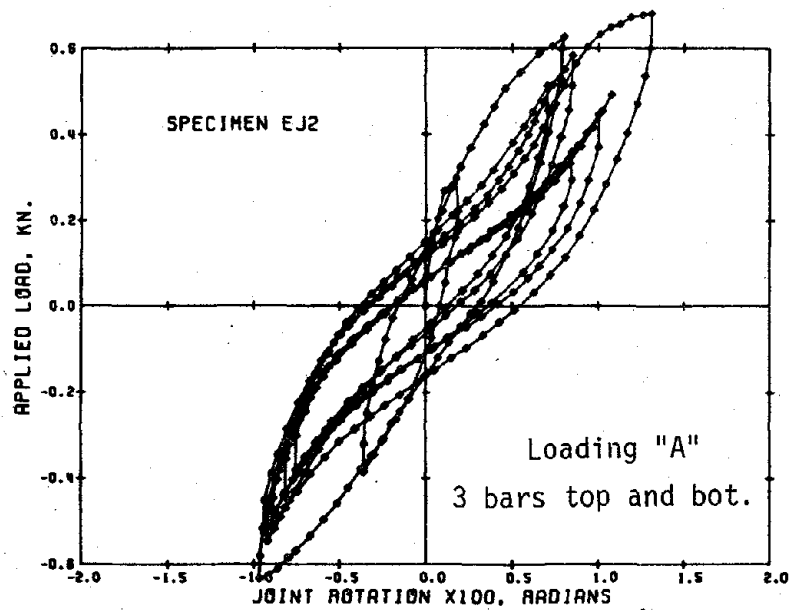


Fig. 4.5(a) Measured Hysteresis Relationships (Exterior Joints)

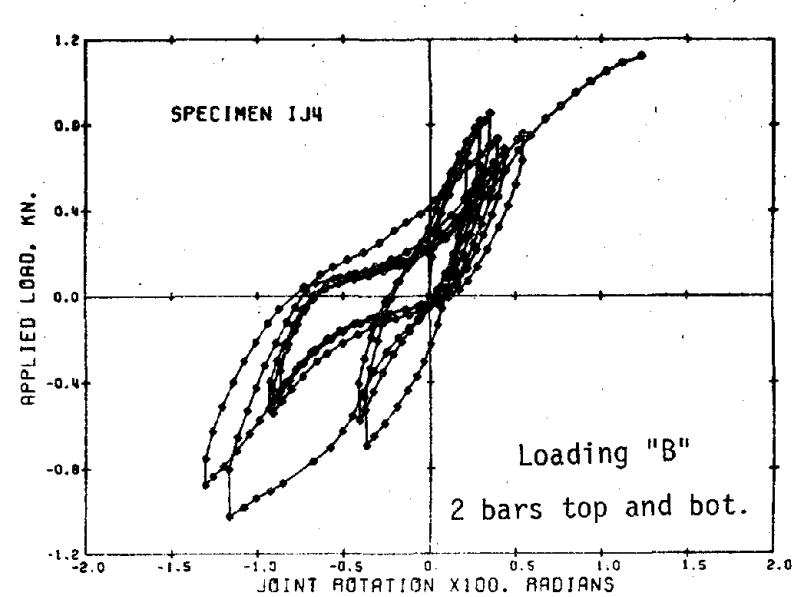
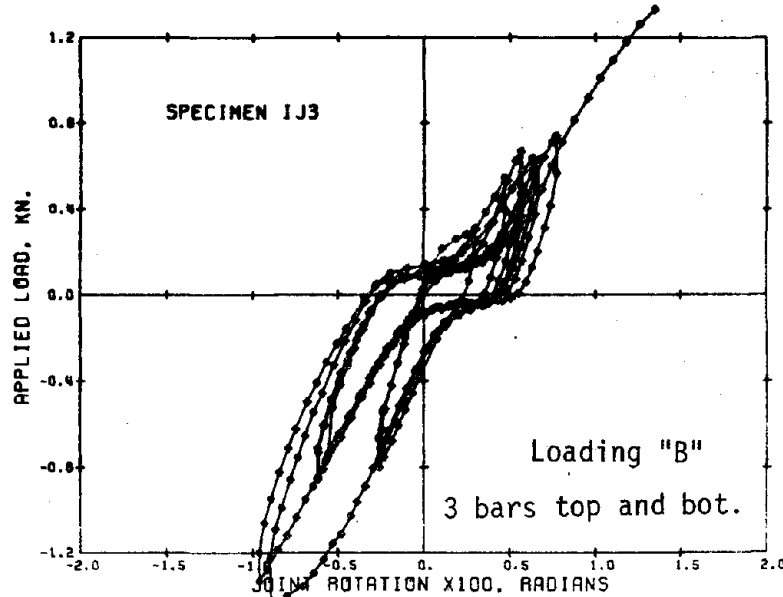
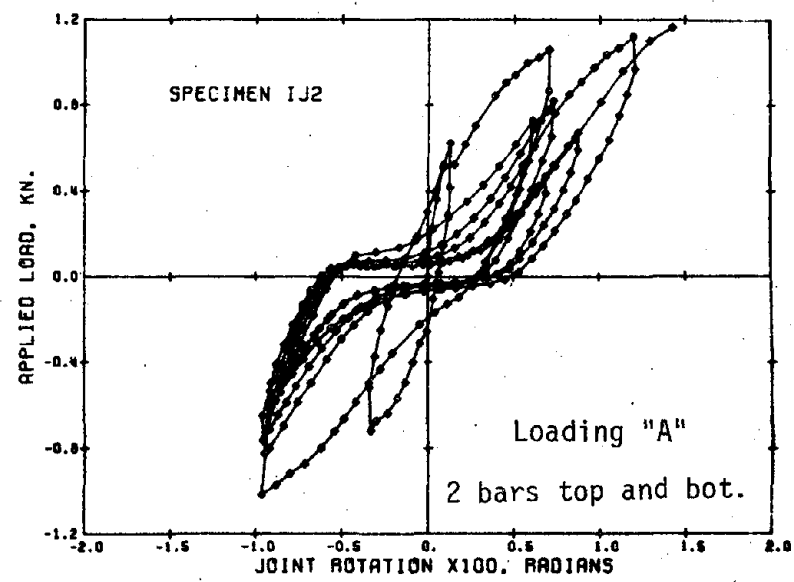
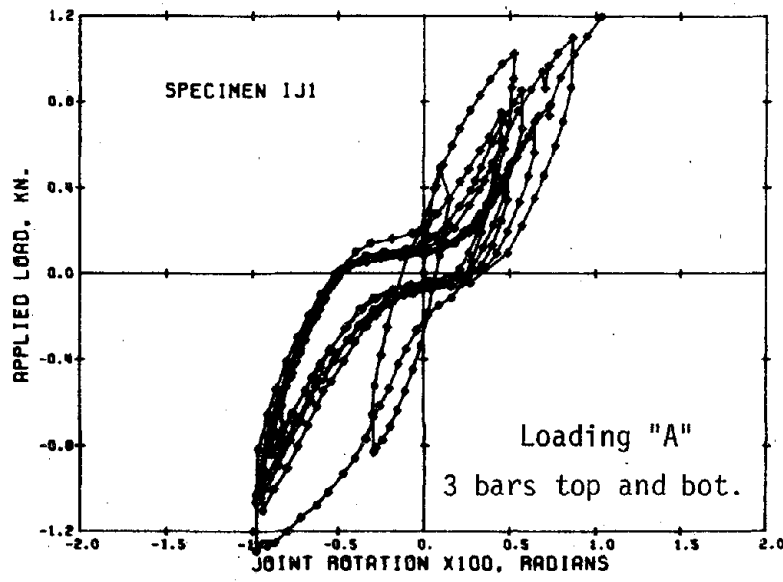


Fig. 4.5(b) Measured Hysteresis Relationships (Interior Joints)

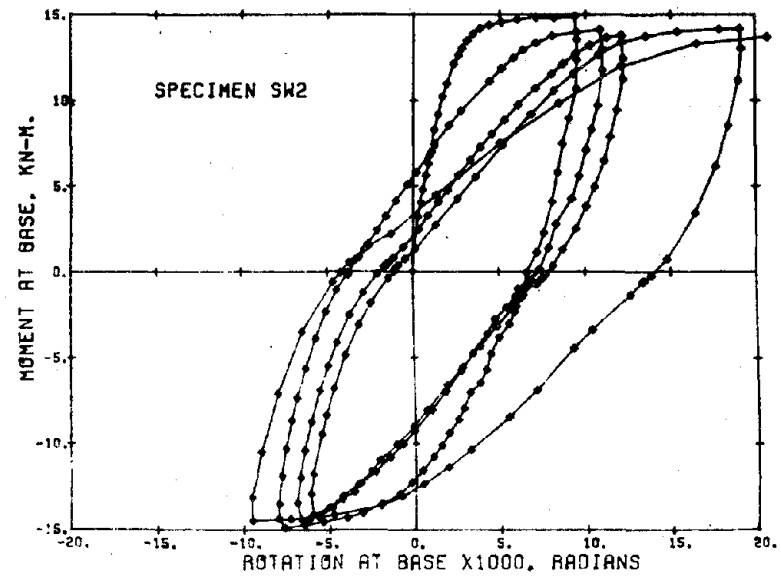
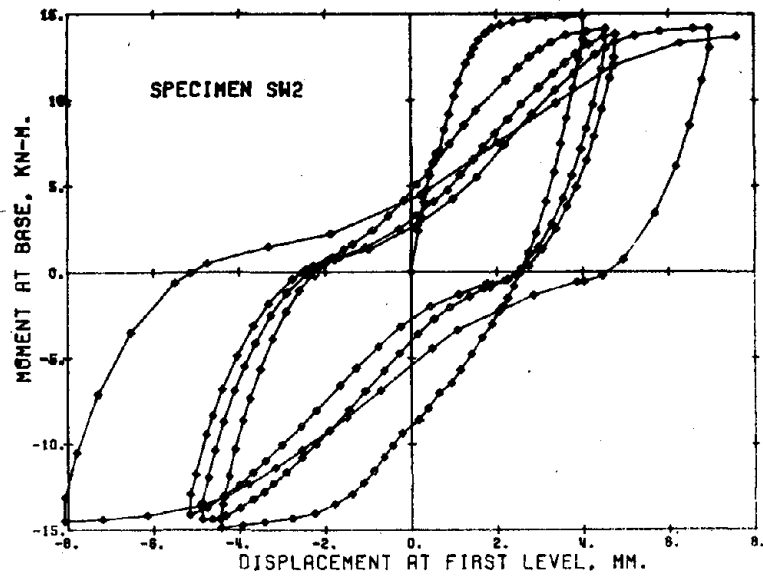
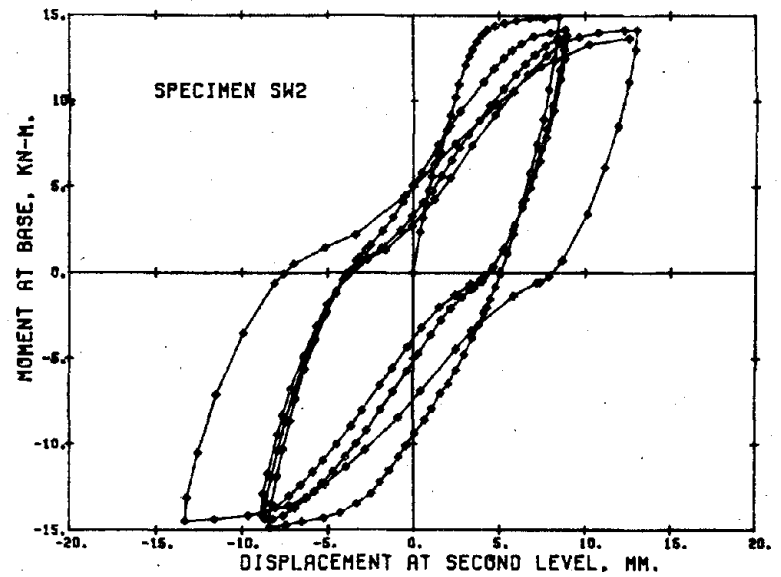
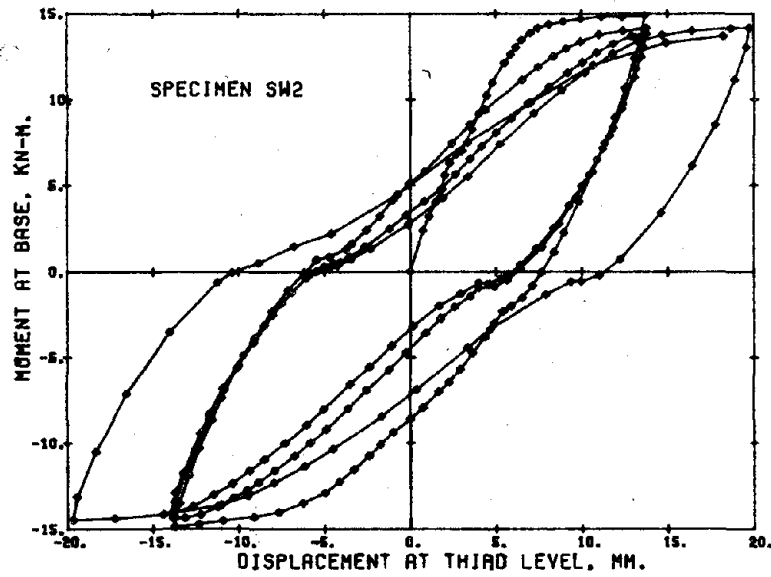


Fig. 4.5(c) Measured Hysteresis Relationships (Heavily Reinforced Wall)

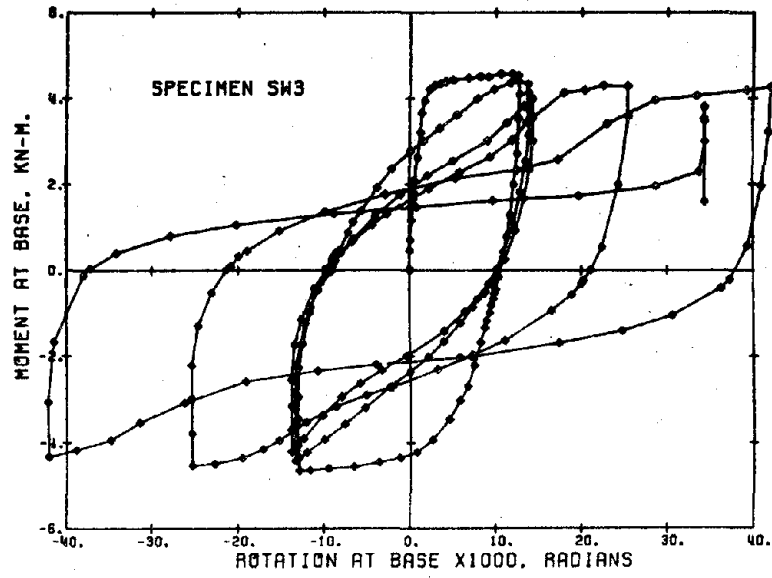
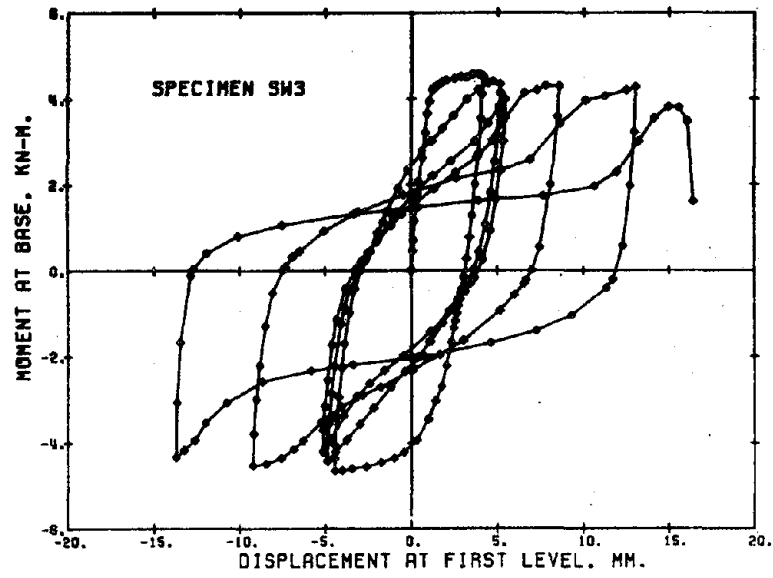
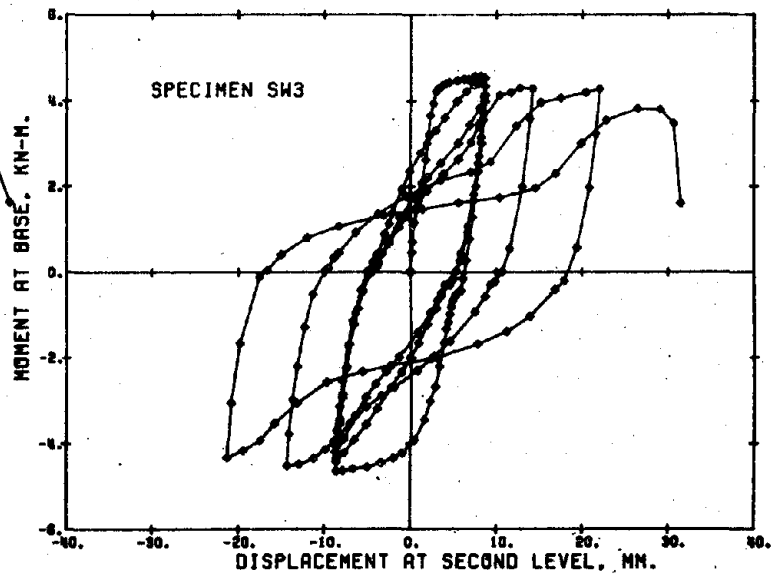
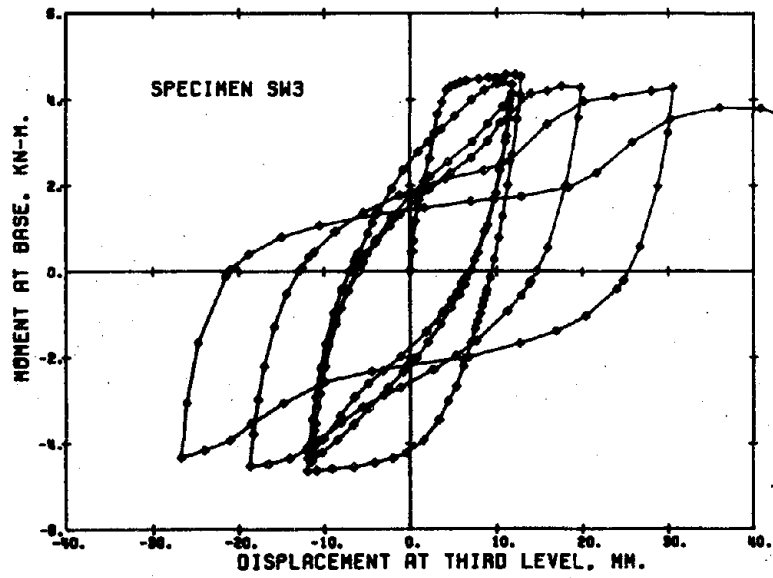
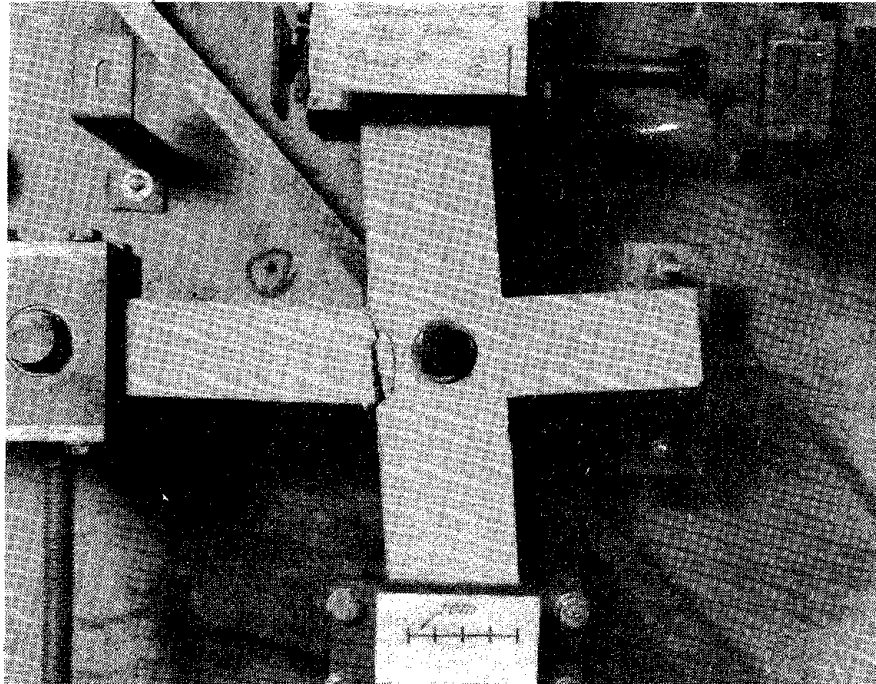
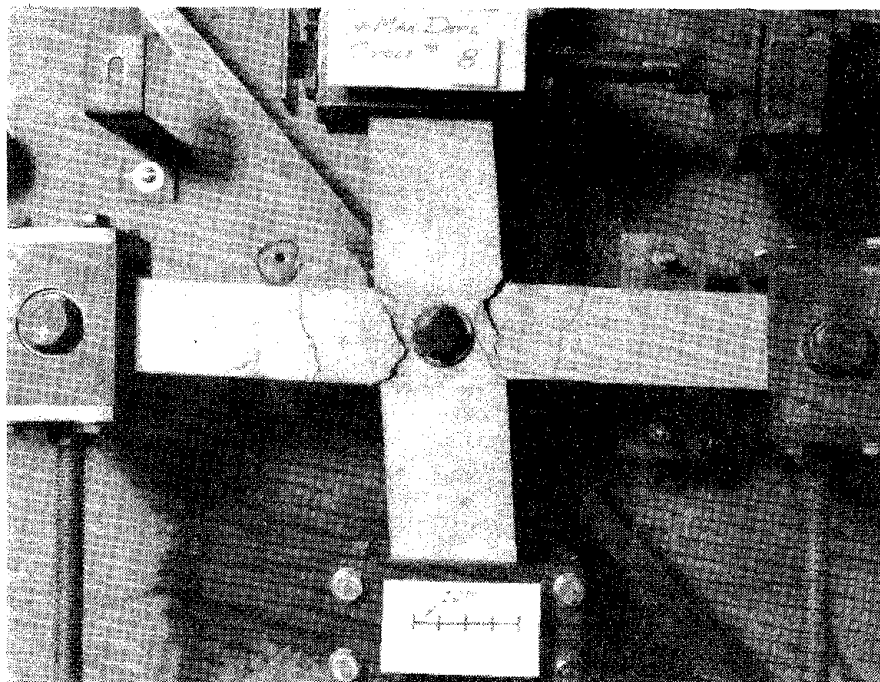


Fig. 4.5(d) Measured Hysteresis Relationships (Lightly Reinforced Wall)

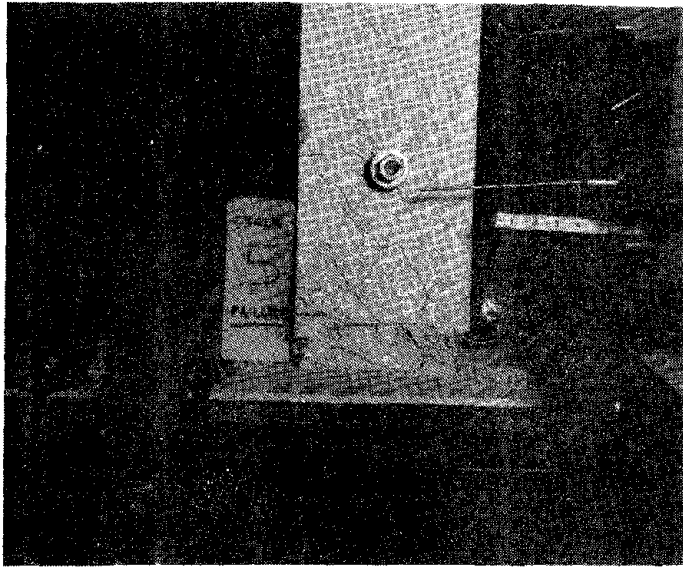


(a) Exterior-Joint Specimen

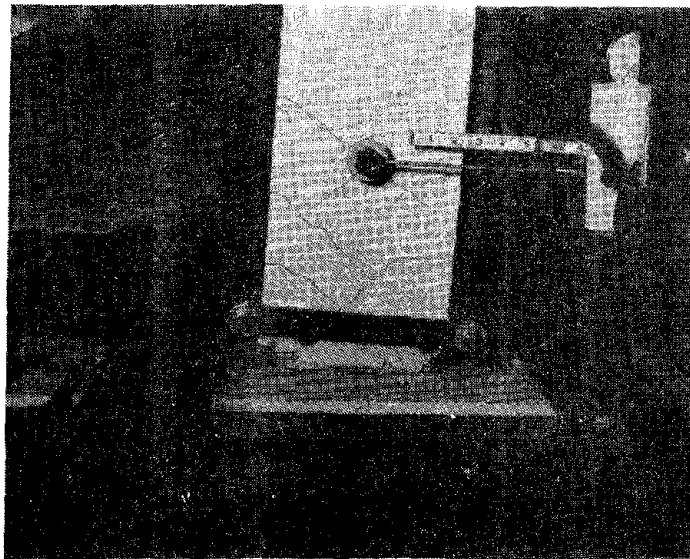


(b) Interior-Joint Specimen

Fig. 4.6 Observed Damage at Maximum Displacement



(c) Heavily Reinforced Wall



(d) Lightly Reinforced Wall

Fig. 4.6 (contd.) Observed Damage at Maximum Displacement

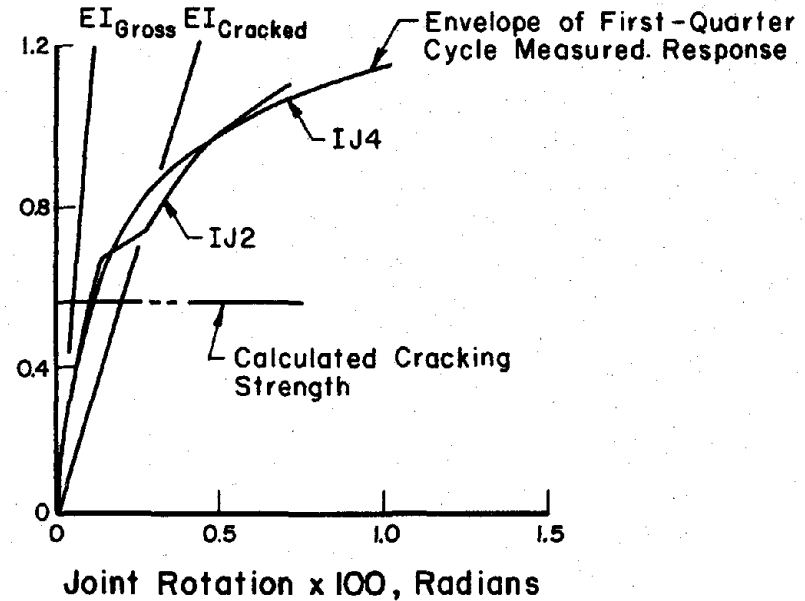
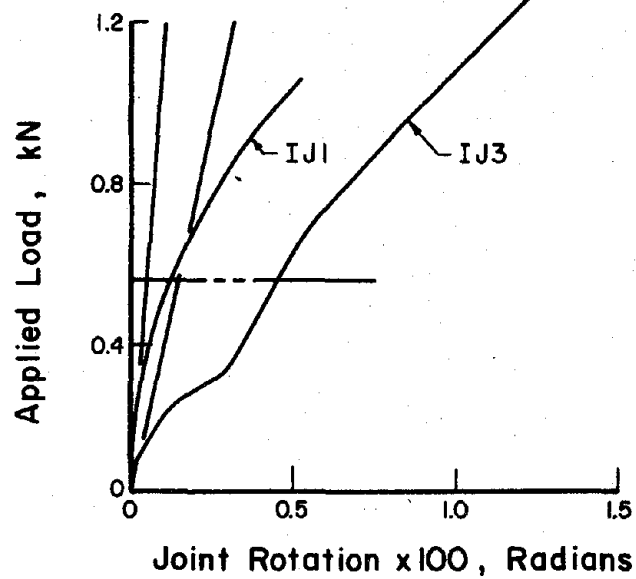
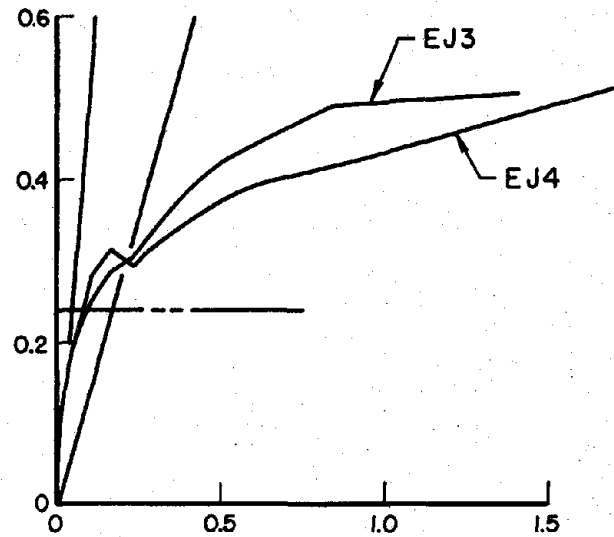
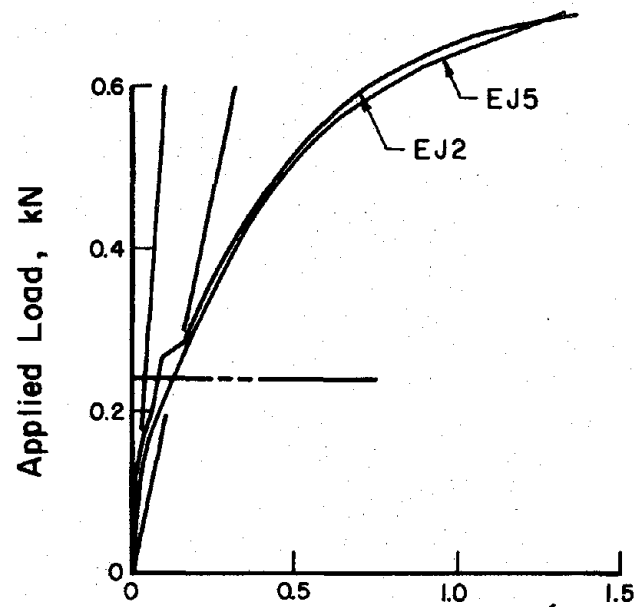


Fig. 4.7 (a) Measured and Calculated Beam Response (Stiffnesses)

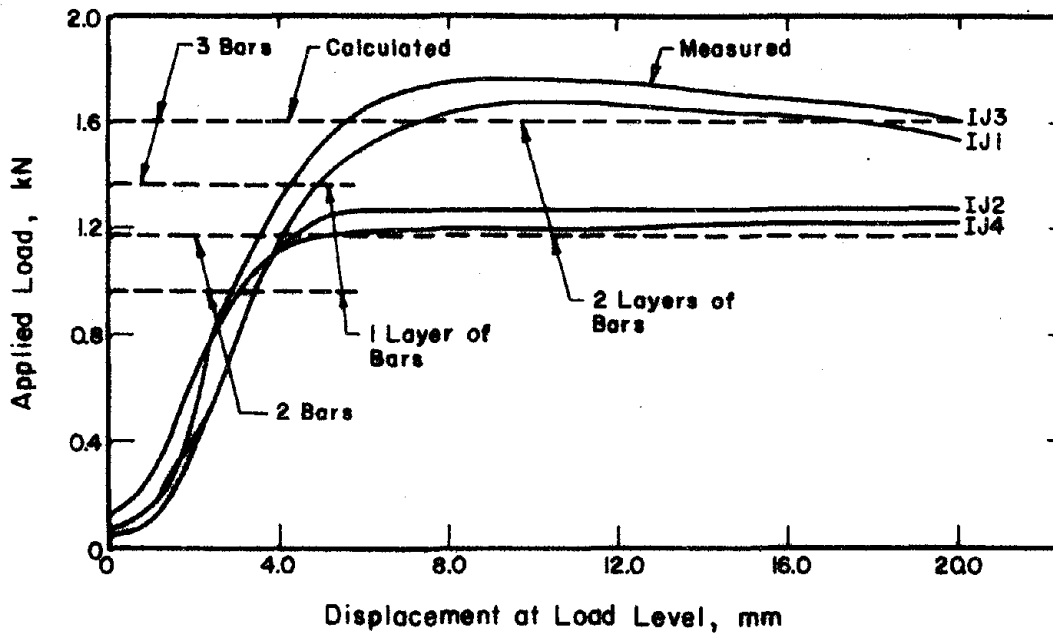
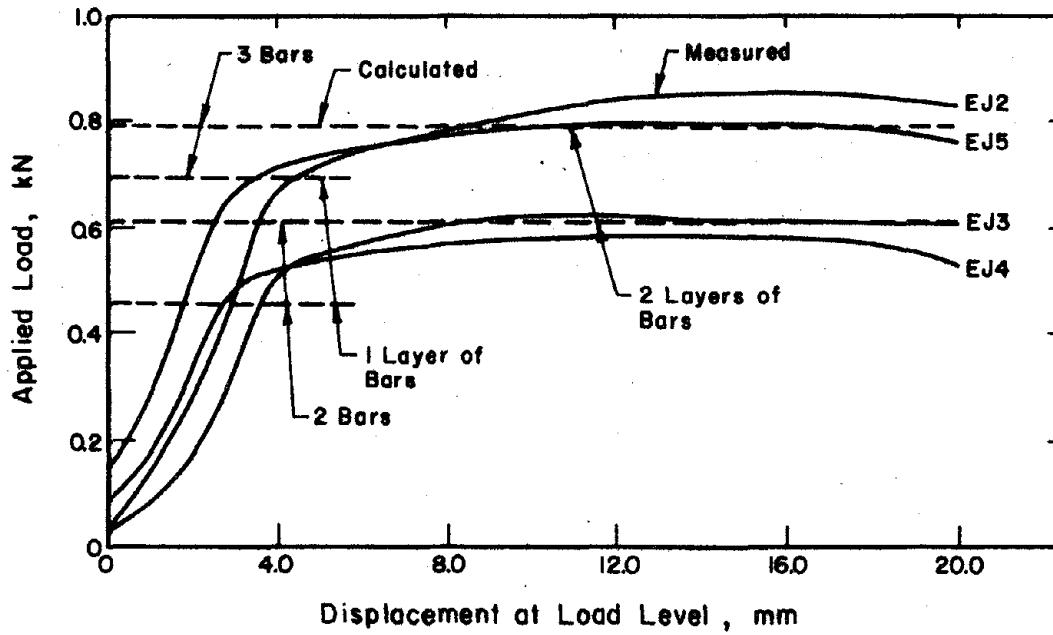


Fig. 4.7(b) Measured and Calculated Beam Response (Strengths)

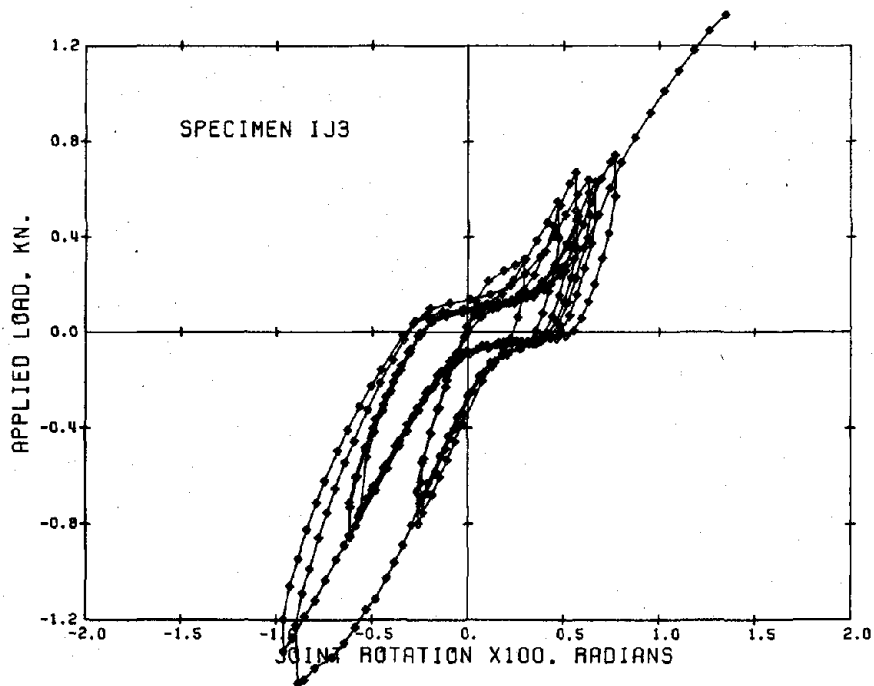
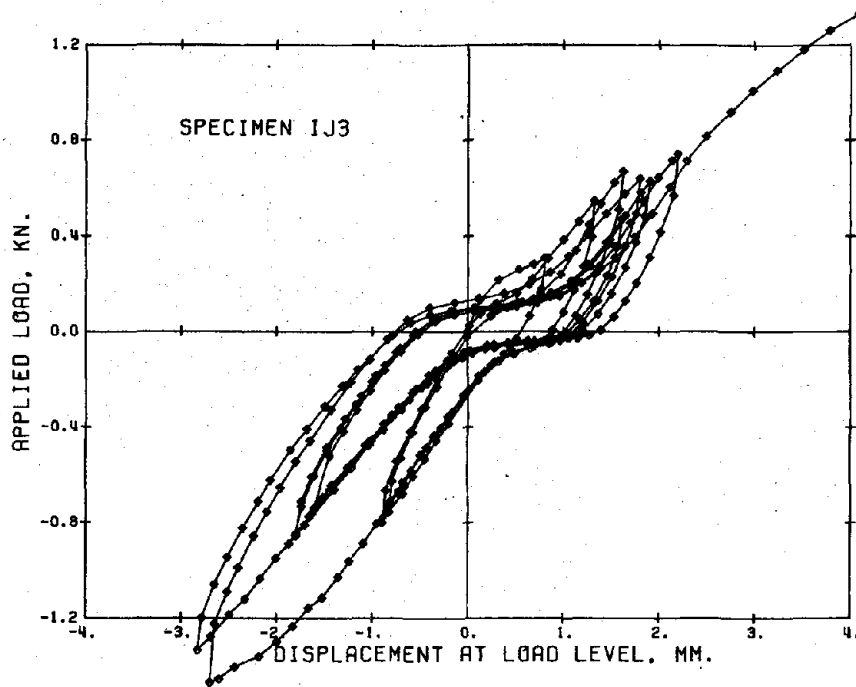


Fig. 4.8 Comparison of Displacement and Rotation Measurements
for Frame Specimens

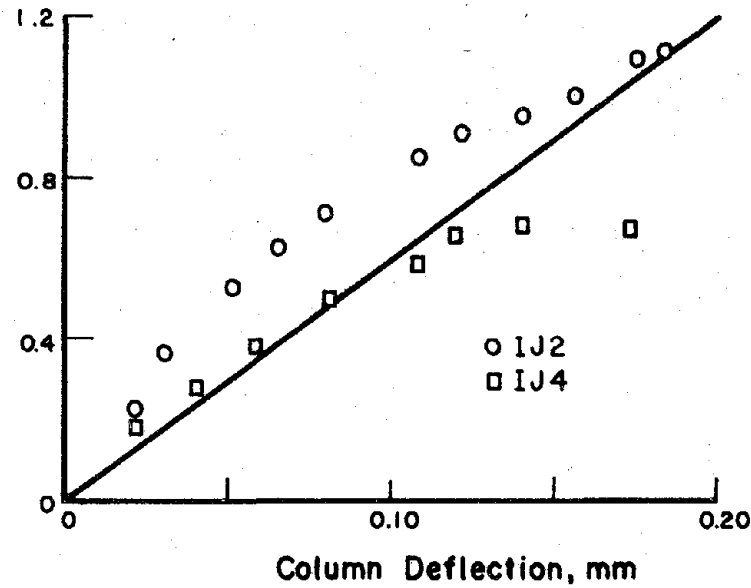
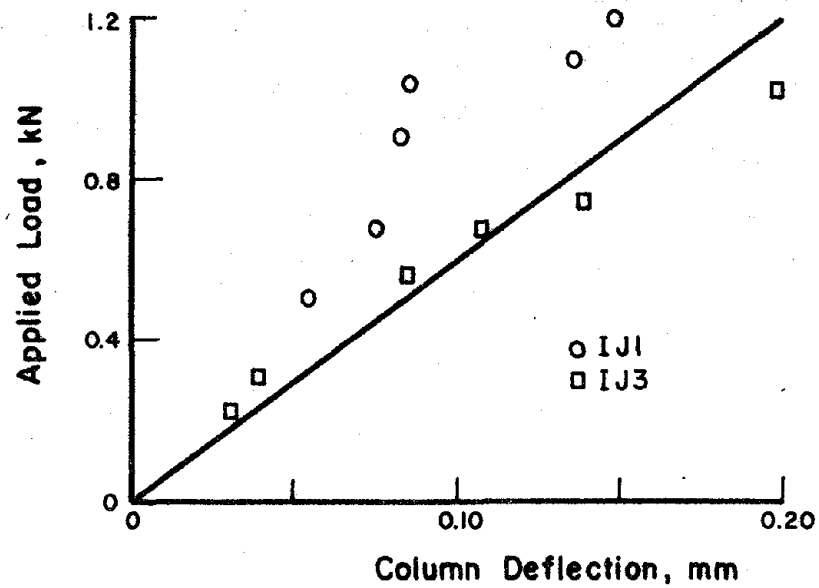
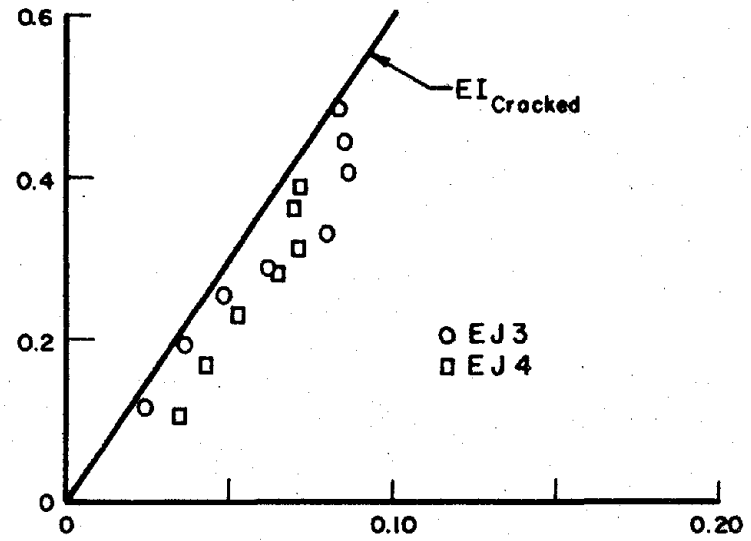
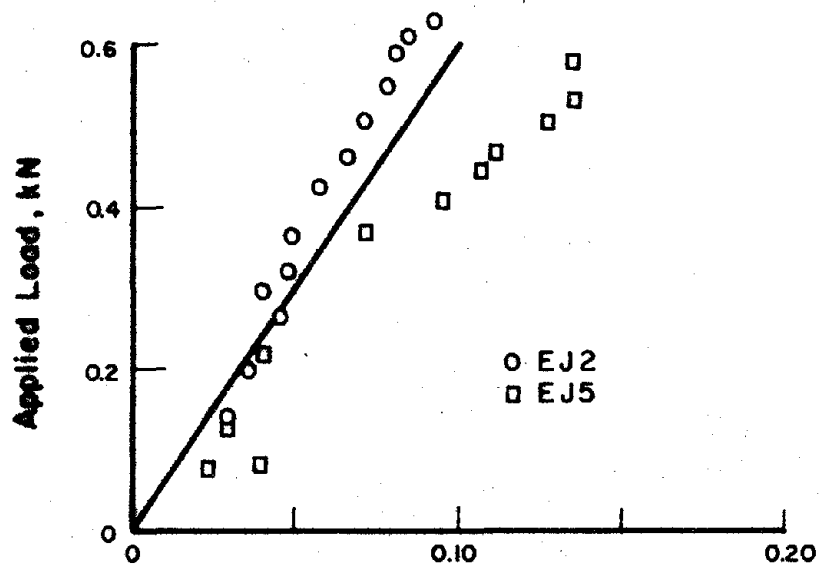
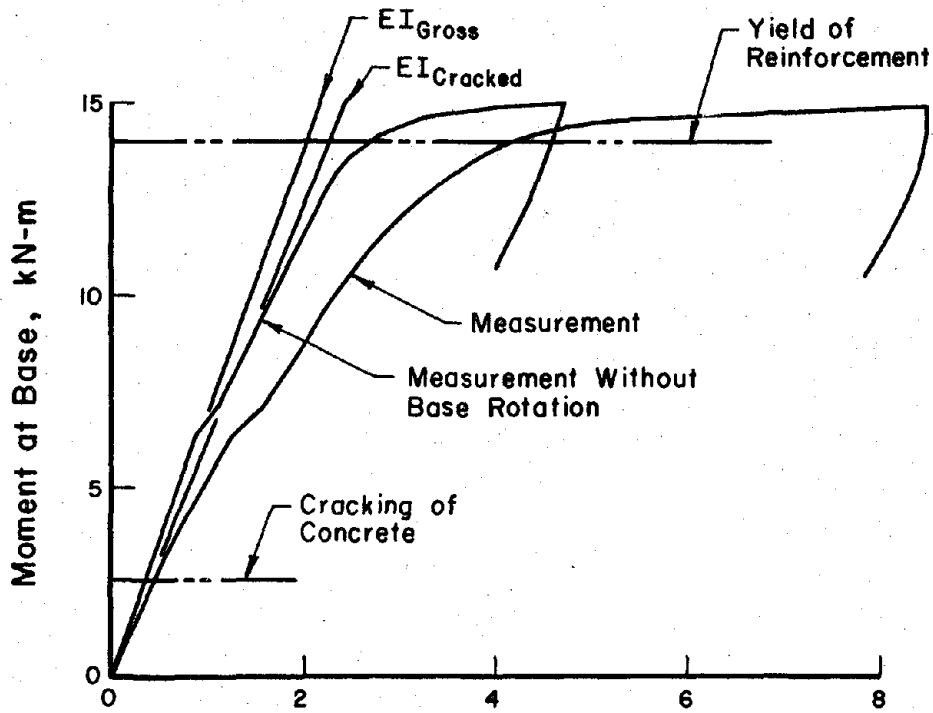
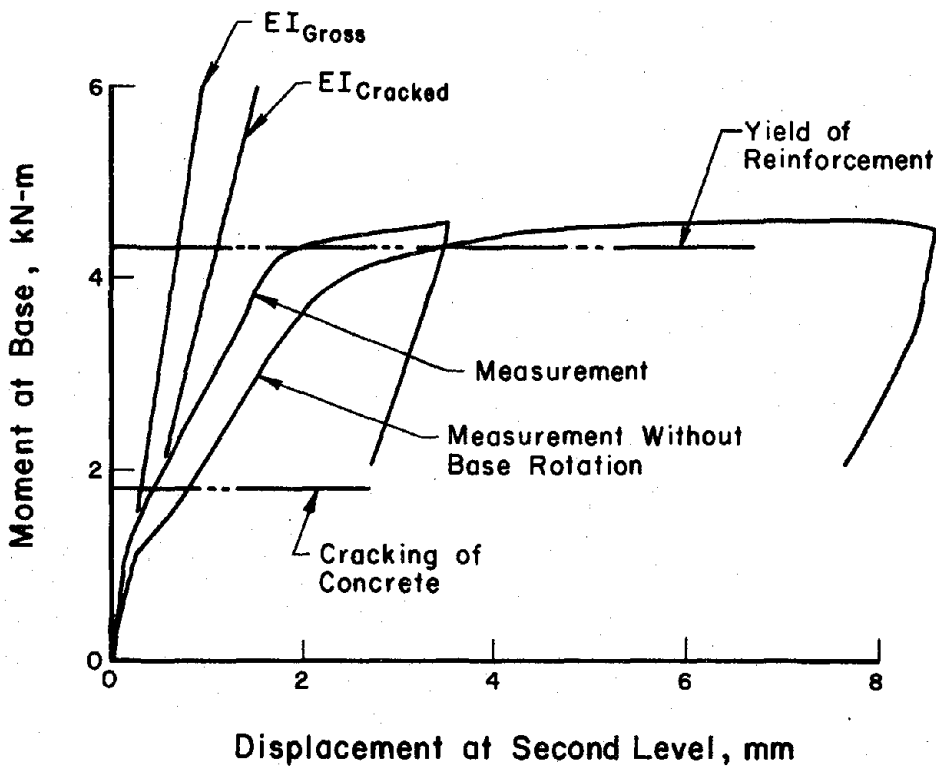


Fig. 4.9 Measured and Calculated Column Stiffnesses



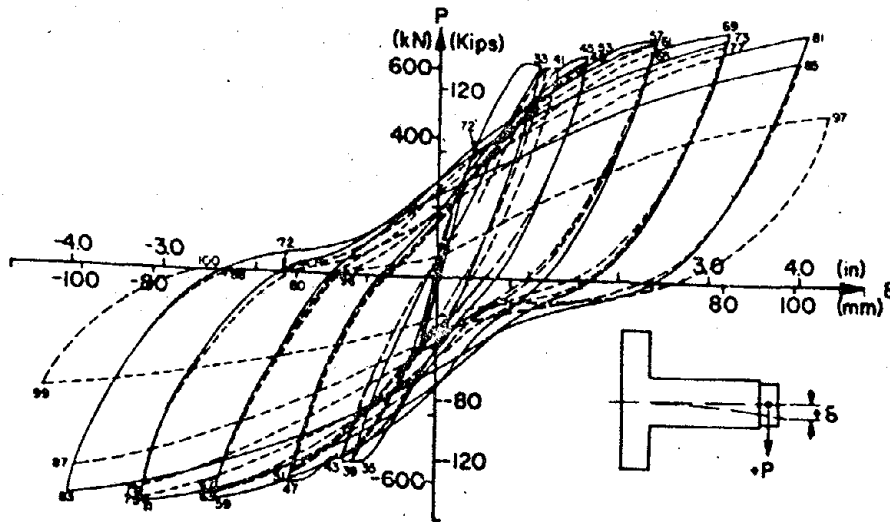
(a) Heavily Reinforced Wall



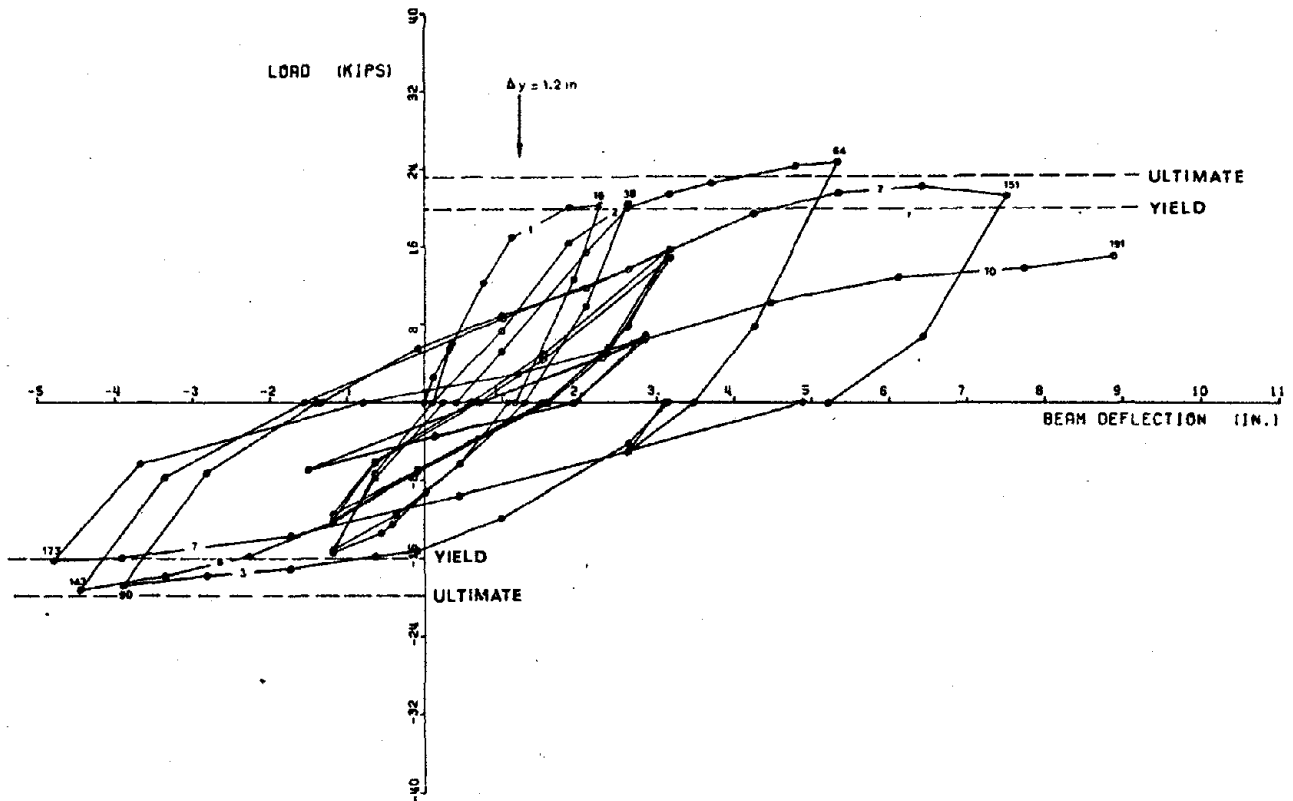
Displacement at Second Level, mm

(b) Lightly Reinforced Wall

Fig. 4.10 Measured and Calculated Wall Response

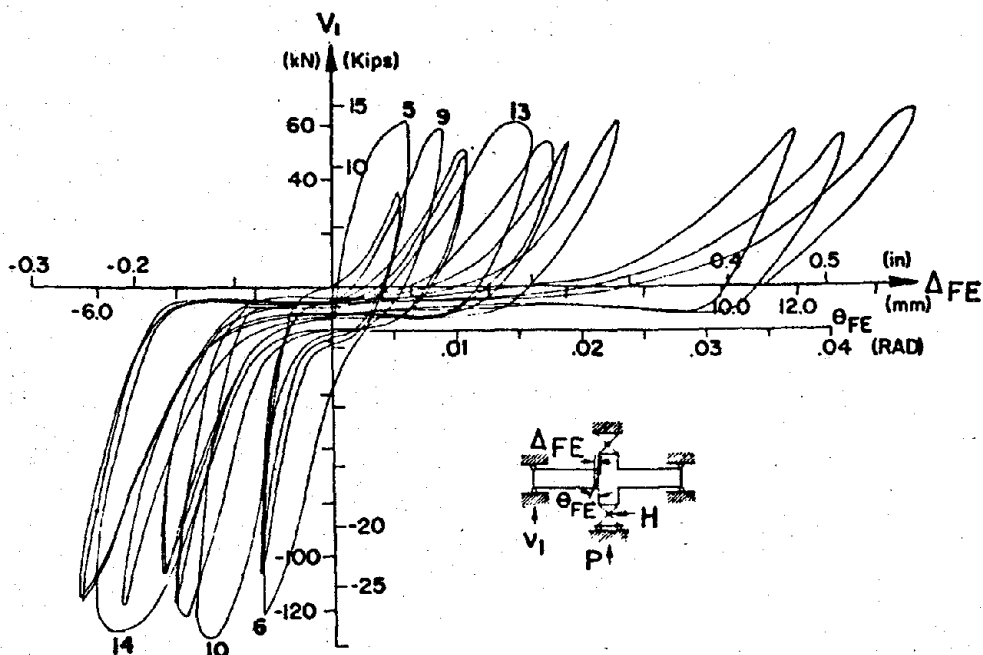


(a) Exterior Beam or Wall (Bertero, Ref. 2)

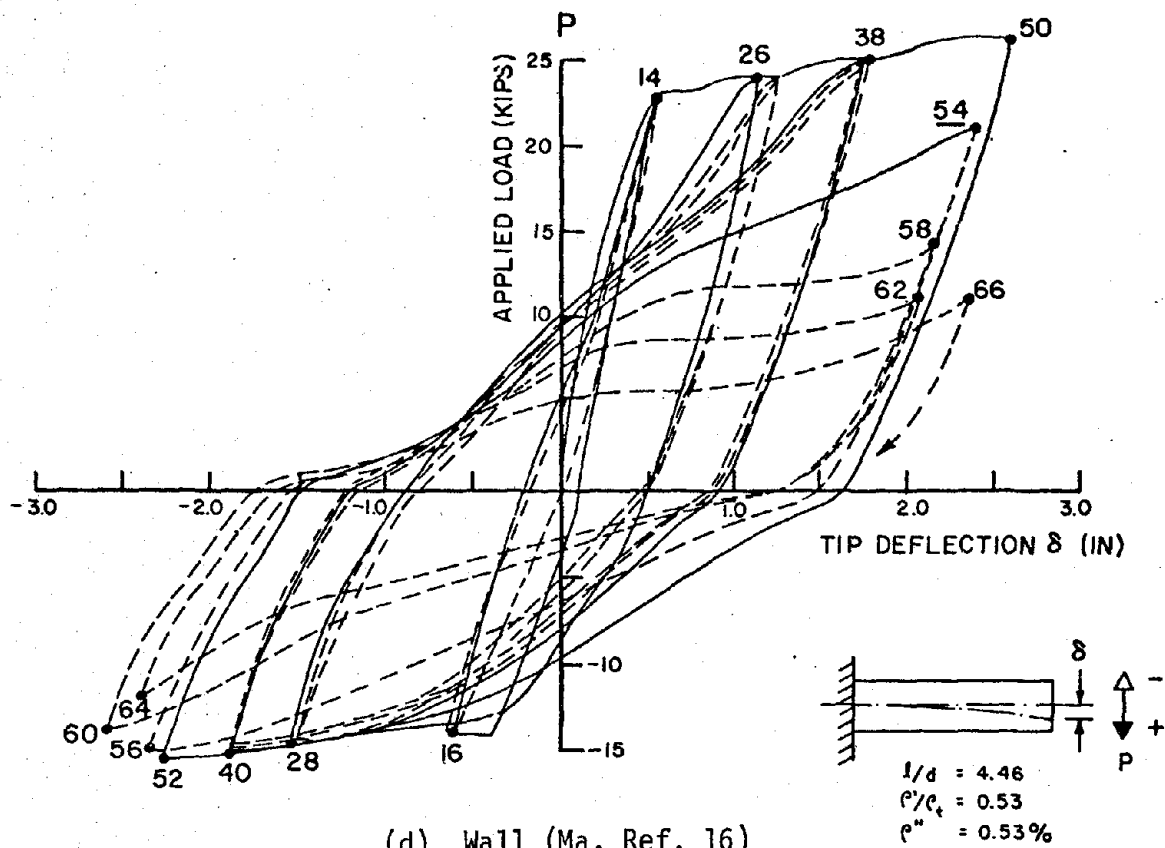


(b) Exterior Beam or Wall (Uzumeri, Ref. 25)

Fig. 4.11 Measured Behavior of Large-Scale Members



(c) Interior Joints (Bertero, Ref. 2)



(d) Wall (Ma, Ref. 16)

Fig. 4.11 (contd.) Measured Behavior of Large-Scale Members

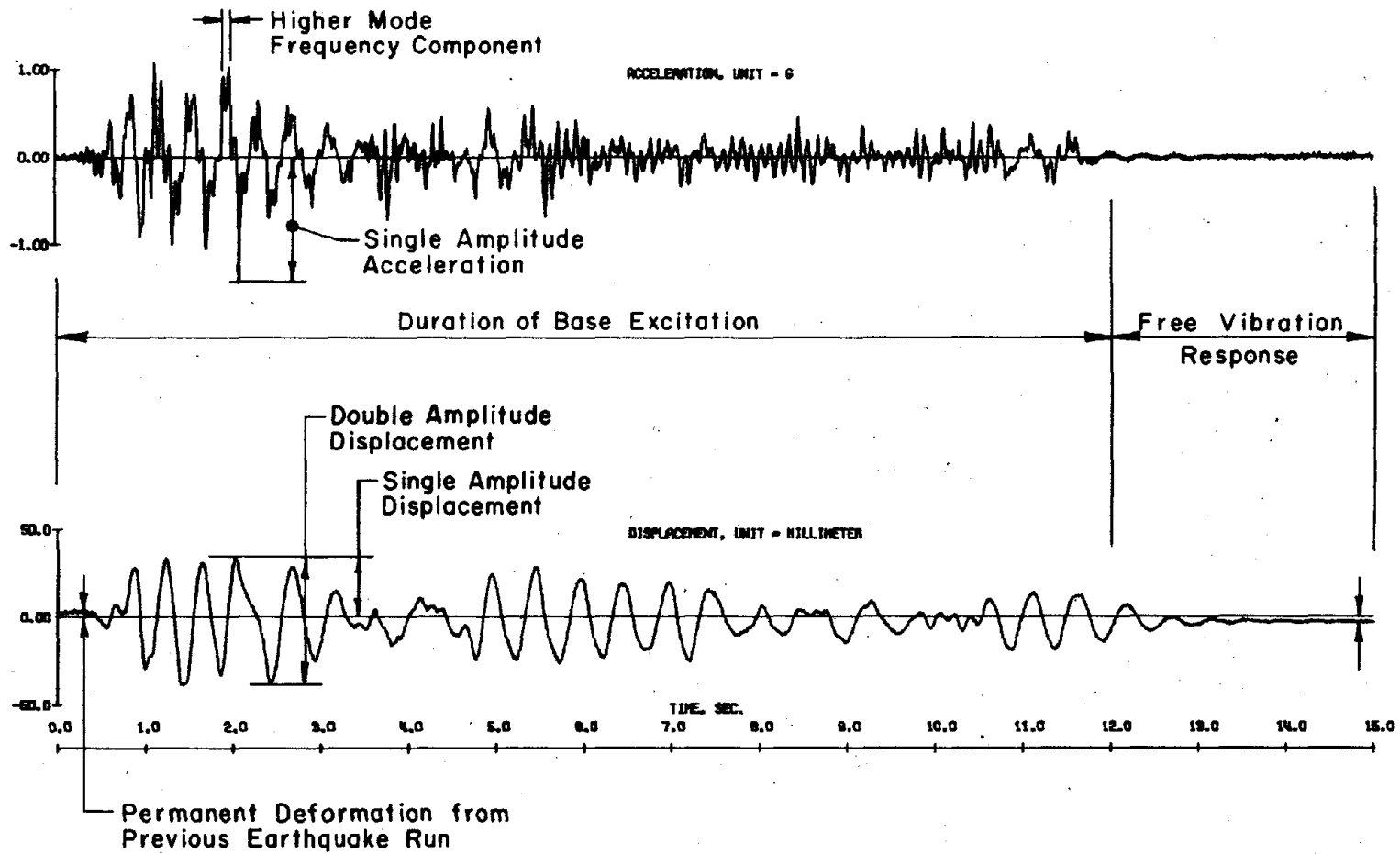
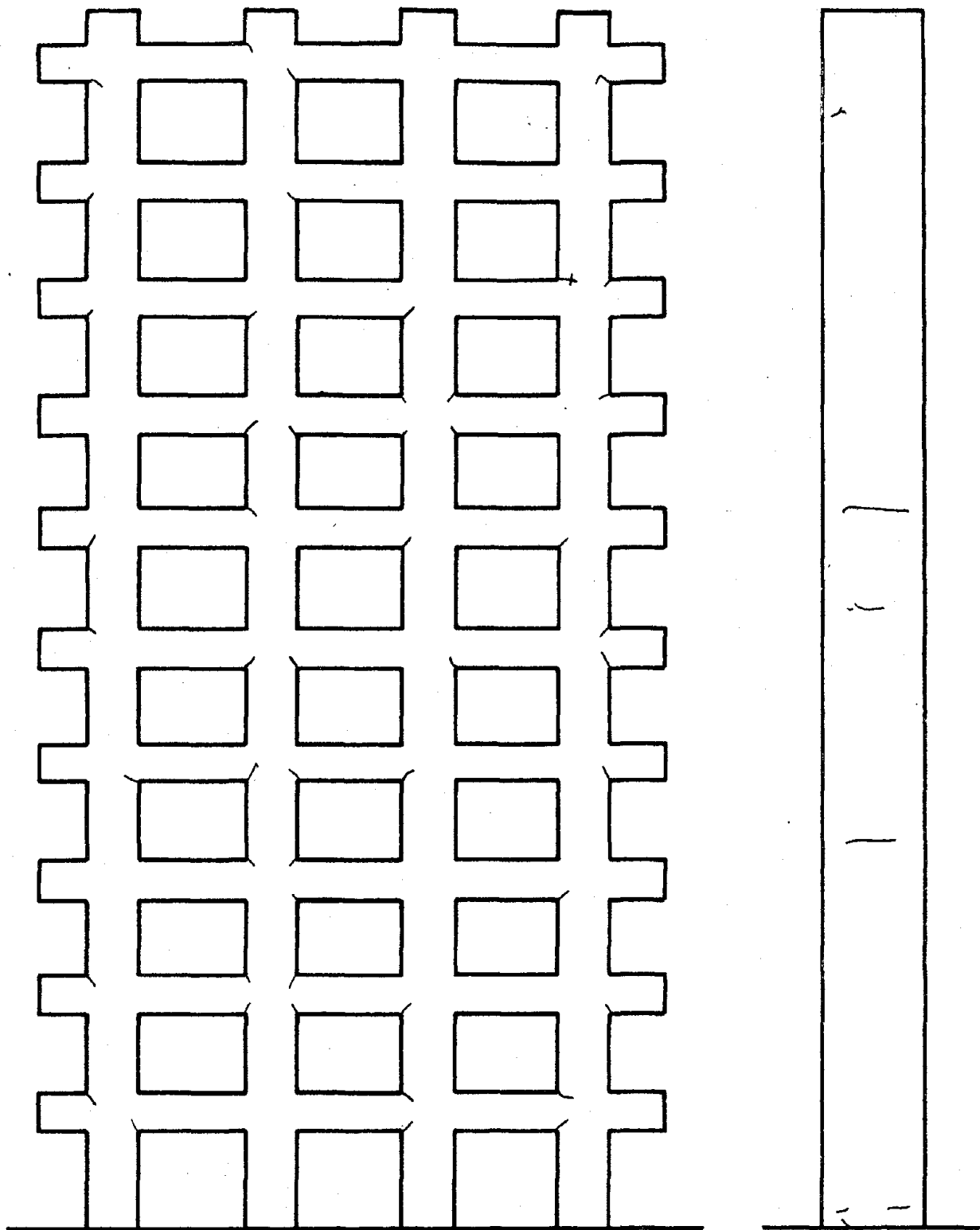


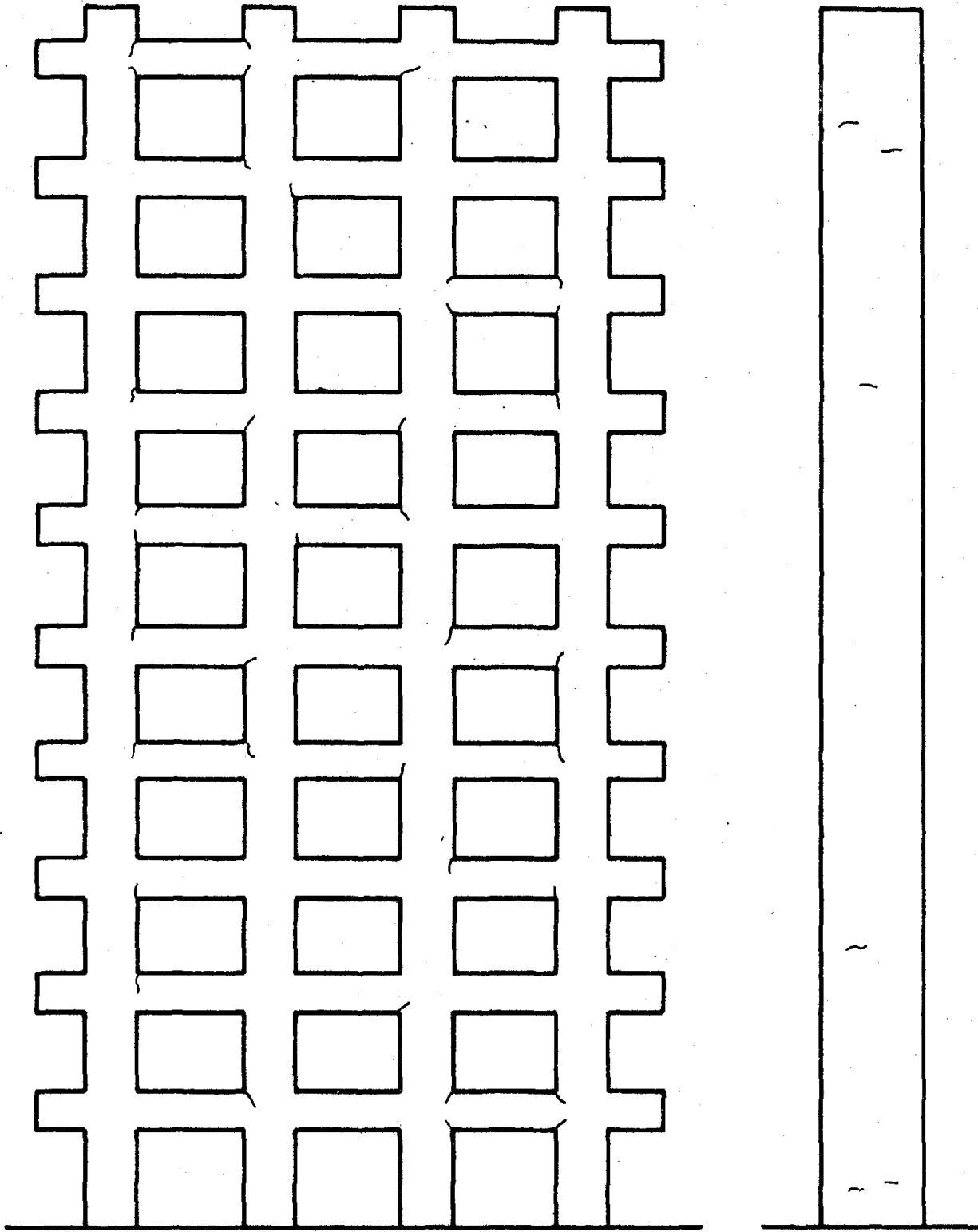
Fig. 5.1 Description of Recorded Waveforms



(Not To Scale)

(a) Structure with Heavily Reinforced Wall

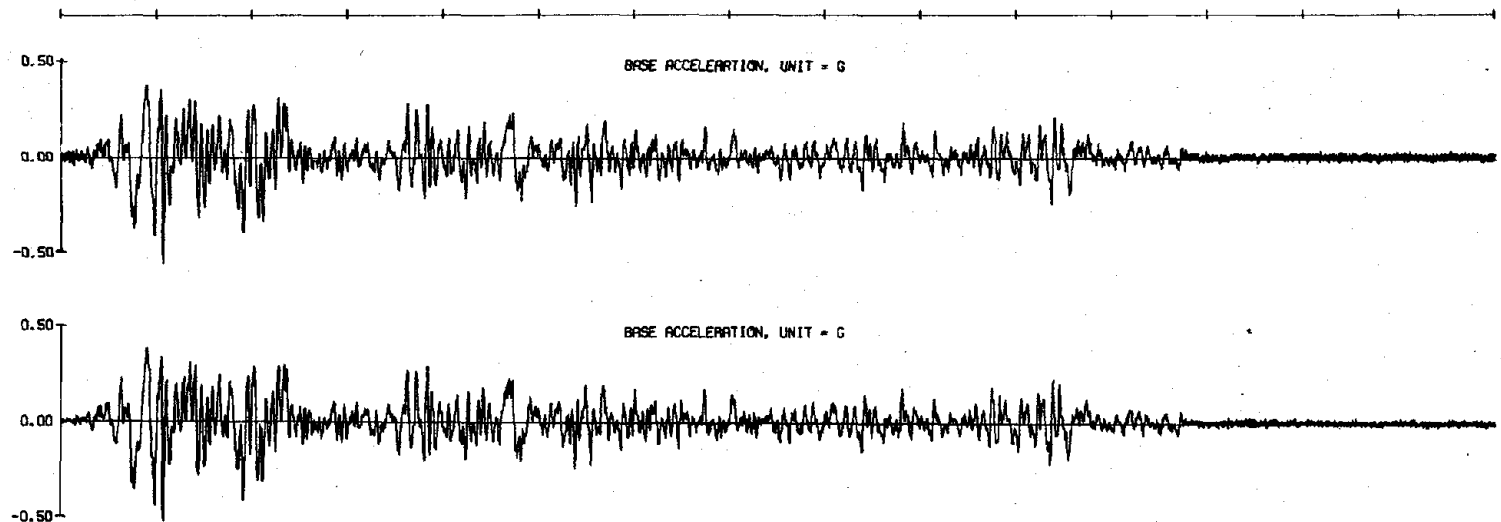
Fig. 5.2 Observed Crack Patterns before Initial El Centro Simulations



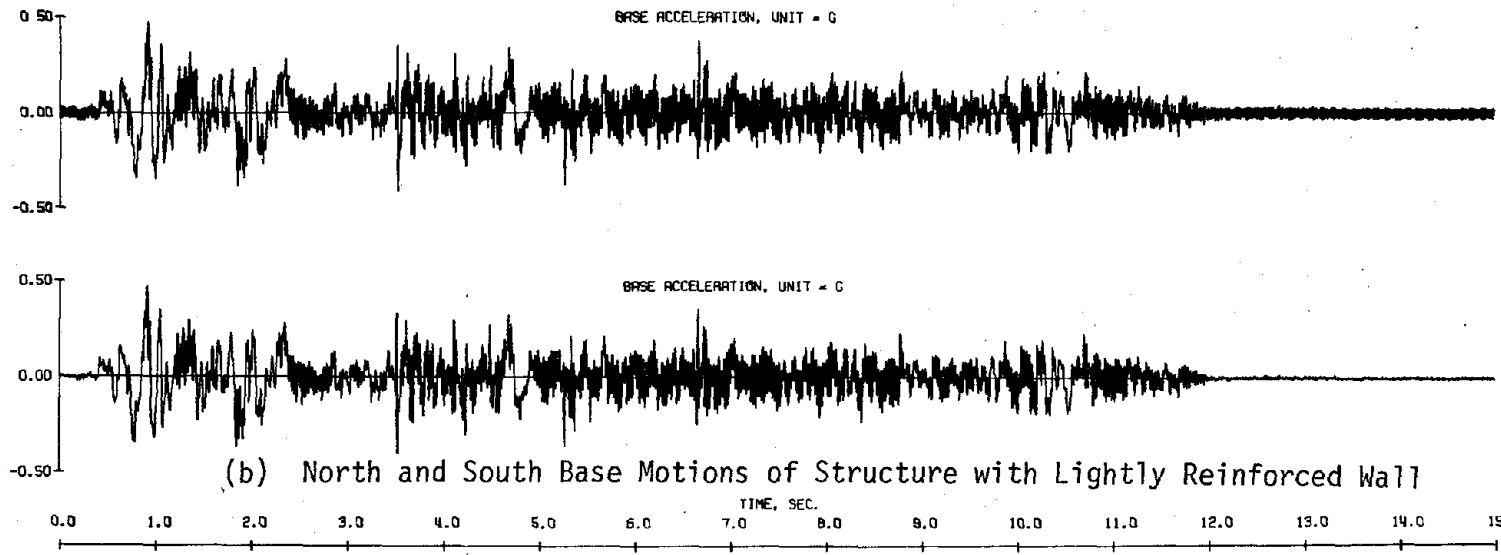
(Not To Scale)

(b) Structure with Lightly Reinforced Wall

Fig. 5.2 (contd.) Observed Crack Patterns before Initial El Centro Simulations



(a) North and South Base Motions of Structure with Heavily Reinforced Wall.



(b) North and South Base Motions of Structure with Lightly Reinforced Wall

0.0 1.0 2.0 3.0 4.0 5.0 6.0 7.0 8.0 9.0 10.0 11.0 12.0 13.0 14.0 15.0
TIME, SEC.

Fig. 5.3 Measured Motions of Initial El Centro Simulations

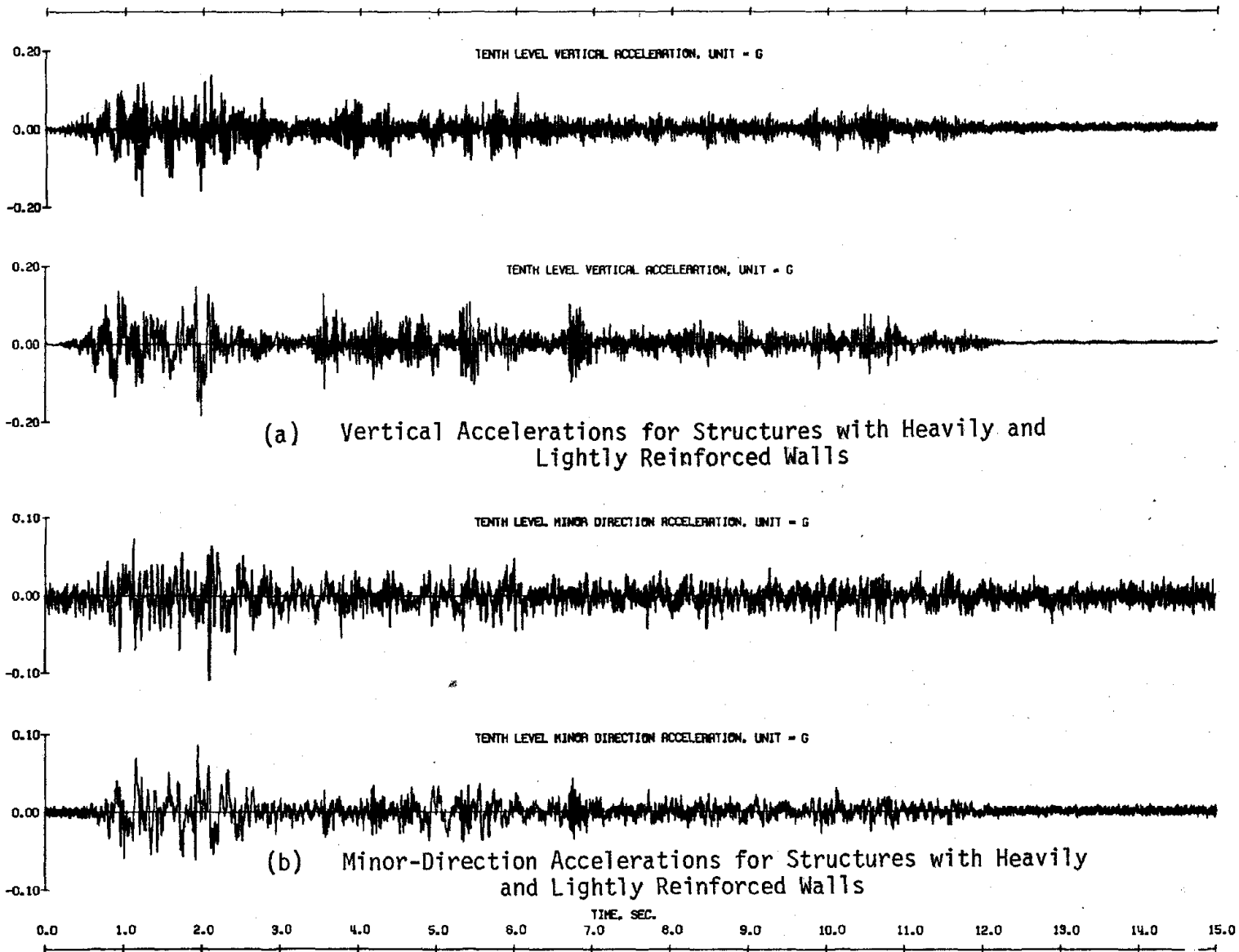
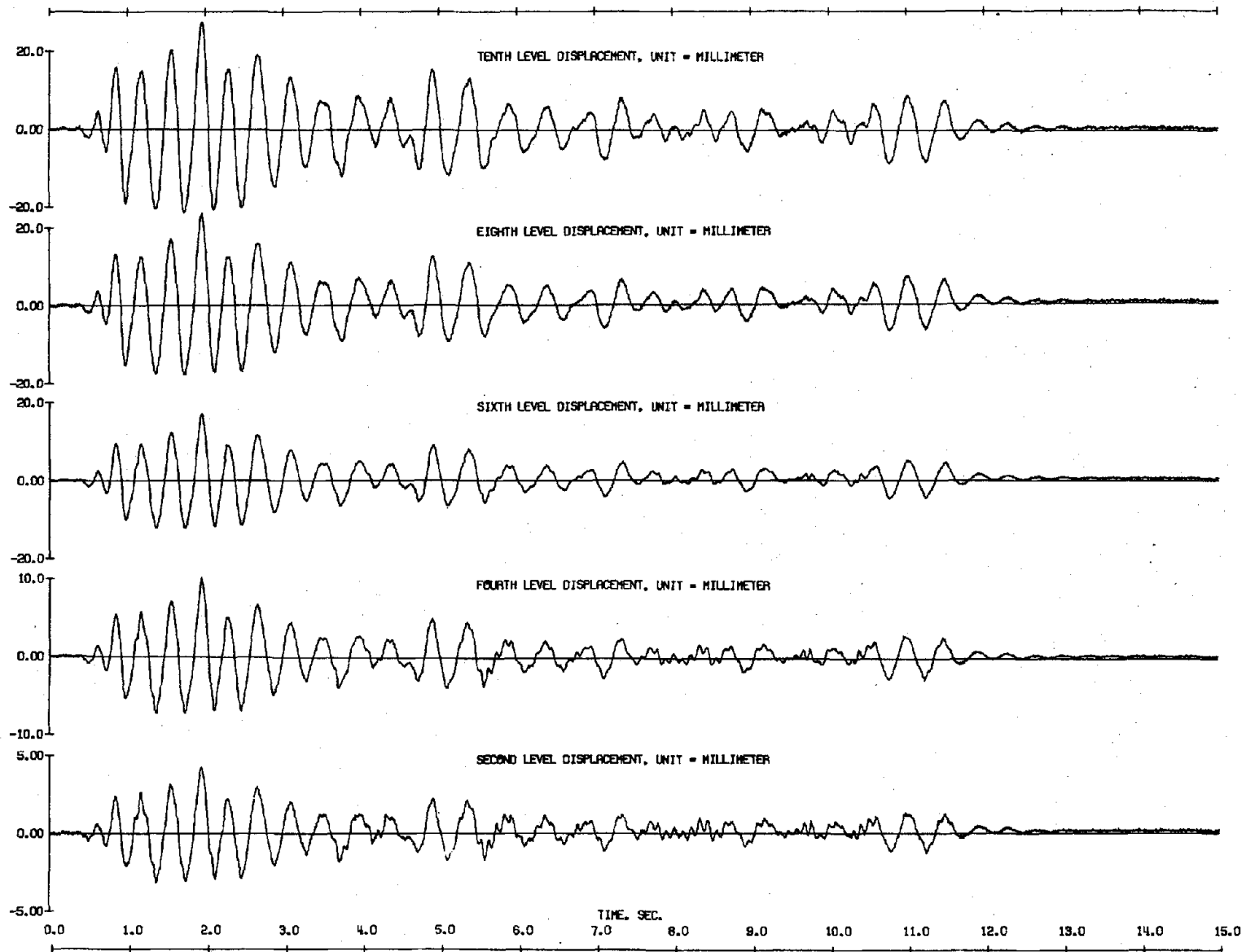
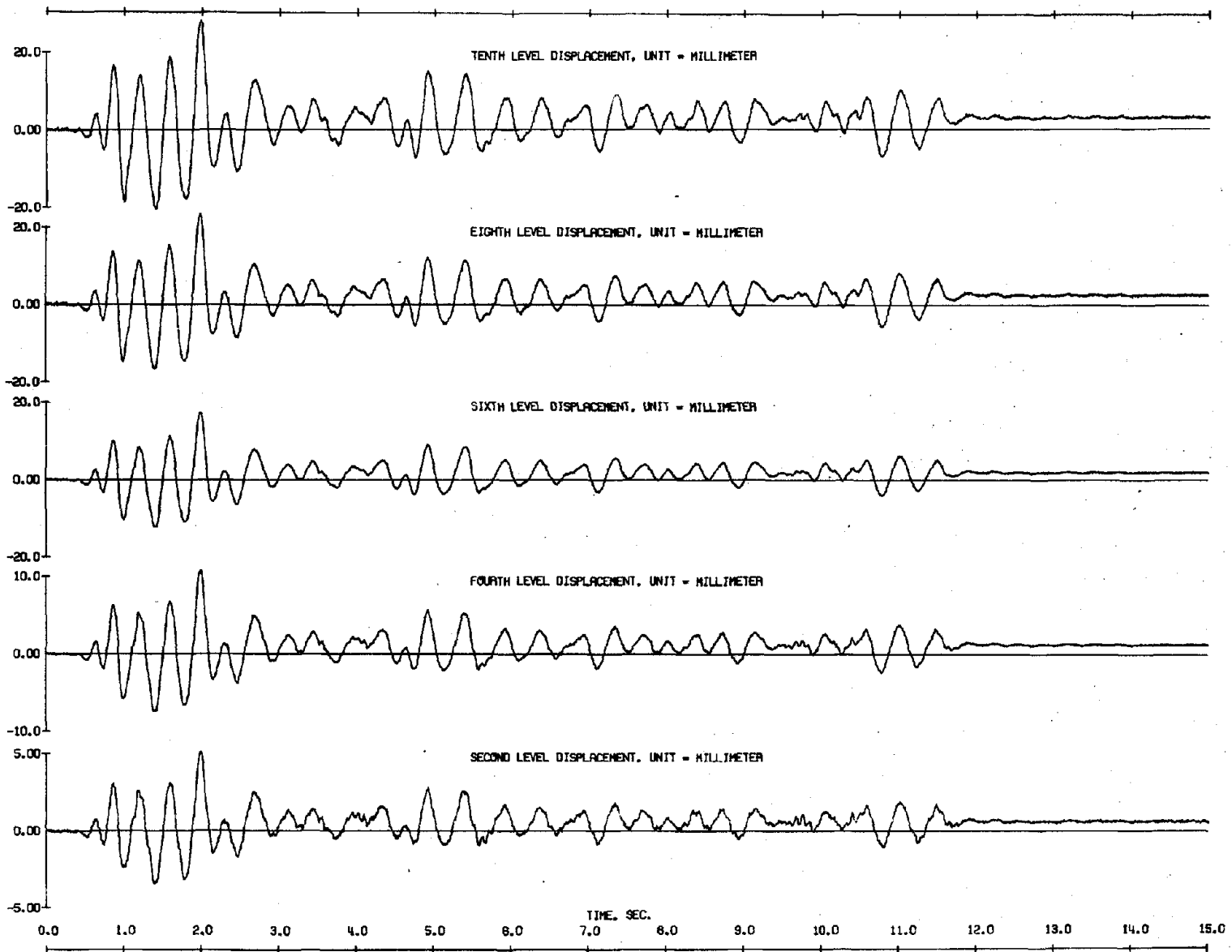


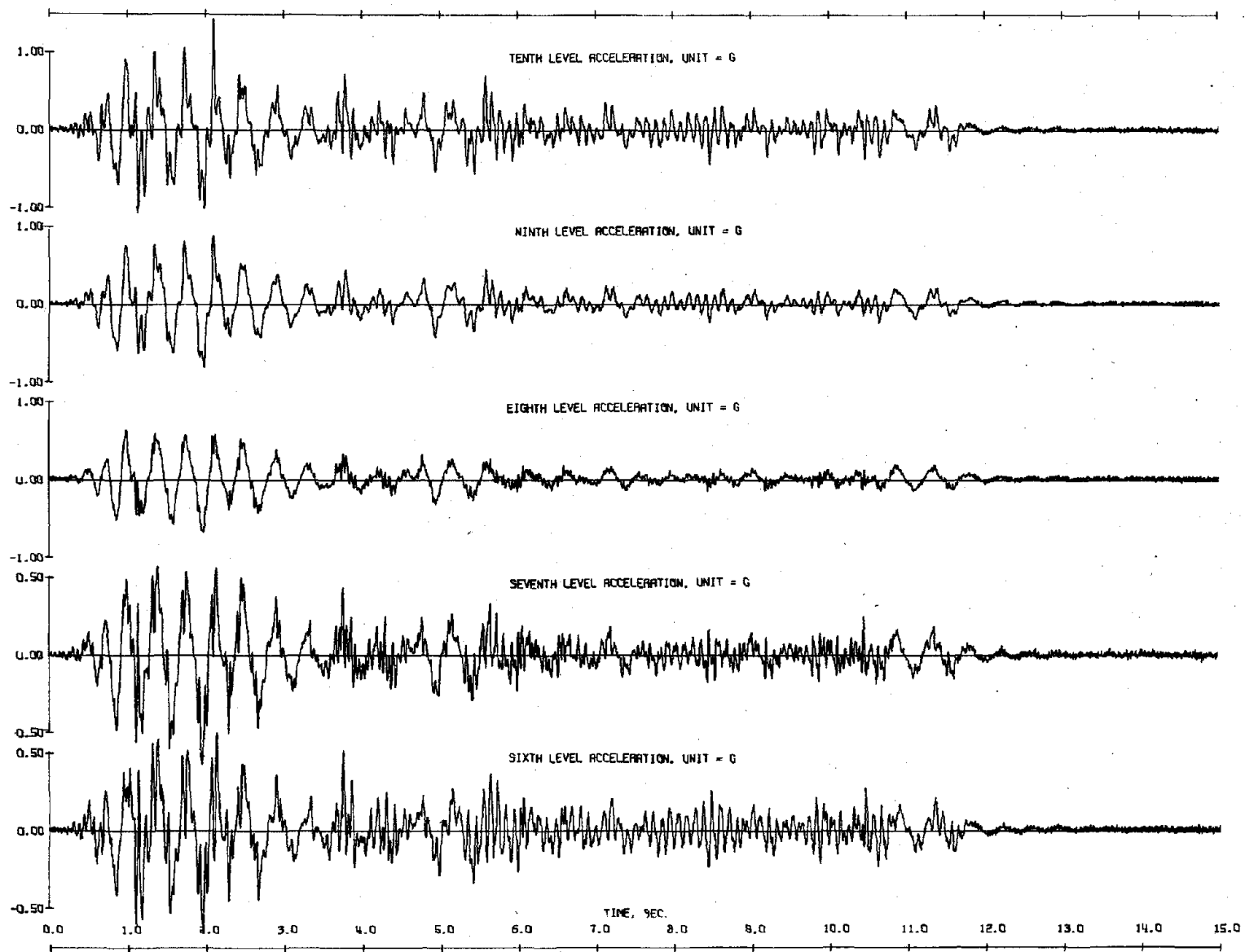
Fig. 5.4 Measured Response to Initial El Centro Simulations



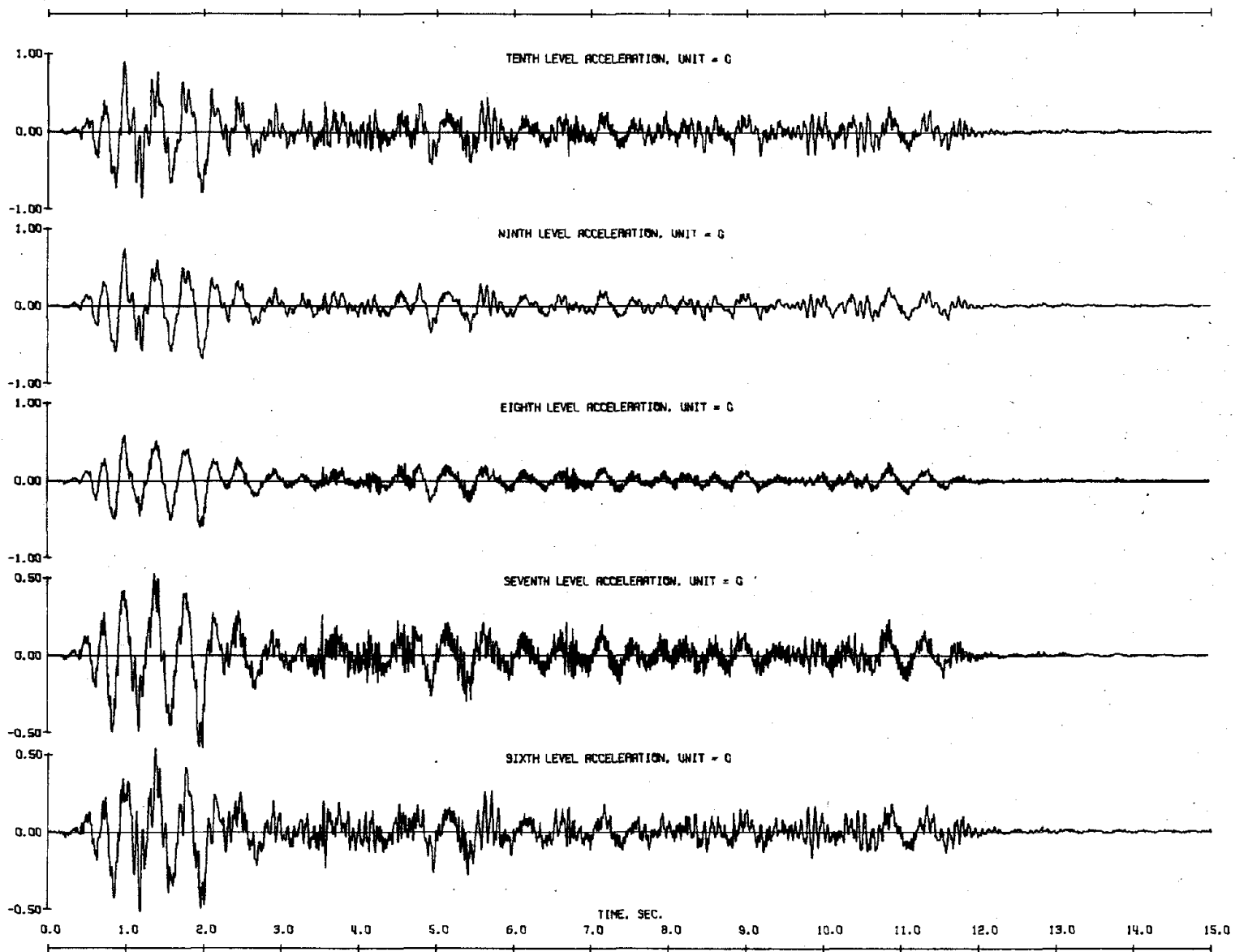
(c) Displacements of Structure with Heavily Reinforced Wall
 Fig. 5.4 (contd.) Measured Response to Initial El Centro Simulations



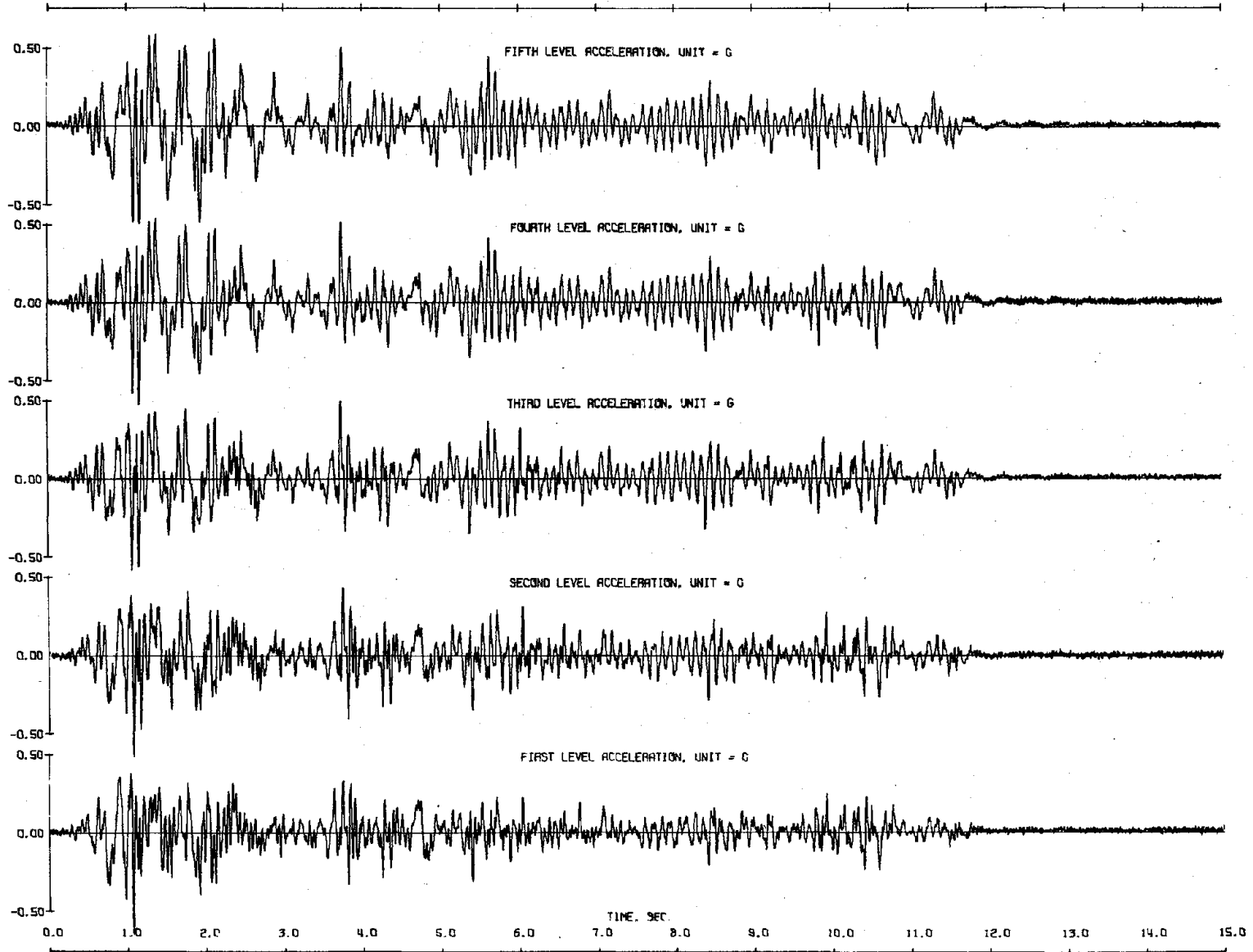
(d) Displacements of Structure with Lightly Reinforced Wall
 Fig. 5.4 (contd.) Measured Response to Initial El Centro Simulations



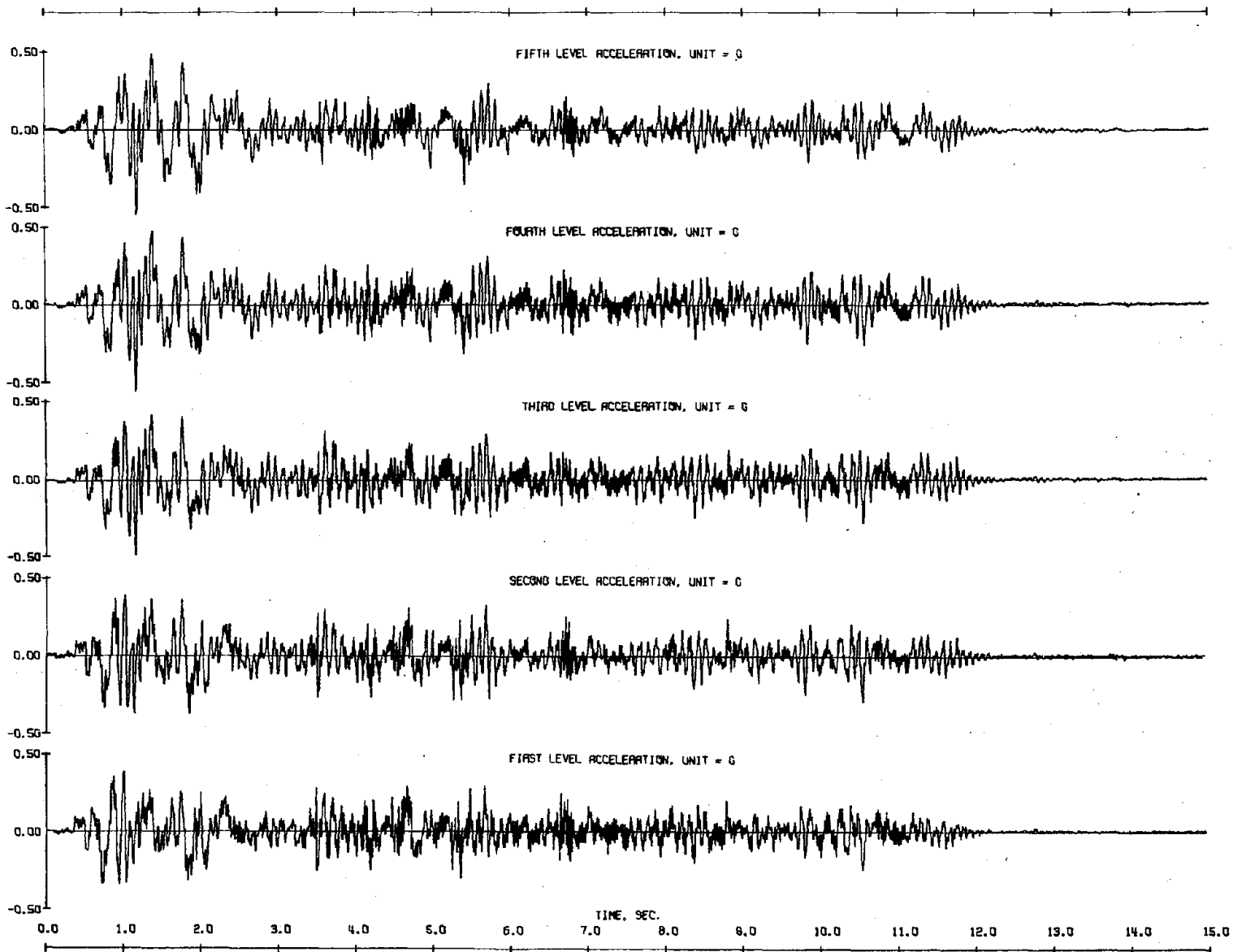
(e) Accelerations of Structure with Heavily Reinforced Wall
 Fig. 5.4 (contd.) Measured Response to Initial El Centro Simulations



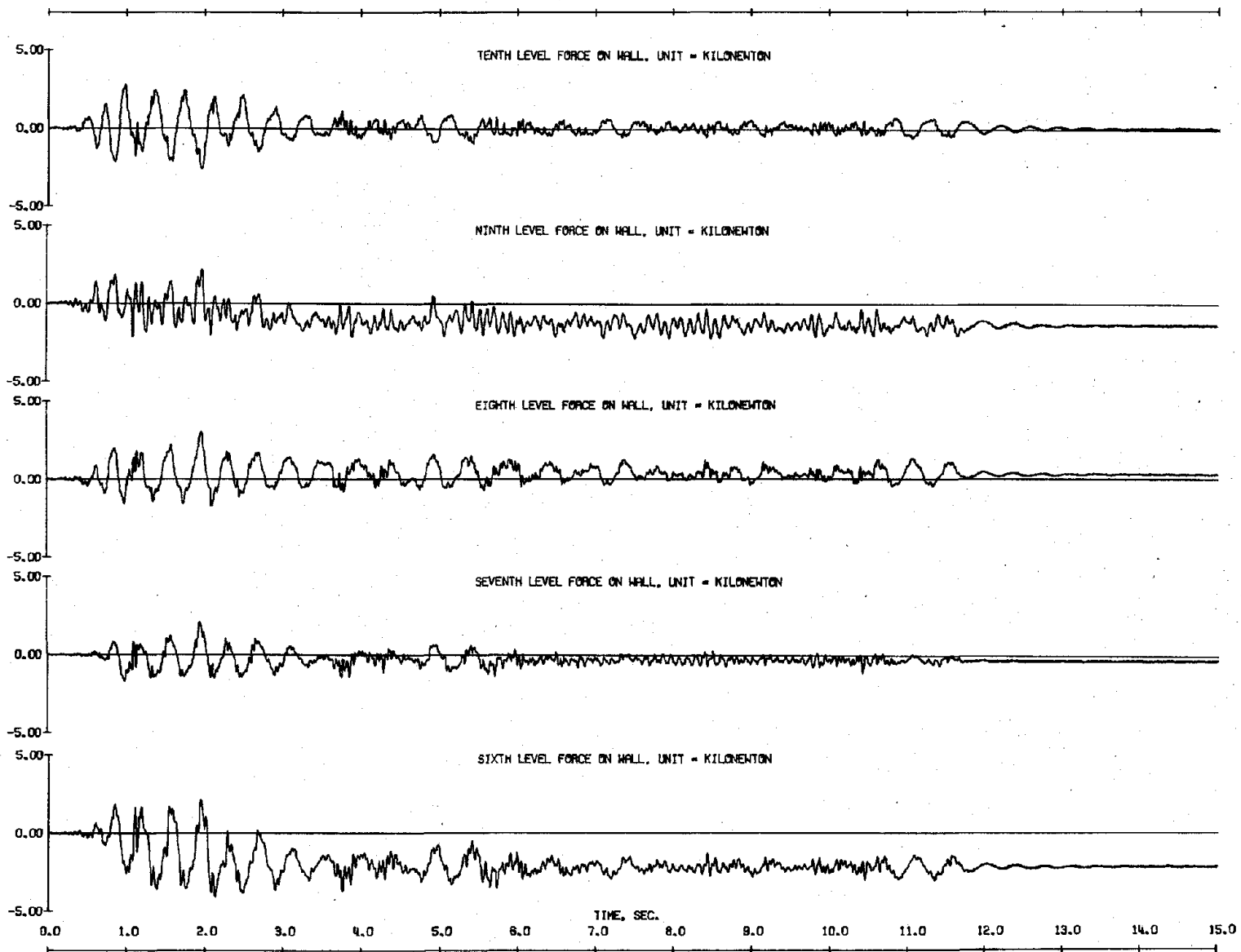
(f) Accelerations of Structure with Lightly Reinforced Wall
 Fig. 5.4 (contd.) Measured Response to Initial El Centro Simulations



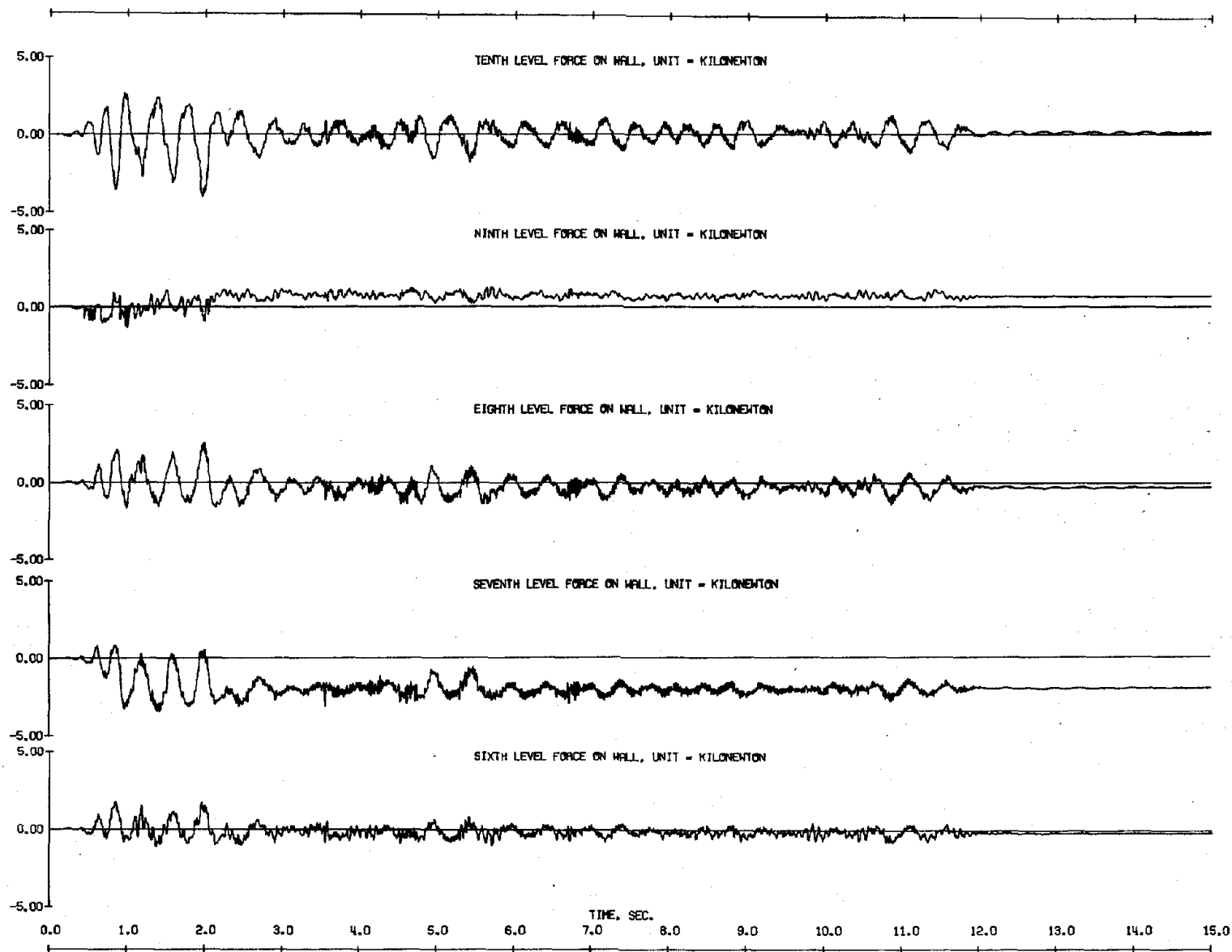
(e) (contd.) Accelerations of Structure with Heavily Reinforced Wall
 Fig. 5.4 (contd.) Measured Response to Initial El Centro Simulations



(f) (contd.) Accelerations of Structure with Lightly Reinforced Wall
 Fig. 5.4 (contd.) Measured Response to Initial El Centro Simulations

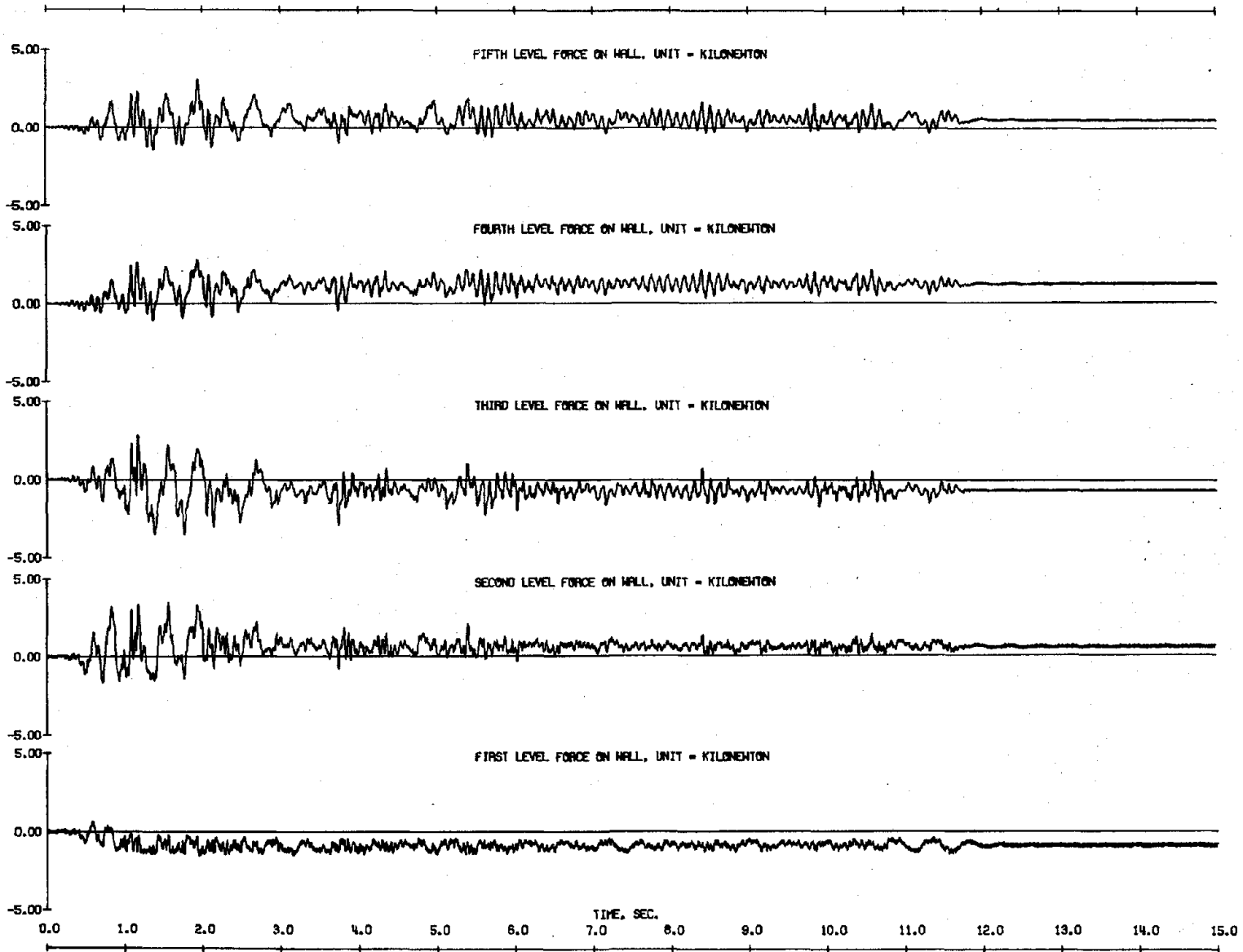


(g) Force Resisted by Heavily Reinforced Wall
 Fig. 5.4 (contd.) Measured Response to Initial El Centro Simulations

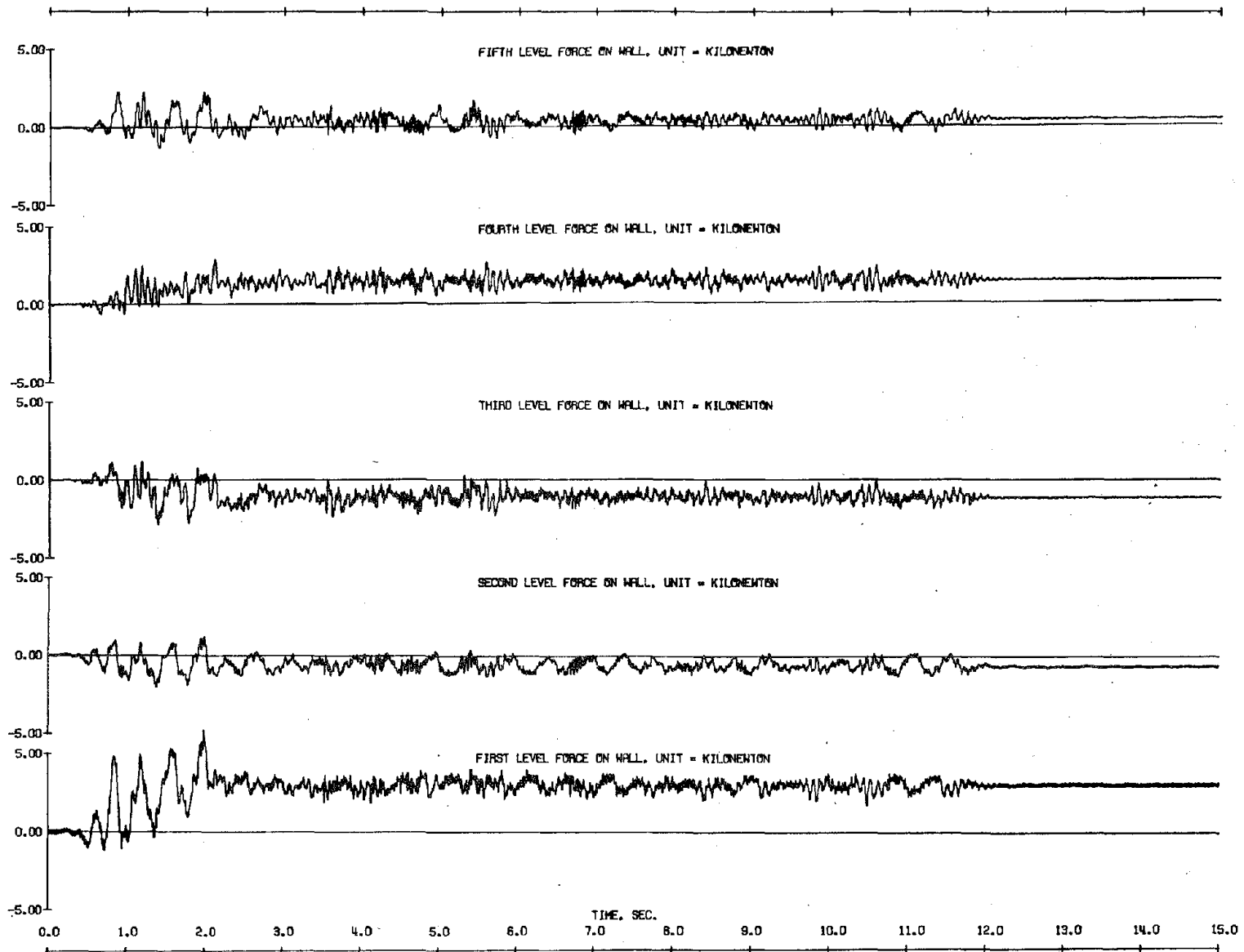


(h) Force Resisted by Lightly Reinforced Wall

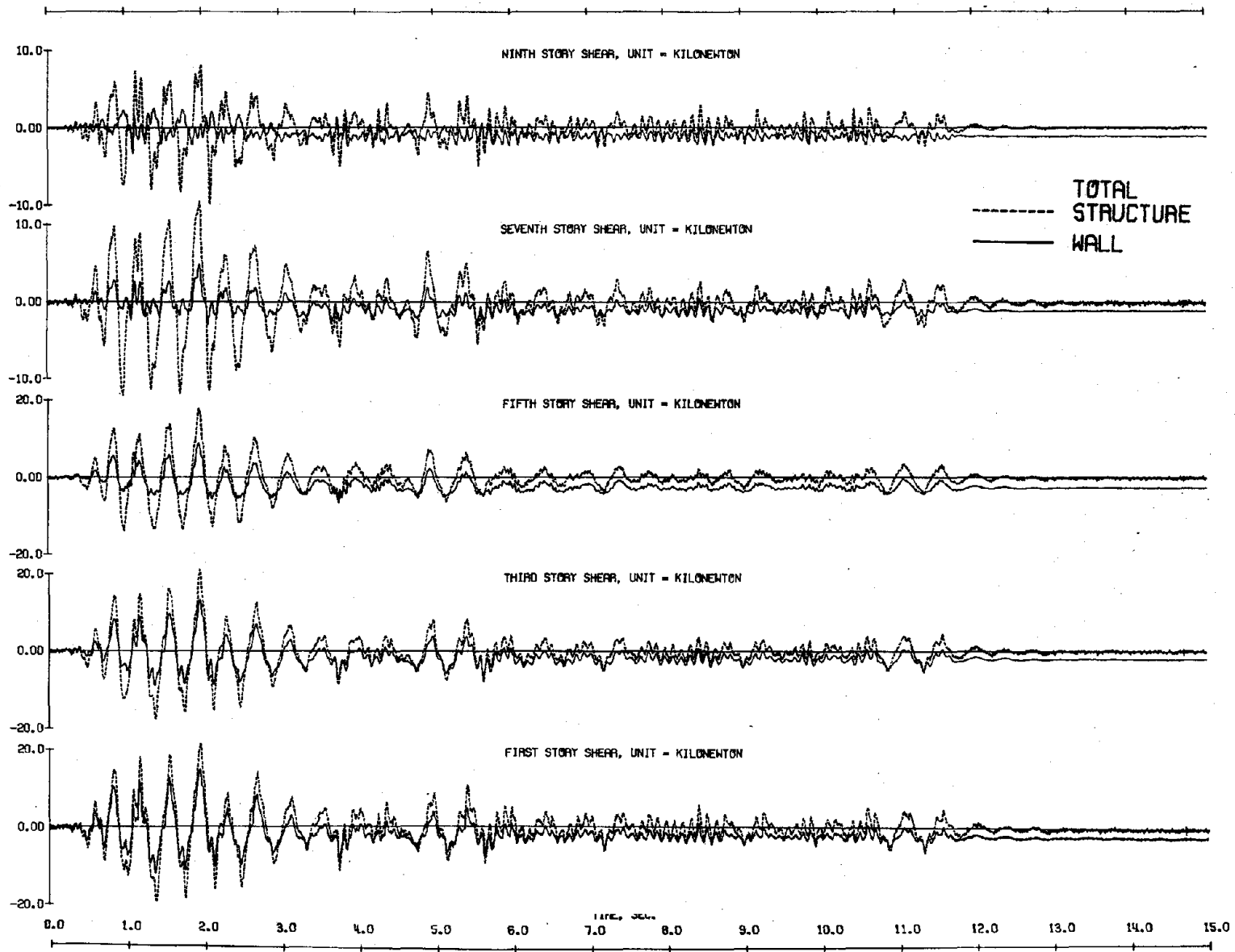
Fig. 5.4 (contd.) Measured Response to Initial El Centro Simulations



(g) (contd.) Force Resisted by Heavily Reinforced Wall
 Fig. 5.4 (contd.) Measured Response to Initial El Centro Simulations

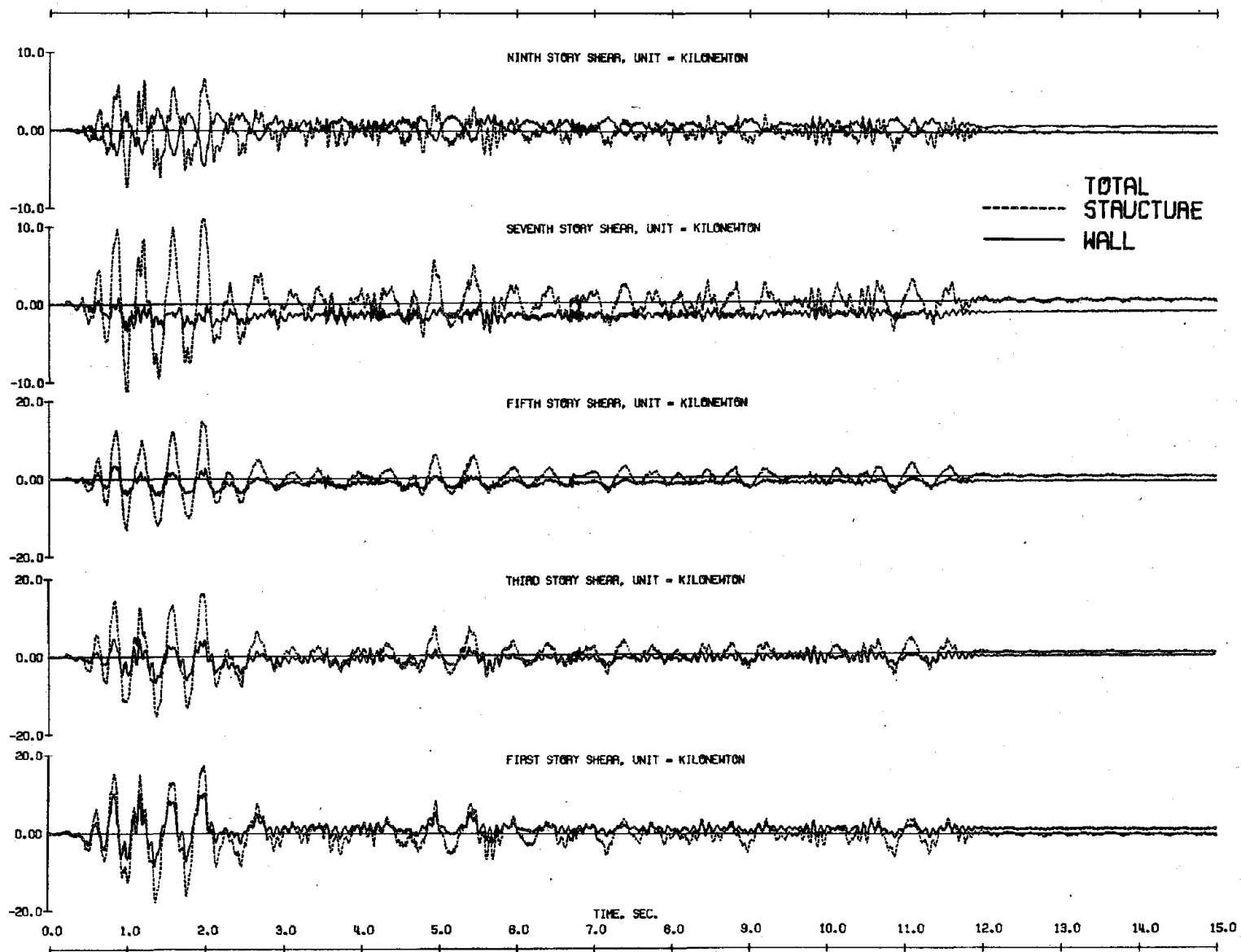


(h) (contd.) Force Resisted by Lightly Reinforced Wall
 Fig. 5.4 (contd.) Measured Response to Initial El Centro Simulations



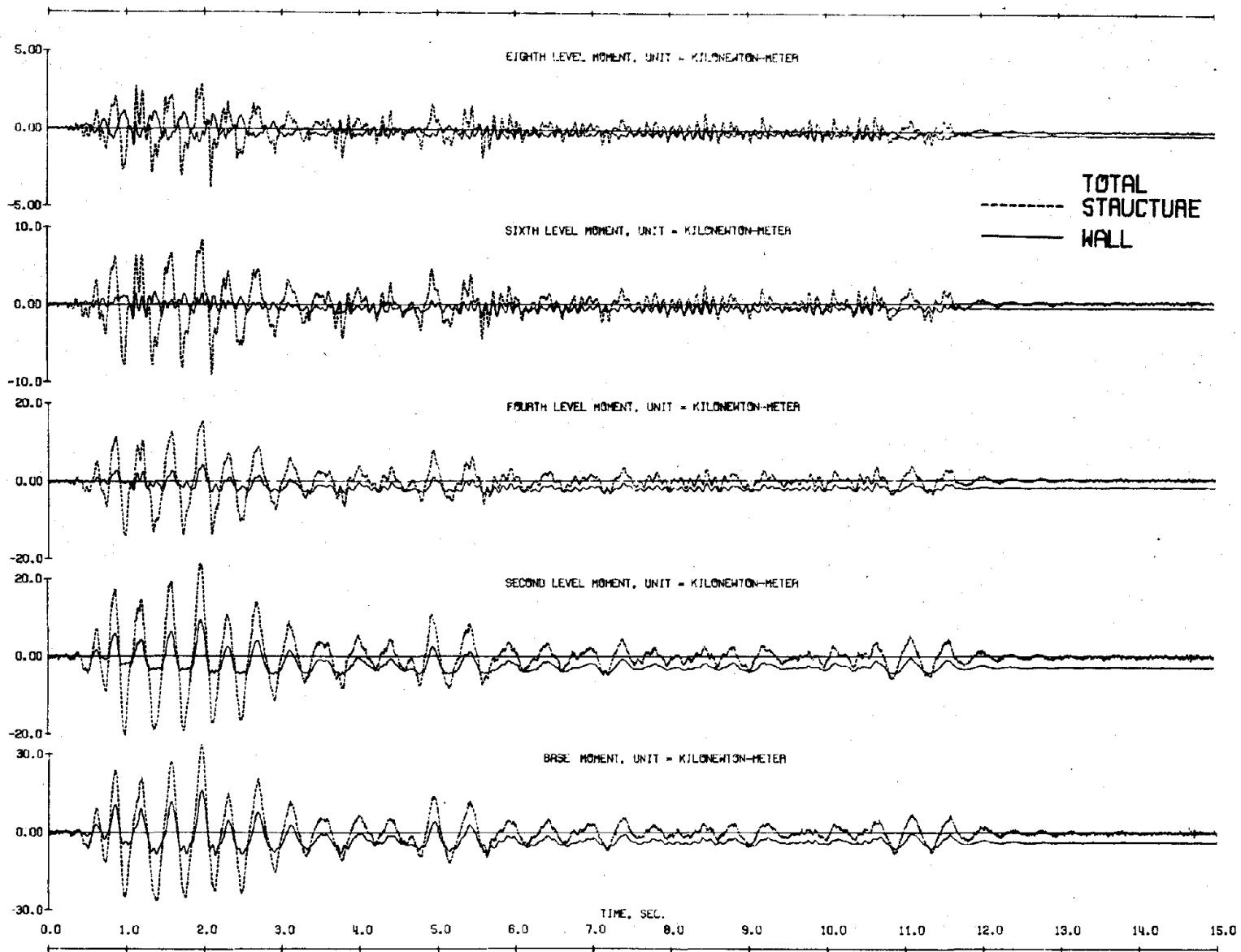
(a) Shears of Structure with Heavily Reinforced Wall

Fig. 5.5 Shear and Moment Response to Initial El Centro Simulations

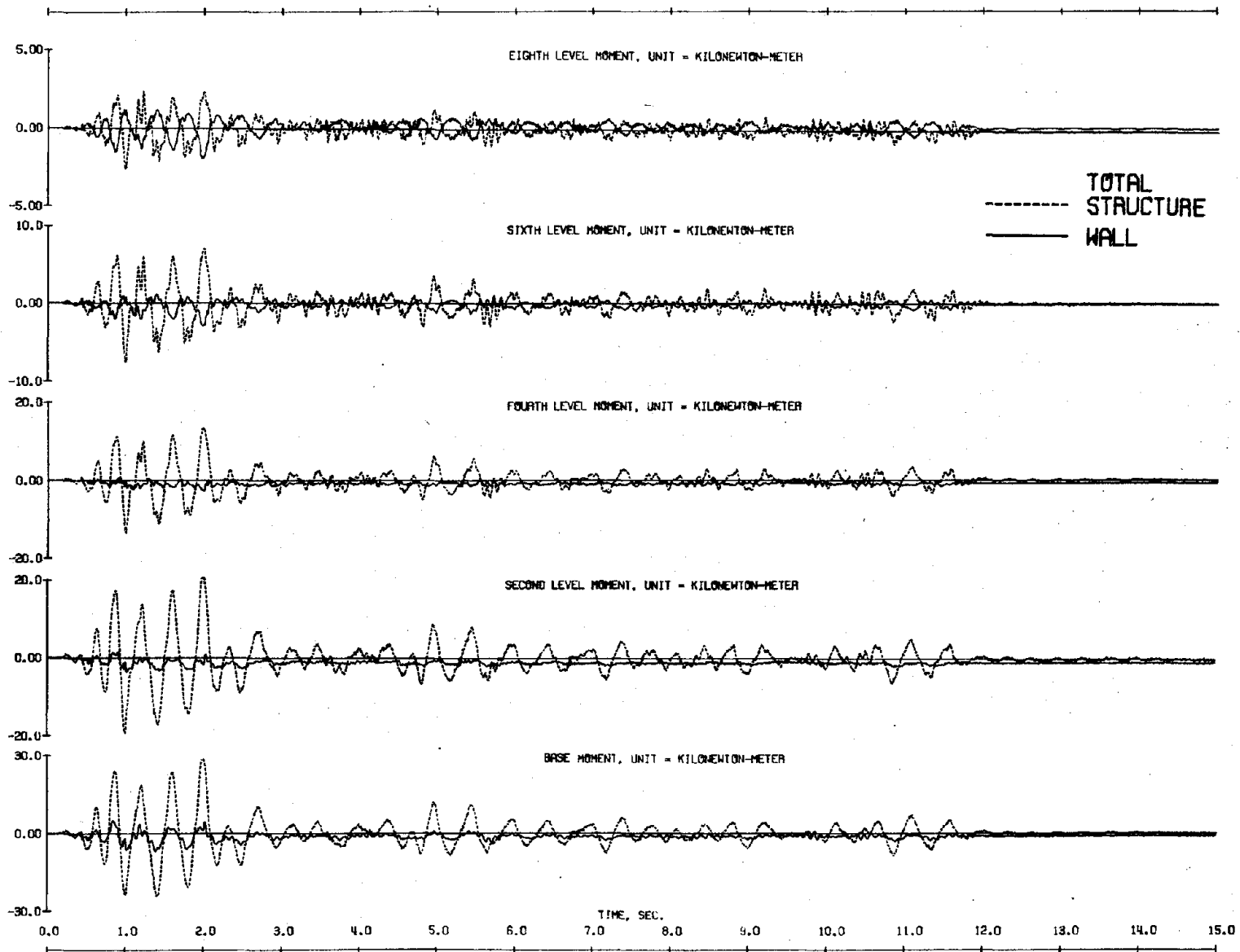


(b) Shears of Structure with Lightly Reinforced Wall

Fig. 5.5 (Contd.) Shear and Moment Response to Initial El Centro Simulations

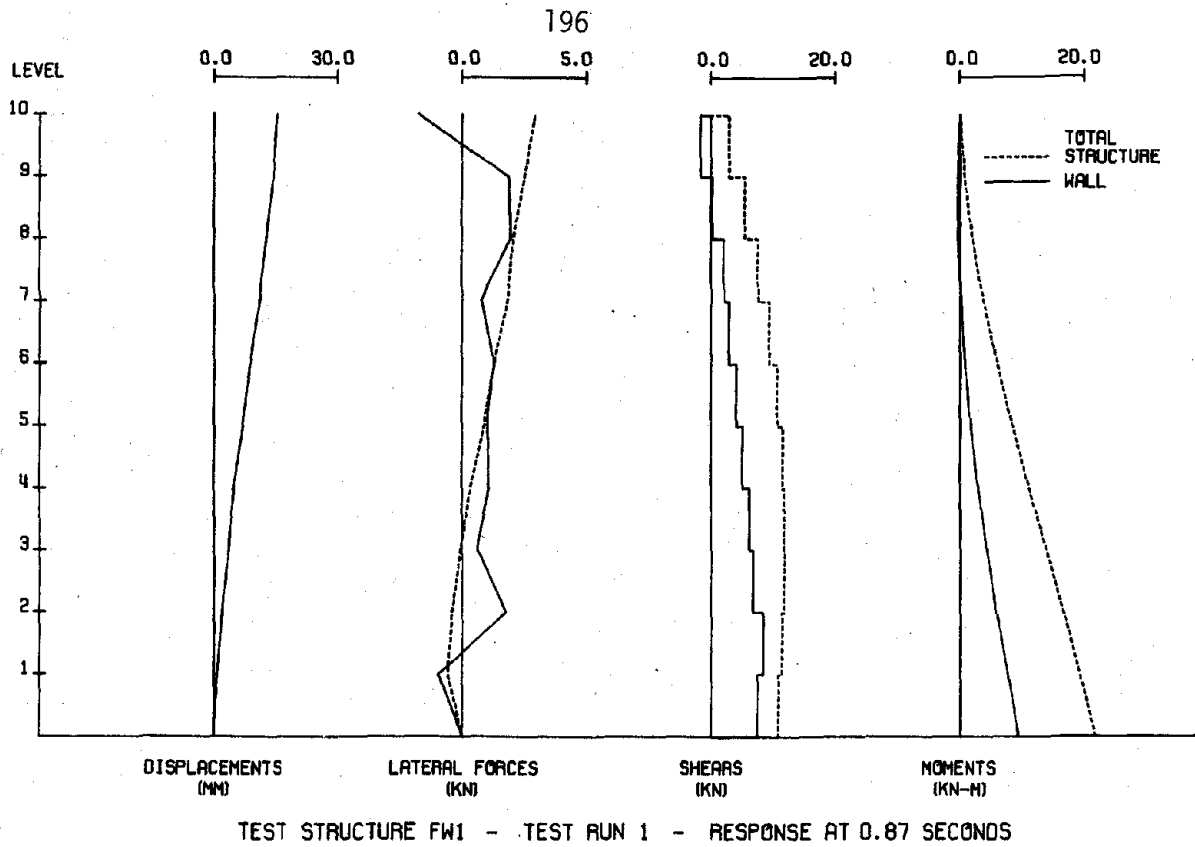


(c) Moments of Structure with Heavily Reinforced Wall
 Fig. 5.5 (Contd.) Shear and Moment Response to Initial El Centro Simulations



(d) Moments of Structure with Lightly Reinforced Wall

Fig. 5.5 (Contd.) Shear and Moment Response to Initial El Centro Simulations



(a) Structure with Heavily Reinforced Wall

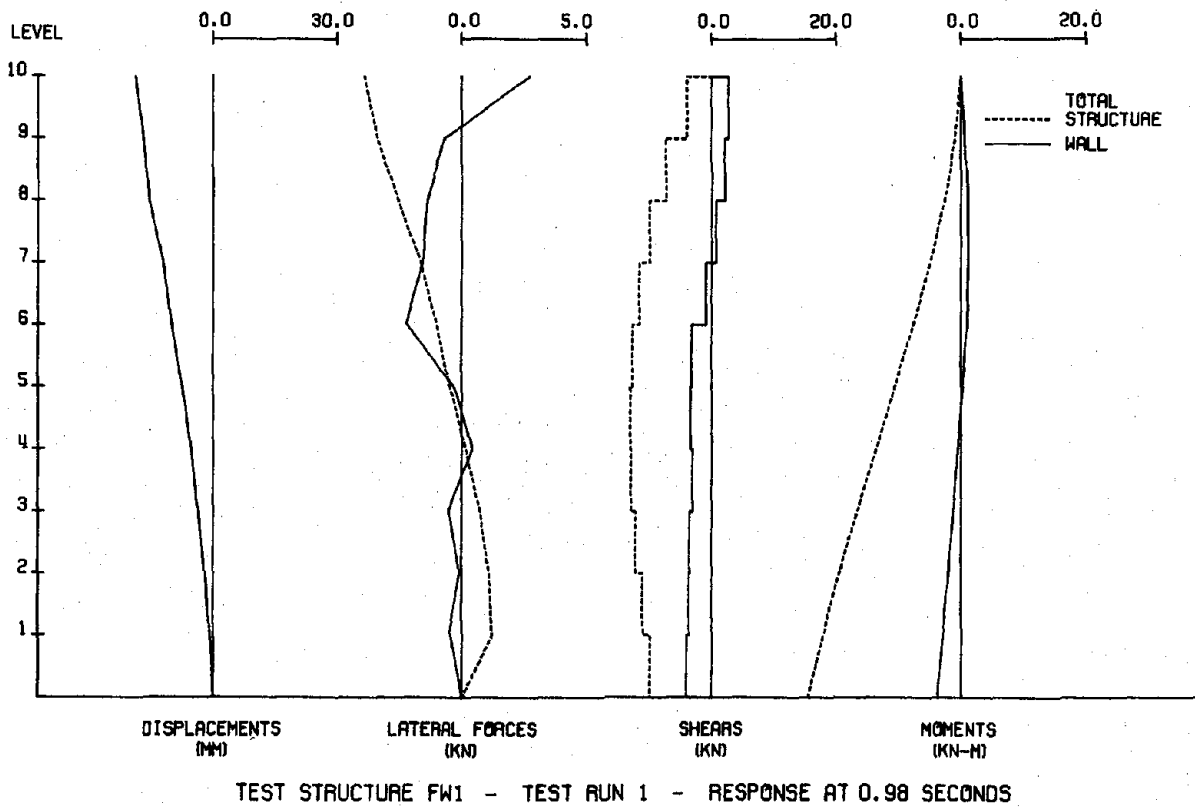
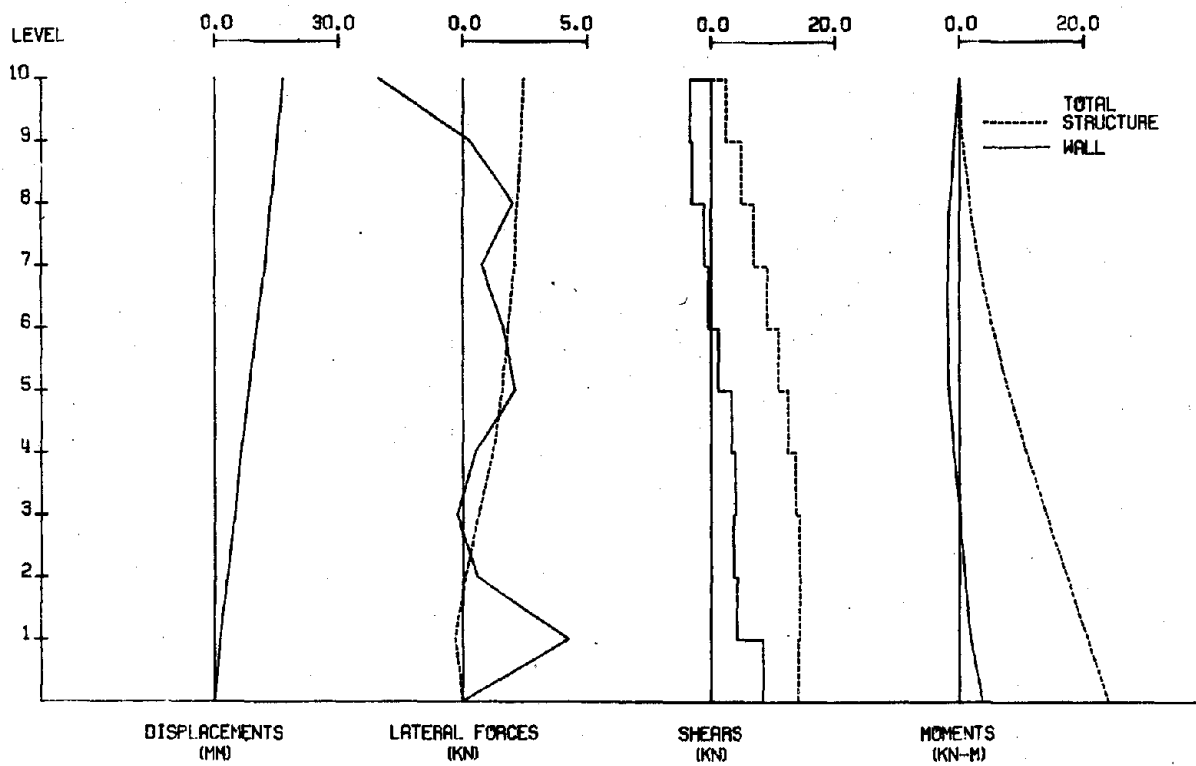
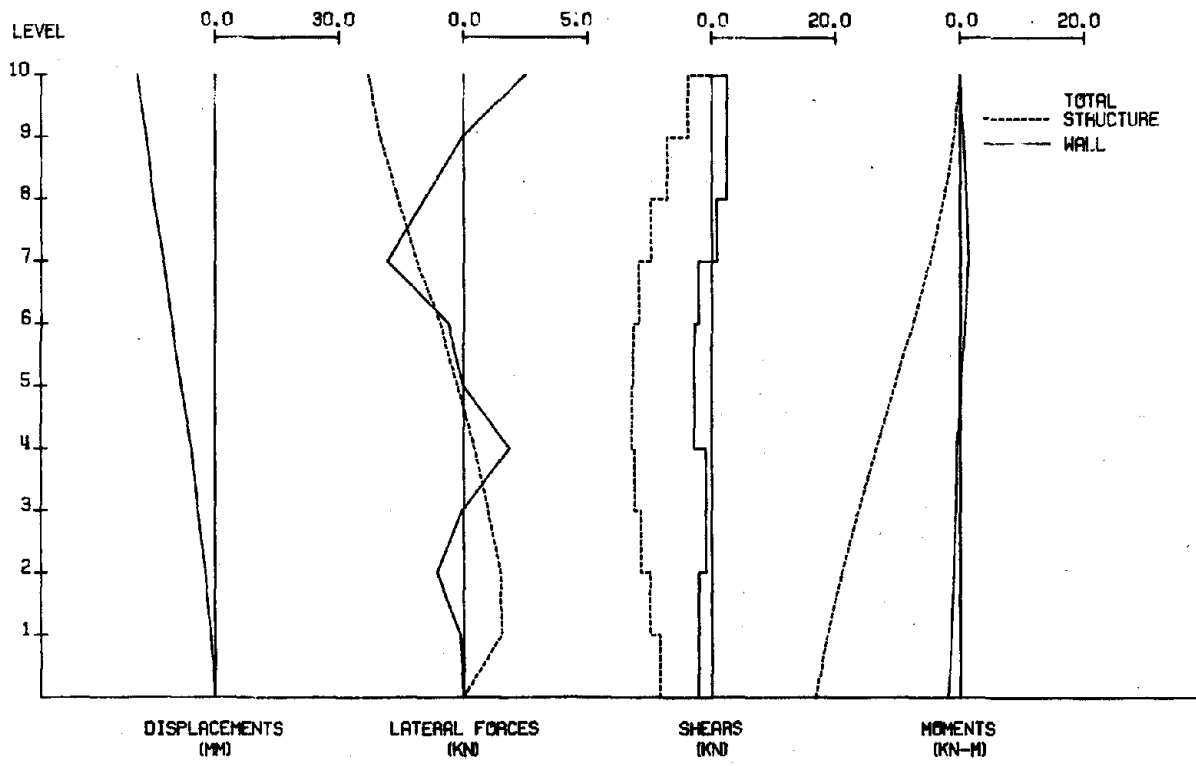


Fig. 5.6 Distributions of Response to Initial El Centro Simulations



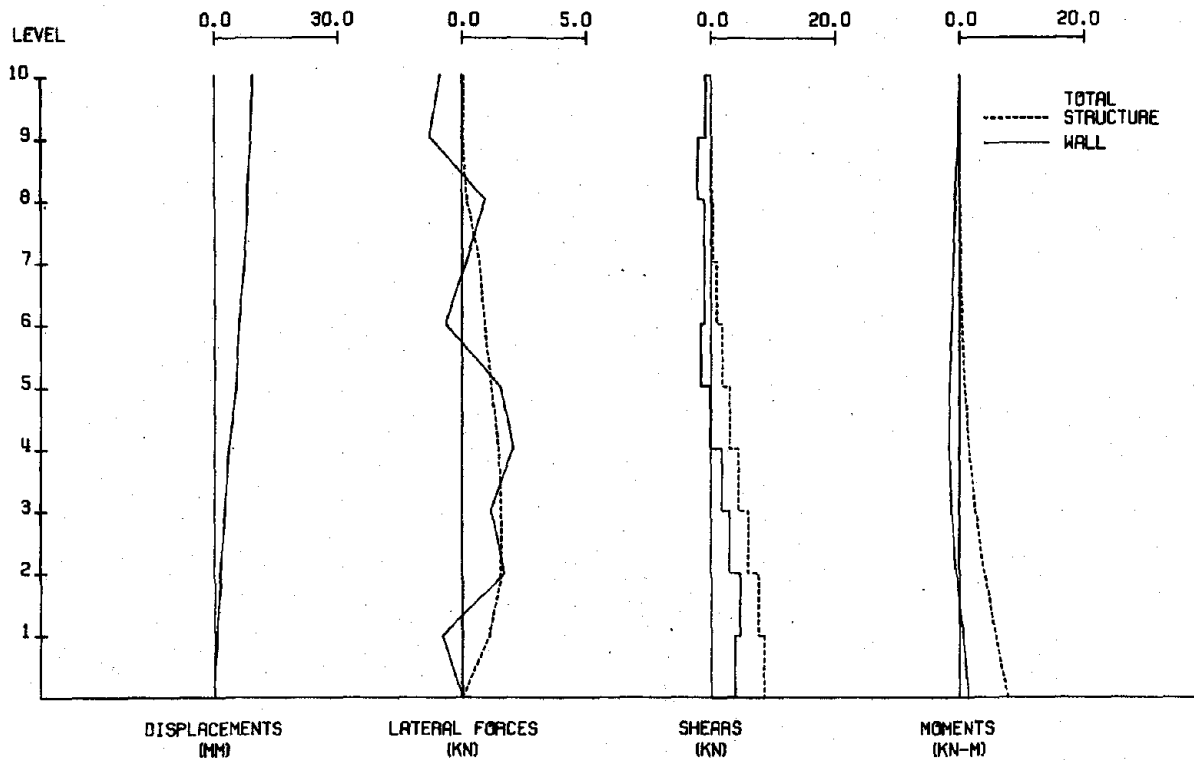
TEST STRUCTURE FW2 - TEST RUN 1 - RESPONSE AT 0.87 SECONDS

(b) Structure with Lightly Reinforced Wall



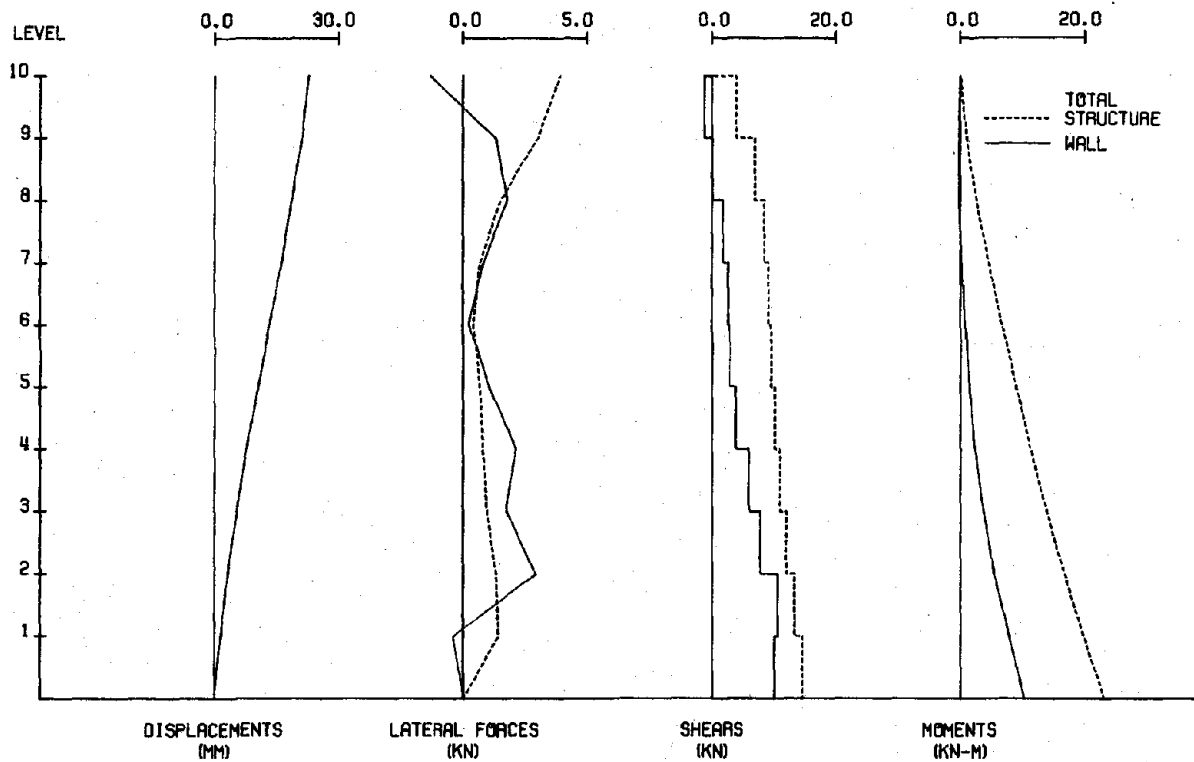
TEST STRUCTURE FW2 - TEST RUN 1 - RESPONSE AT 1.00 SECONDS

Fig. 5.6 (contd.) Distributions of Response to Initial El Centro Simulations



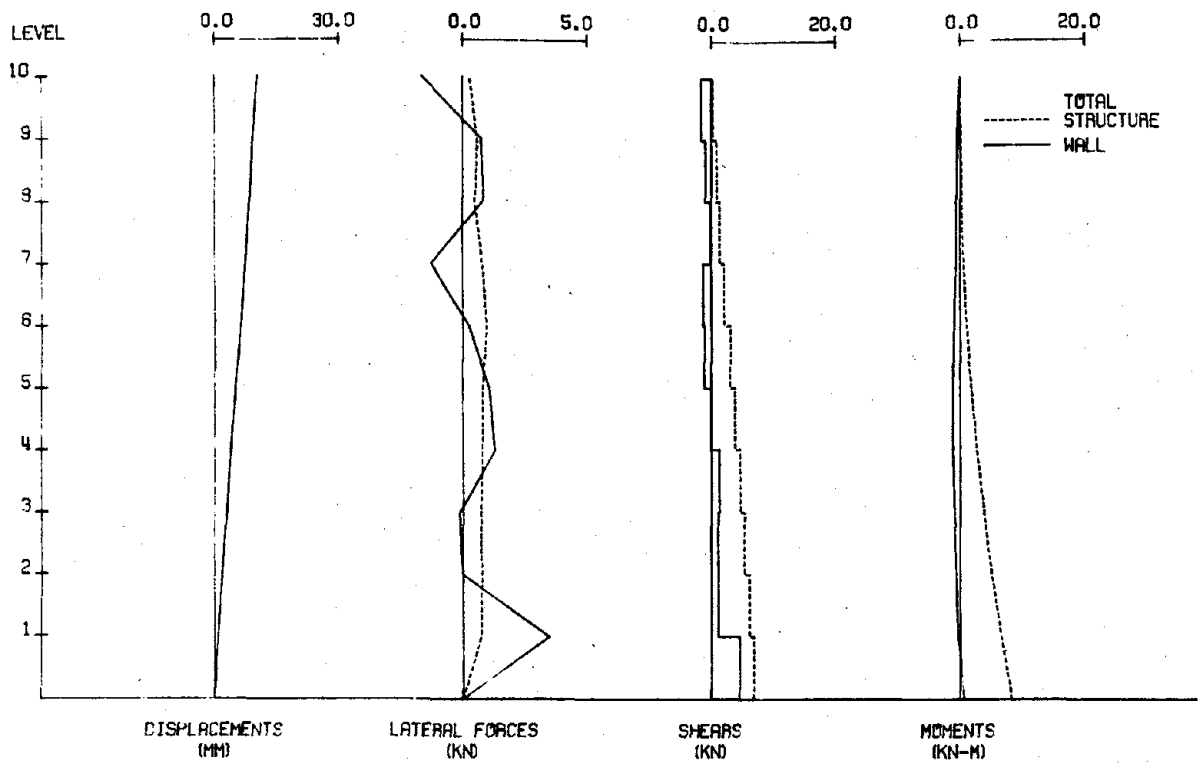
TEST STRUCTURE FW1 - TEST RUN 1 - RESPONSE AT 1.88 SECONDS

(a) Structure with Heavily Reinforced Wall



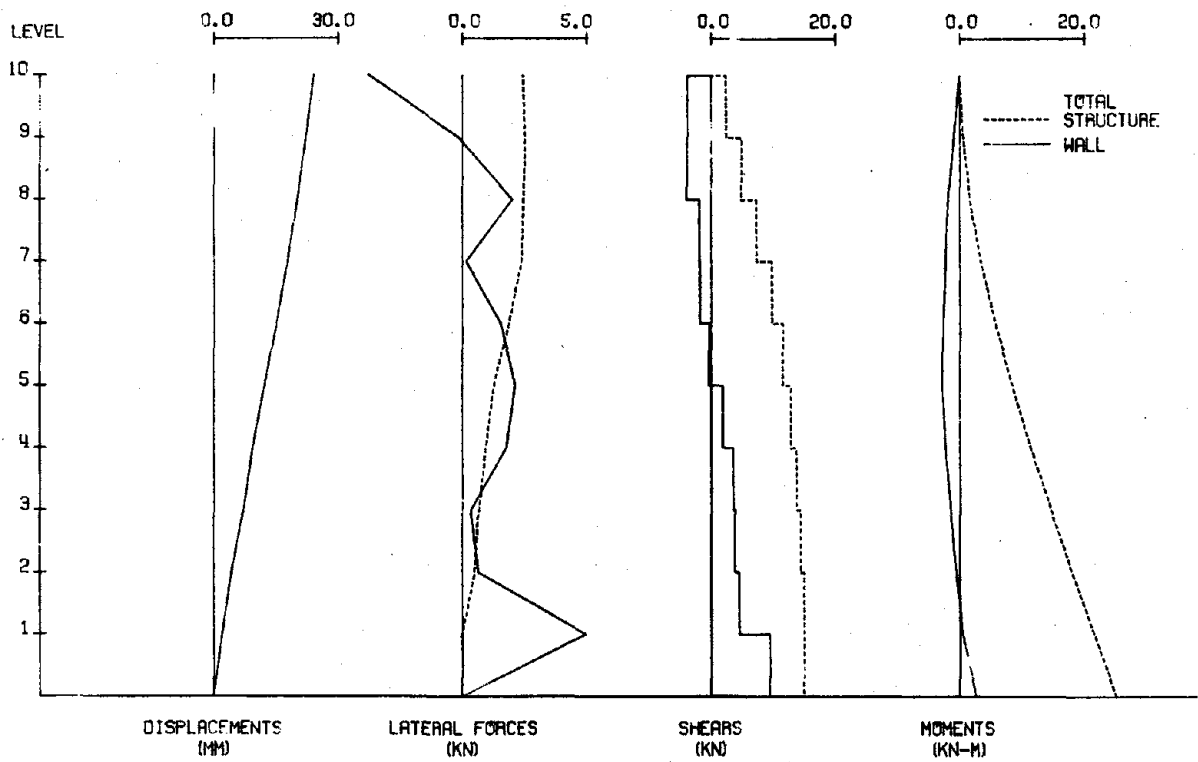
TEST STRUCTURE FW1 - TEST RUN 1 - RESPONSE AT 1.92 SECONDS

Fig. 5.6 (contd.) Distributions of Response to Initial El Centro Simulations



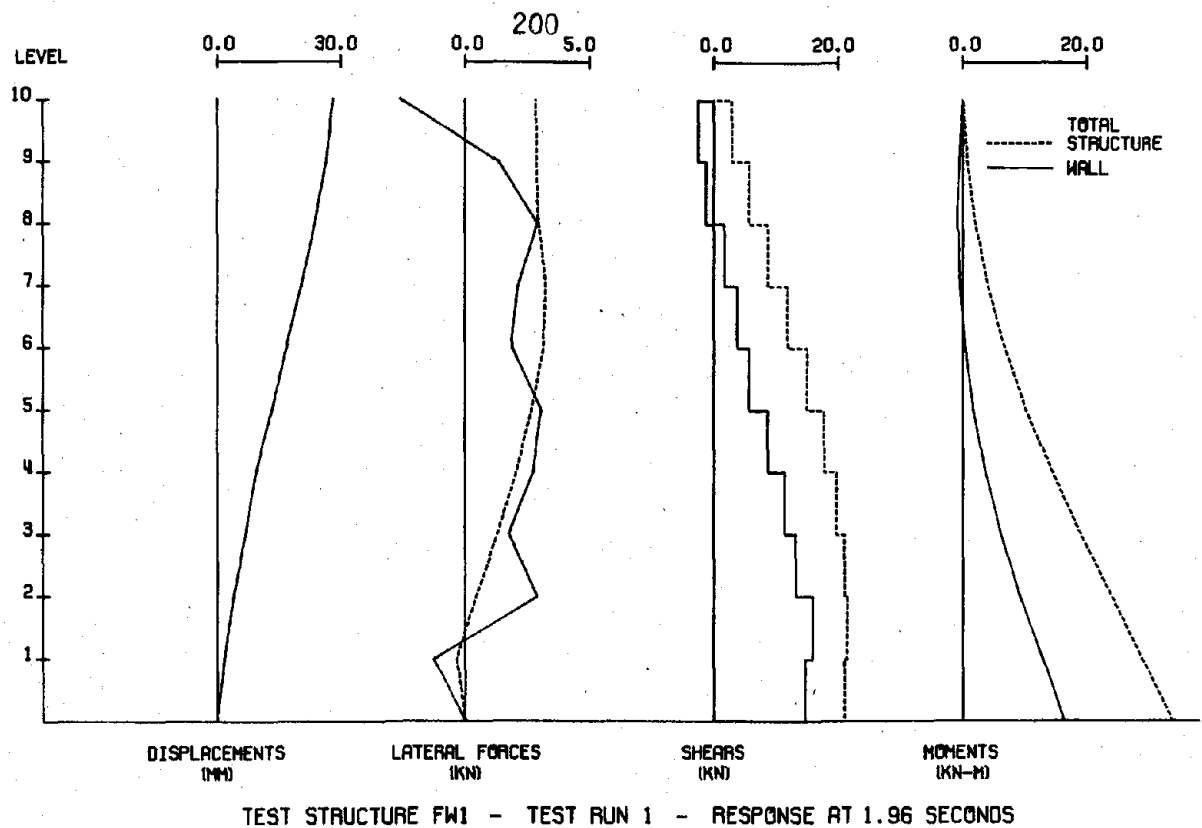
TEST STRUCTURE FW2 - TEST RUN 1 - RESPONSE AT 1.92 SECONDS

(b) Structure with Lightly Reinforced Wall



TEST STRUCTURE FW2 - TEST RUN 1 - RESPONSE AT 1.96 SECONDS

Fig. 5.6 (contd.) Distributions of Response to Initial El Centro Simulations



(a) Structure with Heavily Reinforced Wall

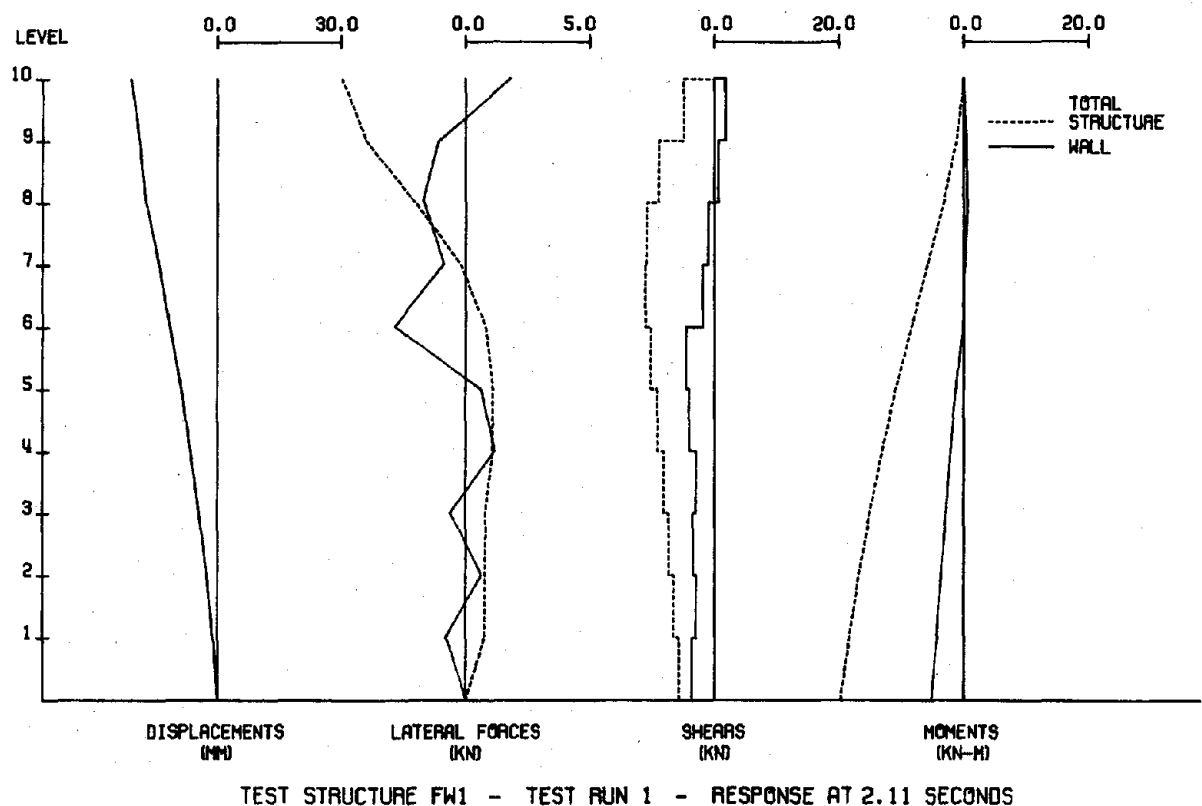
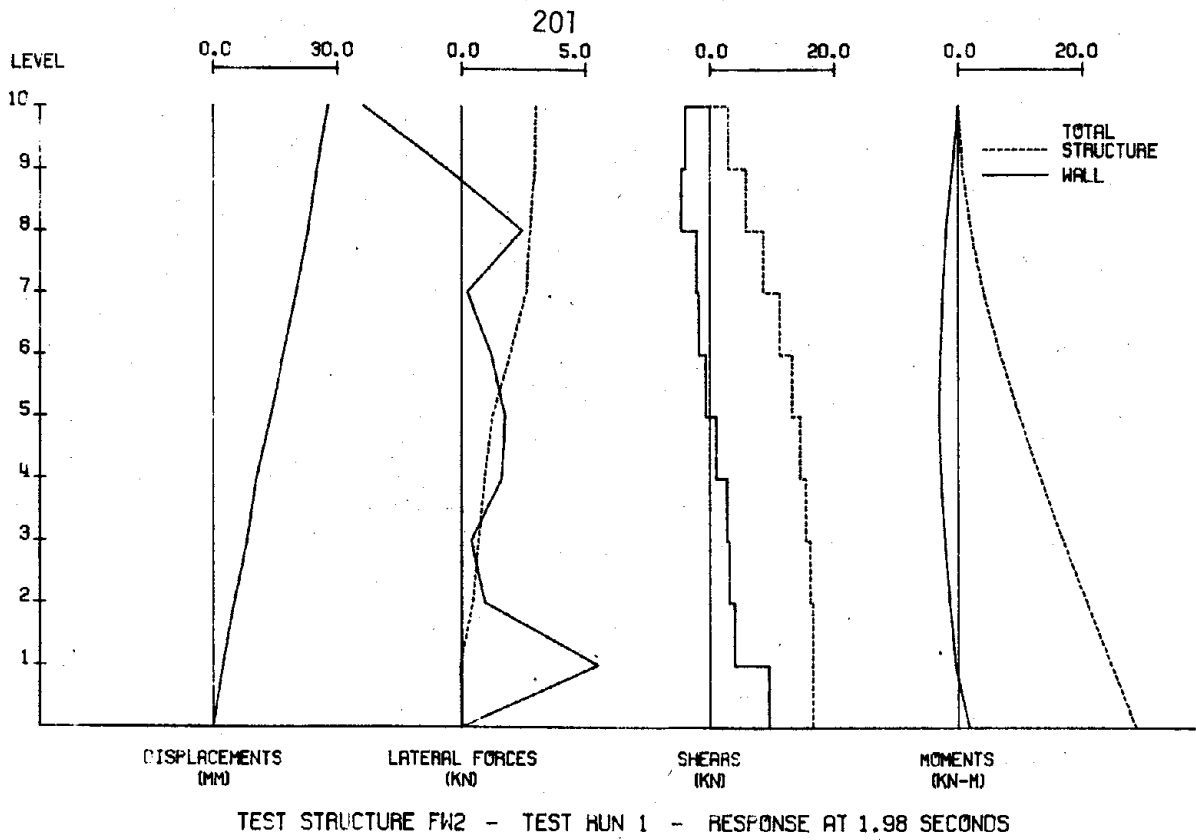


Fig. 5.6 (contd.) Distributions of Response to Initial El Centro Simulations



(b) Structure with Lightly Reinforced Wall

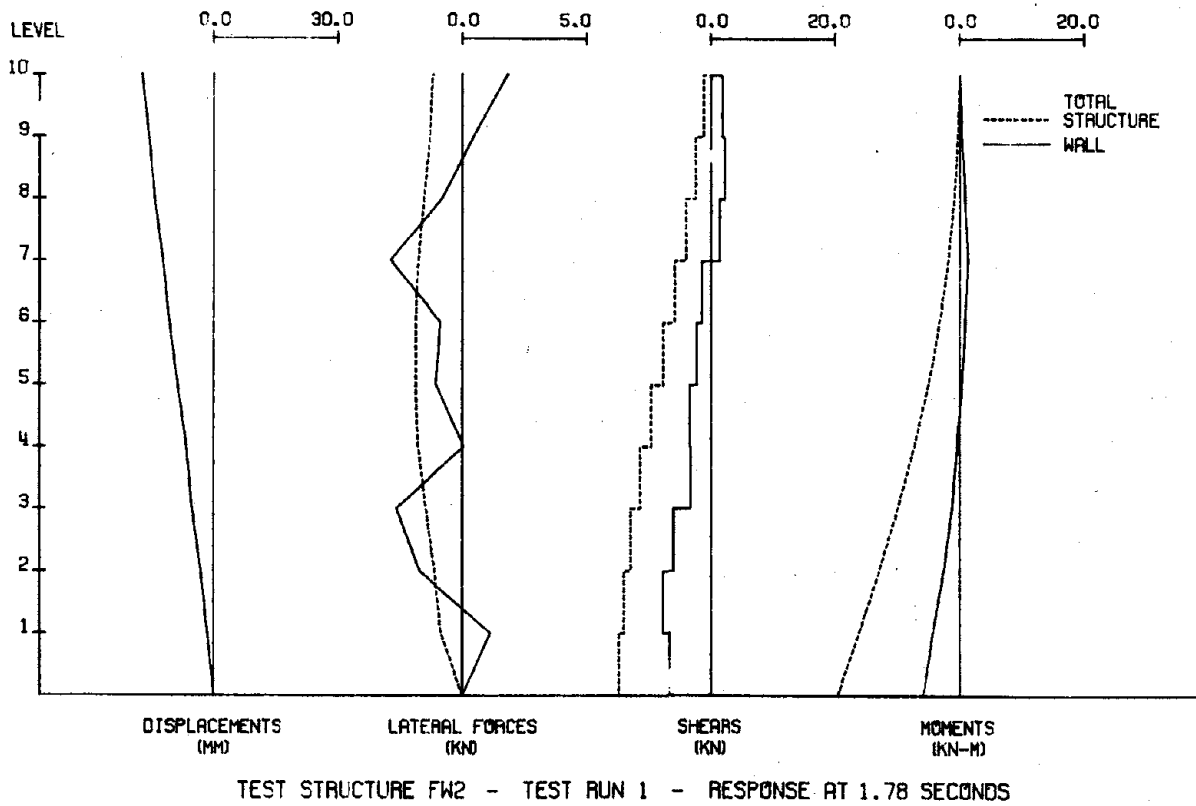
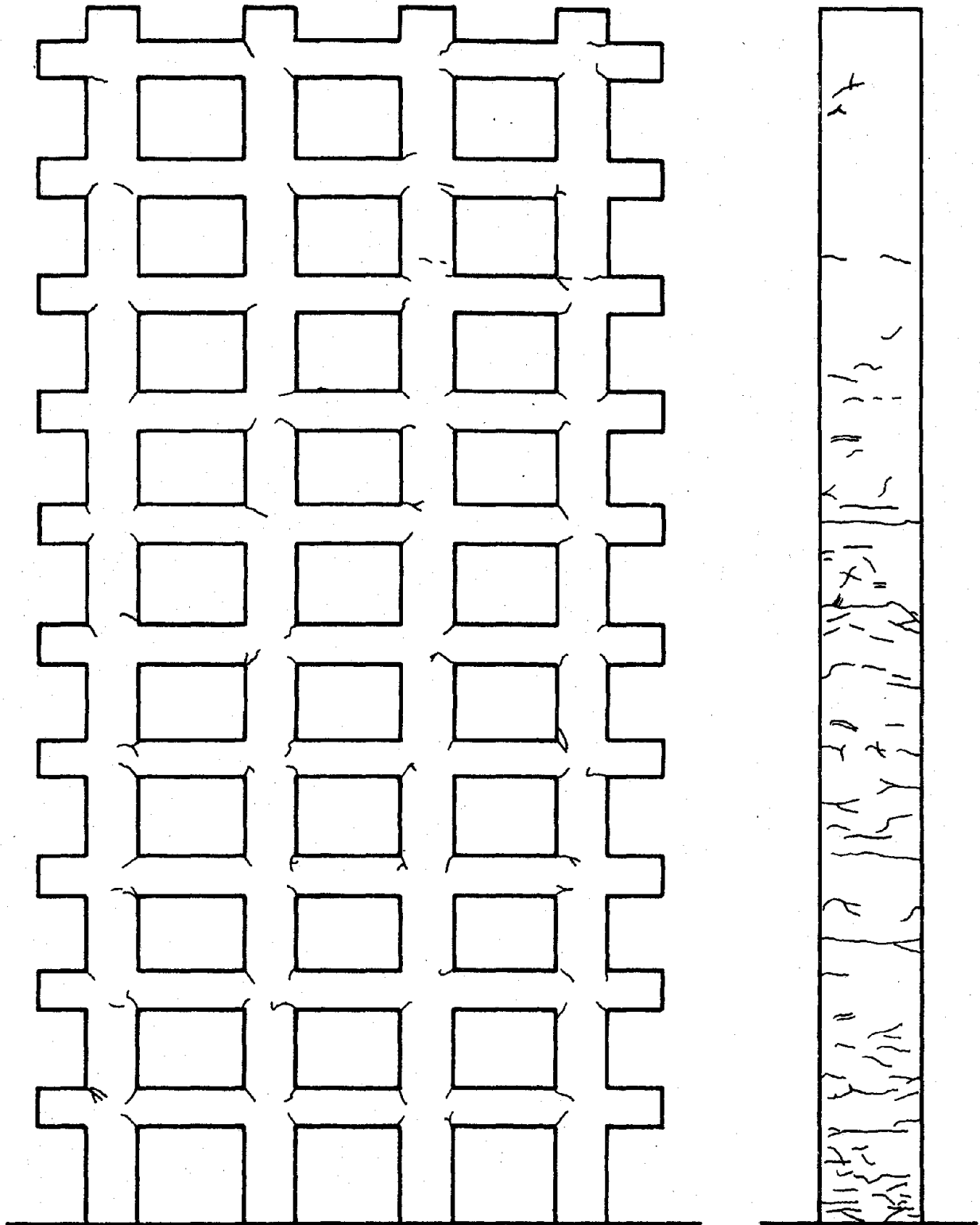


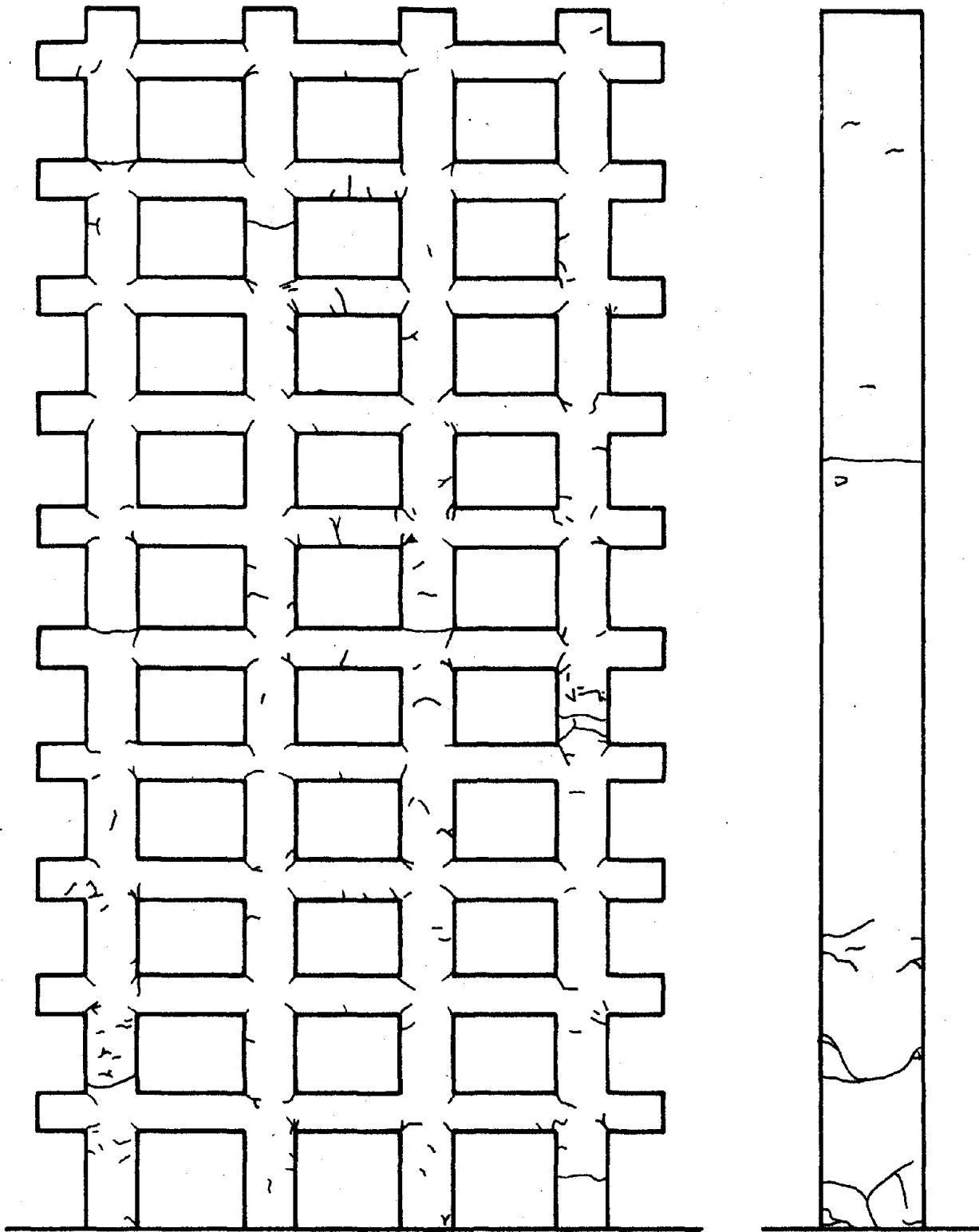
Fig. 5.6 (contd.) Distributions of Response to Initial E1 Centro Simulations



(Not To Scale)

(a) Structure with Heavily Reinforced Wall

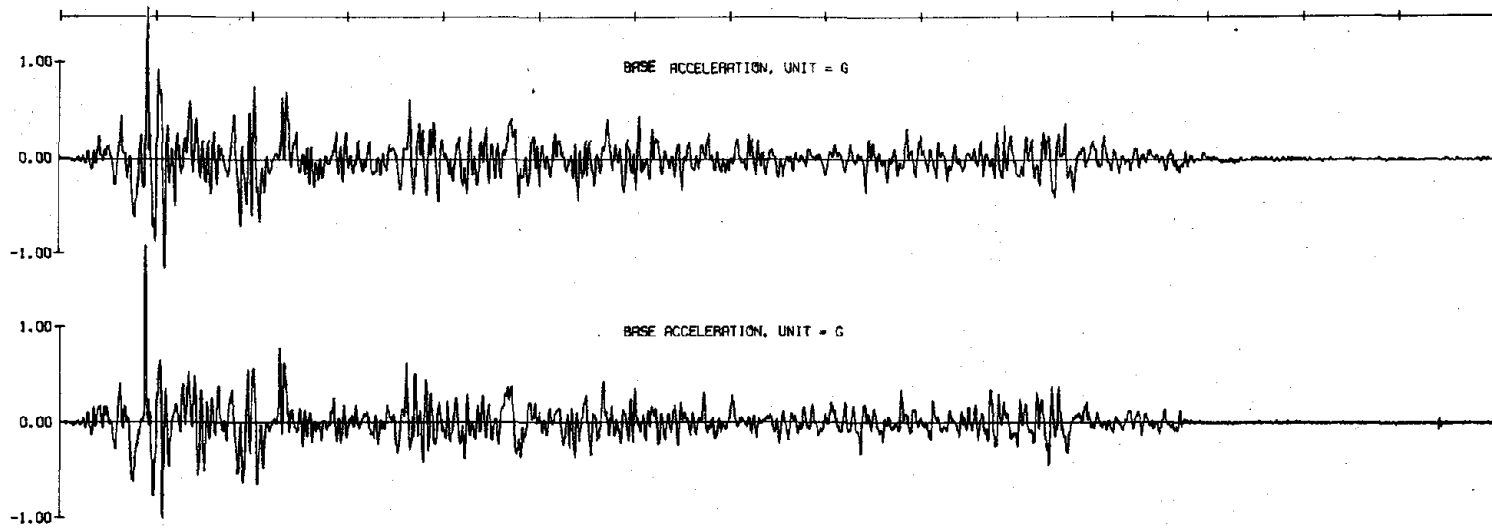
Fig. 5.7 Observed Crack Patterns following Initial El Centro Simulations



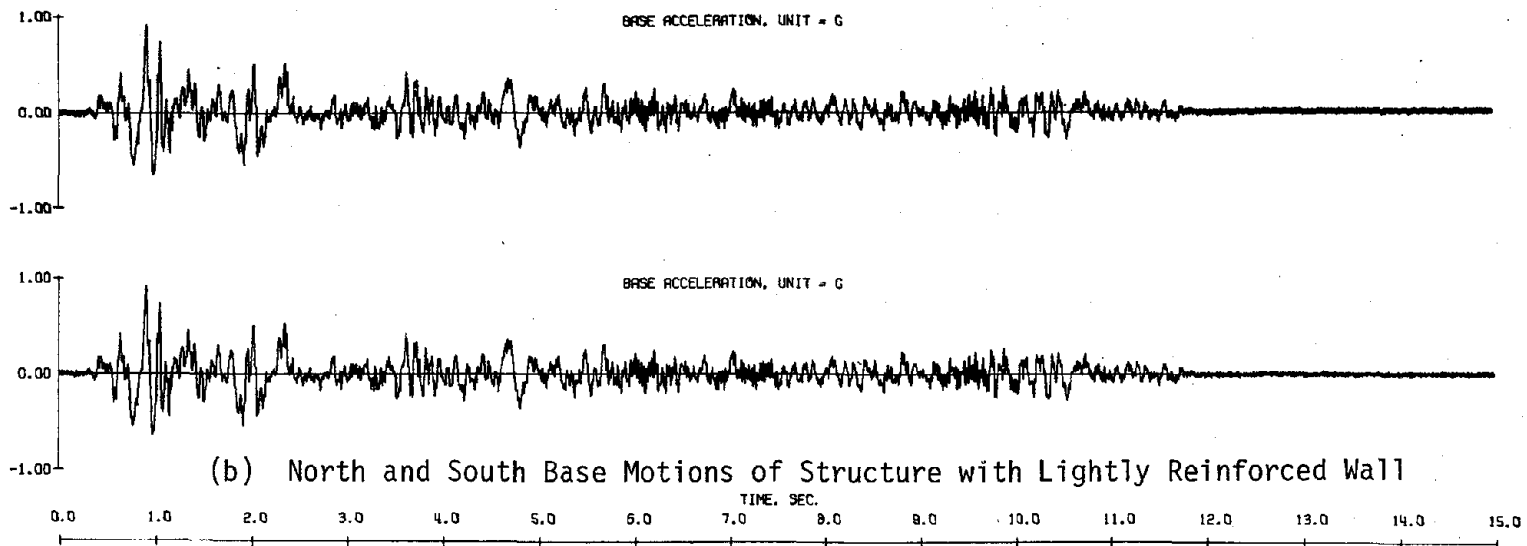
(Not To Scale)

(b) Structure with Lightly Reinforced Wall

Fig. 5.7 (contd.) Observed Crack Patterns following Initial El Centro Simulations



(a) North and South Base Motions of Structure with Heavily Reinforced Wall.



(b) North and South Base Motions of Structure with Lightly Reinforced Wall

Fig. 5.8 Measured Motions of Second El Centro Simulations

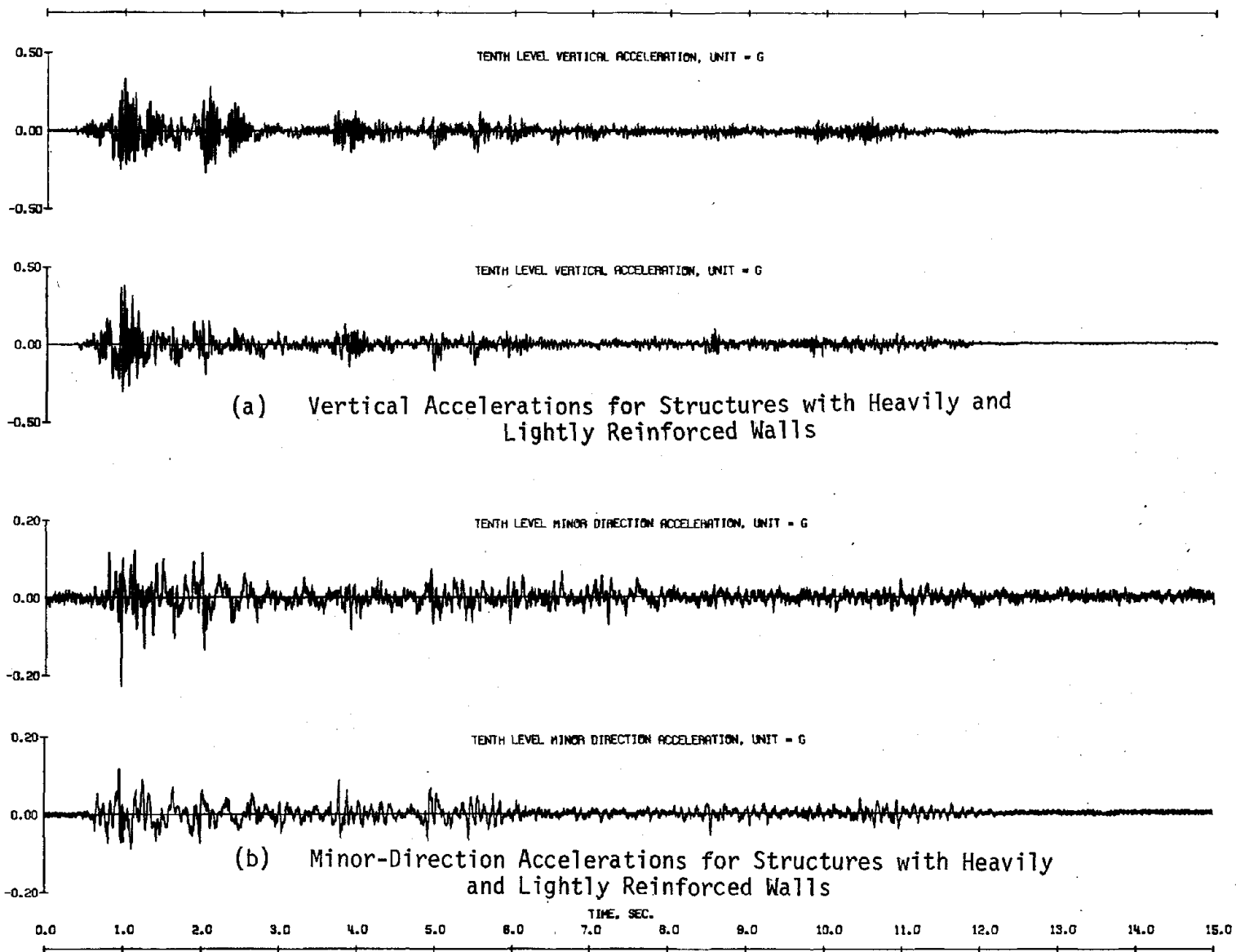
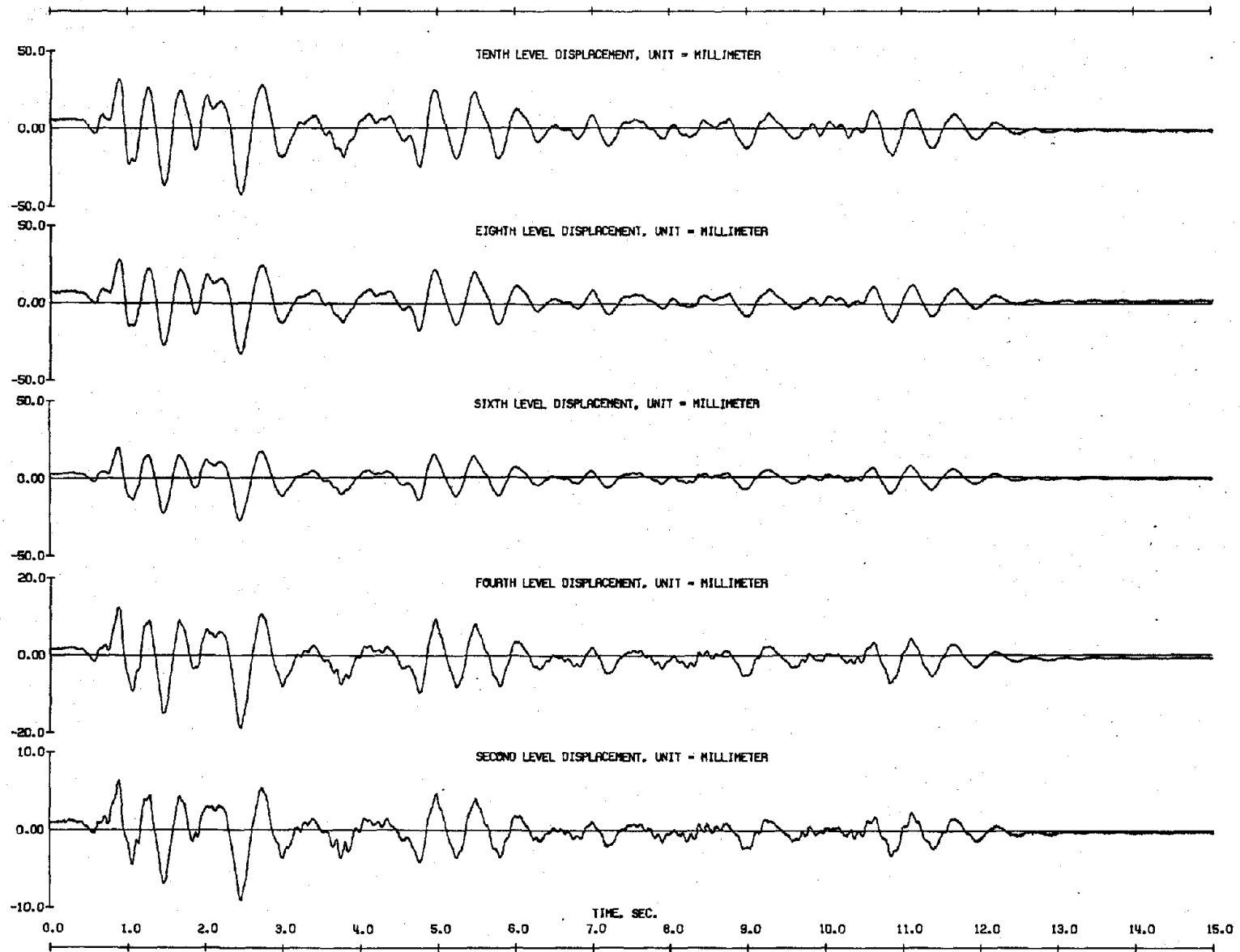
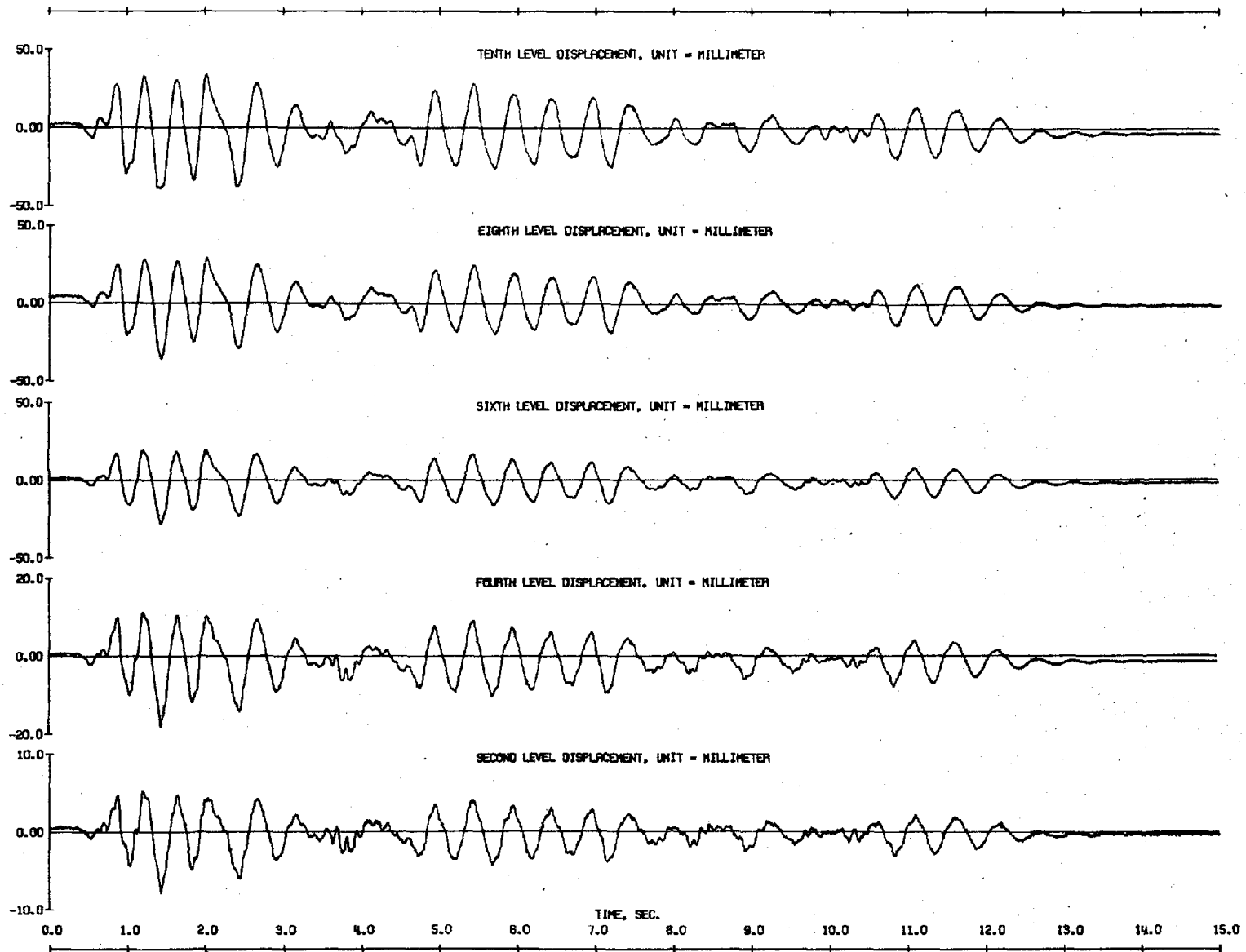


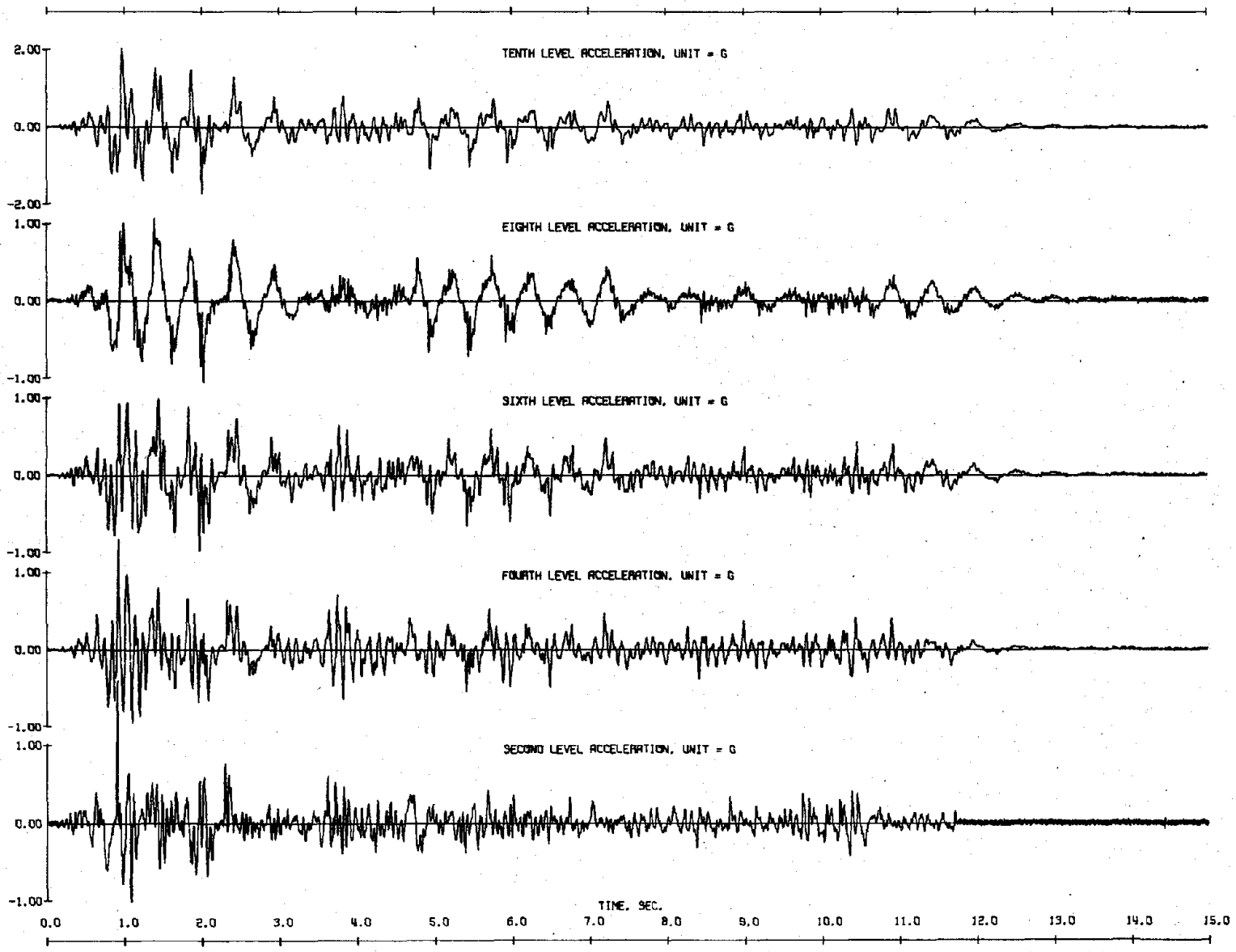
Fig. 5.9 Measured Response to Second El Centro Simulations



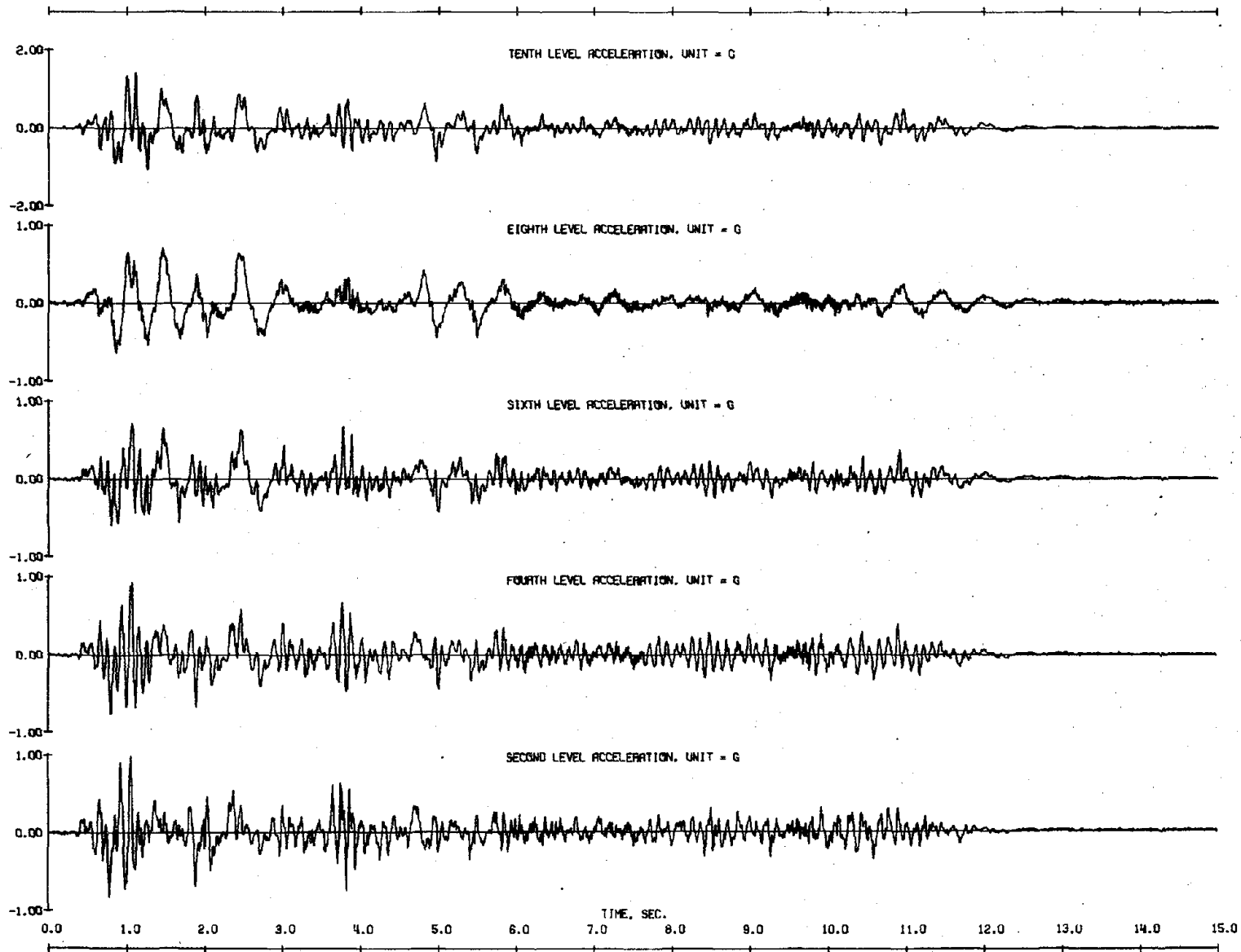
(c) Displacements of Structure with Heavily Reinforced Wall
 Fig. 5.9 (contd.) Measured Response to Second El Centro Simulations



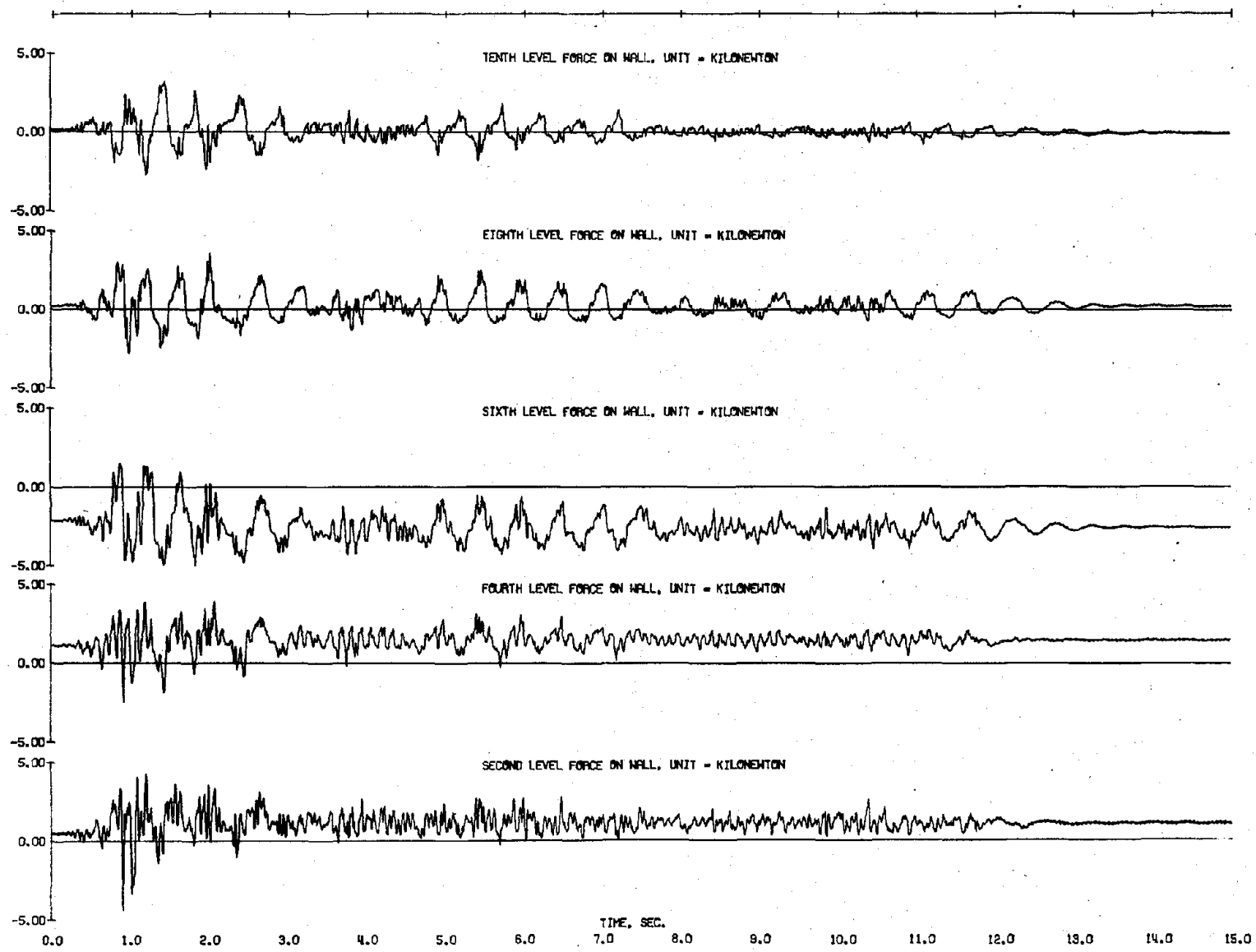
(d) Displacements of Structure with Lightly Reinforced Wall
 Fig. 5.9 (contd.) Measured Response to Second El Centro Simulations



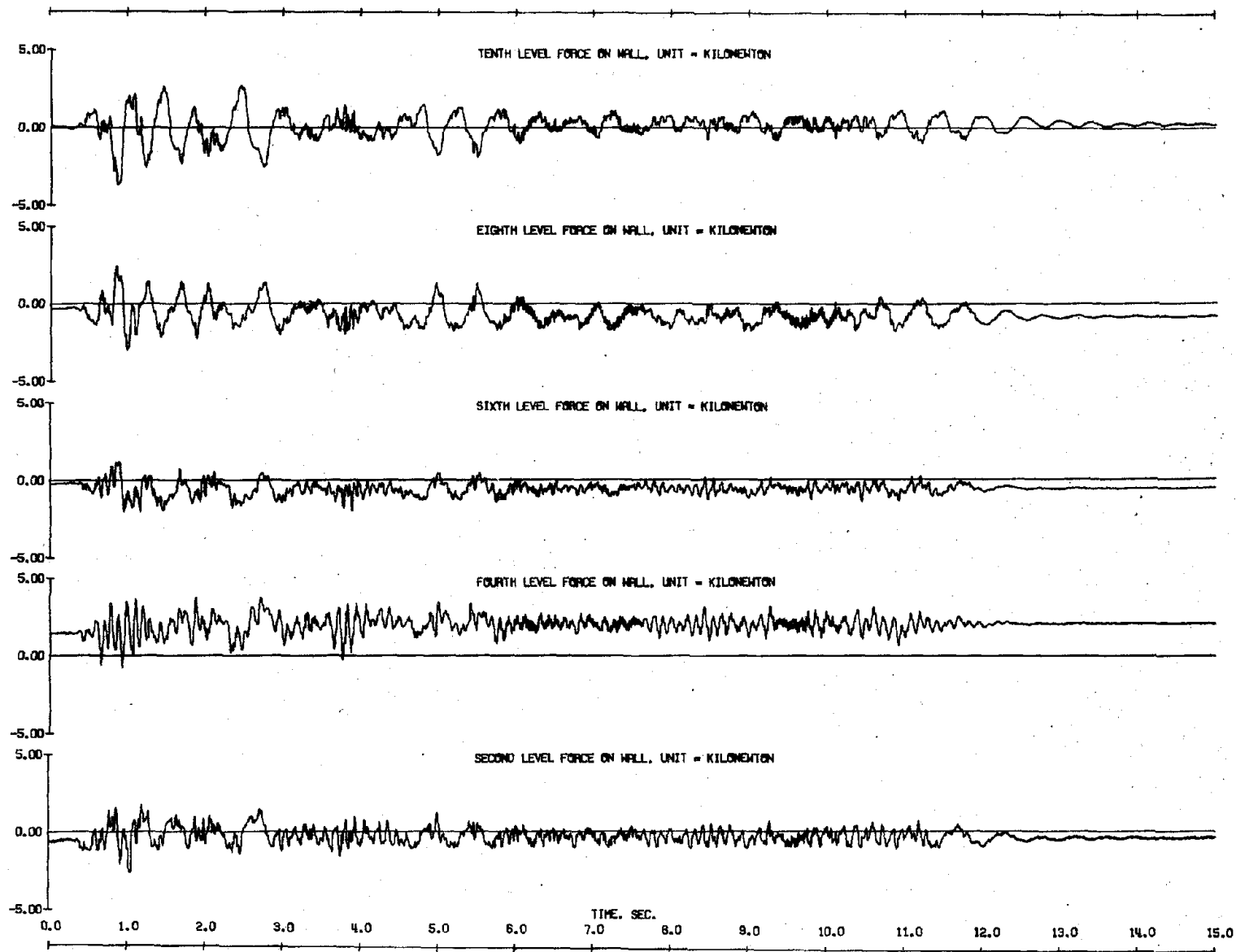
(e) Accelerations of Structure with Heavily Reinforced Wall
 Fig. 5.9 (contd.) Measured Response to Second El Centro Simulations



(f) Accelerations of Structure with Lightly Reinforced Wall
 Fig. 5.9 (contd.) Measured Response to Second El Centro Simulations

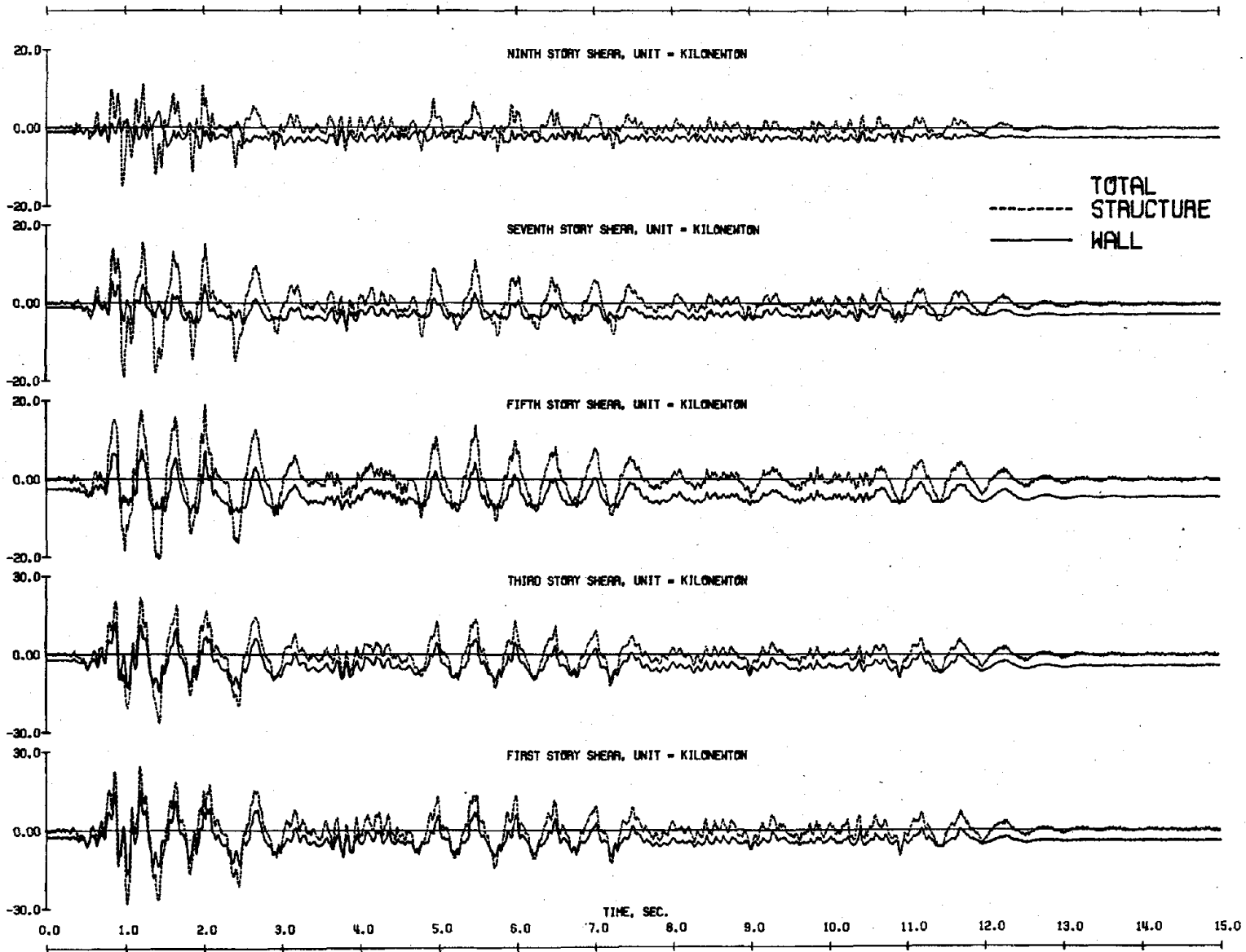


(g) Force Resisted by Heavily Reinforced Wall
 Fig. 5.9 (contd.) Measured Response to Second El Centro Simulations

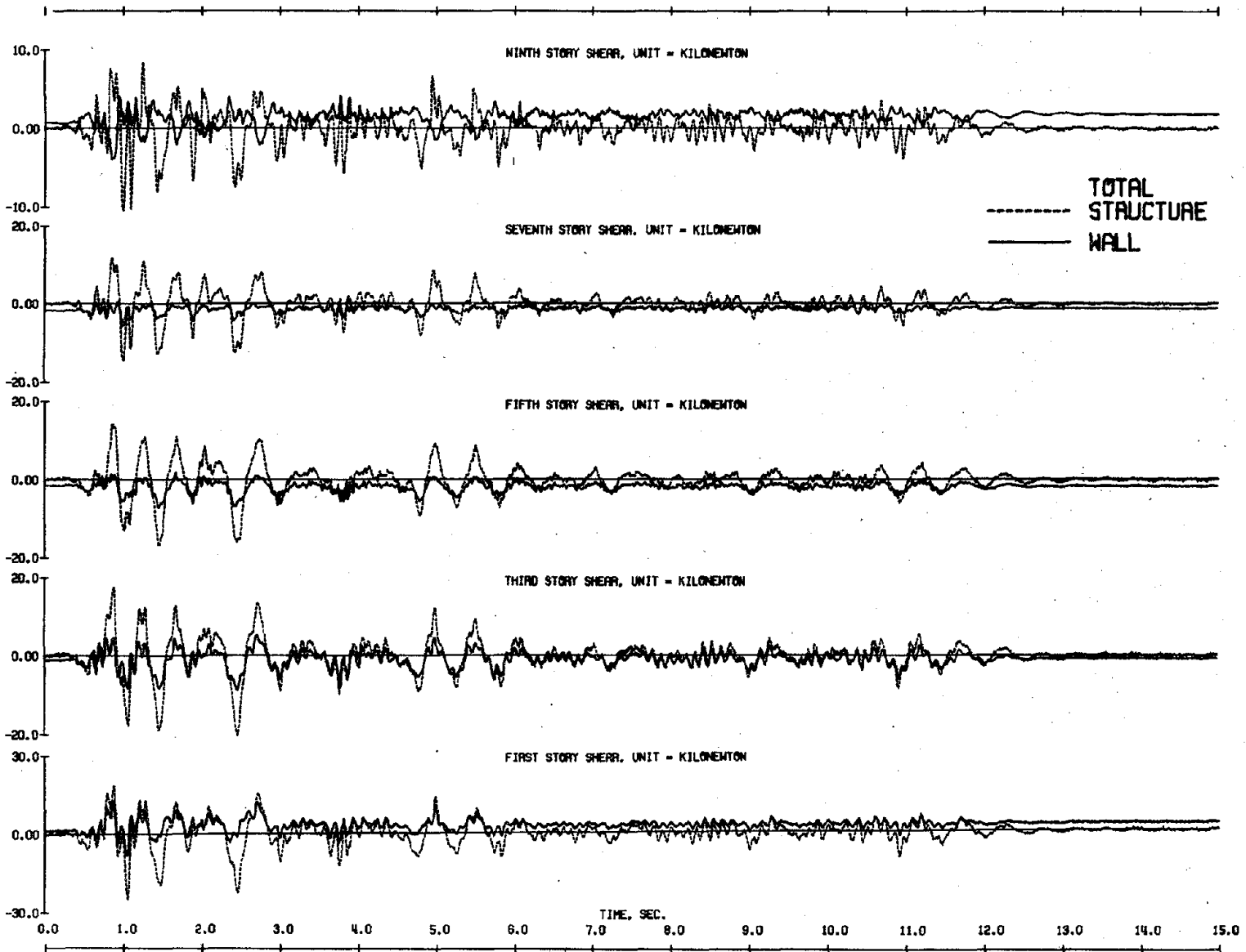


(h) Force Resisted by Lightly Reinforced Wall

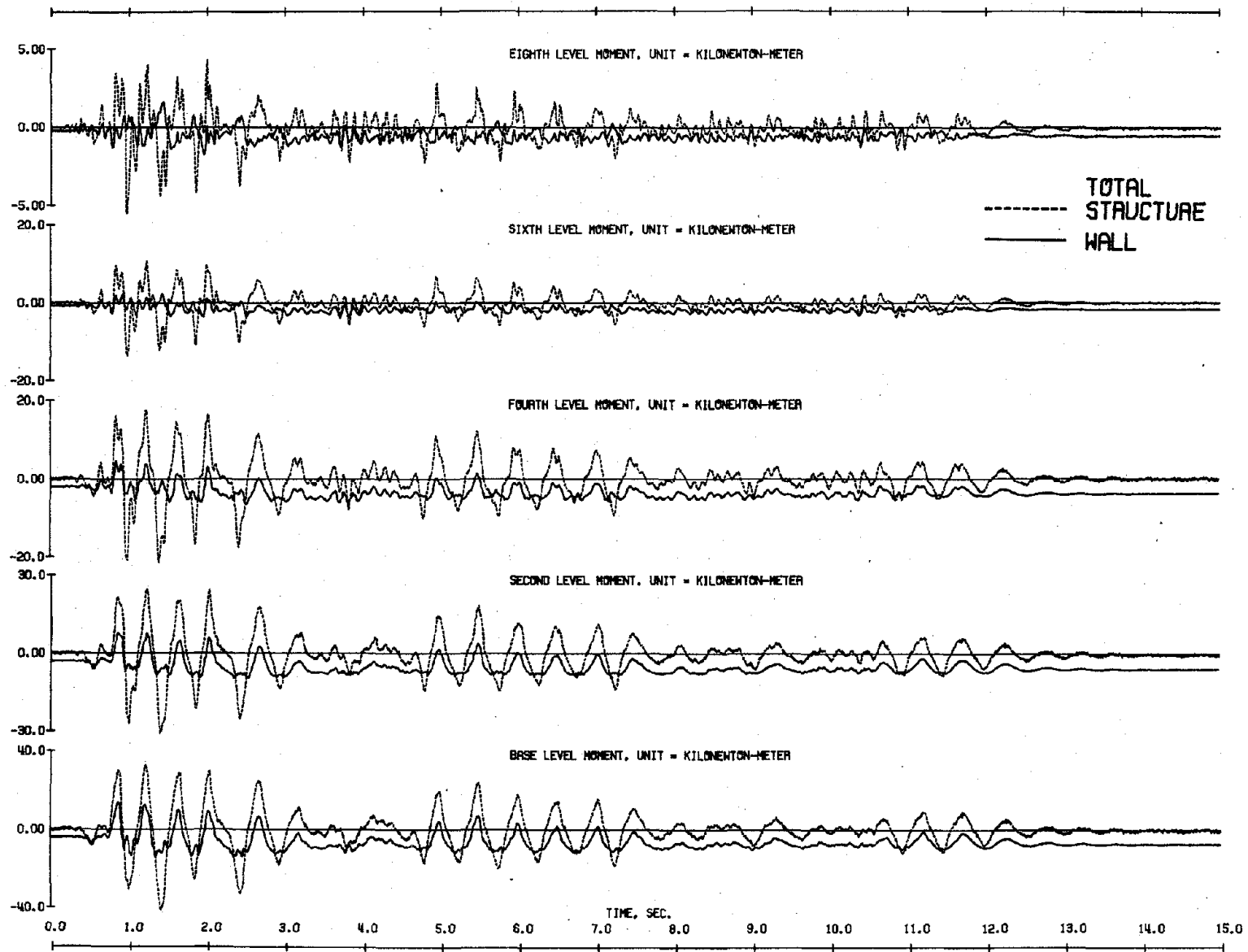
Fig. 5.9 (contd.) Measured Response to Second El Centro Simulations



(a) Shears of Structure with Heavily Reinforced Wall
 Fig. 5.10 Shear and Moment Response to Second El Centro Simulations



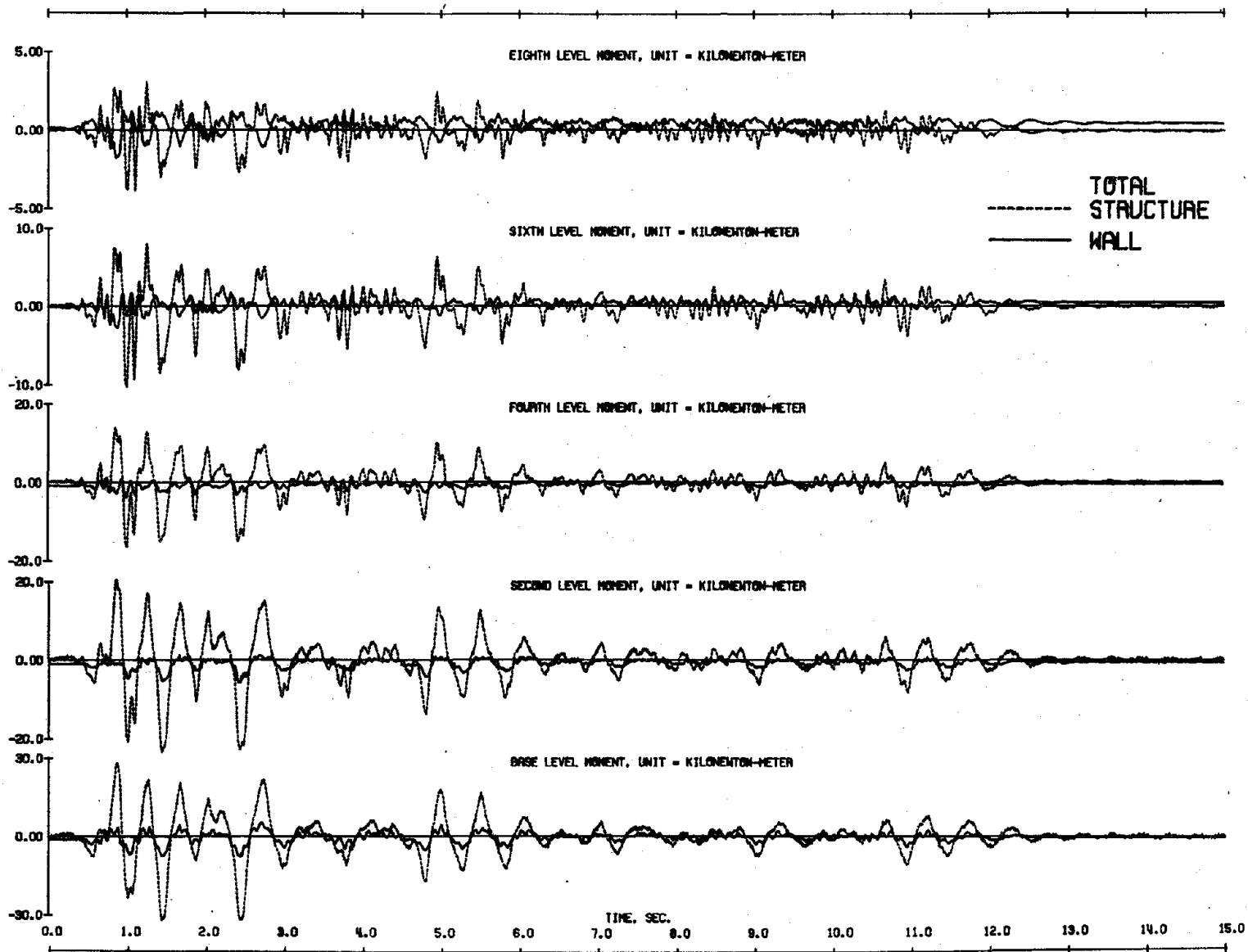
(b) Shears of Structure with Lightly Reinforced Wall
 Fig. 5.10 (contd.) Shear and Moment Response to Second El Centro Simulations



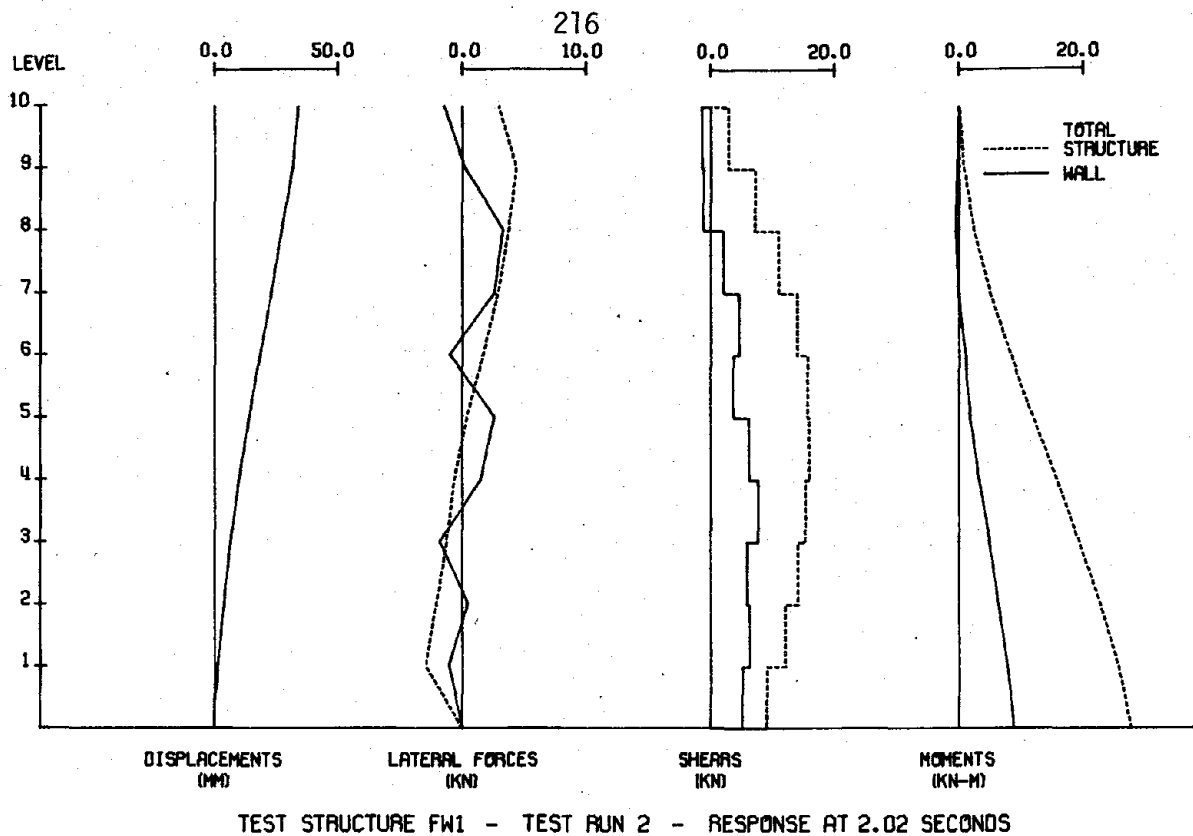
214

(c) Moments of Structure with Heavily Reinforced Wall

Fig. 5.10 (contd.) Shear and Moment Response to Second El Centro Simulations



(d) Moments of Structure with Lightly Reinforced Wall
 Fig. 5.10 (contd.) Shear and Moment Response to Second El Centro Simulations



(a) Structure with Heavily Reinforced Wall

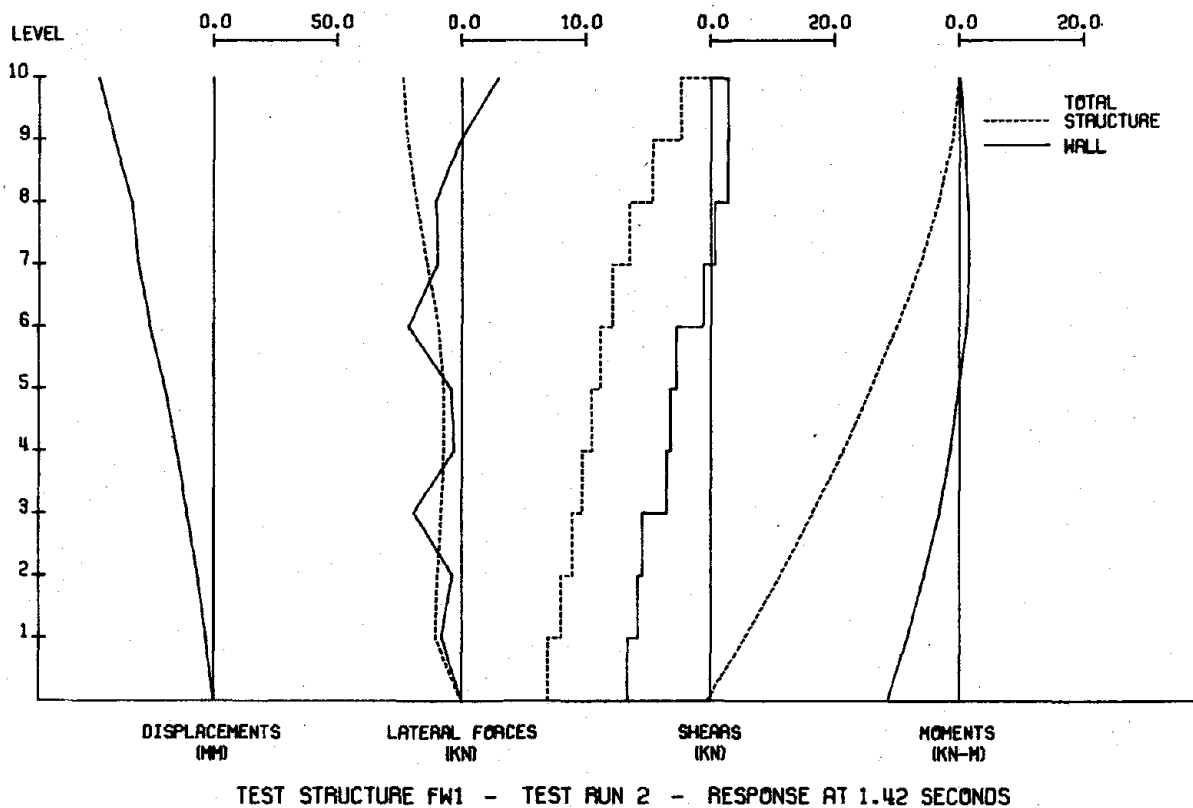
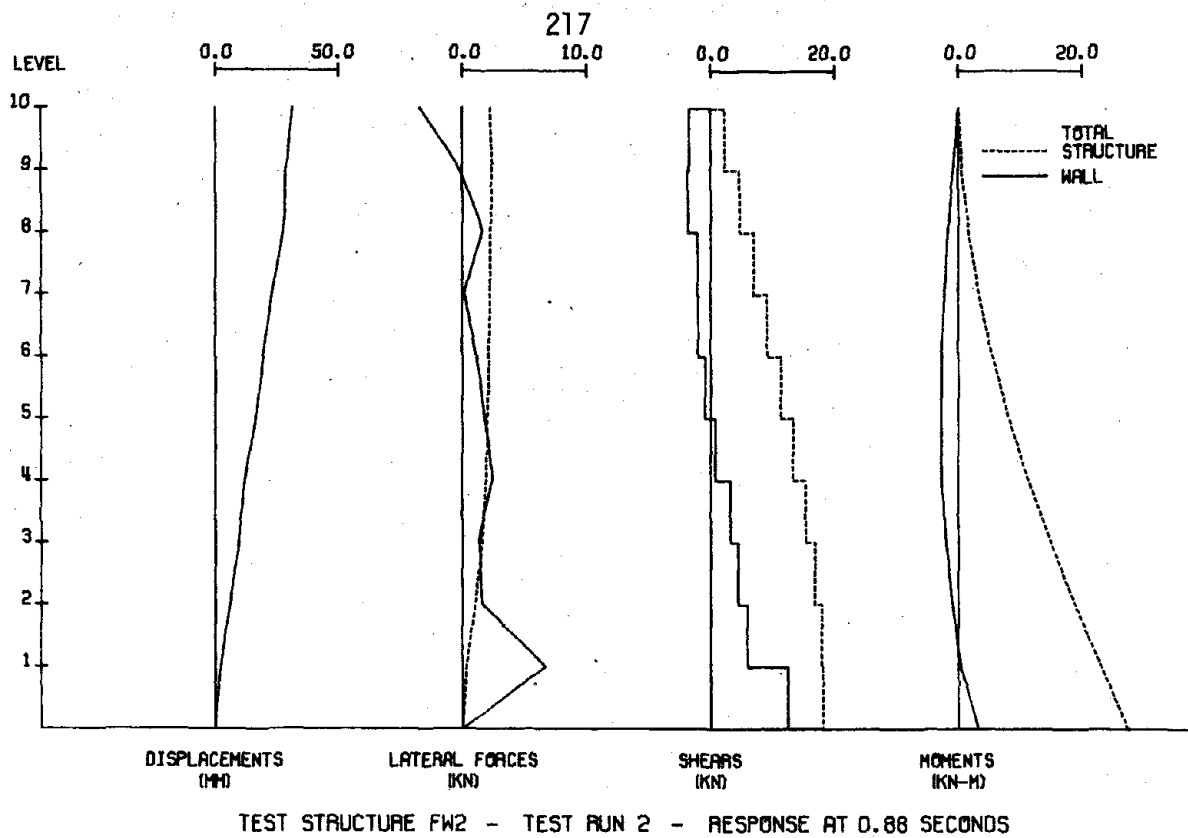


Fig. 5.11 Distributions of Response to Second El Centro Simulations



(b) Structure with Lightly Reinforced Wall

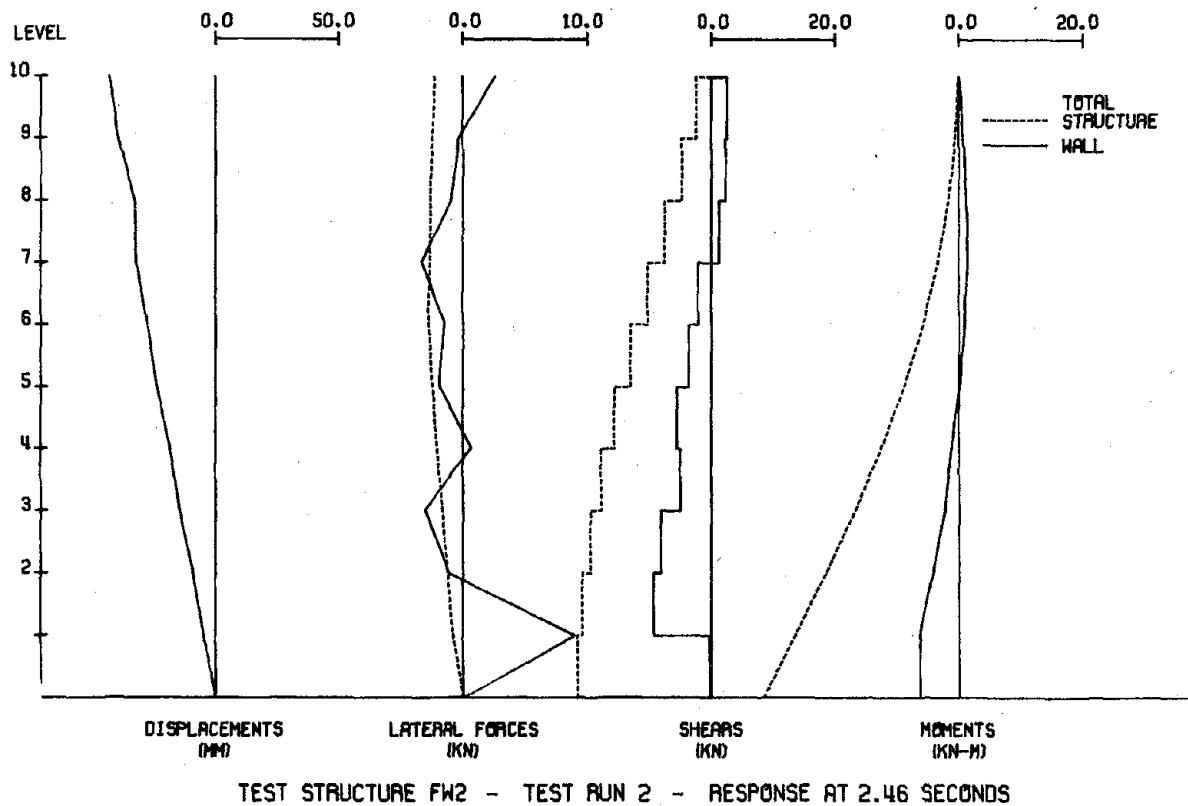
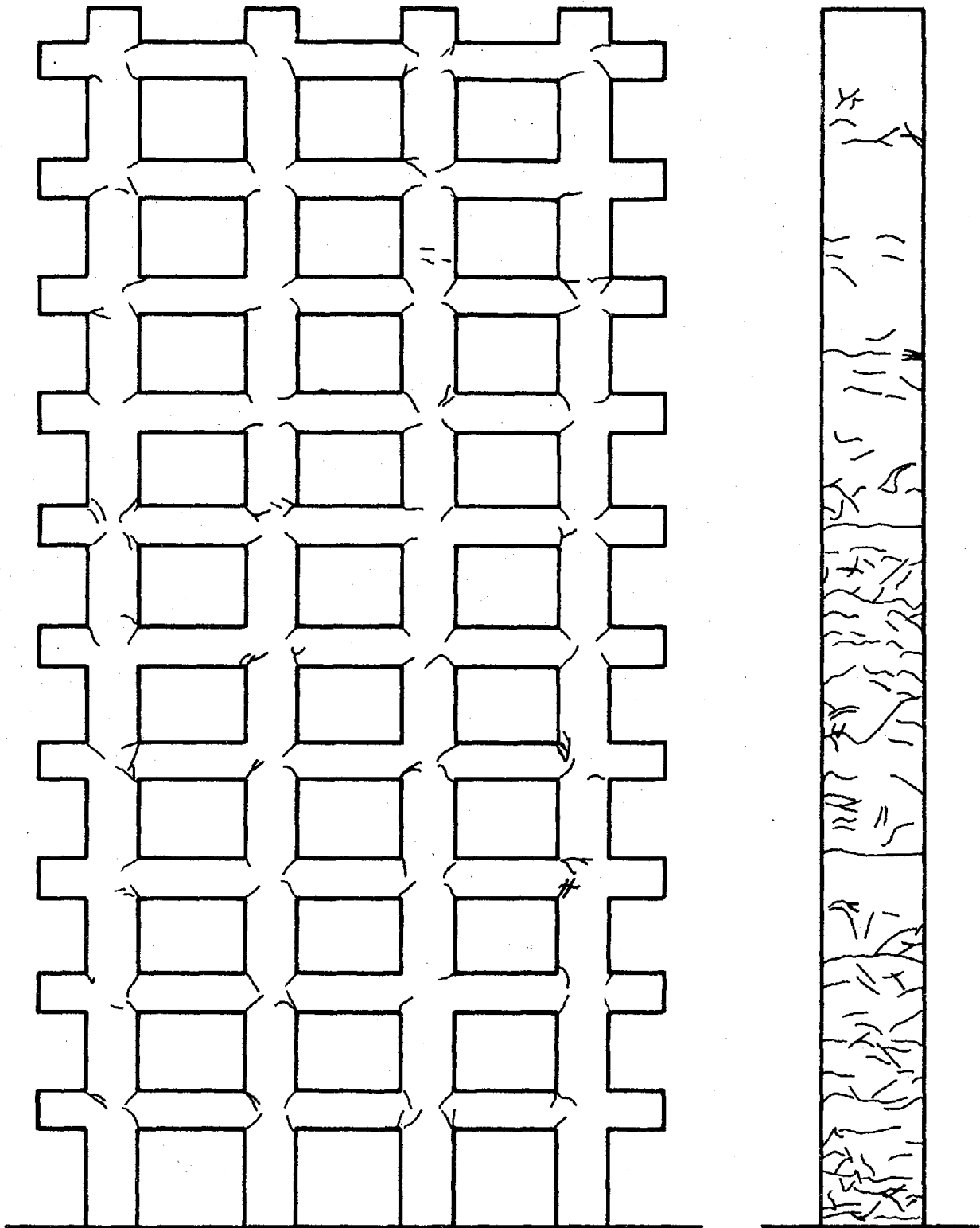


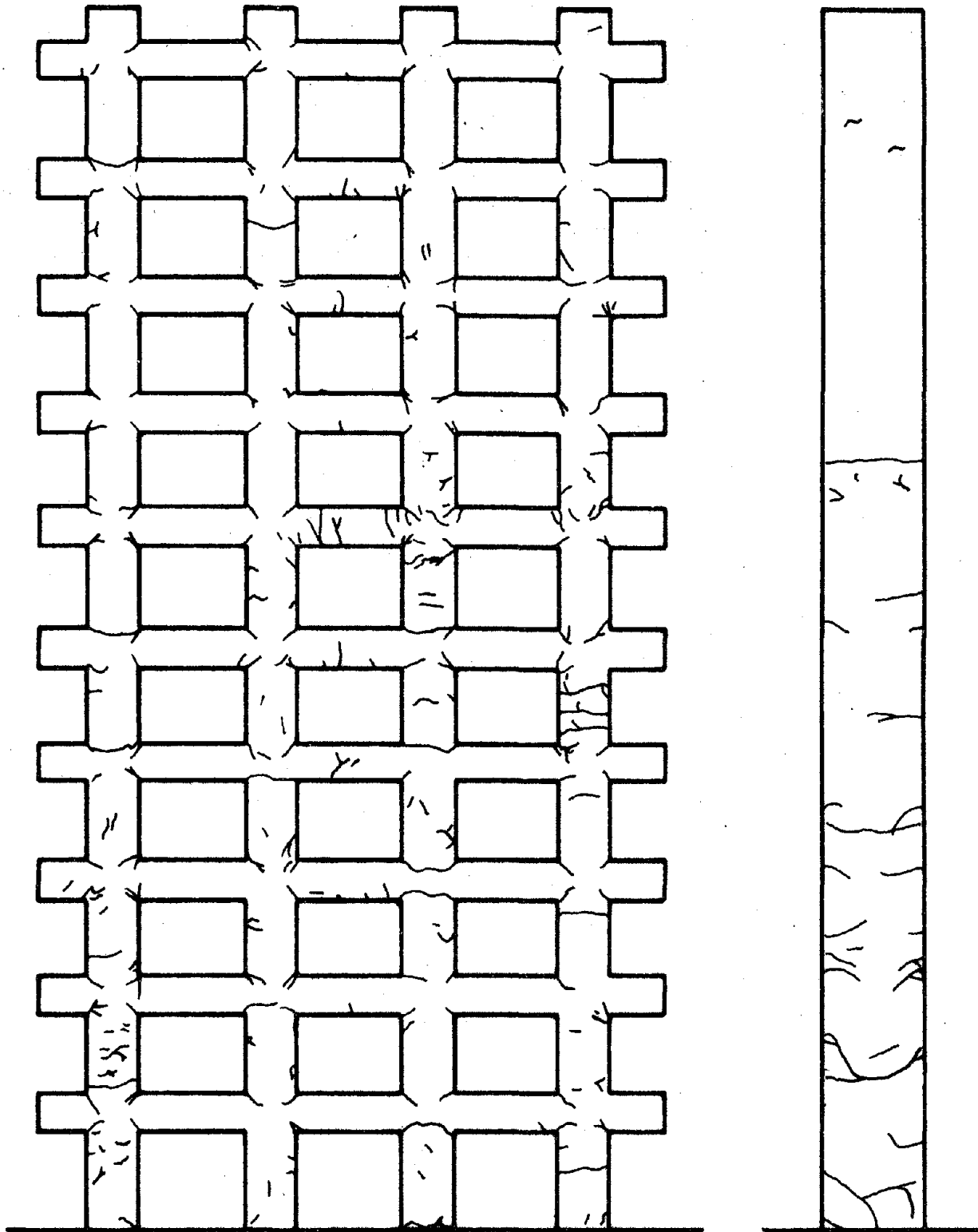
Fig. 5.11 (contd.) Distributions of Response to Second El Centro Simulations



(Not To Scale)

(a) Structure with Heavily Reinforced Wall

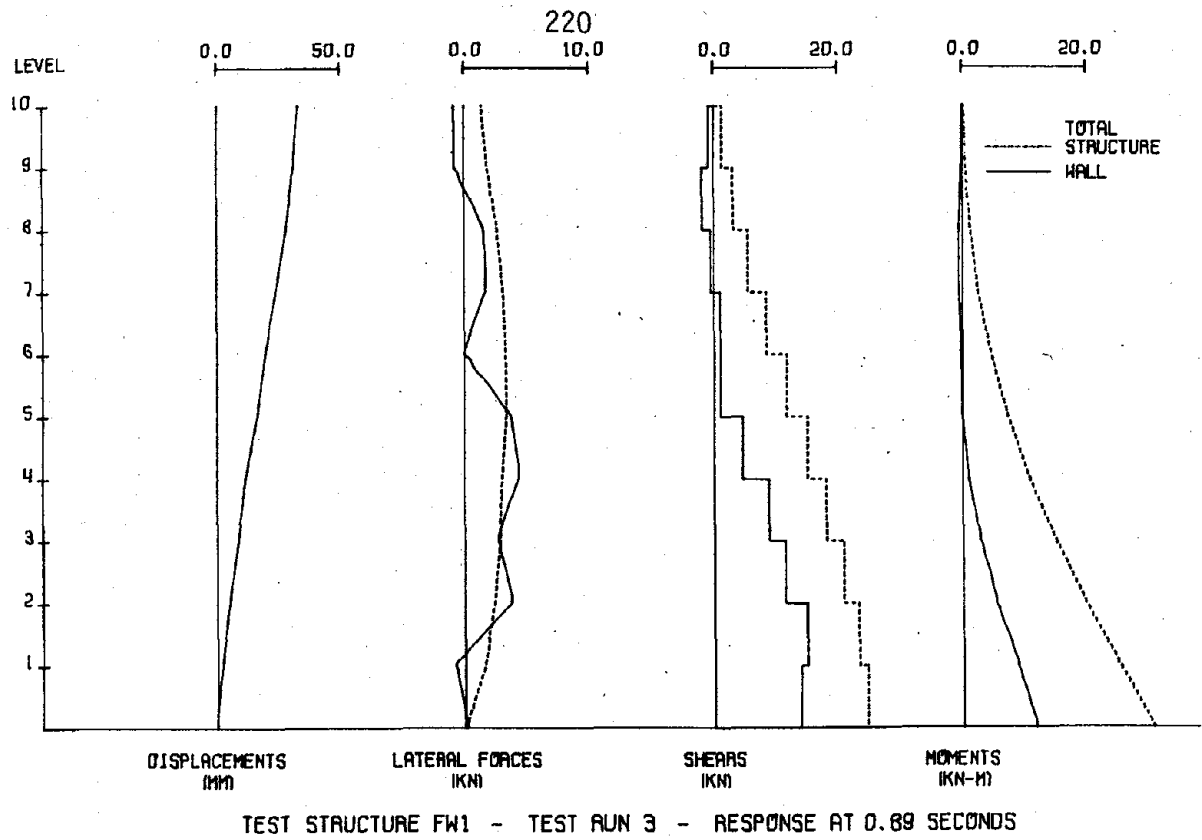
Fig. 5.12 Observed Crack Patterns following Second El Centro Simulations.



(Not To Scale)

(b) Structure with Lightly Reinforced Wall

Fig. 5.12 (contd.) Observed Crack Patterns following Second El Centro Simulations.



(a) Structure with Heavily Reinforced Wall

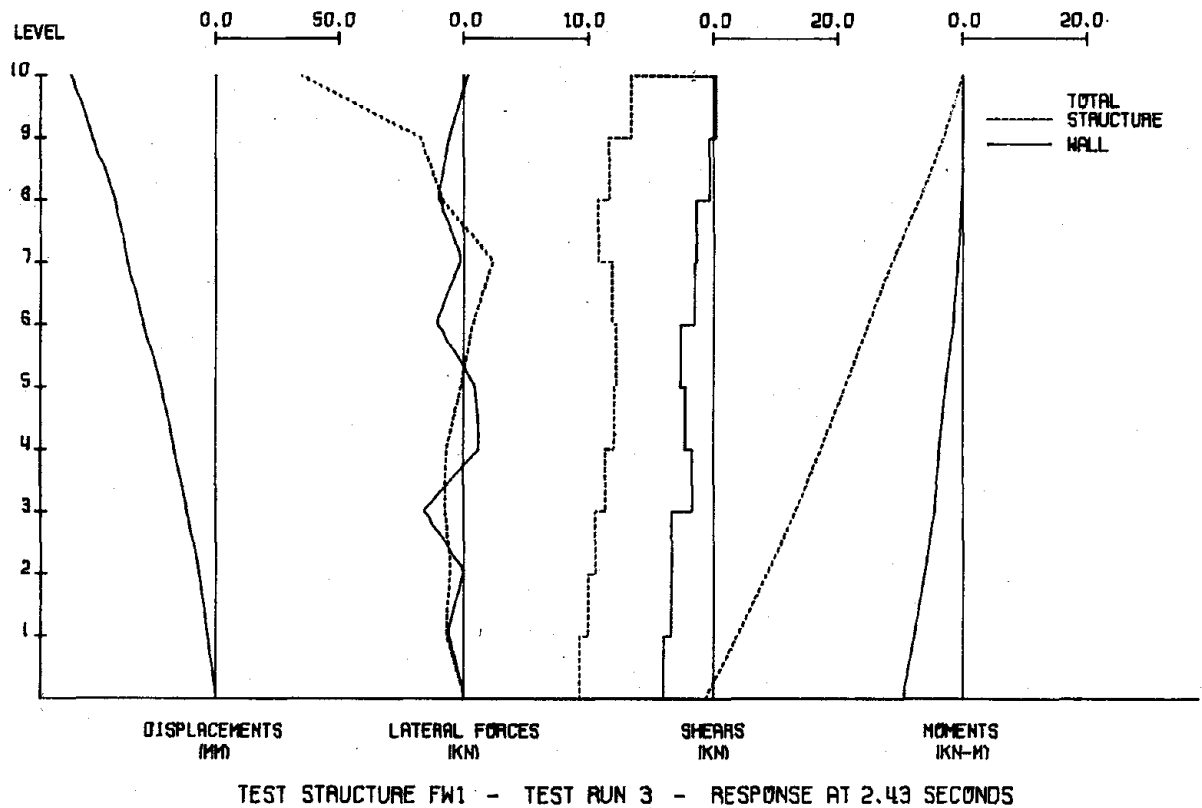
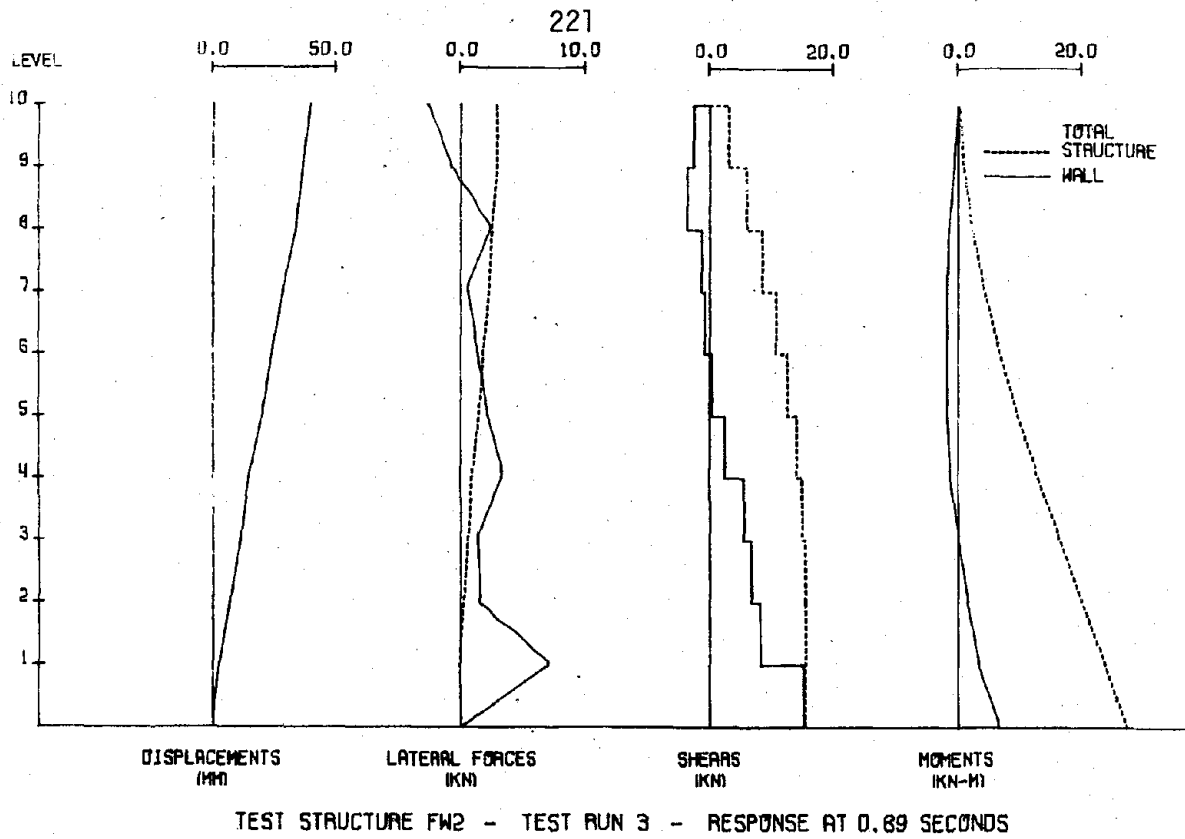


Fig. 5.13 Distributions of Response to Third El Centro Simulations



(b) Structure with Lightly Reinforced Wall

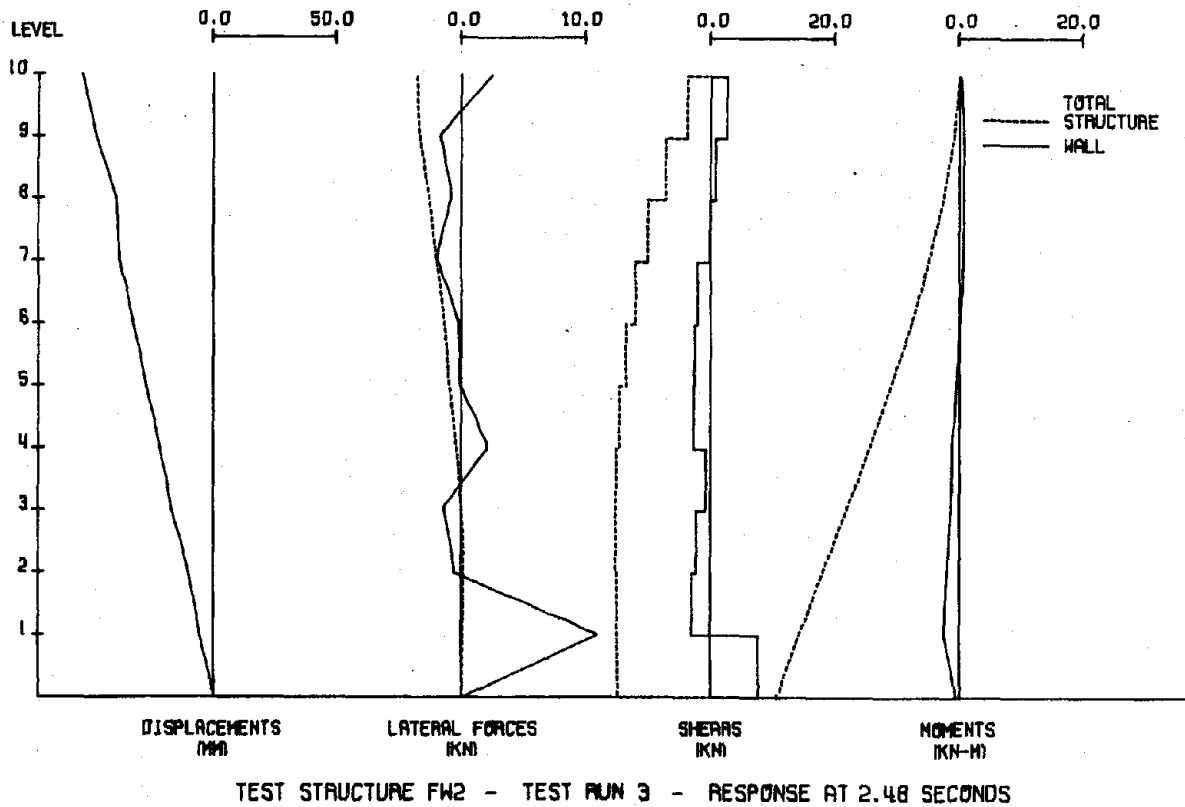
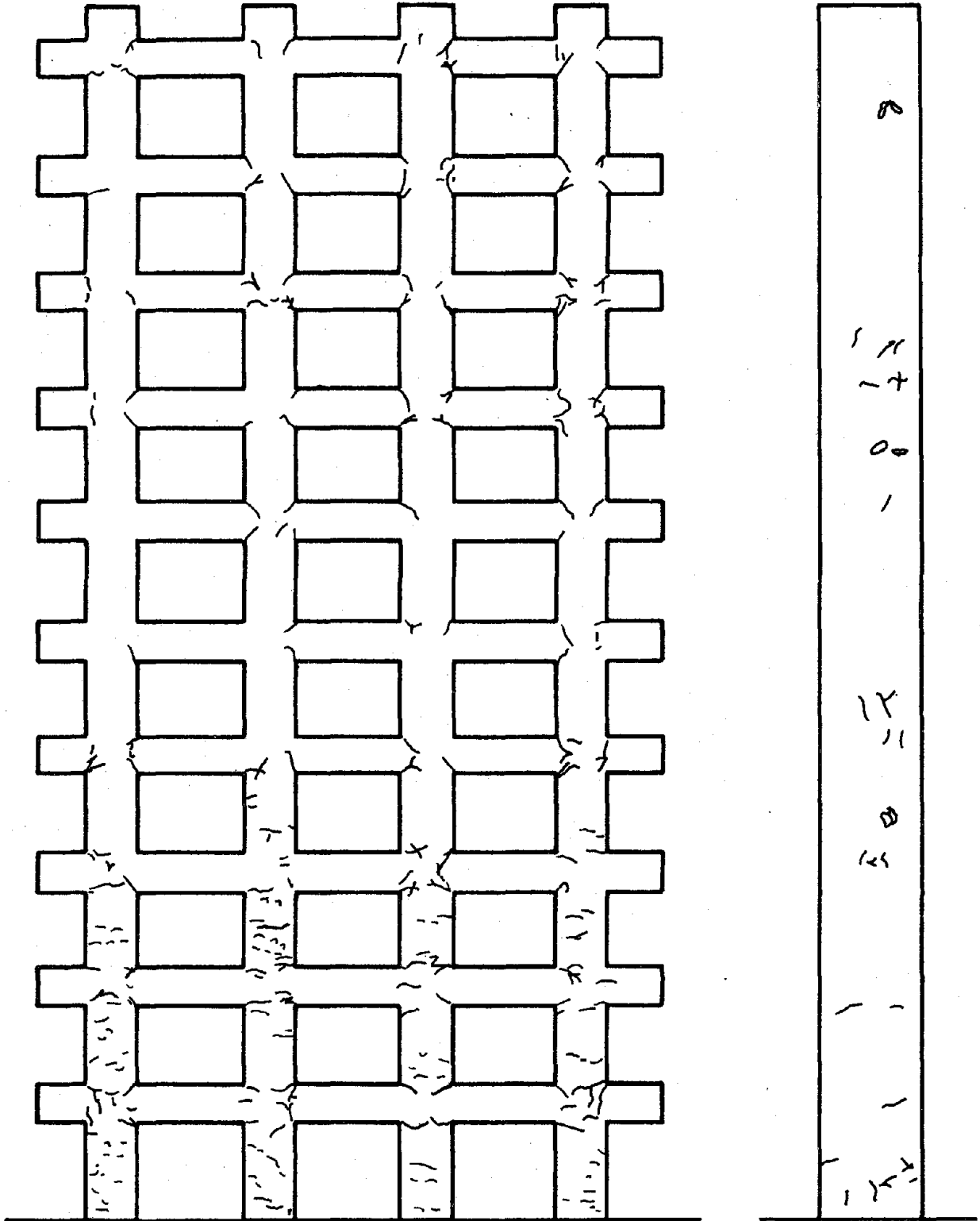


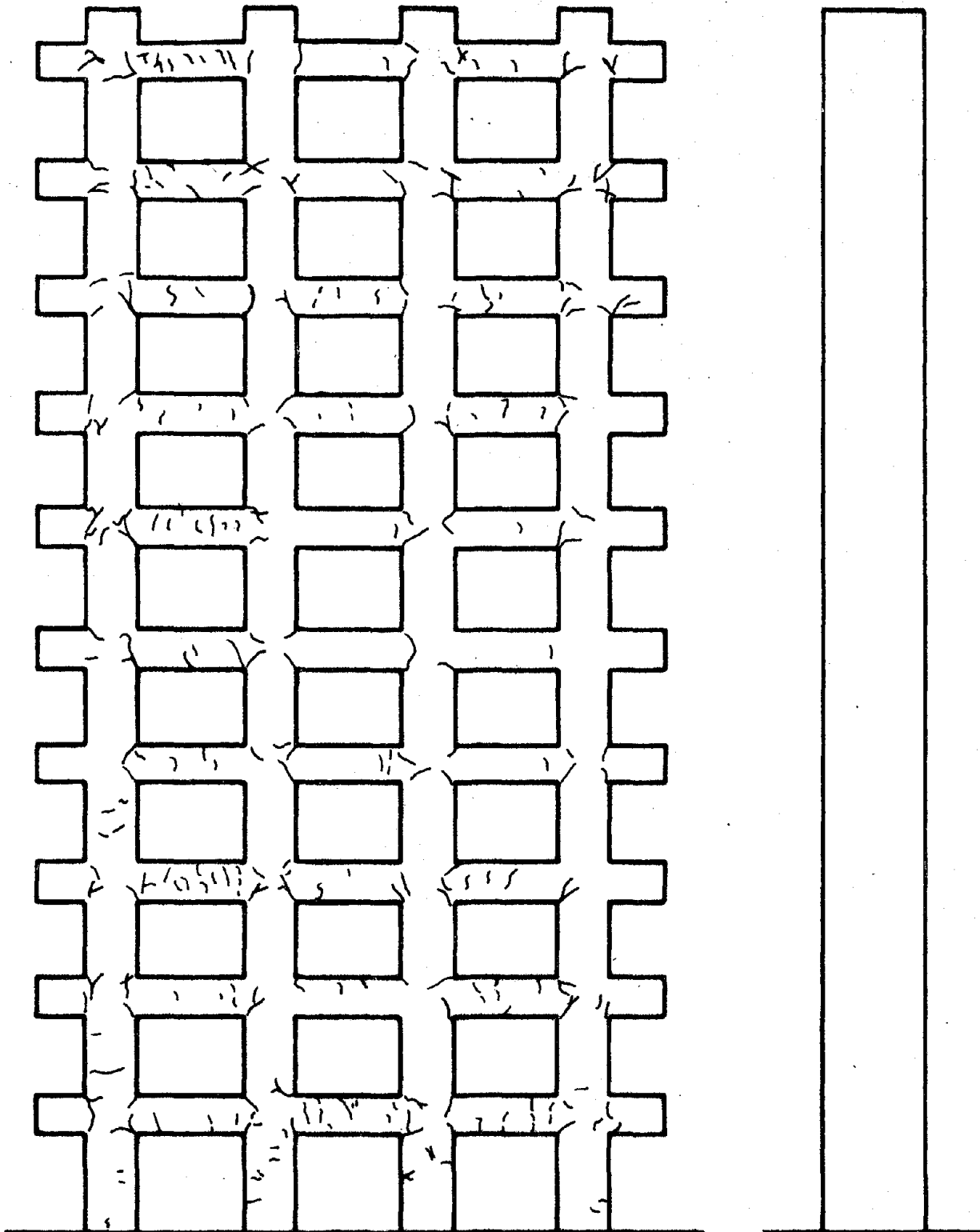
Fig. 5.13 (contd.) Distributions of Response to Third E1 Centro Simulations



(Not To Scale)

(a) Structure with Heavily Reinforced Wall

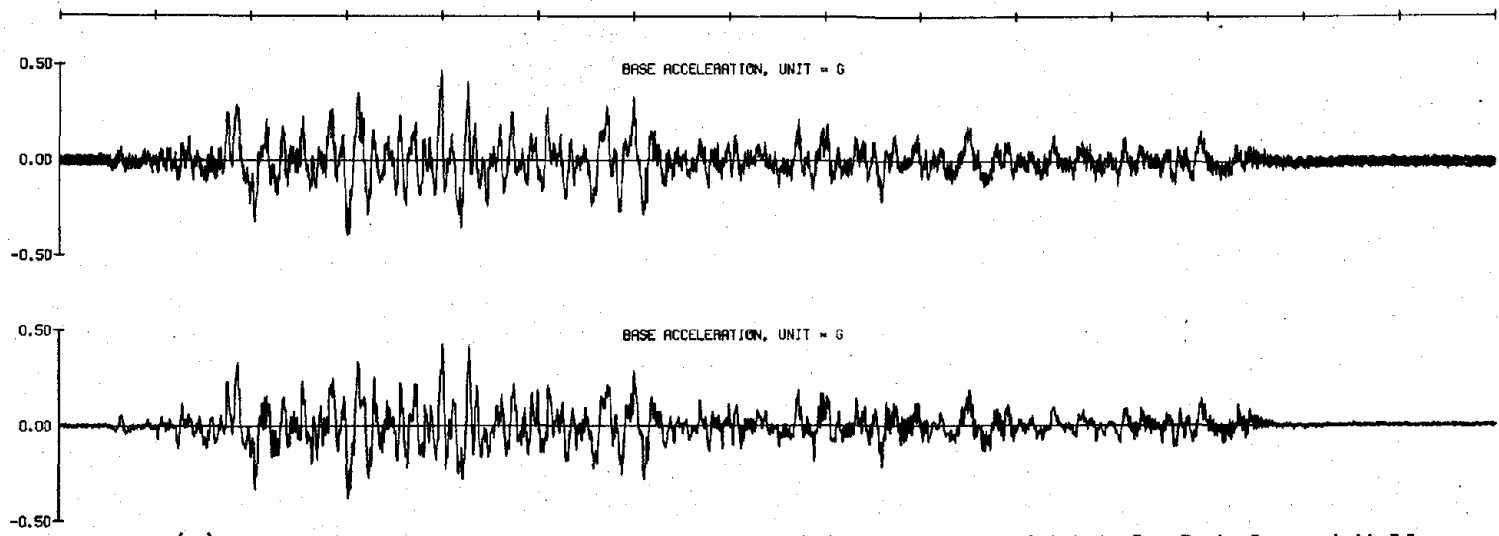
Fig. 5.14 Observed Crack Patterns before Initial Taft Simulations



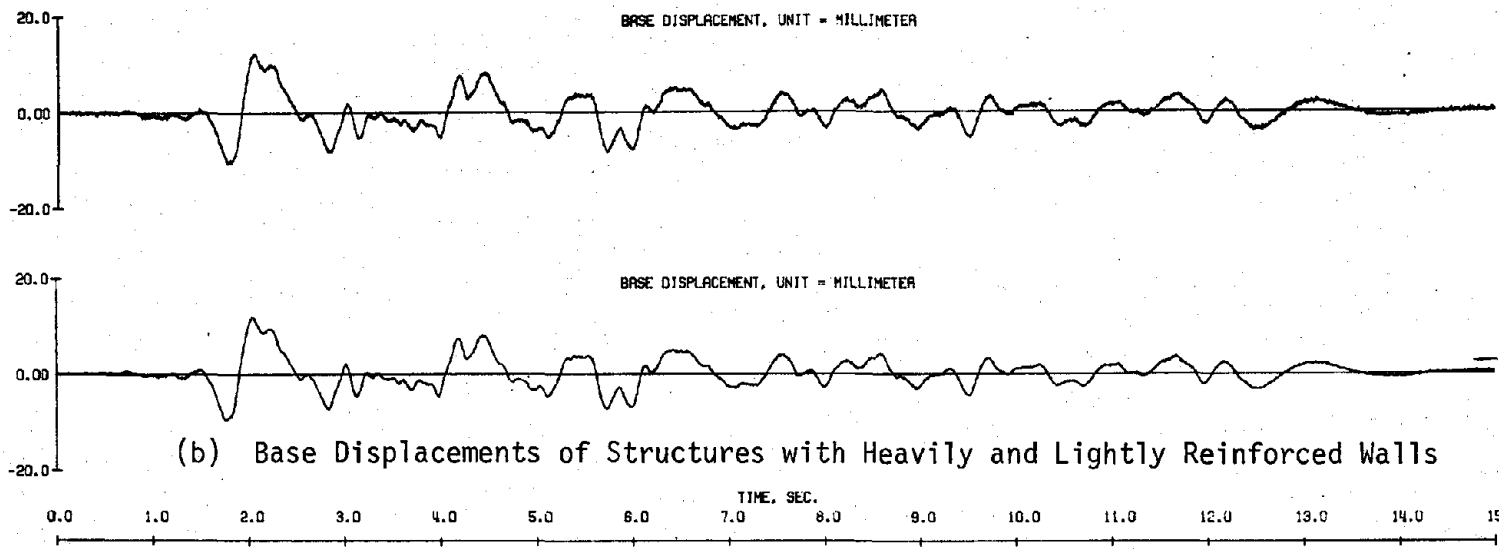
(Not To Scale)

(b) Structure with Lightly Reinforced Wall

Fig. 5.14 (contd.) Observed Crack Patterns before Initial Taft Simulations



(a) Base Accelerations of Structures with Heavily and Lightly Reinforced Walls



(b) Base Displacements of Structures with Heavily and Lightly Reinforced Walls

Fig. 5.15 Measured Motions of Initial Taft Simulations

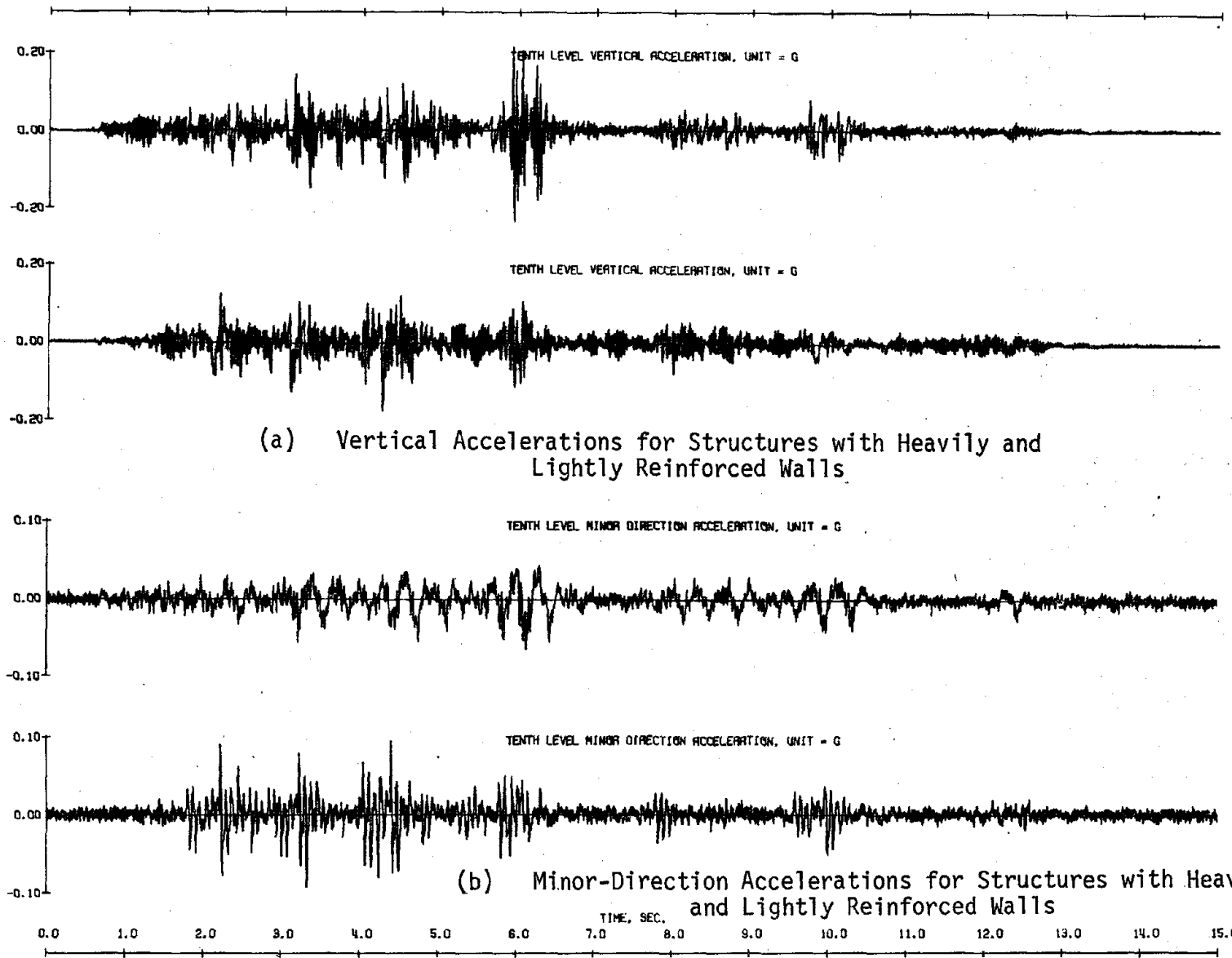
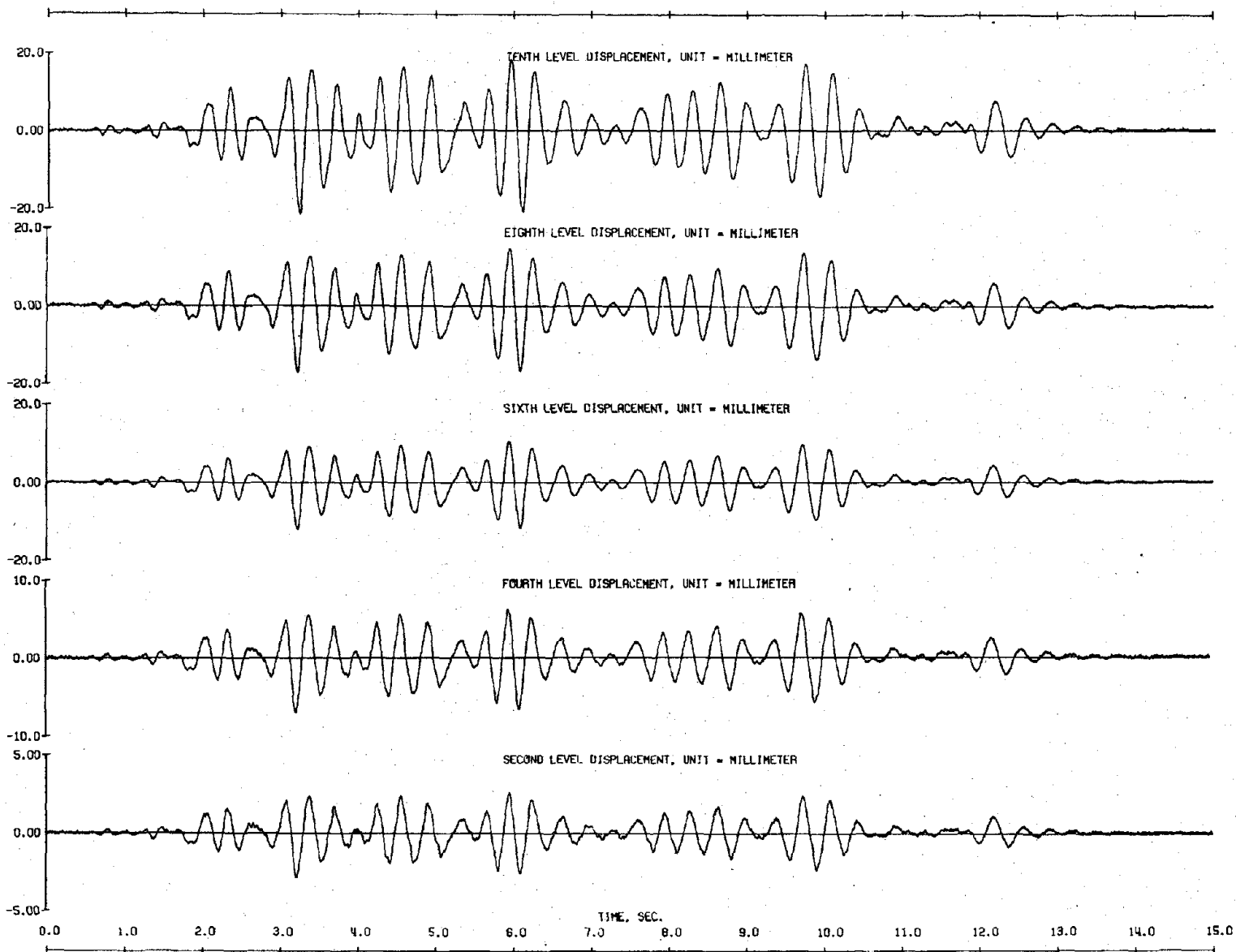
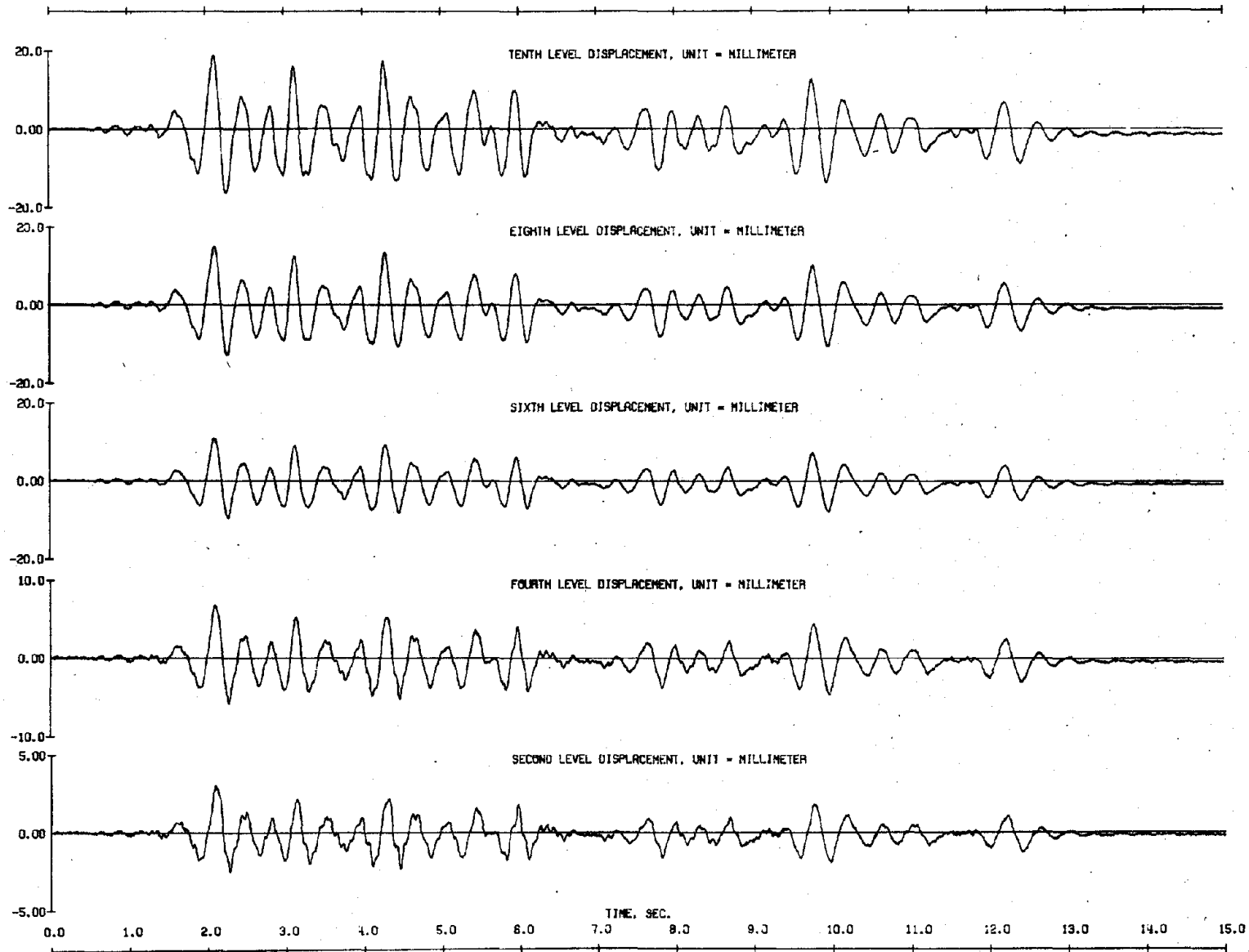


Fig. 5.16 Measured Response to Initial Taft Simulations

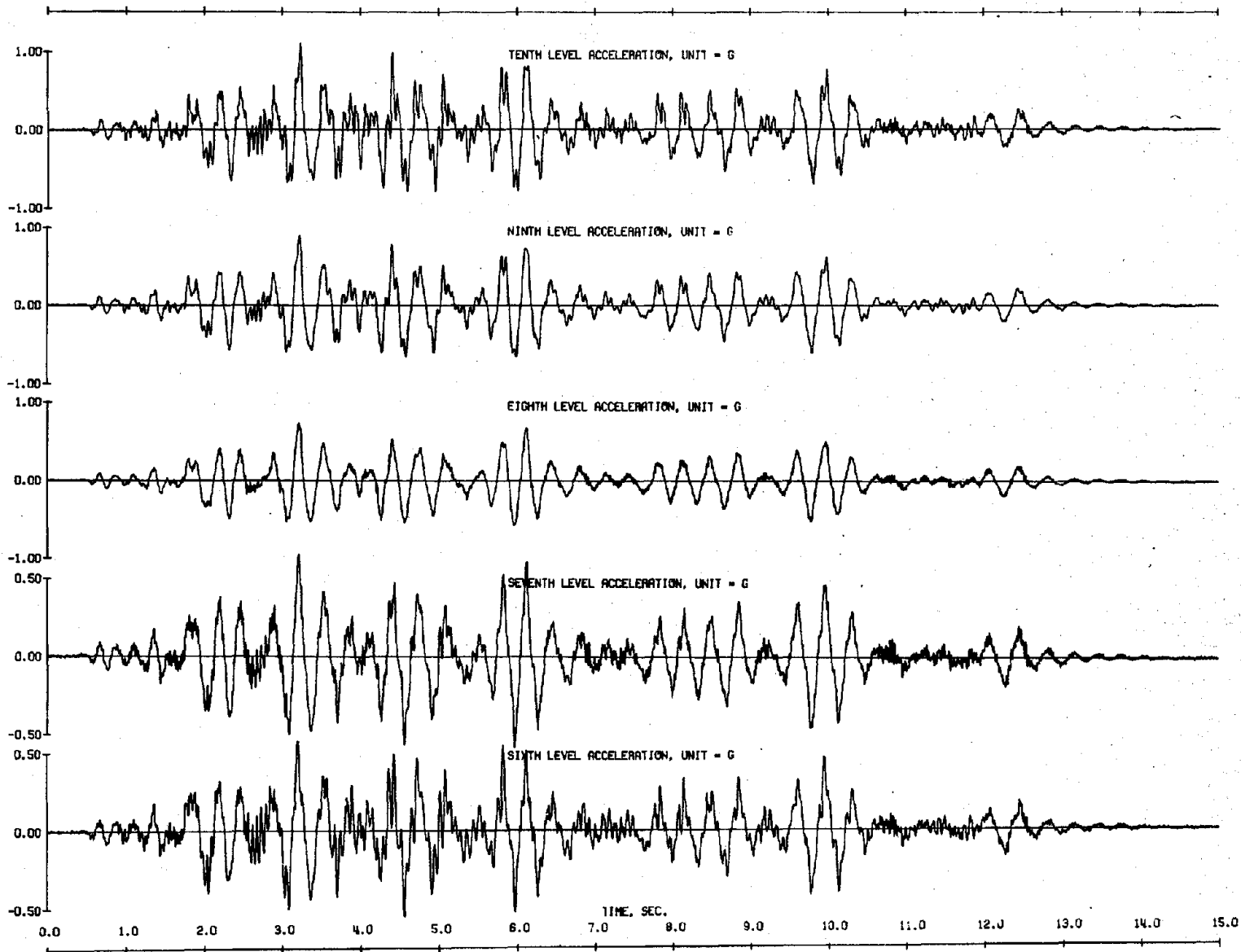


(c) Displacements of Structure with Heavily Reinforced Wall
 Fig. 5.16 (contd.) Measured Response to Initial Taft Simulations

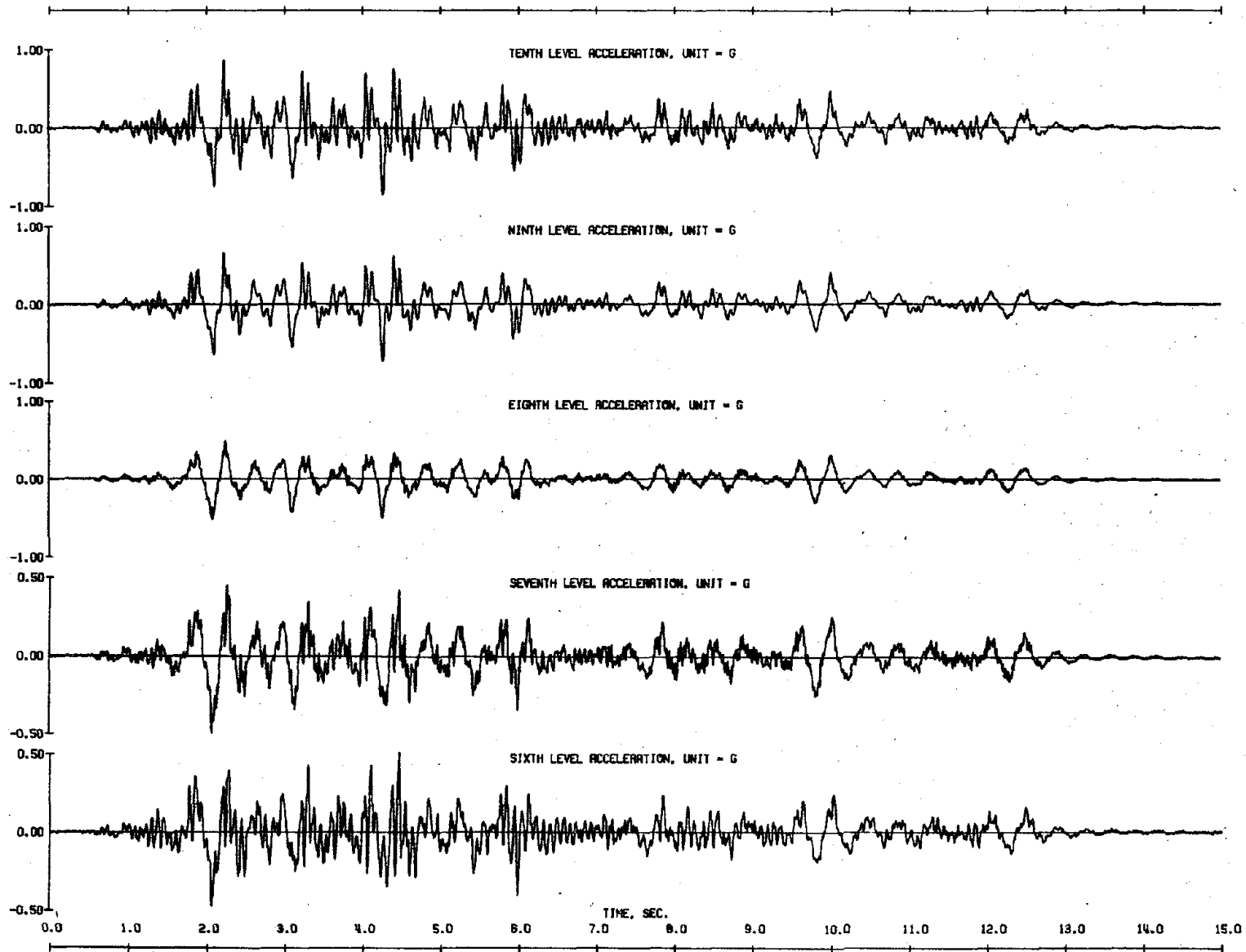


227

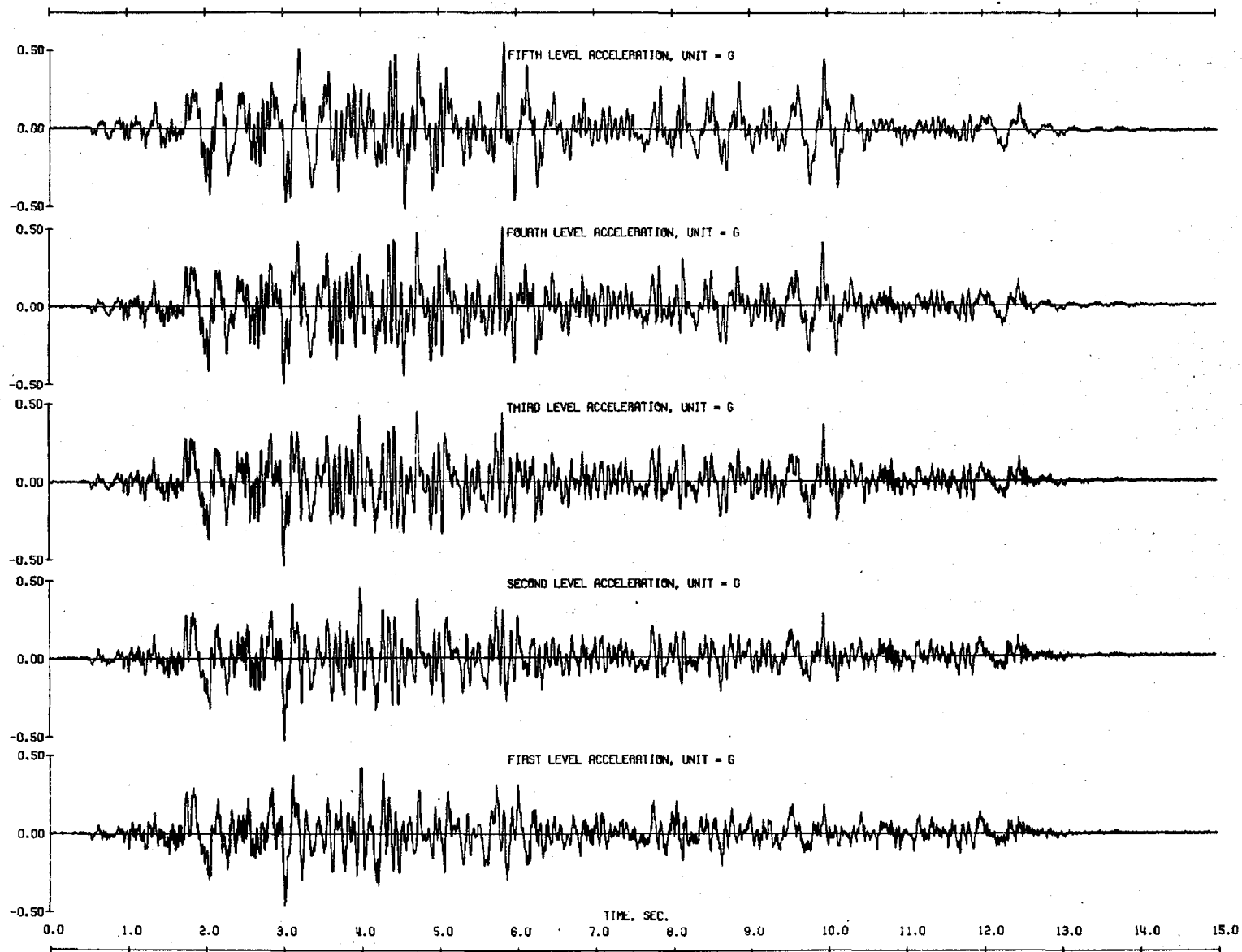
(d) Displacements of Structure with Lightly Reinforced Wall
 Fig. 5.16 (contd.) Measured Response to Initial Taft Simulations



(e) Accelerations of Structure with Heavily Reinforced Wall
 Fig. 5.16 (contd.) Measured Response to Initial Taft Simulations

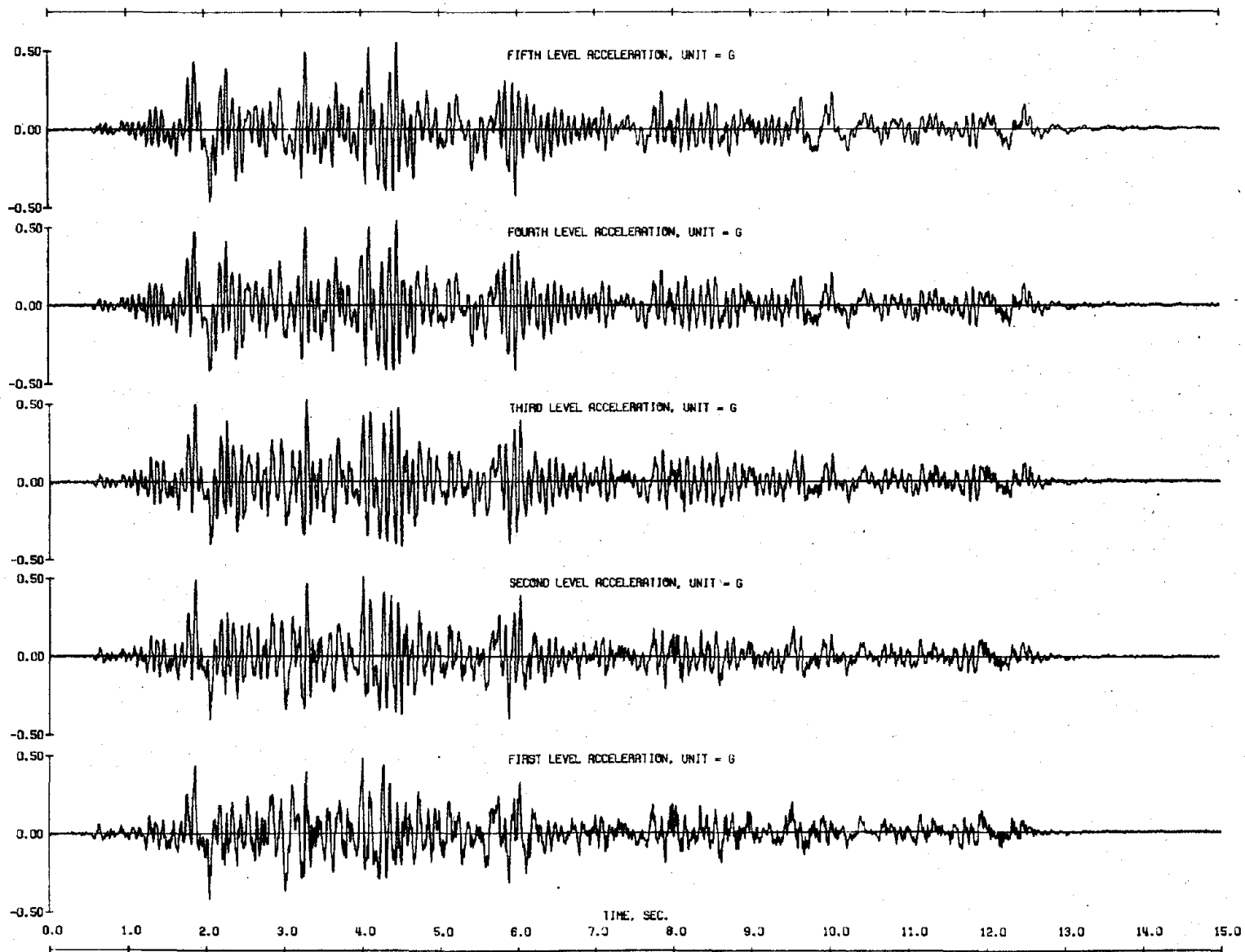


(f) Accelerations of Structure with Lightly Reinforced Wall
 Fig. 5.16 (contd.) Measured Response to Initial Taft Simulations

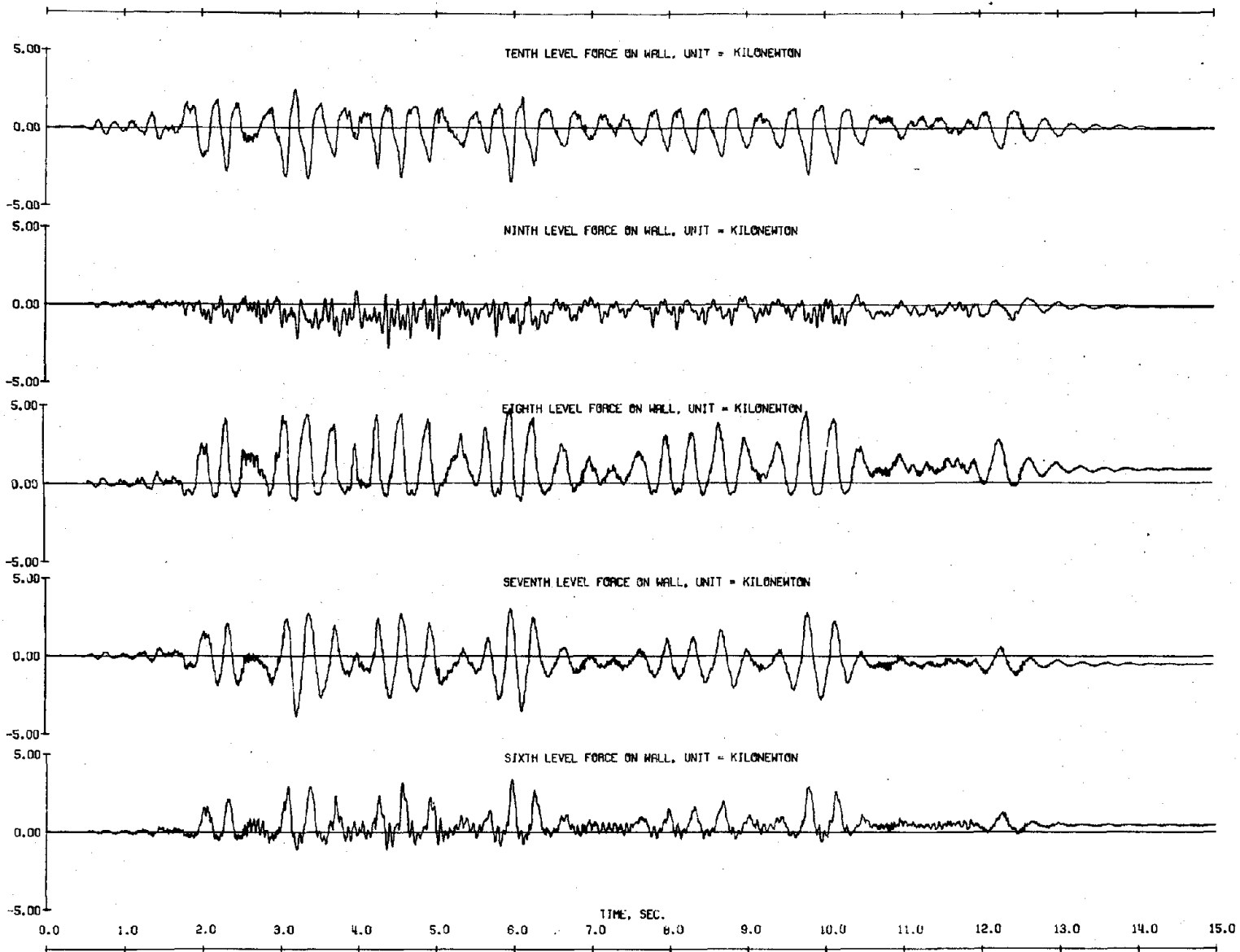


(e) (contd.) Accelerations of Structure with Heavily Reinforced Wall

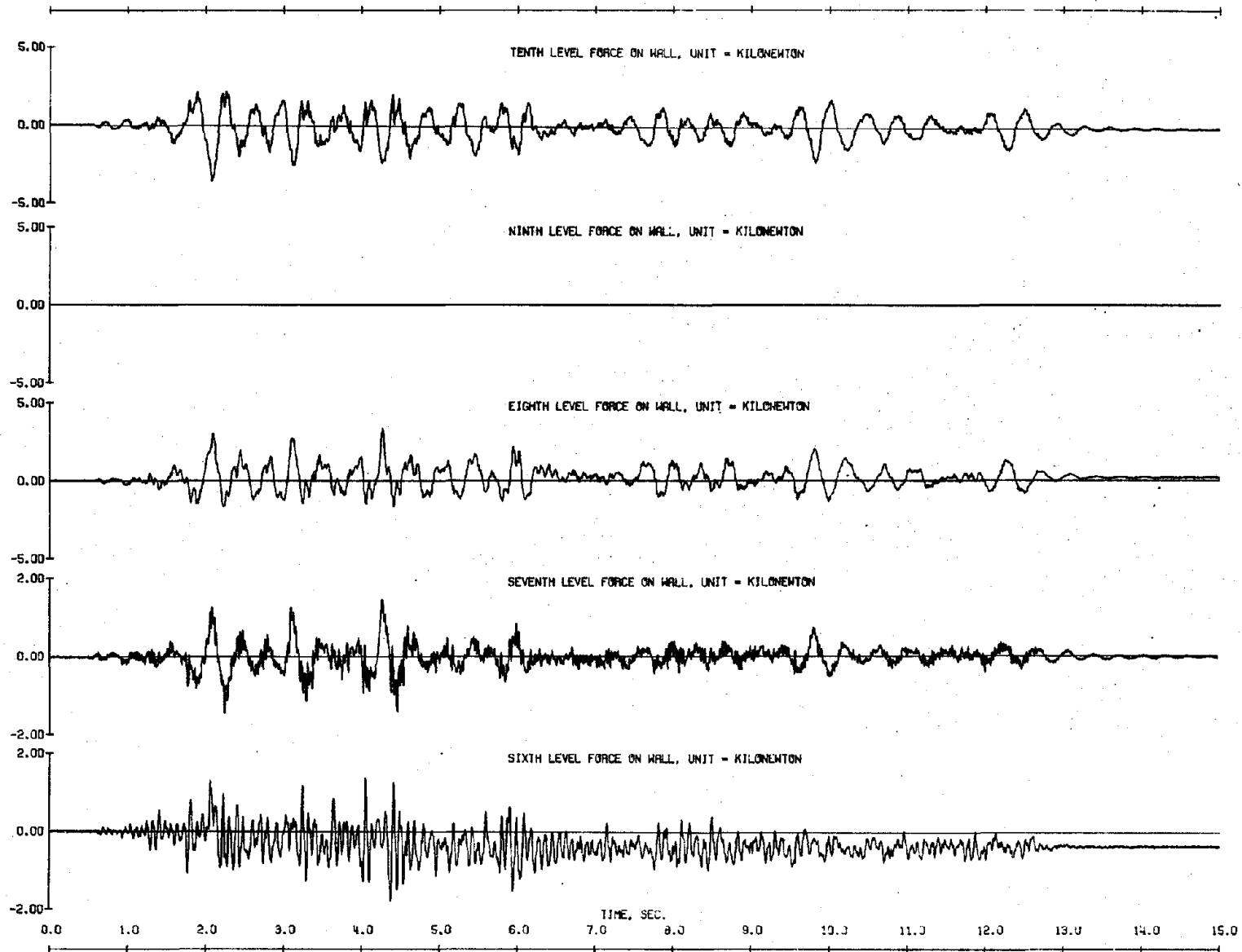
Fig. 5.16 (contd.) Measured Response to Initial Taft Simulations



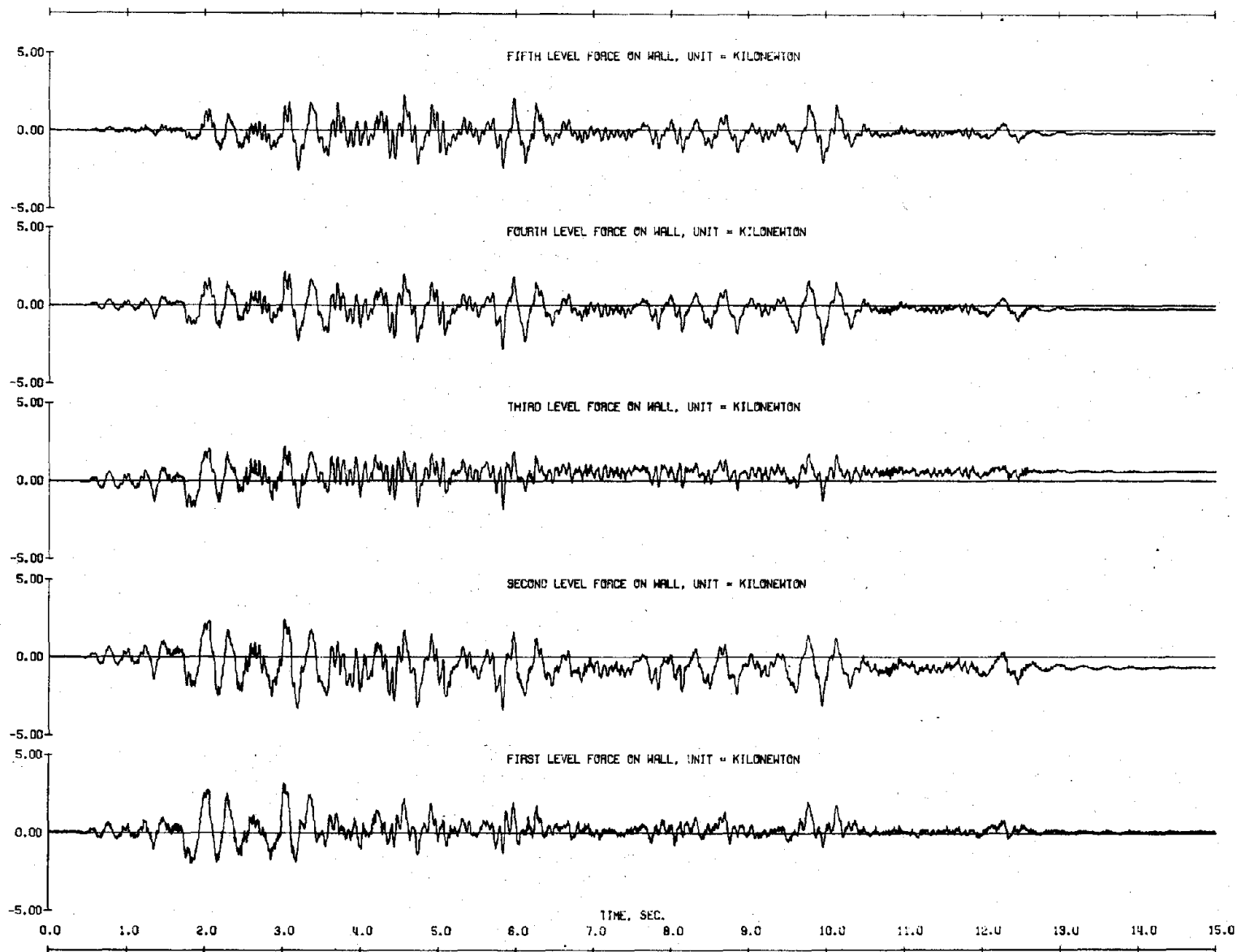
(f) (contd.) Accelerations of Structure with Lightly Reinforced Wall
 Fig. 5.16 (contd.) Measured Response to Initial Taft Simulations



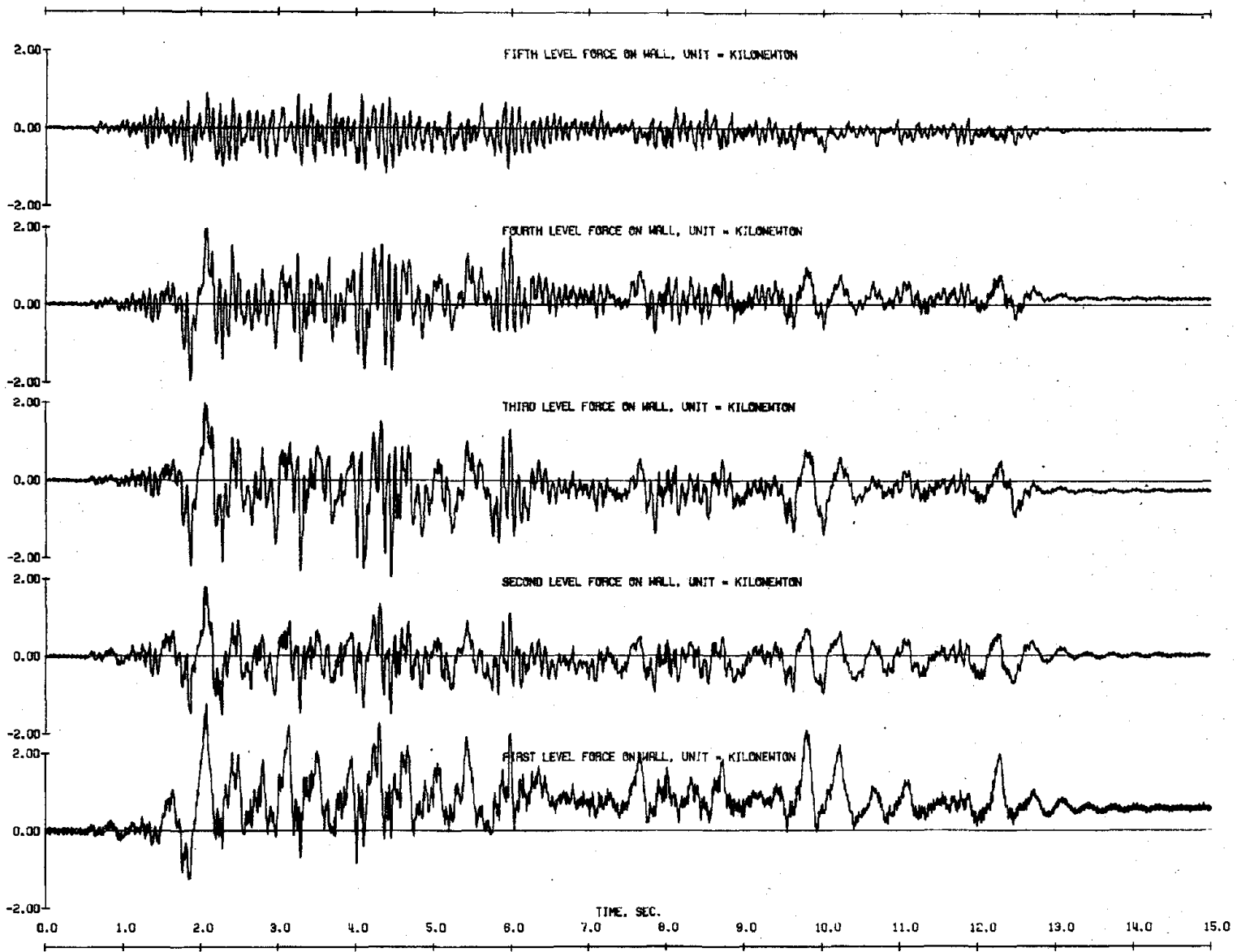
(g) Force Resisted by Heavily Reinforced Wall
 Fig. 5.16 (contd.) Measured Response to Initial Taft Simulations



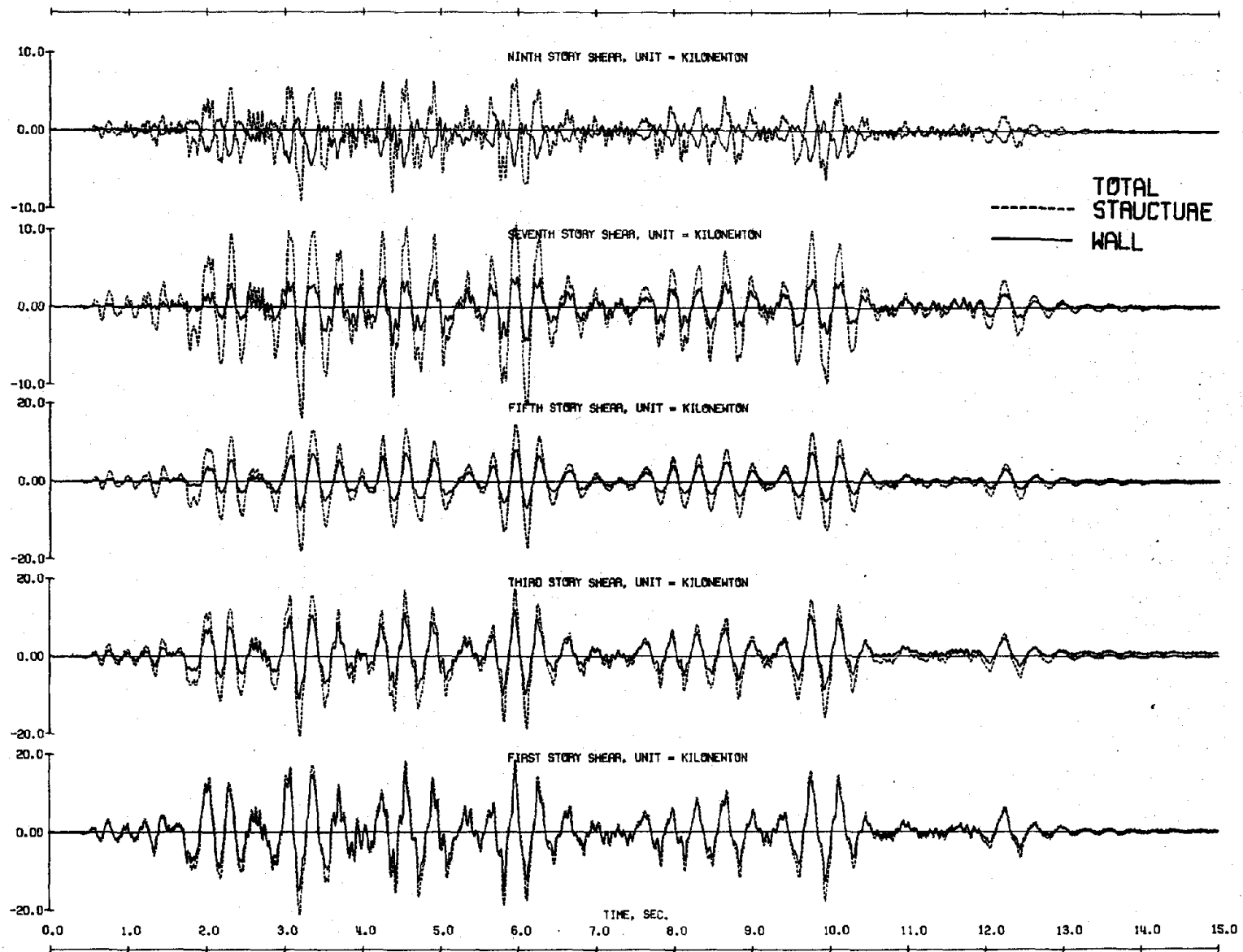
(h) Force Resisted by Lightly Reinforced Wall
 Fig. 5.16 (contd.) Measured Response to Initial Taft Simulations



(g) (contd.) Force Resisted by Heavily Reinforced Wall
 Fig. 5.16 (contd.) Measured Response to Initial Taft Simulations

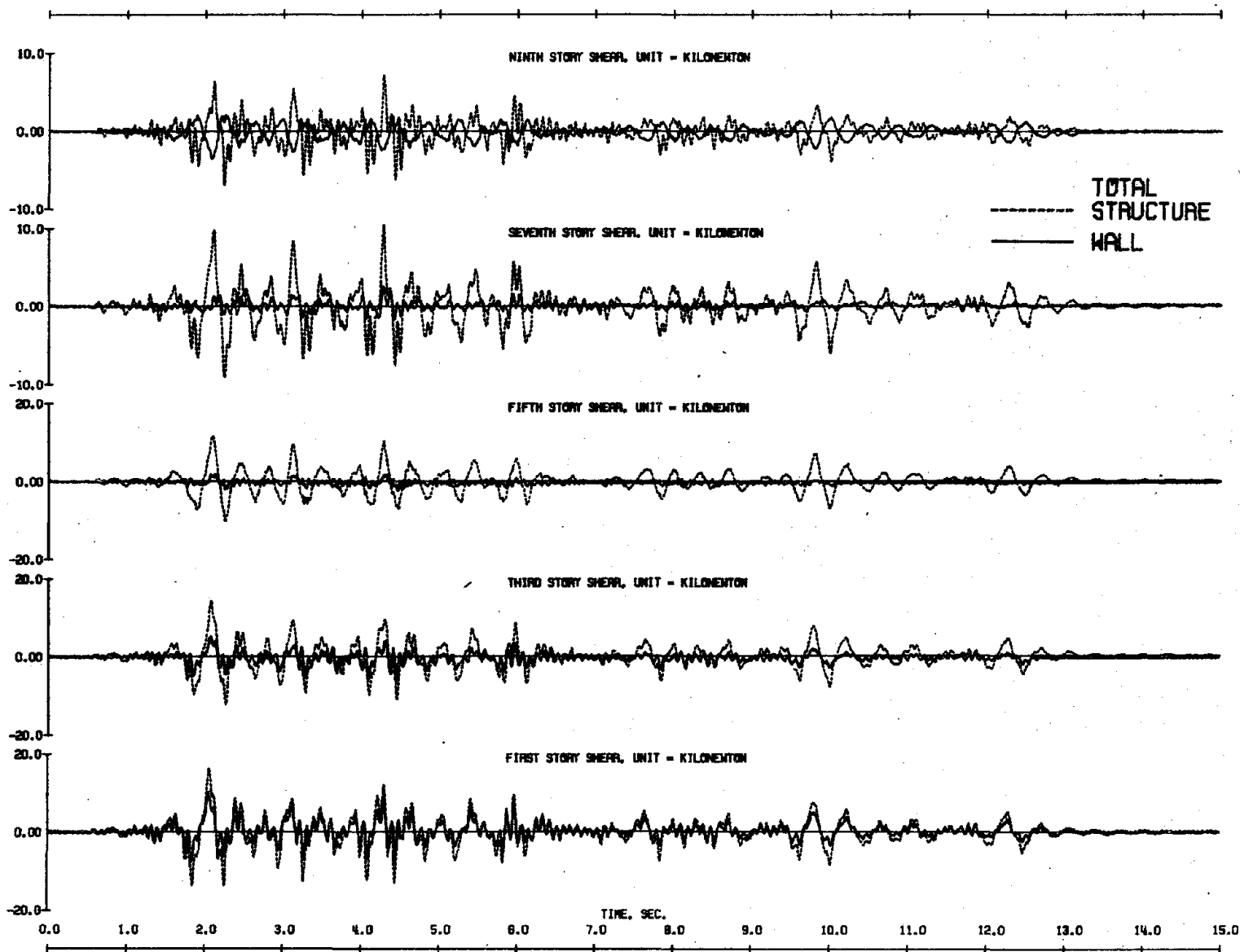


(h) (contd.) Force Resisted by Lightly Reinforced Wall
 Fig. 5.16 (contd.) Measured Response to Initial Taft Simulations



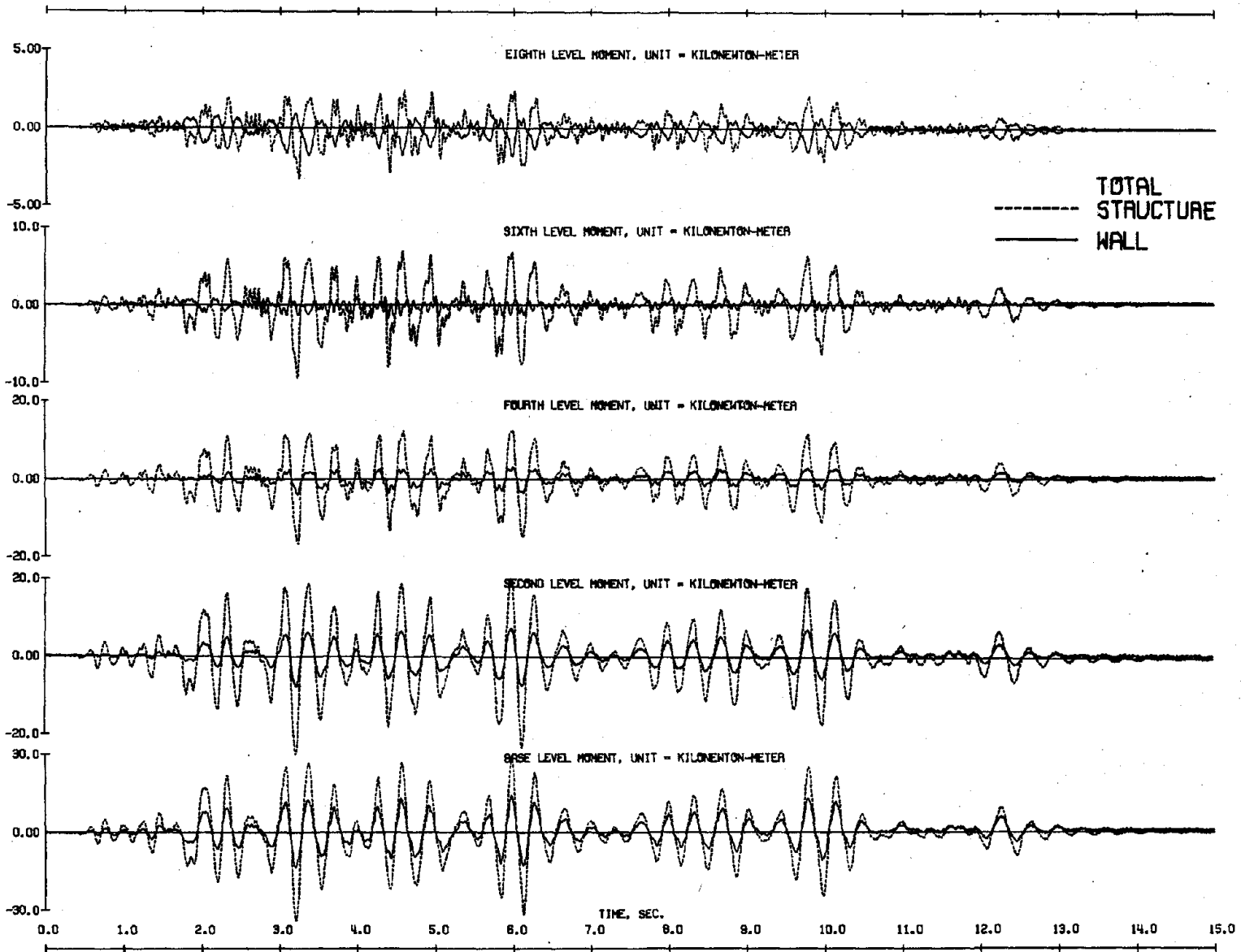
236

(a) Shears of Structure with Heavily Reinforced Wall
 Fig. 5.17 Shear and Moment Response to Initial Taft Simulations



(b) Shears of Structure with Lightly Reinforced Wall

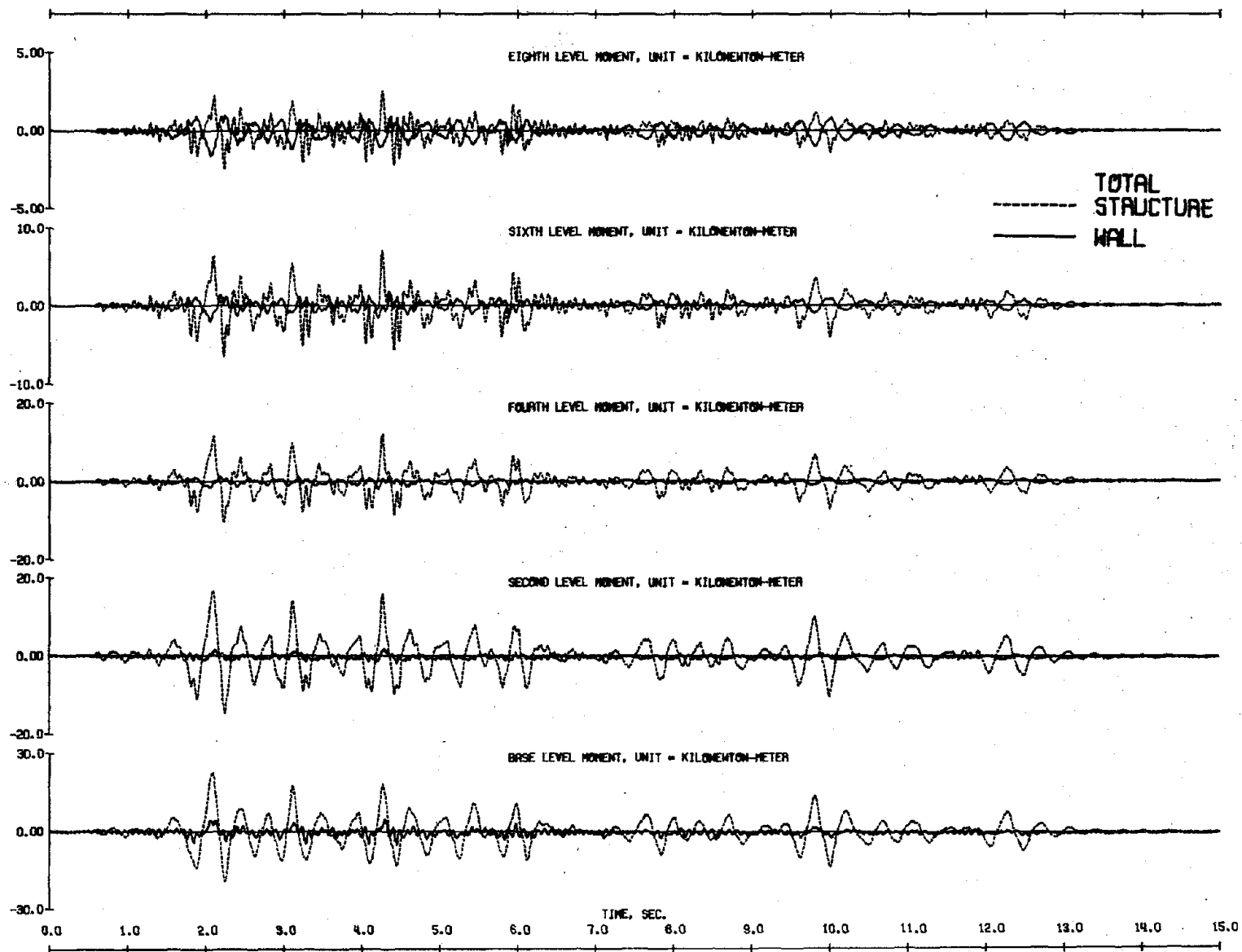
Fig. 5.17 (contd.) Shear and Moment Response to Initial Taft Simulations



238

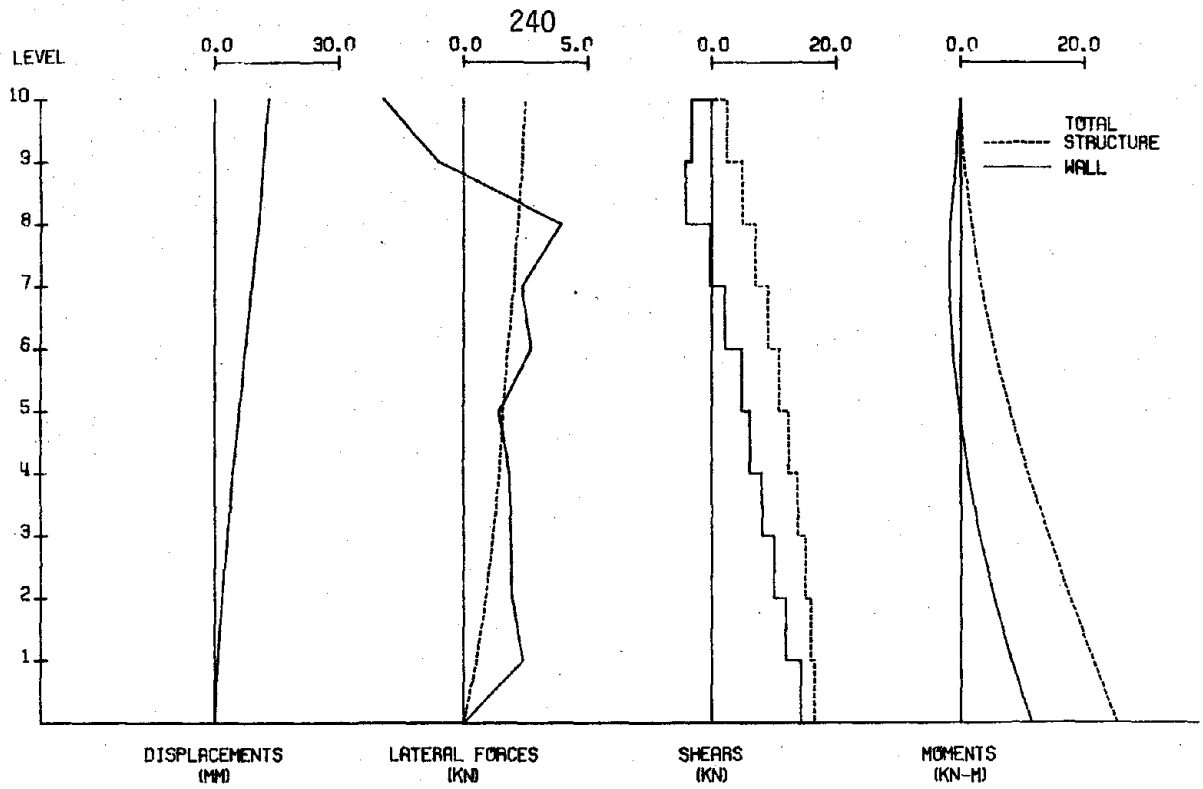
(c) Moments of Structure with Heavily Reinforced Wall

Fig. 5.17 (contd.) Shear and Moment Response to Initial Taft Simulations



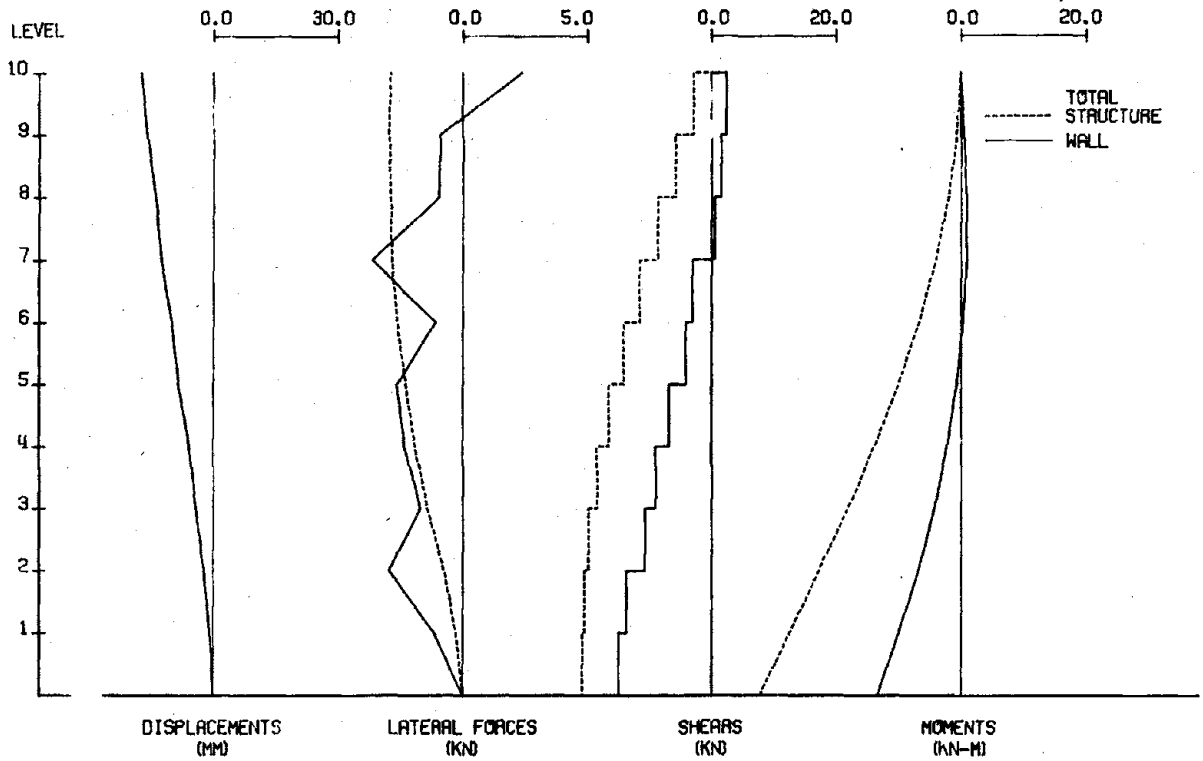
(d) Moments of Structure with Lightly Reinforced Wall

Fig. 5.17 (contd.) Shear and Moment Response to Initial Taft Simulations



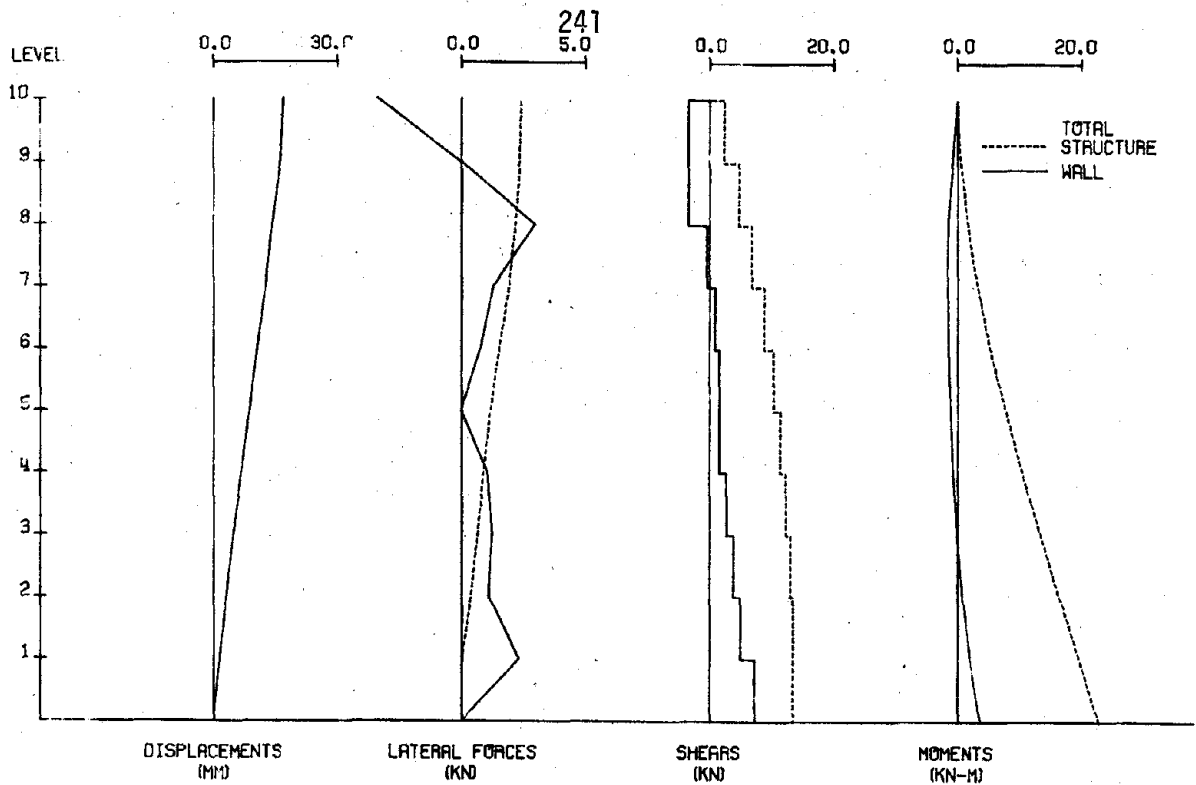
TEST STRUCTURE FW4 - TEST RUN 1 - RESPONSE AT 3.08 SECONDS

(a) Structure with Heavily Reinforced Wall



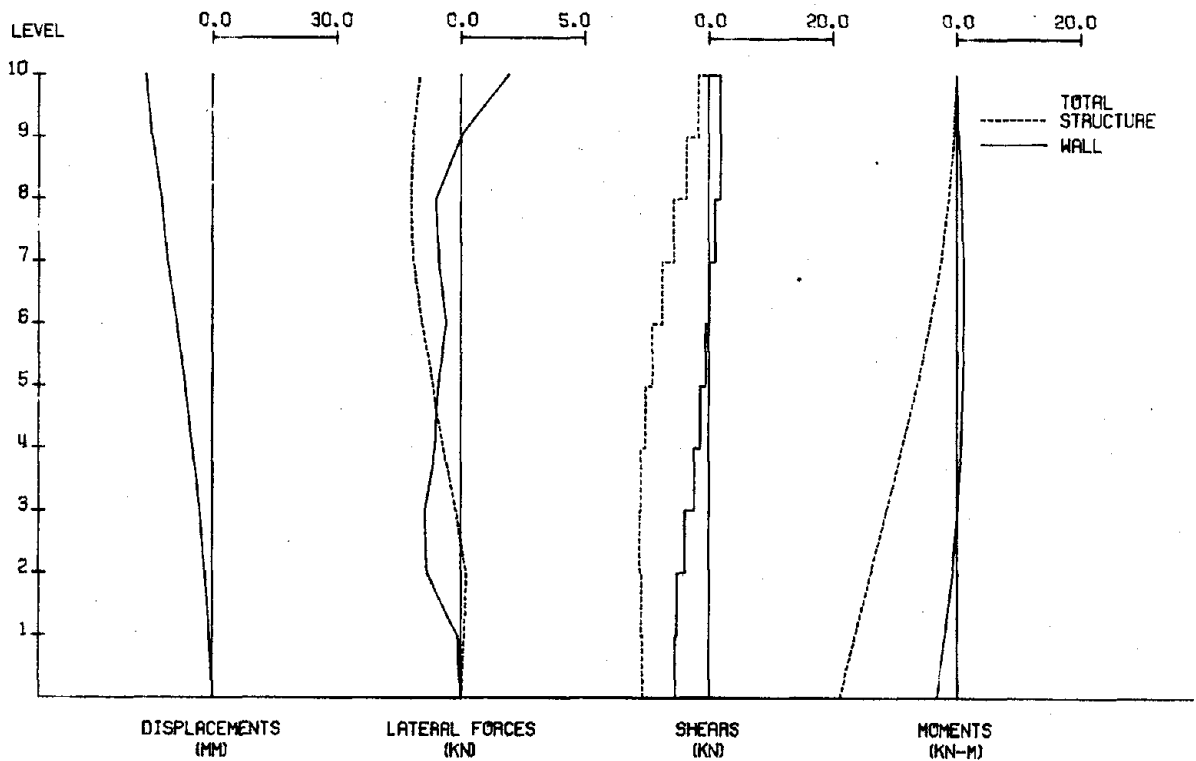
TEST STRUCTURE FW4 - TEST RUN 1 - RESPONSE AT 3.20 SECONDS

Fig. 5.18 Distributions of Response to Initial Taft Simulations



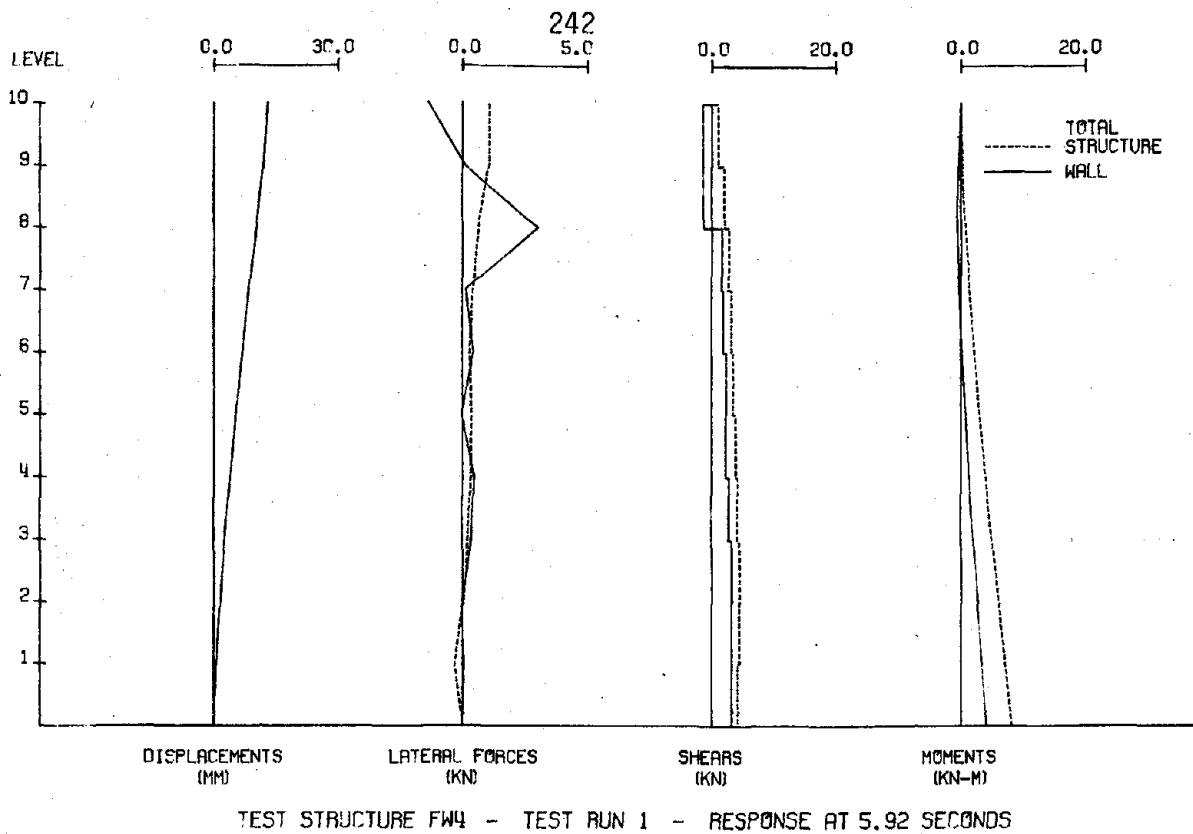
TEST STRUCTURE FW3 - TEST RUN 1 - RESPONSE AT 2.09 SECONDS

(b) Structure with Lightly Reinforced Wall



TEST STRUCTURE FW3 - TEST RUN 1 - RESPONSE AT 2.26 SECONDS

Fig. 5.18 (contd.) Distributions of Response to Initial Taft Simulations



(a) Structure with Heavily Reinforced Wall

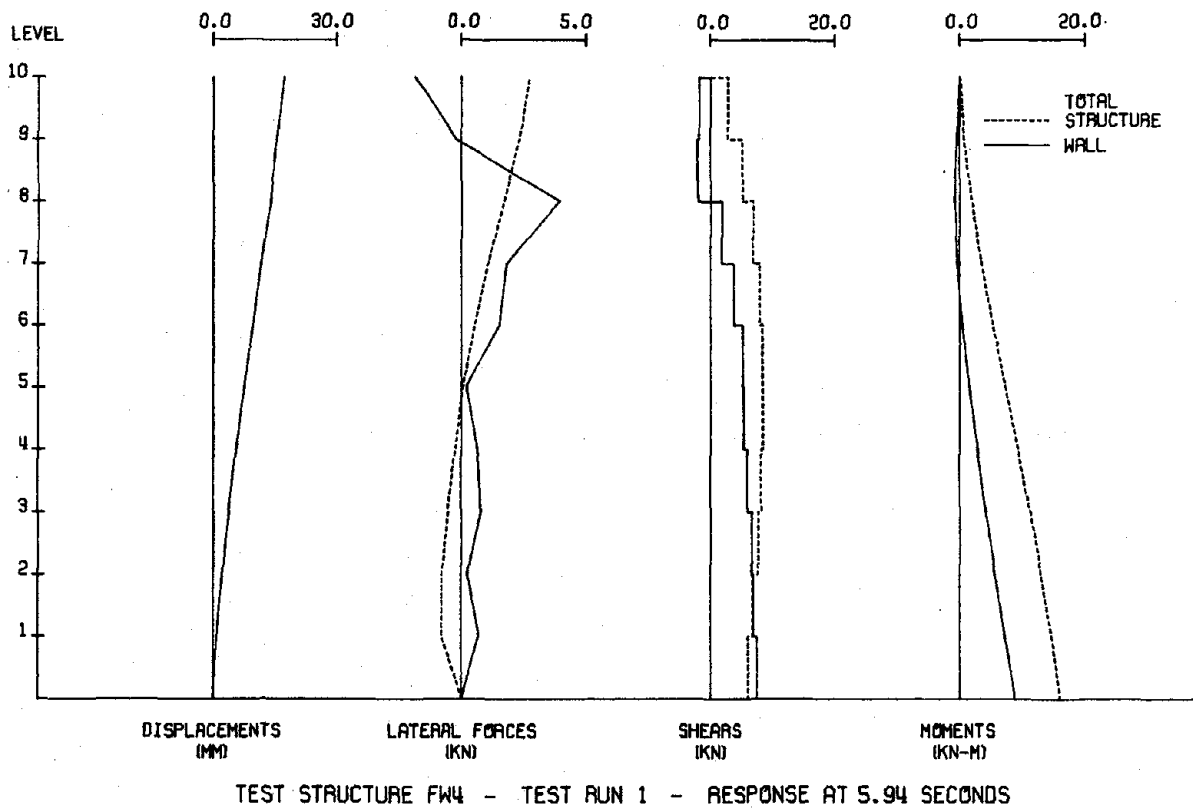
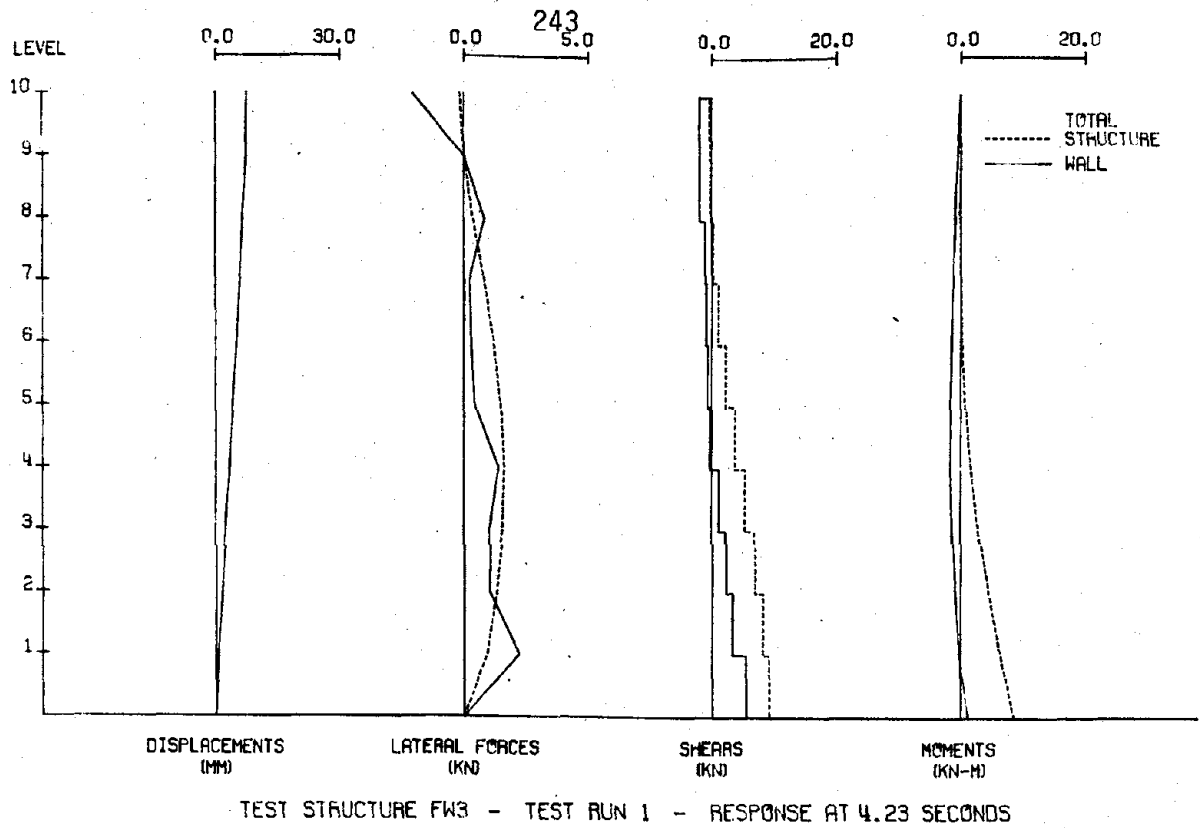


Fig. 5.18 (contd.) Distributions of Response to Initial Taft Simulations



(b) Structure with Lightly Reinforced Wall

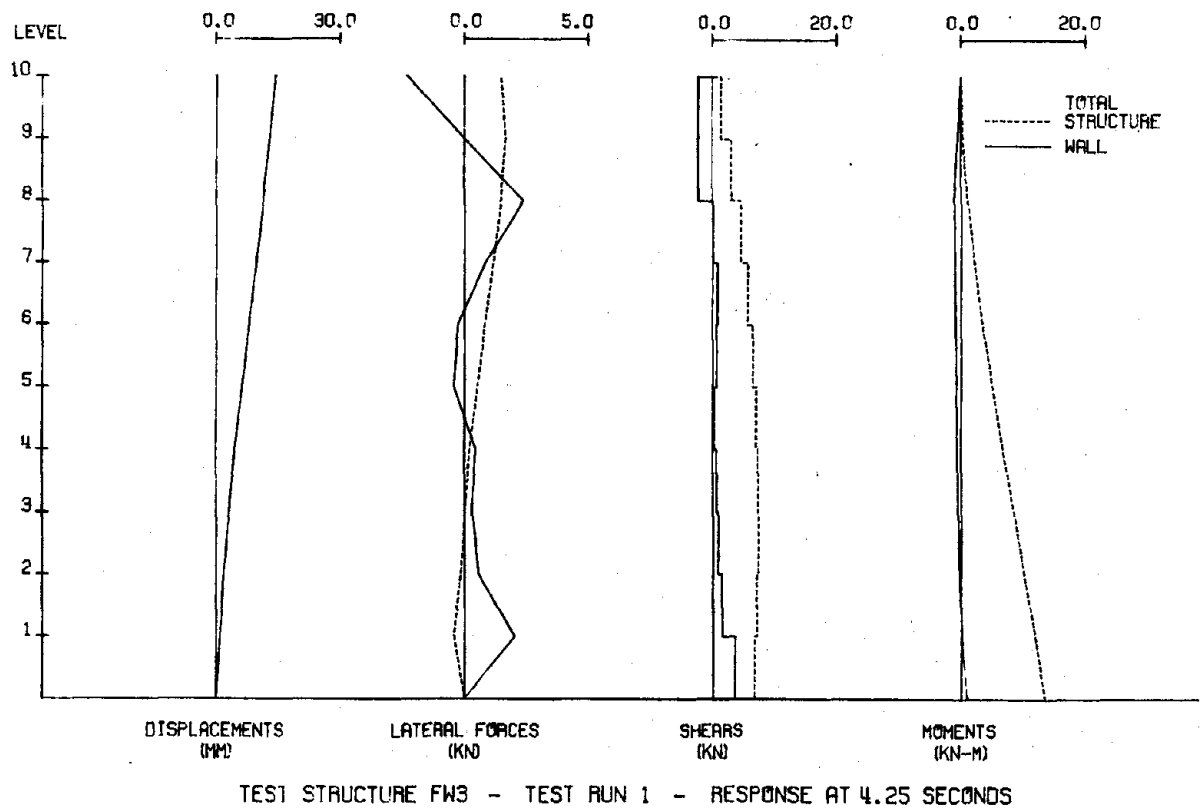
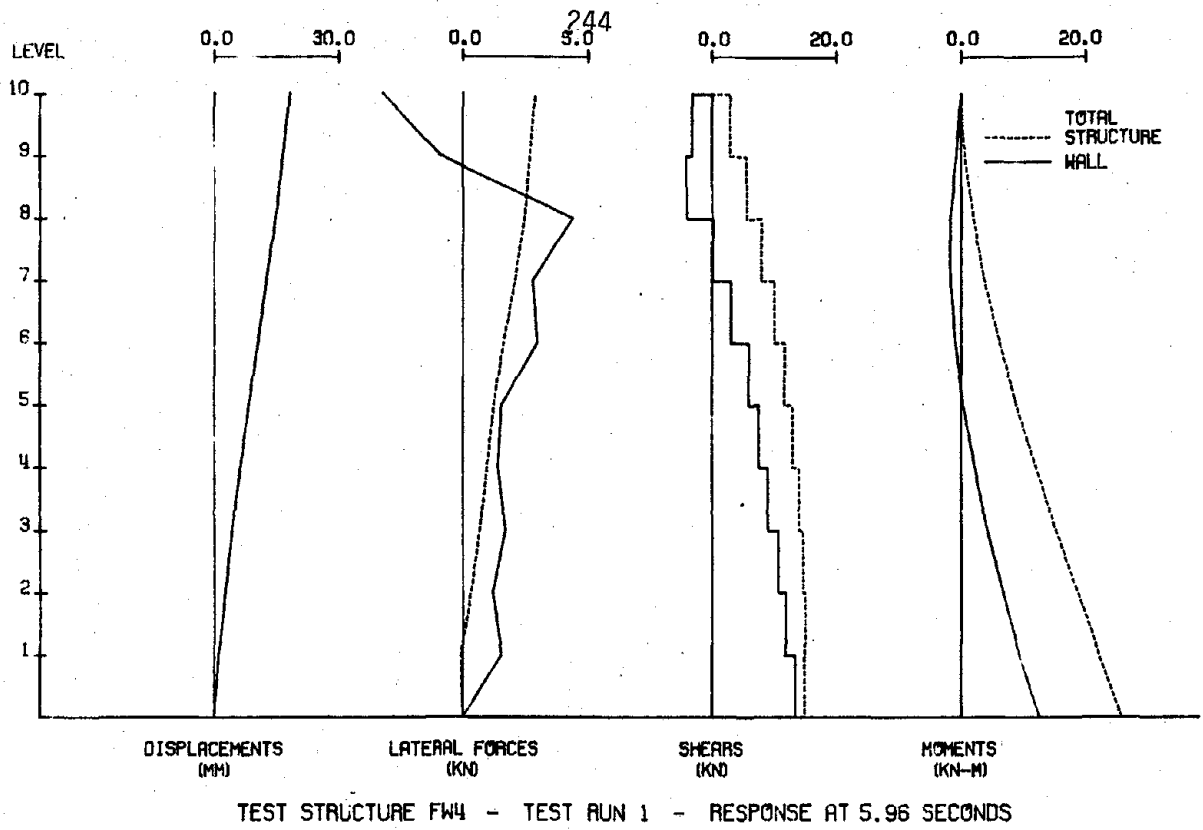


Fig. 5.18 (contd.) Distributions of Response to Initial Taft Simulations



(a) Structure with Heavily Reinforced Wall

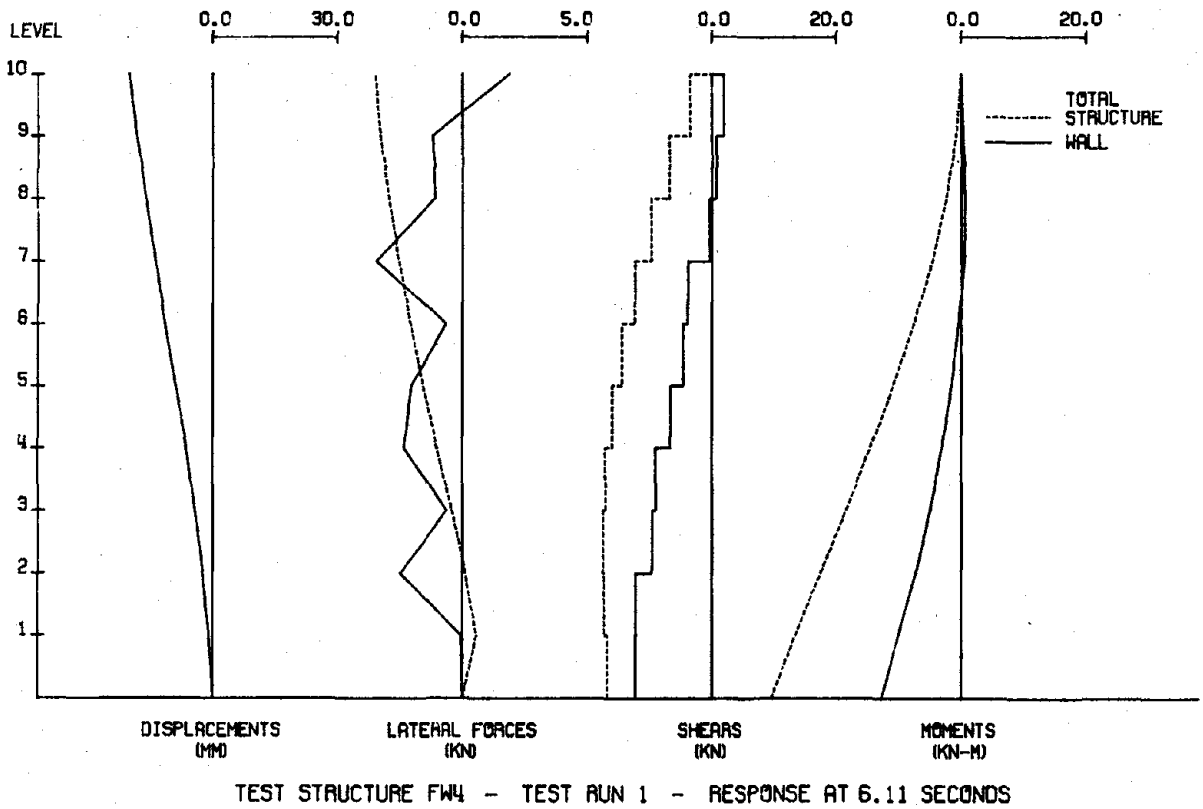
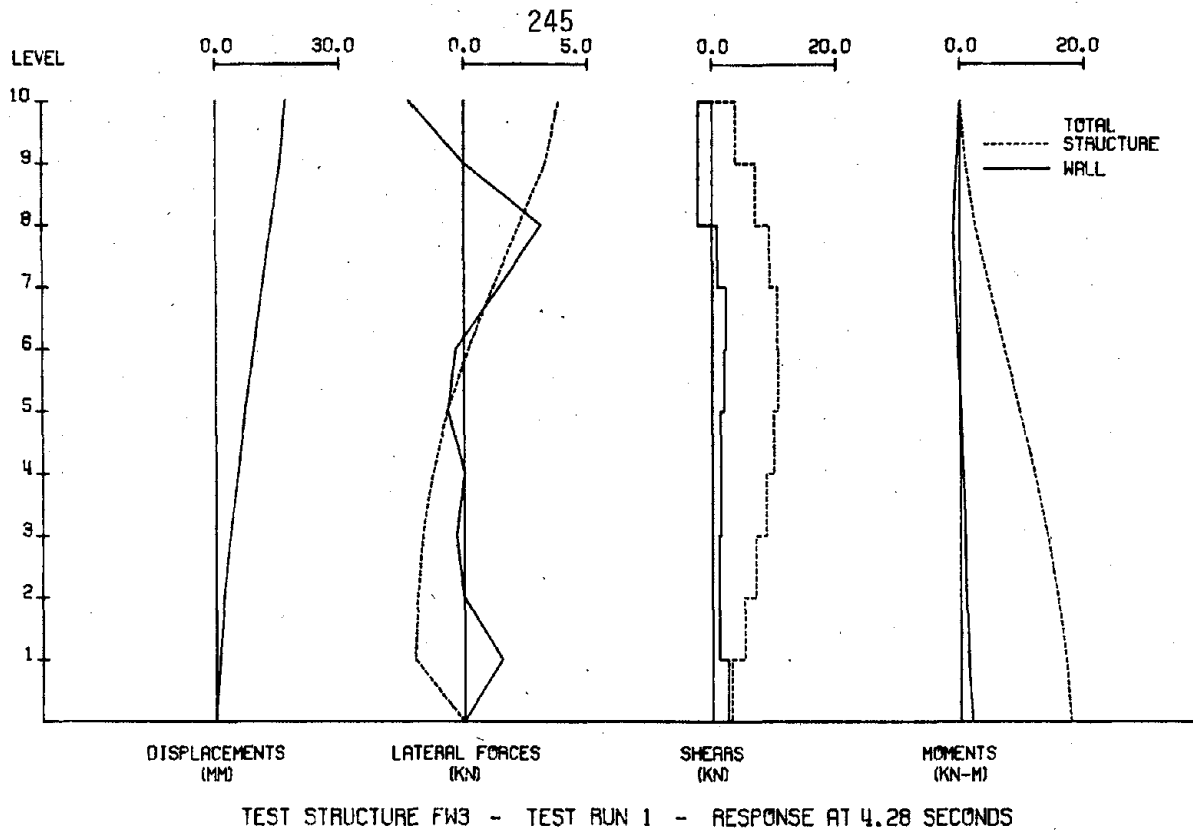


Fig. 5.18 (contd.) Distributions of Response to Initial Taft Simulations



(b) Structure with Lightly Reinforced Wall

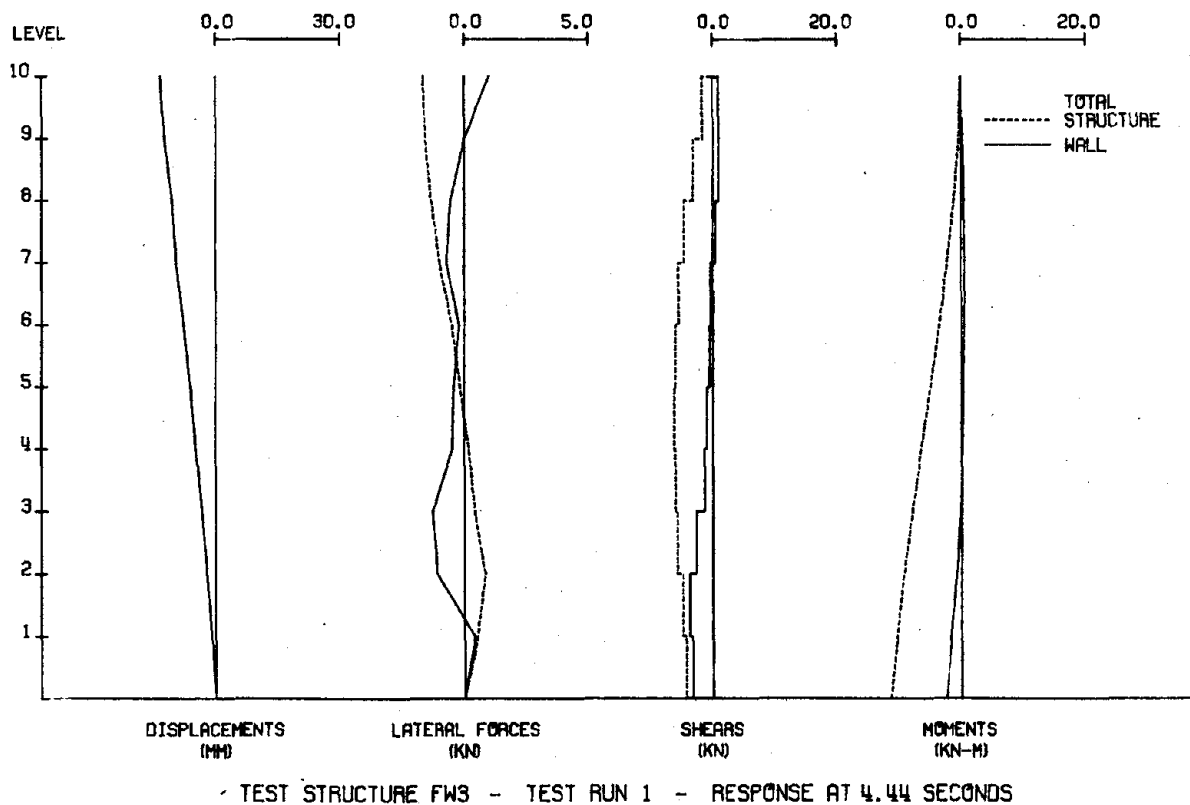
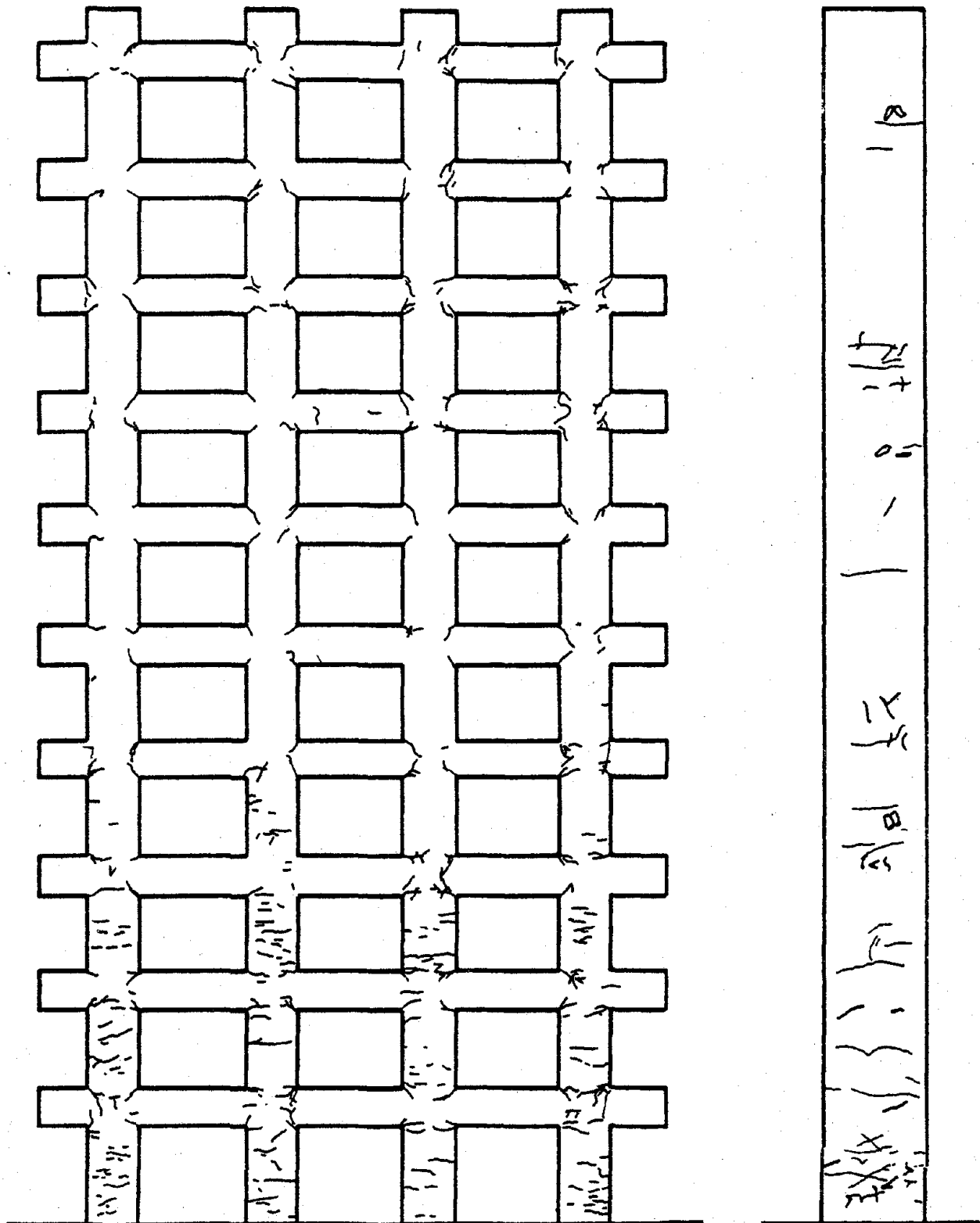


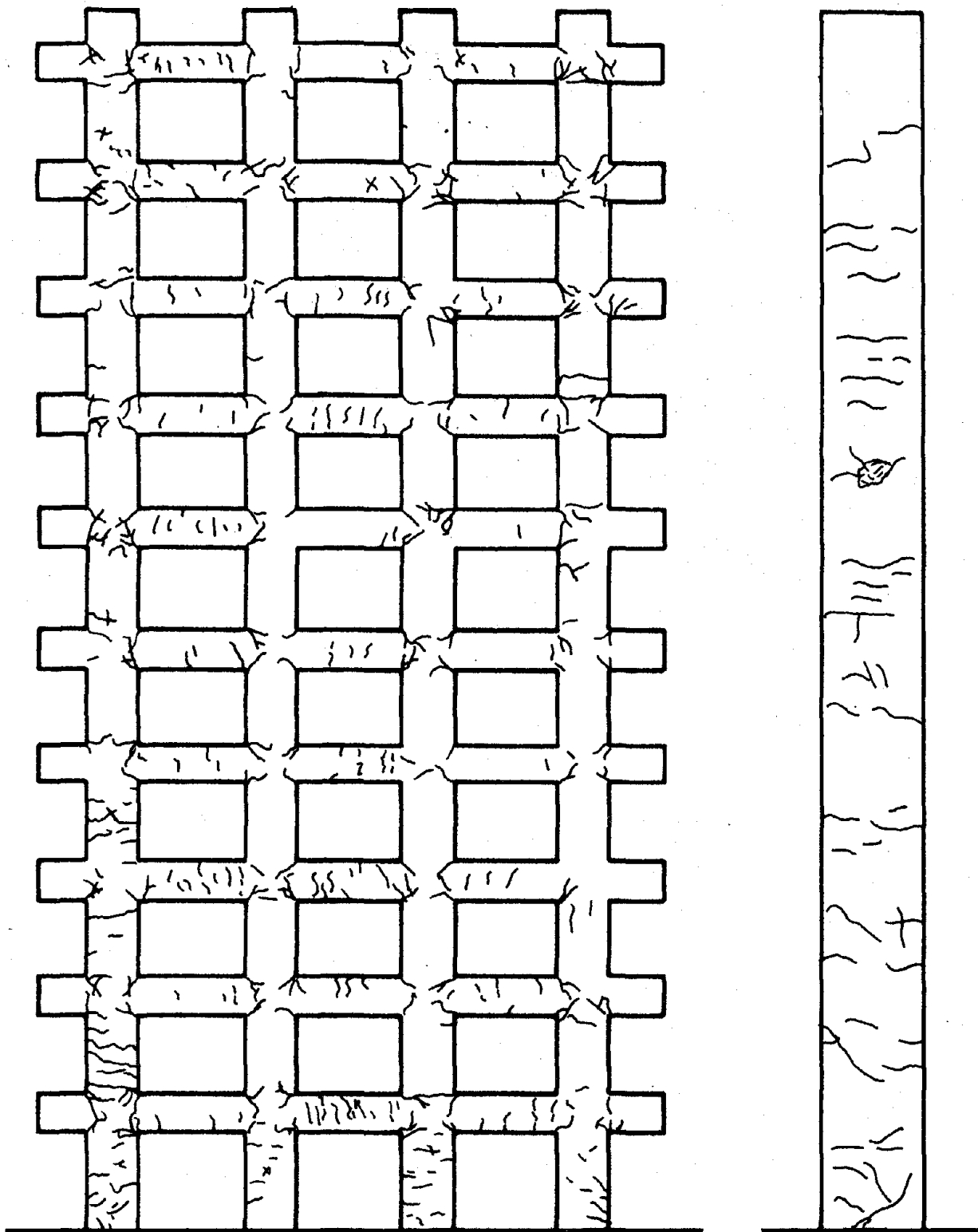
Fig. 5.18 (contd.) Distributions of Response to Initial Taft Simulations



(Not To Scale)

(a) Structure with Heavily Reinforced Wall

Fig. 5.19 Observed Crack Patterns following Initial Taft Simulations



(Not To Scale)

(b) Structure with Lightly Reinforced Wall

Fig. 5.19 (contd.) Observed Crack Patterns following Initial Taft Simulations

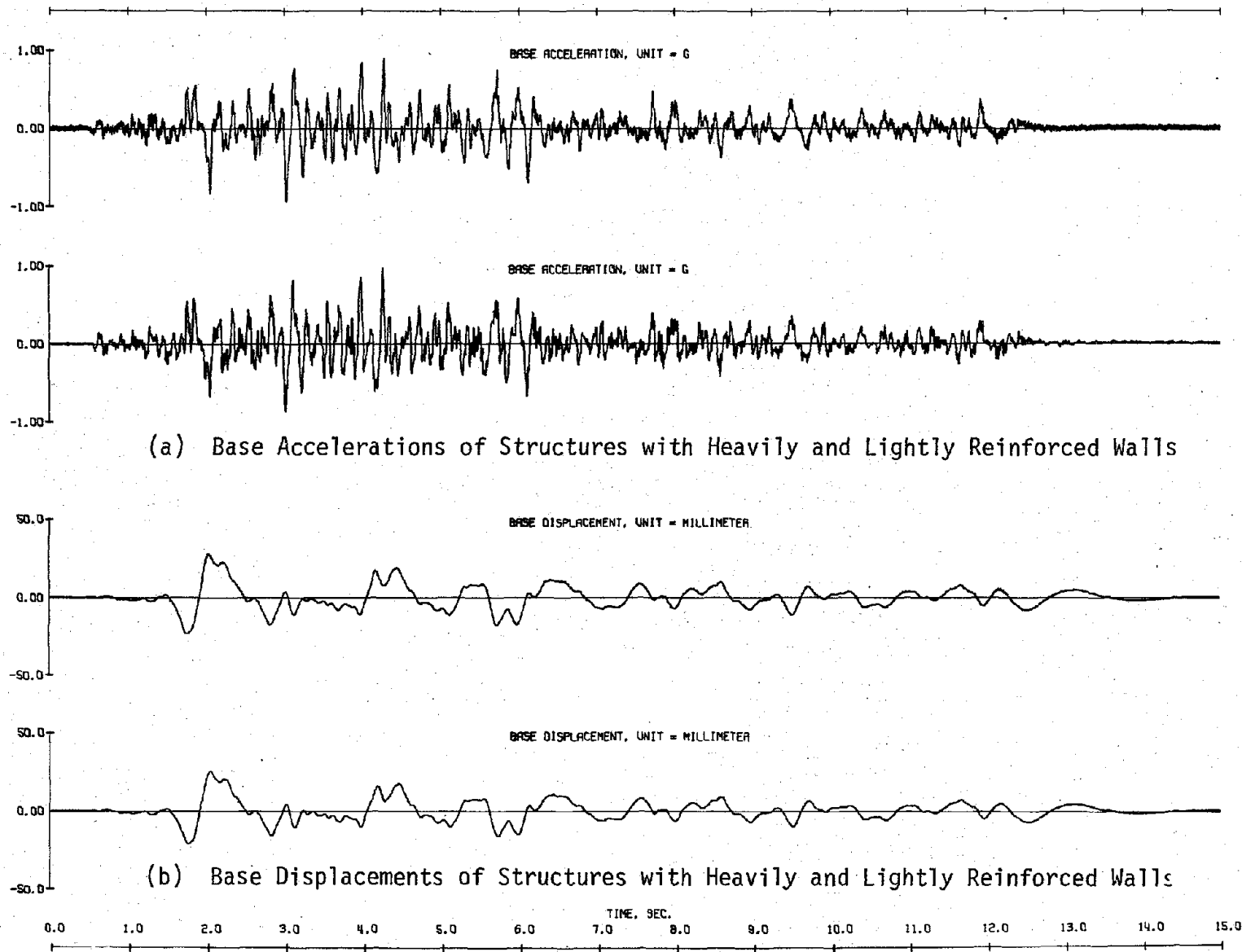


Fig. 5.20 Measured Motions of Second Taft Simulations

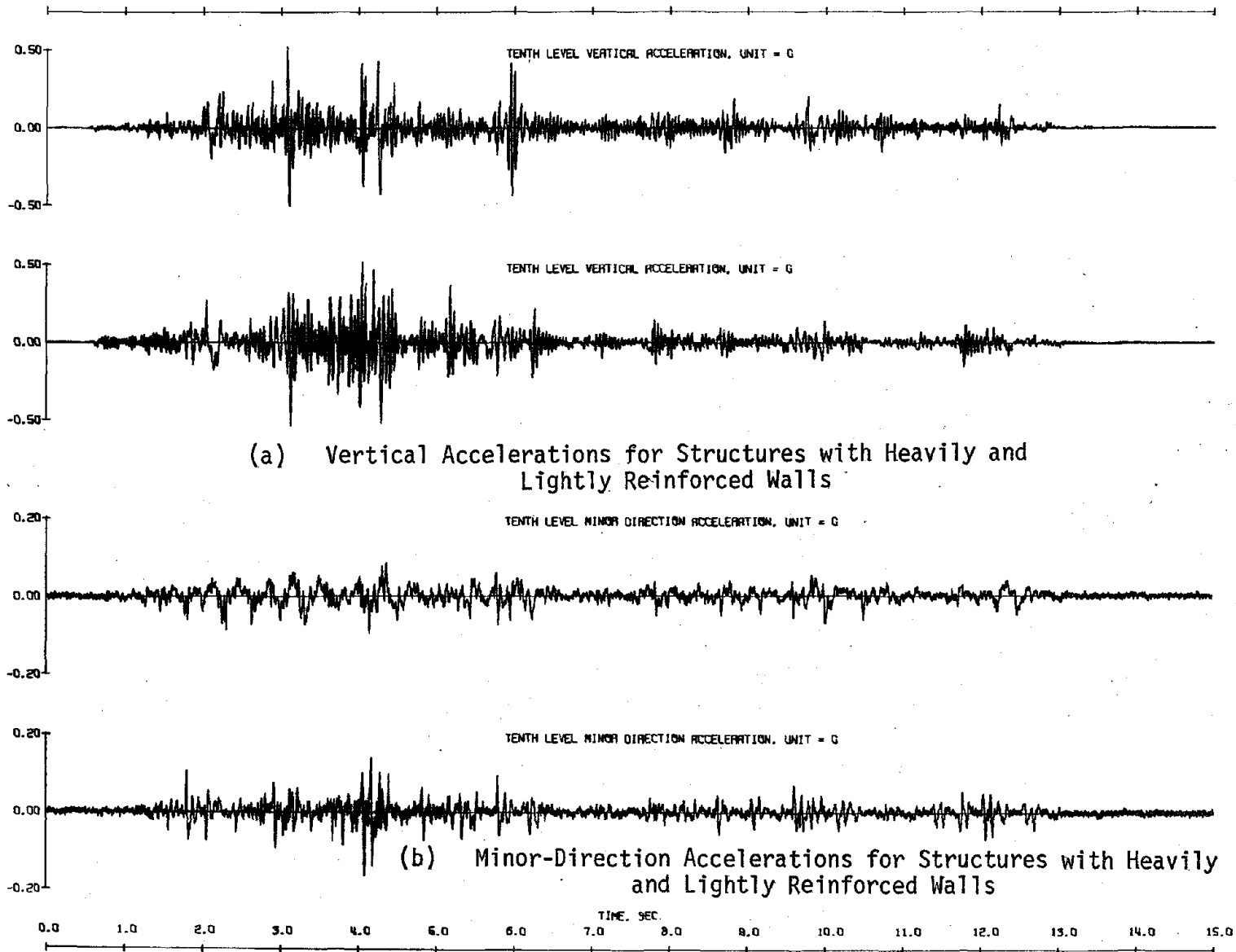
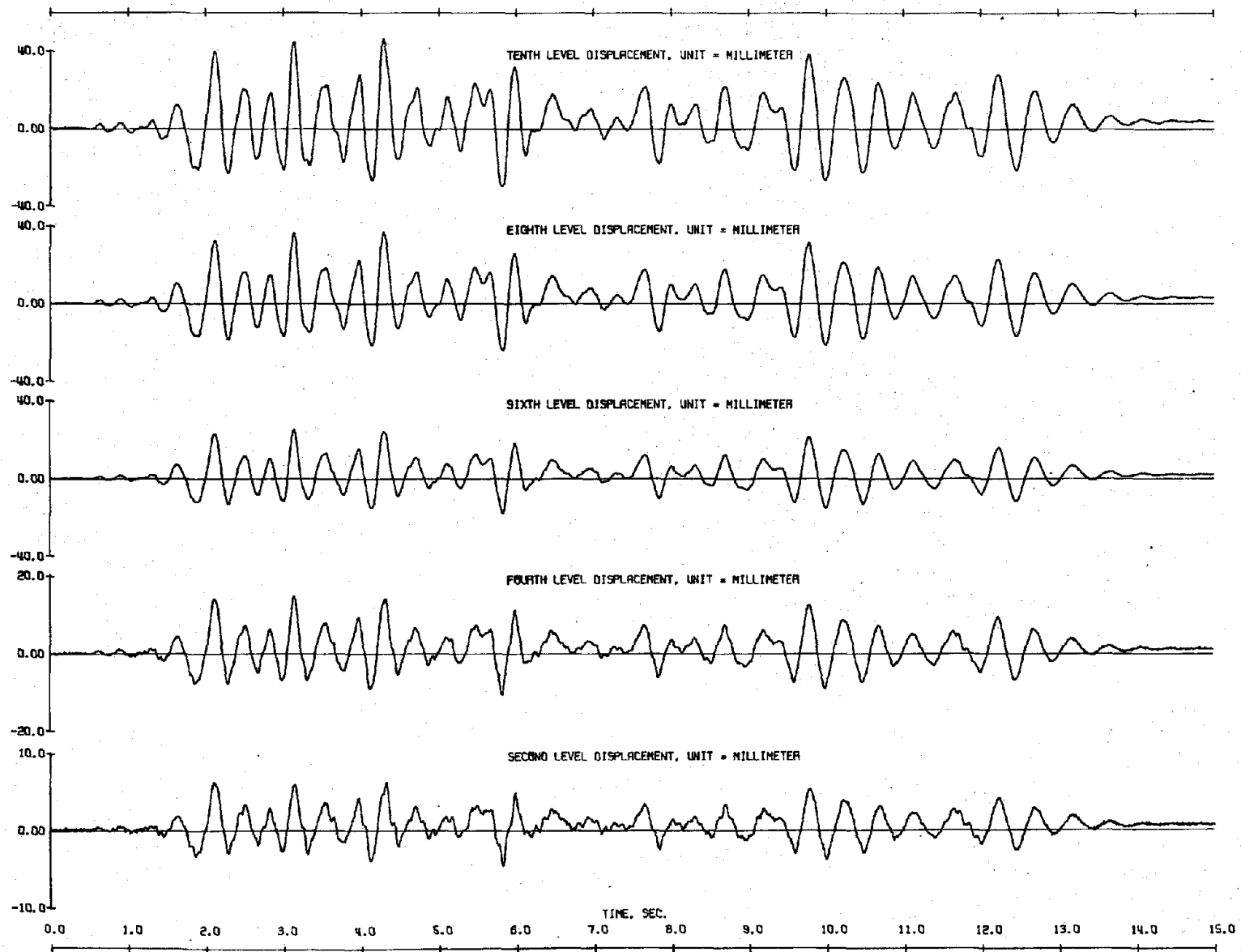
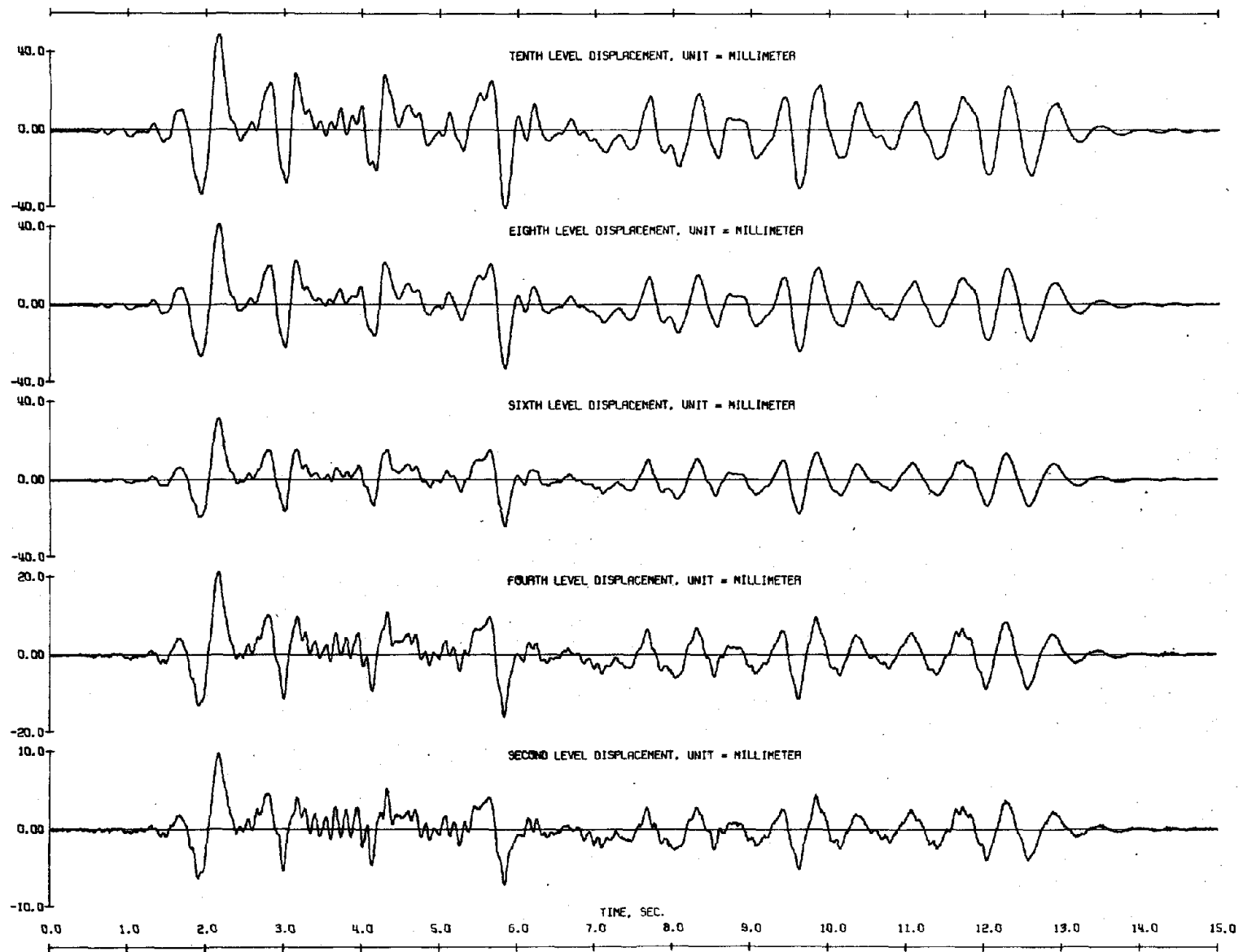


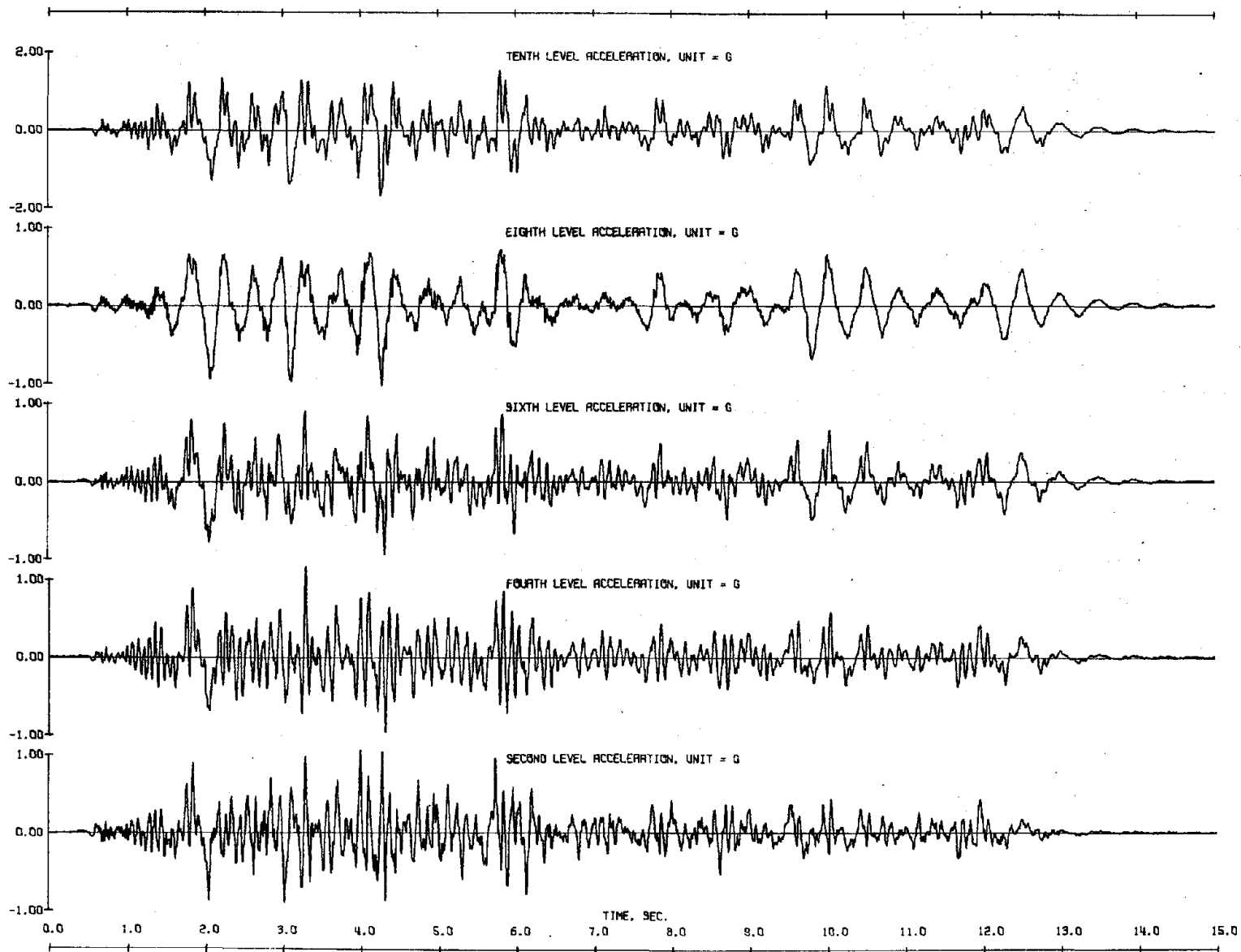
Fig. 5.21 Measured Response to Second Taft Simulations



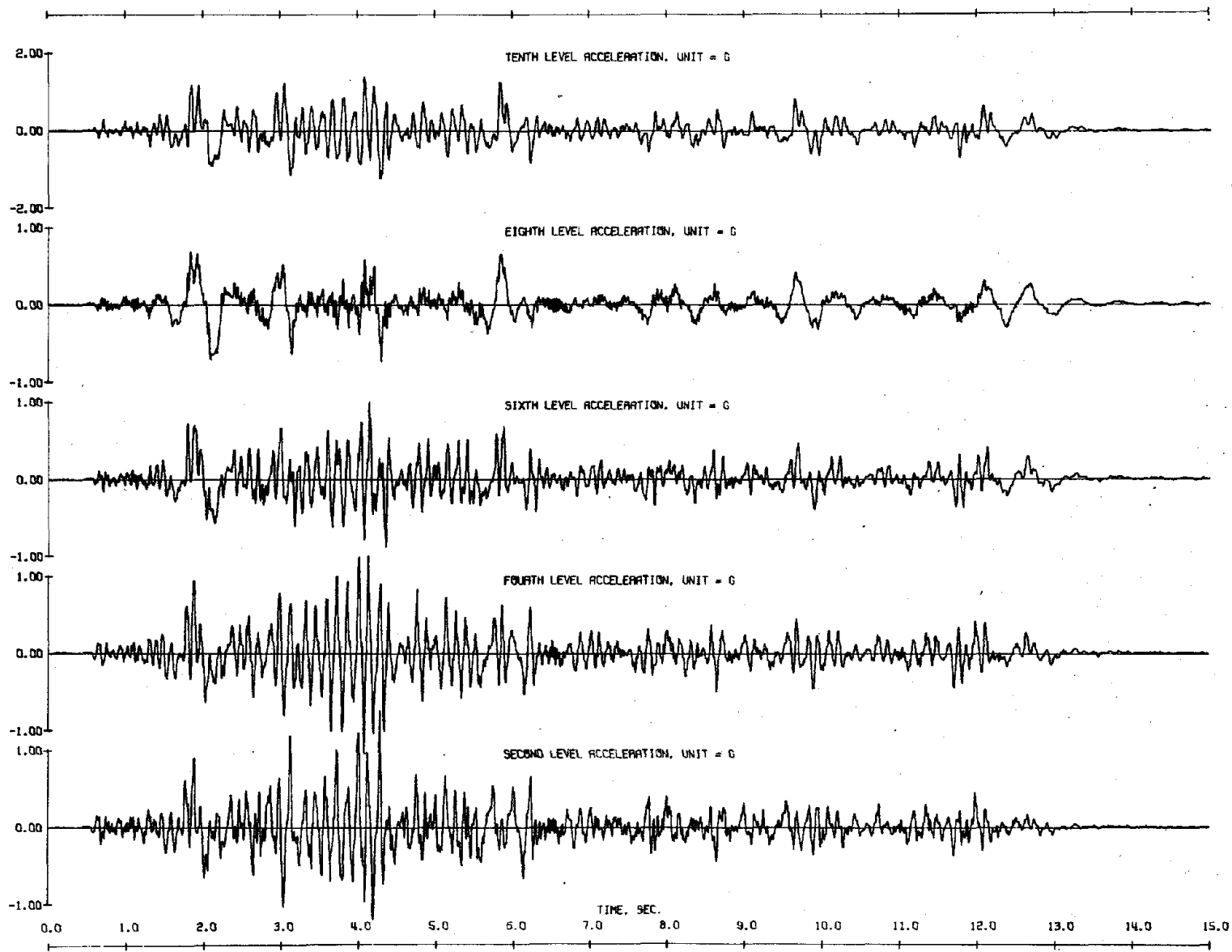
(c) Displacements of Structure with Heavily Reinforced Wall
 Fig. 5.21 (contd.) Measured Response to Second Taft Simulations



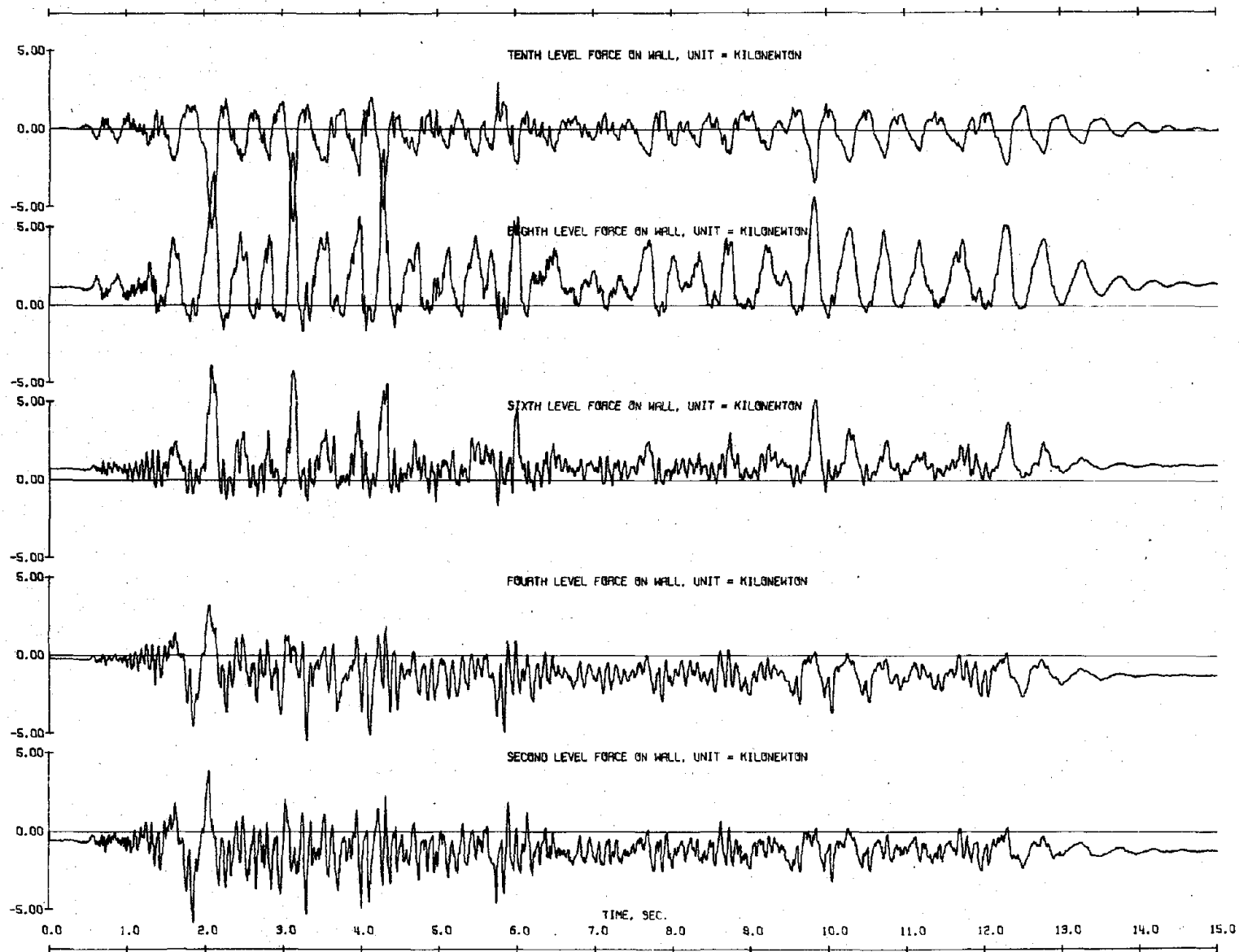
(d) Displacements of Structure with Lightly Reinforced Wall
 Fig. 5.21 (contd.) Measured Response to Second Taft Simulations



(e) Accelerations of Structure with Heavily Reinforced Wall
 Fig. 5.21 (contd.) Measured Response to Second Taft Simulations

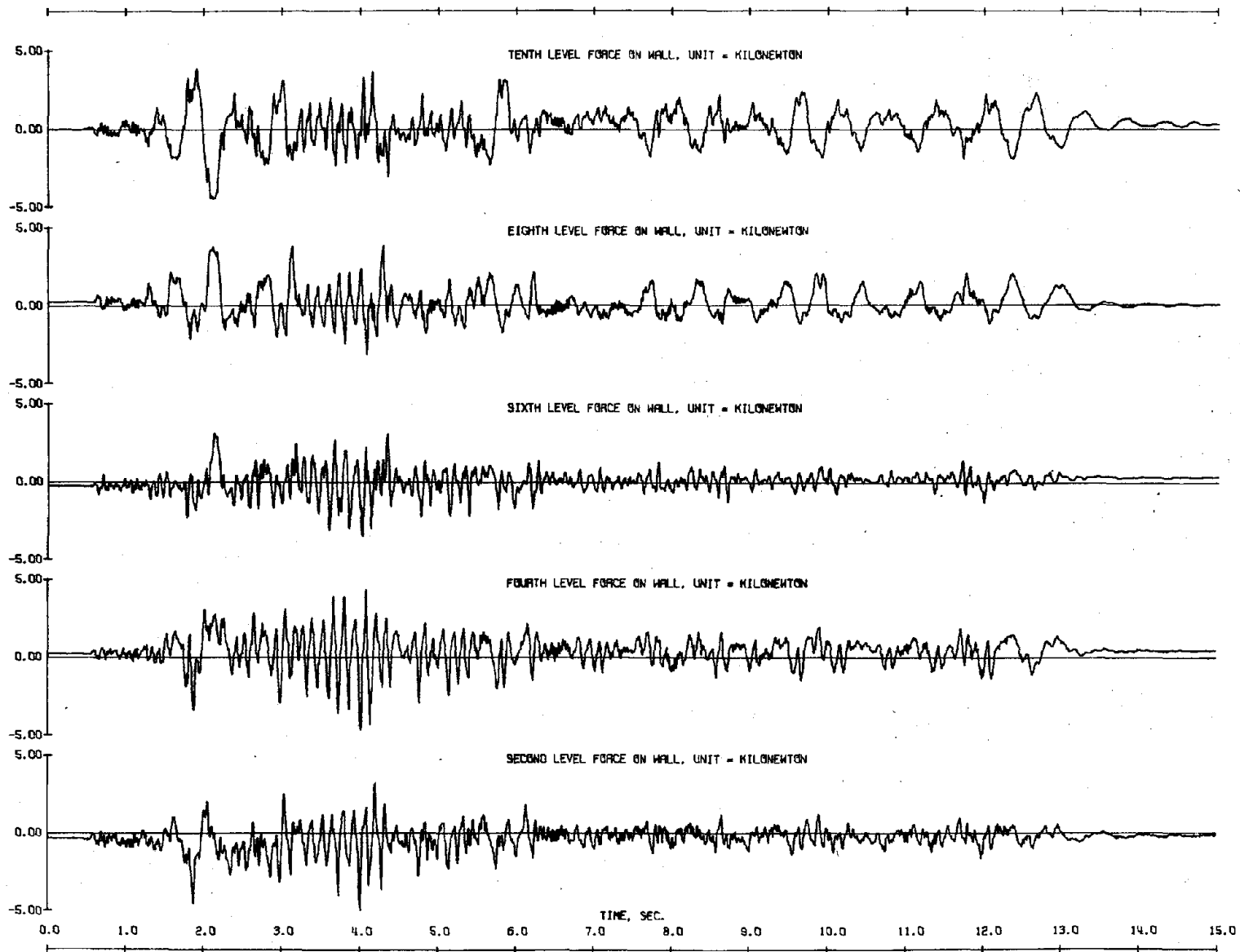


(f) Accelerations of Structure with Lightly Reinforced Wall
 Fig. 5.21 (contd.) Measured Response to Second Taft Simulations



(g) Force Resisted by Heavily Reinforced Wall

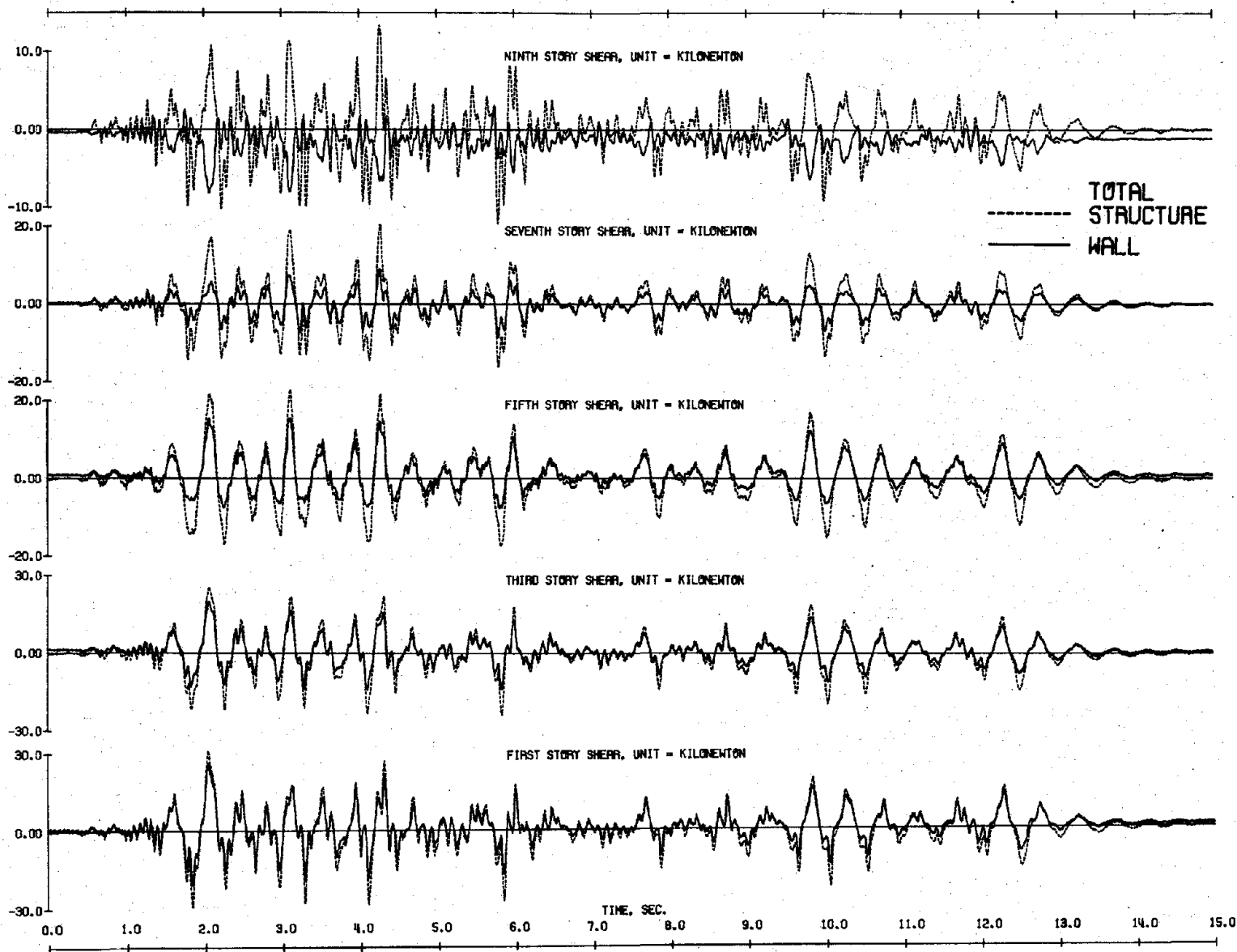
Fig. 5.21 (contd.) Measured Response to Second Taft Simulations



255

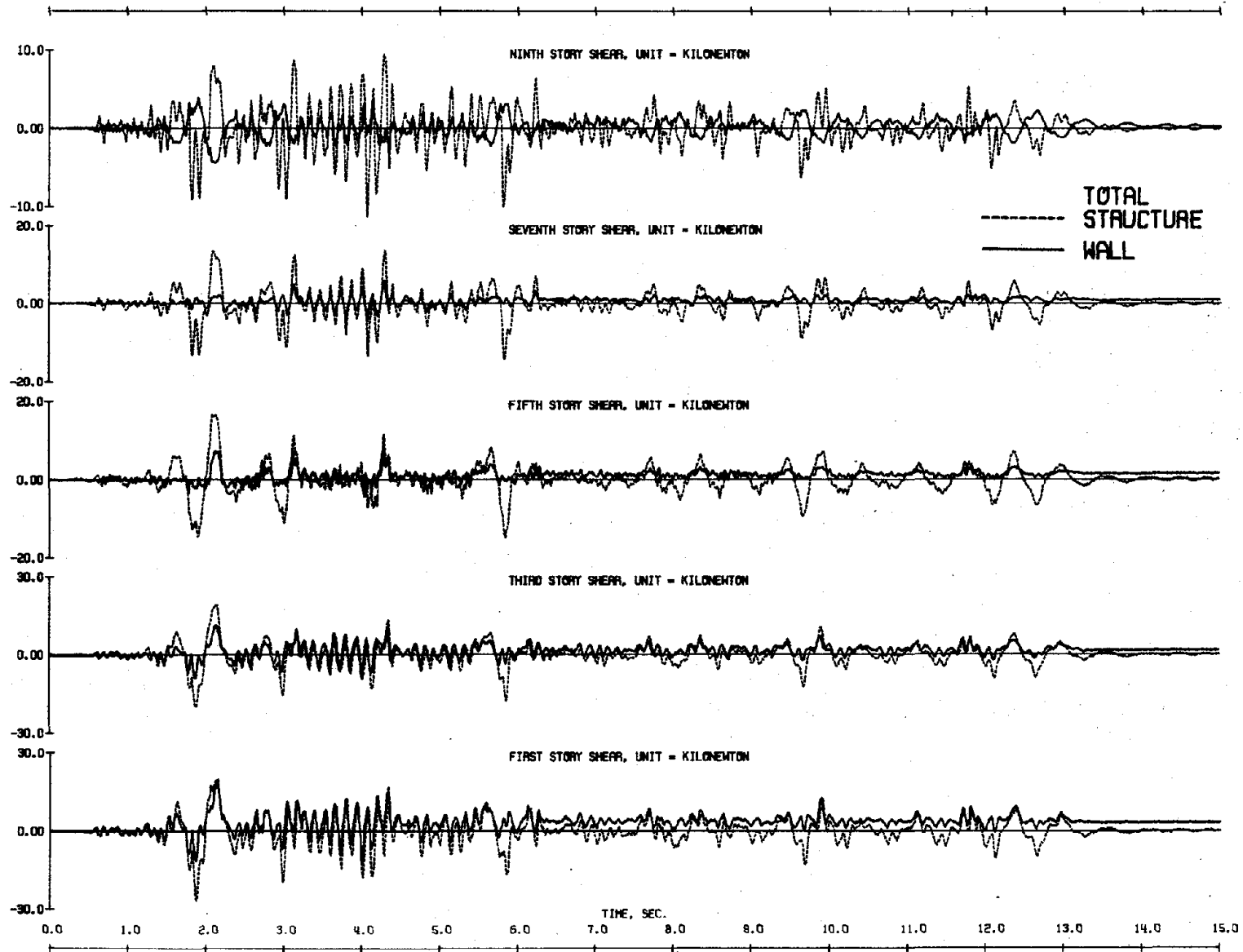
(h) Force Resisted by Lightly Reinforced Wall

Fig. 5.21 (contd.) Measured Response to Second Taft Simulations

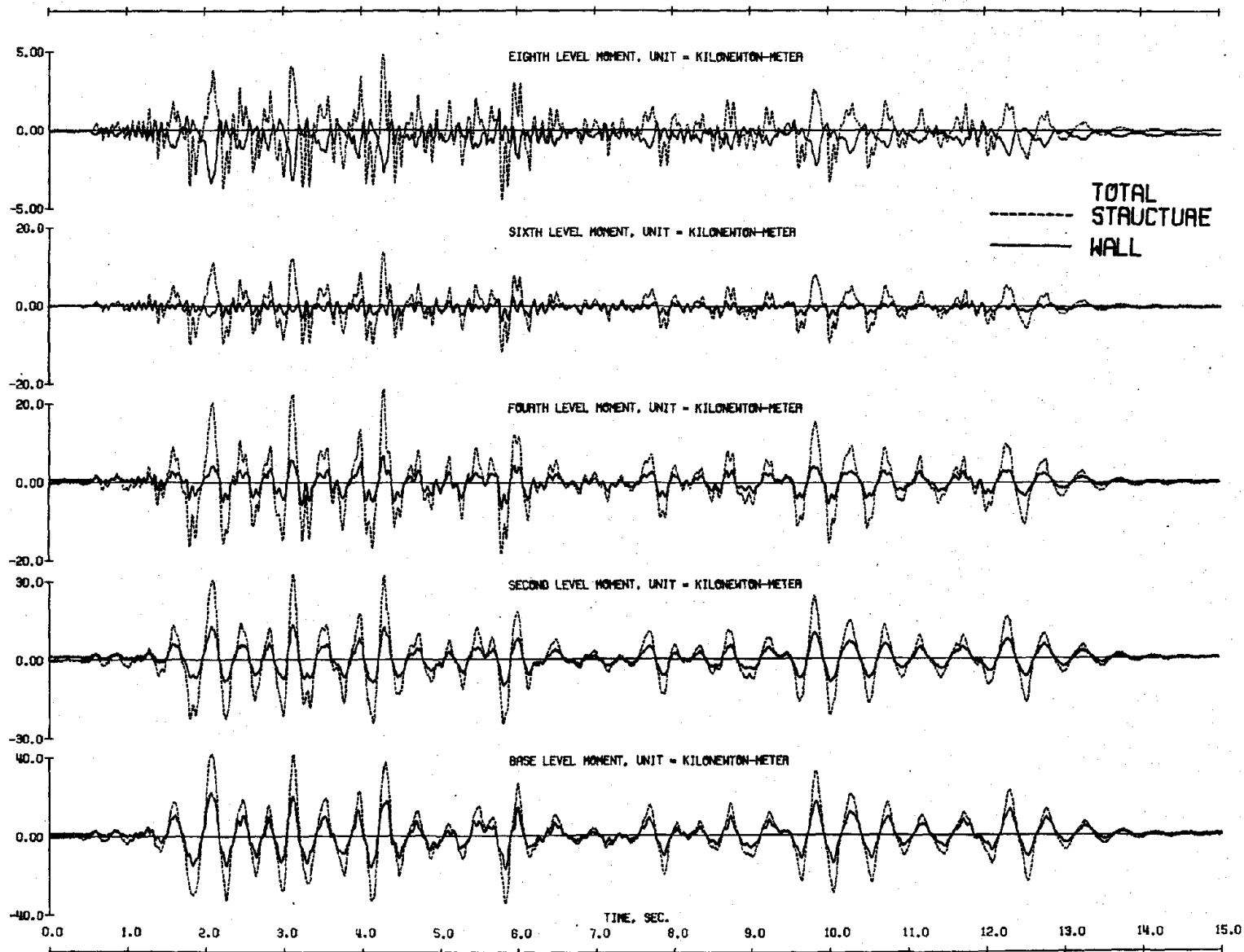


(a) Shears of Structure with Heavily Reinforced Wall

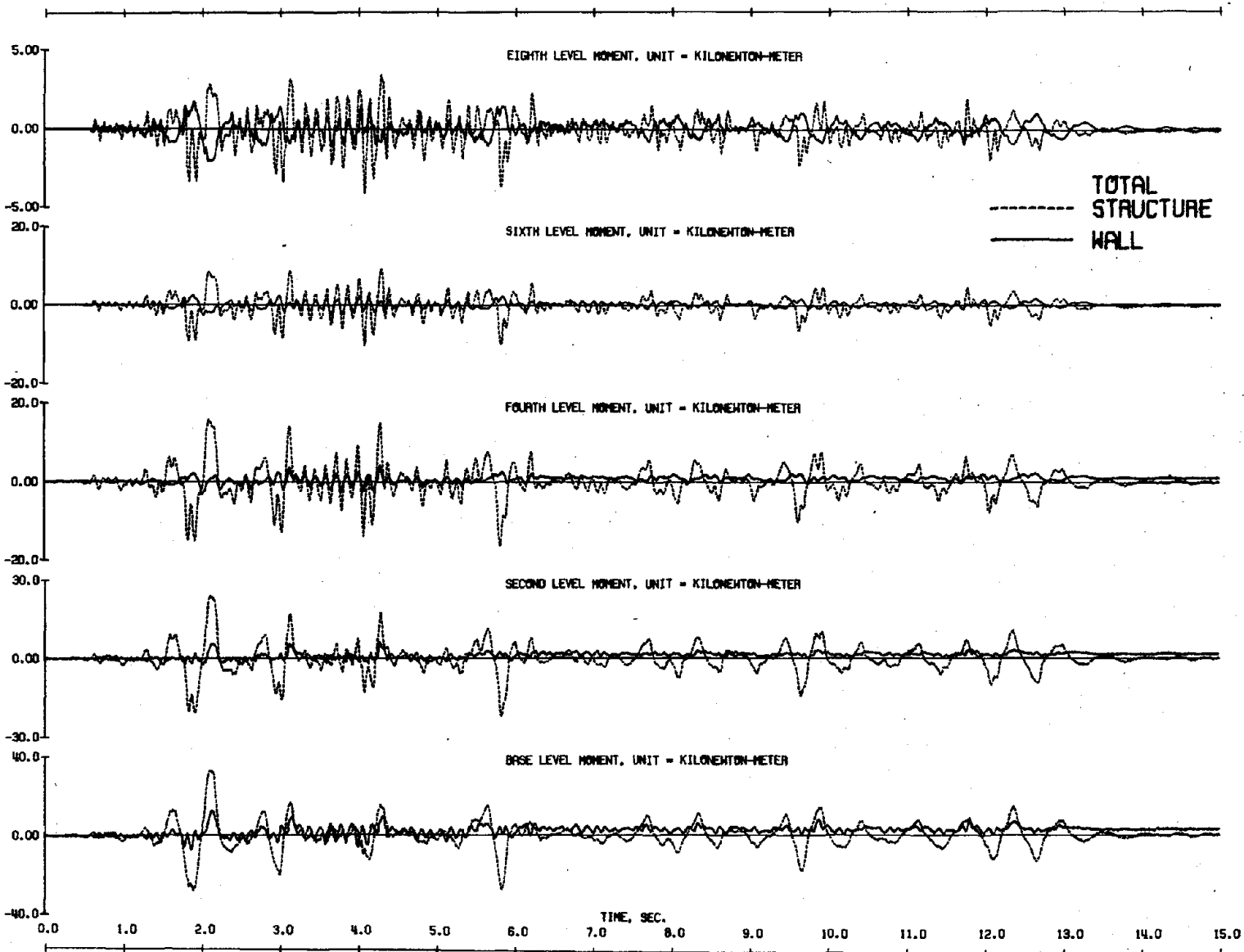
Fig. 5.22 Shear and Moment Response to Second Taft Simulations



(b) Shears of Structure with Lightly Reinforced Wall
 Fig. 5.22 (contd.) Shear and Moment Response to Second Taft Simulations

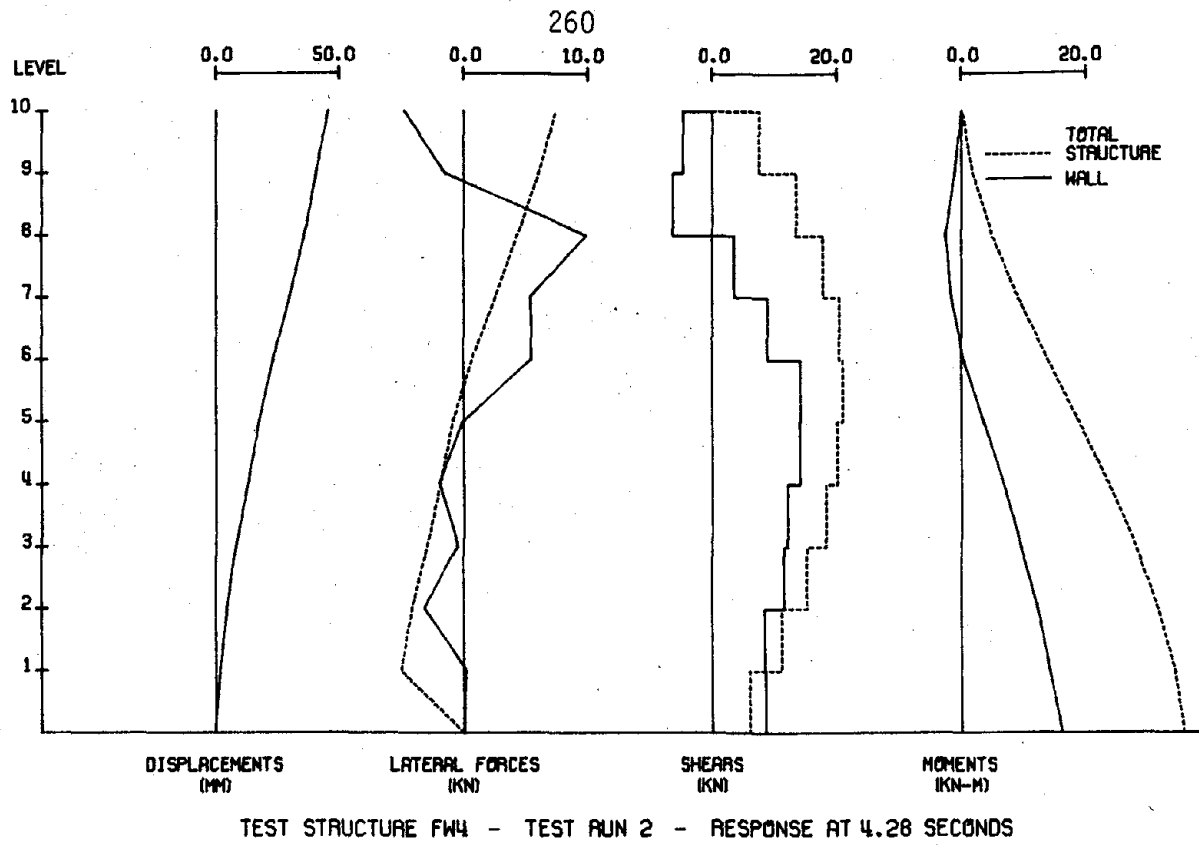


(c) Moments of Structure with Heavily Reinforced Wall
 Fig. 5.22 (contd.) Shear and Moment Response to Second Taft Simulations



(d) Moments of Structure with Lightly Reinforced Wall

Fig. 5.22 (contd.) Shear and Moment Response to Second Taft Simulations



(a) Structure with Heavily Reinforced Wall

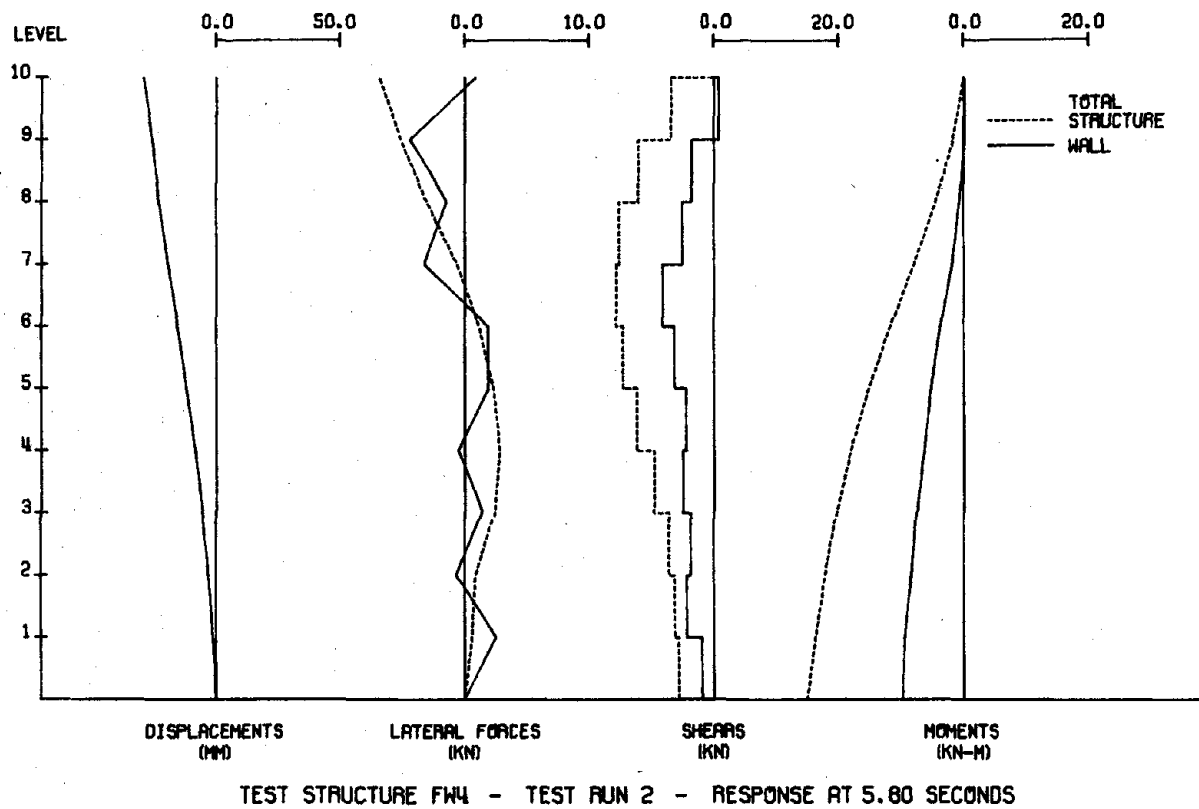
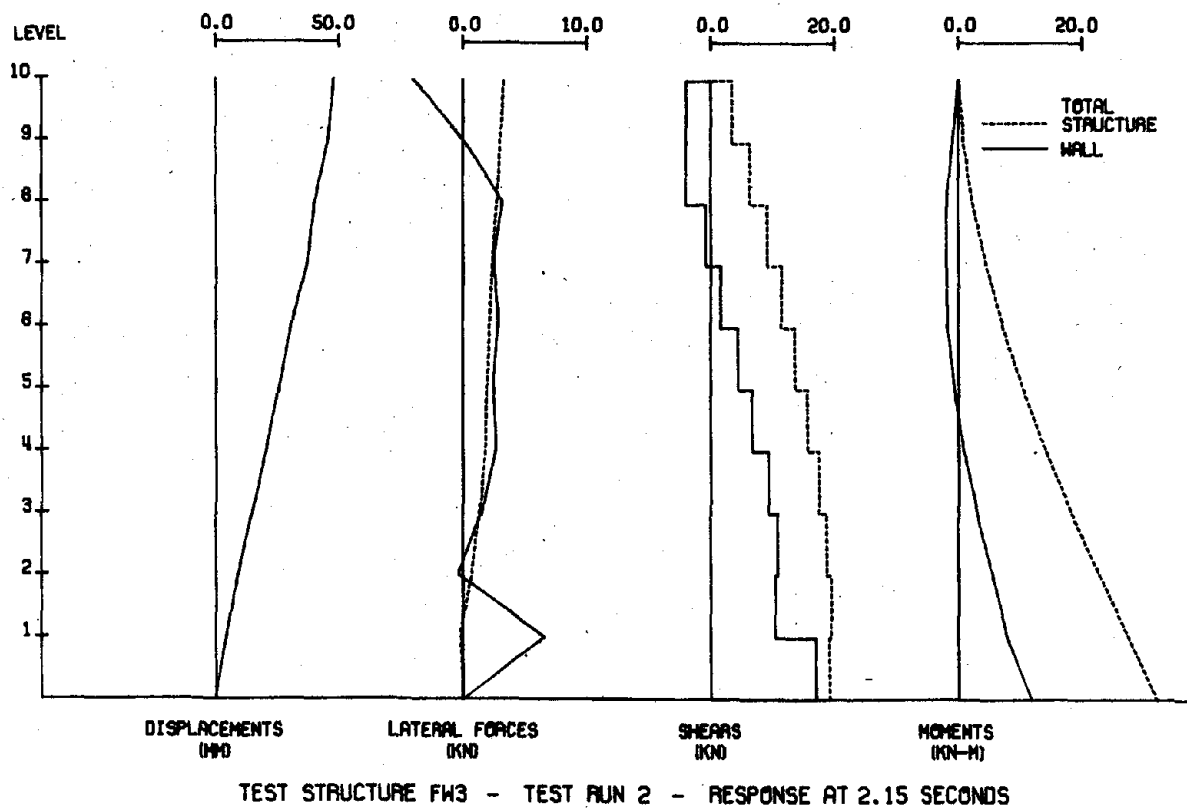


Fig. 5.23 Distributions of Response to Second Taft Simulations



(b) Structure with Lightly Reinforced Wall

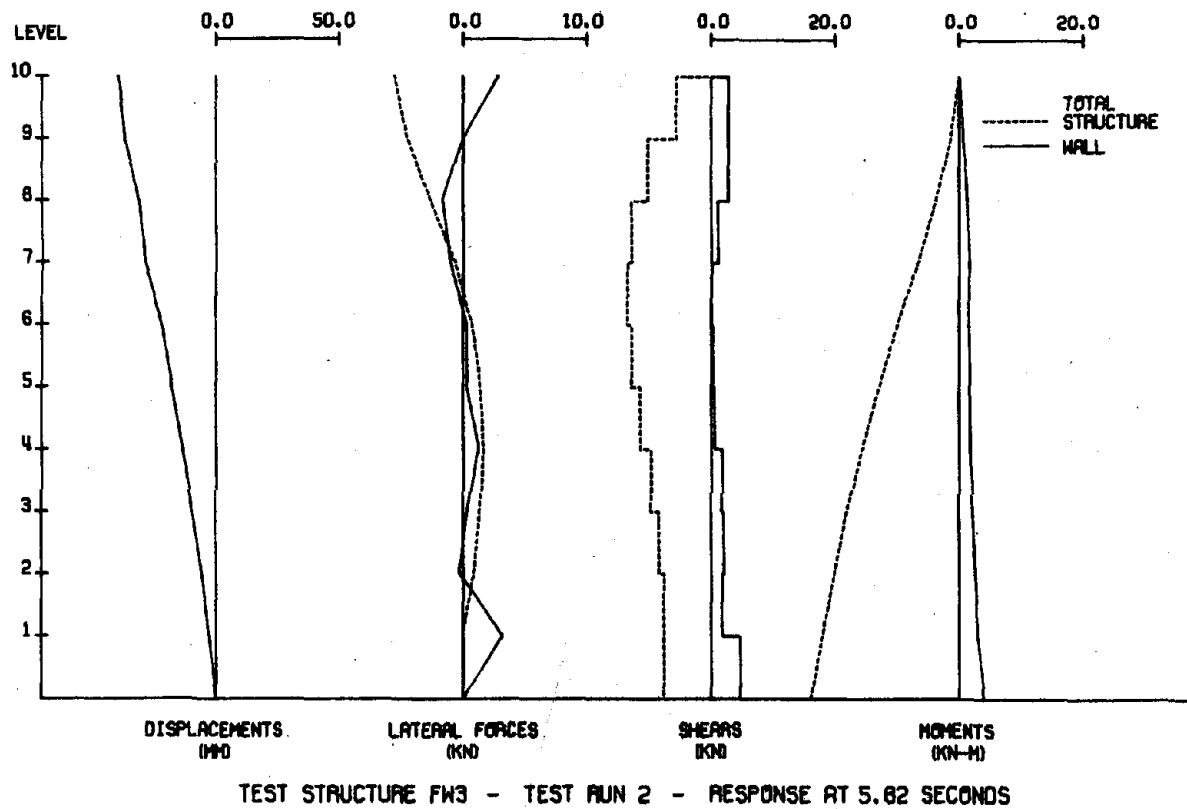
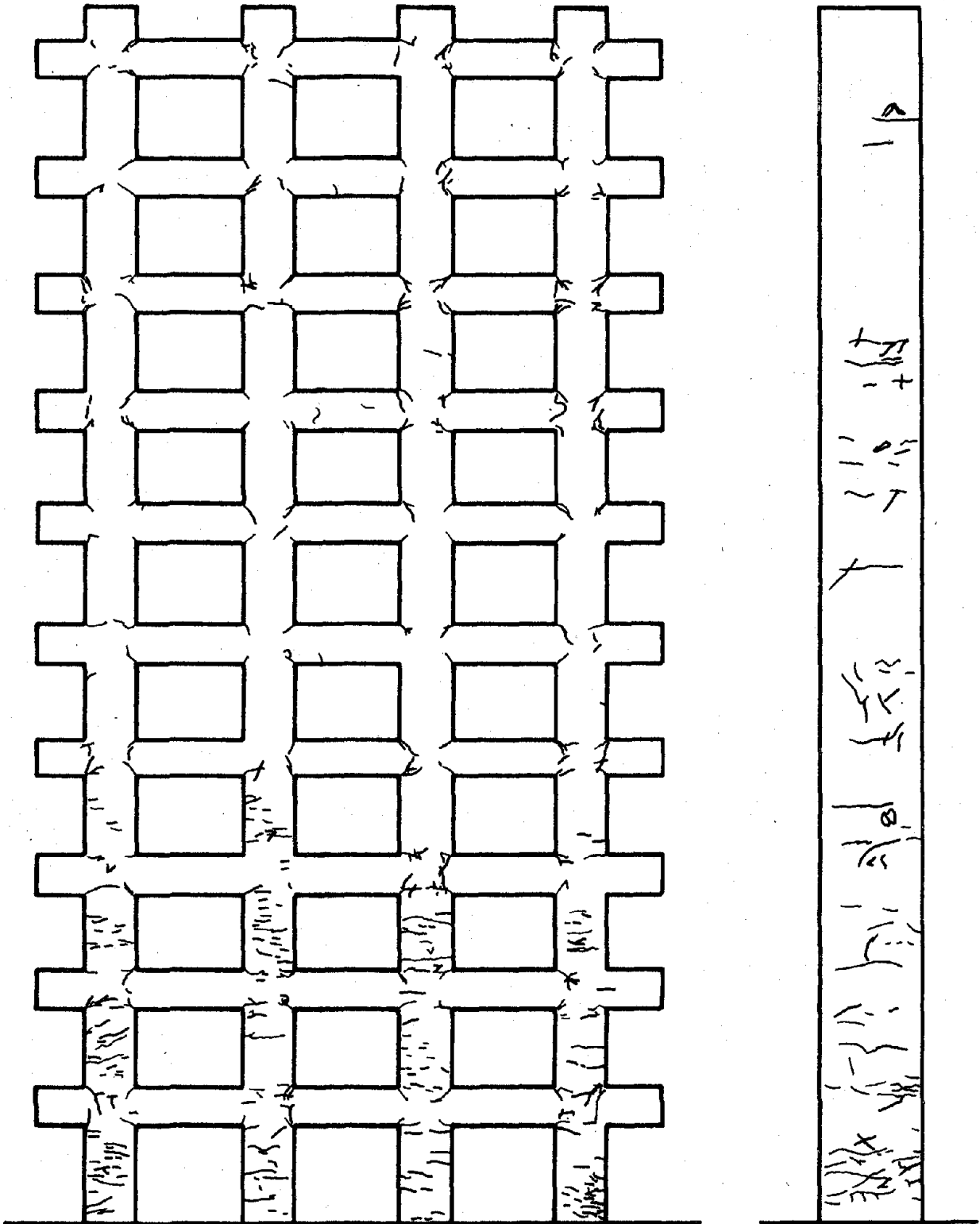


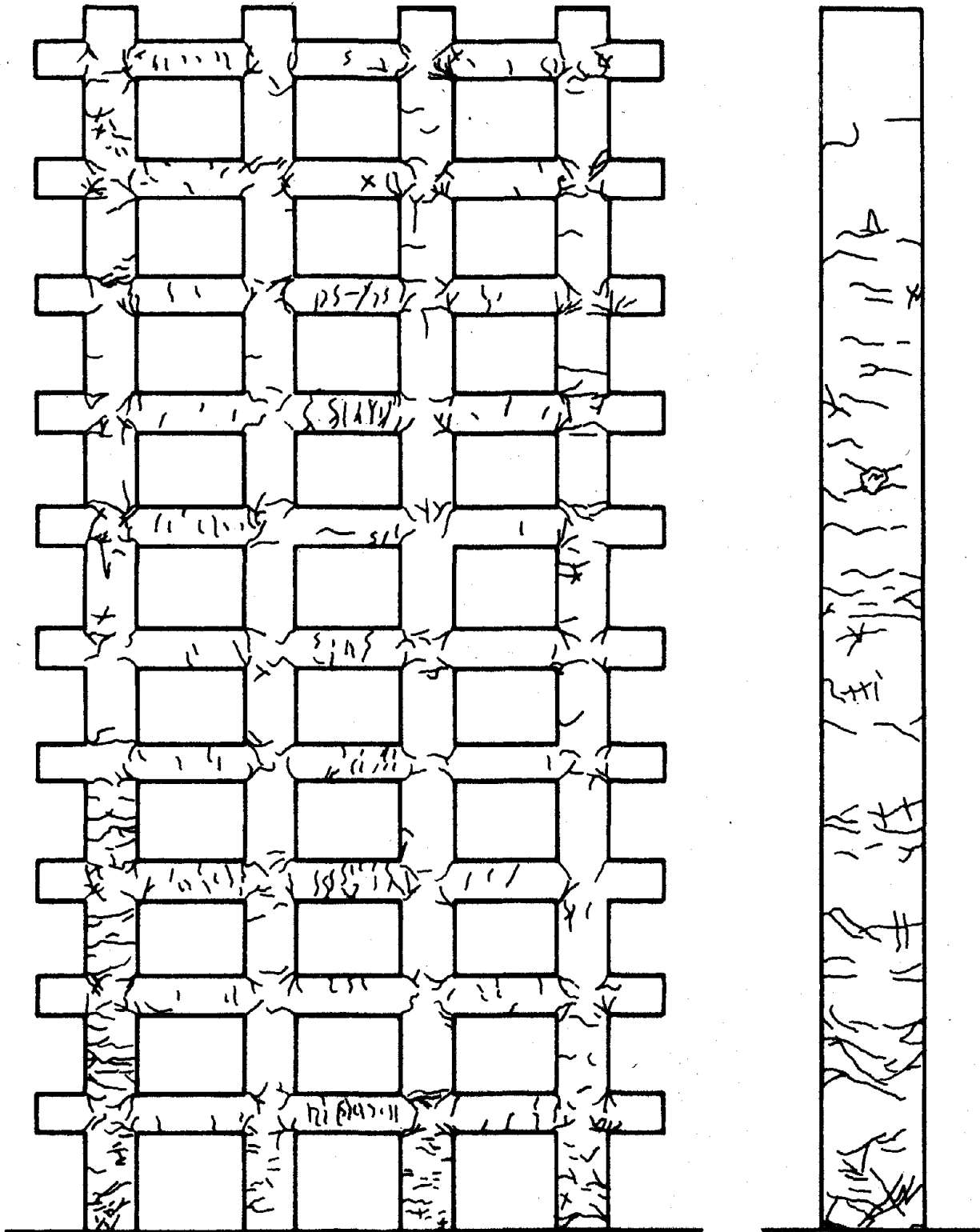
Fig. 5.23 (contd.) Distributions of Response to Second Taft Simulations



(Not To Scale)

(a) Structure with Heavily Reinforced Wall

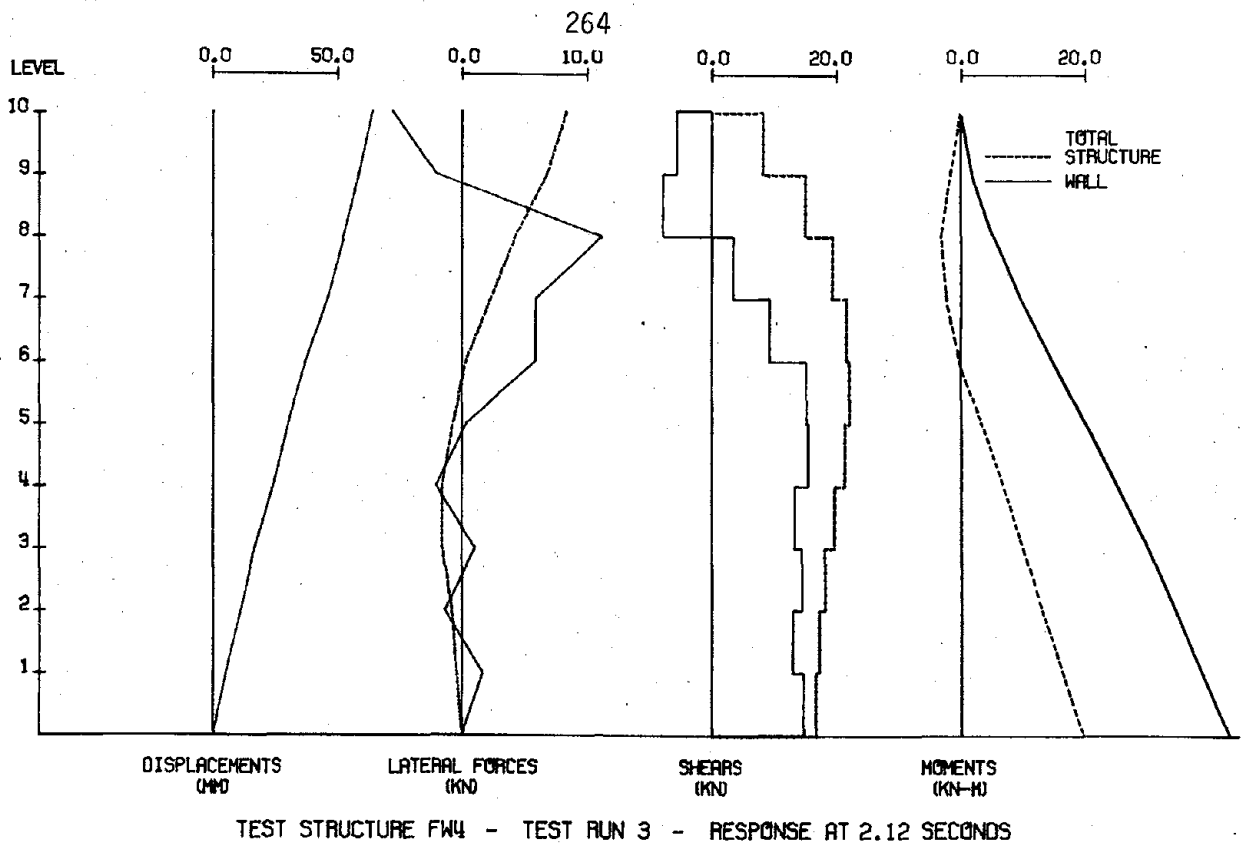
Fig. 5.24 Observed Crack Patterns following Second Taft Simulations



(Not To Scale)

(b) Structure with Lightly Reinforced Wall

Fig. 5.24 (contd.) Observed Crack Patterns following Second Taft Simulations



(a) Structure with Heavily Reinforced Wall

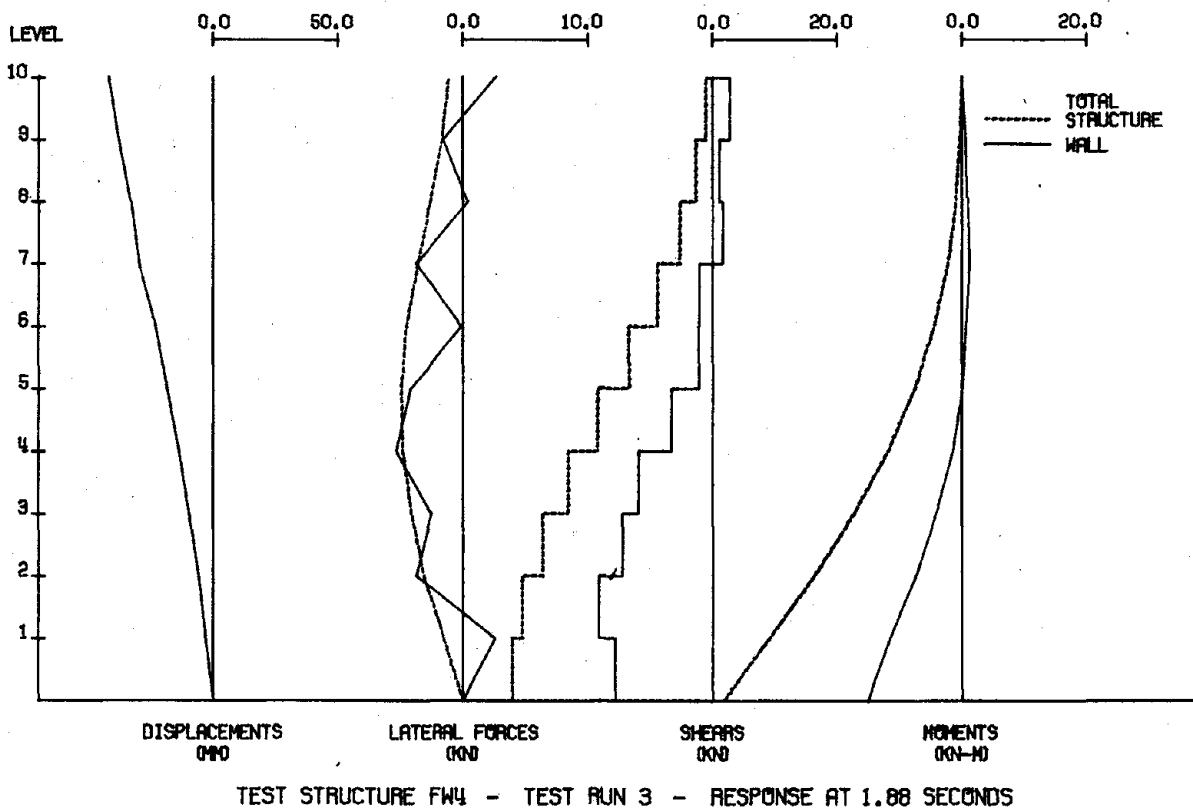
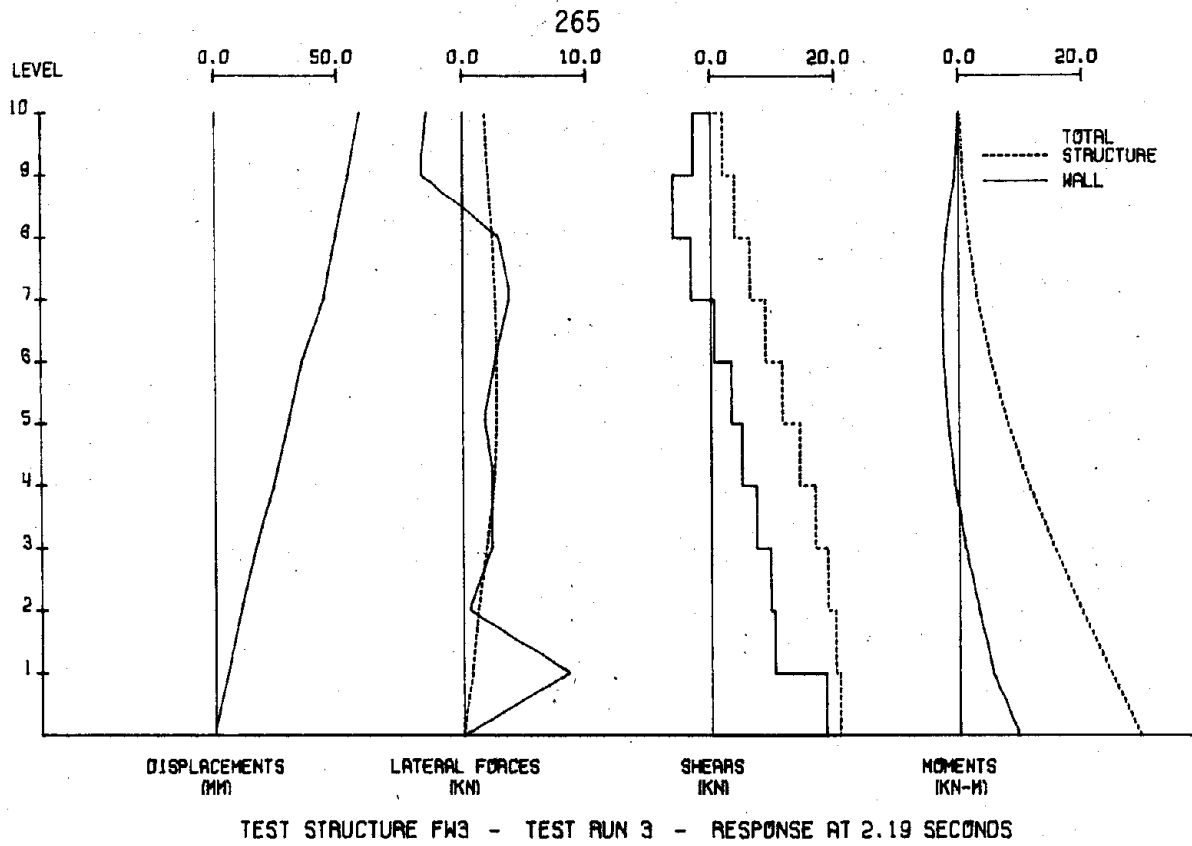


Fig. 5.25 Distributions of Response to Third Taft Simulations



(b) Structure with Lightly Reinforced Wall

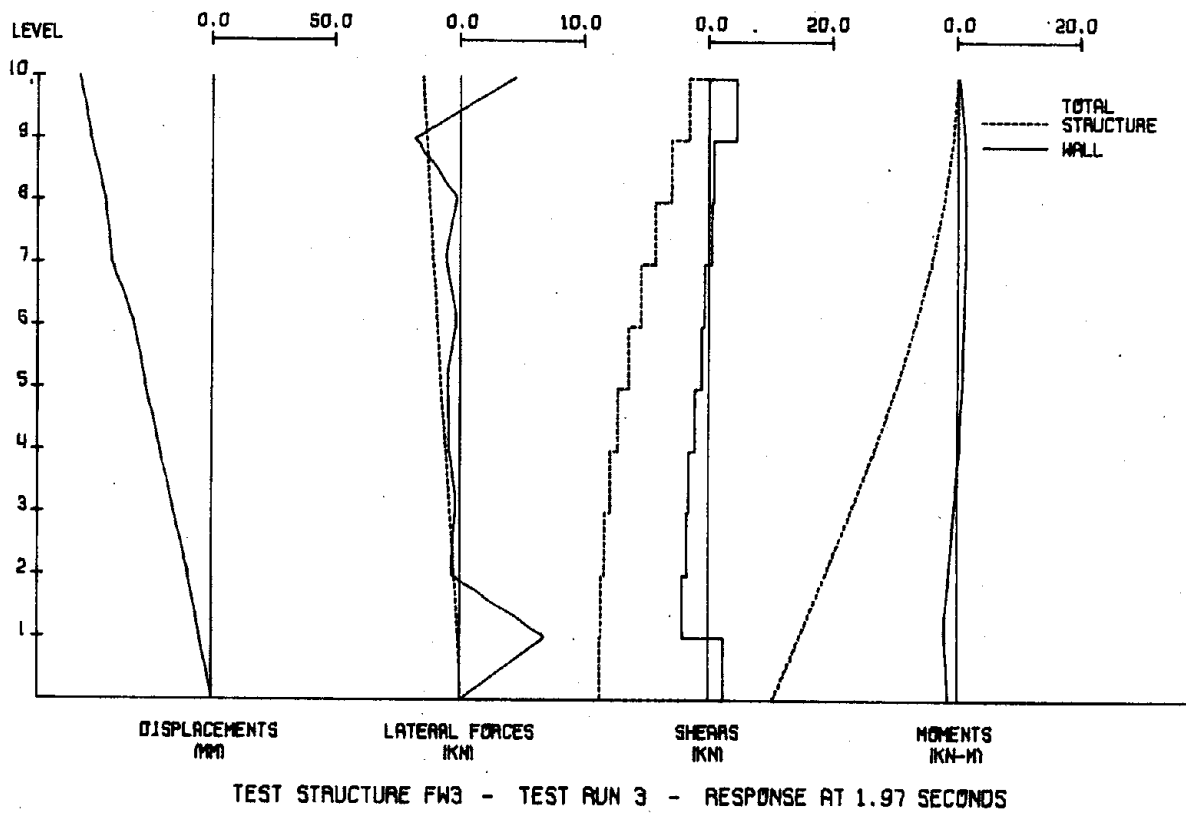


Fig. 5.25 (contd.) Distributions of Response to Third Taft Simulations

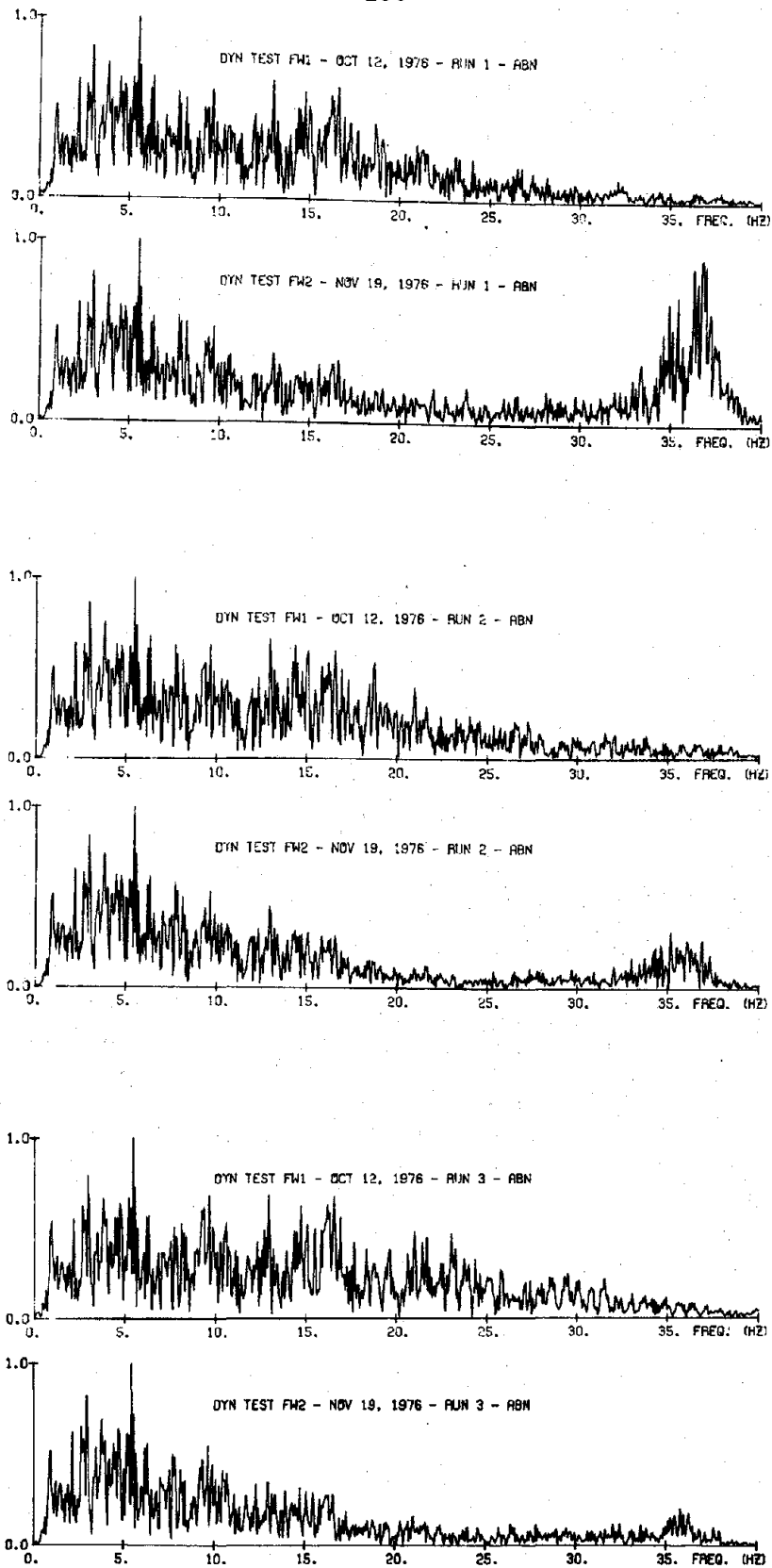


Fig. 6.1 Fourier-Amplitude Spectra of Base Motions

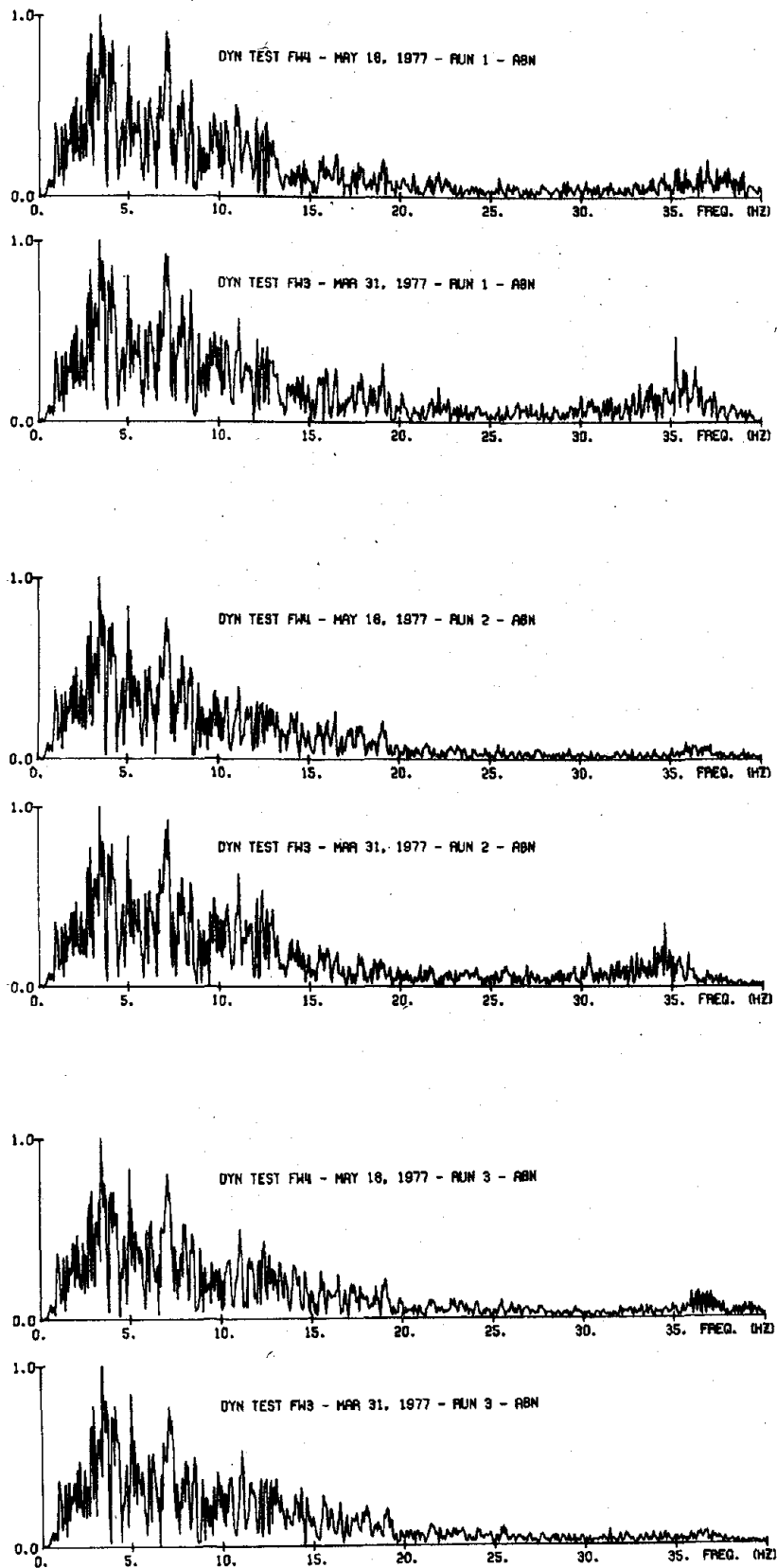
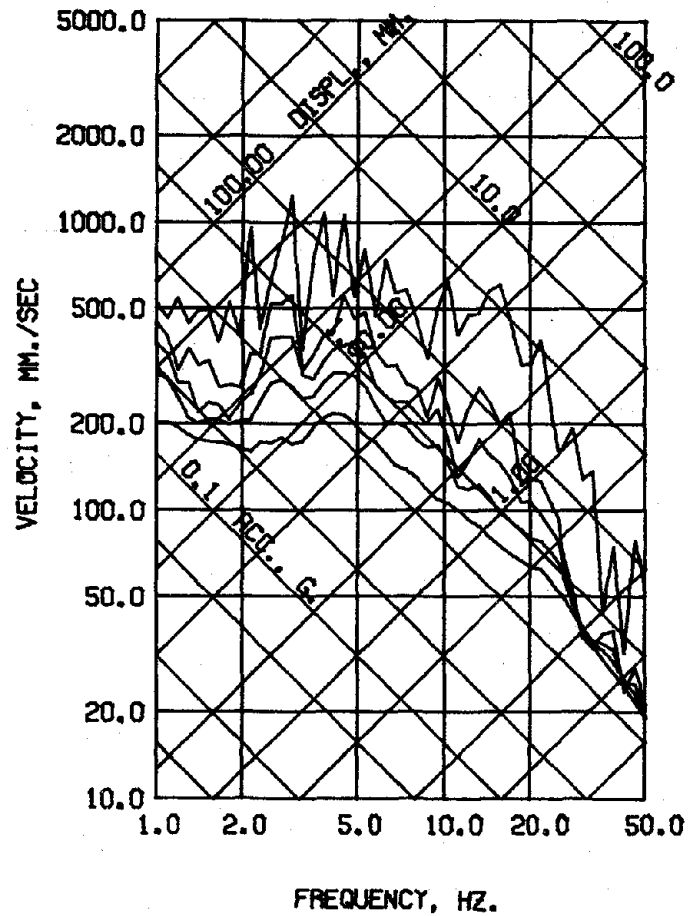
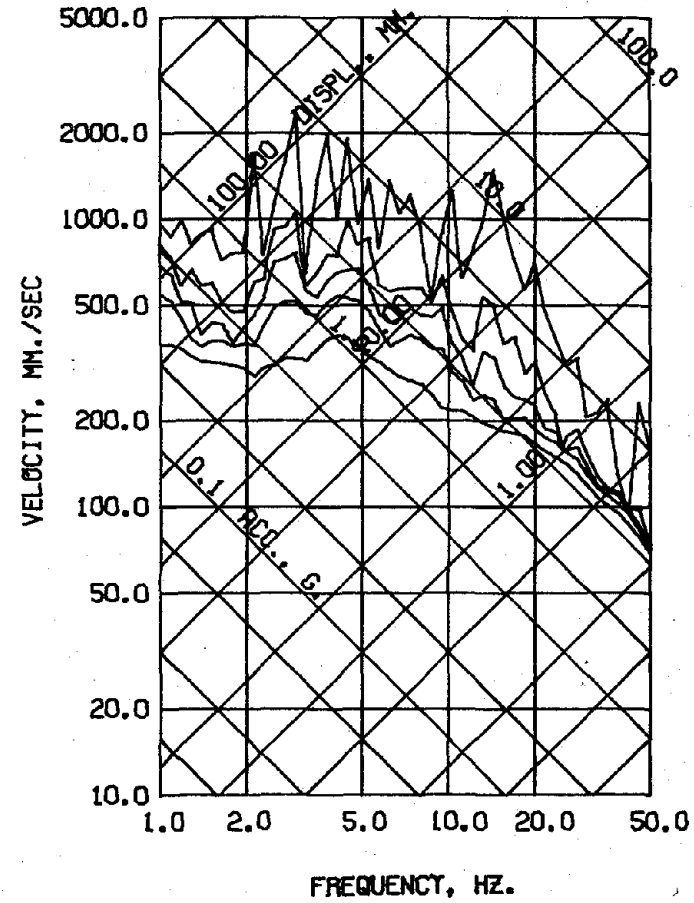


Fig. 6.1 (contd.) Fourier-Amplitude Spectra of Base Motions

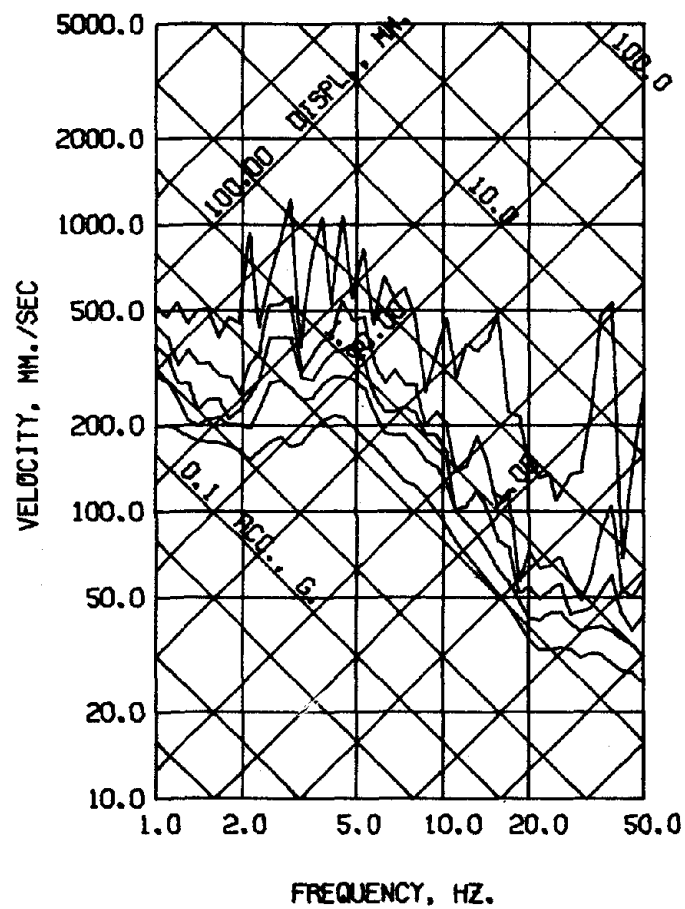


DYN TEST FW1 - OCT 12, 1976 - RUN 1 - ABN
DAMPING FACTOR = 0.00 0.02 0.05 0.10 0.20

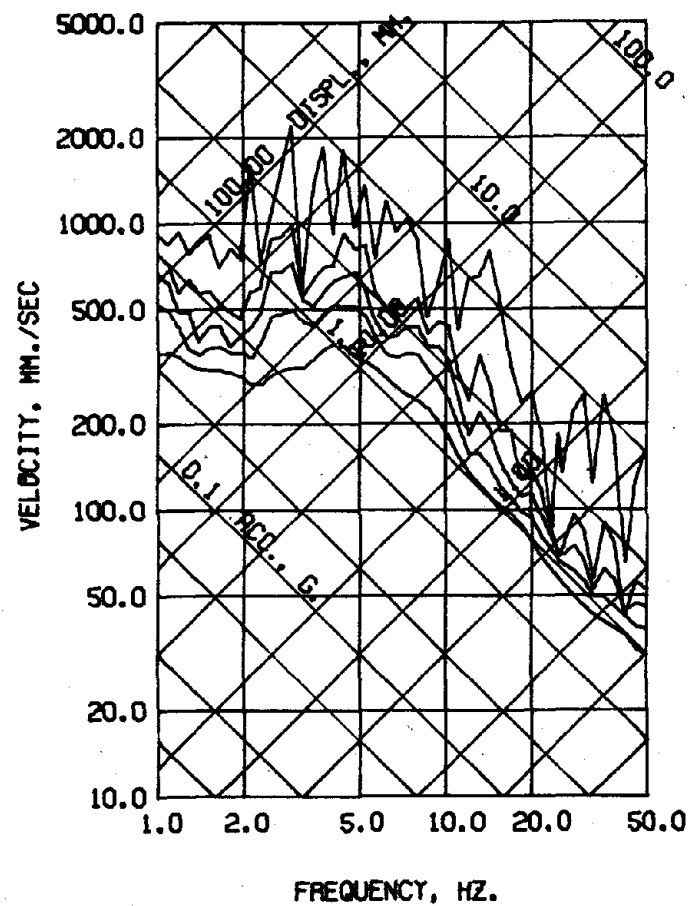


DYN TEST FW1 - OCT 12, 1976 - RUN 2 - ABN
DAMPING FACTOR = 0.00 0.02 0.05 0.10 0.20

Fig. 6.2 Spectral-Response Curves of El Centro Simulations.

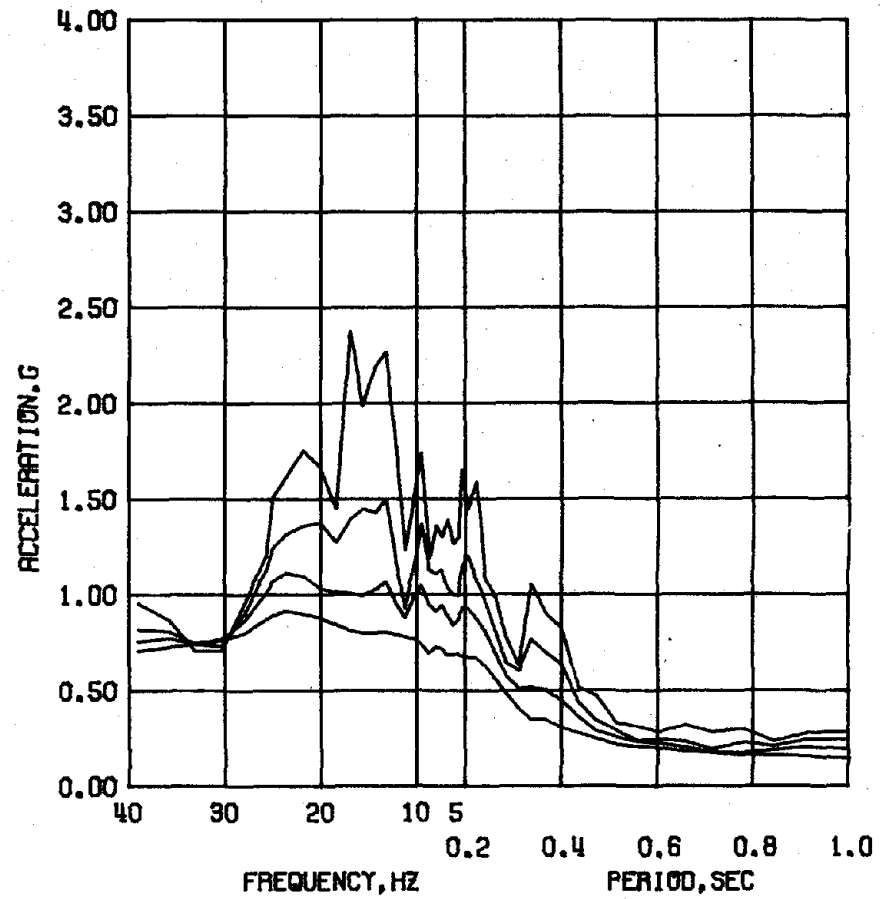
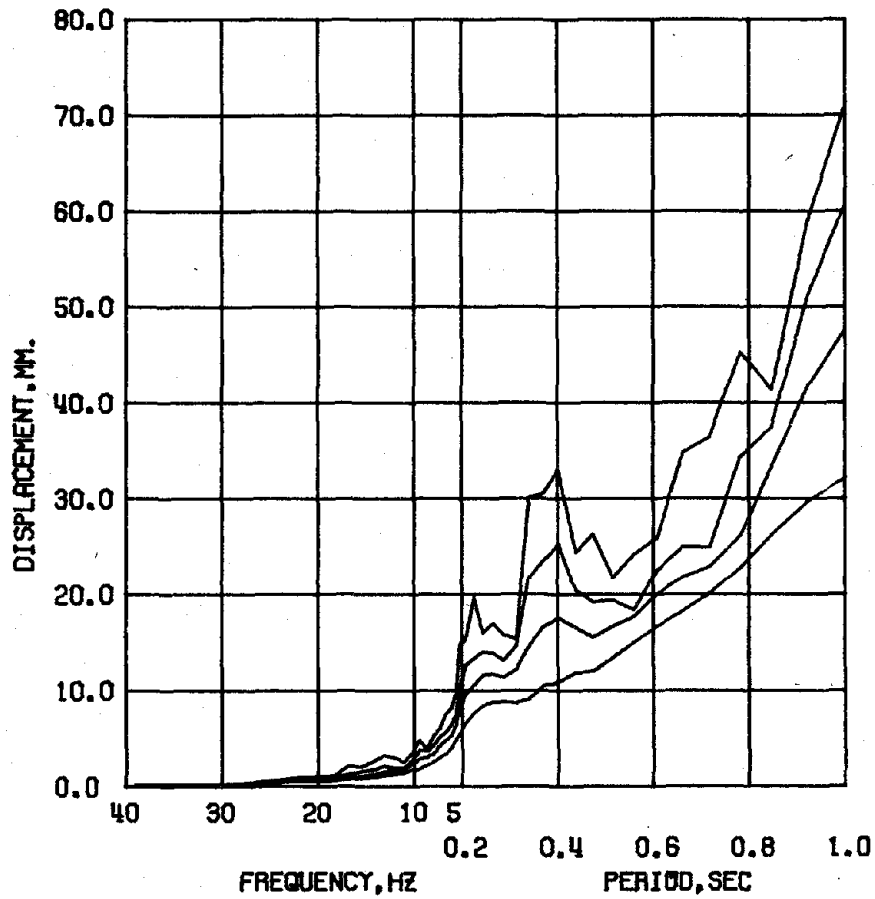


DYN TEST FW2 - NOV 19, 1976 - RUN 1 - ABN
 DAMPING FACTOR = 0.00 0.02 0.05 0.10 0.20



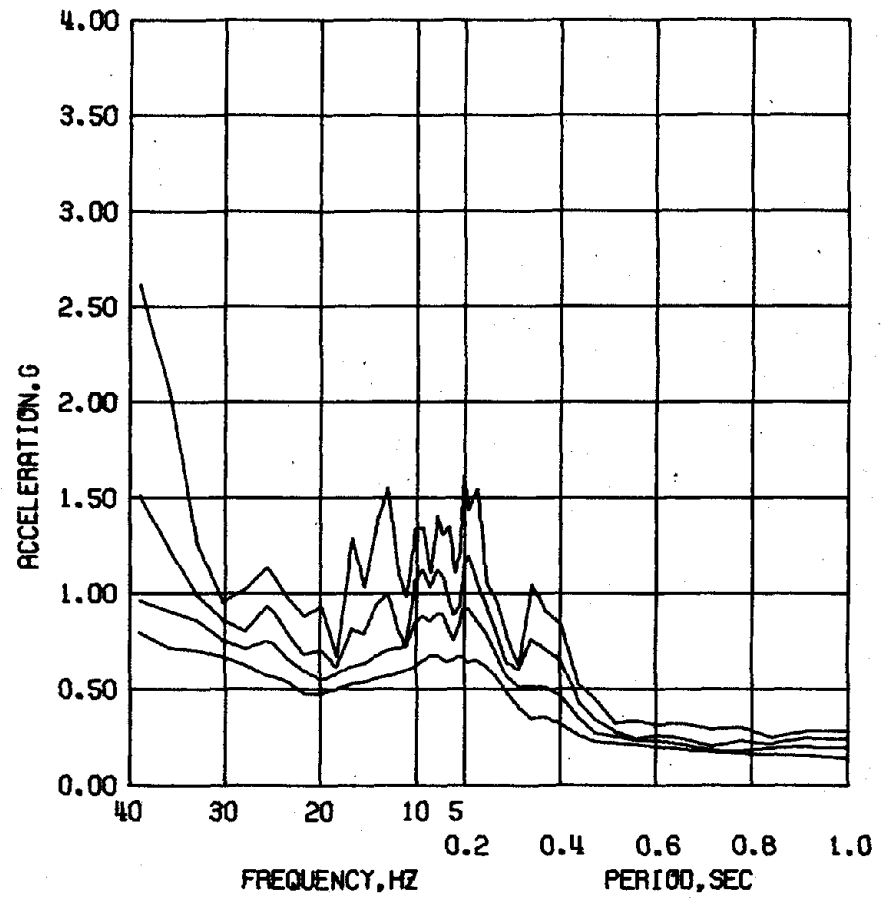
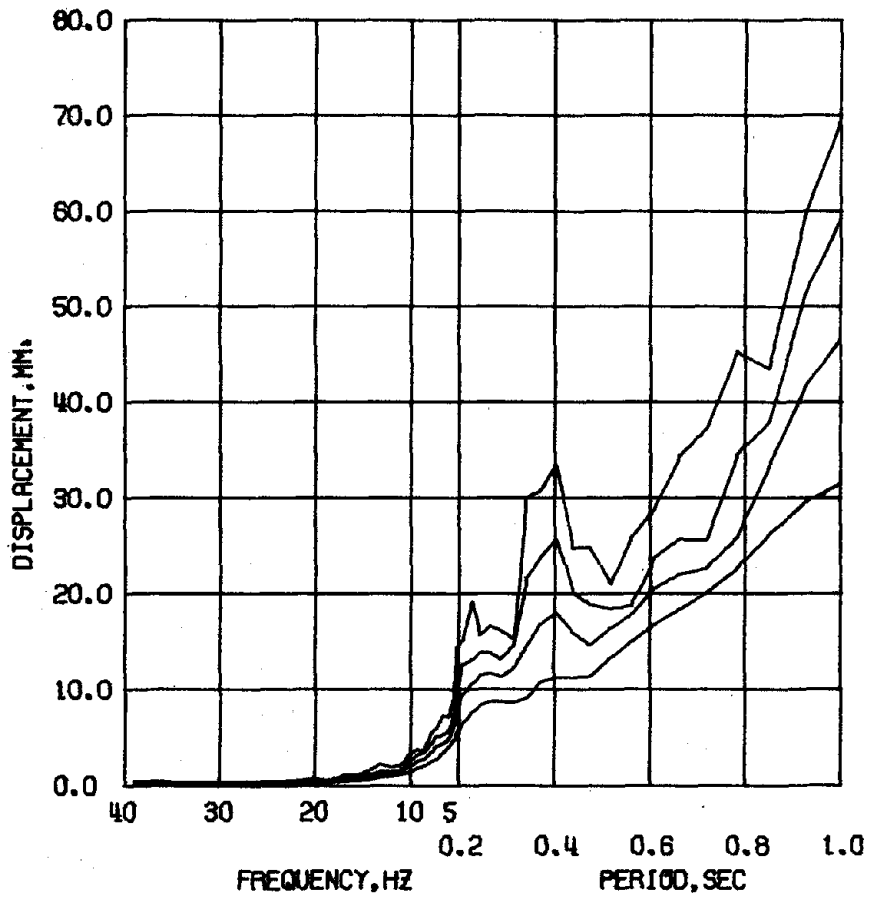
DYN TEST FW2 - NOV 19, 1976 - RUN 2 - ABN
 DAMPING FACTOR = 0.00 0.02 0.05 0.10 0.20

Fig. 6.2 (contd.) Spectral-Response Curves of El Centro Simulations



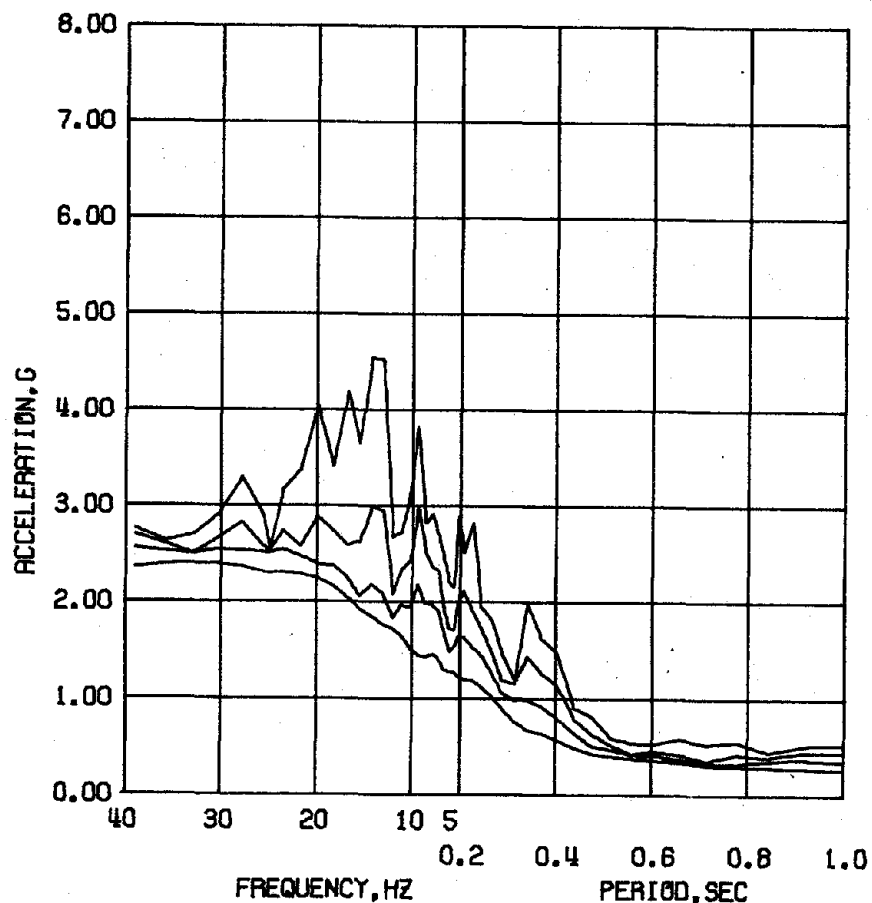
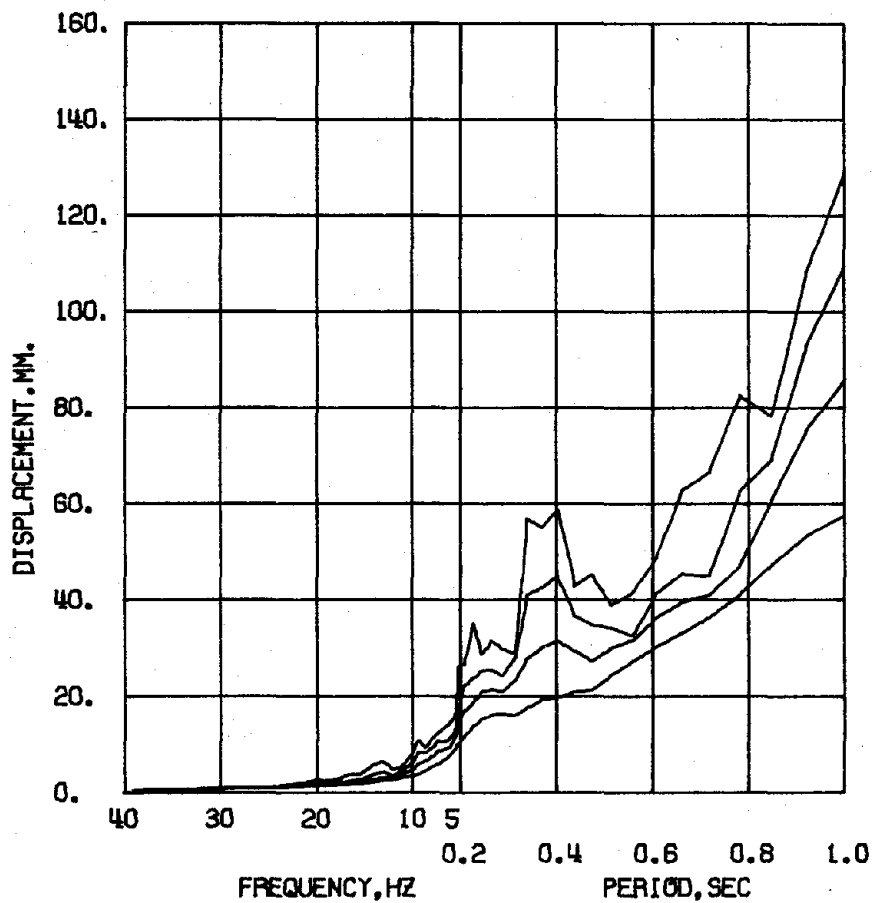
DYN TEST FW1 - OCT 12, 1976 - RUN 1 - ABN
 DAMPING FACTOR = 0.02 0.05 0.10 0.20

Fig. 6.2 (contd.) Spectral-Response Curves of El Centro Simulations



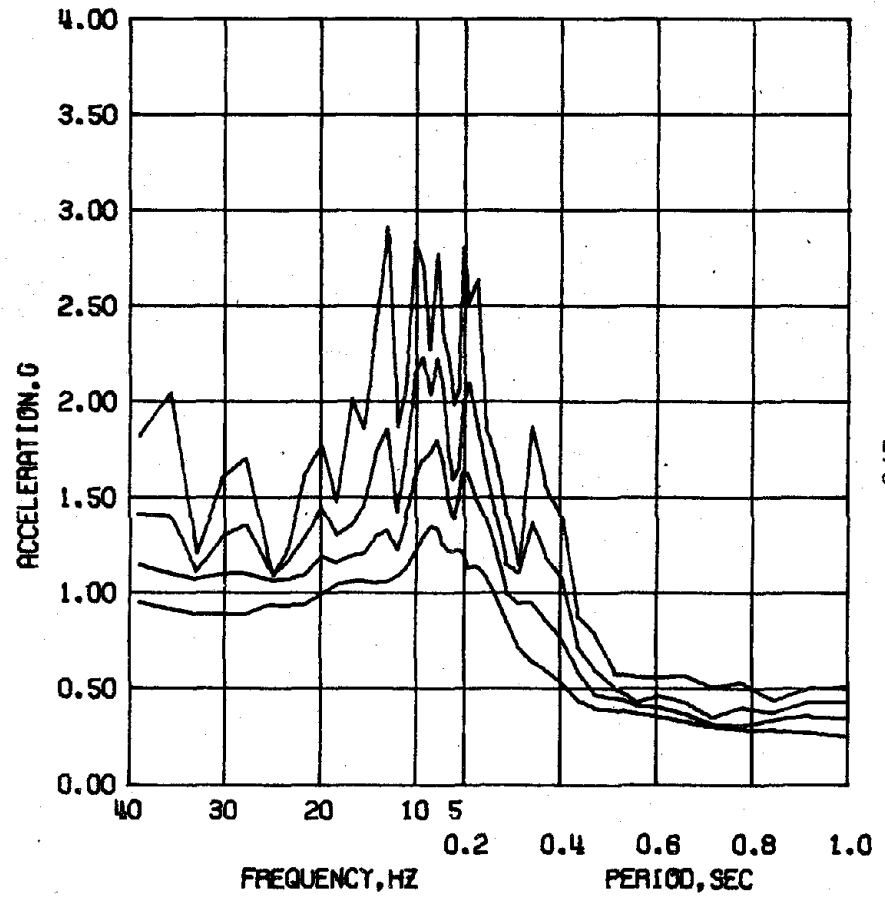
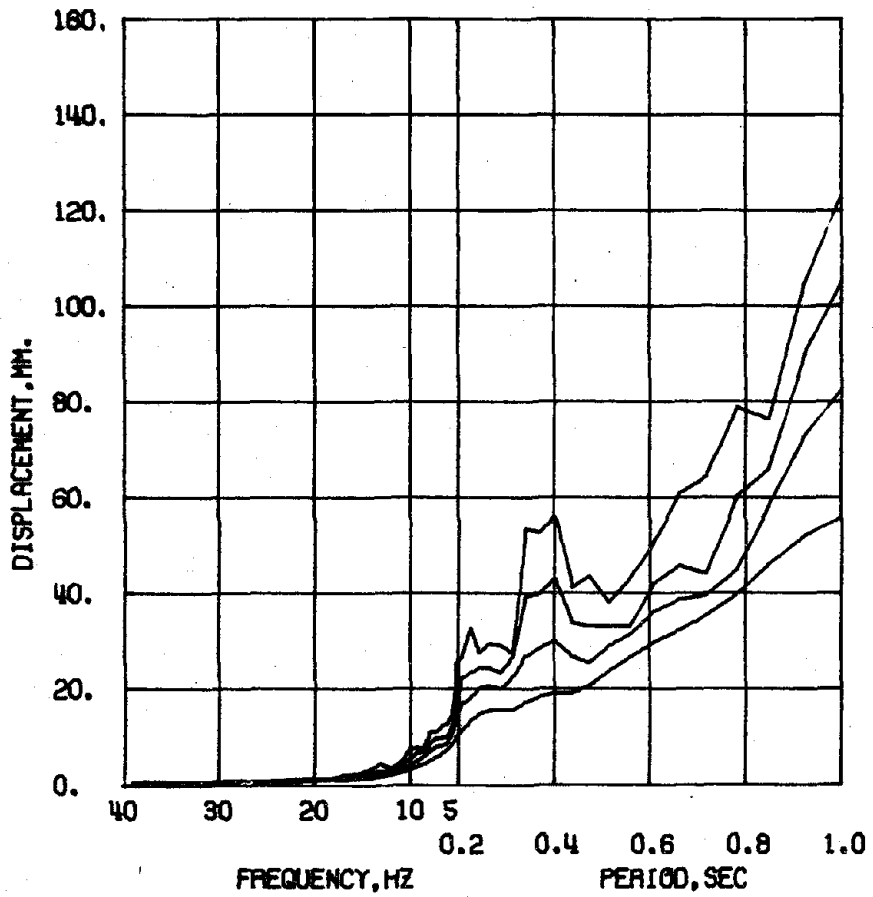
DYN TEST FW2 - NOV 19, 1976 - RUN 1 - ABN
 DAMPING FACTOR = 0.02 0.05 0.10 0.20

Fig. 6.2 (contd.) Spectral-Response Curves of El Centro Simulations



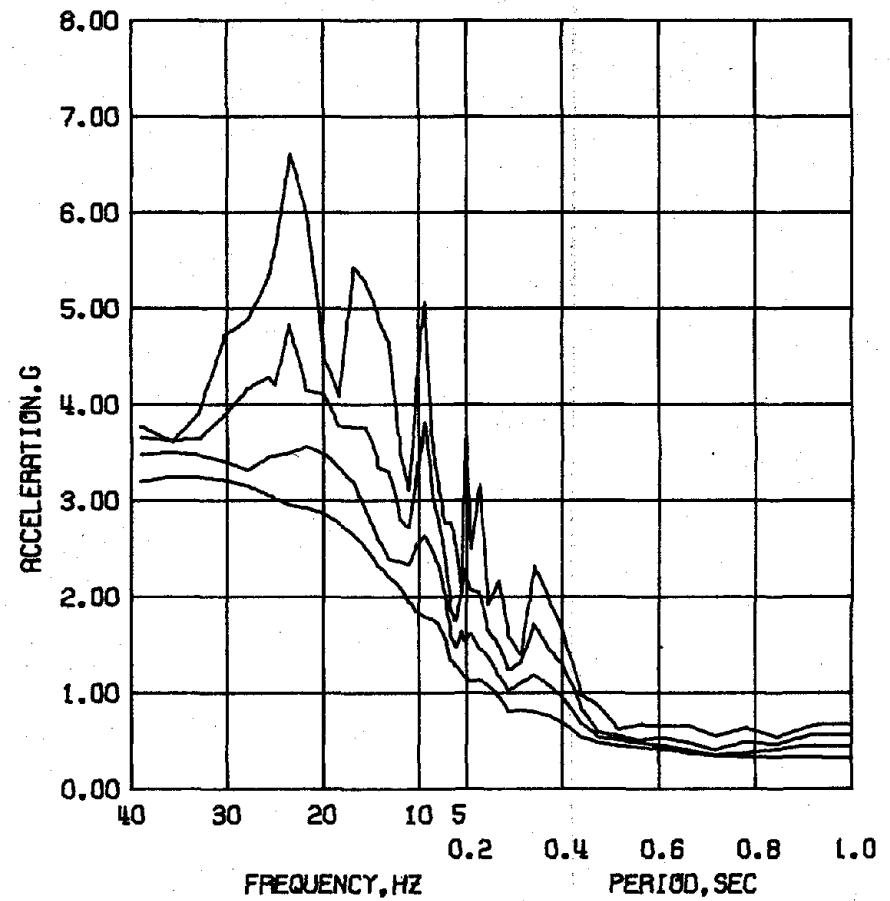
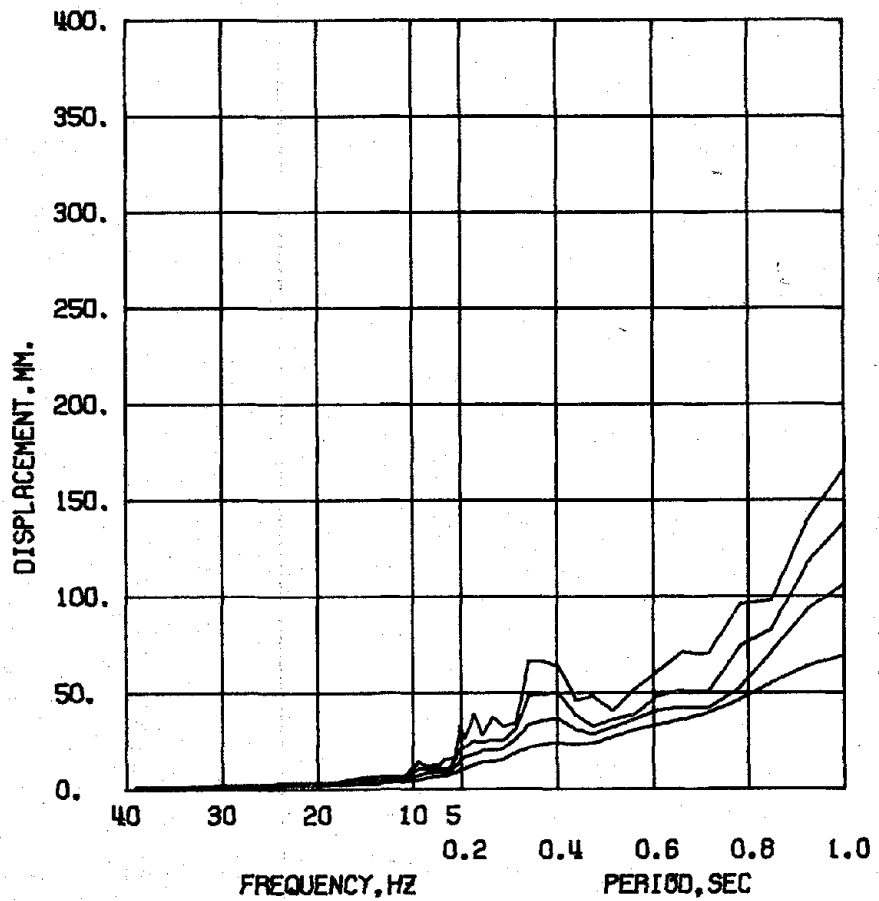
DYN TEST FW1 - OCT 12, 1976 - RUN 2 - ABN
 DAMPING FACTOR = 0.02 0.05 0.10 0.20

Fig. 6.2 (contd.) Spectral-Response Curves of El Centro Simulations



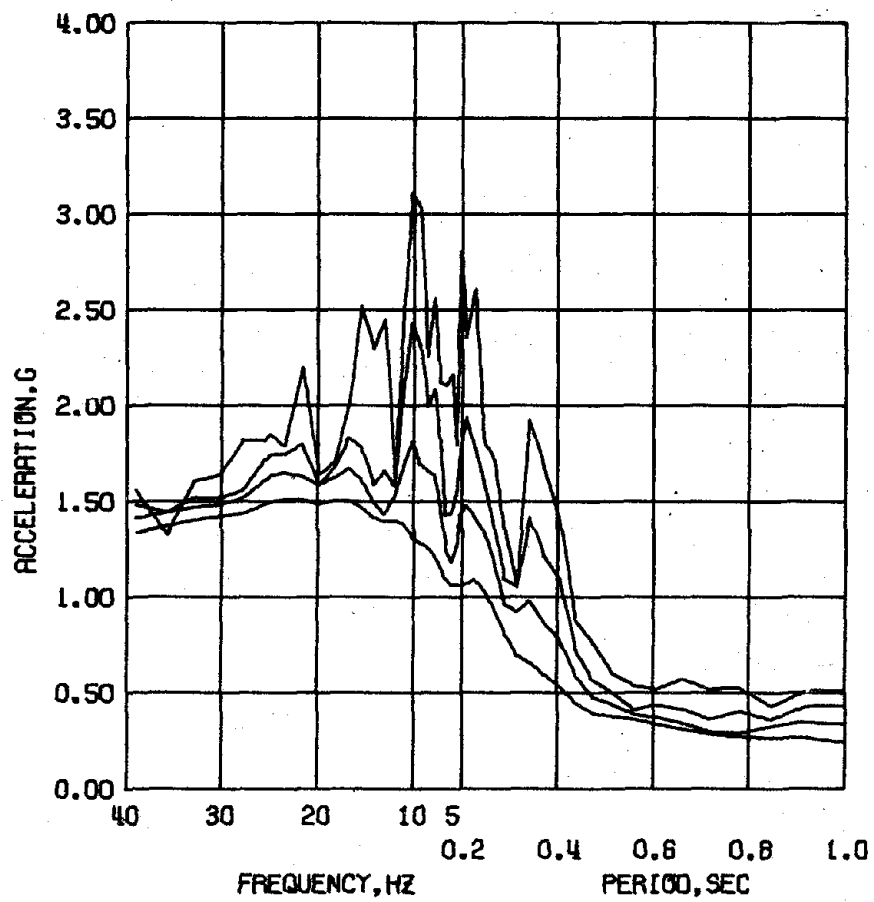
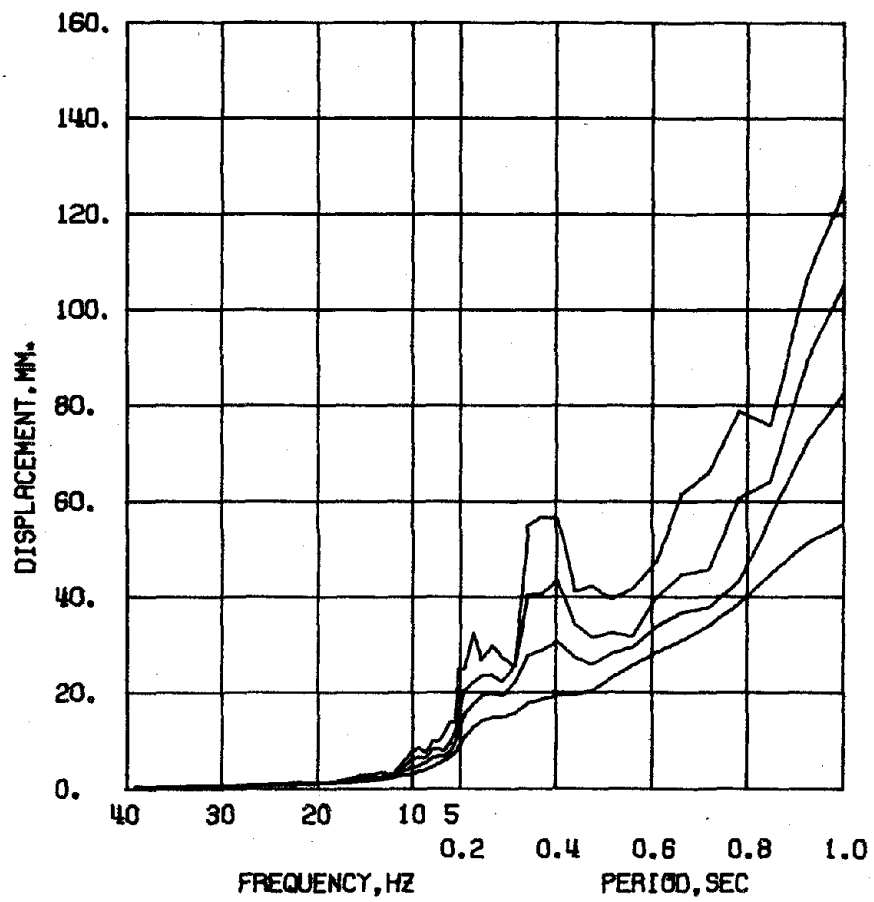
DYN TEST FW2 - NOV 19, 1976 - RUN 2 - ABN
 DAMPING FACTOR = 0.02 0.05 0.10 0.20

Fig. 6.2 (contd.) Spectral-Response Curves of El Centro Simulations



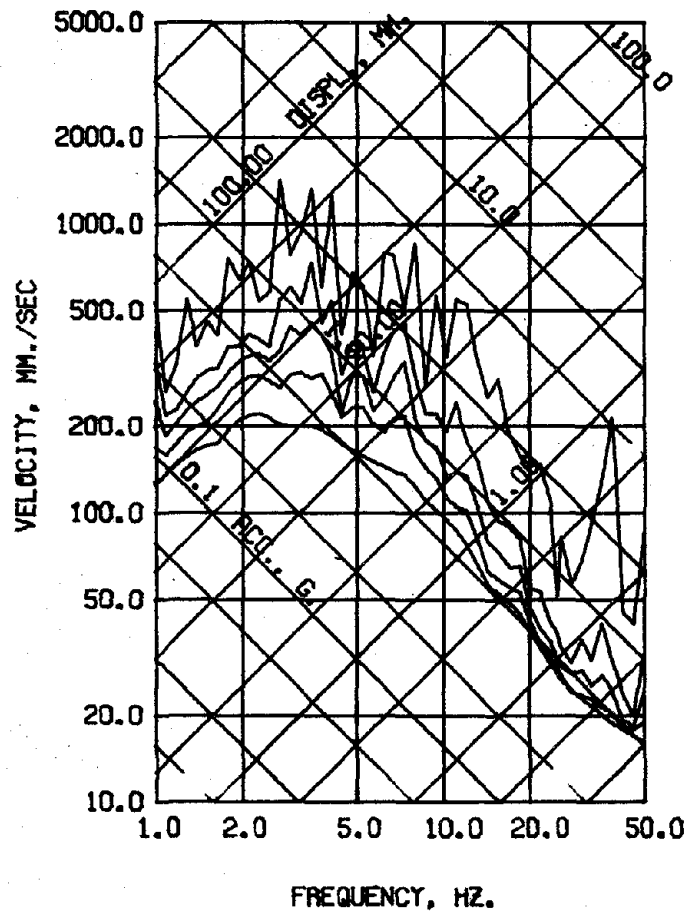
DYN TEST FW1 - OCT 12, 1976 - RUN 3 - ABN
 DAMPING FACTOR = 0.02 0.05 0.10 0.20

Fig. 6.2 (contd.) Spectral-Response Curves of El Centro Simulations

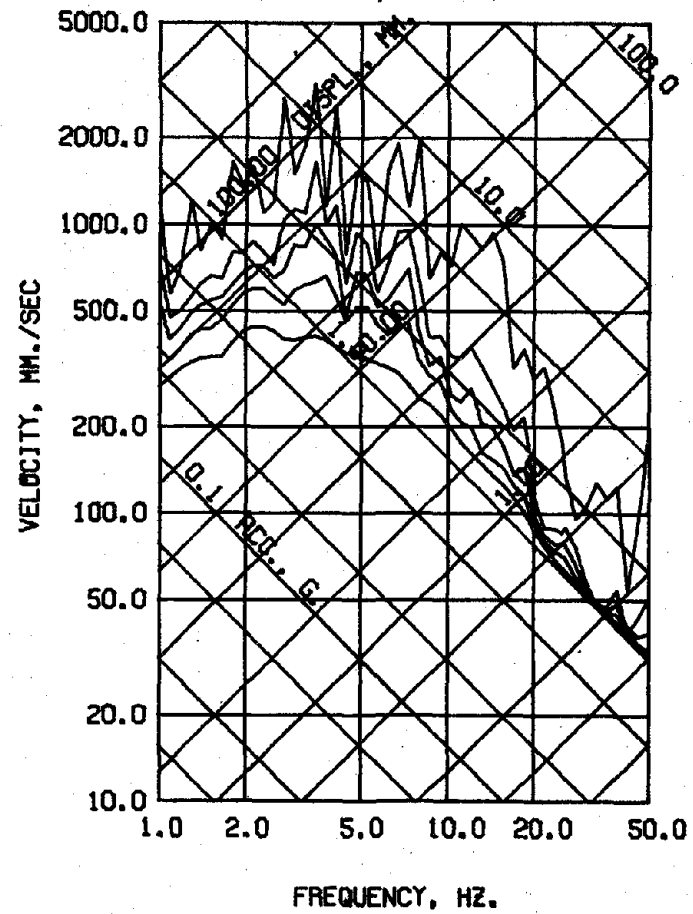


DYN TEST FW2 - NOV 19, 1976 - RUN 3 - ABN
 DAMPING FACTOR = 0.02 0.05 0.10 0.20

Fig. 6.2 (contd.) Spectral-Response Curves of El Centro Simulations

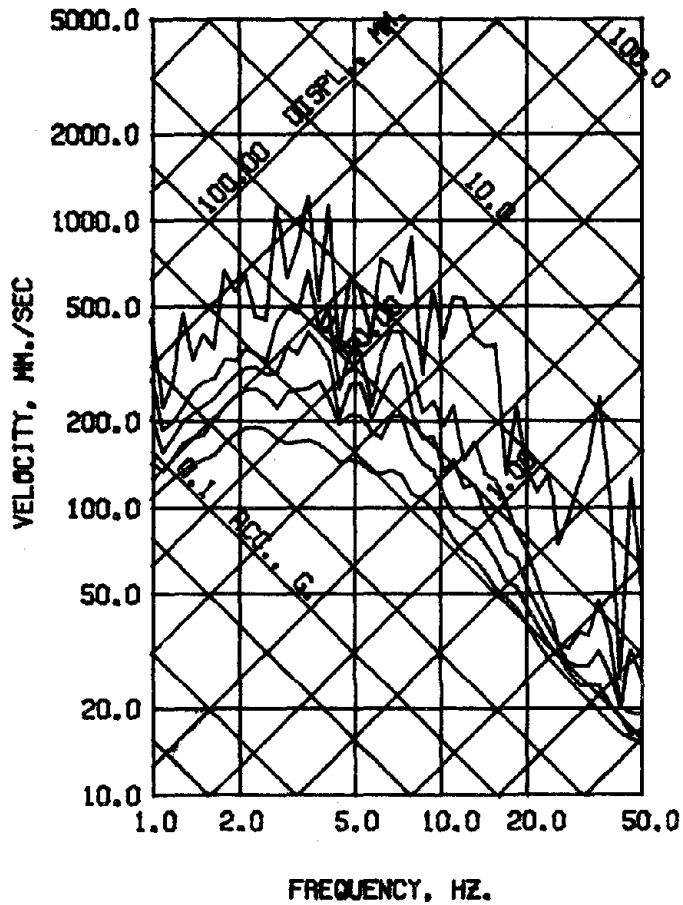


DYN TEST FW4 - MAY 18, 1977 - RUN 1 - ABN
 DAMPING FACTOR = 0.00 0.02 0.05 0.10 0.20

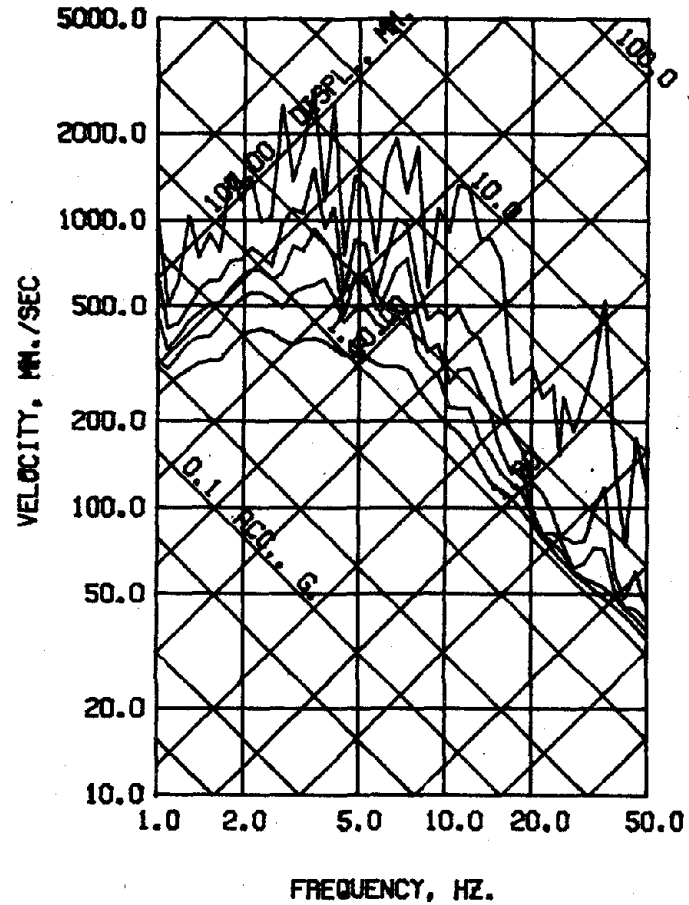


DYN TEST FW4 - MAY 18, 1977 - RUN 2 - ABN
 DAMPING FACTOR = 0.00 0.02 0.05 0.10 0.20

Fig. 6.3 Spectral-Response Curves of Taft Simulations

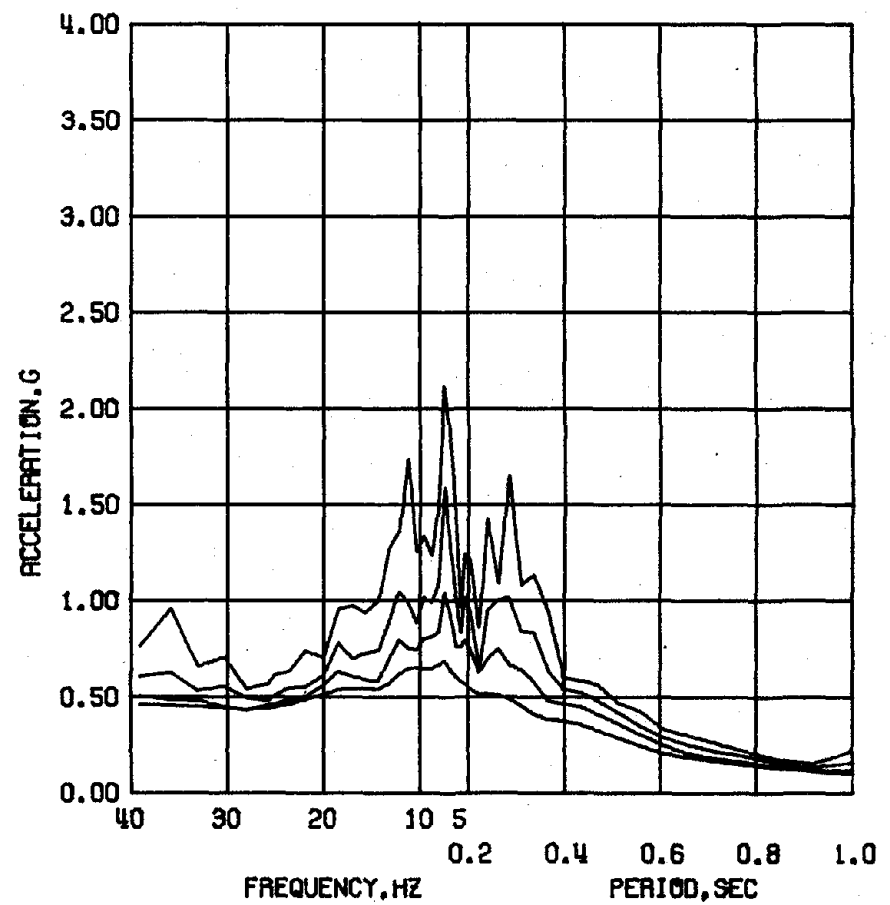
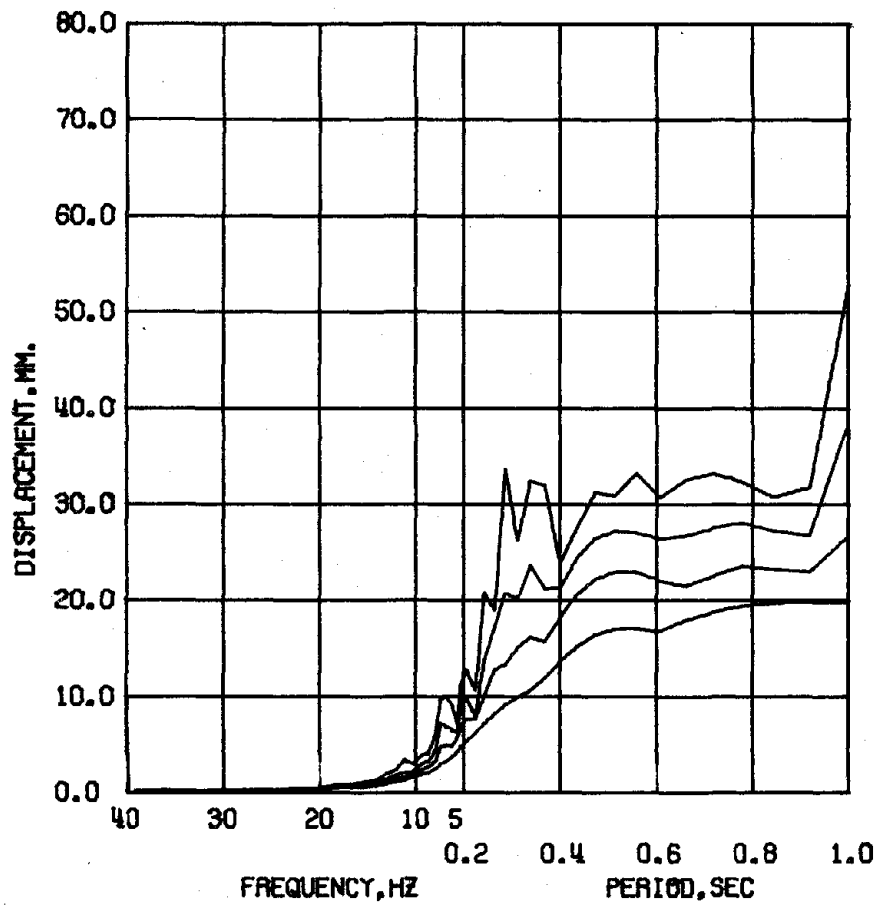


DYN TEST FW3 - MAR 31, 1977 - RUN 1 - ABN
 DAMPING FACTOR = 0.00 0.02 0.05 0.10 0.20



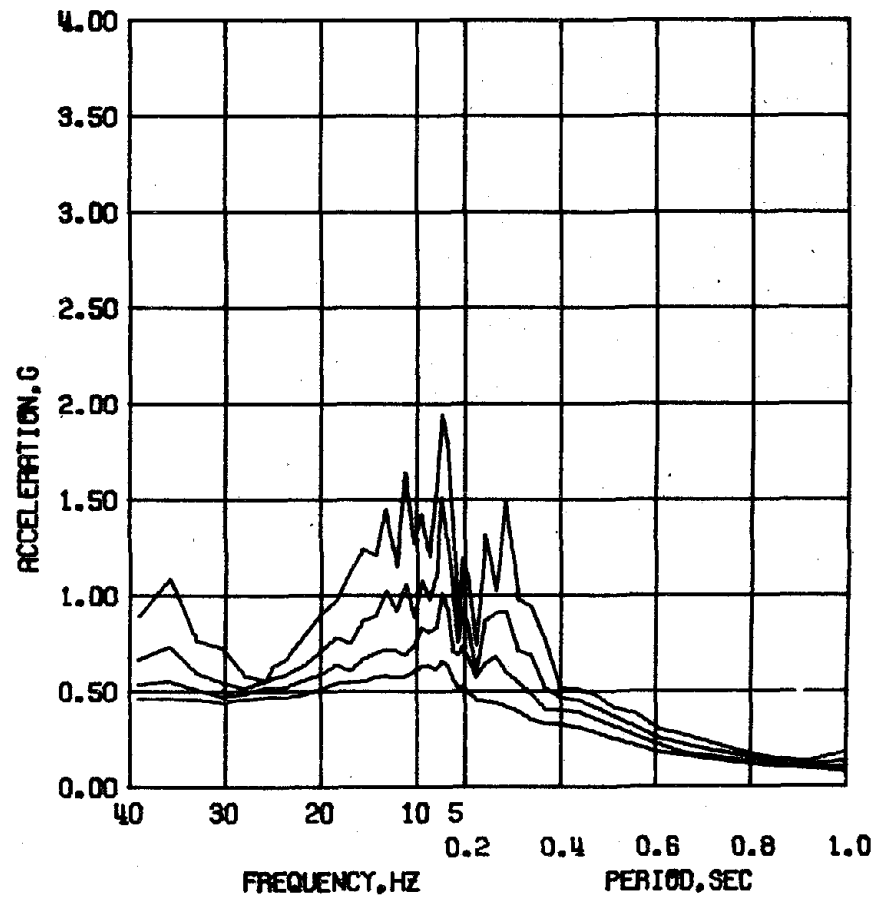
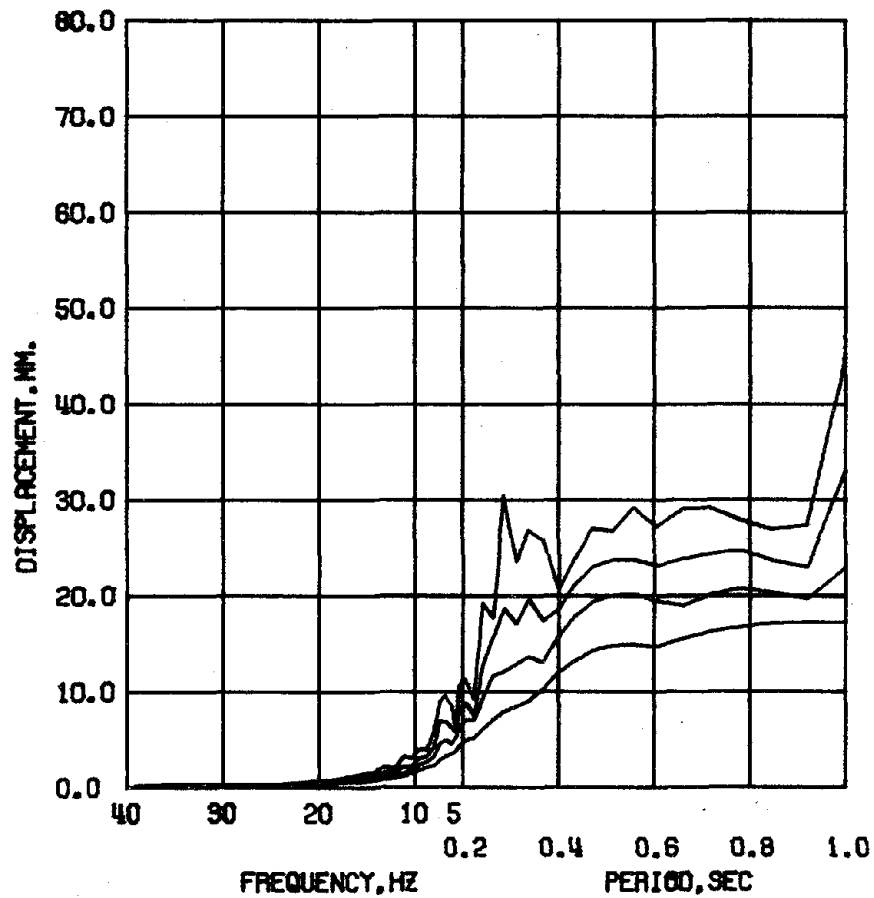
DYN TEST FW3 - MAR 31, 1977 - RUN 2 - ABN
 DAMPING FACTOR = 0.00 0.02 0.05 0.10 0.20

Fig. 6.3 (contd.) Spectral-Response Curves of Taft Simulations



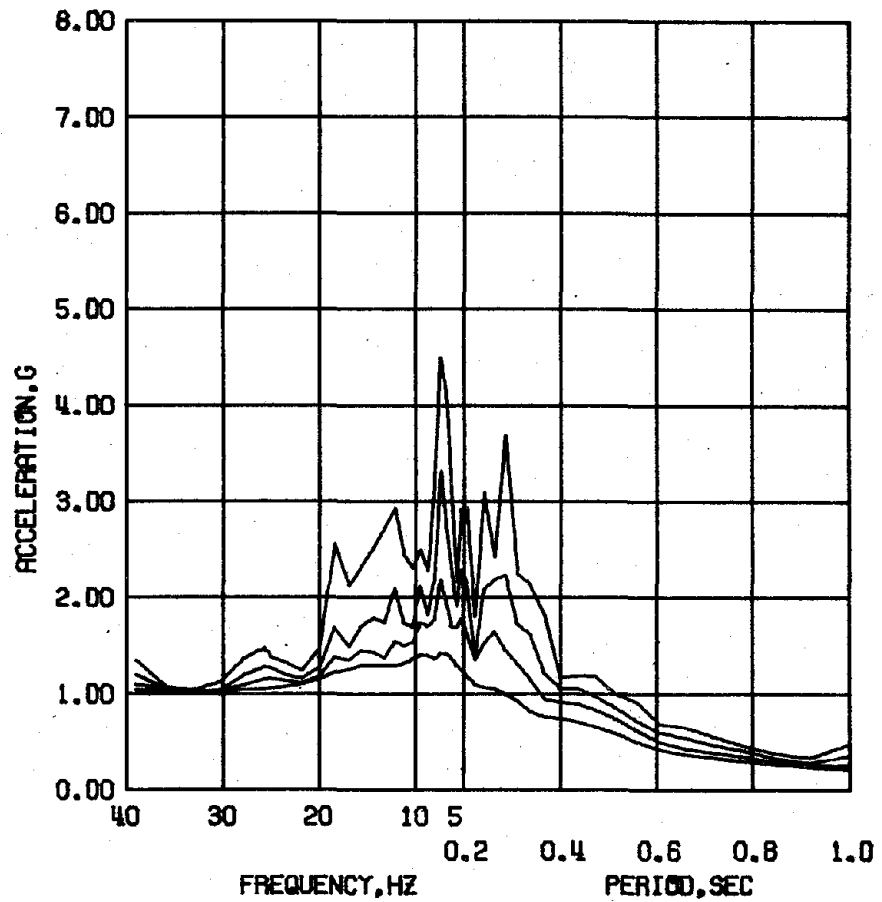
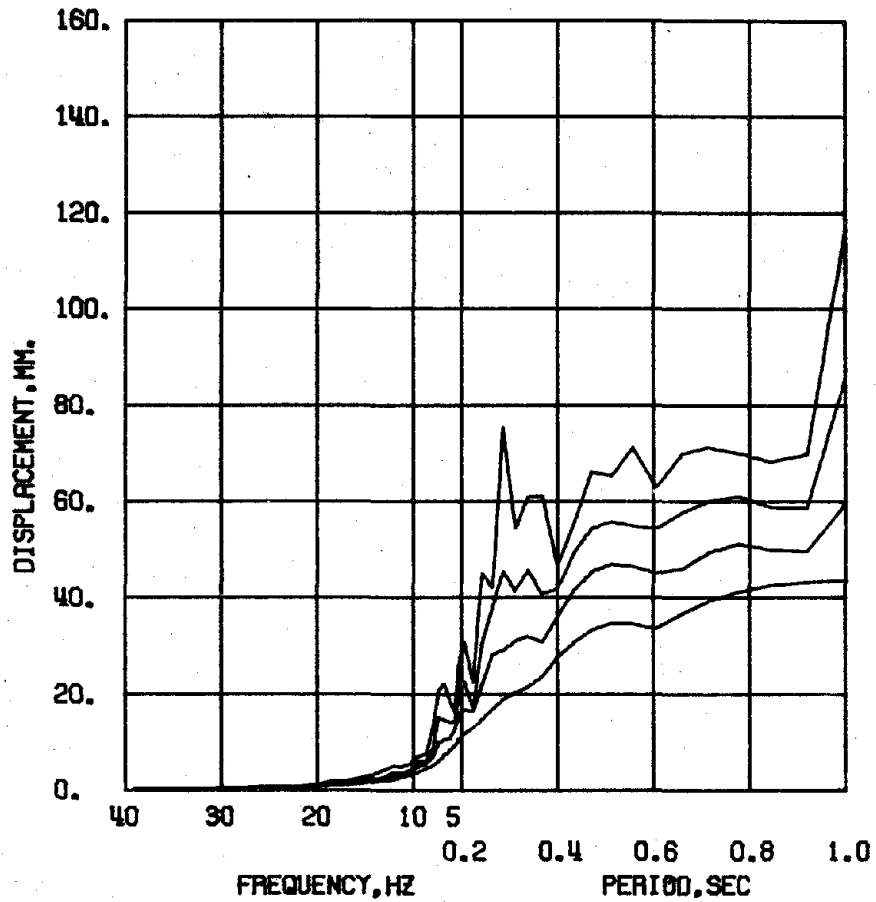
DYN TEST FW4 - MAY 18, 1977 - RUN 1 - ABN
 DAMPING FACTOR = 0.02 0.05 0.10 0.20

Fig. 6.3 (contd.) Spectral-Response Curves of Taft Simulations



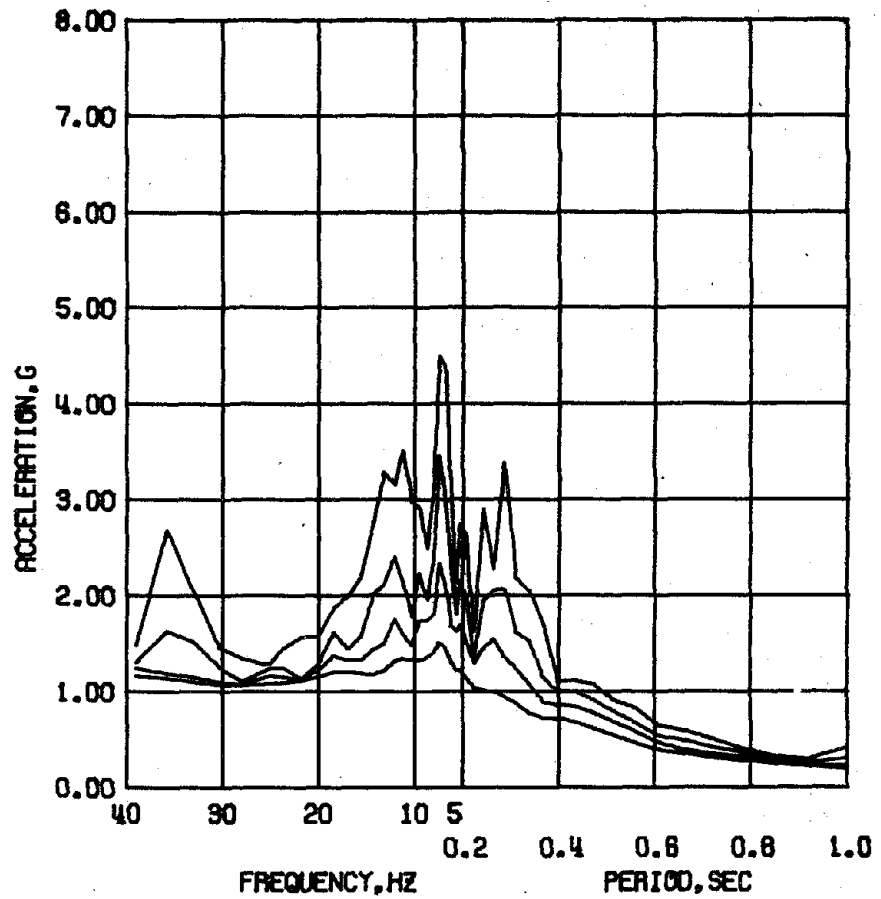
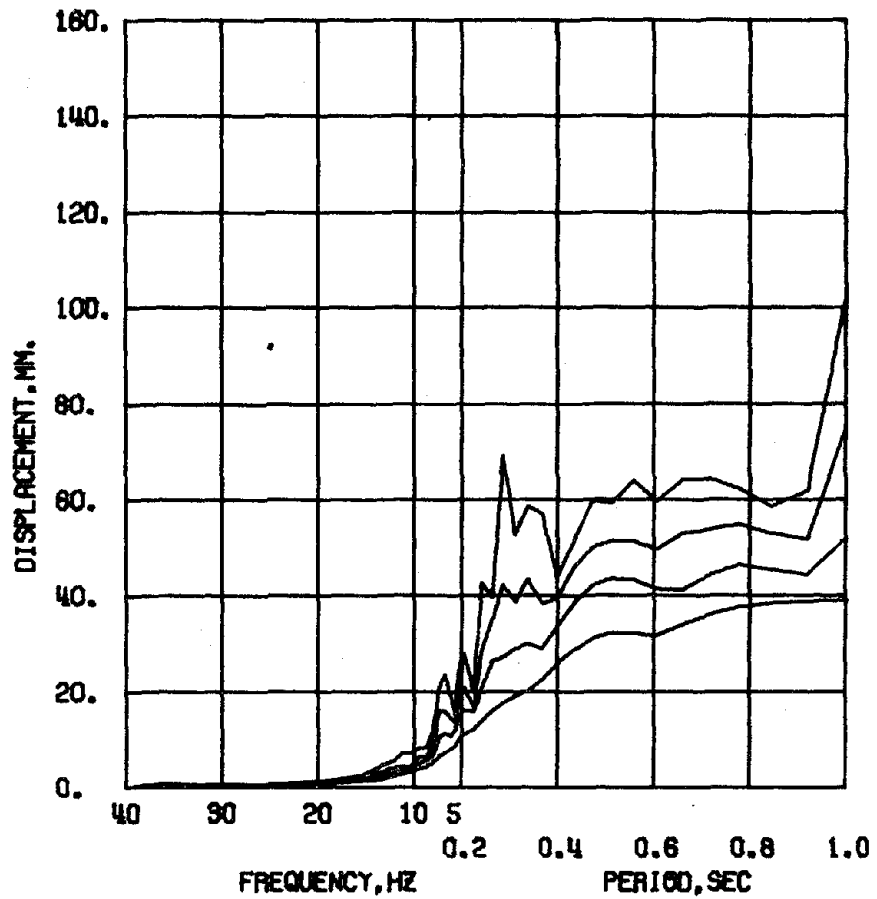
DYN TEST FMS - MAR 31, 1977 - RUN 1 - ABN
 DAMPING FACTOR = 0.02 0.05 0.10 0.20

Fig. 6.3 (contd.) Spectral-Response Curves of Taft Simulations



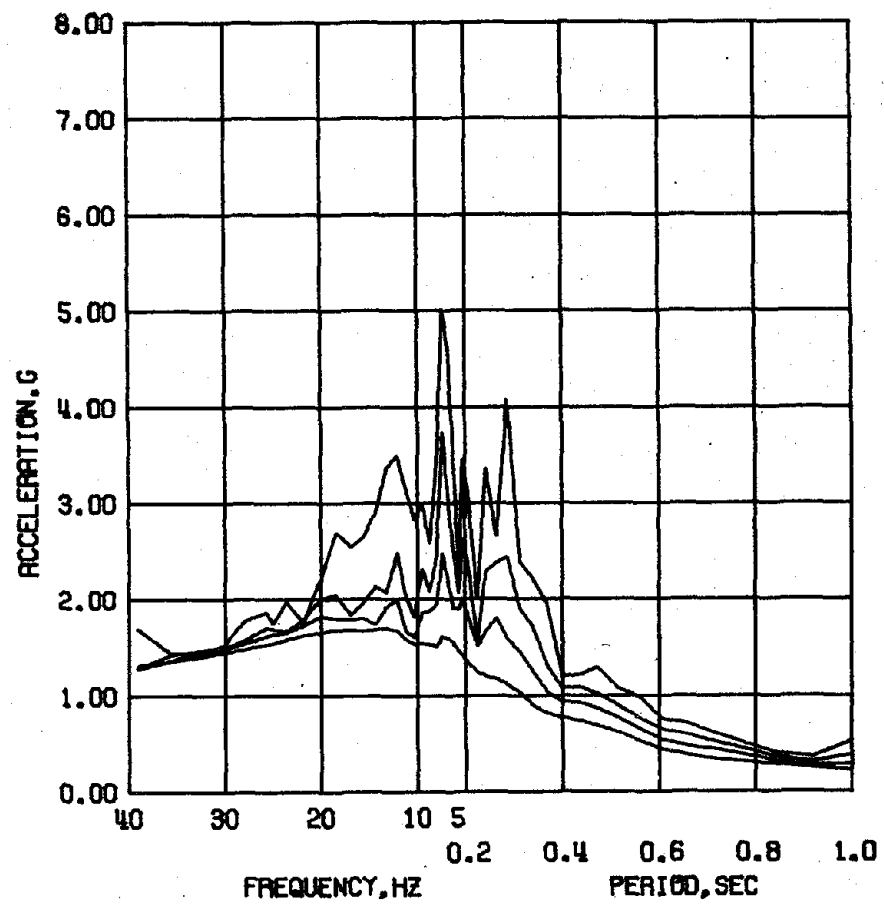
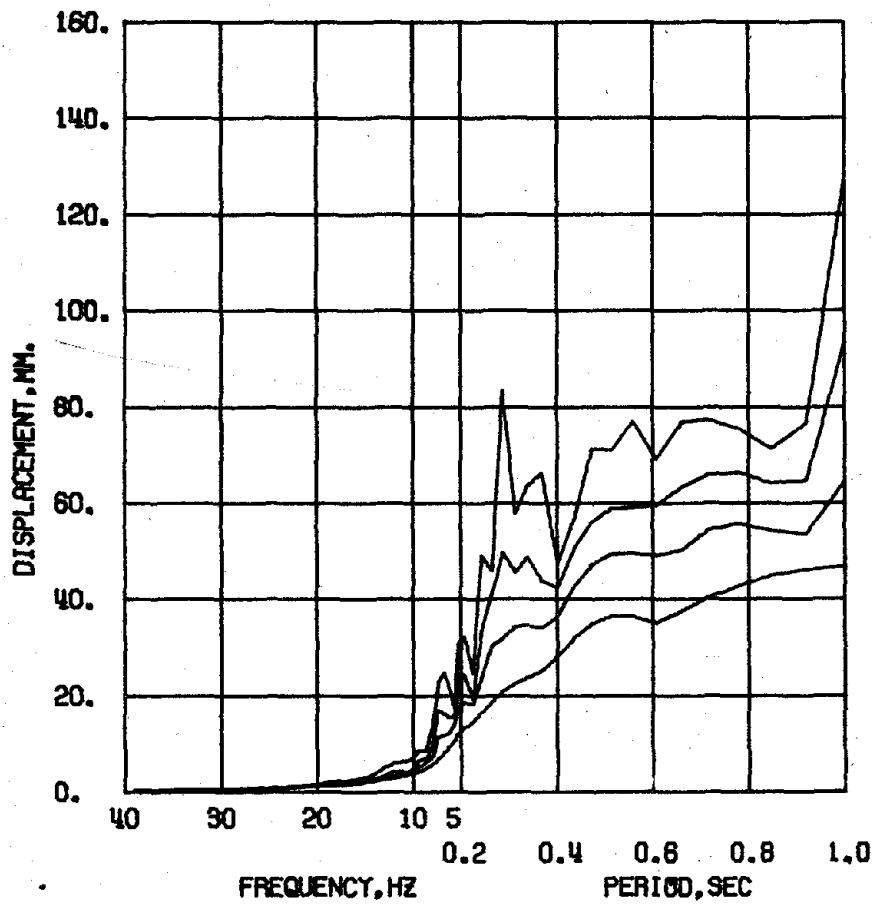
DYN TEST FW4 - MAY 18, 1977 - RUN 2 - ABN
 DAMPING FACTOR = 0.02 0.05 0.10 0.20

Fig. 6.3 (contd.) Spectral-Response Curves of Taft Simulations



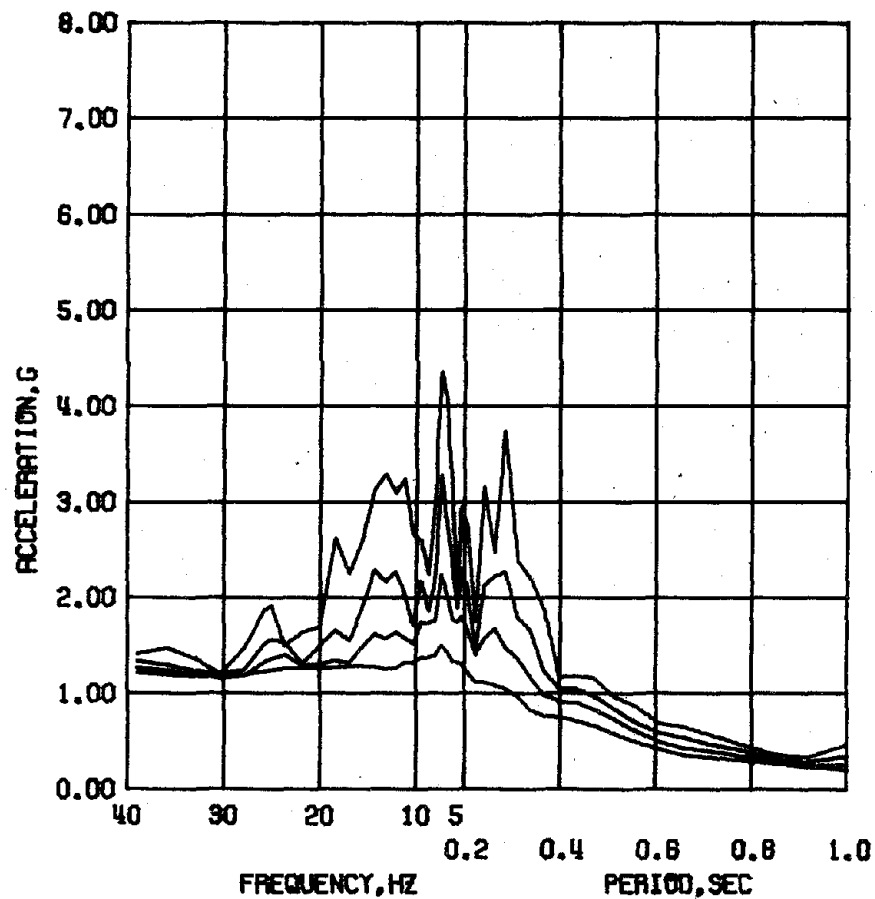
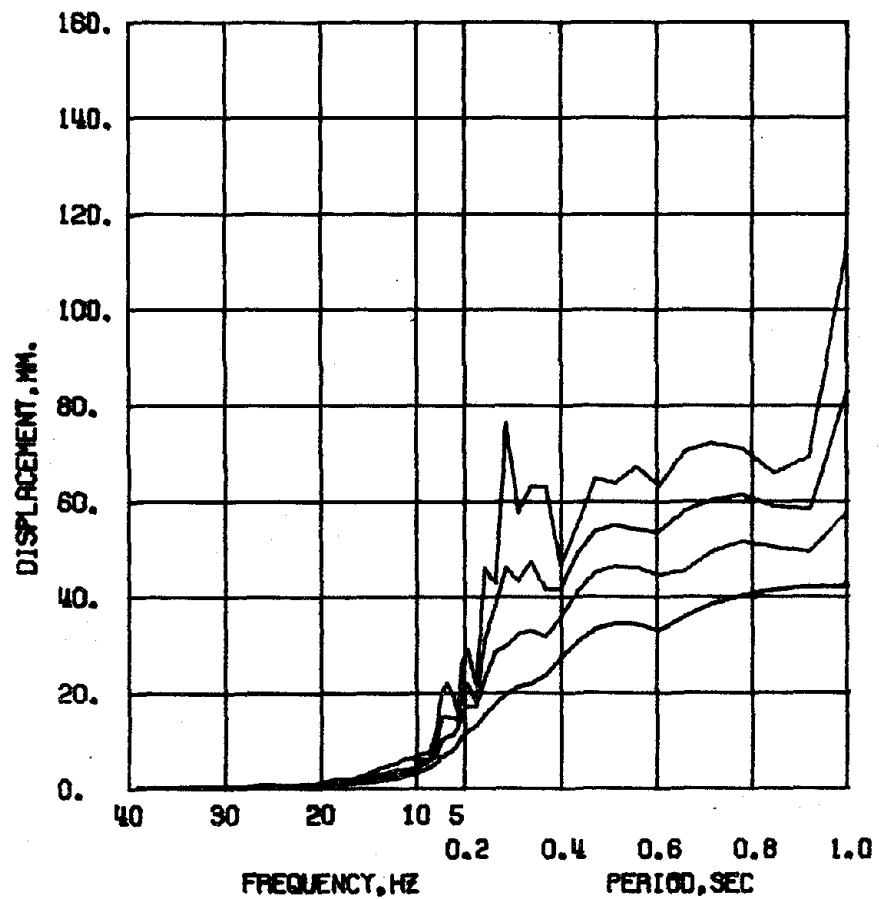
DYN TEST FWS - MAR 31, 1977 - RUN 2 - ABN
 DAMPING FACTOR = 0.02 0.05 0.10 0.20

Fig. 6.3 (contd.) Spectral-Response Curves of Taft Simulations



DYN TEST FW4 - MAY 18, 1977 - RUN 3 - ABN
 DAMPING FACTOR = 0.02 0.05 0.10 0.20

Fig. 6.3 (contd.) Spectral-Response Curves of Taft Simulations



DYN TEST FWS - MAR 31, 1977 - RUN 3 - ABN
 DAMPING FACTOR = 0.02 0.05 0.10 0.20

Fig. 6.3 (contd.) Spectral-Response Curves of Taft Simulations

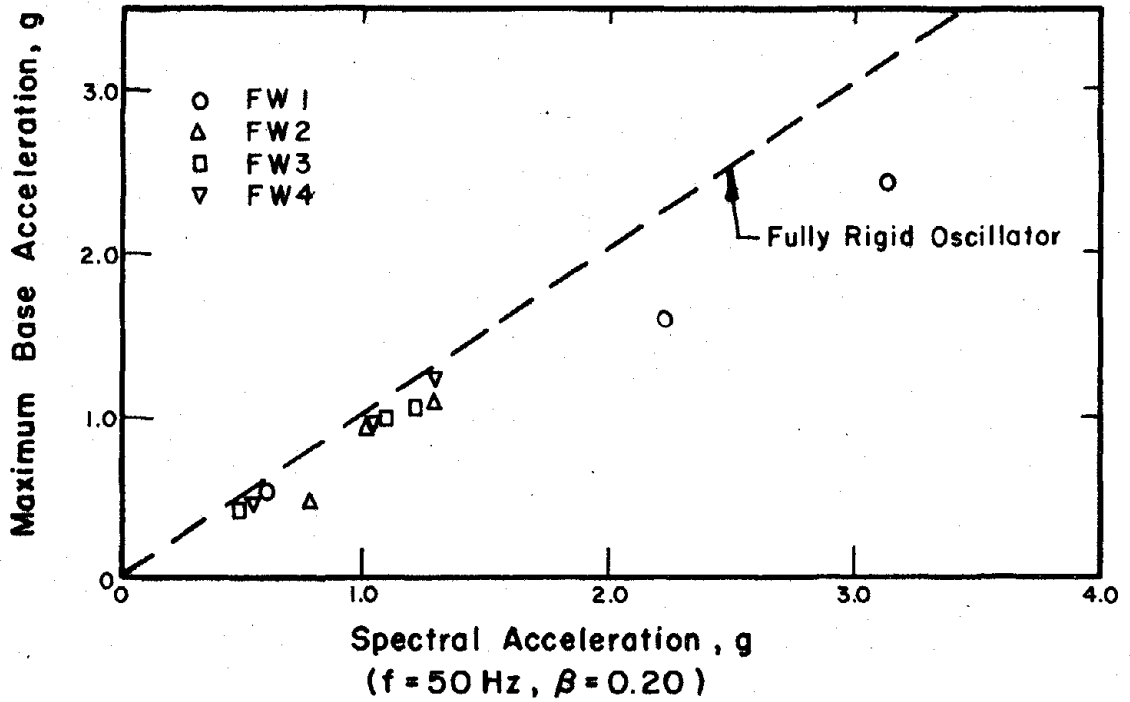


Fig. 6.4 Variation of Maximum Base Acceleration with Spectral Acceleration.

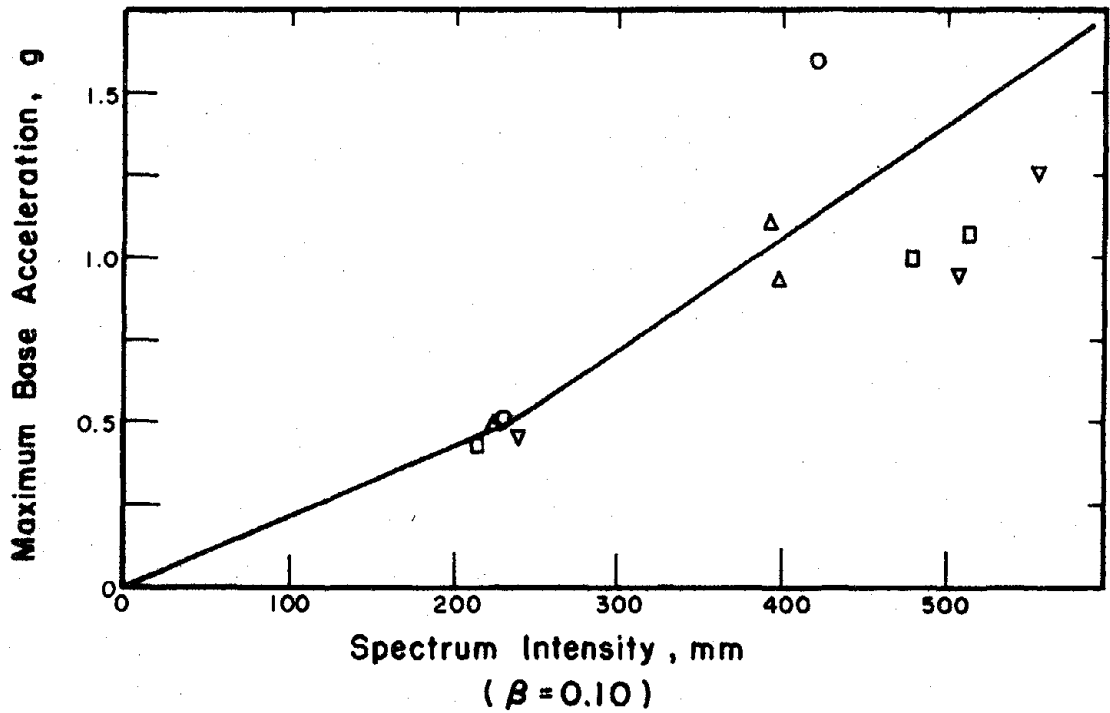


Fig. 6.5 Variation of Maximum Base Acceleration with Spectrum Intensity

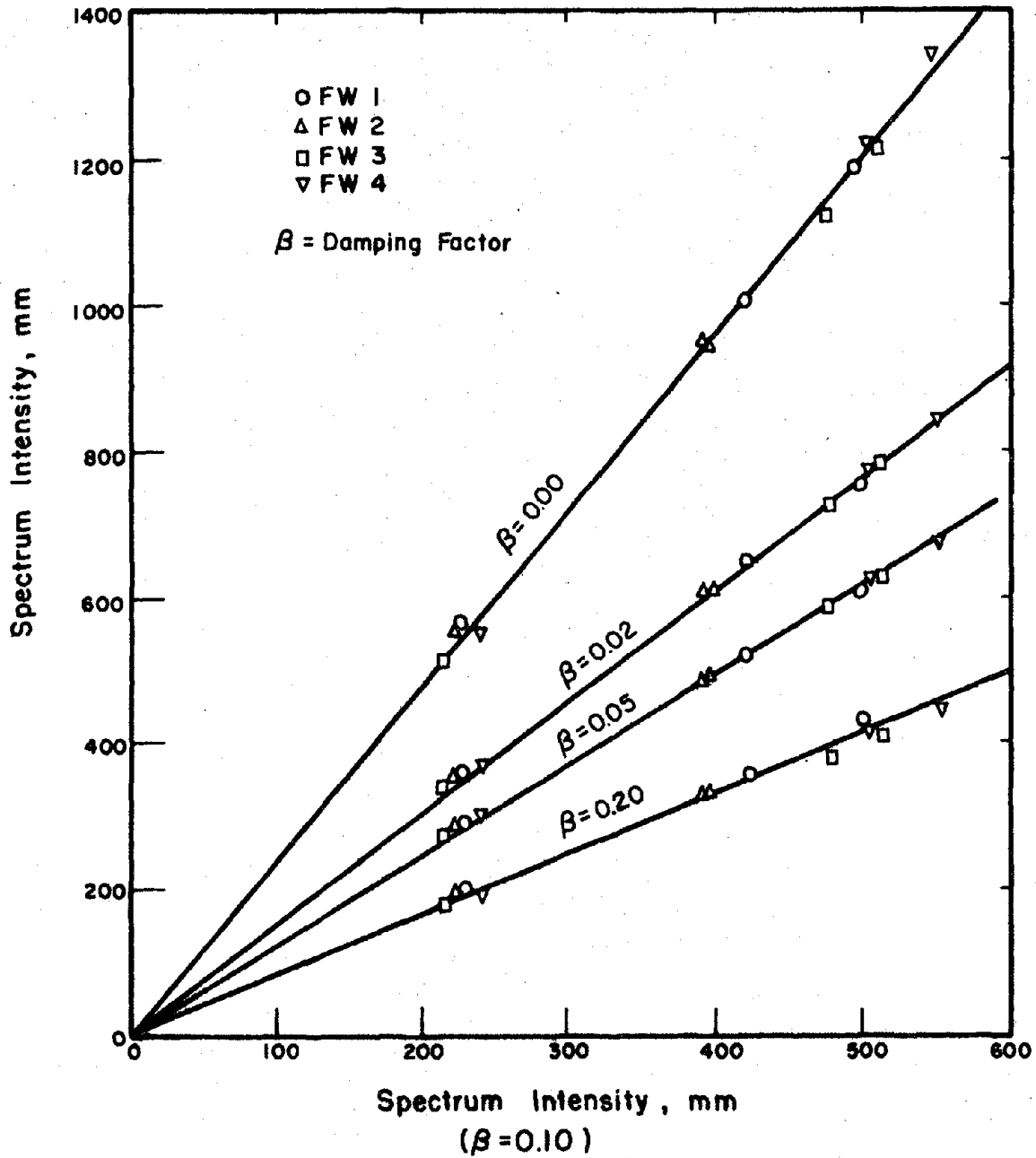
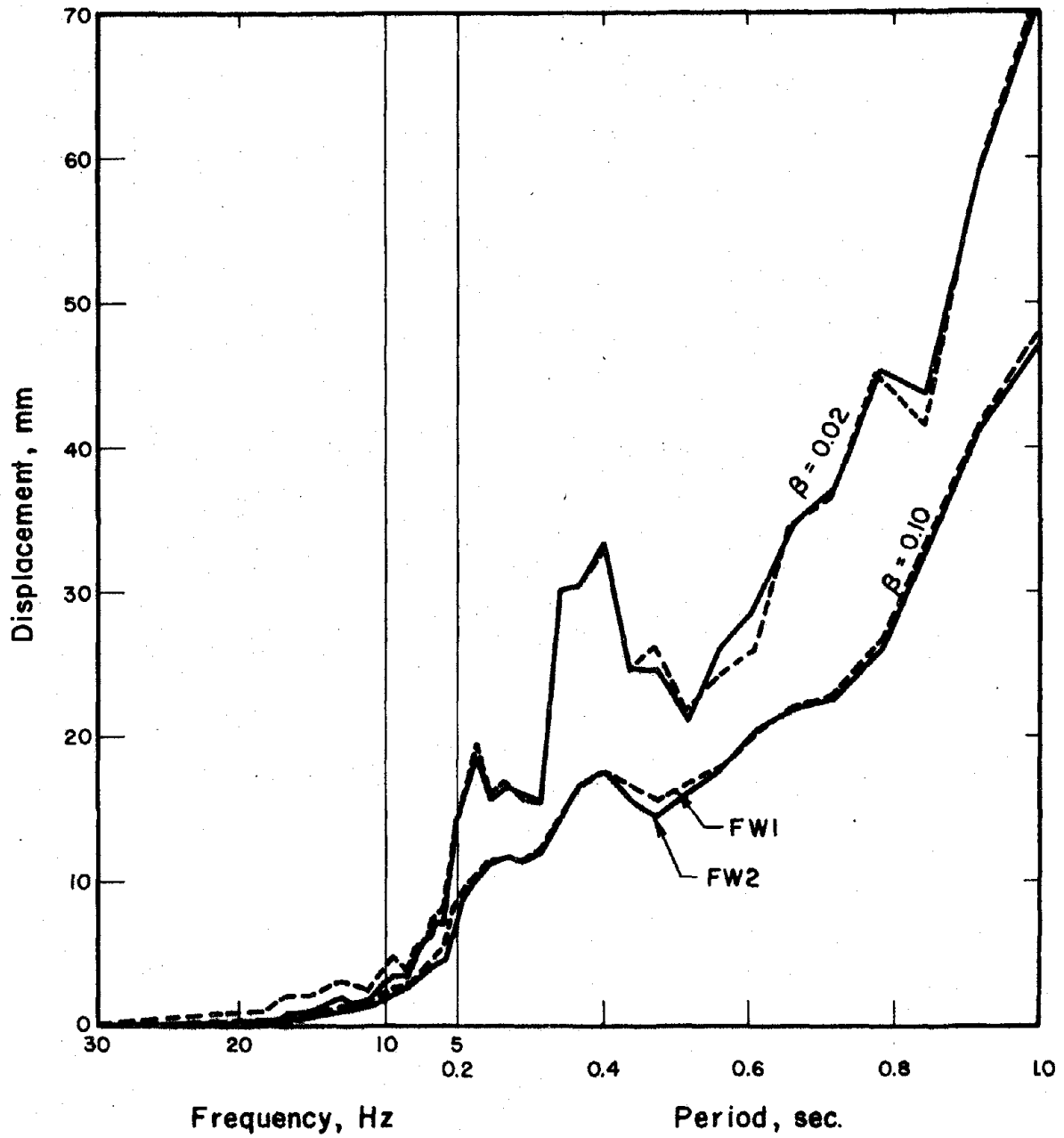
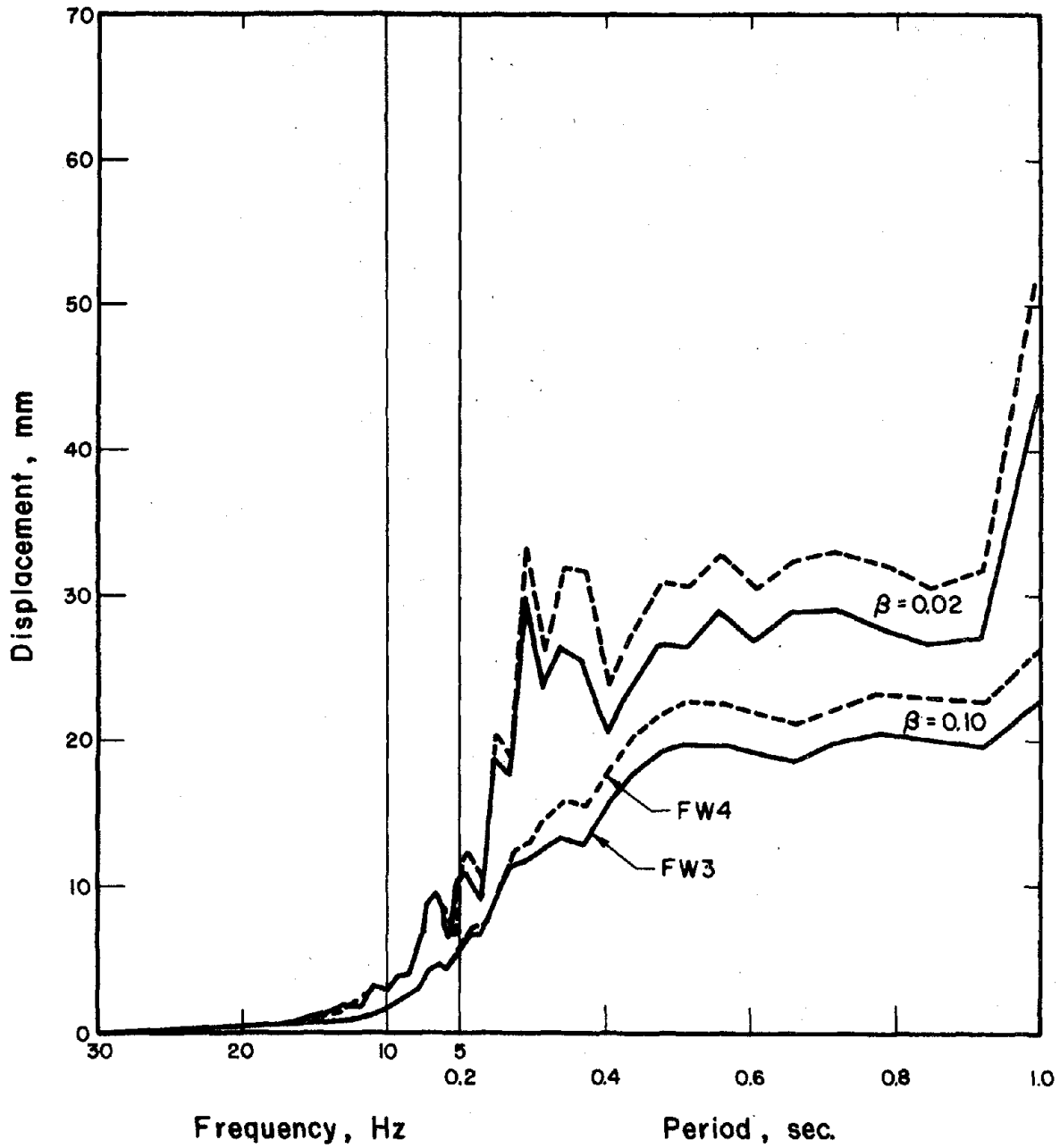


Fig. 6.6 Variation of Spectrum Intensity with Damping Factor.



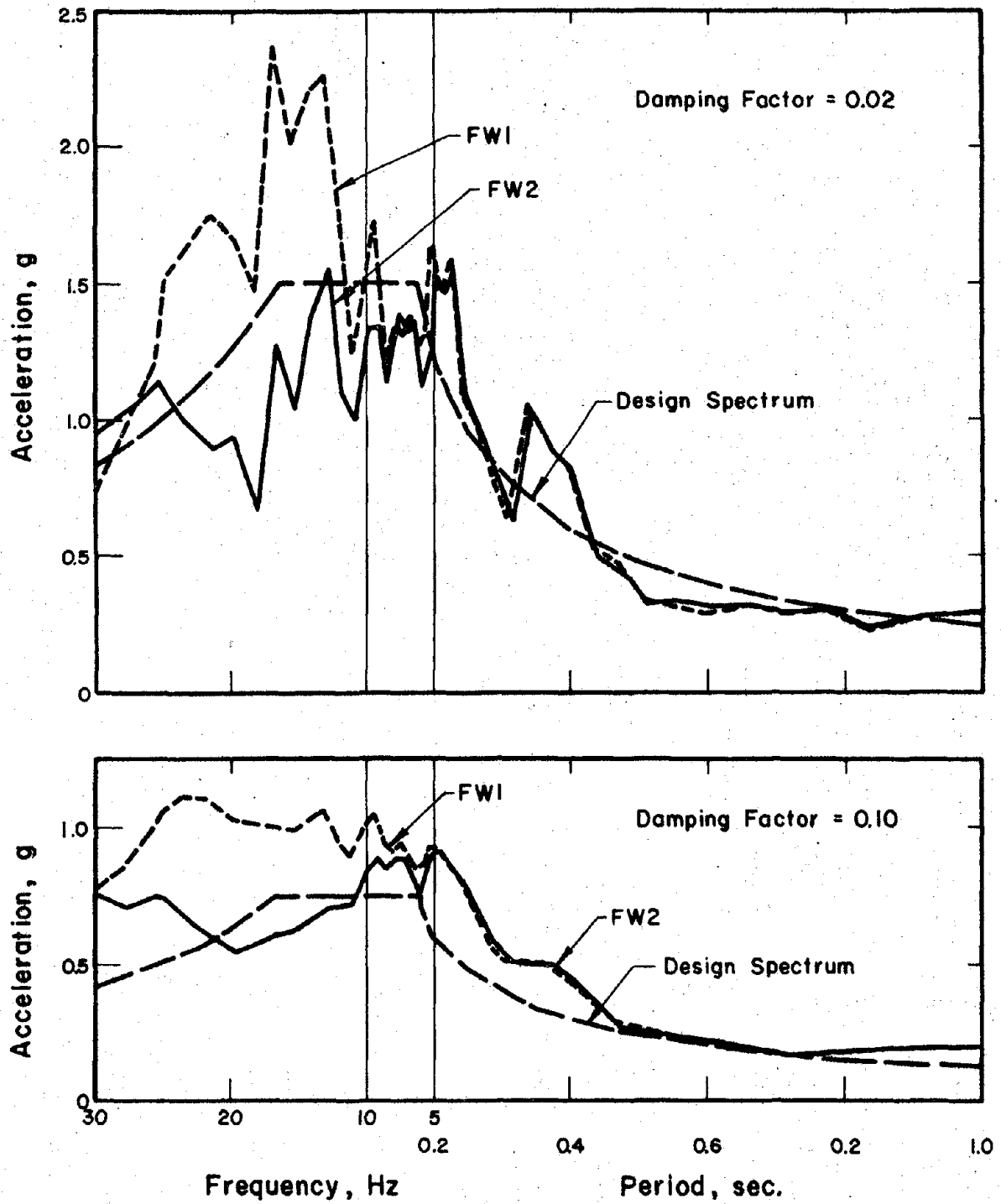
(a) El Centro Base Motions

Fig. 6.7 Comparison of Displacement Spectral Response for Initial Simulations



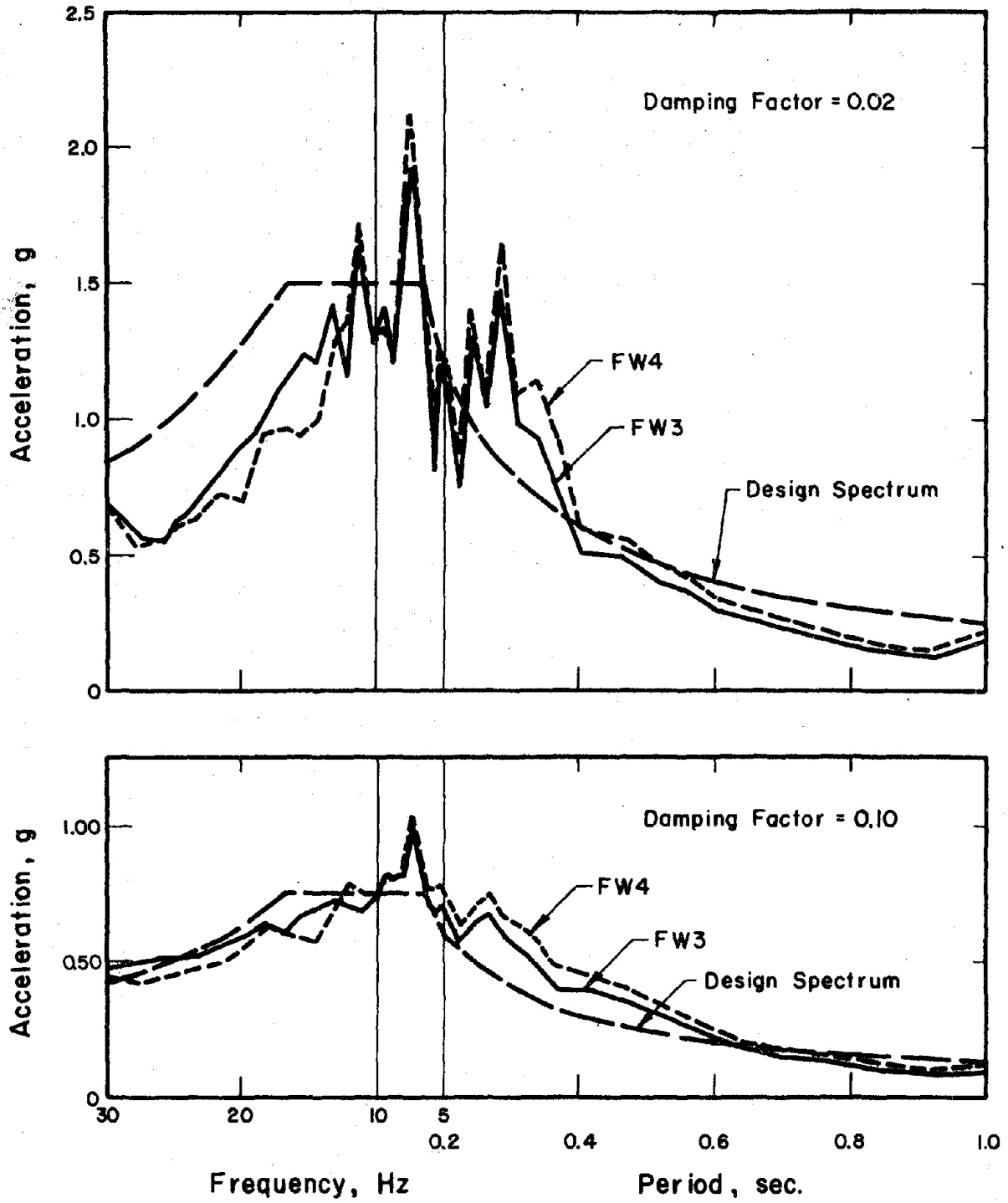
(b) Taft Base Motions

Fig. 6.7 (contd.) Comparison of Displacement Spectral Response for Initial Simulations.



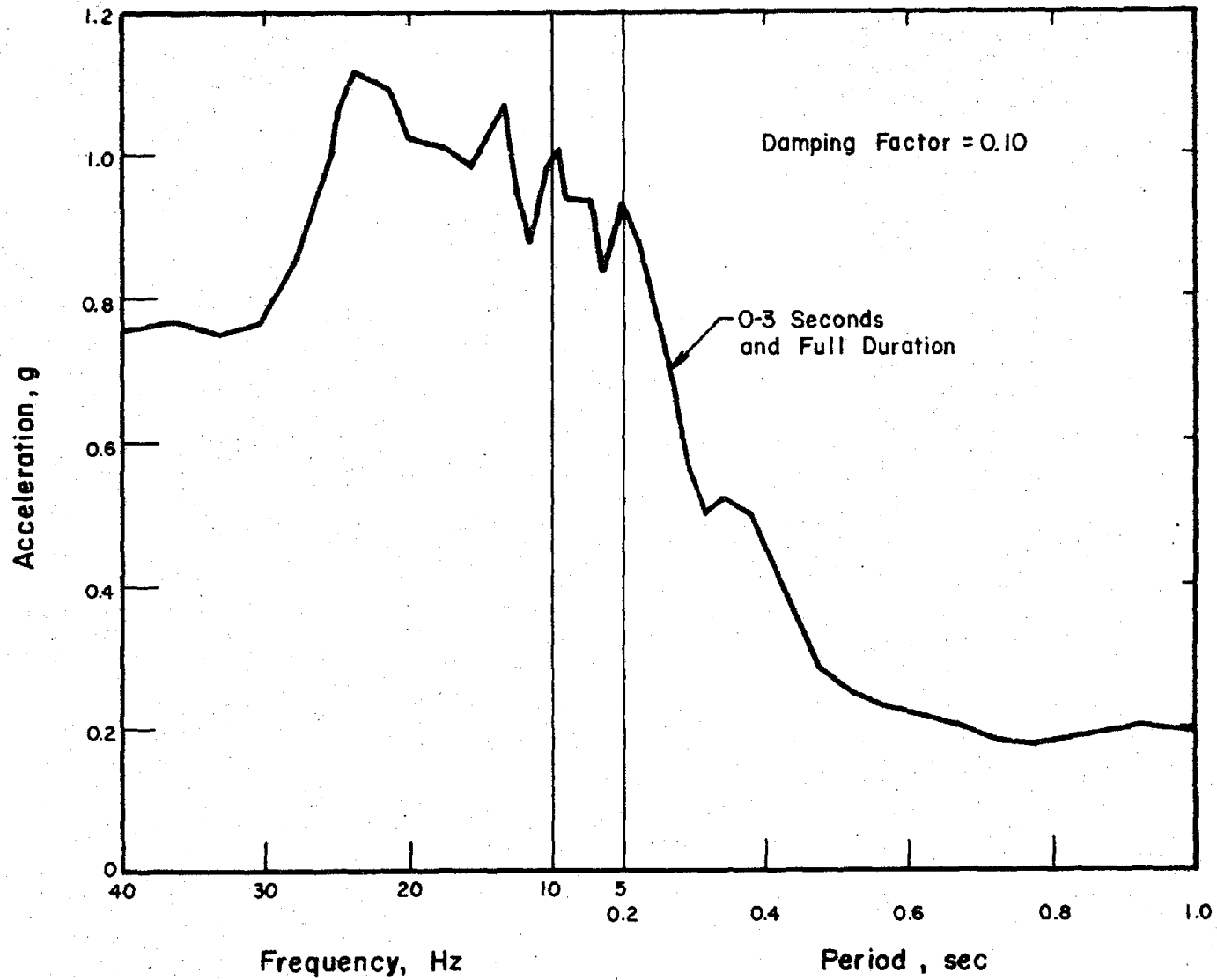
(a) El Centro Base Motions

Fig. 6.8 Comparison of Acceleration Spectral Response for Initial Simulations.



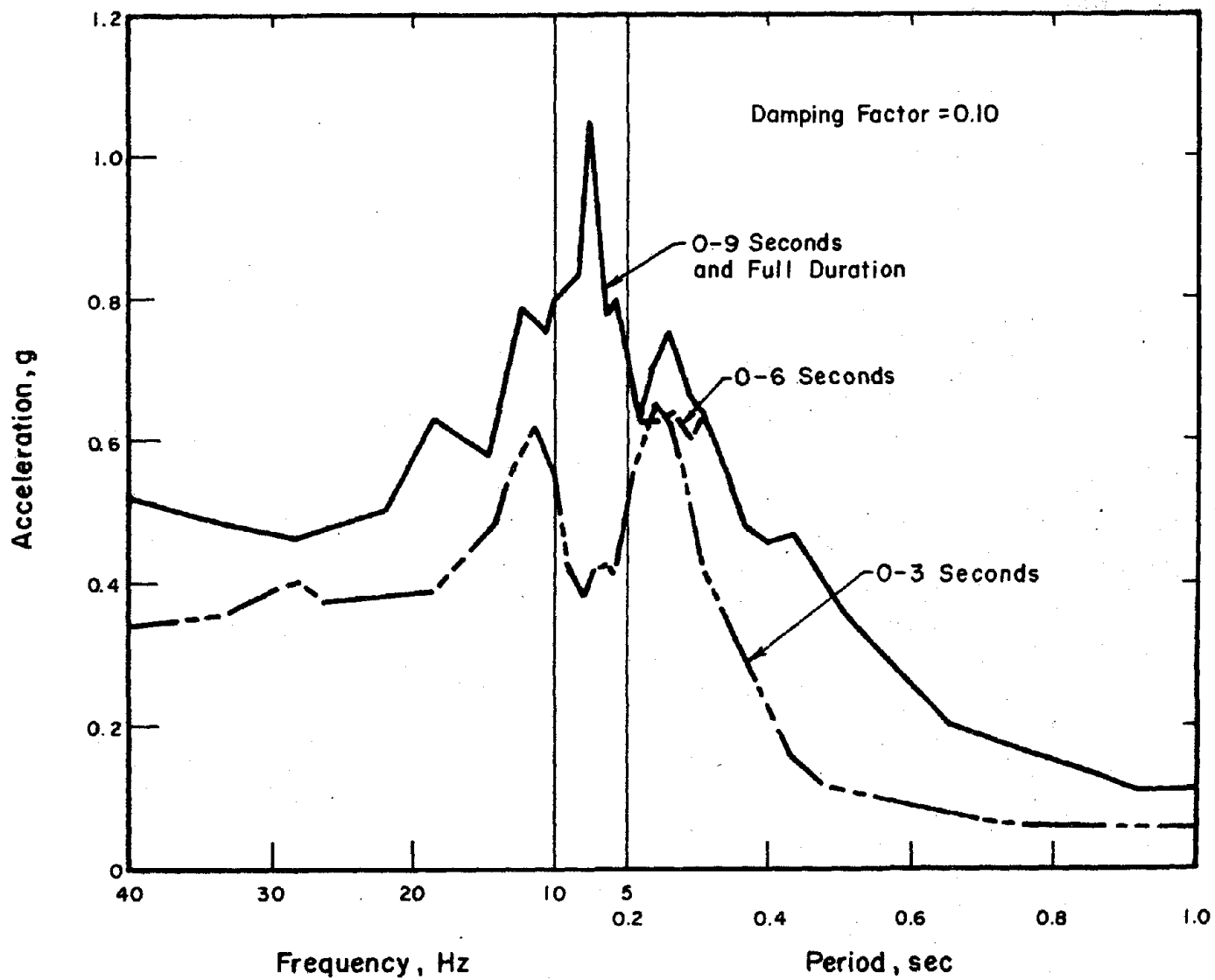
(b) Taft Base Motions

Fig. 6.8 (contd.) Comparison of Acceleration Spectral Response for Initial Simulations



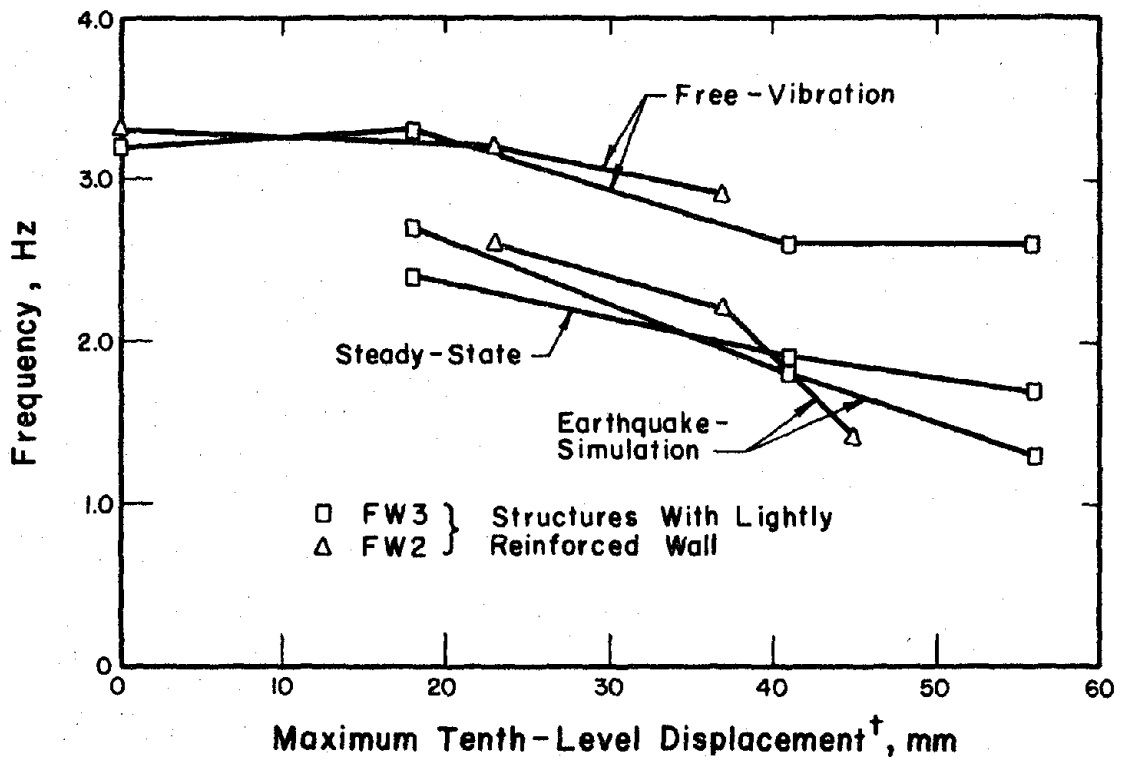
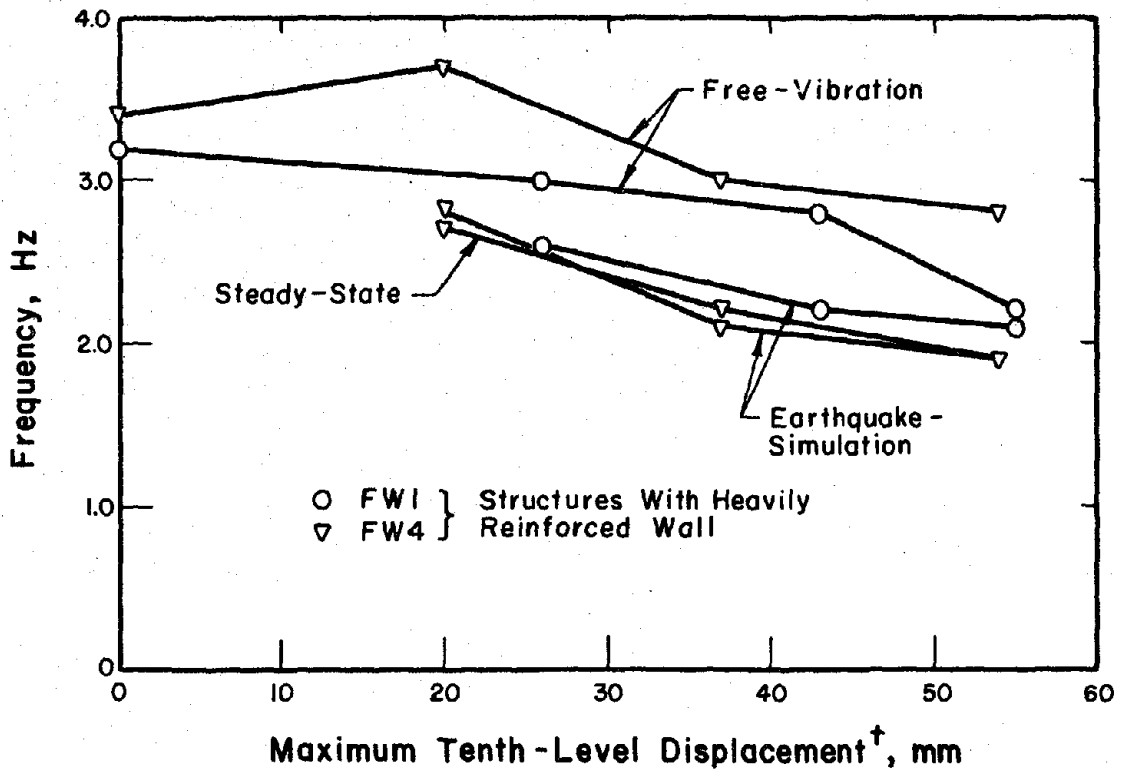
(a) El Centro Base Motions

Fig. 6.9 Spectral-Response Curves for Partial Durations



(b) Taft Base Motions

Fig. 6.9 (contd.) Spectral-Response Curves for Partial Durations



† Double Amplitude/2, Measured During Previous Test Run

Fig. 6.10 Measured Apparent Fundamental Frequencies

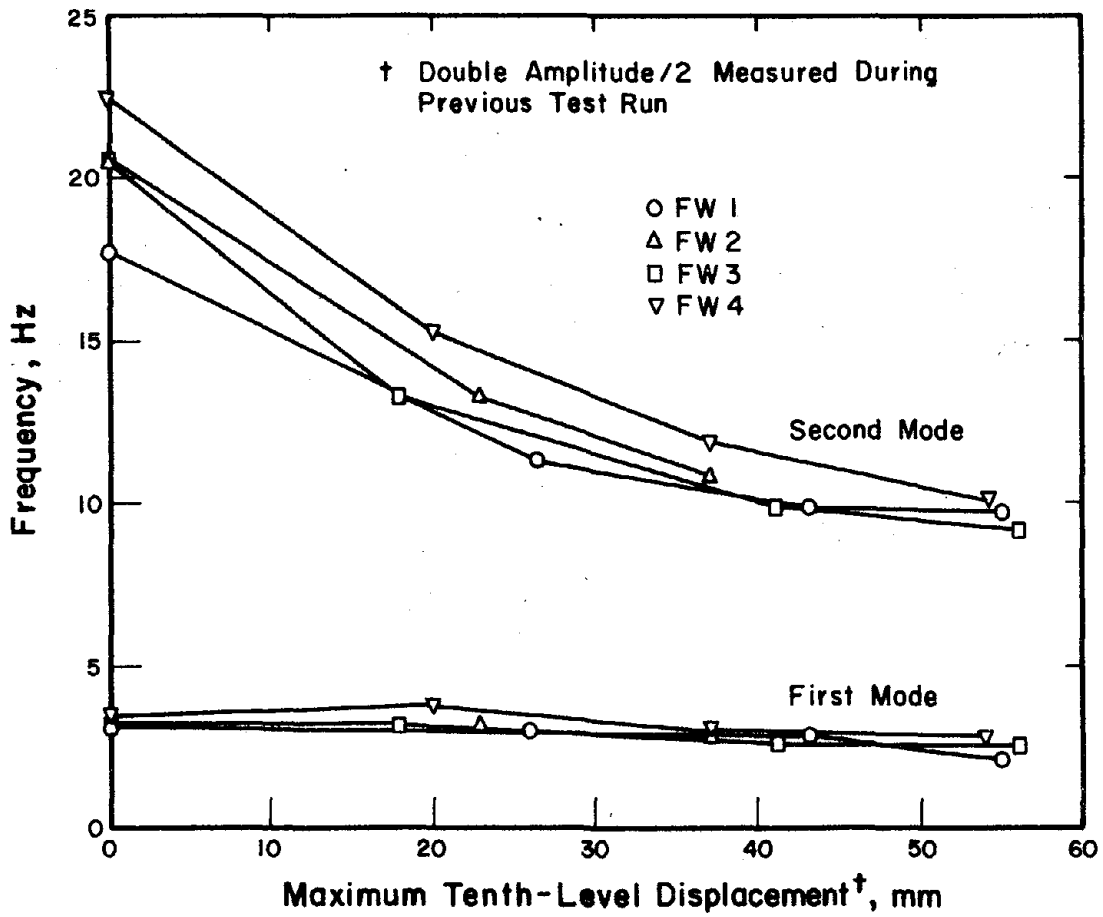


Fig. 6.11 Apparent Frequencies Measured During Free-Vibration Tests

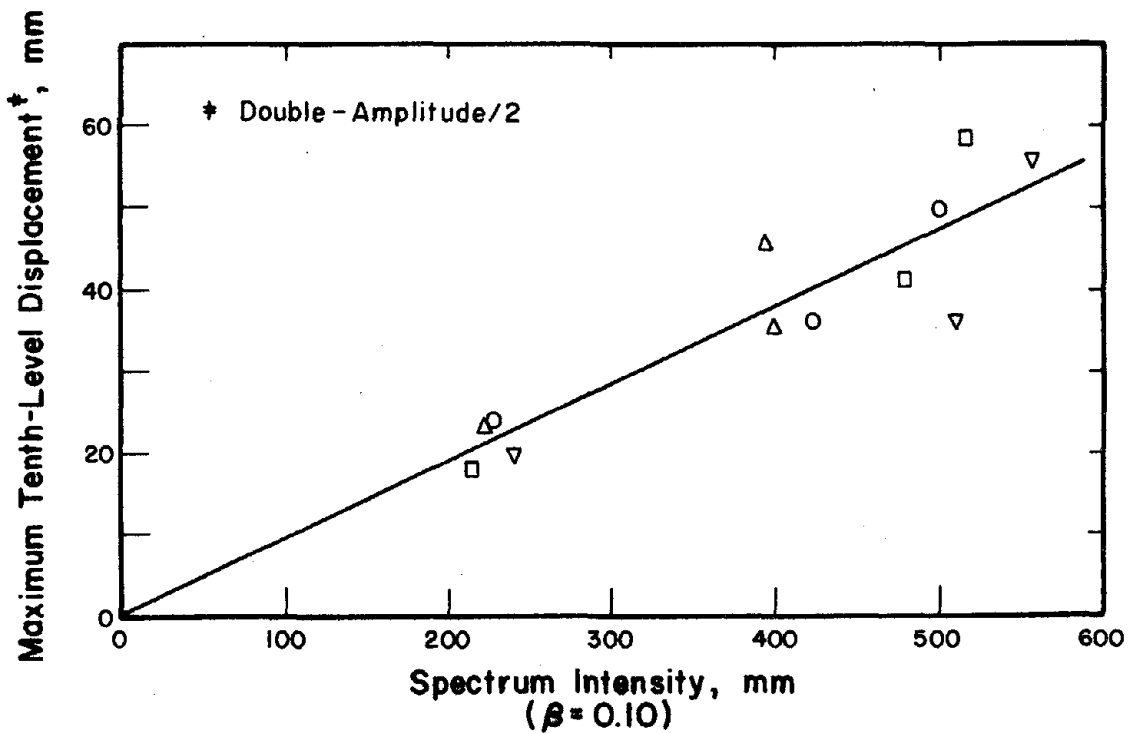
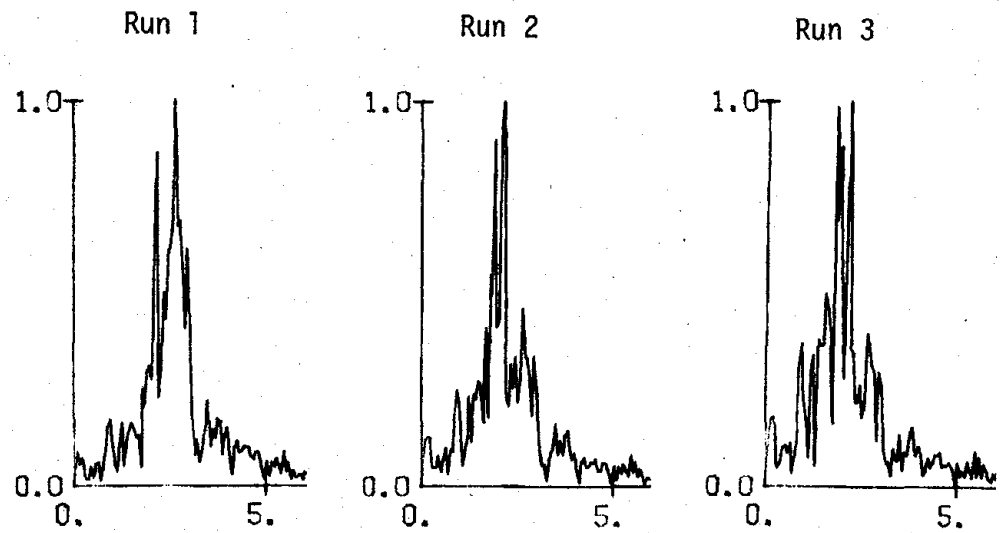
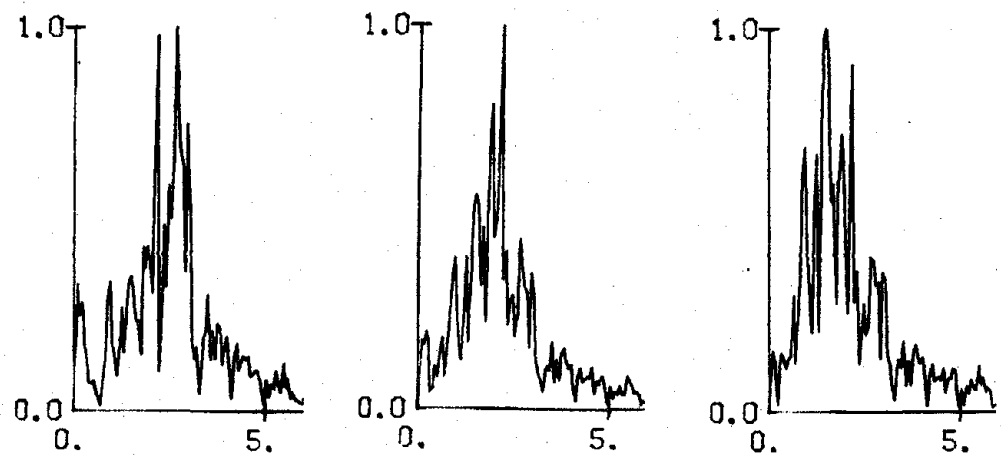


Fig. 6.12 Variation of Displacement with Spectrum Intensity

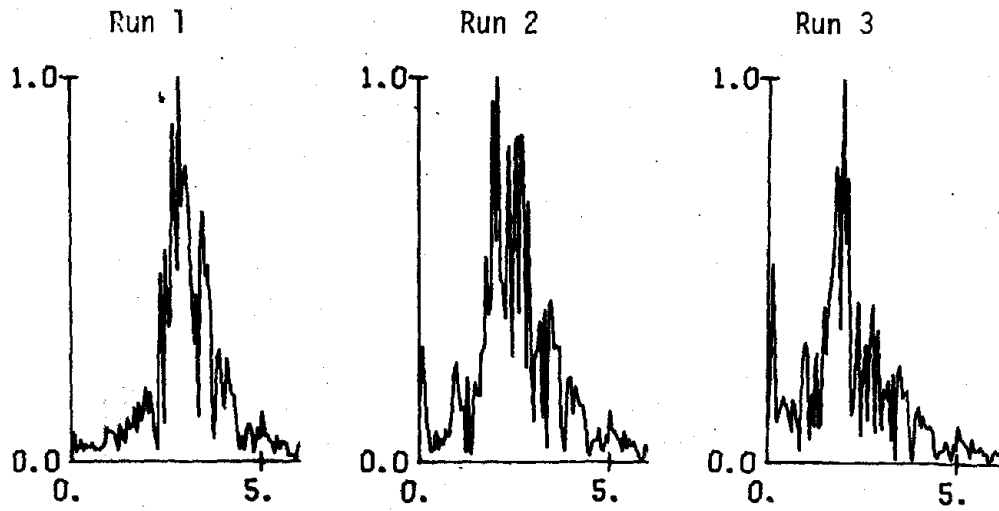


(a) Test Structure FW1

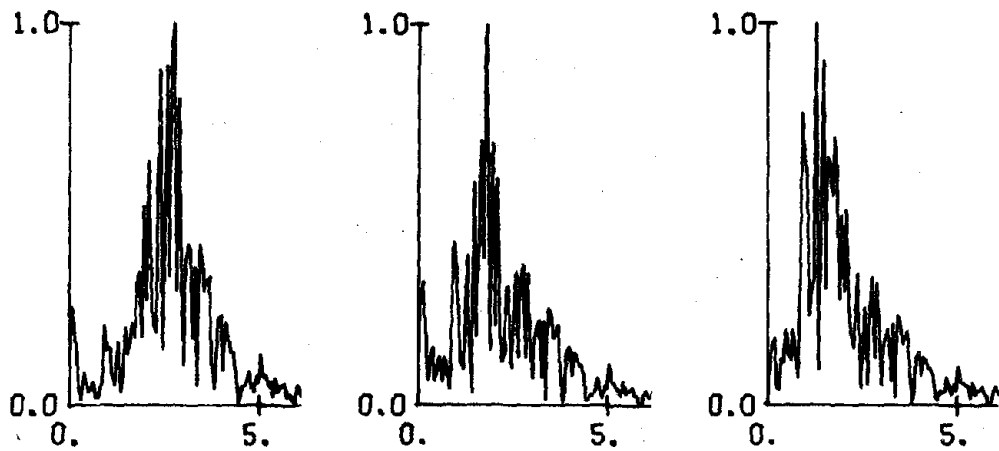


(b) Test Structure FW2

Fig. 6.13 Fourier-Amplitude Spectra of Tenth-Level Displacements Measured During Earthquake Simulations

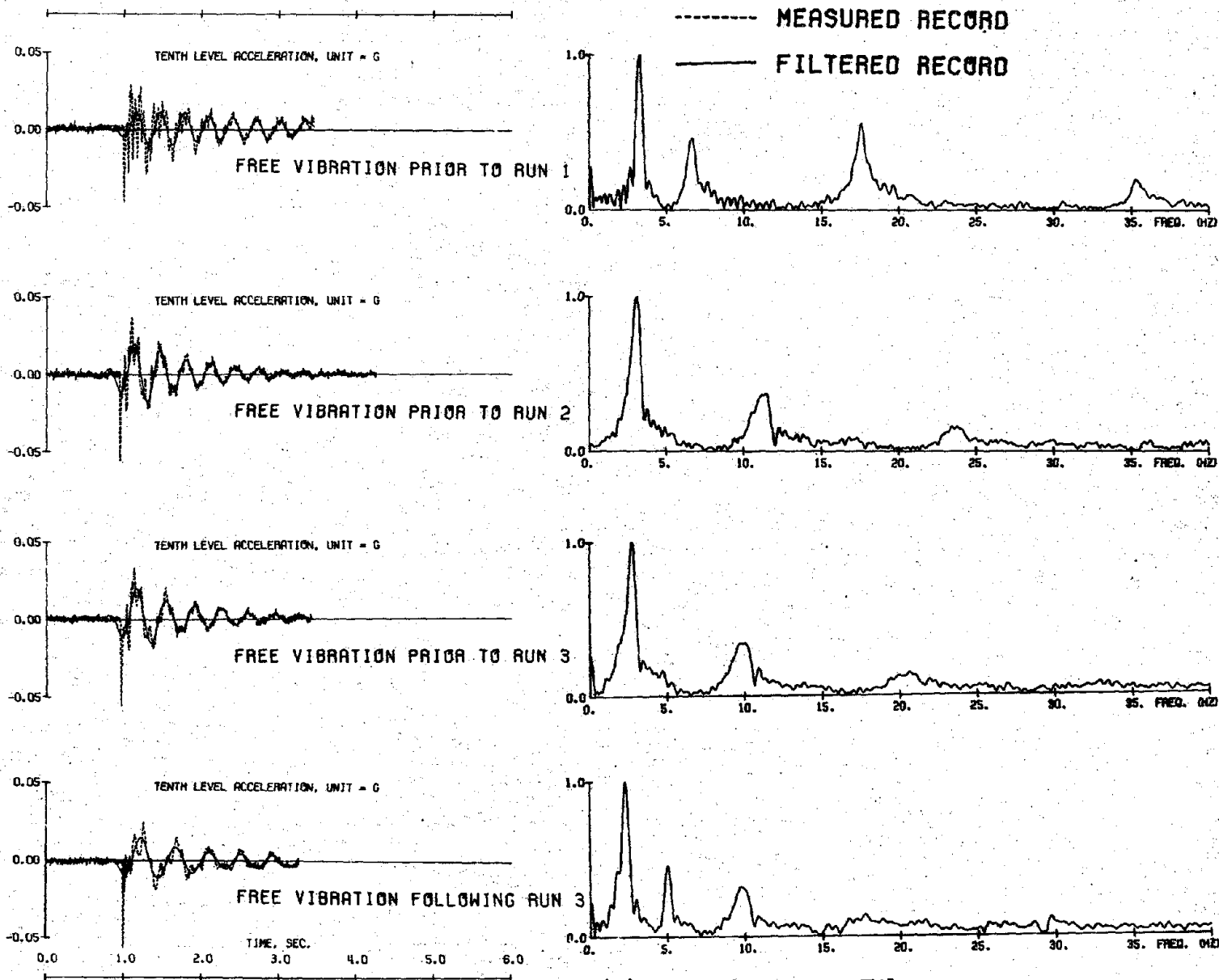


(c) Test Structure FW4



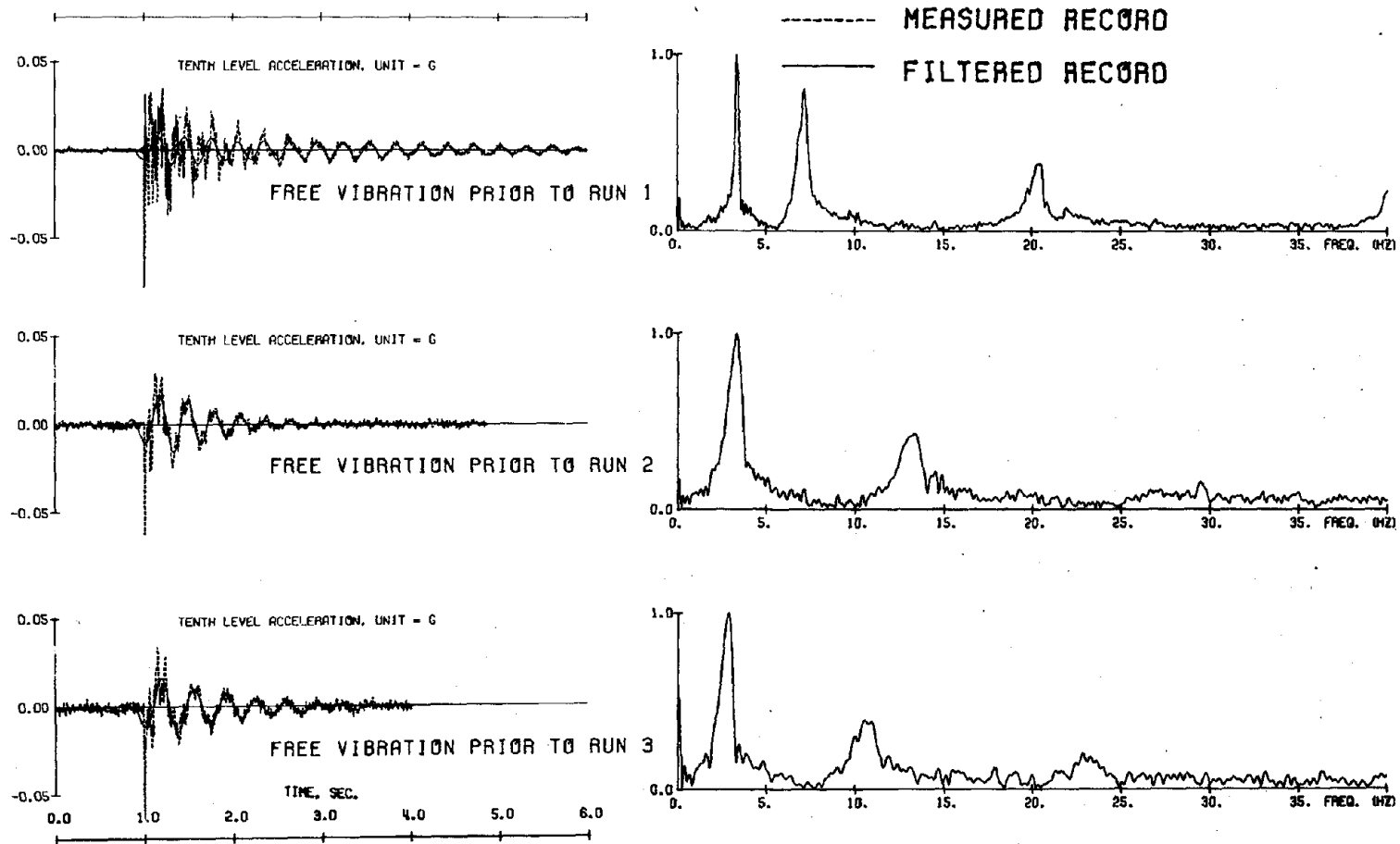
(d) Test Structure FW3

Fig. 6.13 (contd.) Fourier-Amplitude Spectra of Tenth-Level Displacements Measured During Earthquake Simulations



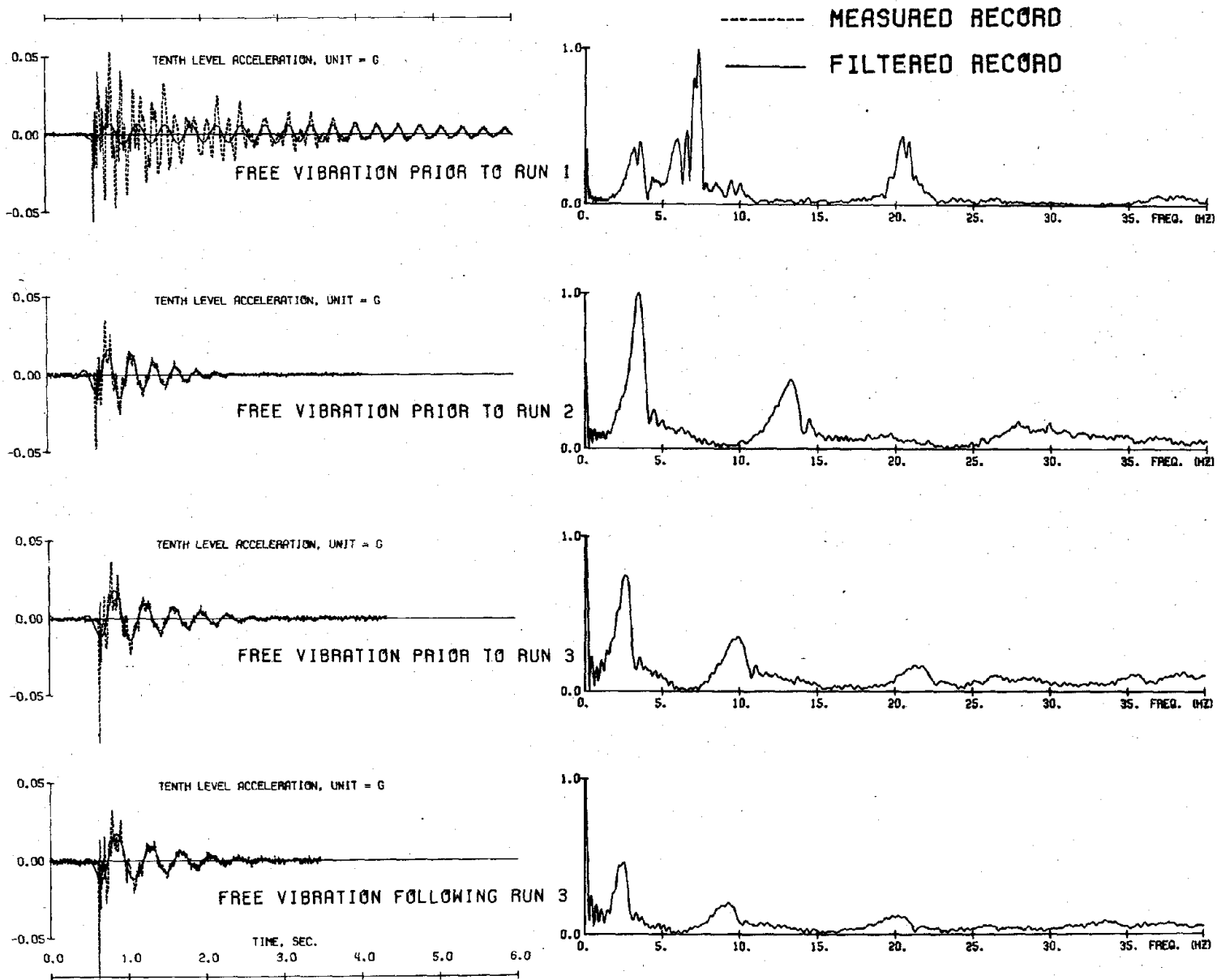
(a) Test Structure FW1

Fig. 6.14 Accelerations and Corresponding Fourier-Amplitude Spectra Measured During Free-Vibration Tests

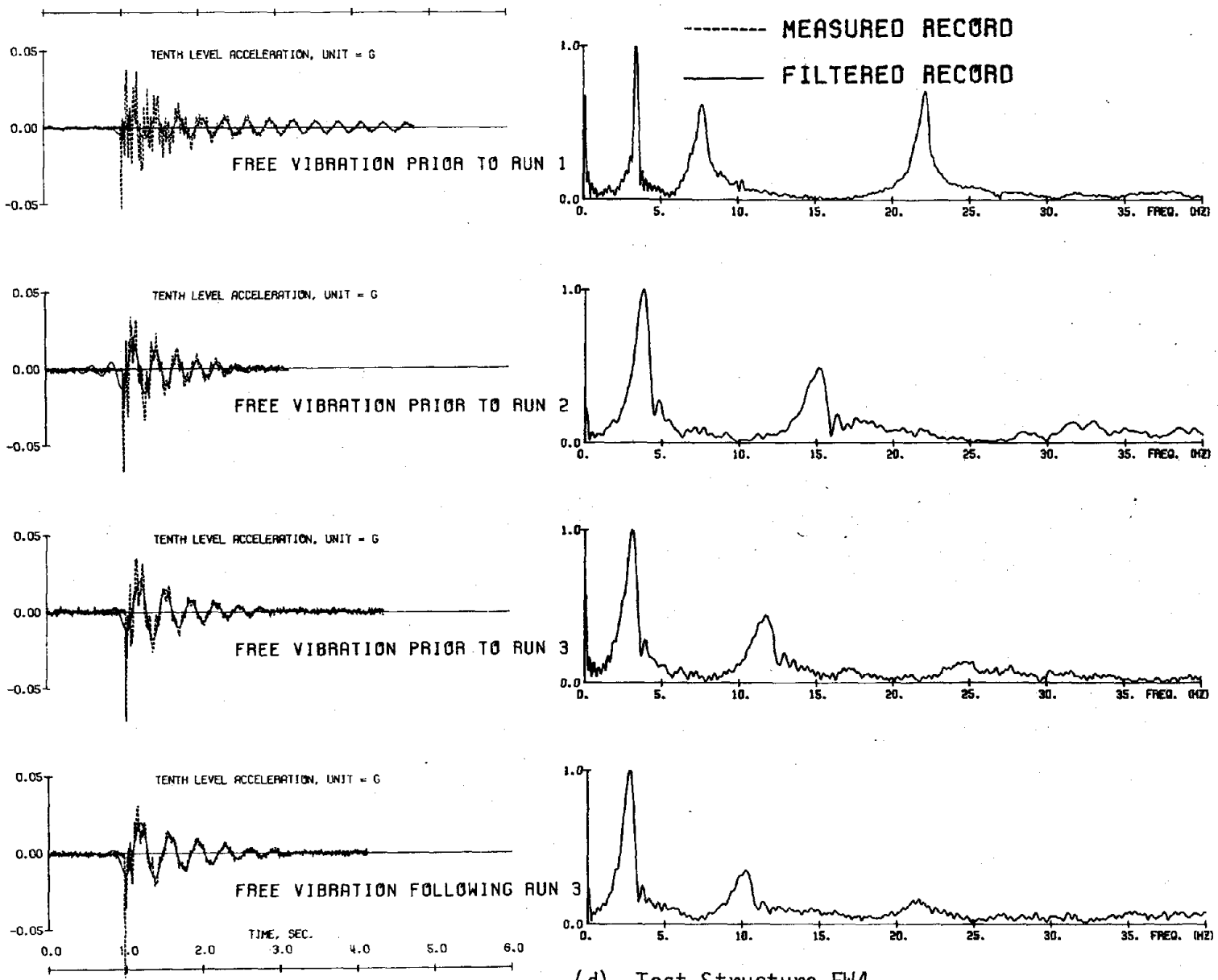


FREE VIBRATION FOLLOWING RUN 3
 (CHANNEL NOT RECORDED BECAUSE OF TAPE RECORDER MALFUNCTION)

(b) Test Structure FW2
 Fig. 6.14 (contd.) Accelerations and Corresponding Fourier-Amplitude Spectra
 Measured During Free-Vibration Tests

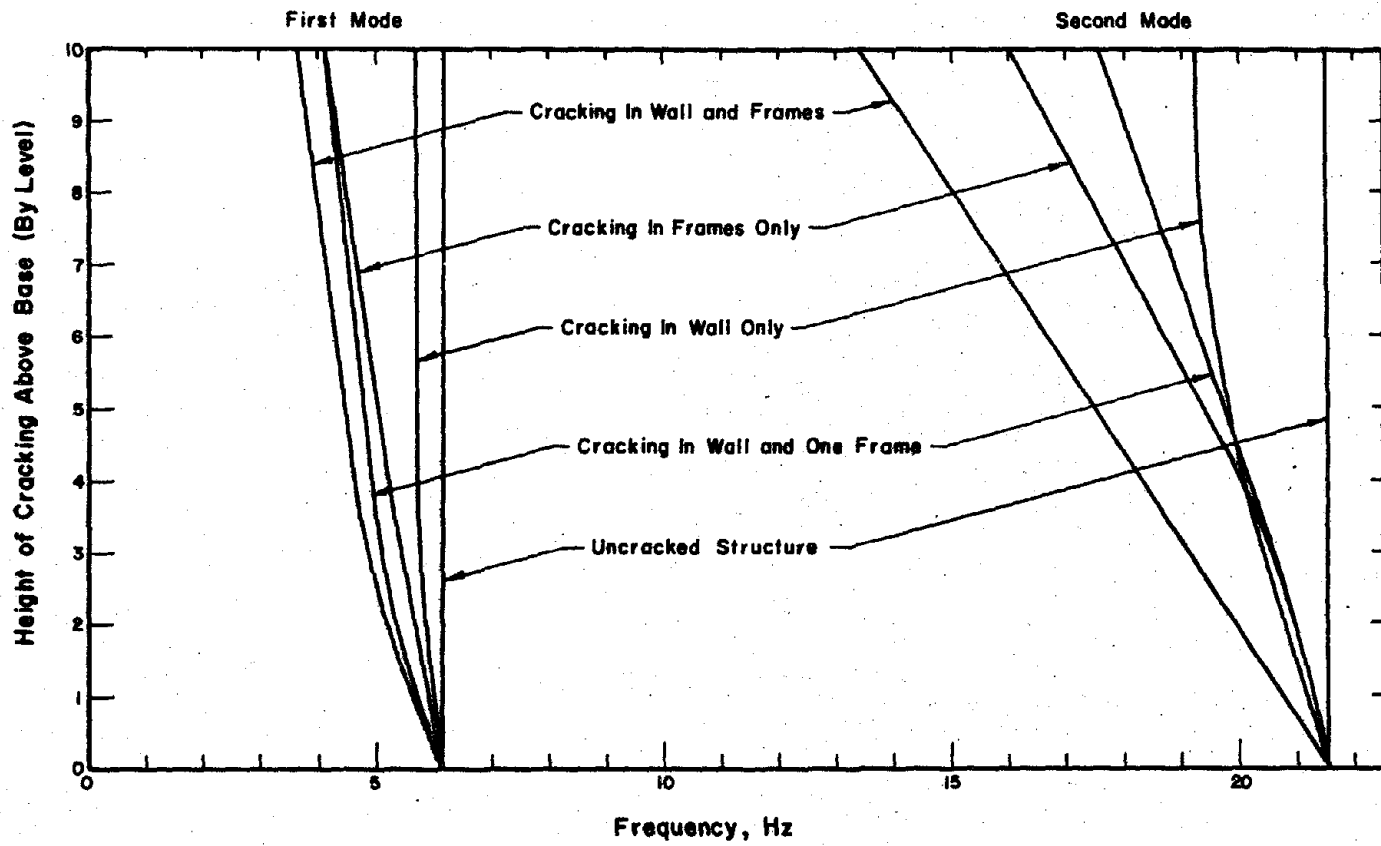


(c) Test Structure FW3
 Fig. 6.14 (contd.) Accelerations and Corresponding Fourier-Amplitude Spectra Measured During Free-Vibration Tests

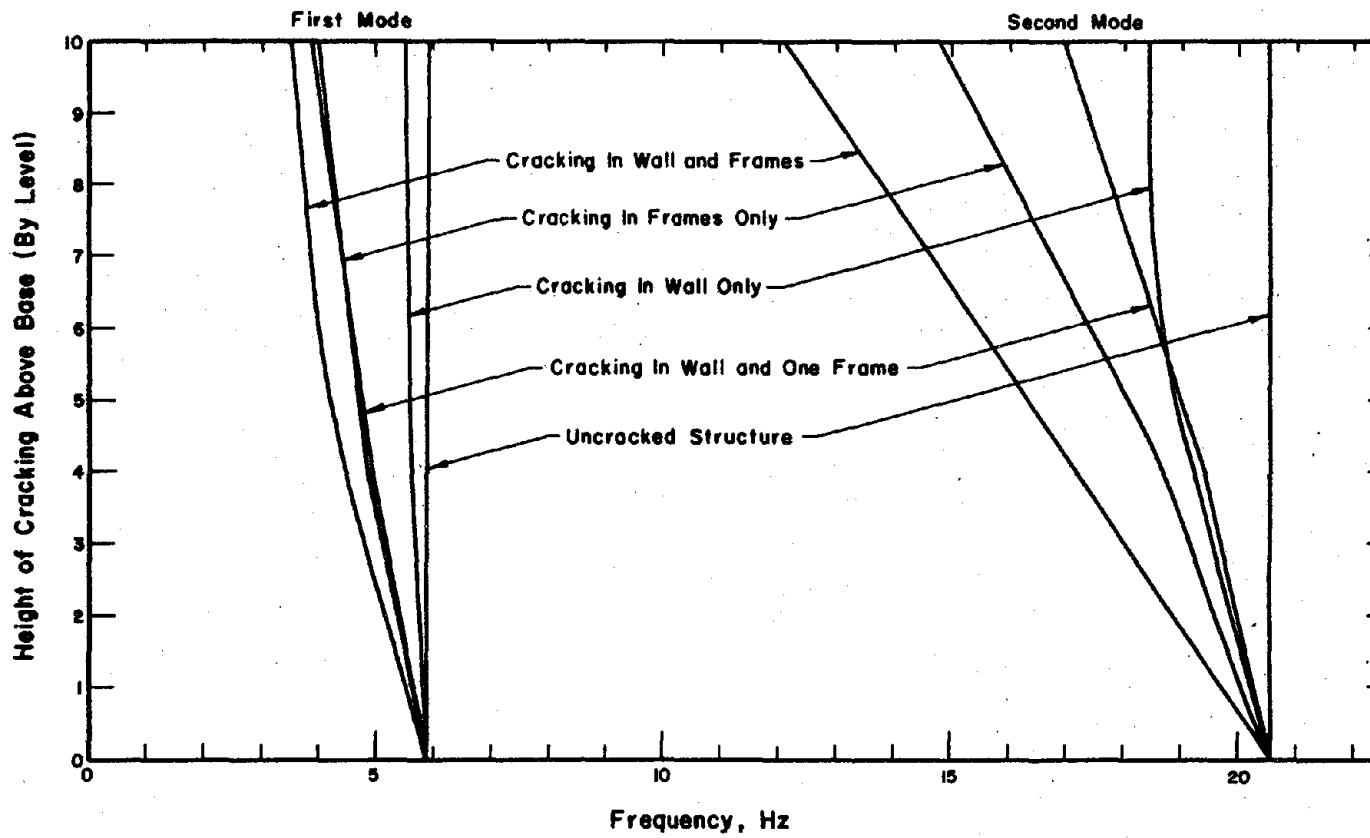


(d) Test Structure FW4

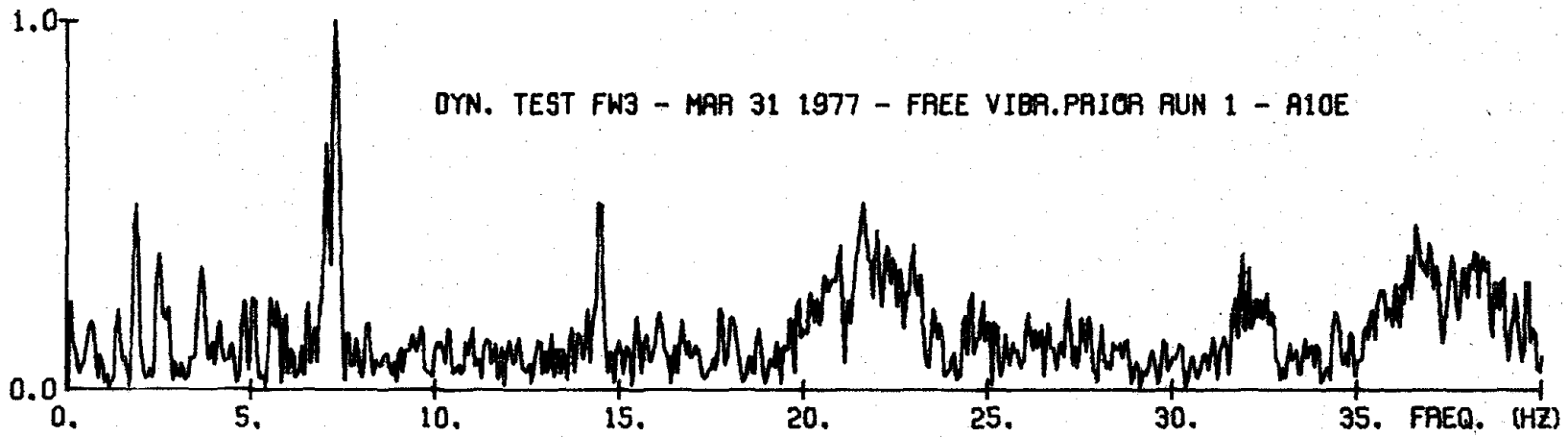
Fig. 6.14 (contd.) Accelerations and Corresponding Fourier-Amplitude Spectra Measured During Free-Vibration Tests



(a) Structure with Heavily Reinforced Wall
 Fig. 6.15 Calculated Natural Frequencies

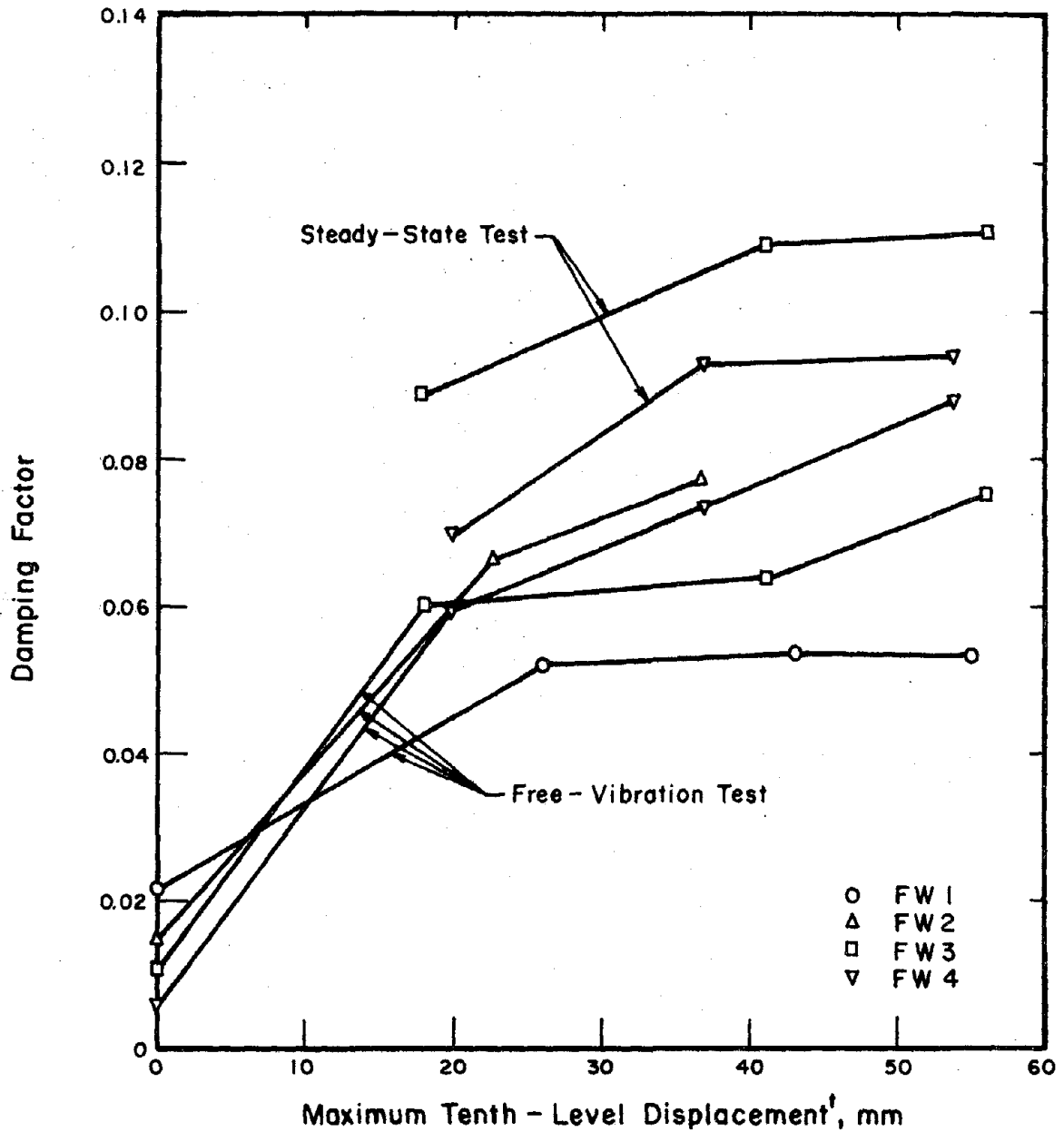


(b) Structure with Lightly Reinforced Wall
 Fig. 6.15 (contd.) Calculated Natural Frequencies



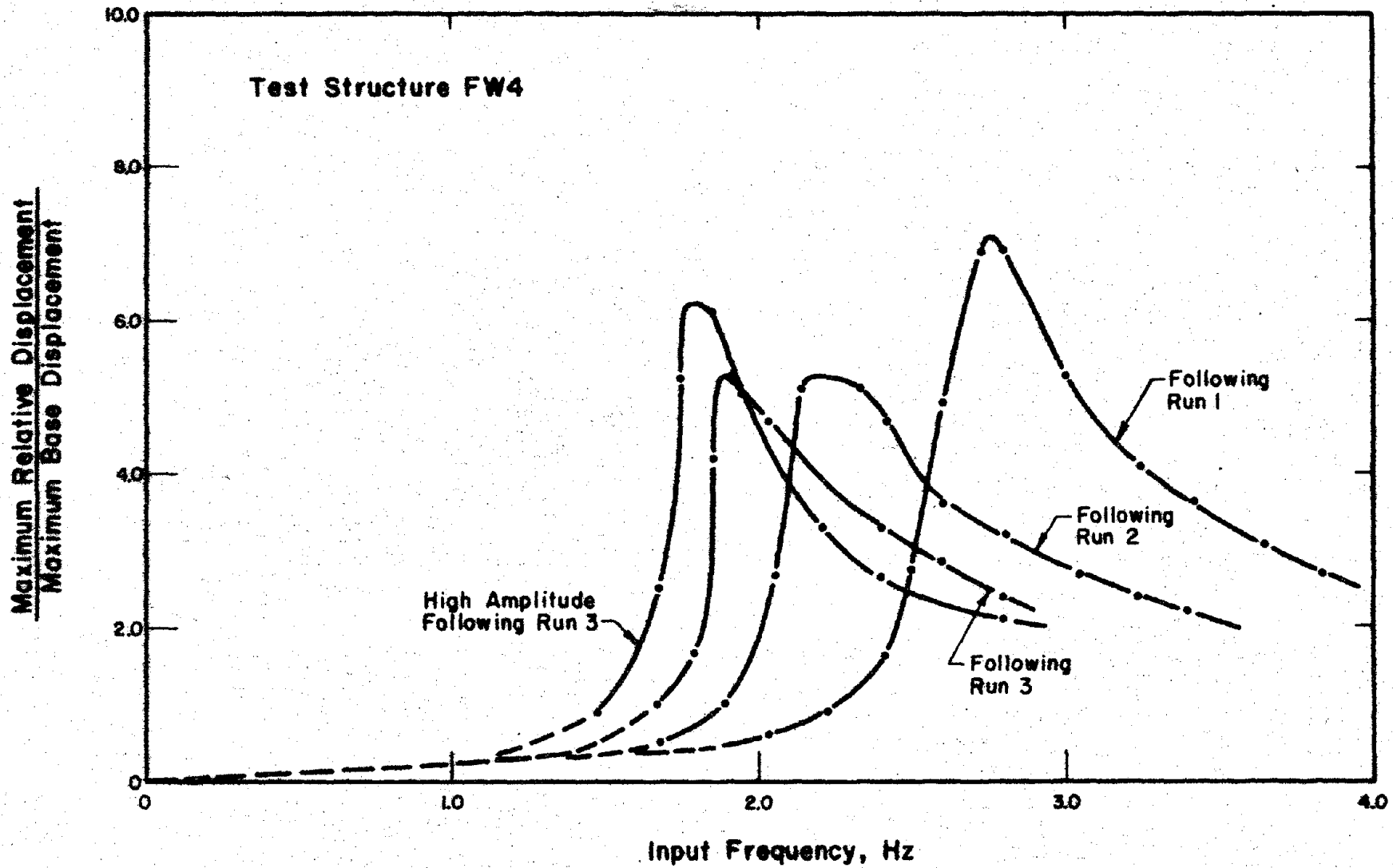
302

Fig. 6.16 Fourier-Amplitude Spectra of Minor Direction Acceleration



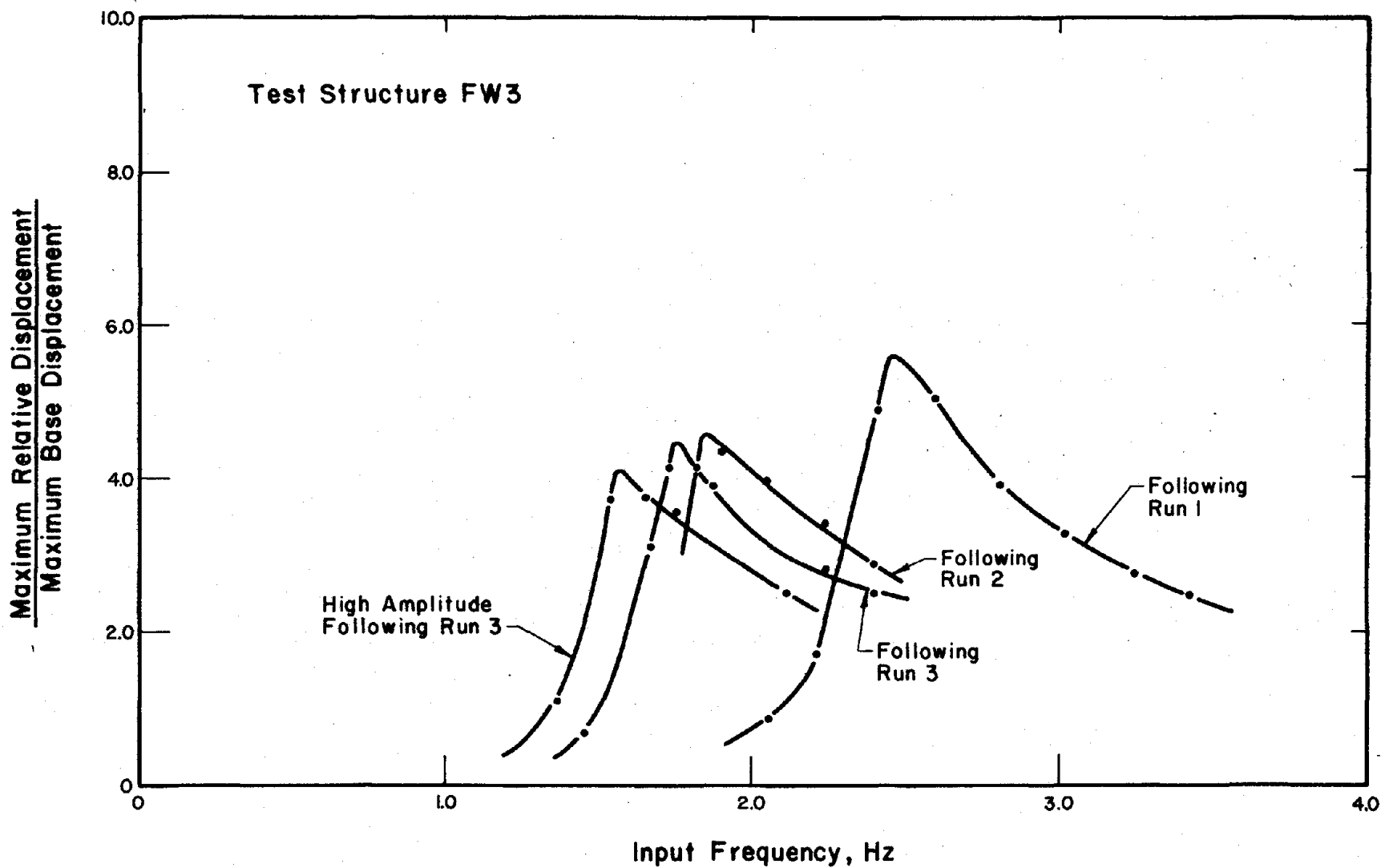
† Double - Amplitude / 2 Measured During Previous Test Run

Fig. 6.17 Equivalent-Viscous Damping Factors Calculated from Measured Response



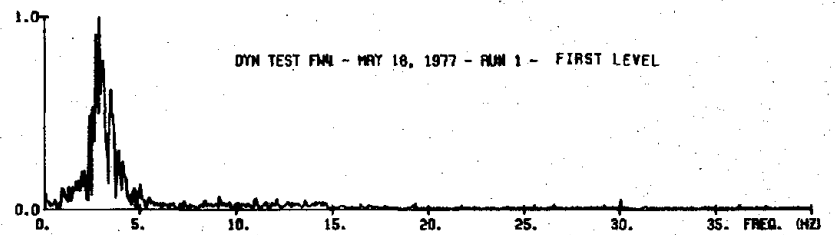
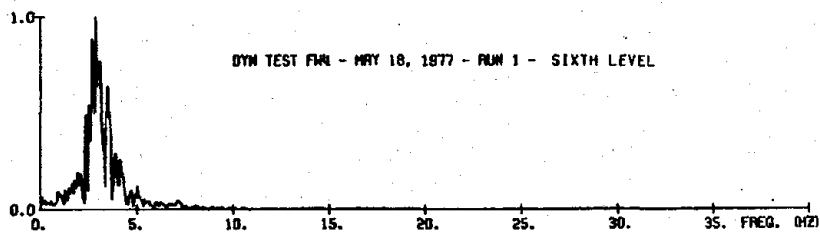
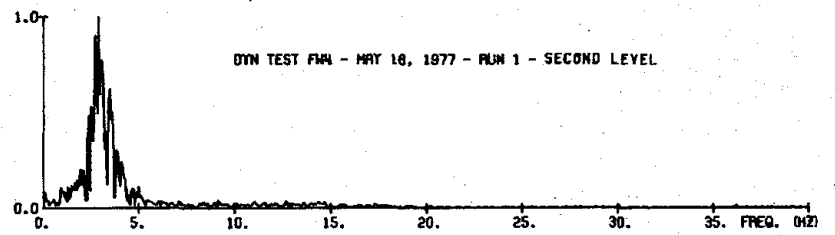
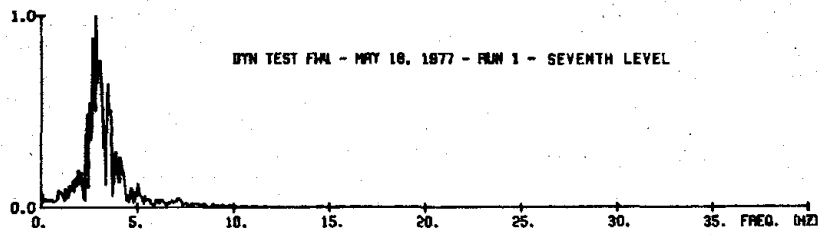
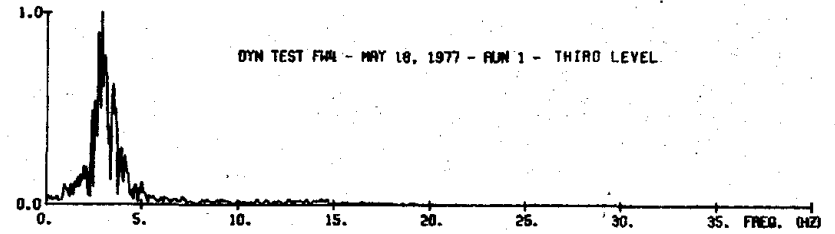
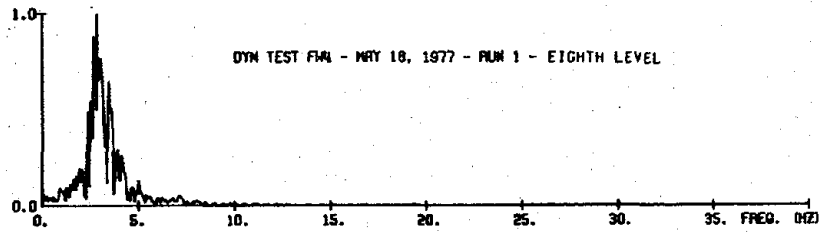
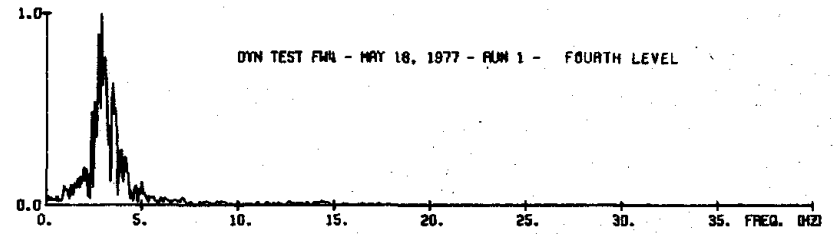
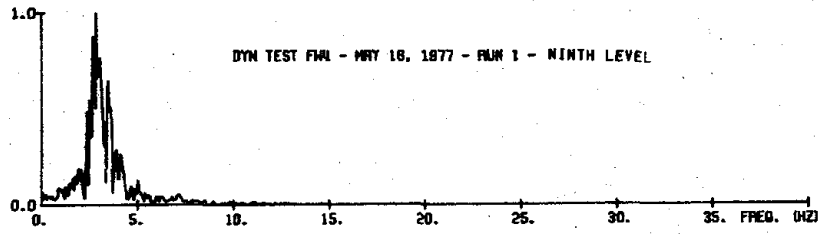
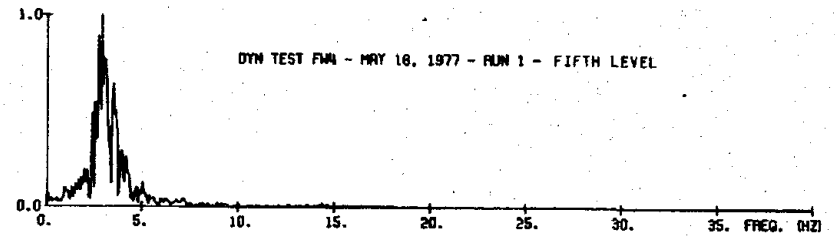
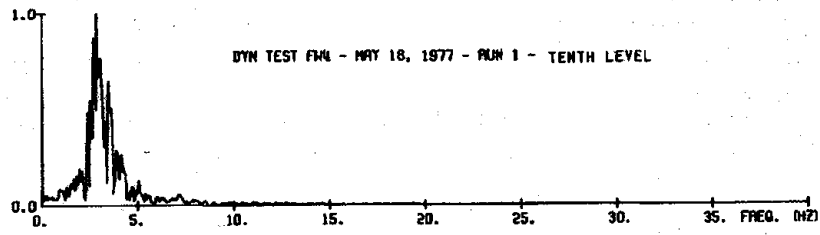
(a) Structure with Heavily Reinforced Wall

Fig. 6.18 Frequency-Response Curves of Response to Steady-State Base Motions



(b) Structure with Lightly Reinforced Wall

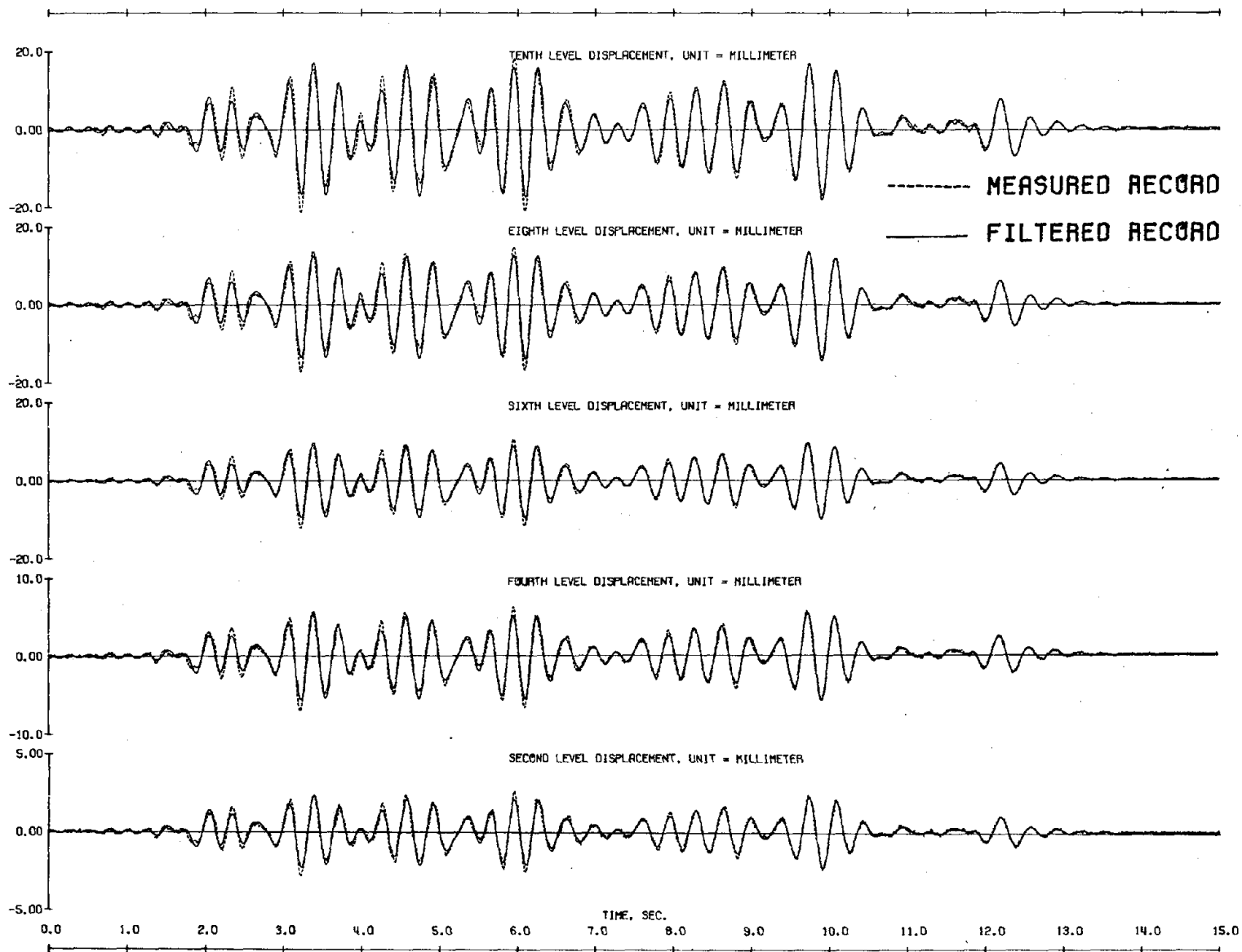
Fig. 6.18 (contd.) Frequency-Response Curves of Response to Steady-State Base Motions



306

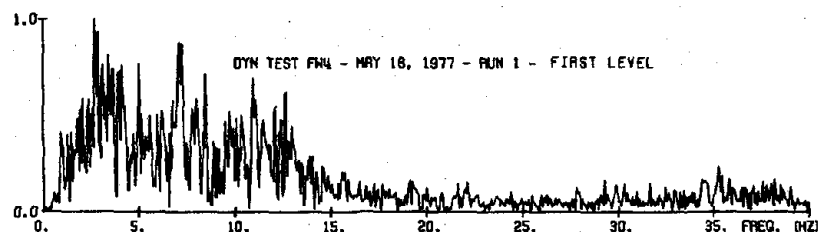
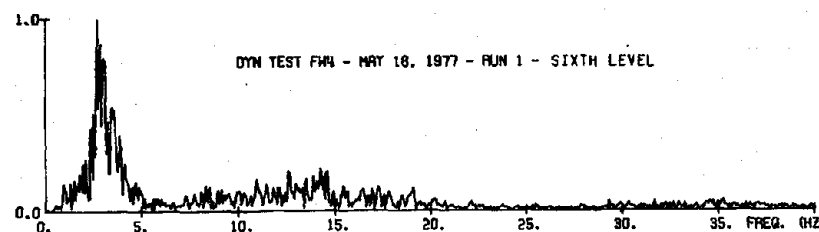
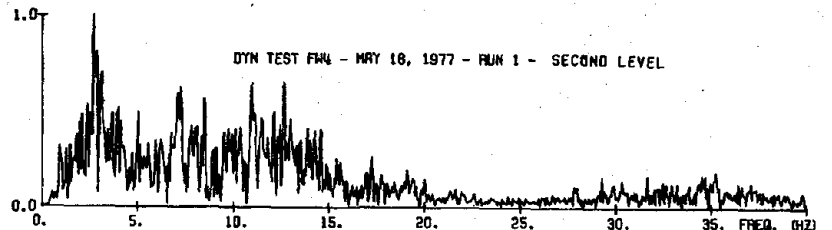
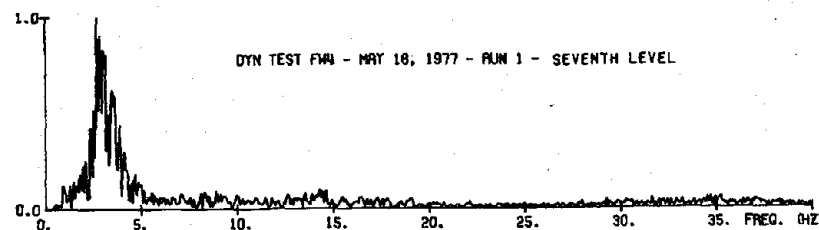
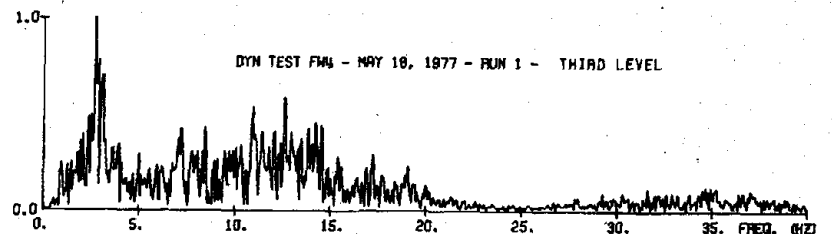
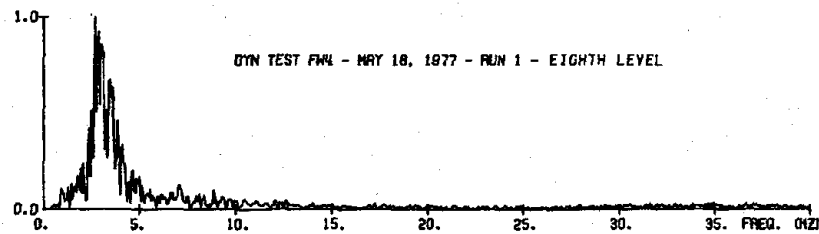
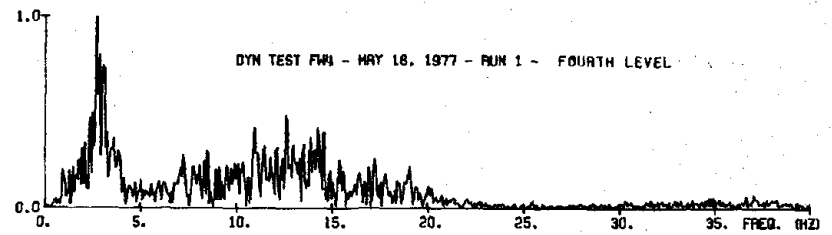
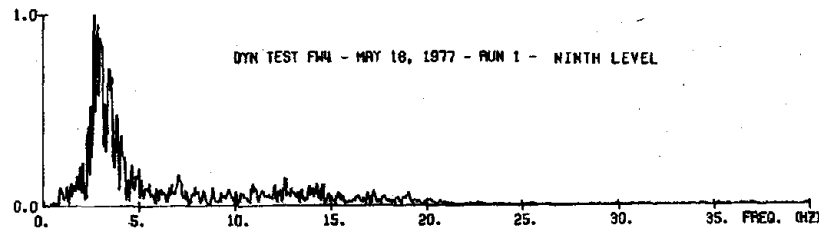
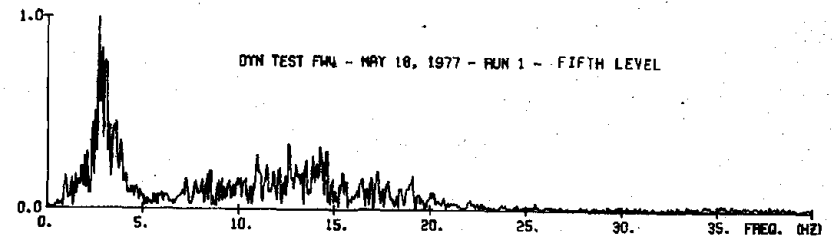
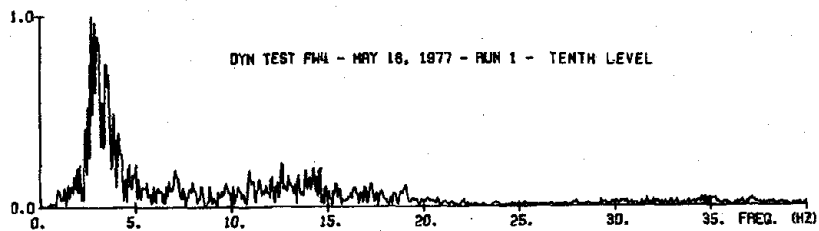
(a) Displacements

Fig. 6.19 Frequency Content of Measured Response



(a) (contd.) Displacements

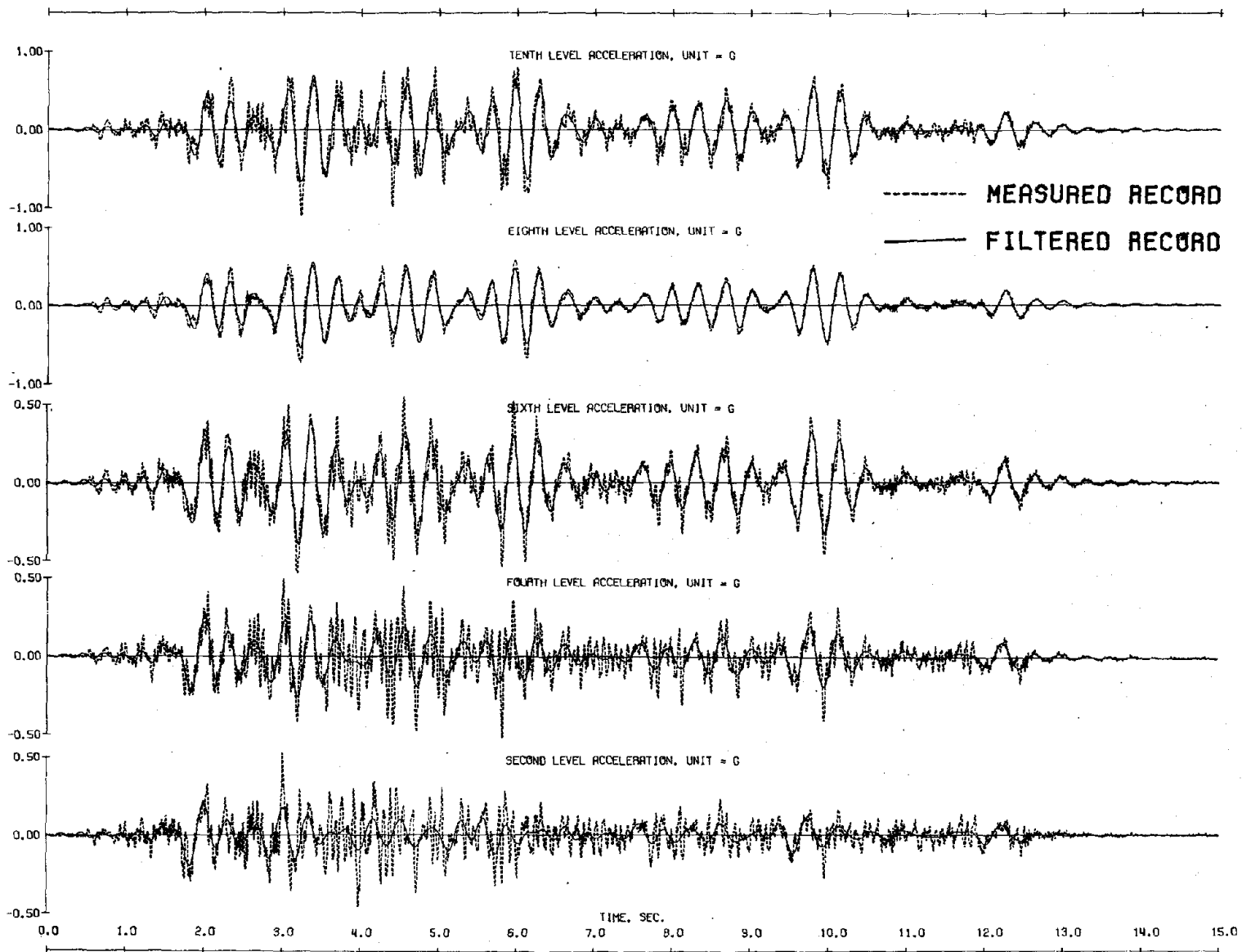
Fig. 6.19 (contd.) Frequency Content of Measured Response



308

(b) Accelerations

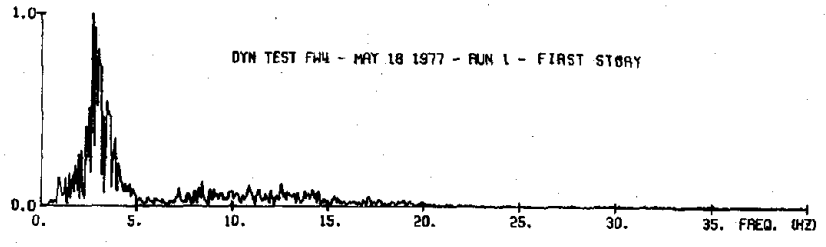
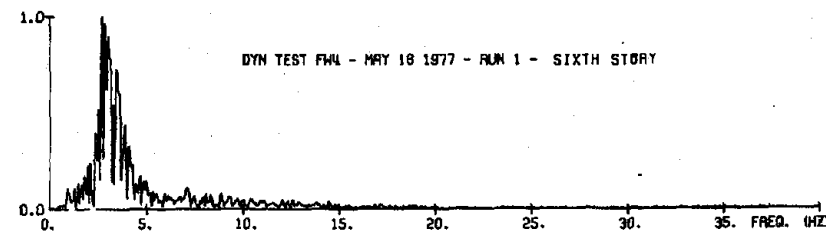
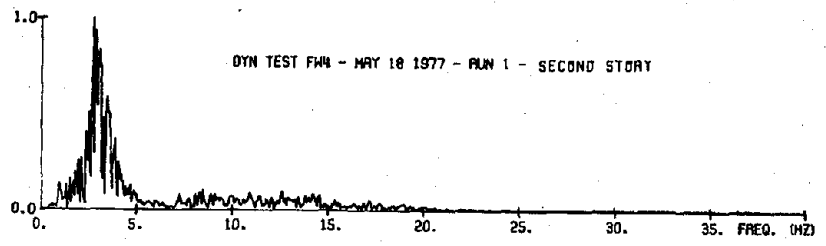
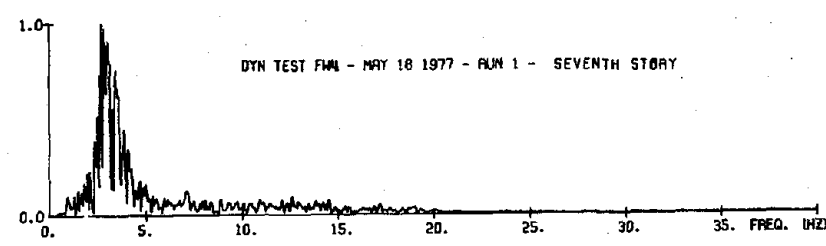
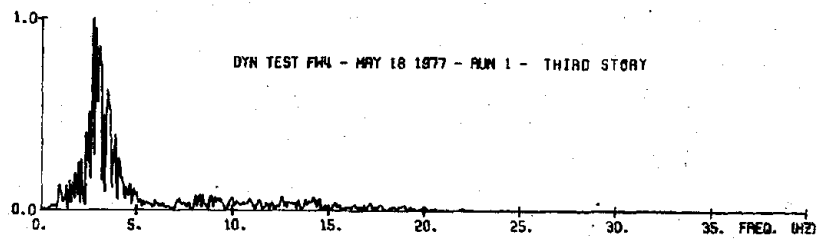
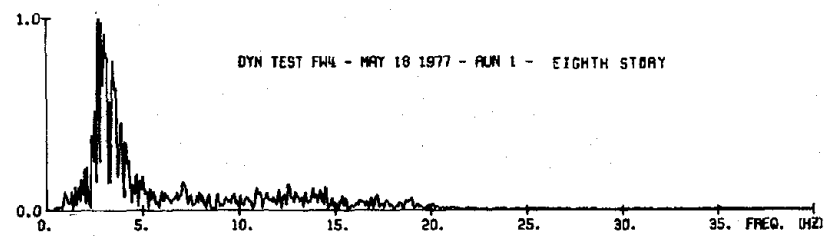
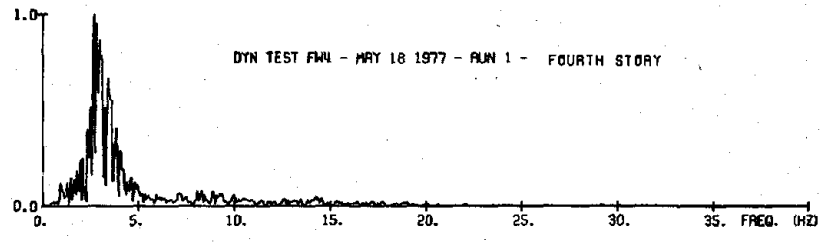
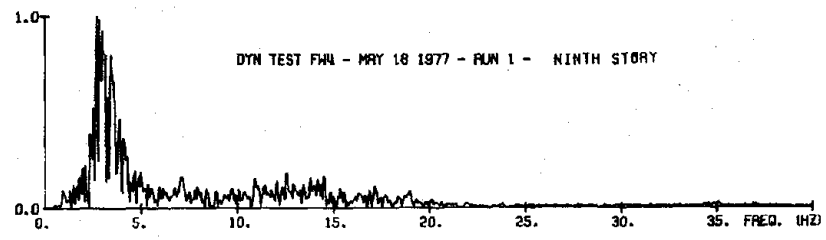
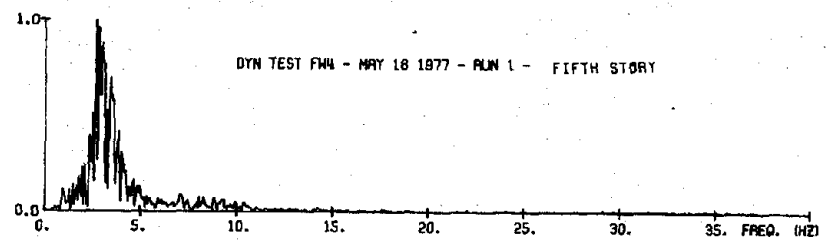
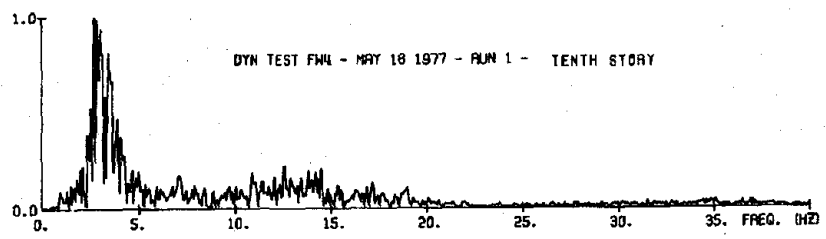
Fig. 6.19 (contd.) Frequency Content of Measured Response



309

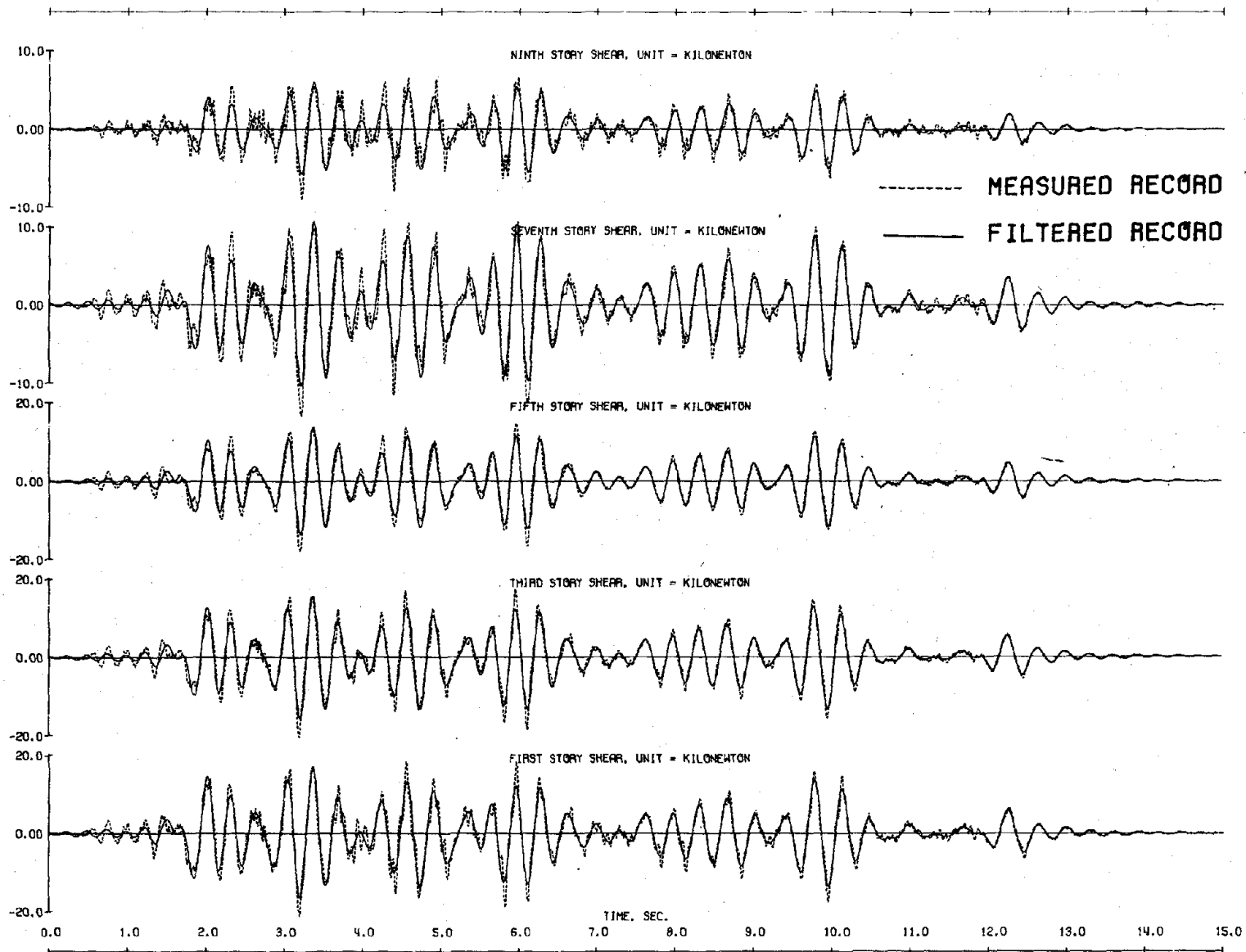
(b) (contd.) Accelerations

Fig. 6.19 (contd.) Frequency Content of Measured Response



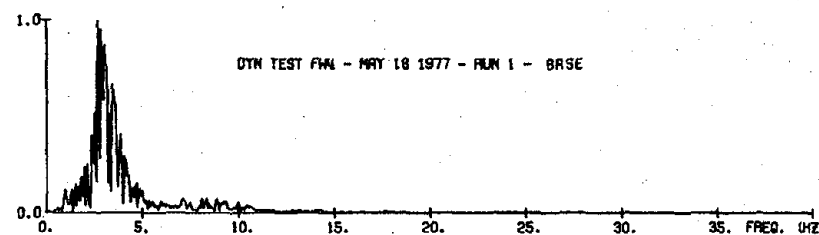
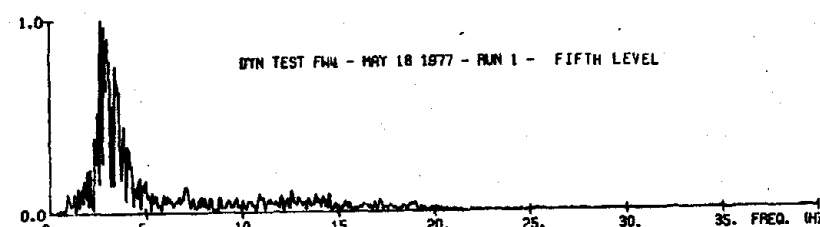
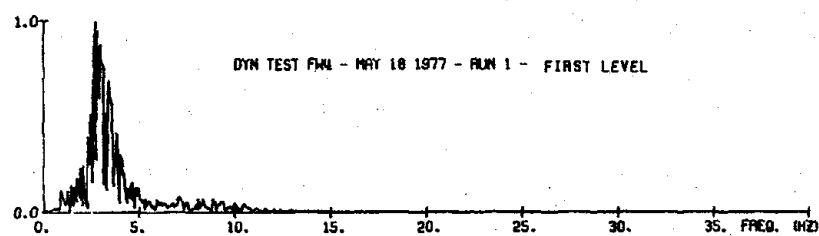
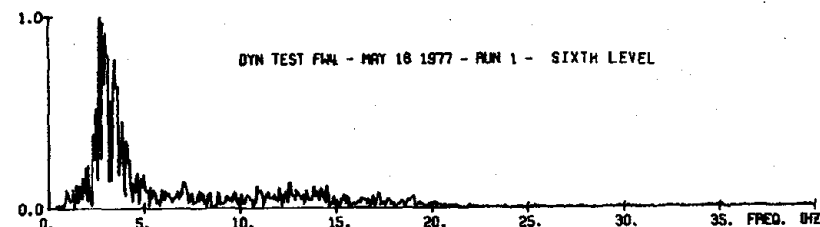
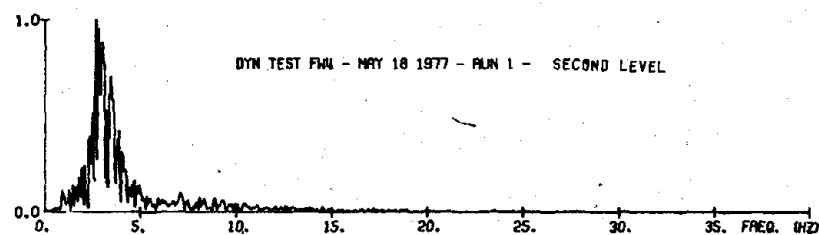
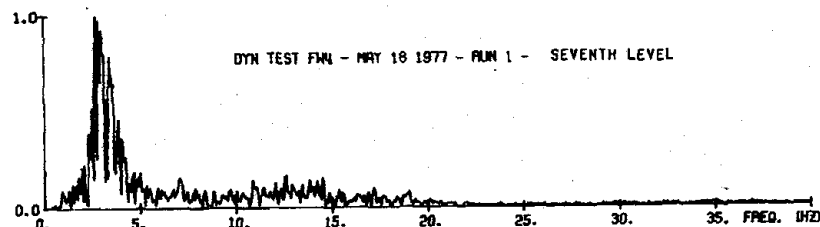
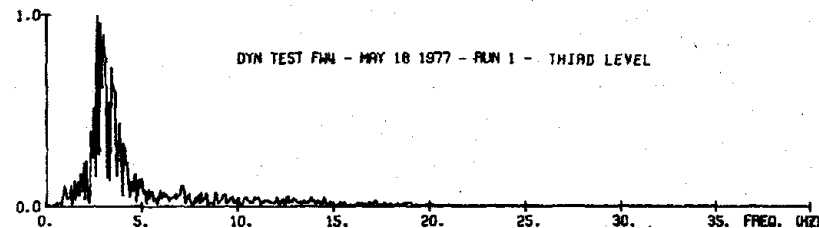
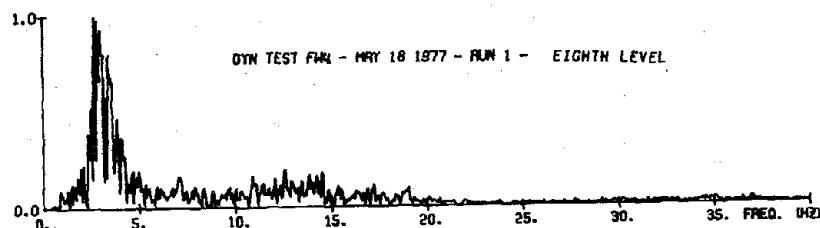
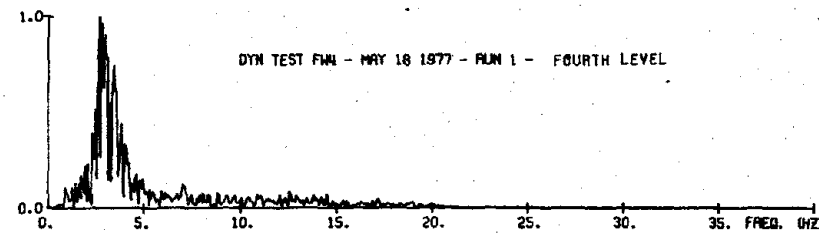
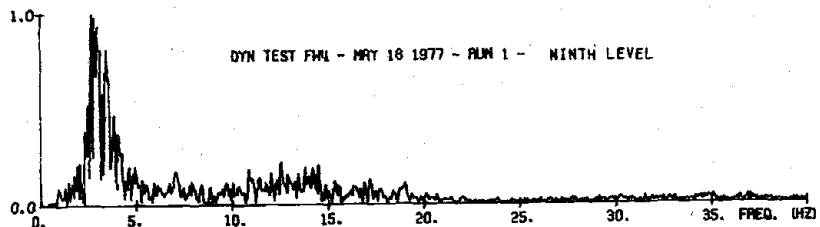
(c) Shears

Fig. 6.19 (contd.) Frequency Content of Measured Response



(c) (contd.) Shears

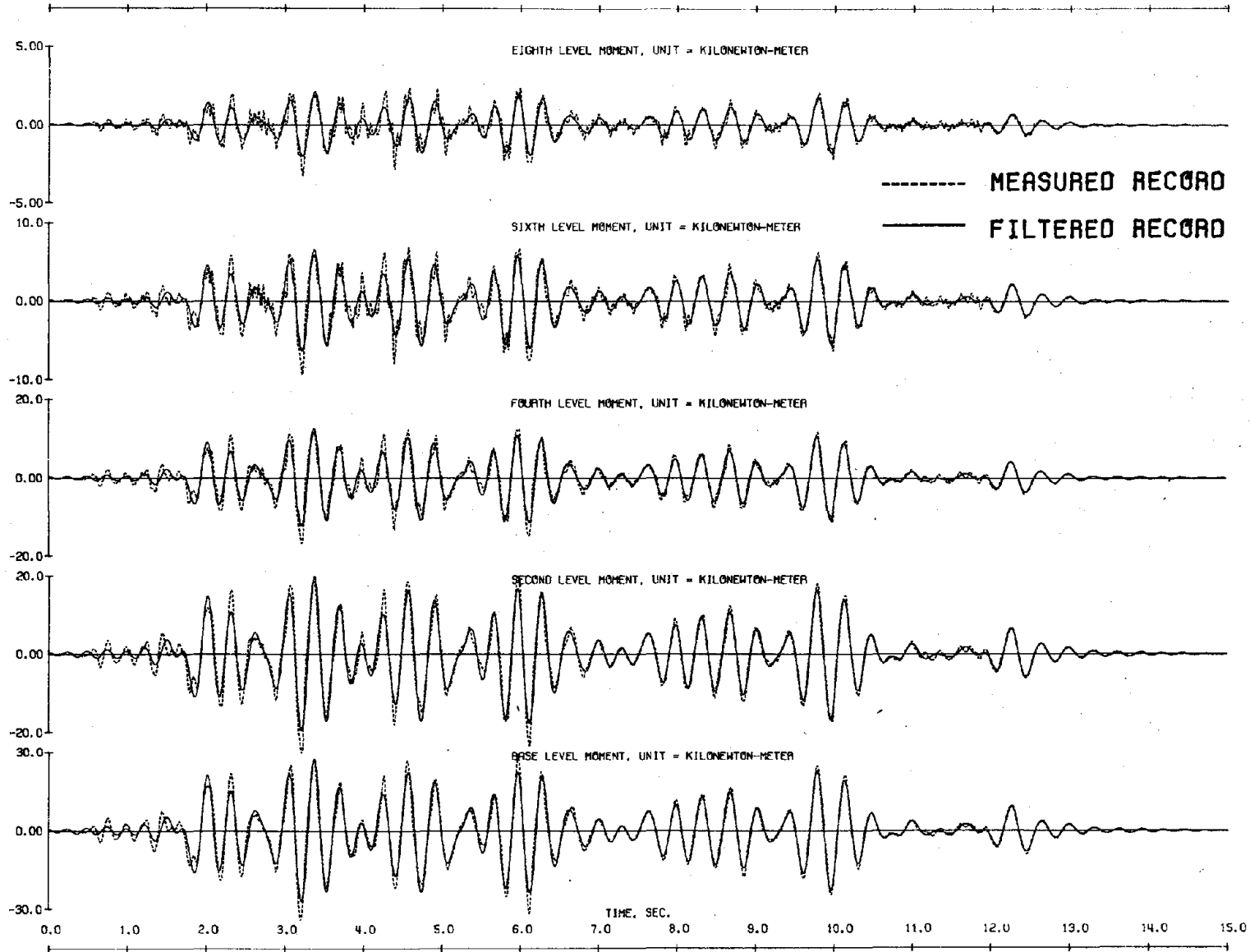
Fig. 6.19 (contd.) Frequency Content of Measured Response



312

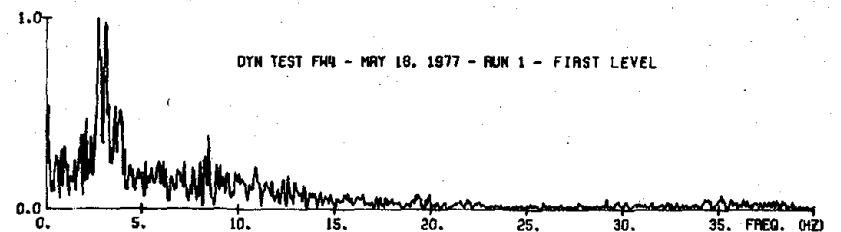
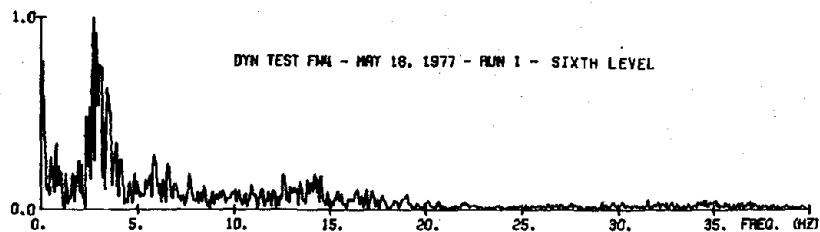
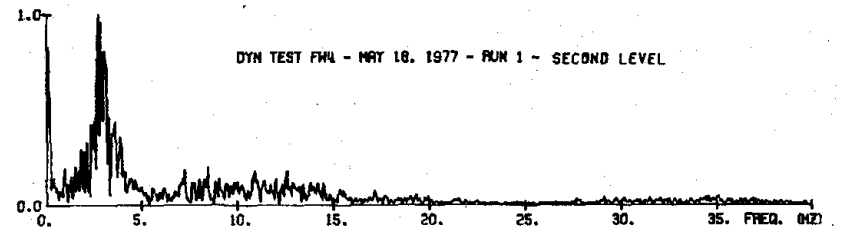
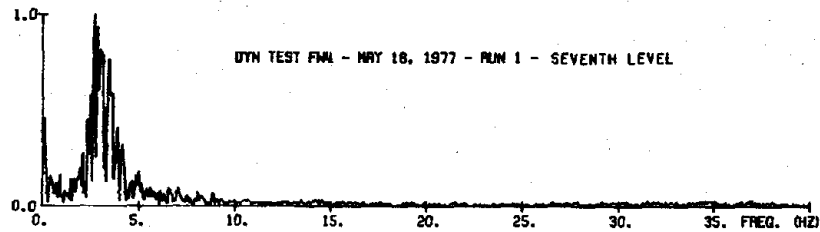
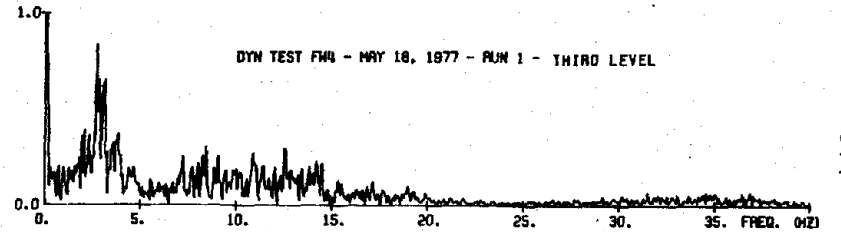
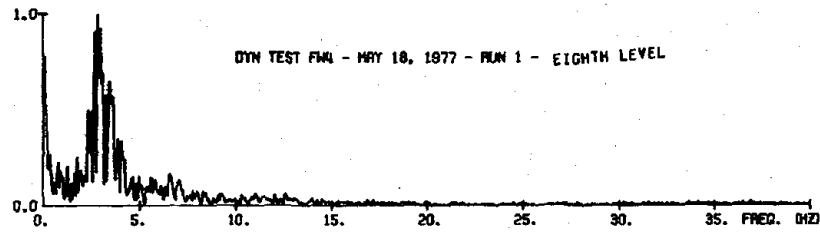
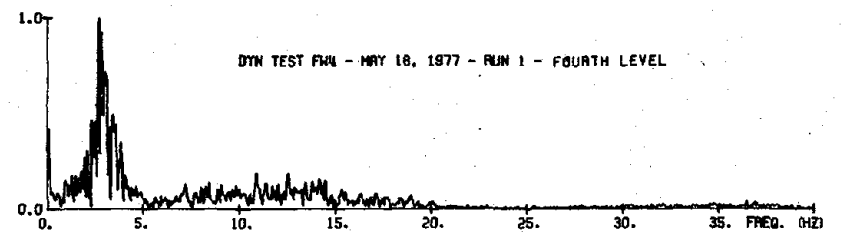
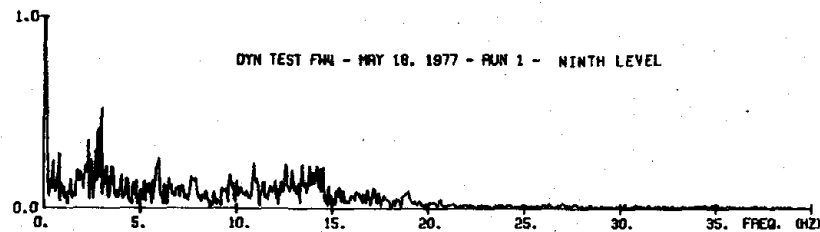
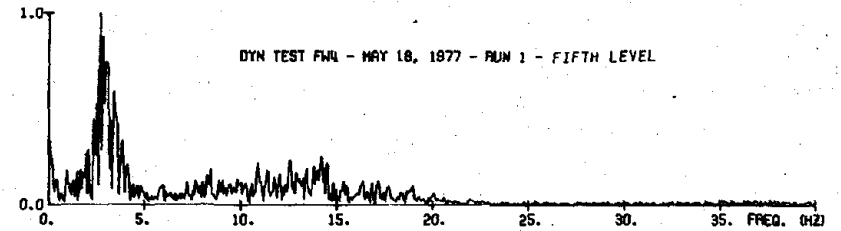
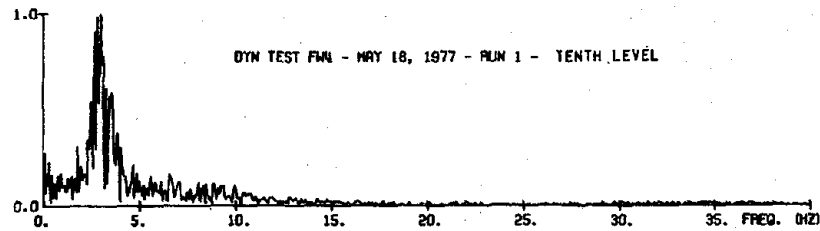
(d) Moments

Fig. 6.19 (contd.) Frequency Content of Measured Response



(d) (contd.) Moments

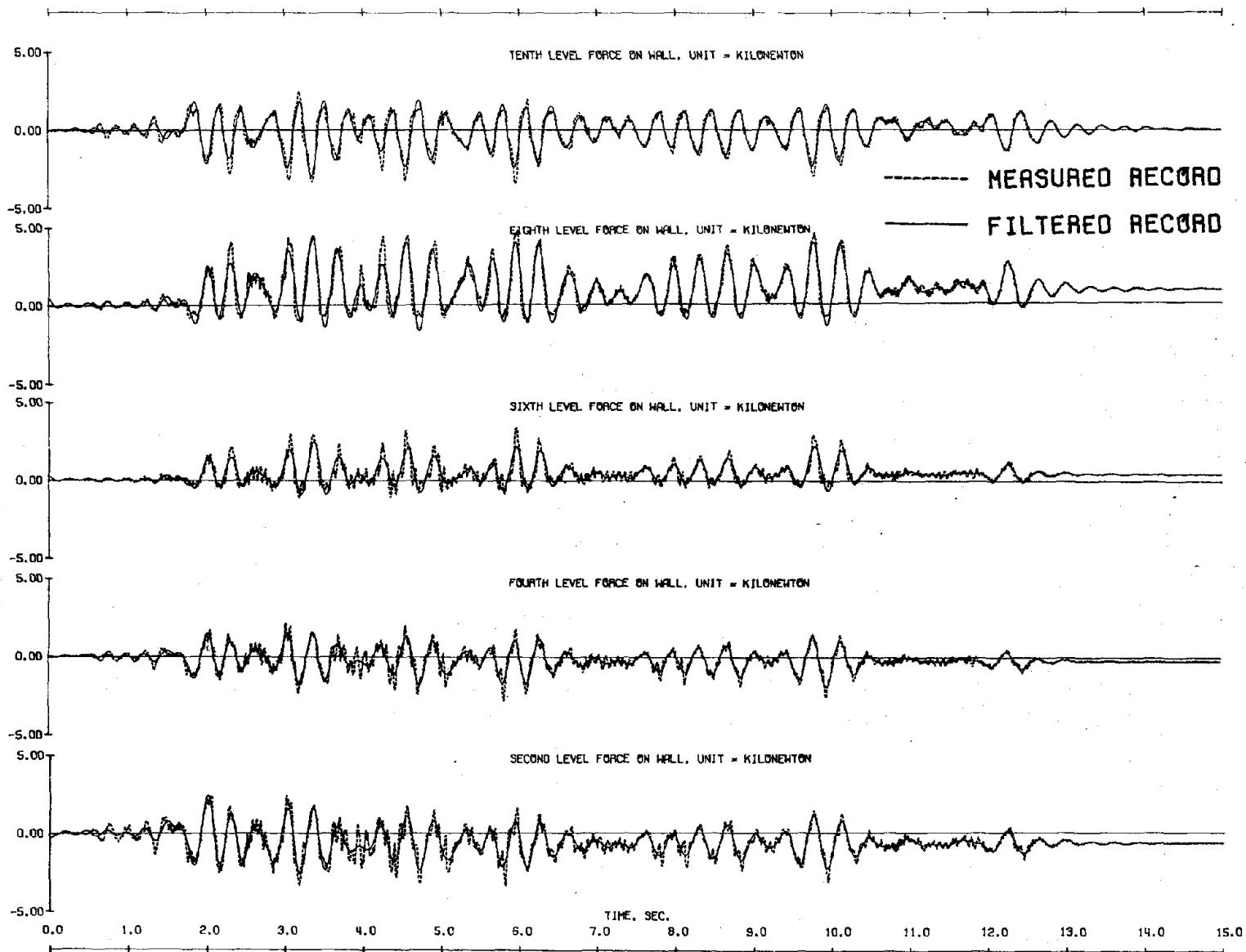
Fig. 6.19 (contd.) Frequency Content of Measured Response



314

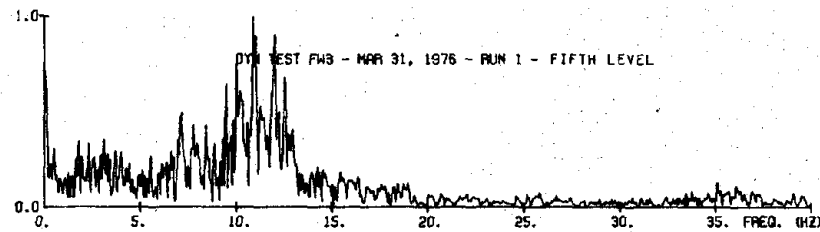
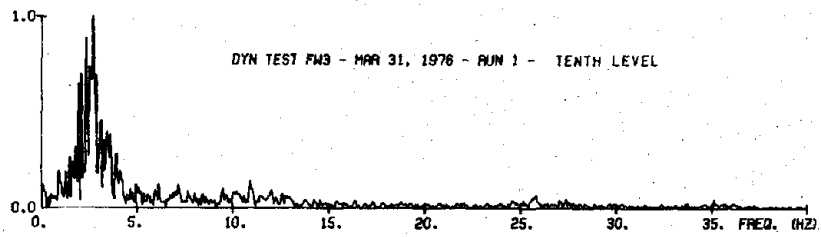
(e) Force Resisted by Heavily Reinforced Wall

Fig. 6.19 (contd.) Frequency Content of Measured Response

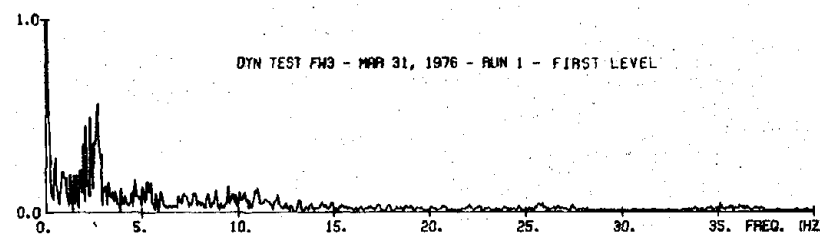
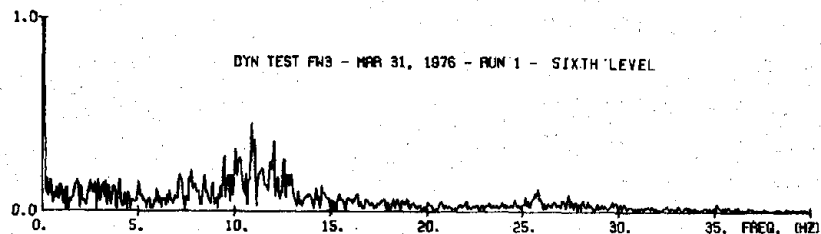
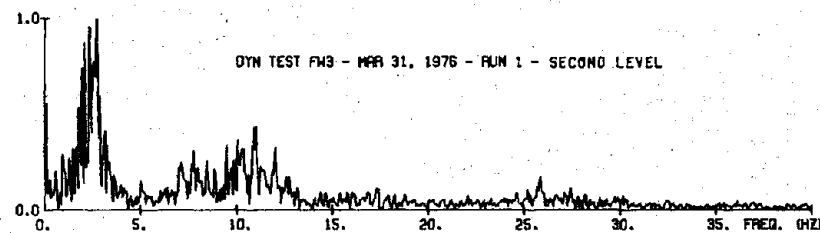
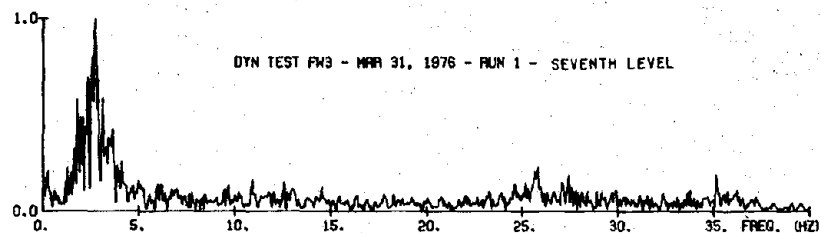
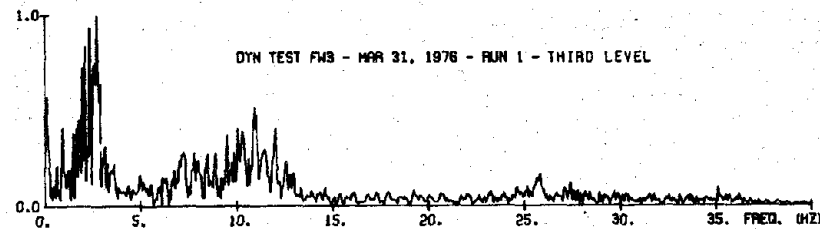
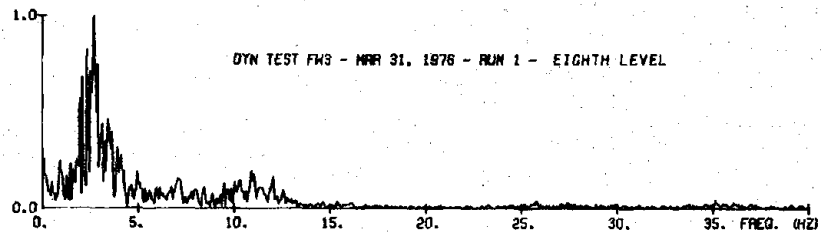
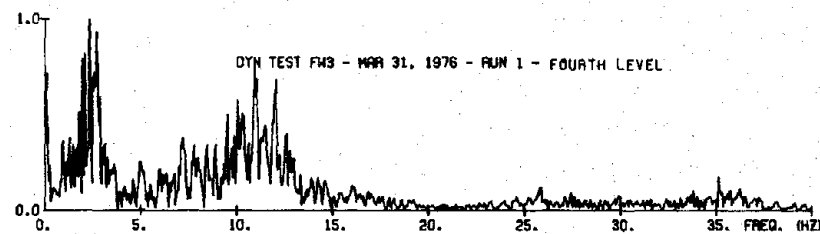


(e) (contd.) Force Resisted by Heavily Reinforced Wall

Fig. 6.19 (contd.) Frequency Content of Measured Response



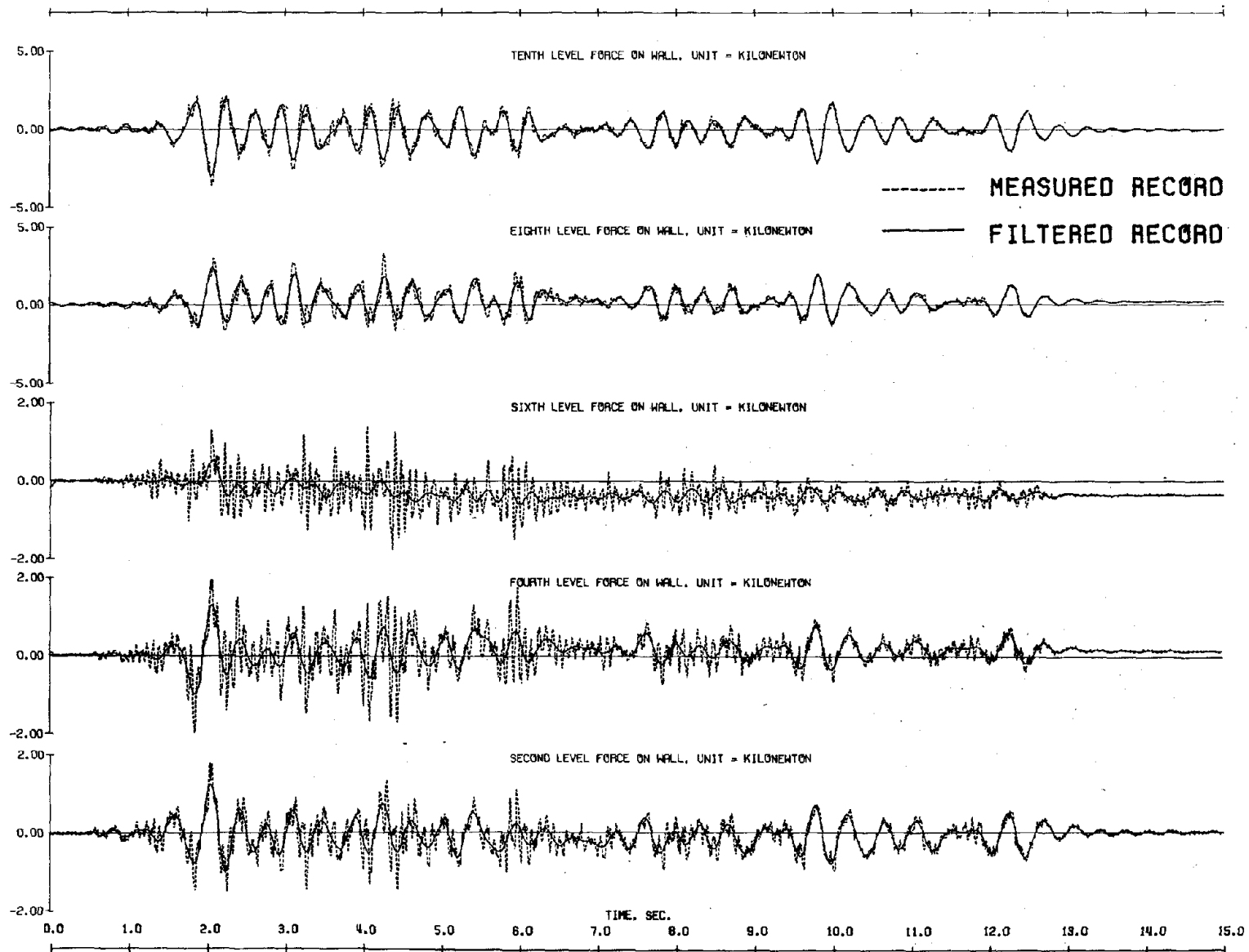
(CHANNEL NOT RECORDED BECAUSE OF
TAPE RECORDER MALFUNCTION)



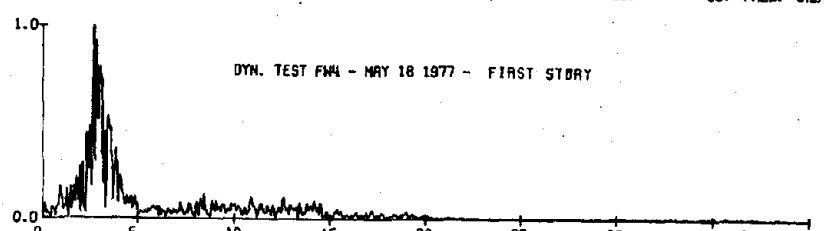
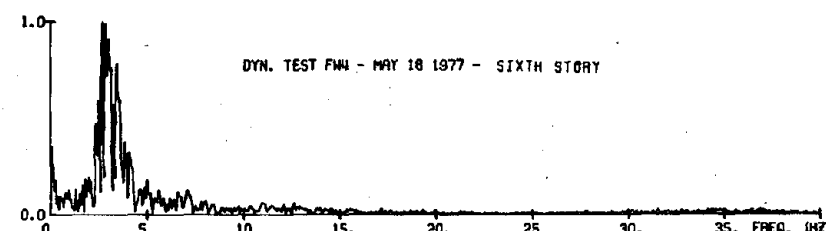
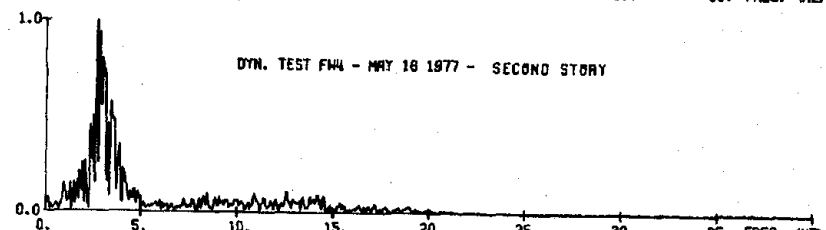
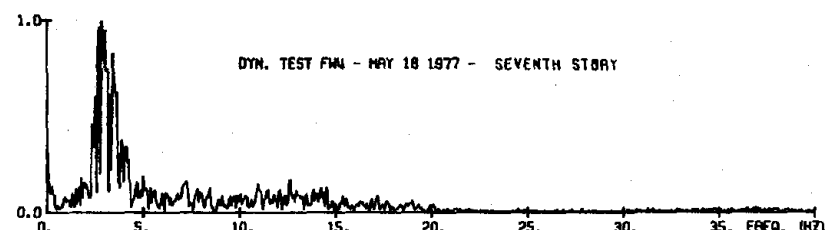
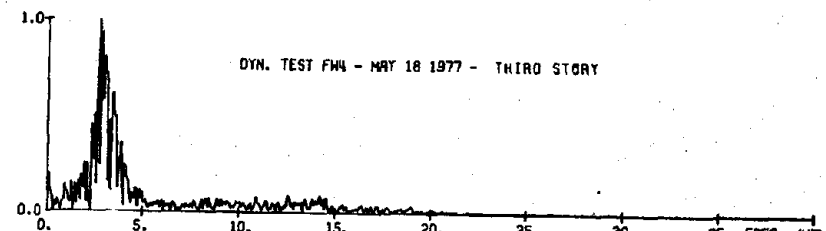
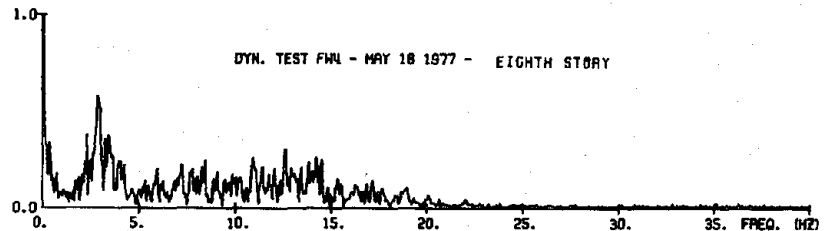
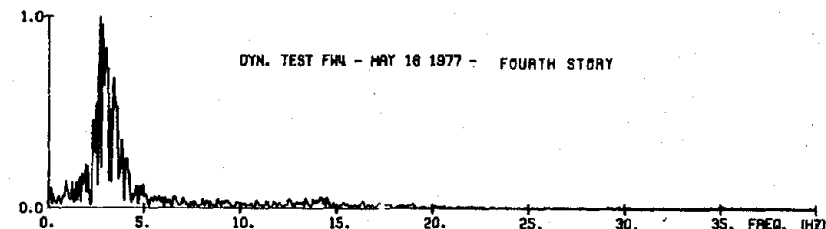
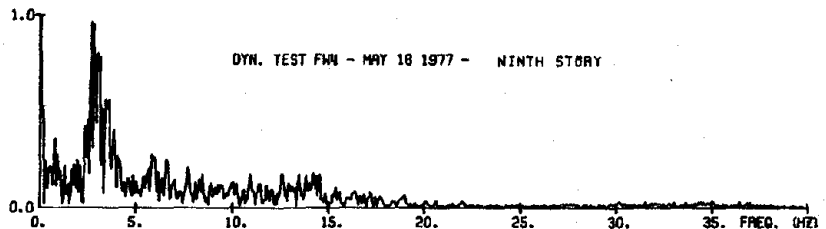
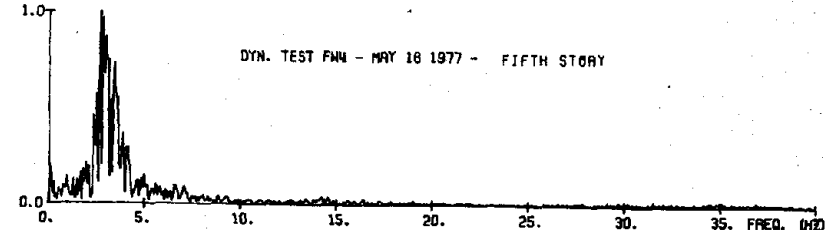
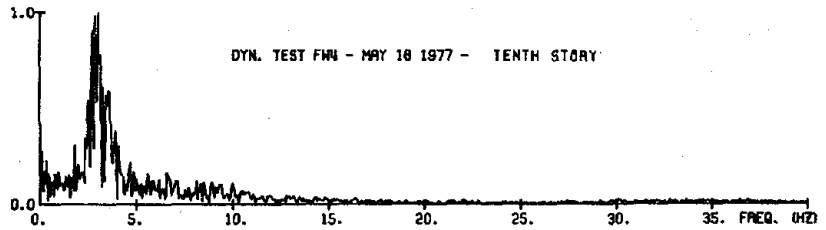
316

(f) Force Resisted by Lightly Reinforced Wall

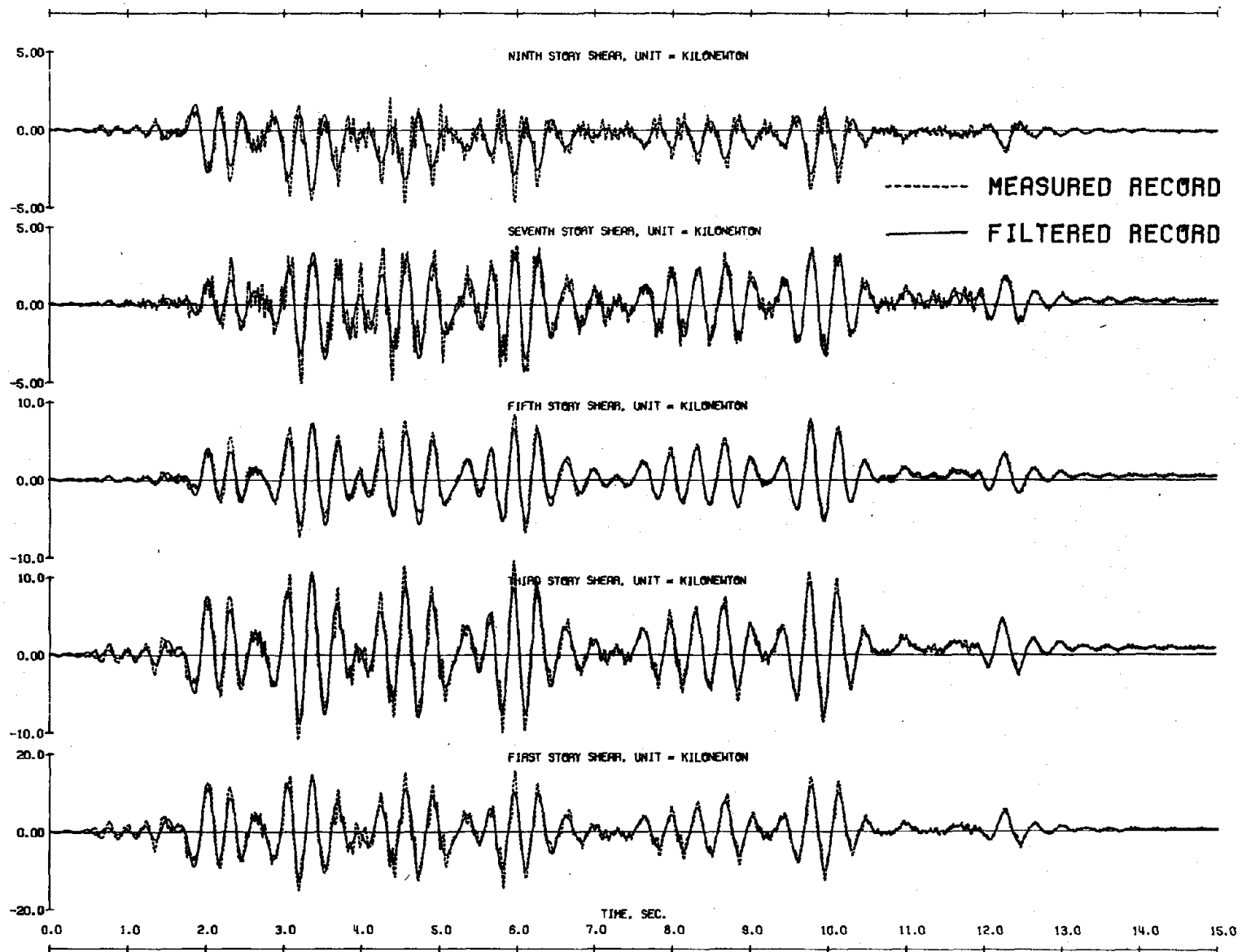
Fig. 6.19 (contd.) Frequency Content of Measured Response



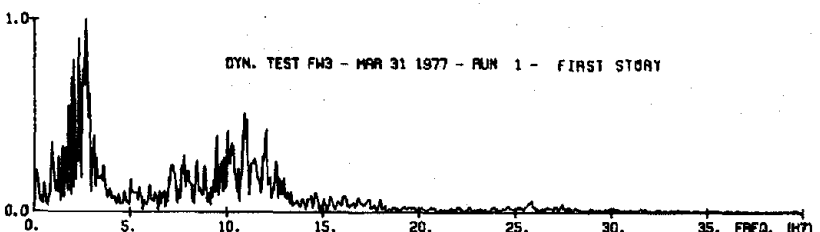
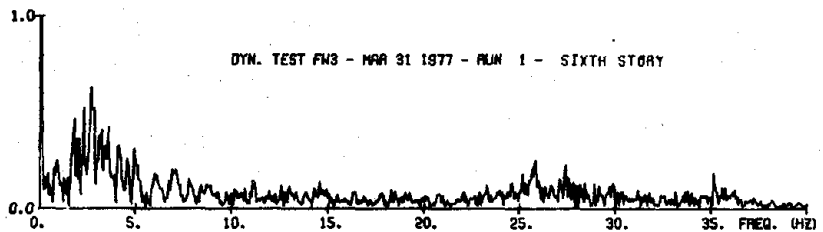
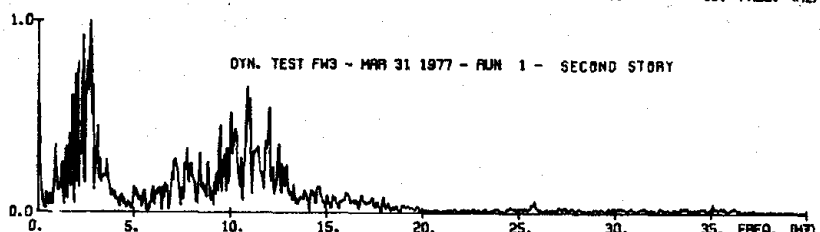
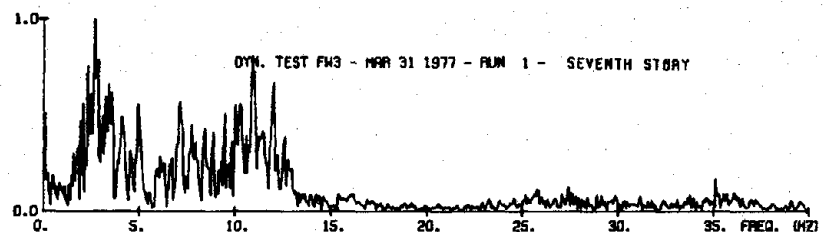
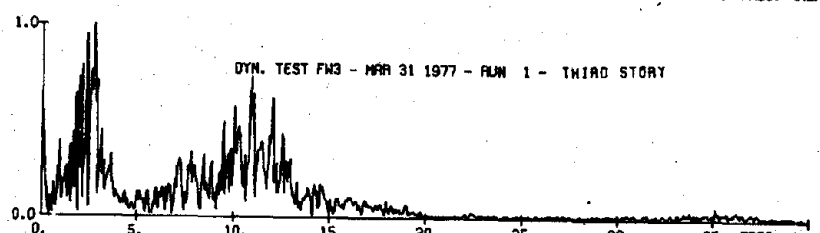
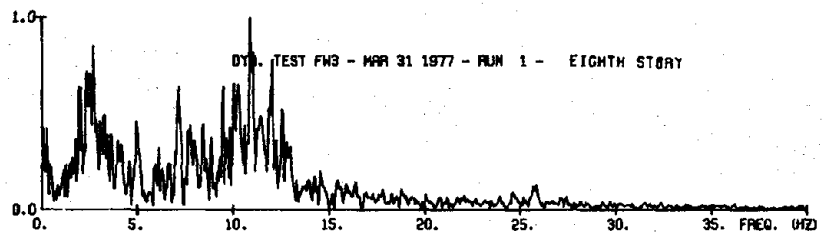
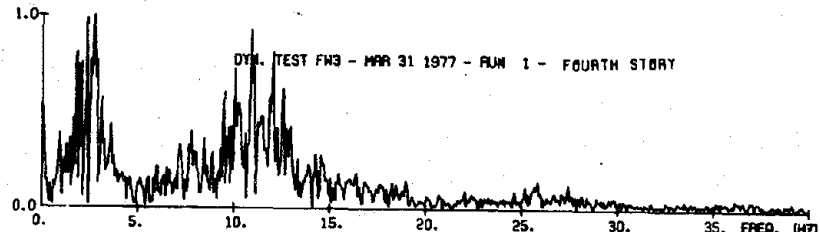
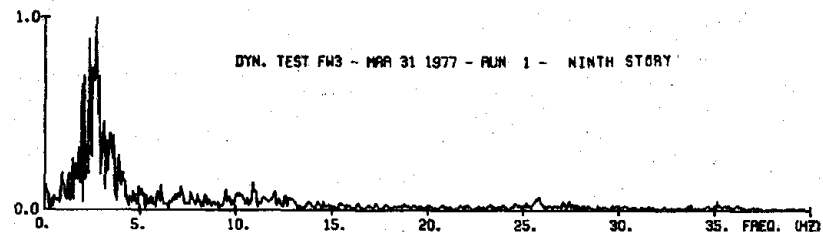
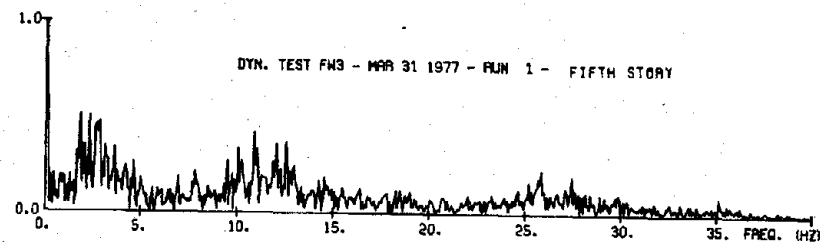
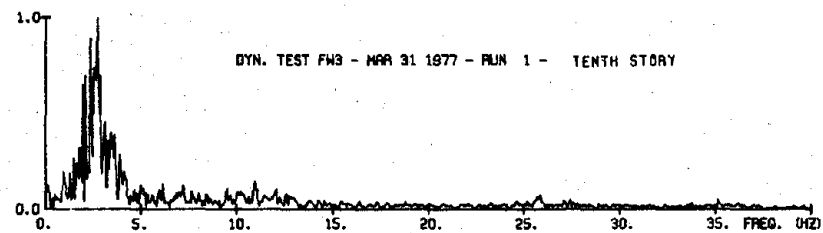
(f) (contd.) Force Resisted by Lightly Reinforced Wall
 Fig. 6.19 (contd.) Frequency Content of Measured Response



(g) Shears Resisted by Heavily Reinforced Wall
 Fig. 6.19 (contd.) Frequency Content of Measured Response



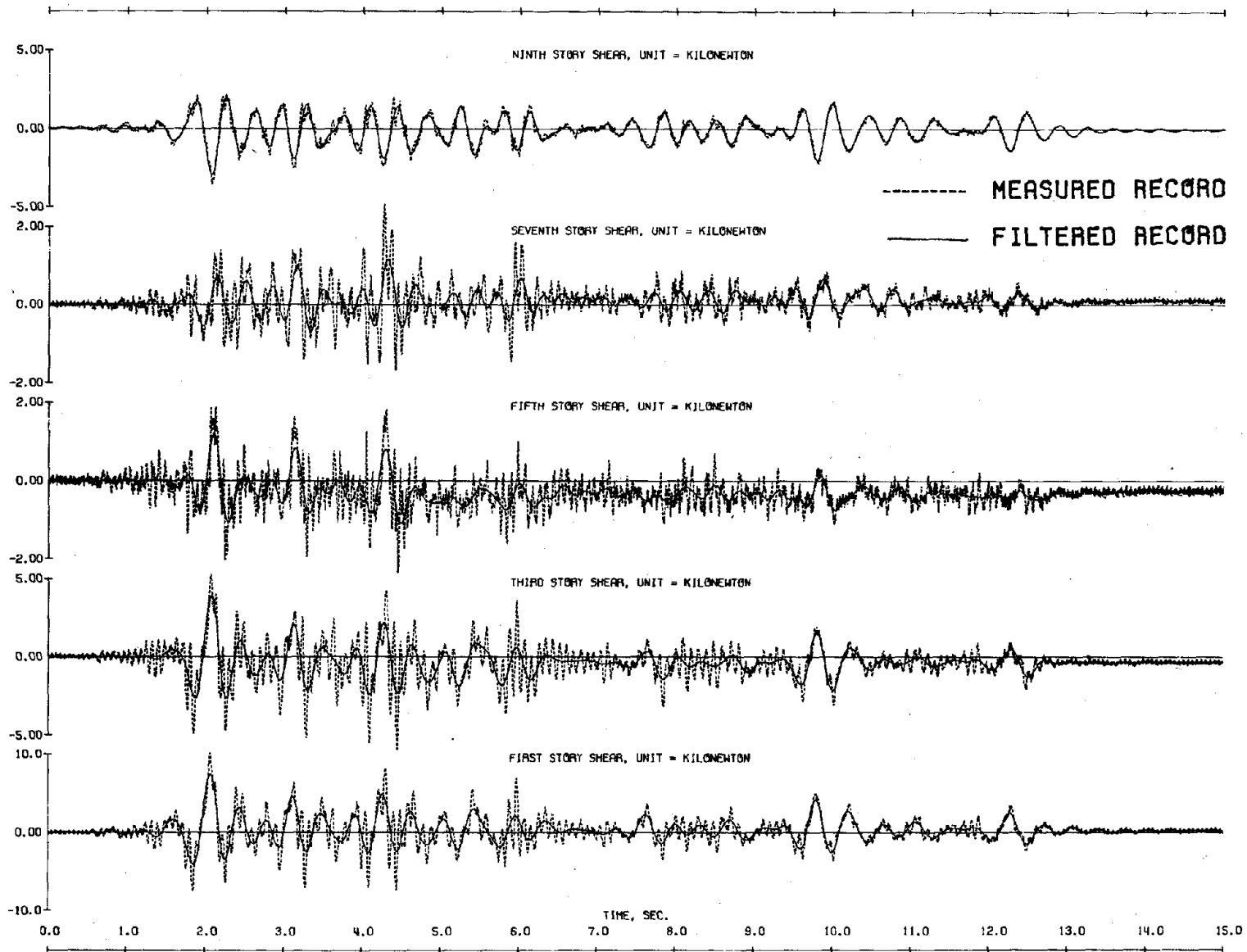
(g) (contd.) Shears Resisted by Heavily Reinforced Wall
 Fig. 6.19 (contd.) Frequency Content of Measured Response



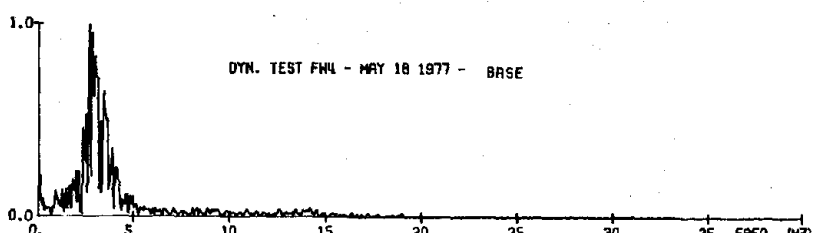
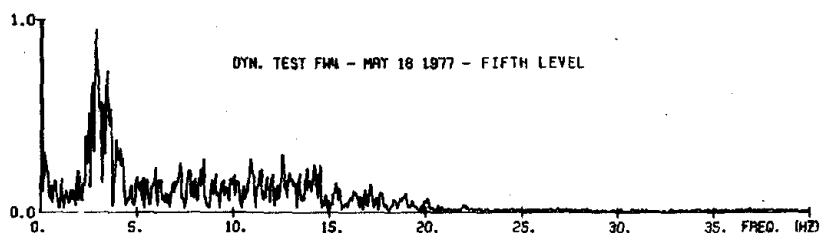
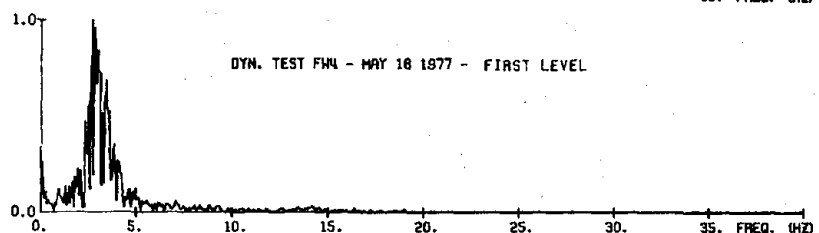
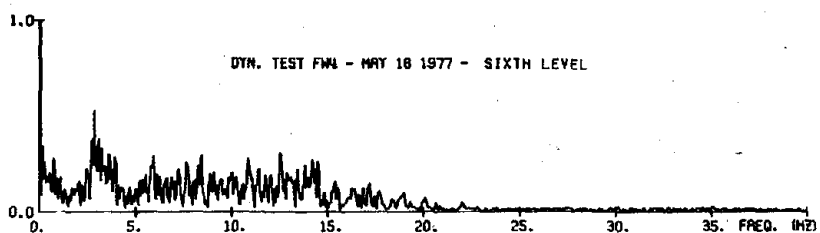
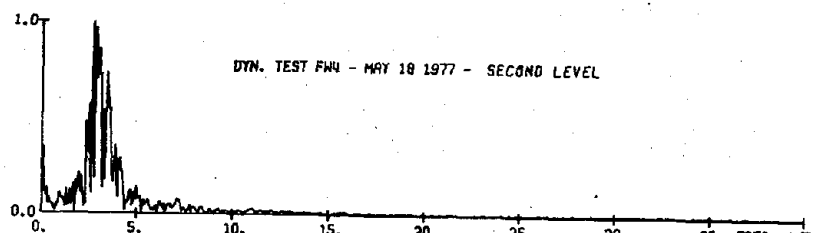
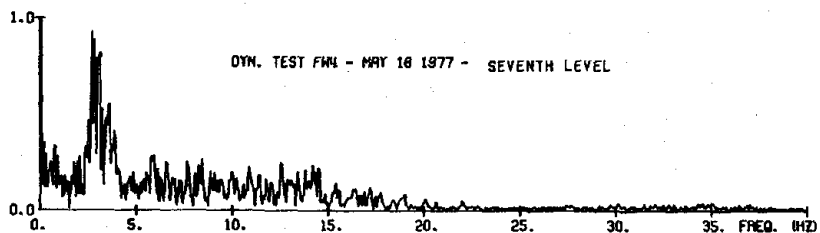
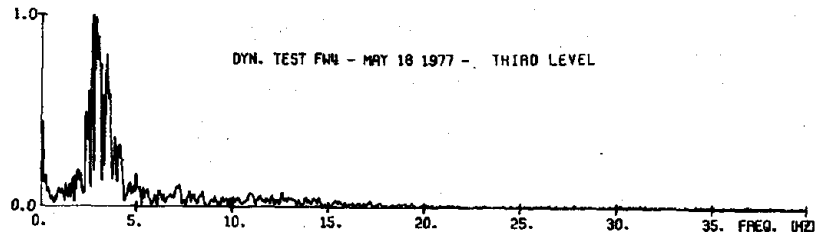
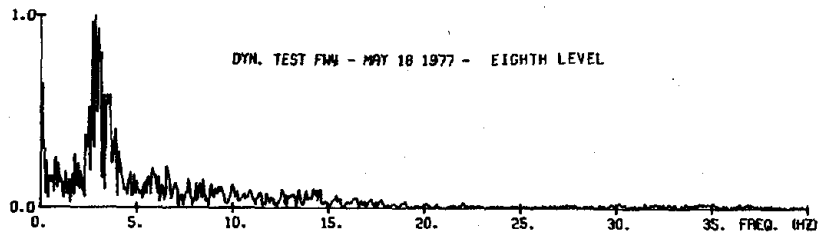
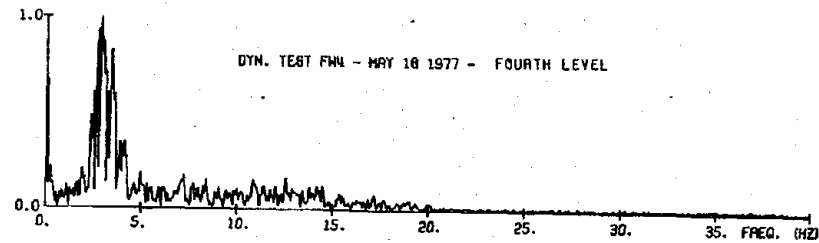
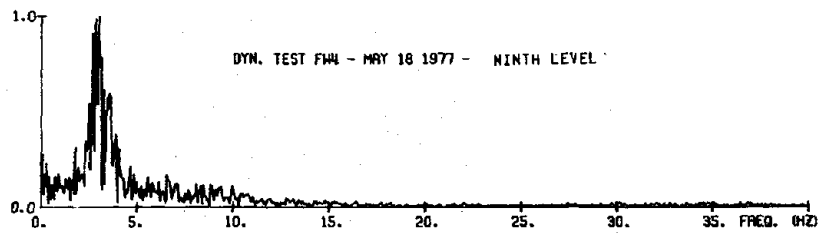
320

(h) Shears Resisted by Lightly Reinforced Wall

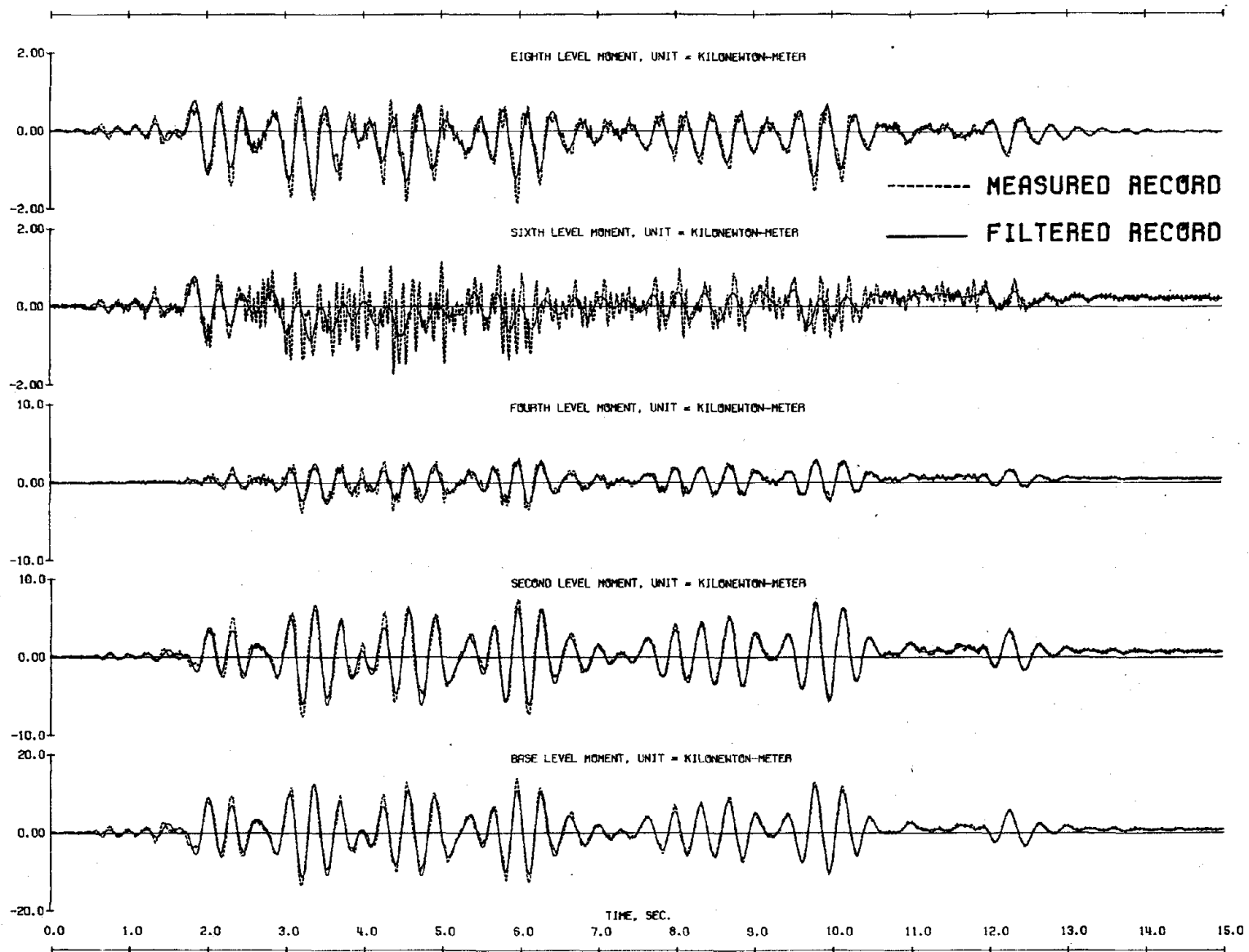
Fig. 6.19 (contd.) Frequency Content of Measured Response



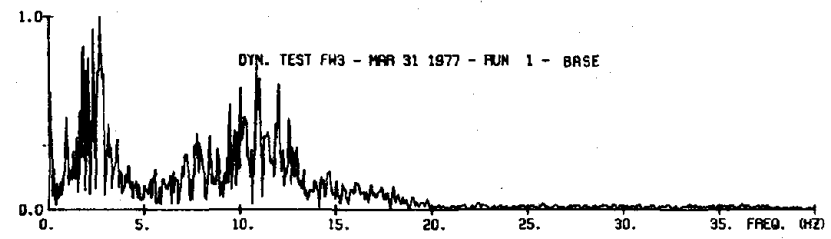
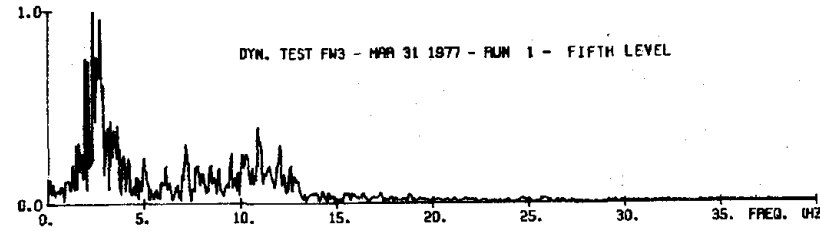
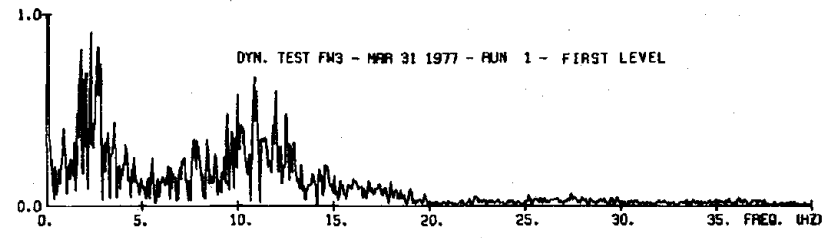
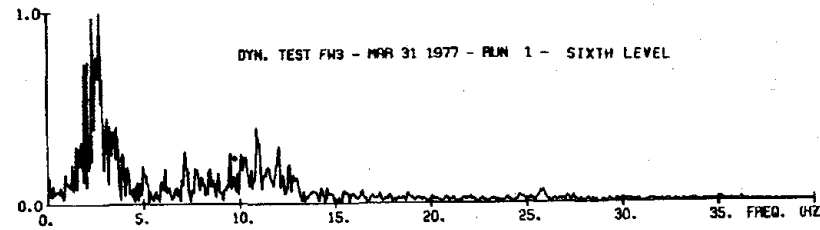
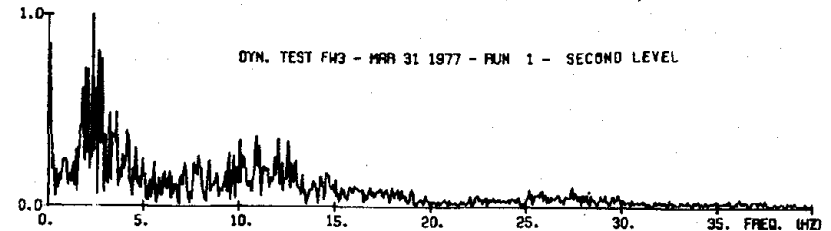
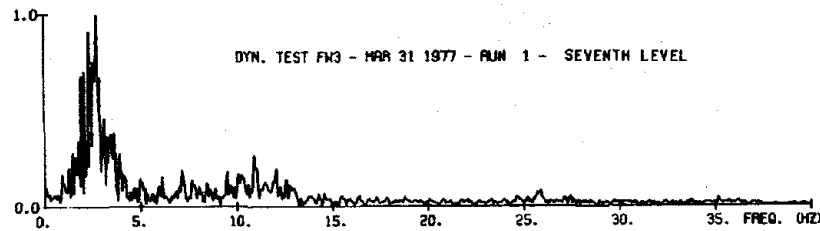
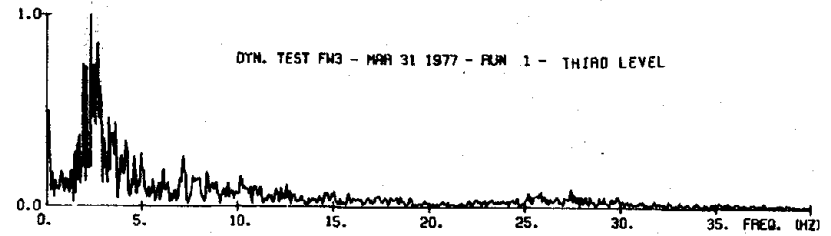
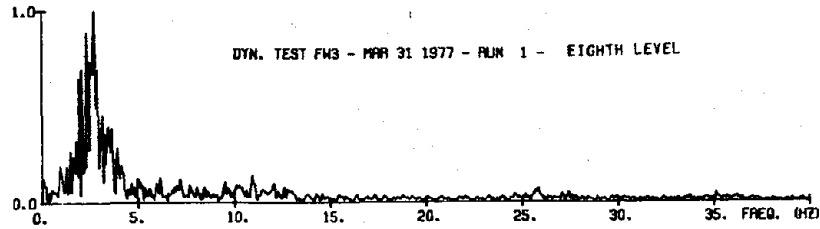
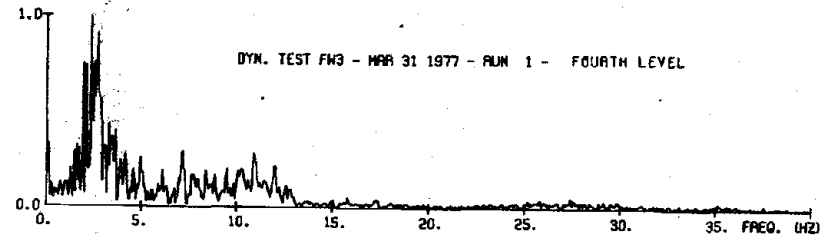
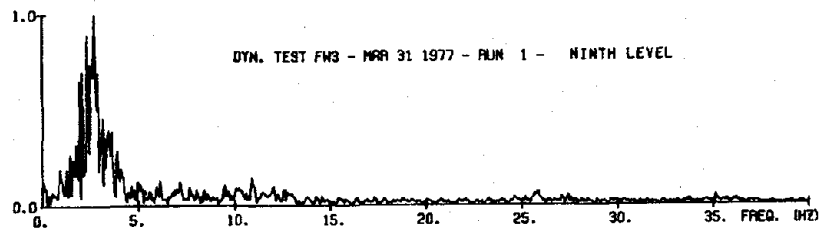
(h) (contd.) Shears Resisted by Lightly Reinforced Wall
 Fig. 6.19 (contd.) Frequency Content of Measured Response



(i) Moments Resisted by Heavily Reinforced Wall
 Fig. 6.19 (contd.) Frequency Content of Measured Response



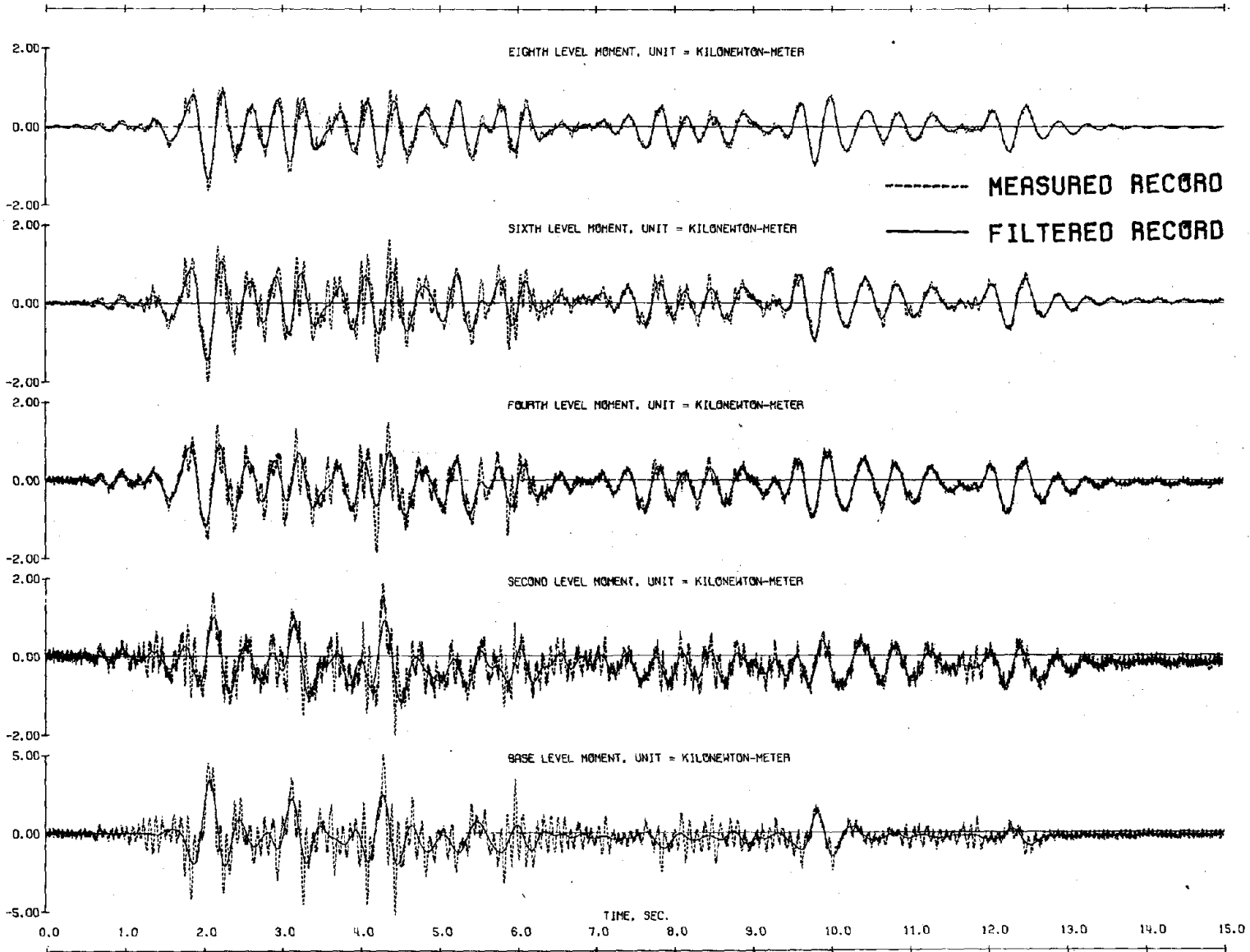
(i) (contd.) Moments Resisted by Heavily Reinforced Wall
 Fig. 6.19 (contd.) Frequency Content of Measured Response



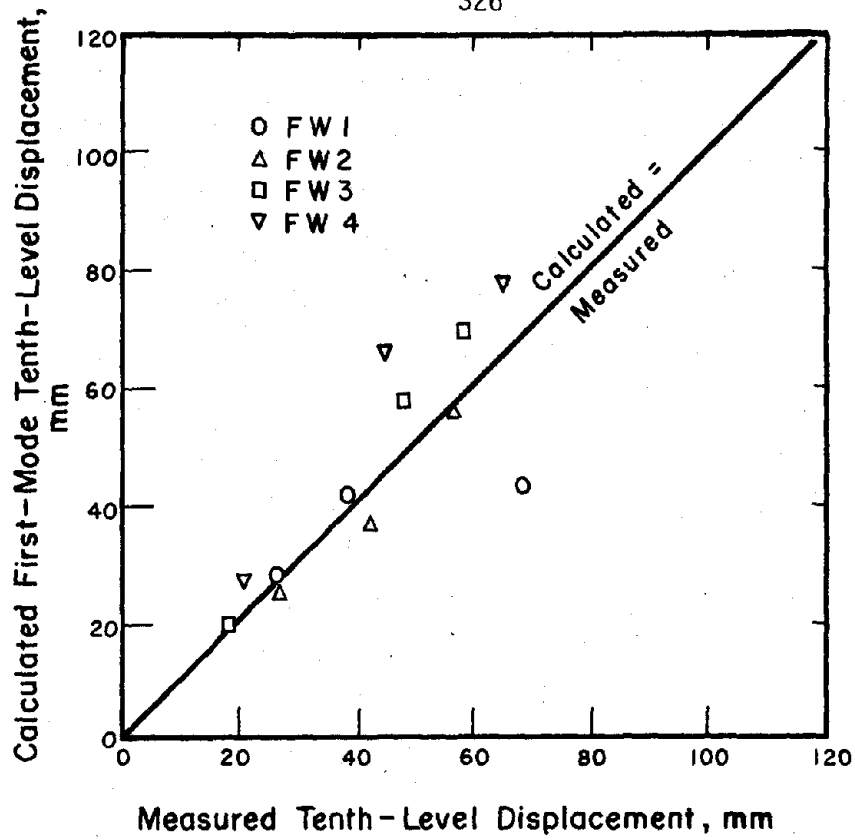
324

(j) Moments Resisted by Lightly Reinforced Wall

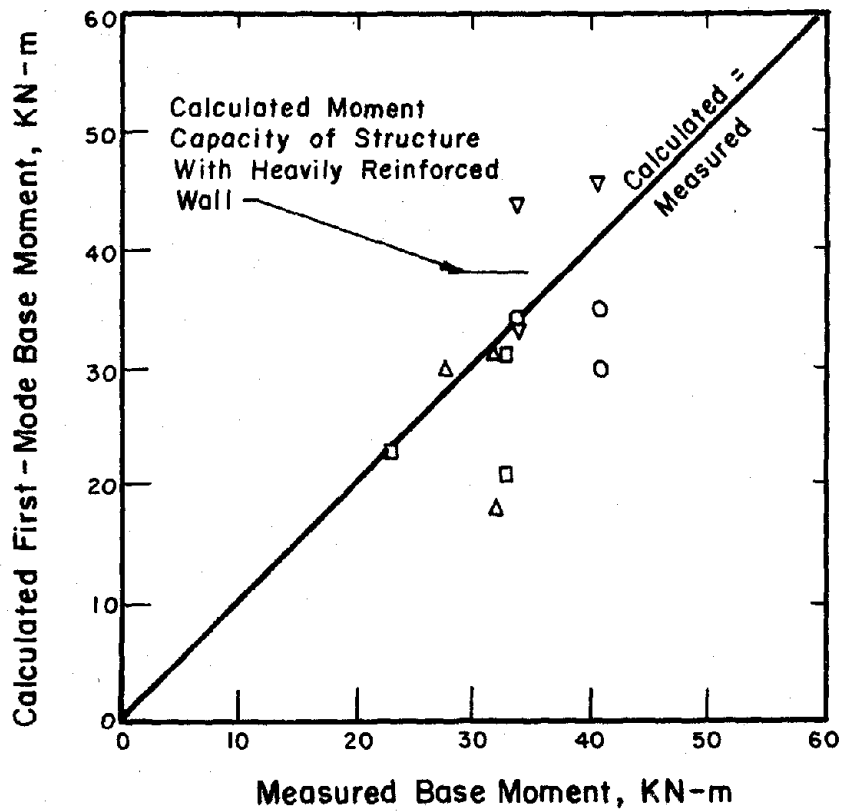
Fig. 6.19 (contd.) Frequency Content of Measured Response



(j) (contd.) Moments Resisted by Lightly Reinforced Wall
 Fig. 6.19 (contd.) Frequency Content of Measured Response

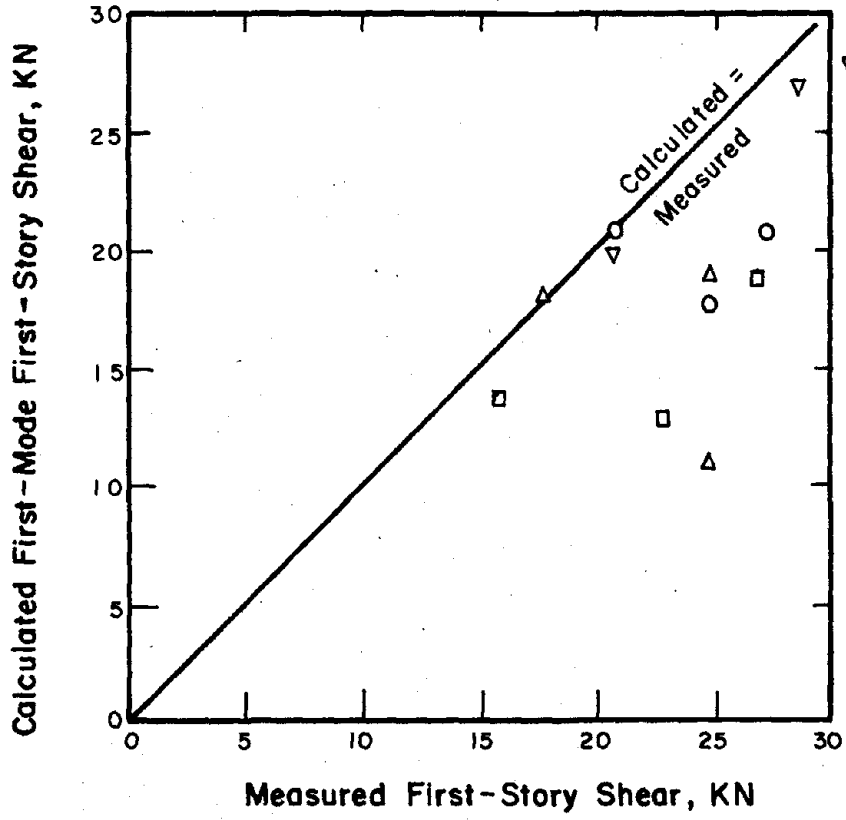


(a) Displacements

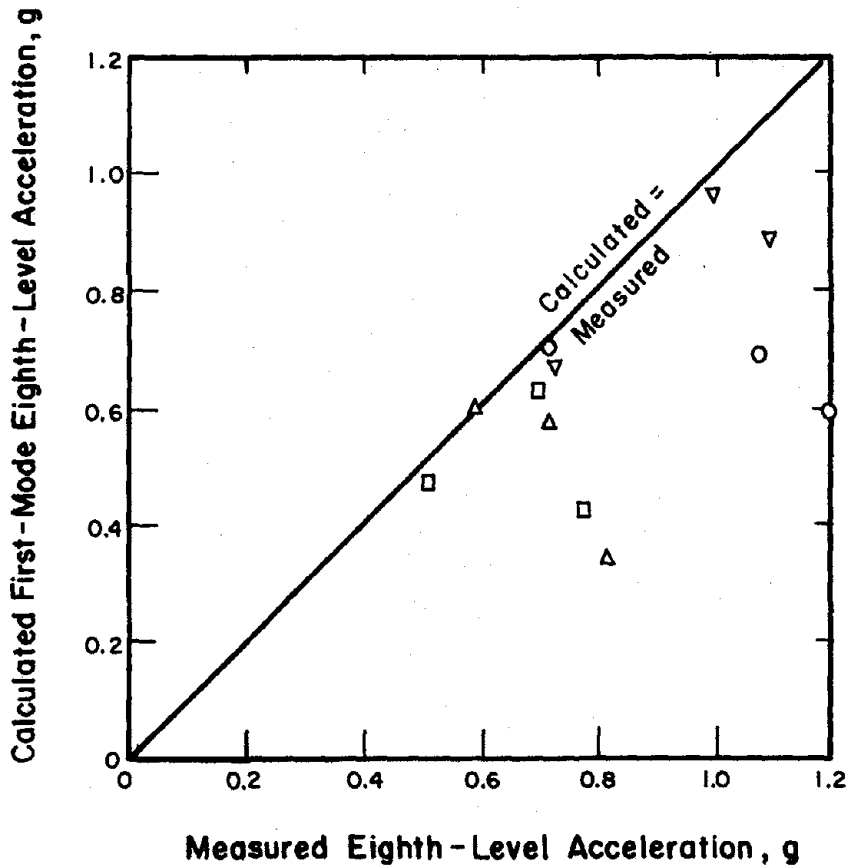


(b) Base Moments

Fig. 6.20 Comparison of Measured and Calculated Response Maxima

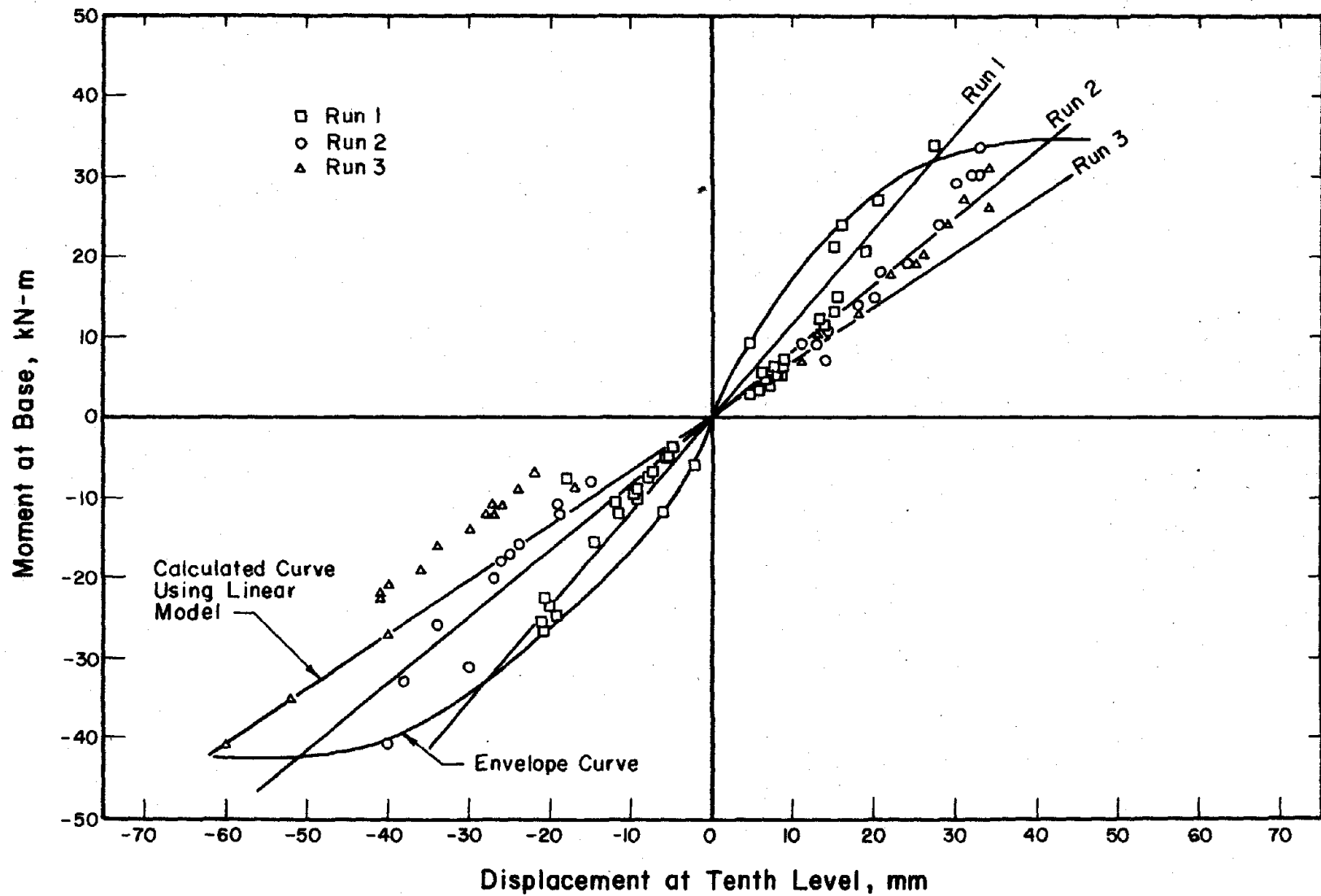


(c) First-Story Shears



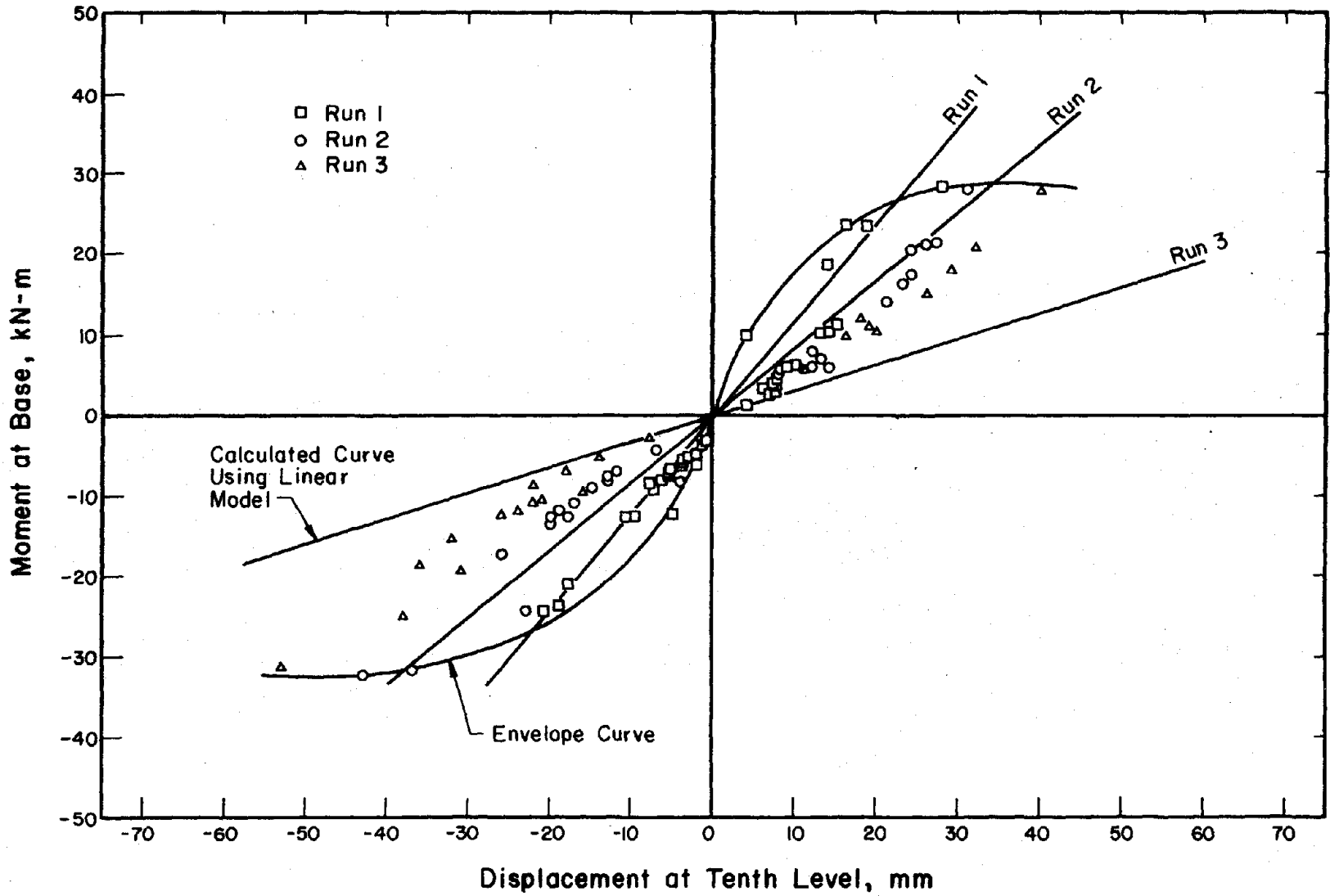
(d) Eighth-Level Accelerations

Fig. 6.20 (contd.) Comparison of Measured and Calculated Response Maxima



(a) Test Structure FW1

Fig. 6.21 Measured and Calculated Variations in Base Moment with Tenth-Level Displacement



(b) Test Structure FW2

Fig. 6.21 (contd.) Measured and Calculated Variations in Base Moment with Tenth-Level Displacement

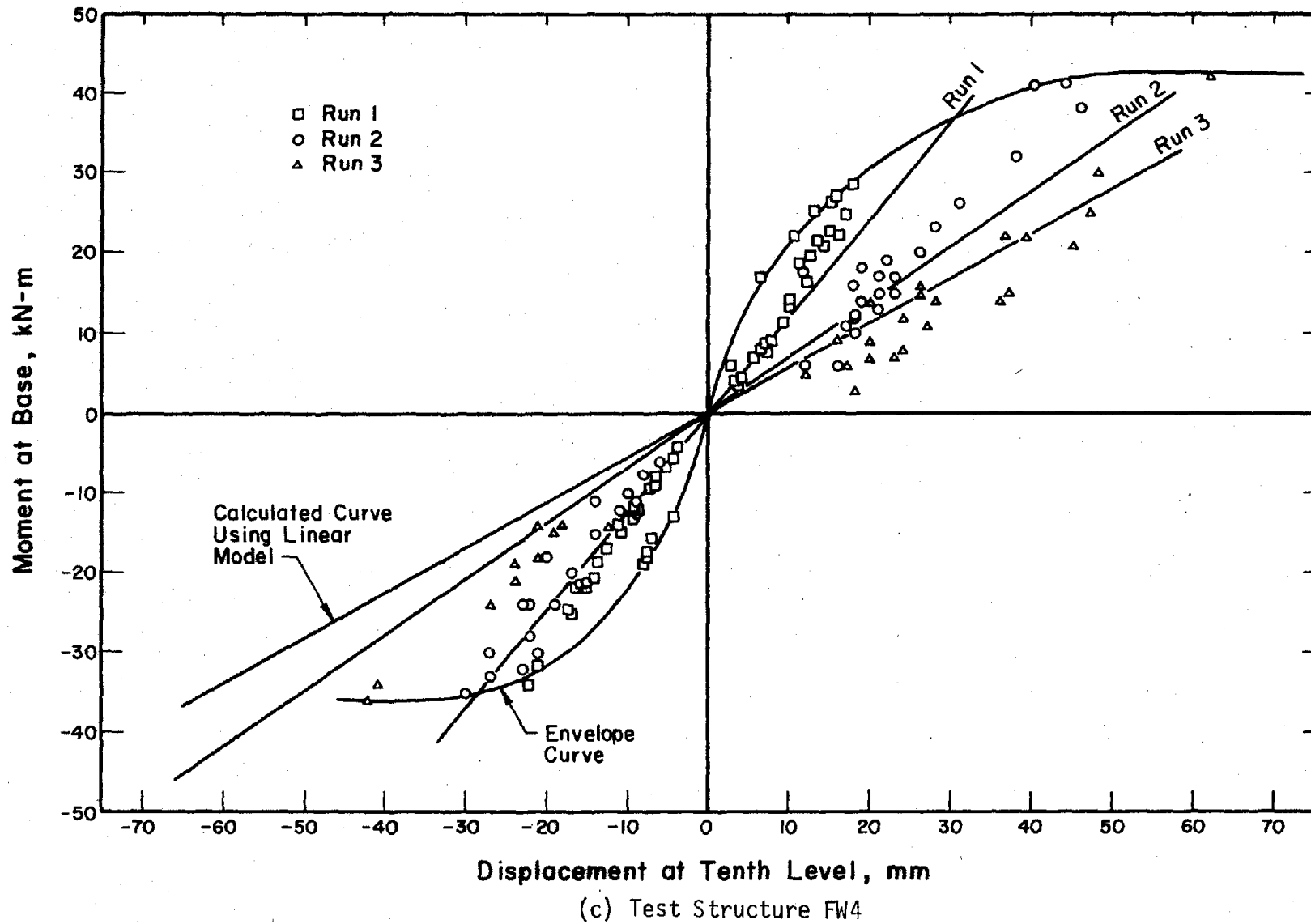
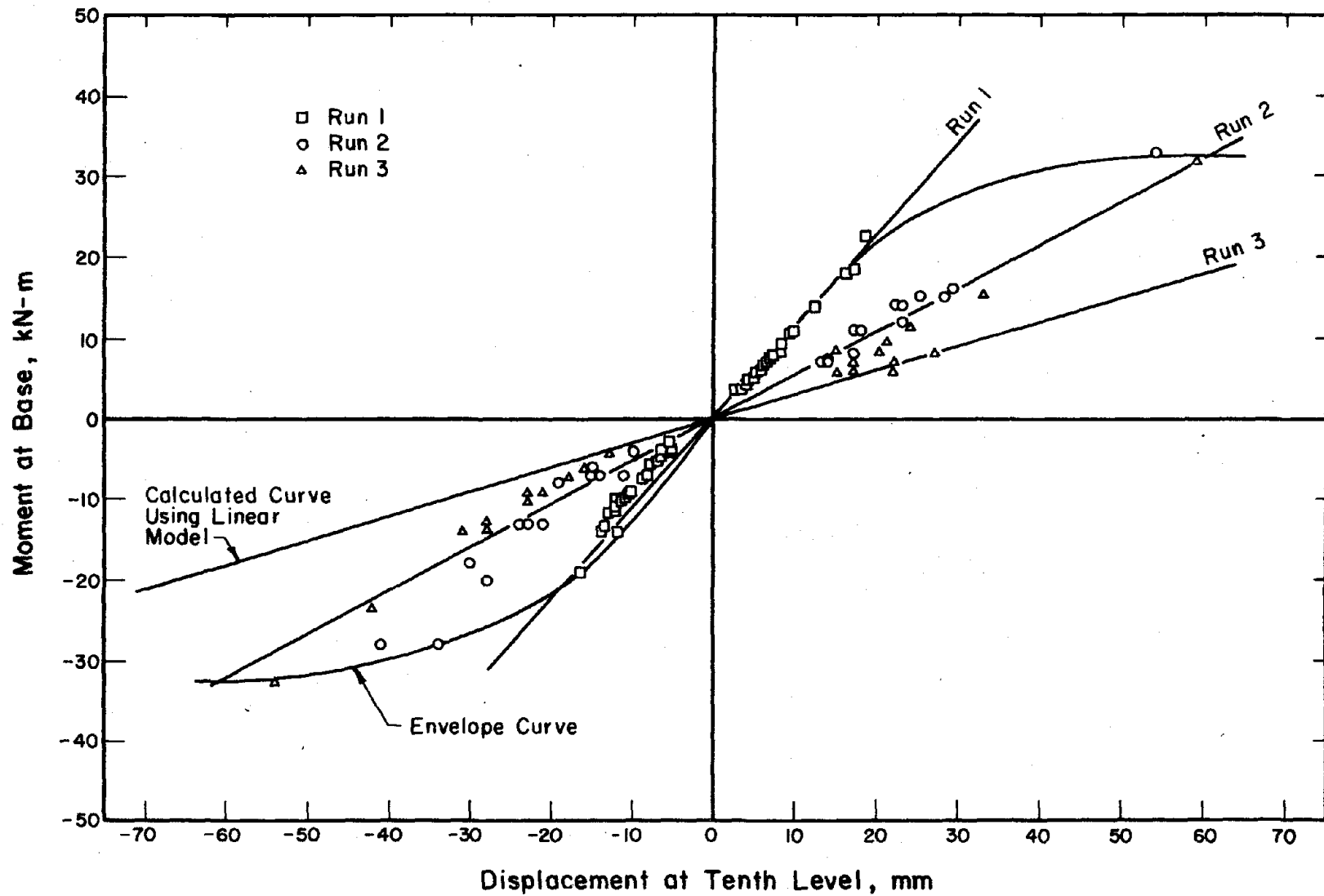
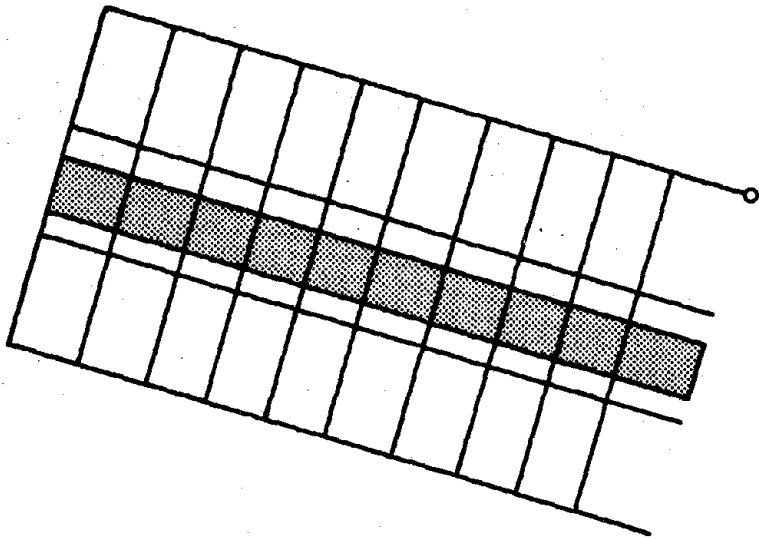


Fig. 6.21 (contd.) Measured and Calculated Variations in Base Moment with Tenth-Level Displacement

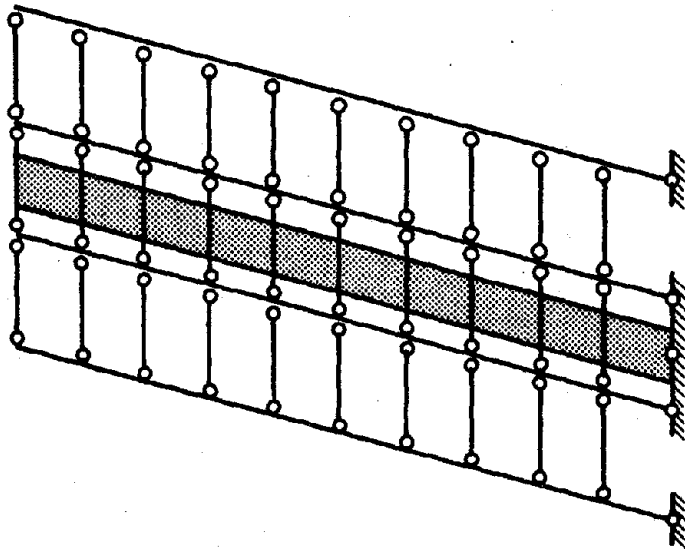


(d) Test Structure FW3

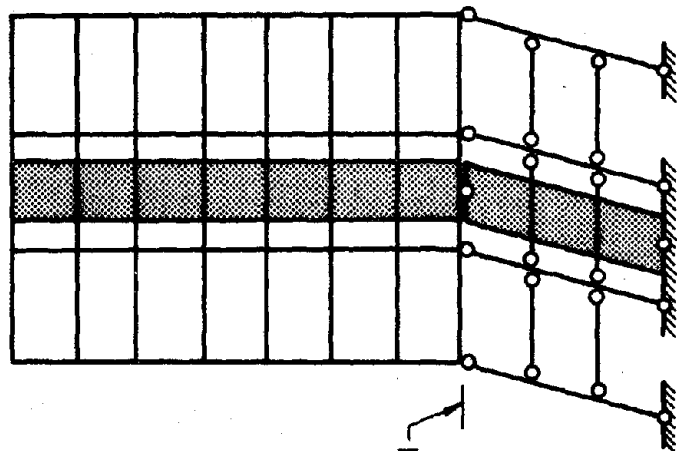
Fig. 6.21 (contd.) Measured and Calculated Variations in Base Moment with Tenth-Level Displacement



(c)



(b)



(a)

Any Level

Fig. 7.1 Possible Collapse Mechanisms

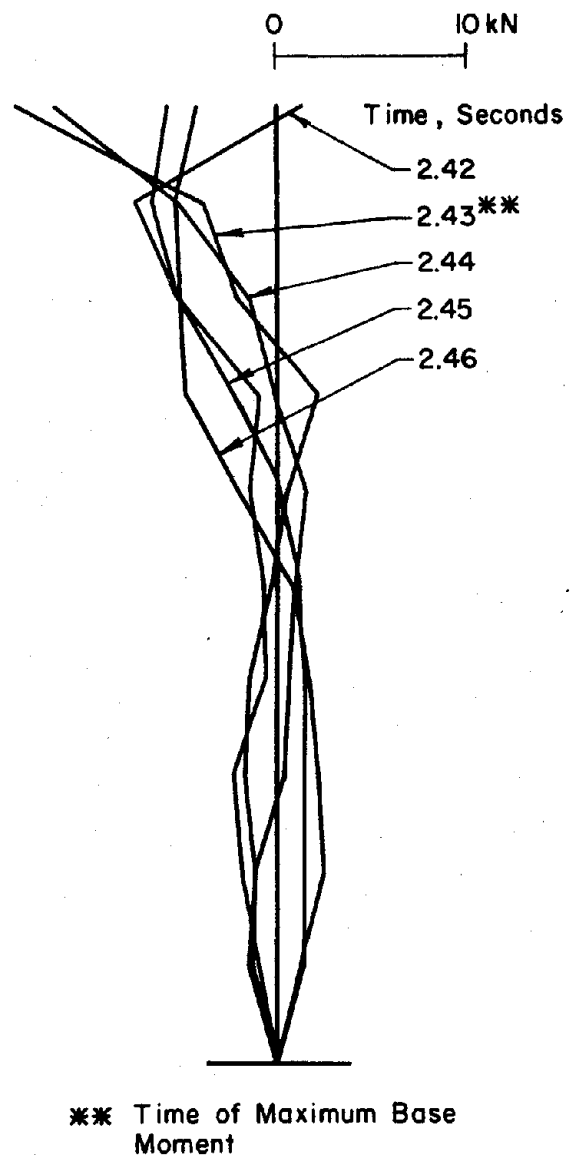
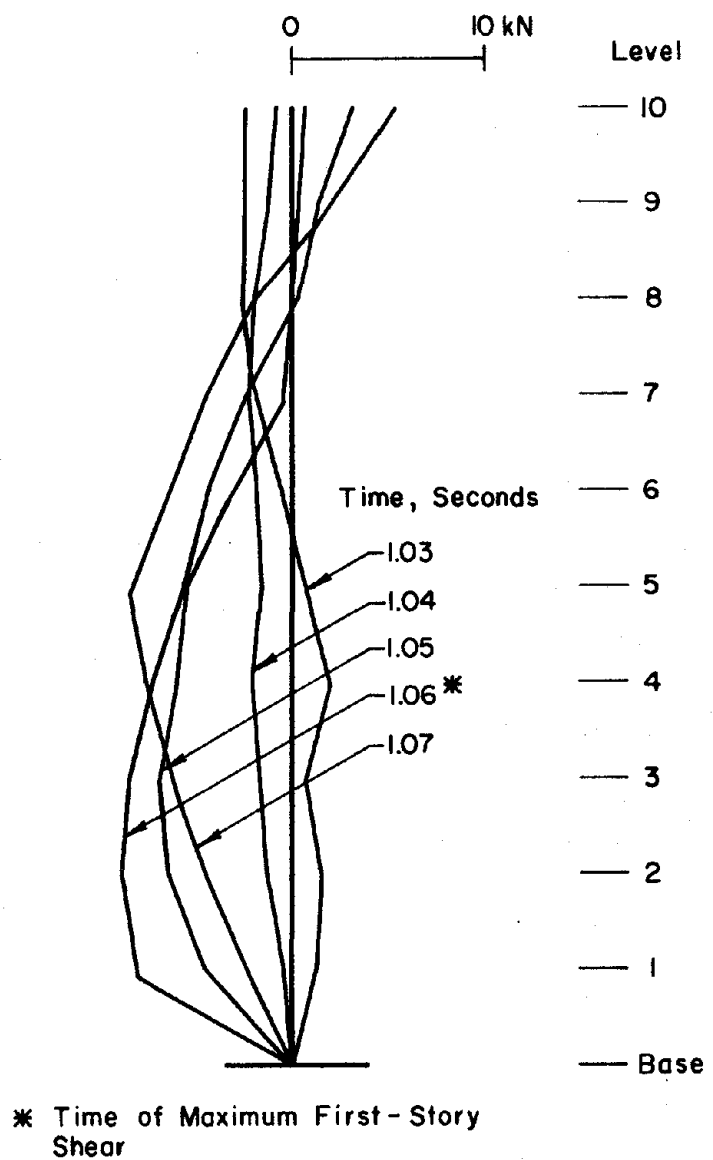
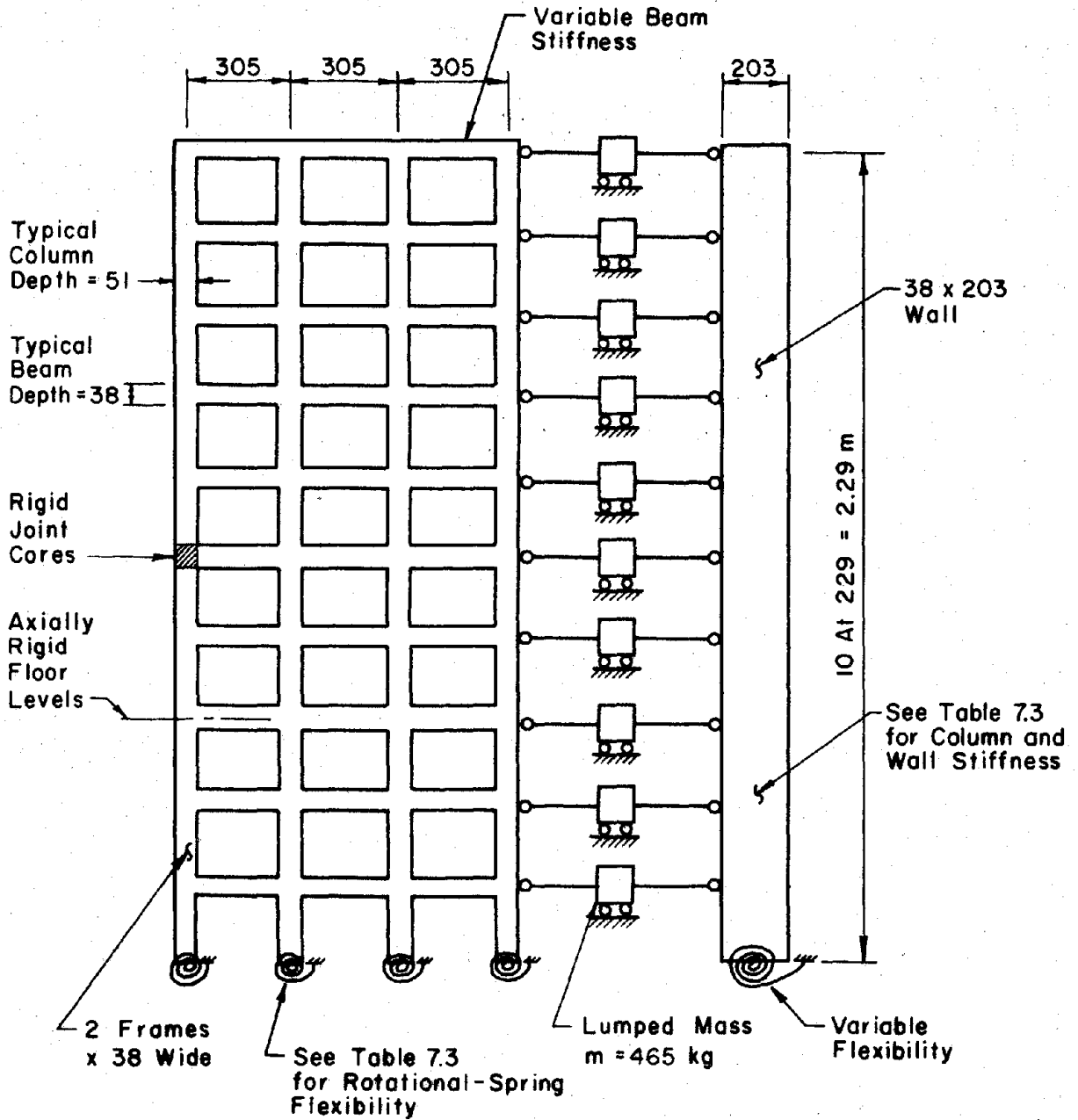
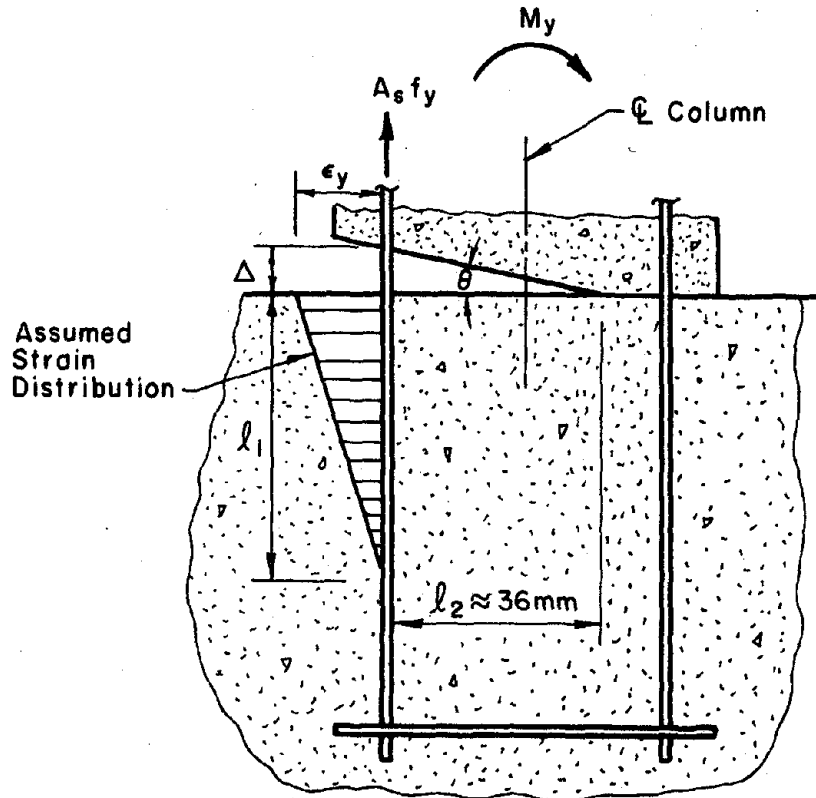


Fig. 7.2 Measured Inertial Forces



(All Dimensions In Millimeters Unless Noted)

Fig. 7.3 Description of Analytical Model



$$\text{Flexibility of Spring} = \frac{\theta}{M_y} ; \theta = \Delta/l_2$$

$$\Delta = \frac{1}{2} \epsilon_y l_1$$

$$l_1 = \frac{A_s f_y}{u_b \pi d_b} = \frac{d_b f_y}{4u_b}$$

where f_y = Yield Stress = 350 MPa

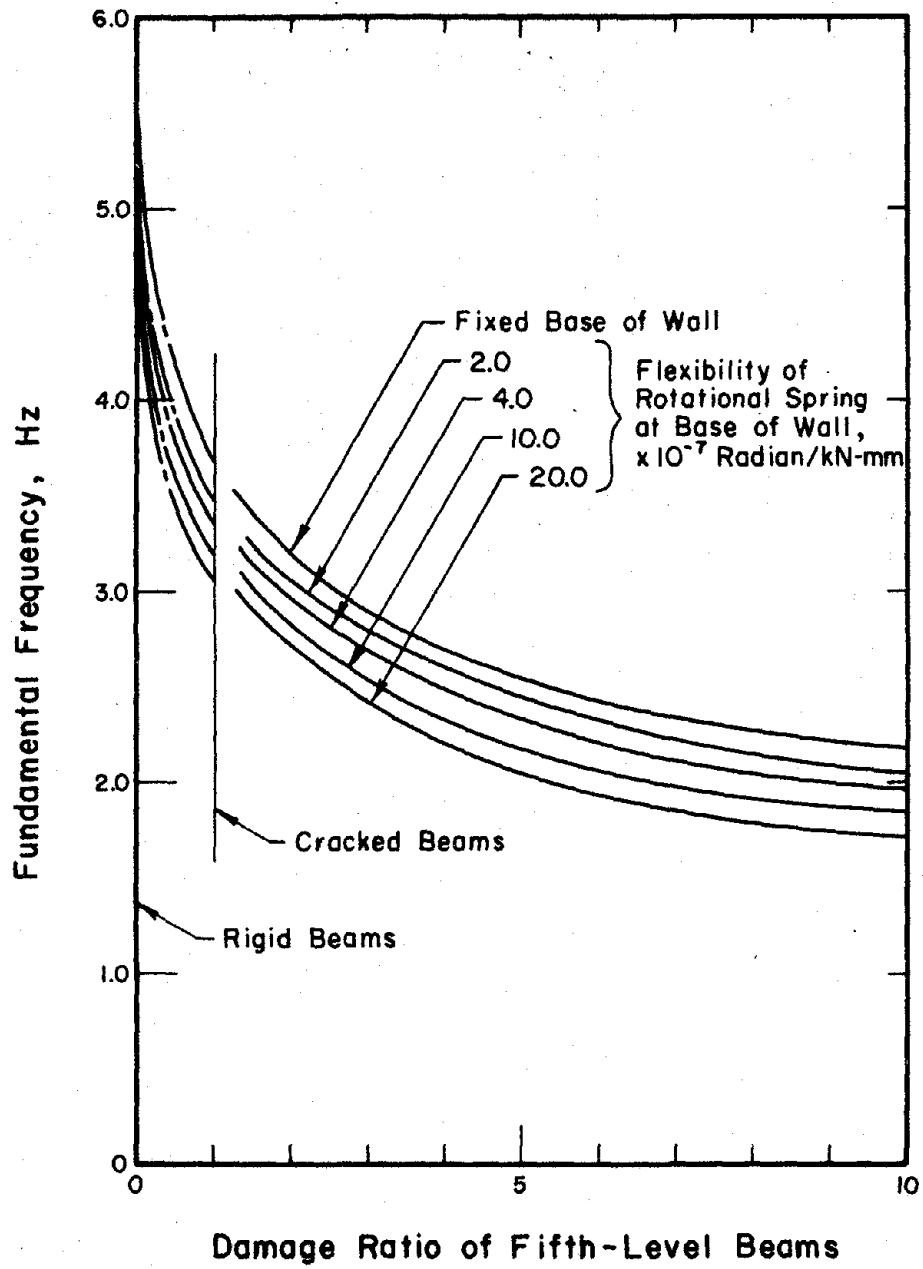
ϵ_y = Yield Strain = 0.002

u_b = Bond Stress = 2.8 MPa

d_b = Diameter of Bar = 2.3 mm

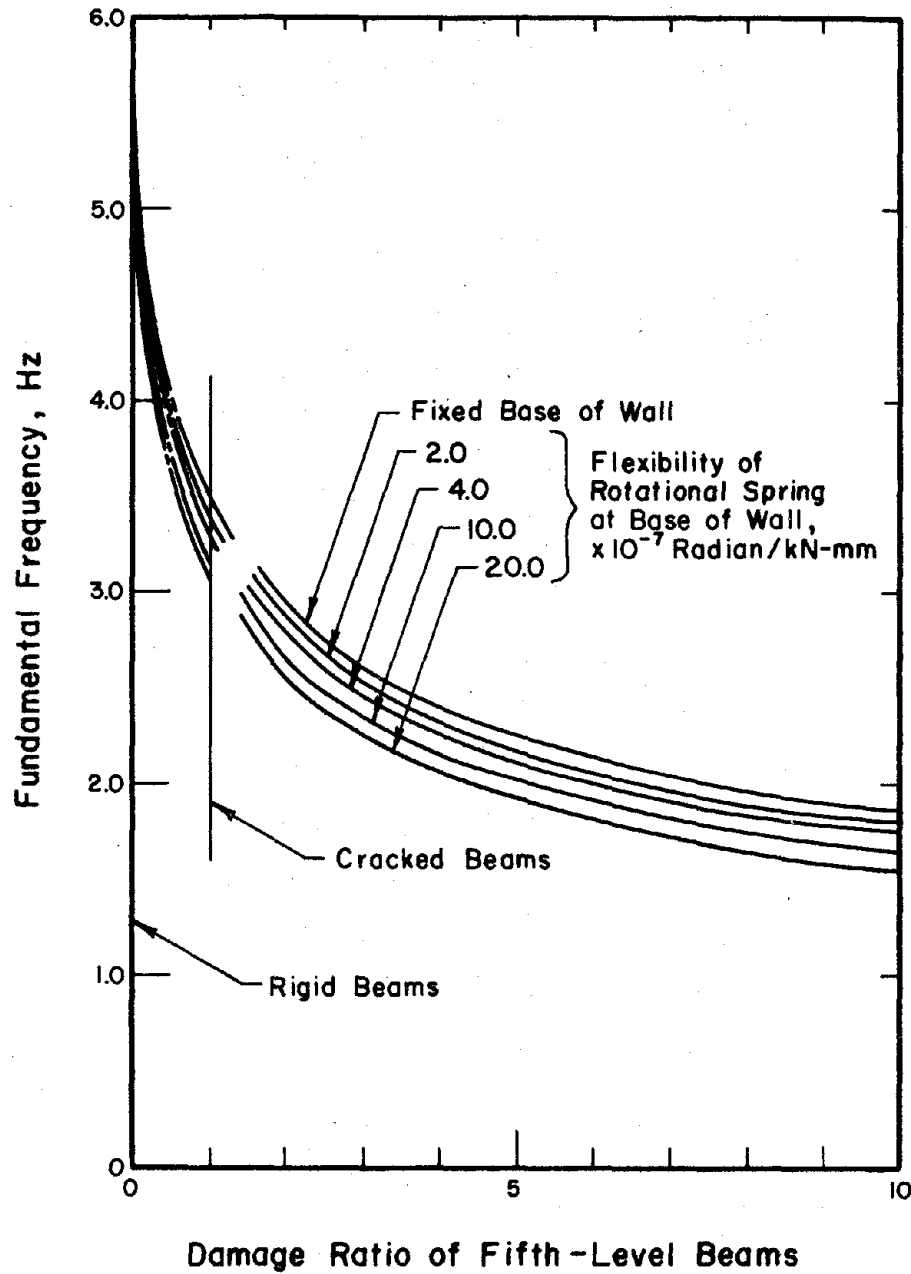
$$\text{Flexibility of Spring} = \frac{\epsilon_y d_b f_y}{8u_b l_2 M_y} = \frac{0.0020}{M_y}$$

Fig. 7.4 Calculation of Spring Flexibility at Base of Columns



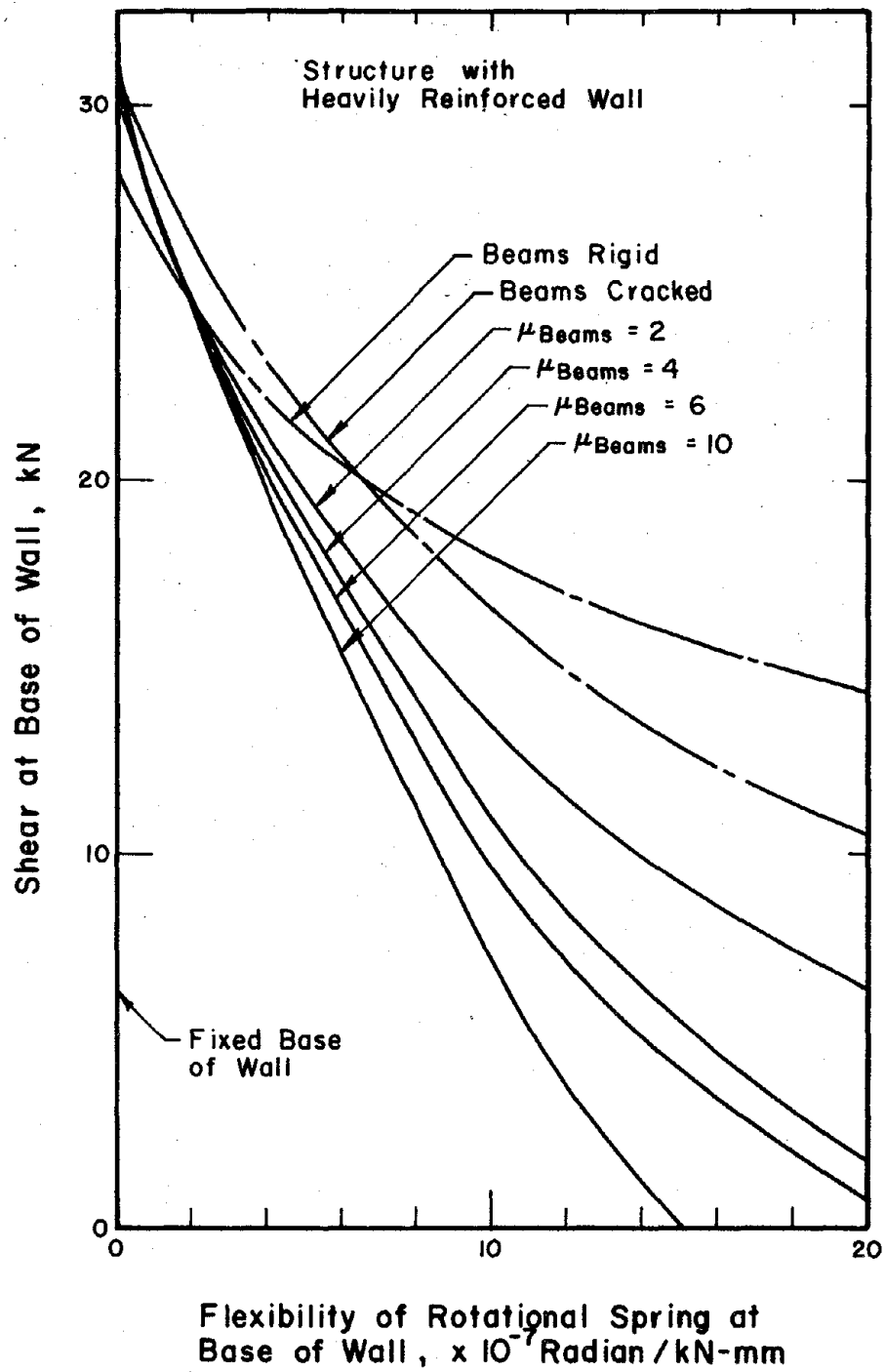
(a) Structure with Heavily Reinforced Wall

Fig. 7.5 Calculated Fundamental Frequencies.



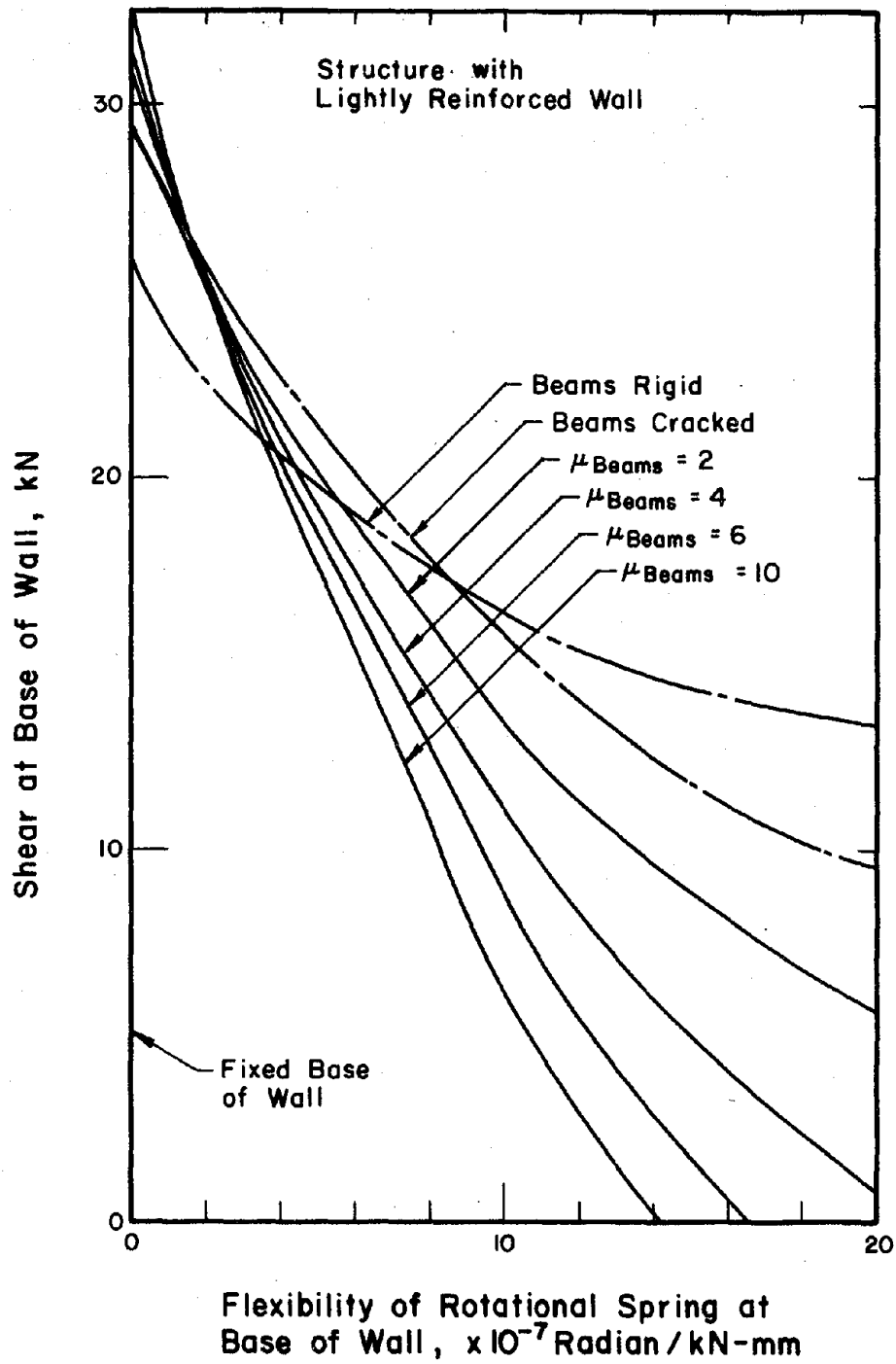
(b) Structure with Lightly Reinforced Wall

Fig. 7.5 (contd.) Calculated Fundamental Frequencies



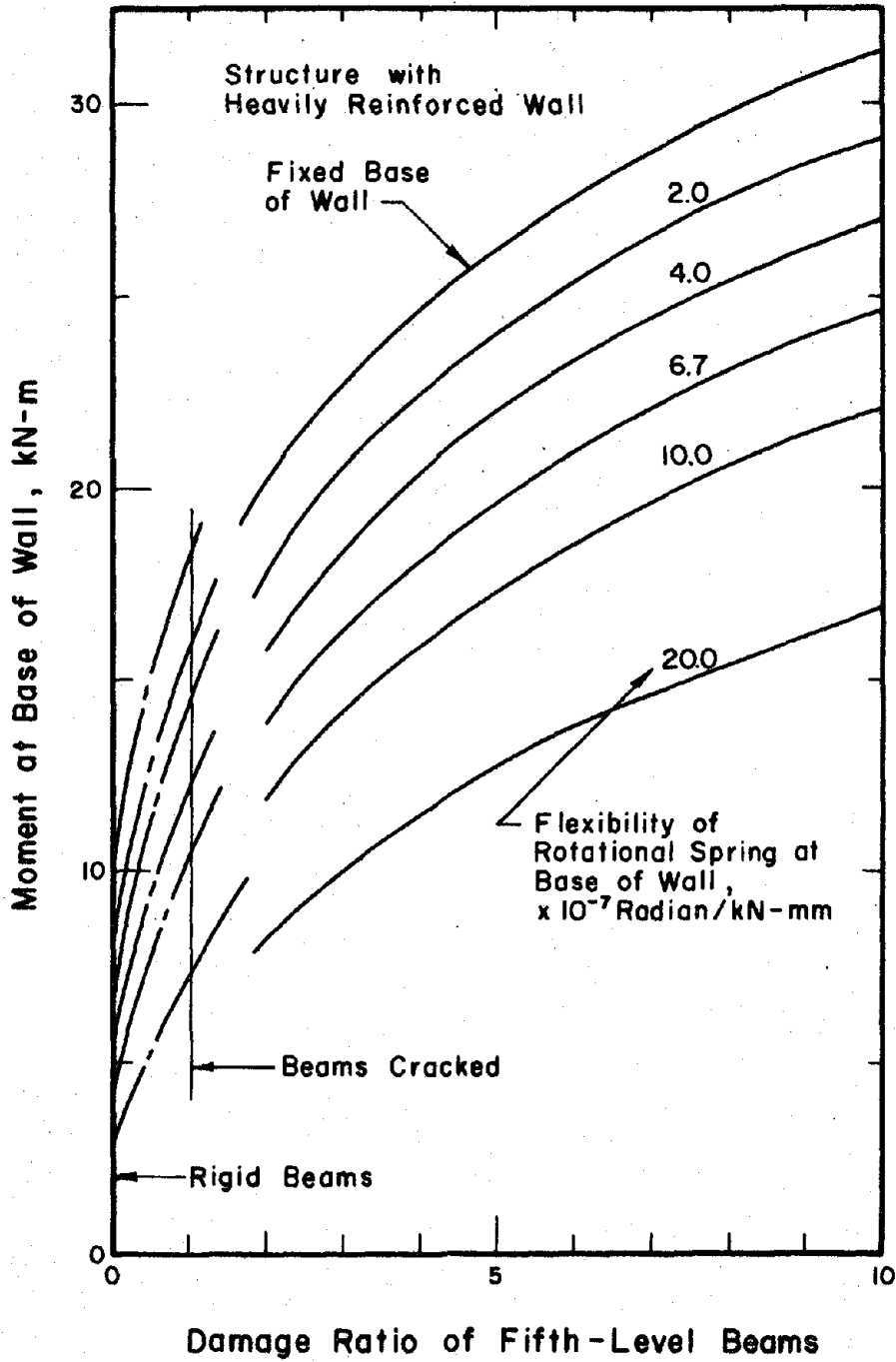
(a) Shear at Base of Wall

Fig. 7.6 Calculated First-Mode Response



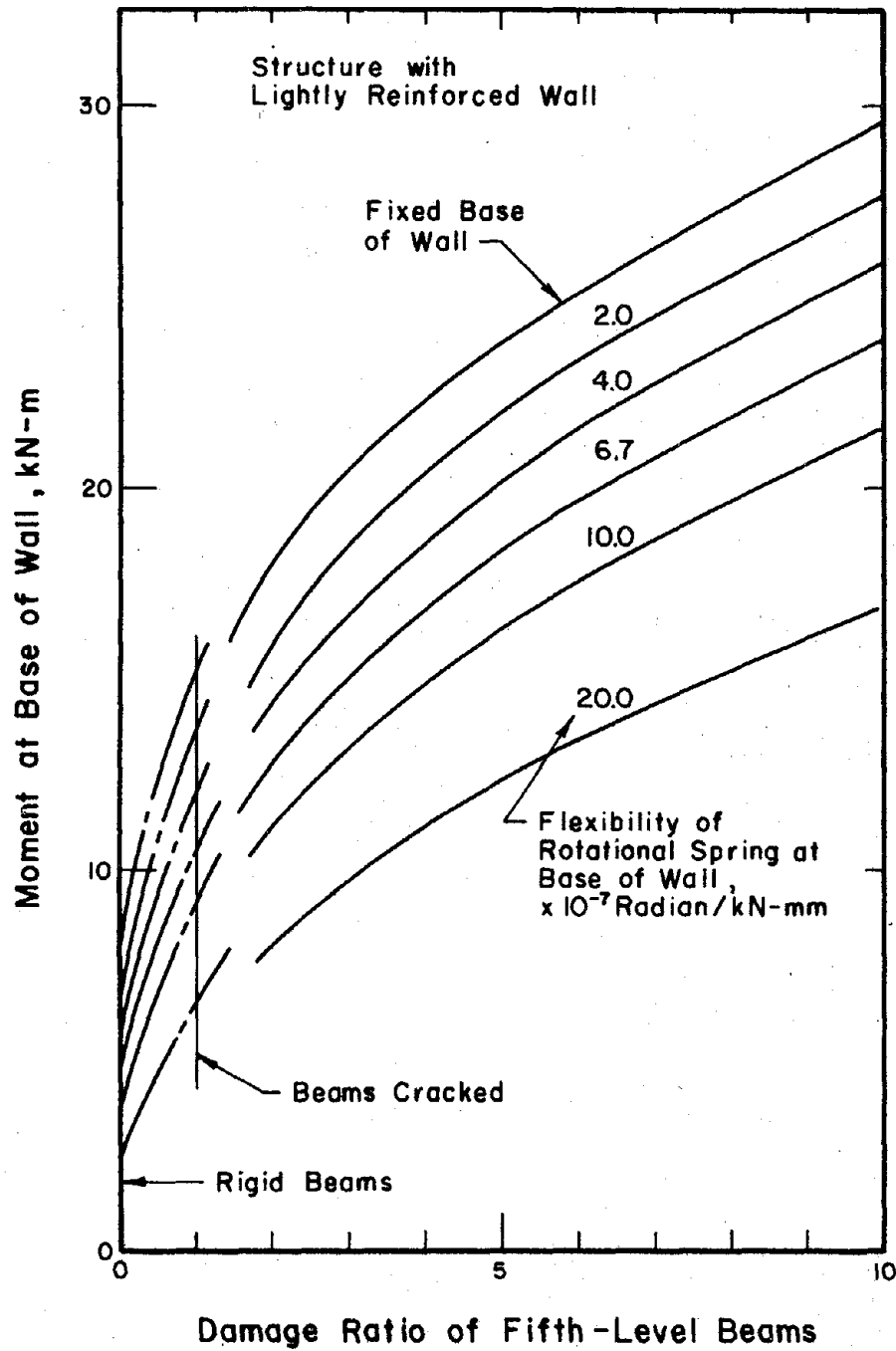
(a) (contd.) Shear at Base of Wall

Fig. 7.6 (contd.) Calculated First-Mode Response



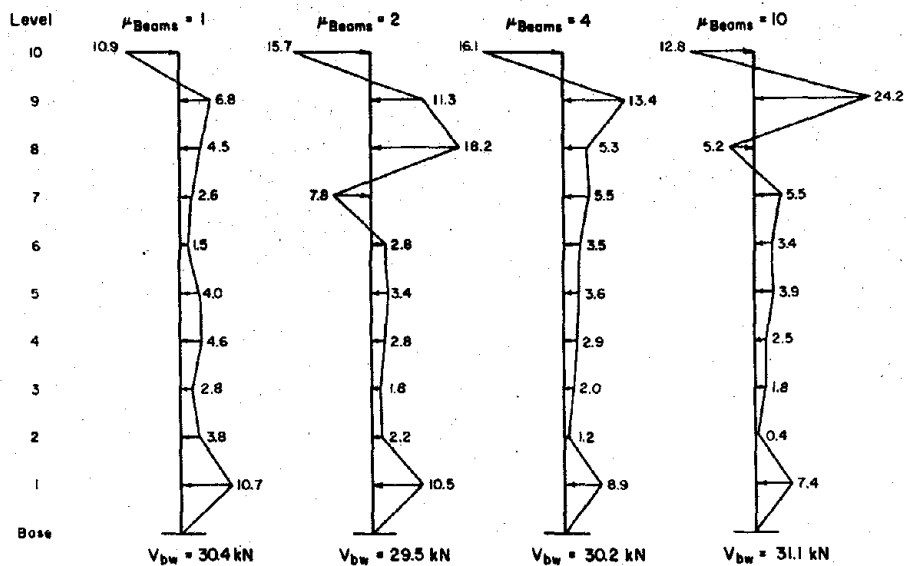
(b) Moment at Base of Wall

Fig. 7.6 (contd.) Calculated First-Mode Response

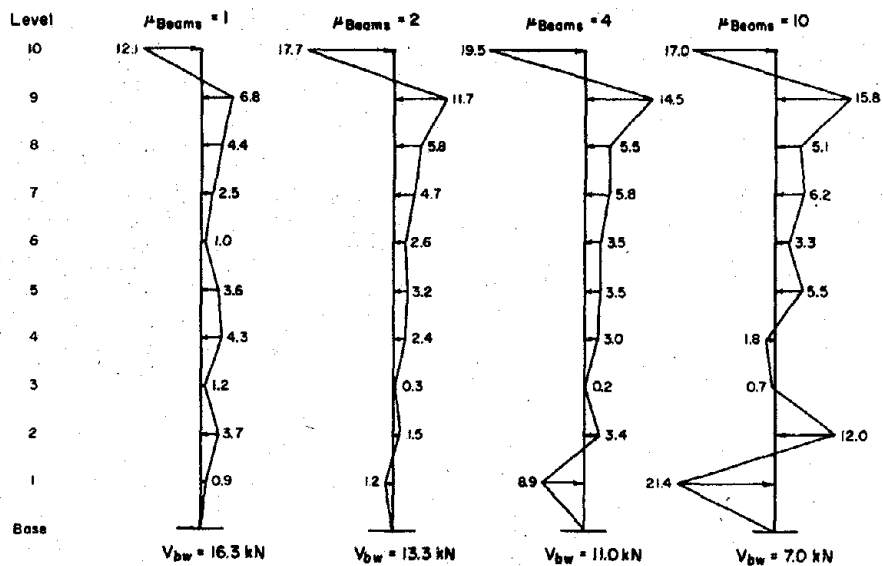


(b) (contd.) Moment at Base of Wall

Fig. 7.6 (contd.) Calculated First-Mode Response

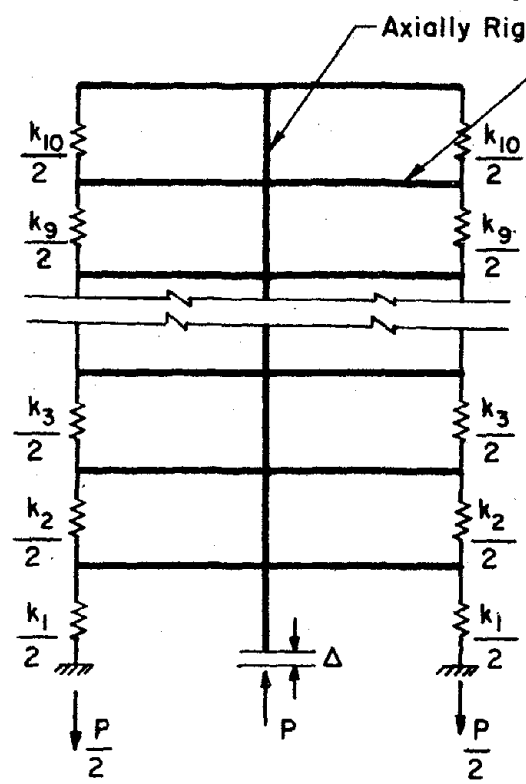


(a) Wall Fixed at Base



(b) Flexibility of Spring at Base of Wall = 10×10^{-7} Radian/KN-mm

Fig. 7.7 Calculated Force Distributions on Wall.



$k_1, k_2, k_3, \dots, k_{10}$ = Axial Stiffness of Columns in Tension

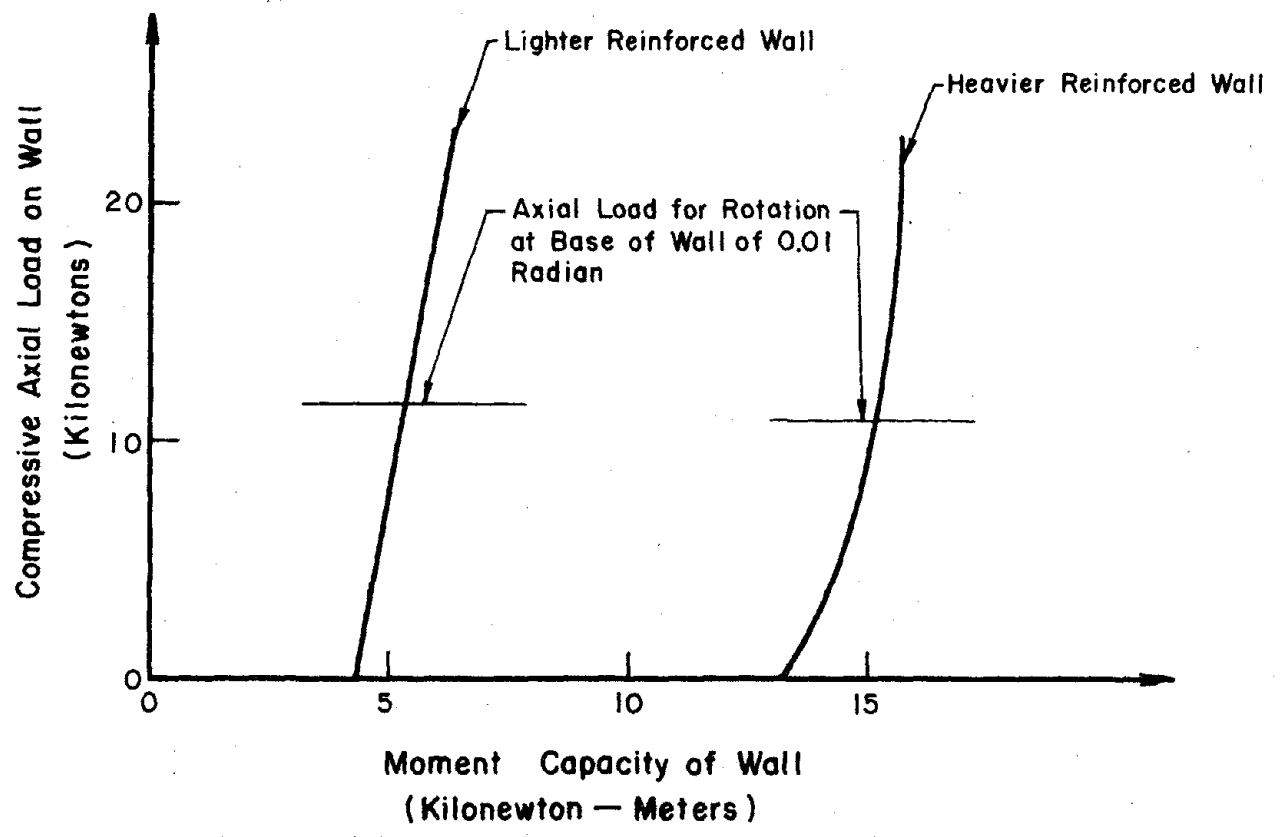
$$\Delta = \frac{W}{2} \tan \theta$$

Where W = Width of Wall
 θ = Rotation at Base of Wall

$$P = k_e \Delta$$

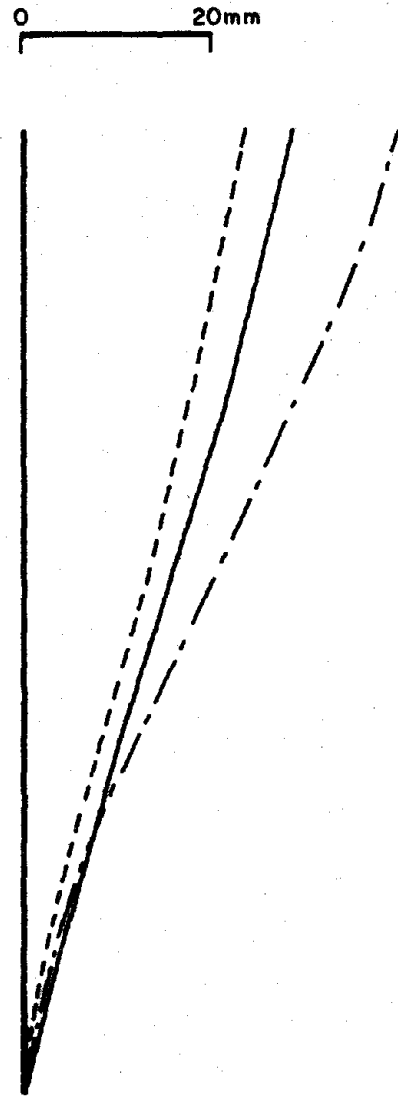
$$\frac{1}{k_e} = \frac{1}{k_1} + \frac{1}{k_2} + \dots + \frac{1}{k_{10}}$$

(a) Analytical Model

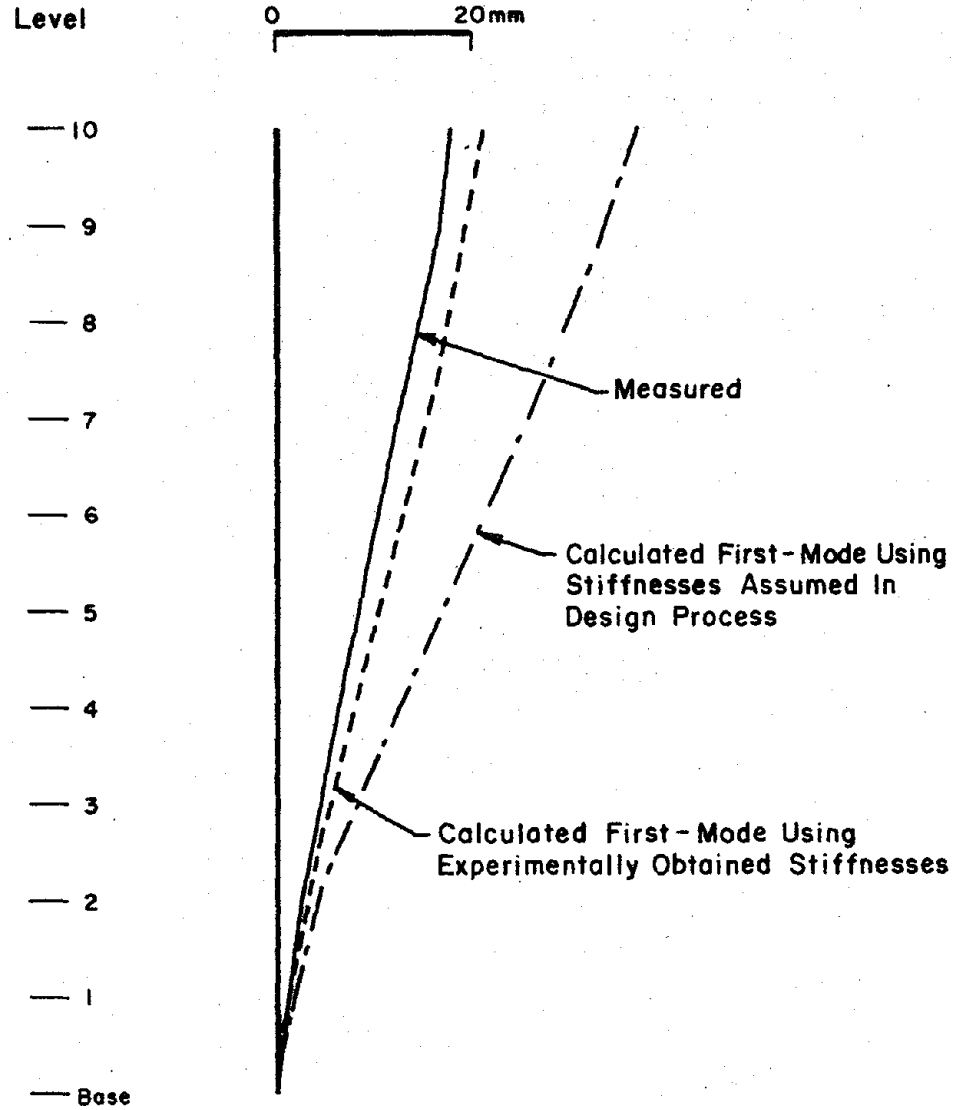


(b) Wall Interaction Diagram

Fig. 7.8 Increase in Moment Capacity of Wall with Axial Load

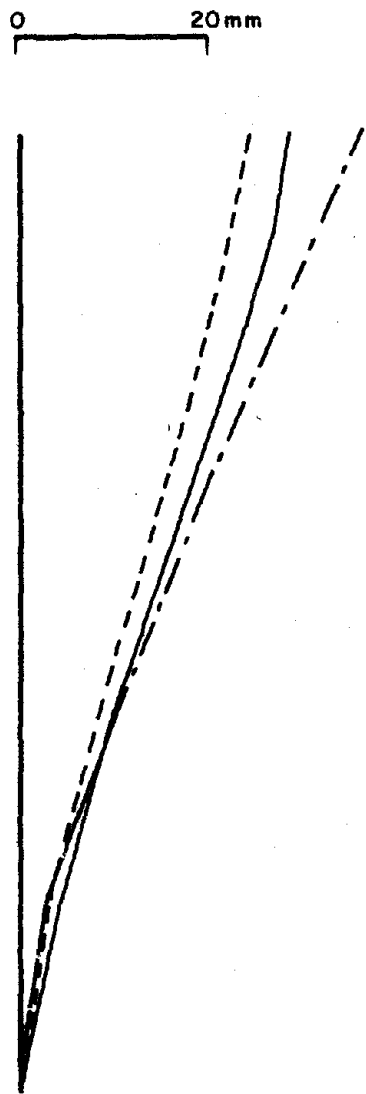


(a) Test Structure FW1

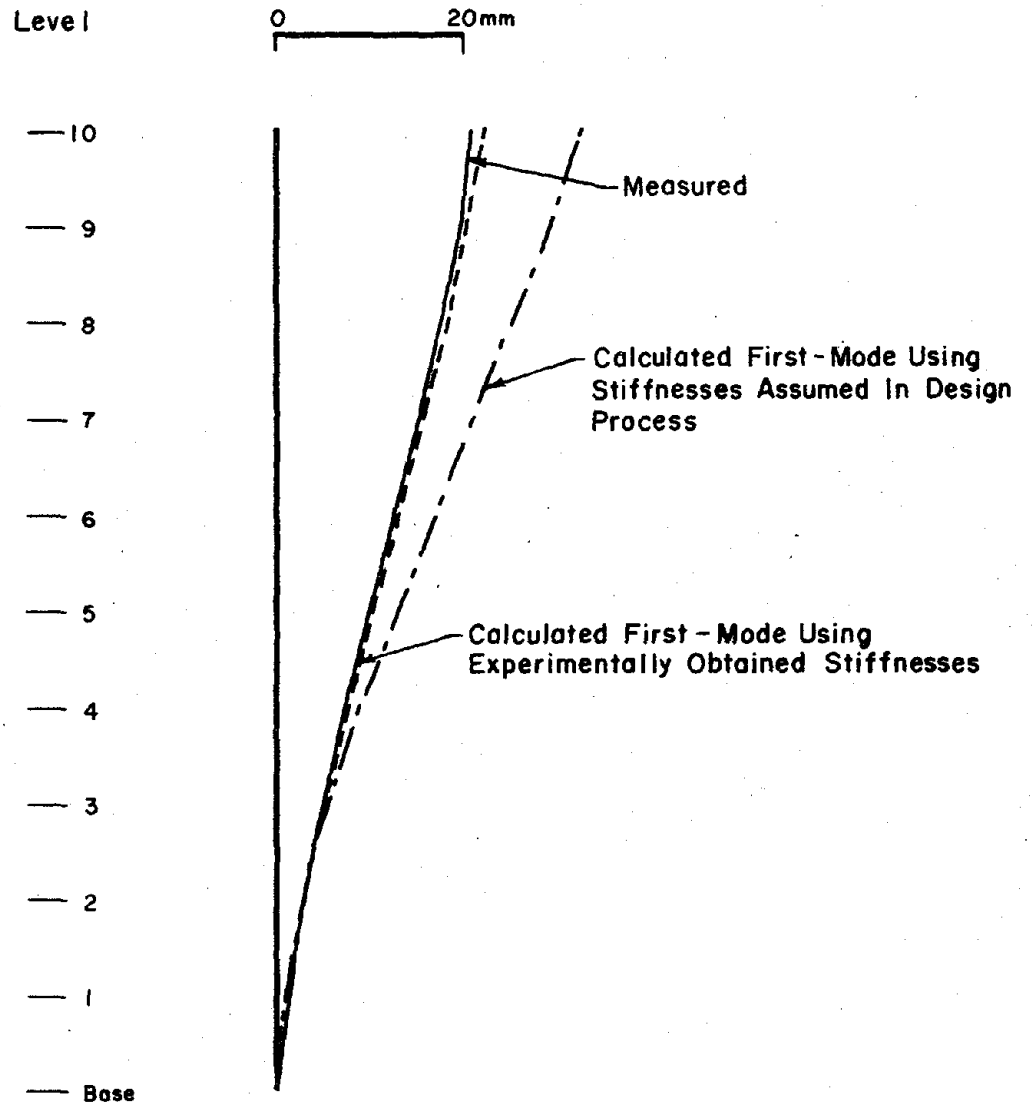


(b) Test Structure FW4

Fig. 7.9 Comparison of Measurements with Calculated Displacements



(c) Test Structure FW2



(d) Test Structure FW3

Fig. 7.9 (contd.) Comparison of Measurements with Calculated Displacements.

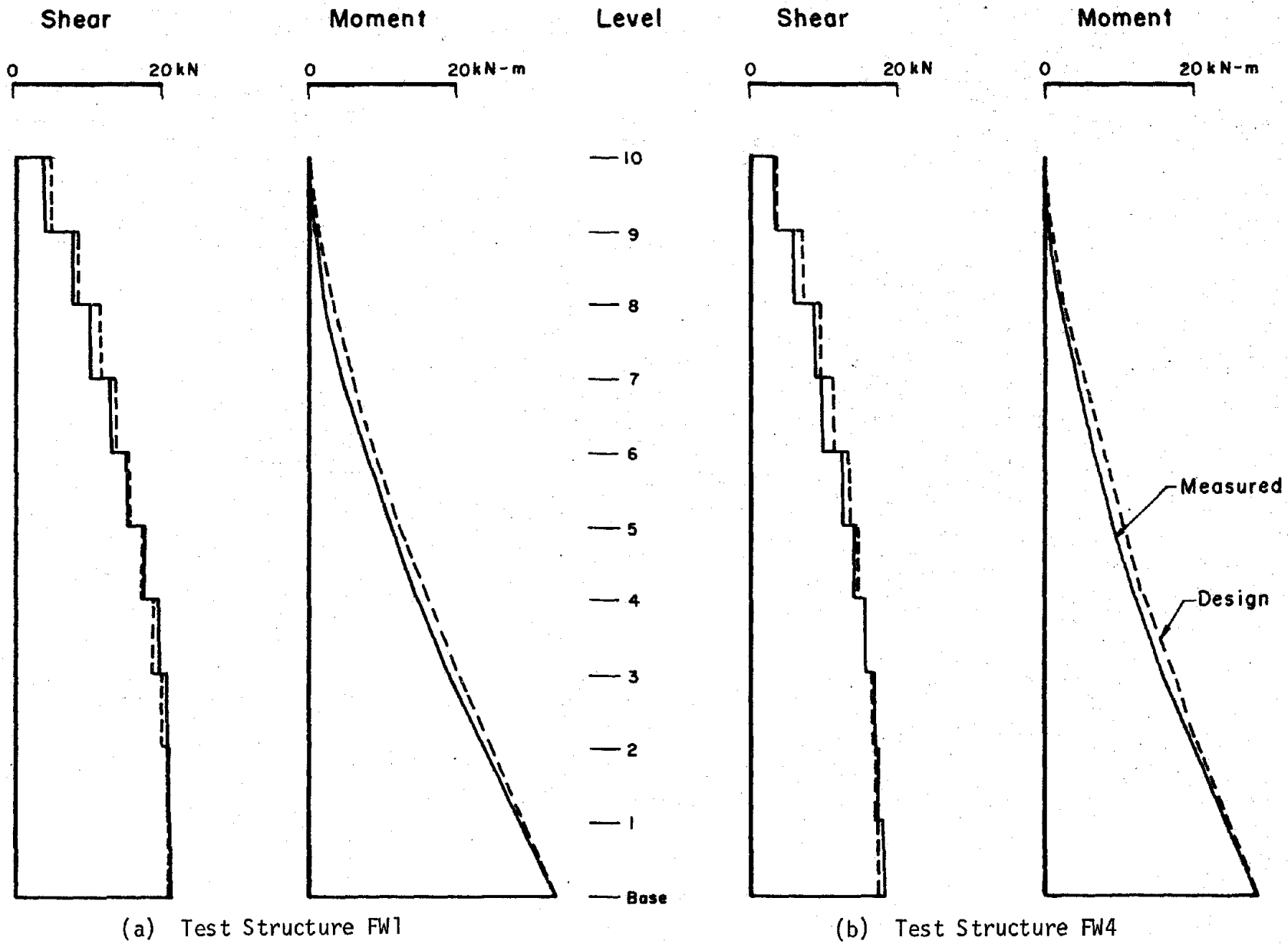
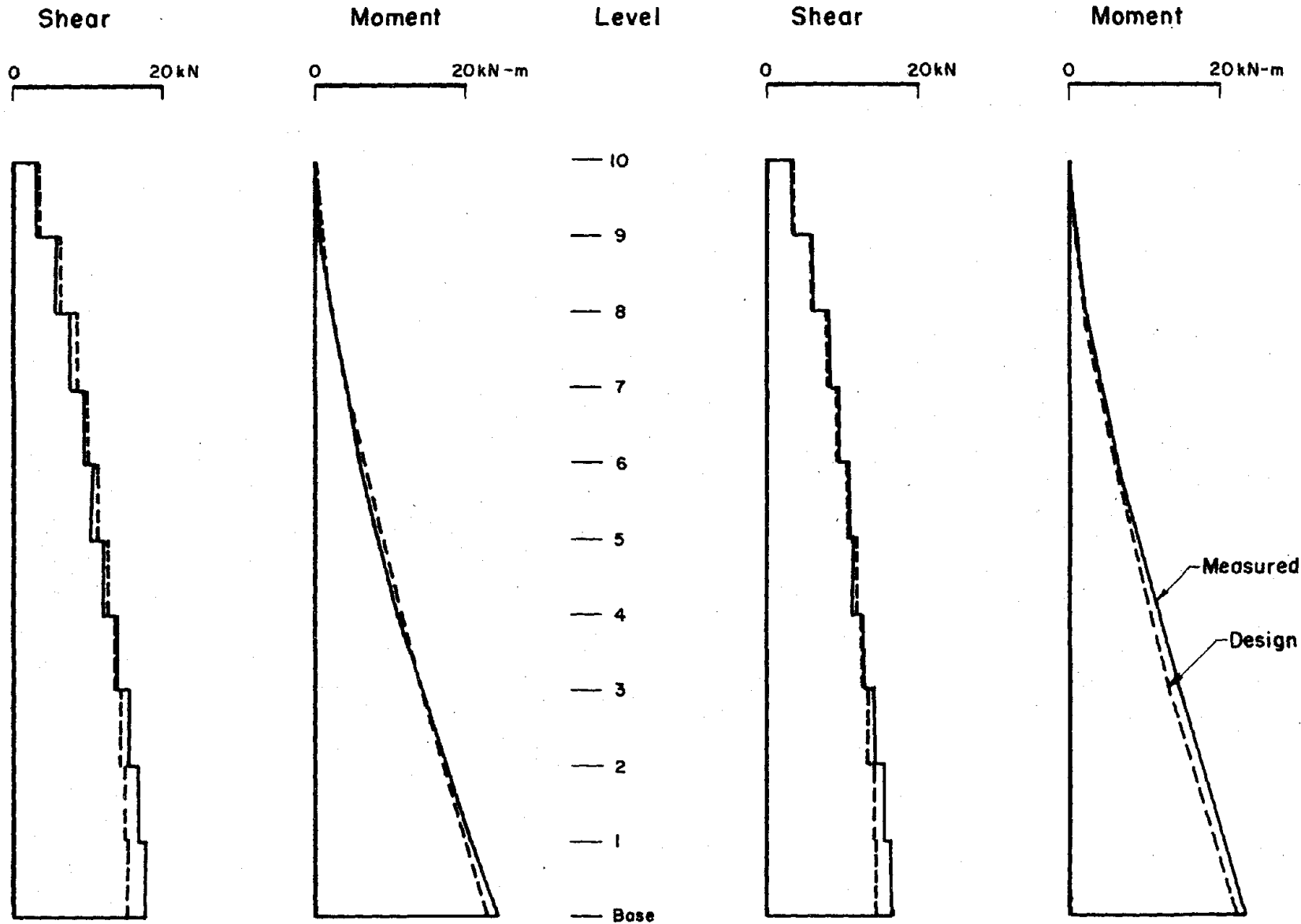


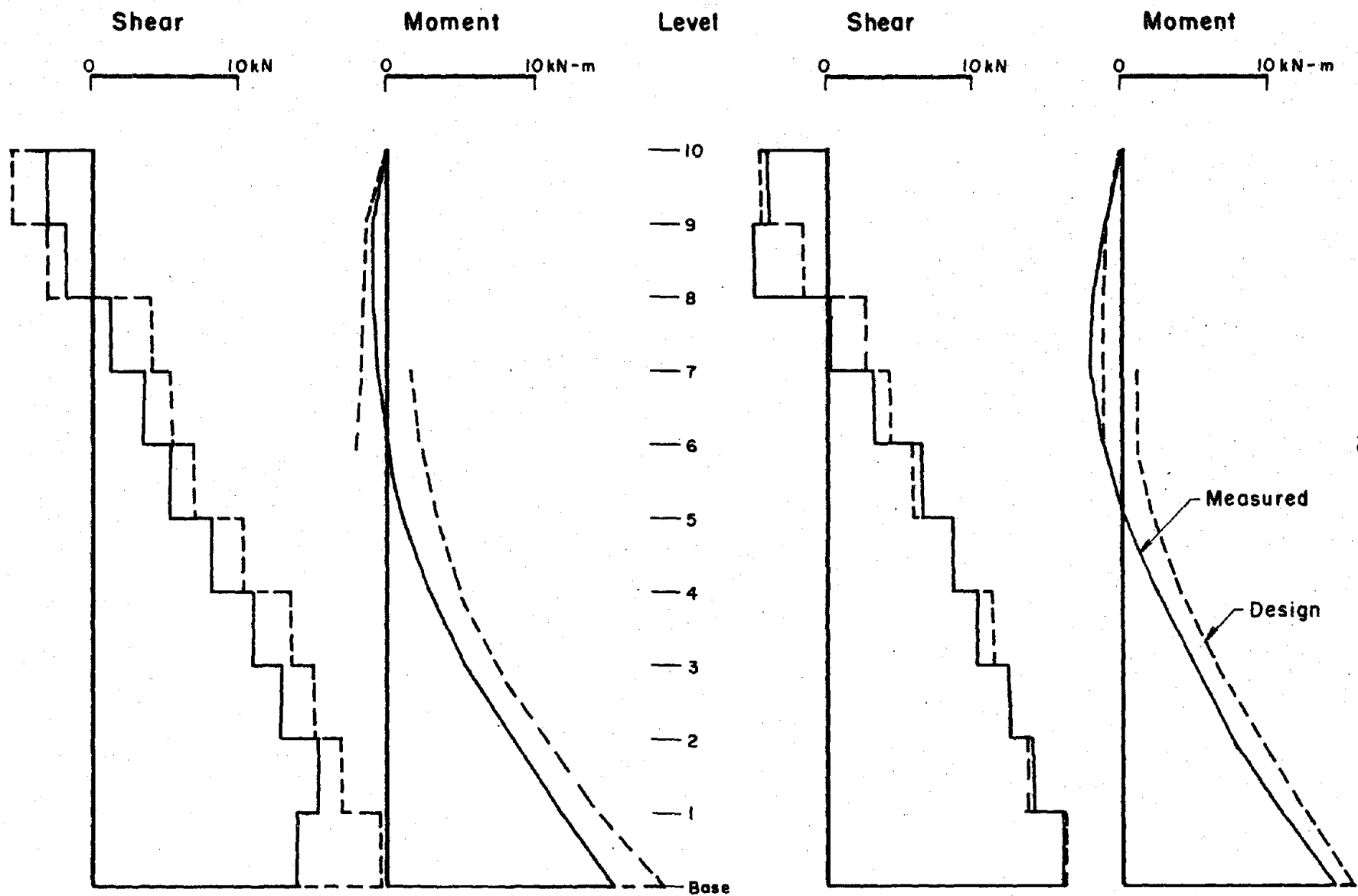
Fig. 7.10 Comparison of Measurements with Design Shears and Moments Resisted by Entire Structure



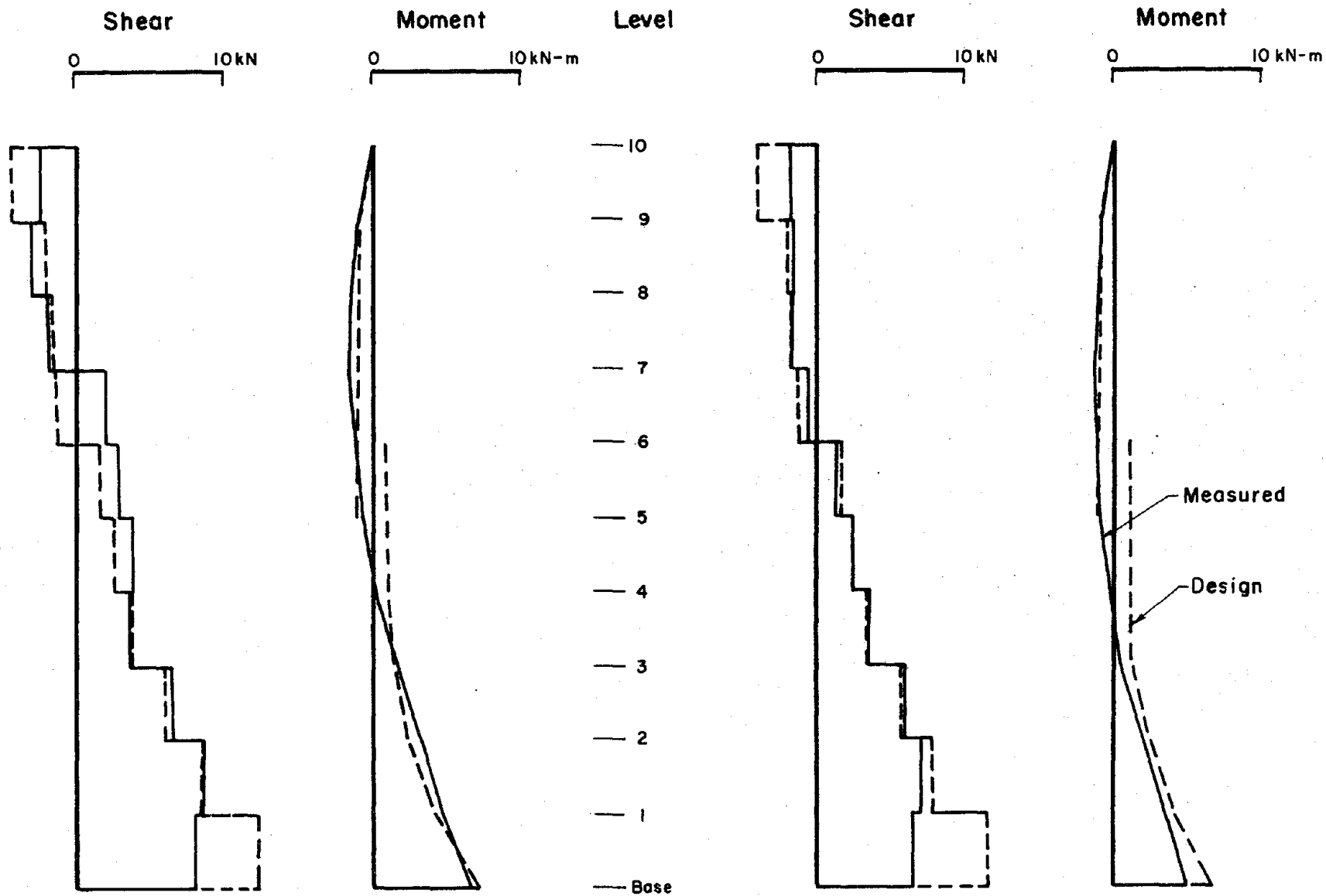
(c) Test Structure FW2

(d) Test Structure FW3

Fig. 7.10 (contd.) Comparison of Measurements with Design Shears and Moments Resisted by Entire Structure



(a) Test Structure FW1
 (b) Test Structure FW4
 Fig. 7.11 Comparison of Measurements with Design Shears and Moments Resisted by Wall.



(c) Test Structure FW2
 (d) Test Structure FW3
 Fig. 7.11 (contd.) Comparison of Measurements with Design Shears and Moments Resisted by Wall

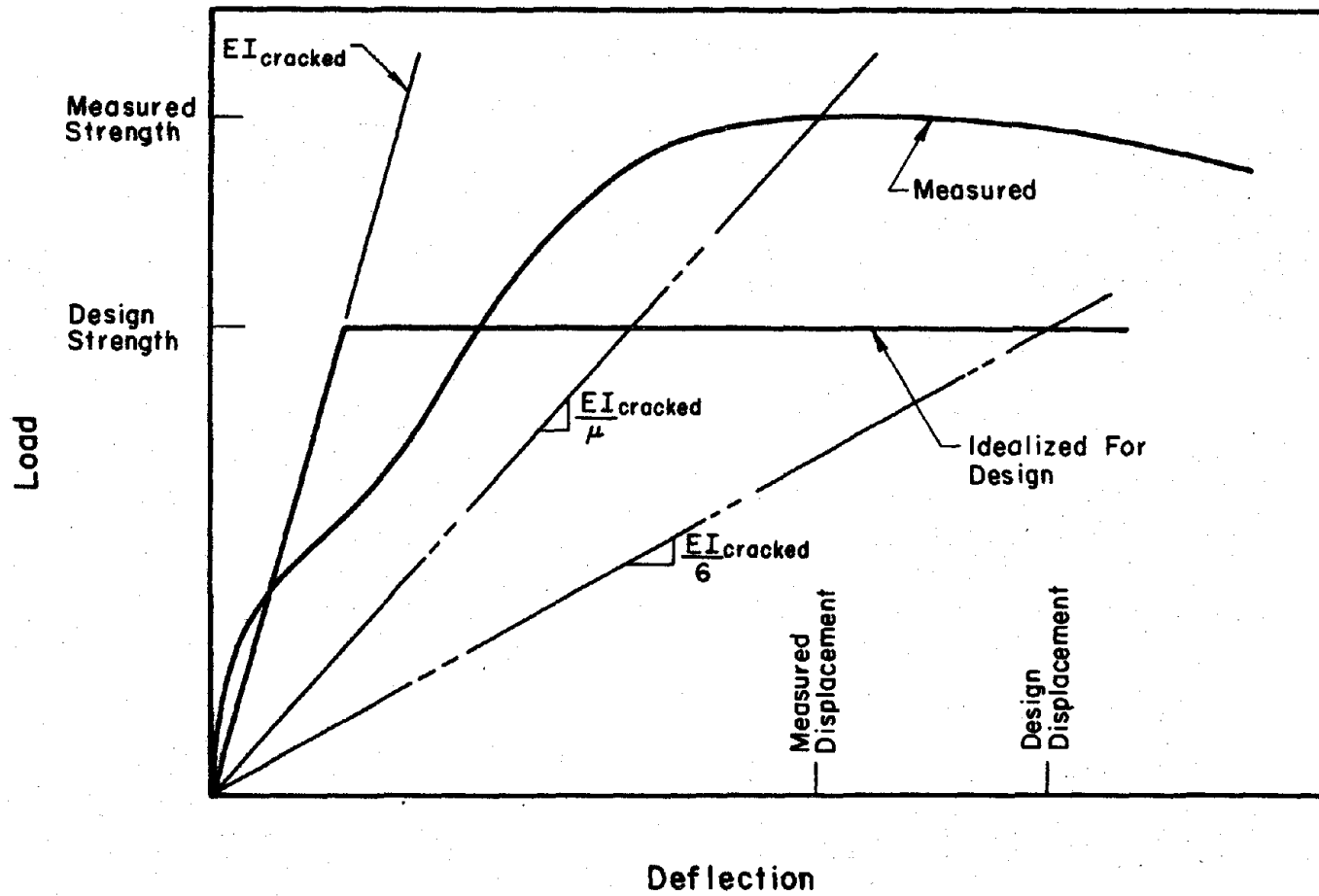


Fig. 7.12 Representative Load-Deflection Relationship for Beams

APPENDIX

DESCRIPTION OF EXPERIMENTAL WORK

A.1 Test Apparatus(a) Earthquake Simulator

The test structures were subjected to earthquake motions generated by the University of Illinois Earthquake Simulator. Each test structure was secured to the simulator platform (Fig. A.1) which was activated by a hydraulic servoram (330 kN capacity) operated in displacement control from input signals recorded on magnetic tape. The frequency range of the simulator response was rated between zero and 100 Hz. Maximum single-amplitude displacement of the platform was limited to 65 mm. Further details of performance of the simulator are presented by Otani [20].

A steel reference frame was secured to the simulator platform so that displacements relative to the base could be measured. Natural frequencies of the frame were measured at 50 Hz.

(b) Free-Vibration Test Set-up

The test structures were excited in small-amplitude free vibration by hanging a weight (45 kg) from a wire which was attached to the story weight at the tenth level (Fig. A.2). The wire was cut to release the structure in free vibration. Response was measured with a tenth-level accelerometer with increased sensitivity.

A.2 Description of Test Structures

A brief description of the test structures is presented in Sec. 2.1 where nominal dimensions of the structures are shown (Fig. 2.1). Detailed descriptions of specimen dimensions, story weights, connections and anchorage of structures at base are presented in this section.

(a) Measured Dimensions of Specimens

Cross-sectional dimensions of each member were measured with a dial gage precise to 0.03 mm. Widths and depths of beams and columns were measured at ends of members and averaged by story level (Table A.1). A summary of measured dimensions showed that means of measured values were essentially the same as nominal values. Dimensions of story heights and bay widths were also measured and were within a 0.5 mm precision.

(b) Story Weights

Story weights were used to couple wall and frames and to provide mass for attainment of inertial loads. Nominal dimensions of the story weights are presented in Fig. A.3 (a). To increase weight and diaphragm stiffness, steel liner plates (51 mm) and No. 11 reinforcing bars were provided. Embedded bent bars (No. 4) were welded to the liner plates to insure composite action of steel and concrete. Story weights were cast from a single batch of concrete so that uniformity of weight at all levels would result. The concrete mix included high-strength cement and pea-gravel aggregate for high density. Measured weights (including the weight of all connections and lumped portions of the specimens) are presented in Table A.2 in terms of mass units. Channel sections (MC3x9) were welded to the underside of each weight for connection with frames. An

opening at the center of each mass was provided for penetrations of the wall.

(c) Connections

Stiffnesses of connections used to transfer forces from the story weights to the frames and wall were established so that natural frequencies of the connecting system would be beyond the range of estimated third-mode frequencies of the test structures. Connections were also designed to assure negligible resistances to rotation within the principal plane of the frame and wall.

A series of channels (Fig. A.3 (b)) were used to transfer horizontal and vertical reactions from the story weights to the centroid of each frame joint. The channels were attached to the frames with 7/16 inch diameter bolts that were tightened snugly by hand. Oversized holes in the channels permitted attachment of the frames to the story weights with negligible forces applied to specimen.

The wall was connected to the story weights with an assembly of steel members that transferred force to the center of the wall (Fig. A.3 (c)). A ball bearing connection was provided so that rotation within the plane of the wall could occur with insignificant lateral translation due to slippage. The "jacket" of steel members secured to the wall was prestressed against the walls of the opening of the story weight with one-inch diameter high-strength bolts. Compression in the bolts was approximately 10kN. Strain gages were placed on necked-down regions of these bolts to indicate force being resisted by the wall.

(d) Base Anchorage

Foundation portions of frames and wall were secured to the simulator

platform with a series of angles (4 inch) and channels (12 inch) that were stressed heavily during erection of the model structures (Fig. 2.2). No slippage or uplift of the foundation was observed during testing as indicated by uncracked dabs of hydrocal placed at interfaces of members of the base anchorage system.

A.3 Instrumentation

(a) Measurements

Response of the structures to simulated earthquake motions was monitored on forty-eight channels of four analog tape recorders. Measured response consisted of accelerations, displacements and strain in the bolts of the connecting system for the wall. A layout of instrumentation is presented in Fig. A.4 (e). Accelerometers were placed on the frame connections at each level (Fig. A.4 (c)) of north and south frames. Vertical accelerations were also measured at the tops of the north-east and south-west columns. Accelerations in the minor direction were measured at the tenth level. Displacements were measured with LVDT's mounted on the reference frame and attached to each story weight (Fig. A.4 (d)). To detect torsional motions an additional two LVDT's were placed at the tenth level and attached to each frame. Strain gages were attached to bolts of the wall connection which were termed "wall dynamometers" (Fig. A.4 (a)). A four-arm bridge of strain gages was used so that strains resulting from flexure of the bolt would cancel. Dynamometers at each level were wired so that an increase in compression of one bolt would add with a decrease in compression of the other bolt.

(b) Instrument Ratings

Accelerometers were of two types. Instruments used to measure second through tenth level accelerations were Endevco Piezoresistive accelerometers. All other accelerometers were Endevco Q-Flex's. Manufacturer's ratings are listed below.

<u>Parameter</u>	<u>Piezoresistive Type Accelerometers</u>	<u>Q-Flex Type Accelerometers</u>
Range	+ 25 g	+ 15 g
Linearity	1.0%	0.03%
Frequency Response (5%)	0-750 Hz	0-500 Hz
Natural Frequency	2500 Hz	1000 Hz
Damping	0.7	0.6

It should be noted that precisions of measured data were in most cases limited by sensitivities of tape recorders and not by precisions of instruments.

(c) Recording of Data

Accelerations of north frames, accelerations of south frames, displacements and wall forces were each recorded on a separate fourteen track tape recorder. One channel of each was used to record a common signal (the simulator input signal) for synchronization. Another channel of each tape recorder was used to store a signal which activated a digitizing process for later reduction of data.

Full-scale settings of each channel were established from estimated response maxima of the structures. Settings were increased between earthquake test runs. Full-scale settings of channels recording wall forces were

established conservatively high because of the anticipated accumulation of residual forces resulting from nonlinear behavior of the structures.

Each channel was calibrated prior to the day of testing. A physical unit was measured by a particular instrument and recorded on tape. Accelerometers were pointed towards the floor to provide a standard calibration of plus and minus 1.0 g. LVDT's were displaced a known amount equal to the full-scale setting of the first test run. Wall dynamometers were calibrated by applying a known force to the connection (Fig. A.4 (b)) before erection of the test structure. In addition to these mechanical calibrations a common step voltage was recorded before each earthquake simulation to serve as an index of the full-scale setting.

(d) Data Reduction

After the day of testing analog data was played back through a Spiras-65 computer which digitized the records at a resolution of a thousand points per second. Data was stored on magnetic tapes which were copied using a Burrough's 6700 system so that the data could be read by an IBM 360-75 system. Calibration factors and zero levels were applied to the data which was then stored on a permanent IBM magnetic tape. Measured response was plotted from this tape using Calcomp subroutines, and further reduced to give shear and moment response histories, Fourier-amplitude spectra, filtered records and spectral-response curves.

A.4 Fabrication and Erection of Models

(a) Reinforcing Cages

Longitudinal reinforcement (Fig. A.5) was tied to rectangularly shaped spirals which were fabricated from 1.8 meter lengths of No. 16 gage wire. The spirals were turned about a mandrel on a lathe and twisted straight by hand. Reinforcement was soaked in solvent and wiped clean with acetone to remove grease and dirt. Longitudinal reinforcement was purchased in 3 meter lengths to avoid splicing. Welding of reinforcing wire was done only at connection points with anchorage plates. Helical reinforcement (Fig. 3.12 (a)) which reinforced joints consisted of No. 16 gage wire.

(b) Casting and Curing

Two frames and one wall were cast from the same batch of concrete. Specimens were cast in the horizontal position with steel forms (Fig. A.5 (a)) consisting of bars screwed to a flat cold-rolled plate. Concrete was placed by hand, vibrated twice with a stud vibrator (placed against the upper face of the cages), and hand troweled to a smooth finish. The entire casting process lasted approximately three hours. Twelve test cylinders (100 x 150 mm) and ten test prisms (50 x 50 x 200 mm) were also cast from the same batch to measure material properties at the day of testing. Approximately eight hours after casting, the steel bars were removed from the forms so that the specimens could shrink without being restrained.

The specimens were cured under wet burlap for two weeks to prevent warping. The forms were lifted to a vertical position at the end of this time (Fig. A.6 (a))

and removed from the specimens. The specimens were left standing in the temperature- and humidity-controlled laboratory for an additional two weeks to allow for uniform drying on each face.

(c) Erection of Test Structures

Erection of the test structures followed a standard procedure that was used for all four structures. The wall was placed first (Fig. A.6 (b)) on the simulator platform, aligned, and secured temporarily with bolts to the steel plate of the platform. Story weights were then stacked about the wall (Fig. A.6 (c)) using collapsible wooden blocks. As each story weight was placed, the wall connection was secured to the wall and pre-stressed against the sides of the opening of the story weight. A temporary construction cage was erected from steel angles and cables for horizontal alignment of each story weight. After stacking all ten weights, each frame was placed on the simulator platform and guided into position (Fig. A.6 (d)). The base-anchorage system of steel angles and channels was then installed and secured to the platform. Connection of the frames to the story weights followed with the wooden erection blocks still in place. The construction cage and blocks were removed immediately before testing.

A.5 Test Procedures

The entire series of testing lasted approximately eight hours. Before starting the series, all bolts were checked for tightness and retightened if necessary. Initial condition of each structure was recorded by marking cracks with a felt tip pen. Cracks were identified using a fluorescent liquid and a "black light."

Each test run, of which there were three, consisted of subjecting each test structure to the following array of motions (as depicted in Fig. 2.3).

- (1) a low-amplitude free vibration using the set-up shown in Fig. A.2
- (2) an earthquake simulation of progressively increasing intensity for each successive simulation
- (3) another low-amplitude free vibration
- (4) a low-amplitude steady-state base excitation which varied in frequency over the range of first-mode frequencies of the structures

The first two test structures were subjected to the steady-state motions after the third test run only. Crack patterns and widths were recorded after each test run.

In addition to recording measurements on analog tape, 16 mm and video cameras recorded visual observations on motion-picture film and tape.

A.6 Material Properties

(a) Concrete

Concrete of the model structures was actually a mortar consisting of coarse Wabash River sand and fine lake sand as aggregate. Cement used in the mix design was Type III - high early strength so that the specimens could be lifted from the forms as soon as possible to prevent warping resulting from unequal shrinkage on formed and finished faces. Mix proportions by dry weight were 1.00:0.96:3.83 (cement:fine aggregate:coarse aggregate). The water-cement ratio was 0.80. The concrete was mixed in a one-ton capacity Koehring Cyclo-Mixer.

Several test cylinders and prisms were cast and cured with the test specimens for measurement of material properties. Age at testing (same day as dynamic testing), slump, compressive strength, secant modulus, modulus of rupture, and tensile strength measurements are presented in Table A.3. Stress-strain relationships for the concrete (Fig. A.7 (c)) were determined from compression tests of cylinders using (1) a 1300 kN-capacity Riehle testing machine with a 0.001-inch mechanical dial gage, and (2) a 2600 kN-capacity MTS servohydraulic testing machine with a 12 mm-gage length extensometer. Relationships were essentially the same for control samples tested by either method.

(b) Reinforcement

Reinforcement for the model structures consisted of No. 13 gage (frames) and No. 2 gage (wall) annealed and processed, bright-basic wire. The wire was purchased from Wire Sales Company, Chicago, in 3 meter lengths. Annealing of the wire was done at the factory in coil form which resulted in very uniform properties along the length of the wire. Stress-strain relationships were measured for plain and knurled wire at strain rates of 0.001 and 0.005 strain per second. Relationships presented in Fig. A.7 are from measurements at a strain rate of 0.005 strain per second for knurled No. 2 gage wire and plain No. 13 gage wire. A summary of wire testing is presented in Table A.4.

Because design of shear reinforcement was based on conservatively high safety factors, only a few samples of No. 16 gage wire were tested. Yield stress of shear reinforcement was nominally 750 MPa.

A.7 Cyclic-Load Test of Wall Specimens

(a) Test Set-up

The test set-up (Fig. 4.2 (b)) consisted of a 110 kN-capacity MTS servohydraulic ram mounted on a 480 mm wall of the foundation of the structural research laboratory. The ram applied lateral loads slowly through a controlled displacement program to the cantilevered specimens. Specimens were fixed to a stiff concrete test floor with prestressed angles similar to those anchoring the ten-story walls.

(b) Instrumentation

Measurements included applied loads and resulting displacements of the specimen at each level (Fig. 4.4 (b)). Displacements were measured electronically using LVDT's and mechanically using 0.001-inch dial gages. Signals from the load cell and LVDT's were input to a VIDAR data acquisition system for punching on paper tape and later plotting on a Calcomp device. Rotation of a bar attached to the specimen 51 mm above the base was also measured to indicate the concentration of curvature near the base. Complementary measurements using 0.0001-inch dial gages indicated negligible uplift or slippage of the foundation beam.

(c) Fabrication

Procedures for fabricating the wall specimens were identical with those of the ten-story walls.

(d) Test Procedures

Each specimen was displaced through a history (Fig 4.3 (c) and (d))

that was monitored with an x-y plotter which signaled load and displacement. Specimens were subjected to displacements beyond yield for the first cycle and progressively increasing displacements of subsequent cycles. Crack patterns and widths were recorded throughout the duration of testing.

(e) Material Properties

Reinforcement was from the same stock as reported in Sec. A.6. Concrete was mixed using the same design as reported in Sec. A.6, and had essentially the same strength and stiffness characteristics.

Table A.1 Summary of Measured Gross Cross-Sectional Member Dimensions

(a) Test Structure FW1

Level or Story	Dimensions, mm.									
	North Frame				South Frame				Wall	
	Beams*		Columns**		Beams		Columns		Mean	Std. Dev.
	Mean	Std. Dev.	Mean	Std. Dev.	Mean	Std. Dev.	Mean	Std. Dev.		
WIDTHS										
10	38.0	0.5	38.4	0.4	39.3	0.4	39.1	0.4	38.8	0.2
9	38.7	0.3	38.7	0.3	39.3	0.6	39.2	0.3	38.8	0.1
8	38.7	0.2	38.5	0.4	39.1	0.8	39.1	0.3	39.2	0.0
7	38.7	0.2	38.7	0.4	38.9	0.3	39.0	0.5	38.9	0.1
6	38.6	0.1	38.6	0.3	39.0	0.2	39.3	0.3	38.9	0.2
5	38.7	0.4	38.5	0.2	39.2	0.1	39.4	0.3	38.8	0.0
4	38.7	0.3	38.6	0.5	39.2	0.5	39.3	0.4	38.5	0.1
3	38.9	0.7	38.6	0.5	39.7	0.1	39.6	0.6	38.3	0.1
2	38.4	0.4	38.4	0.4	39.4	0.3	39.5	0.6	38.3	0.1
1	38.3	0.4	38.2	0.8	39.2	0.6	38.9	0.8	38.6	0.0
DEPTHS										
10	37.9	0.3	50.8	0.4	38.0	0.5	50.8	0.5	204.0	--
9	38.5	0.3	50.7	0.5	38.1	0.3	50.7	0.5	203.7	--
8	37.9	0.5	50.5	0.5	38.2	0.1	50.7	0.4	203.2	--
7	37.9	0.5	50.8	0.7	38.2	0.5	50.6	0.5	202.2	--
6	37.9	0.3	50.8	0.6	38.2	0.4	50.6	0.6	203.2	--
5	38.2	0.3	50.5	0.8	38.0	0.4	50.6	0.9	203.2	--
4	37.9	0.5	50.7	0.4	38.2	0.3	51.1	0.5	202.9	--
3	38.0	0.7	50.7	0.6	38.3	0.1	50.8	0.7	202.7	--
2	38.2	0.4	50.6	0.4	38.3	0.8	50.7	0.8	202.2	--
1	38.0	0.6	50.6	0.5	38.2	0.6	50.7	0.6	201.9	--

*Sample Size = 6

**Sample Size = 8

Table A.1 (contd.) Summary of Measured Gross Cross-Sectional Member Dimensions

(b) Test Structure FW2

Level or Story	Dimensions, mm.									
	North Frame				South Frame				Wall	
	Beams*		Columns**		Beams		Columns			
	Mean	Std. Dev.	Mean	Std. Dev.	Mean	Std. Dev.	Mean	Std. Dev.	Mean	Std. Dev.
WIDTHS										
10	38.8	0.3	39.1	0.6	39.3	0.3	39.2	0.3	38.7	0.4
9	39.0	0.3	39.3	0.5	39.2	0.4	39.1	0.3	38.9	0.3
8	39.4	0.4	39.4	0.6	39.1	0.3	38.9	0.4	39.4	0.5
7	39.1	0.8	38.9	0.2	39.2	0.4	39.0	0.5	39.1	0.1
6	38.7	0.6	38.9	0.7	38.8	0.2	39.4	0.9	39.1	0.1
5	39.0	0.5	39.2	1.1	39.7	0.4	39.5	0.3	38.9	0.5
4	38.8	0.4	38.9	0.4	39.6	0.3	39.3	0.3	39.1	0.0
3	39.2	0.3	38.9	0.3	39.0	0.4	38.9	0.3	39.0	0.4
2	39.1	0.4	39.0	0.4	39.2	0.3	39.0	0.4	38.7	0.0
1	38.7	0.2	38.6	0.5	39.4	0.4	39.1	0.4	38.8	0.3
DEPTHS										
10	37.8	0.6	50.6	0.4	38.3	0.3	50.8	0.3	204.2	--
9	38.4	0.2	50.6	0.5	38.3	0.1	51.0	0.5	203.7	--
8	38.3	0.2	50.5	0.6	38.2	0.2	51.1	0.5	203.7	--
7	38.2	0.7	50.8	0.6	38.1	0.3	51.0	0.5	203.5	--
6	38.1	0.4	50.4	0.4	38.3	0.1	51.1	0.5	203.5	--
5	38.4	0.3	50.5	0.5	38.4	0.2	51.1	0.5	203.7	--
4	37.8	0.4	50.7	0.4	38.1	0.4	51.1	0.2	204.0	--
3	38.0	0.3	51.0	0.3	38.3	0.2	51.1	0.3	203.5	--
2	38.3	0.4	50.7	0.2	38.4	0.1	51.1	0.3	203.7	--
1	37.9	0.4	50.7	0.5	38.2	0.4	51.2	0.3	203.5	--

*Sample Size = 6

**Sample Size = 8

Table A.1 (contd.) Summary of Measured Gross Cross-Sectional Member Dimensions

(c) Test Structure FW3

Level or Story	Dimensions, mm.									
	North Frame				South Frame				Wall	
	Beams*		Columns**		Beams		Columns		Mean	Std. Dev.
	Mean	Std. Dev.	Mean	Std. Dev.	Mean	Std. Dev.	Mean	Std. Dev.		
WIDTHS										
10	38.5	0.6	39.0	0.5	39.2	0.5	39.2	0.3	37.6	0.7
9	39.0	0.5	39.0	0.8	39.0	0.3	39.3	0.4	37.6	0.4
8	39.0	0.6	39.0	0.5	39.3	0.2	39.2	0.6	38.2	0.2
7	39.4	0.6	39.3	0.5	39.2	0.4	39.2	0.5	38.4	0.4
6	39.5	0.4	39.4	0.6	39.5	0.3	39.5	0.3	38.2	1.3
5	39.5	0.4	39.5	0.5	39.4	0.4	39.4	0.3	38.7	0.2
4	39.6	0.2	39.4	0.6	39.3	0.3	39.4	0.4	38.1	0.4
3	39.5	0.4	38.9	0.5	39.7	0.3	39.3	0.4	38.4	0.4
2	39.0	0.2	39.2	0.4	39.3	0.4	39.8	0.5	38.2	0.2
1	39.1	0.2	39.4	0.5	39.4	0.6	39.1	0.4	38.1	0.4
DEPTHS										
10	38.0	0.6	51.2	0.3	38.1	0.8	50.9	0.5	203.2	--
9	38.9	0.3	51.2	0.4	38.5	0.3	51.1	0.4	202.9	--
8	38.4	0.5	51.1	0.3	38.4	0.4	50.9	0.5	203.2	--
7	38.5	0.2	51.3	0.3	38.4	0.3	51.0	0.4	203.2	--
6	38.4	0.2	51.3	0.4	38.4	0.3	51.1	0.6	202.4	--
5	38.3	0.4	51.1	0.3	38.3	0.3	51.0	0.3	203.2	--
4	38.4	0.3	51.2	0.3	37.8	0.2	51.2	0.4	202.7	--
3	38.1	0.7	51.1	0.3	38.4	0.2	51.1	0.2	203.5	--
2	38.3	0.6	51.2	0.4	38.4	0.2	50.9	0.4	203.2	--
1	38.0	0.4	51.1	0.3	37.9	0.4	51.0	0.6	202.7	--

*Sample Size = 6

**Sample Size = 8

Table A.1 (contd.) Summary of Measured Gross Cross-Sectional Member Dimensions

(d) Test Structure FW4

	Dimensions, mm.									
	North Frame				South Frame				Wall	
	Beams*		Columns**		Beams		Columns		Mean	Std. Dev.
	Mean	Std. Dev.	Mean	Std. Dev.	Mean	Std. Dev.	Mean	Std. Dev.		
WIDTHS										
10	39.1	1.1	38.8	0.8	39.7	0.7	39.8	0.6	37.6	0.0
9	38.8	0.8	38.6	0.5	39.5	0.9	39.6	0.9	37.7	0.2
8	39.0	0.6	38.8	0.8	39.6	0.7	39.1	0.8	38.0	0.2
7	39.2	0.6	38.8	1.0	39.3	0.2	39.3	1.0	38.4	0.4
6	38.7	0.2	39.0	0.4	40.0	0.6	39.6	0.7	38.2	0.5
5	39.1	0.9	38.6	0.7	39.6	0.3	39.3	0.6	37.8	0.7
4	38.5	0.7	38.9	0.4	39.5	0.5	39.5	0.6	38.4	0.4
3	38.9	0.3	38.6	0.4	39.5	0.6	39.2	0.7	38.4	0.0
2	39.0	0.4	38.9	0.4	39.7	0.4	39.0	0.5	38.6	0.0
1	39.0	0.3	38.9	0.6	39.1	0.4	38.8	0.5	38.7	0.2
DEPTHS										
10	38.9	0.4	50.4	0.5	39.1	0.7	50.5	0.8	203.5	--
9	38.4	0.5	50.9	0.5	38.2	0.4	50.4	0.7	202.9	--
8	38.9	0.4	50.6	0.4	38.3	0.4	50.5	0.6	202.7	--
7	38.4	0.4	50.3	0.7	38.2	0.5	50.6	0.5	202.4	--
6	38.6	0.6	50.7	0.7	38.0	0.3	50.5	0.3	202.7	--
5	38.3	0.2	50.8	0.4	38.1	0.4	50.7	0.8	202.4	--
4	37.8	0.5	50.6	0.6	37.8	0.1	50.7	0.4	202.7	--
3	38.3	0.4	50.6	0.5	38.0	0.3	50.5	0.2	202.7	--
2	38.2	0.4	50.5	0.3	38.1	0.4	50.5	0.3	203.2	--
1	37.8	0.5	51.1	0.8	38.8	0.9	50.8	0.4	202.9	--

*Sample Size = 6

**Sample Size = 8

Table A.1 (contd.) Summary of Measured Gross Cross-Sectional Member Dimensions

(e) Composite Summary

Dimensions, mm.						
	Nominal	Number of Samples	Mean	Maximum	Minimum	Standard Deviation
Beam Depth	38.1	480	38.2	39.9	37.1	0.4
Beam Width	38.1	480	39.1	40.6	37.3	0.4
Column Depth	50.8	640	50.8	51.8	49.3	0.5
Column Width	38.1	640	39.1	40.4	37.9	0.5
Wall Depth	203.2	40	203.1	204.2	201.9	0.3
Wall Width	38.1	80	38.5	39.2	37.1	--

Table A.2
Measured Story Masses

Level	Mass(kg)
10	461
9	464
8	463
7	466
6	464
5	465
4	465
3	462
2	465
1	460

Table A.3 Measured Properties of Concrete

Parameter	Test Structure			
	FW1	FW2	FW3	FW4
Age at Testing (days)	84	65	30	27
Slump (mm)	57	102	64	64
Compressive Strength, f'_c (MPa)				
Mean	33.0	42.1	32.1	33.8
Standard Deviation	2.4	1.0	5.1	1.5
Number of Coupons	10	9	7	10
Secant Modulus*, E_c ($\times 10^3$ MPa)				
Mean	18.6	23.0	20.2	19.1
Standard Deviation	1.4	2.5	3.2	1.2
Number of Coupons	10	9	7	10
Modulus of Rupture, f_r (MPa)				
Mean	6.7	7.4	6.5	6.5
Standard Deviation	0.8	0.8	0.6	0.6
Number of Coupons	7	7	7	12
Tensile Strength, f_{sp} (MPa)				
Mean	3.6	4.0	3.2	3.2
Standard Deviation	0.2	0.3	0.7	0.6
Number of Coupons	4	4	5	6

*Measured at a compressive stress = 20 MPa

Table A.4 Measured Properties of Reinforcement

Wire Type	Strain Rate (1/Sec.)	Number of Coupons	Yield Stress f_y (MPa)		Ultimate Stress f_u (MPa)	
			Mean	Std. Dev.	Mean	Std. Dev.
No. 13 gage						
Plain	0.001	10	351	10	368	13
	0.005	10	358	5	373	4
Knurled	0.001	4	350	4	370	4
	0.005	5	360	4	379	5
No. 2 gage						
Plain	0.001	5	330	5	351	11
	0.005	10	345	8	371	7
Knurled	0.001	5	338	6	325	5
	0.005	10	340	4	366	3

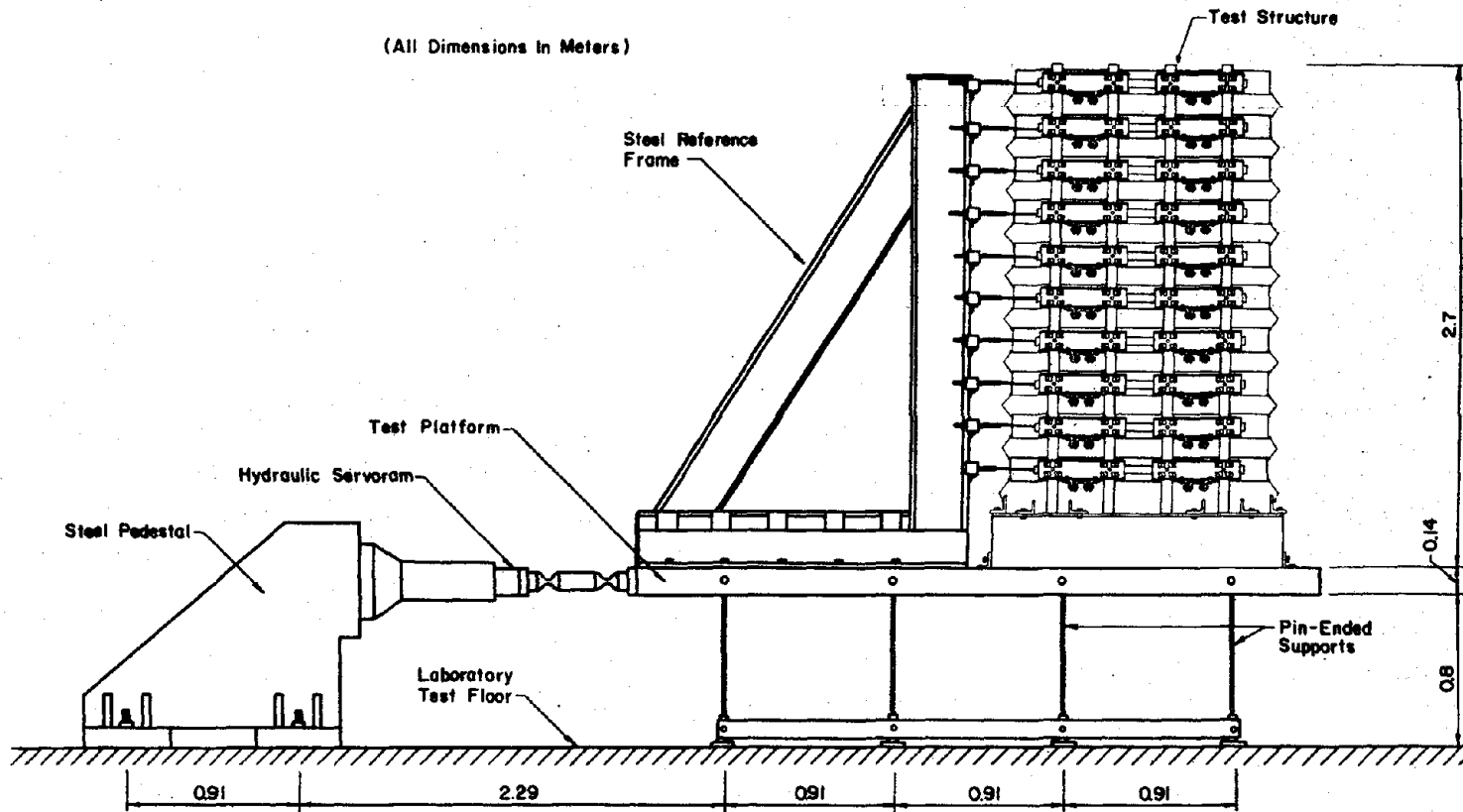
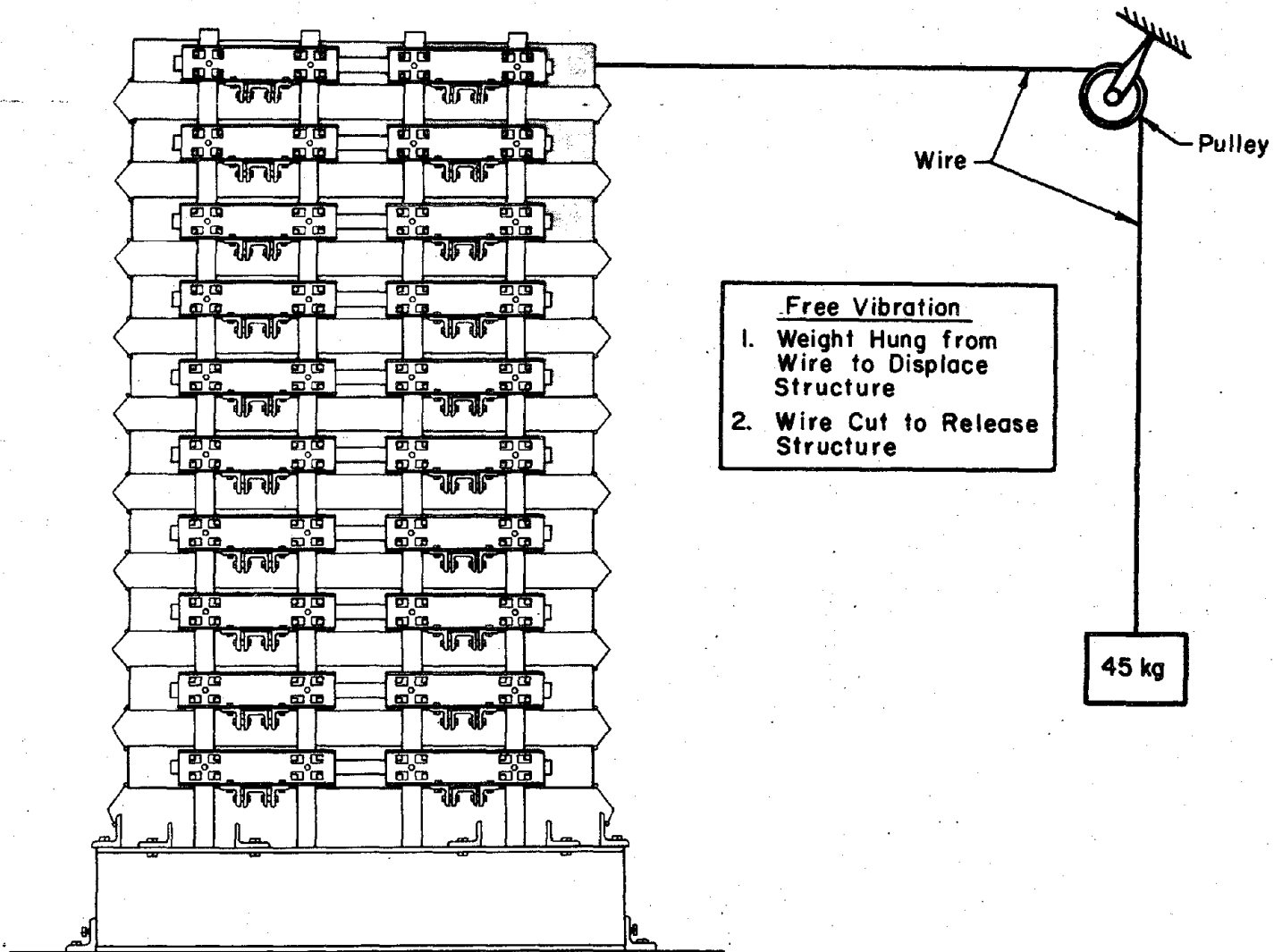
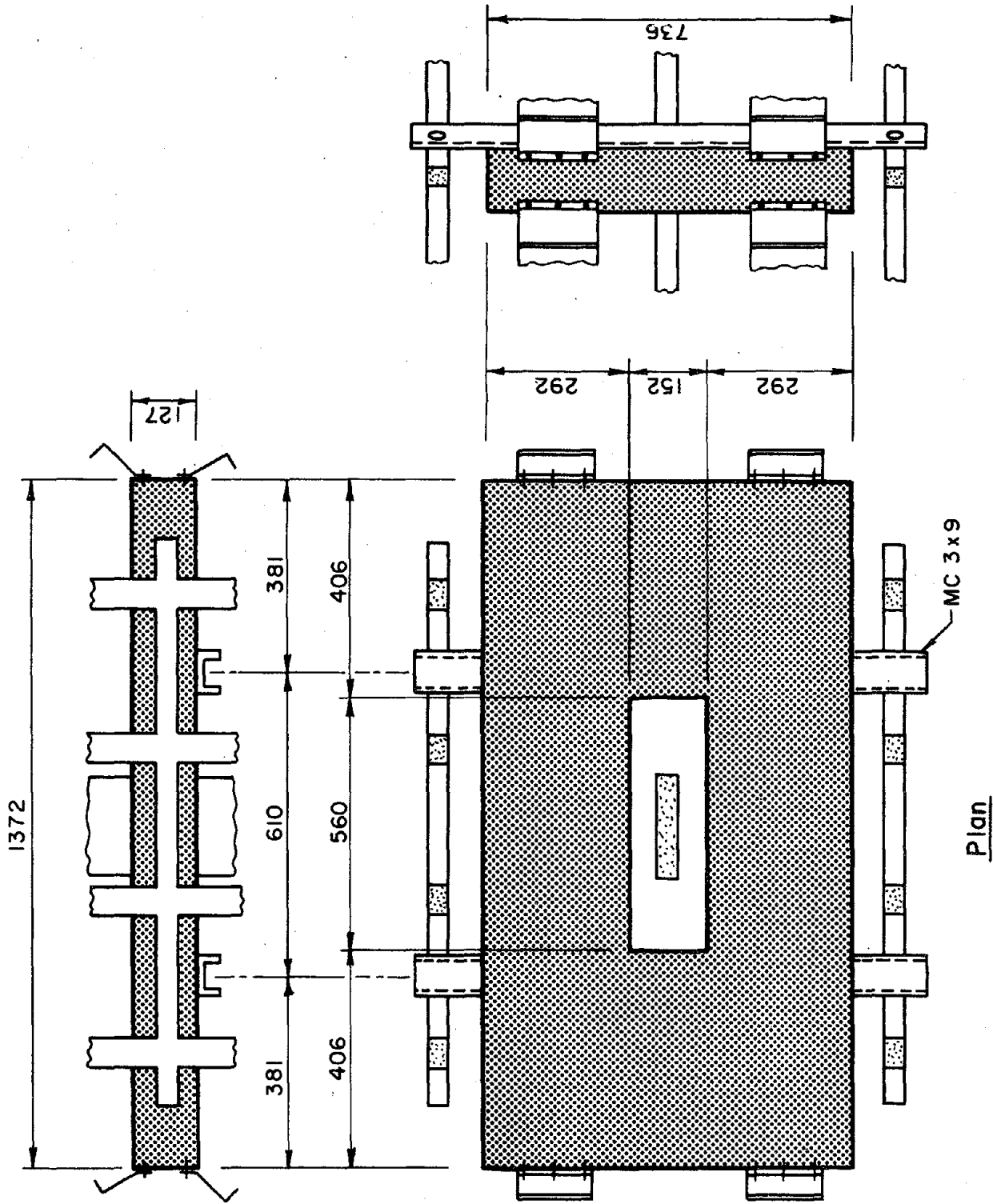


Fig. A.1 Test Apparatus

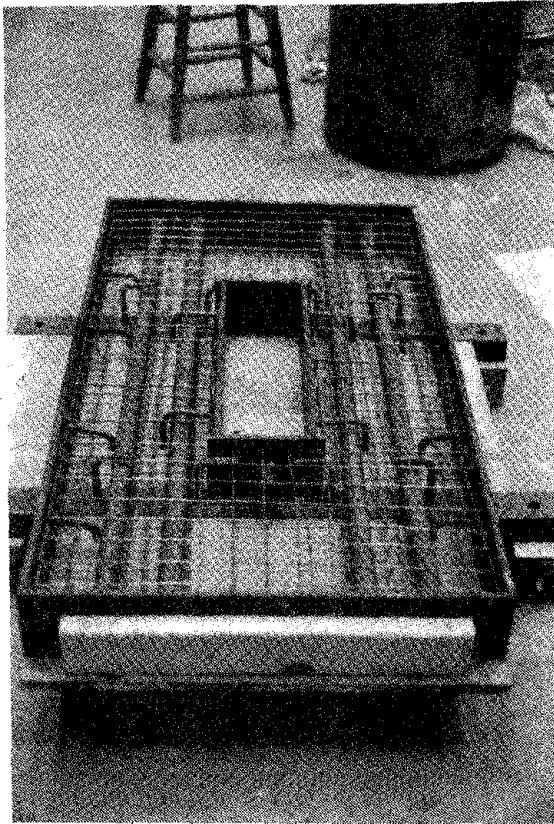


372

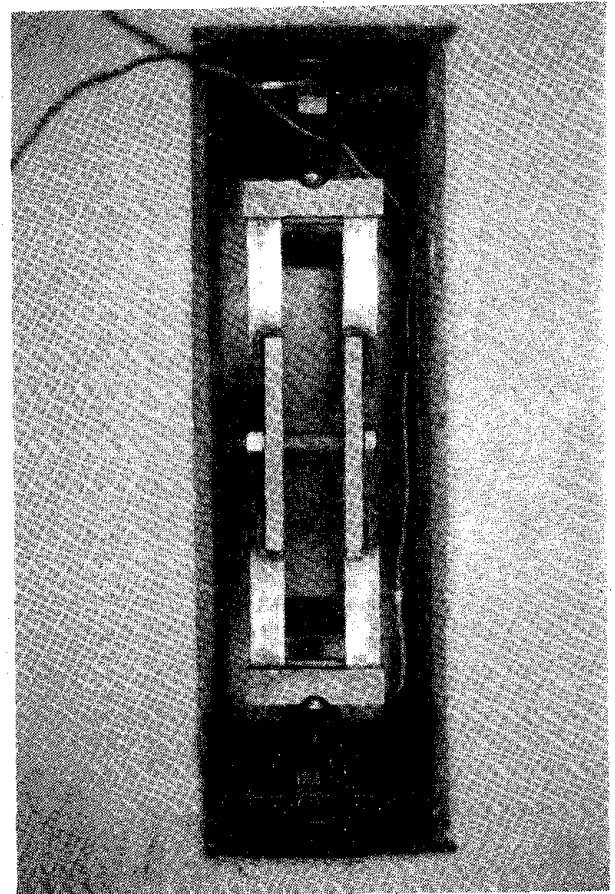
Fig. A.2 Free-Vibration Test



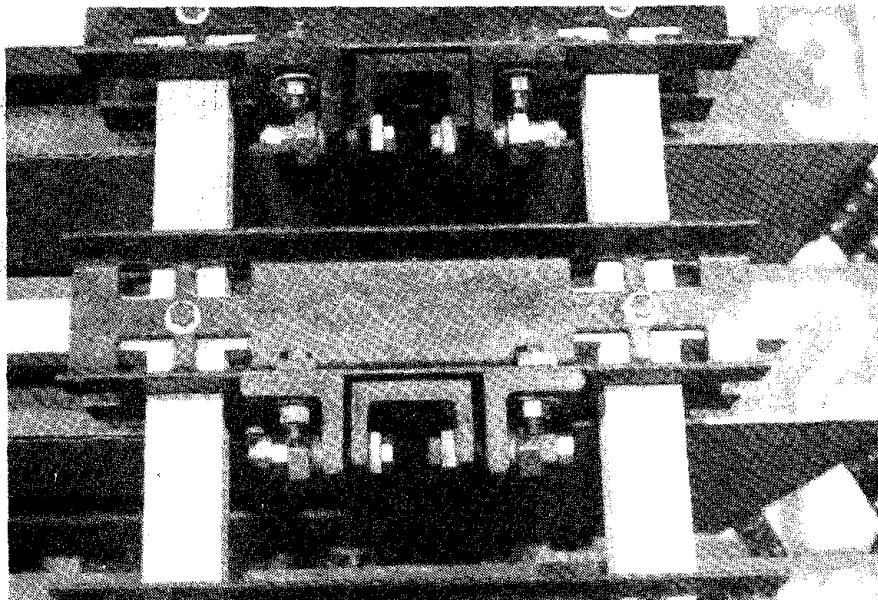
(a) Story Weights
Fig. A.3 Test-Structure Components



(a) (contd.) Story Weights

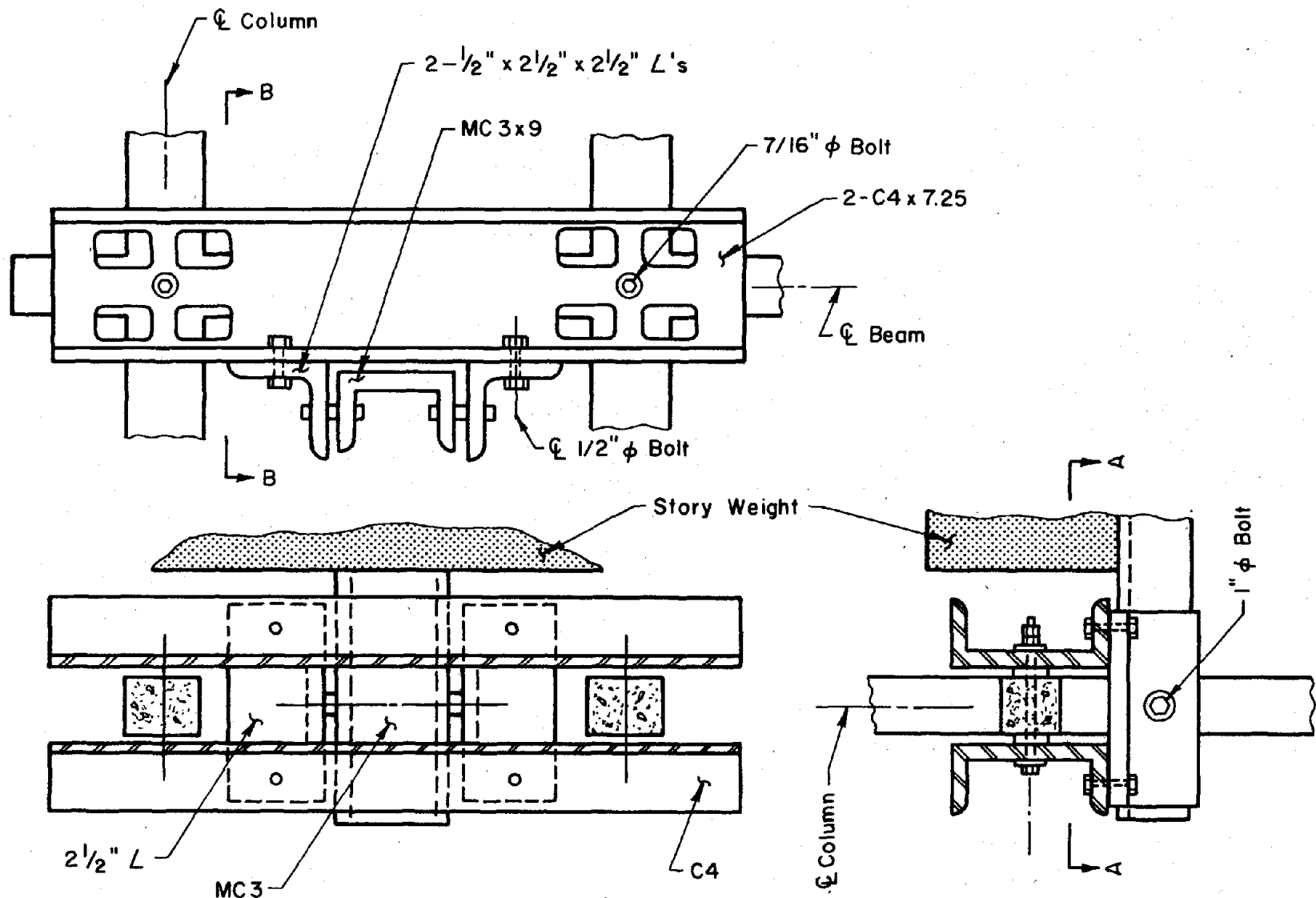


(c) Wall Connection



(b) Frame Connection

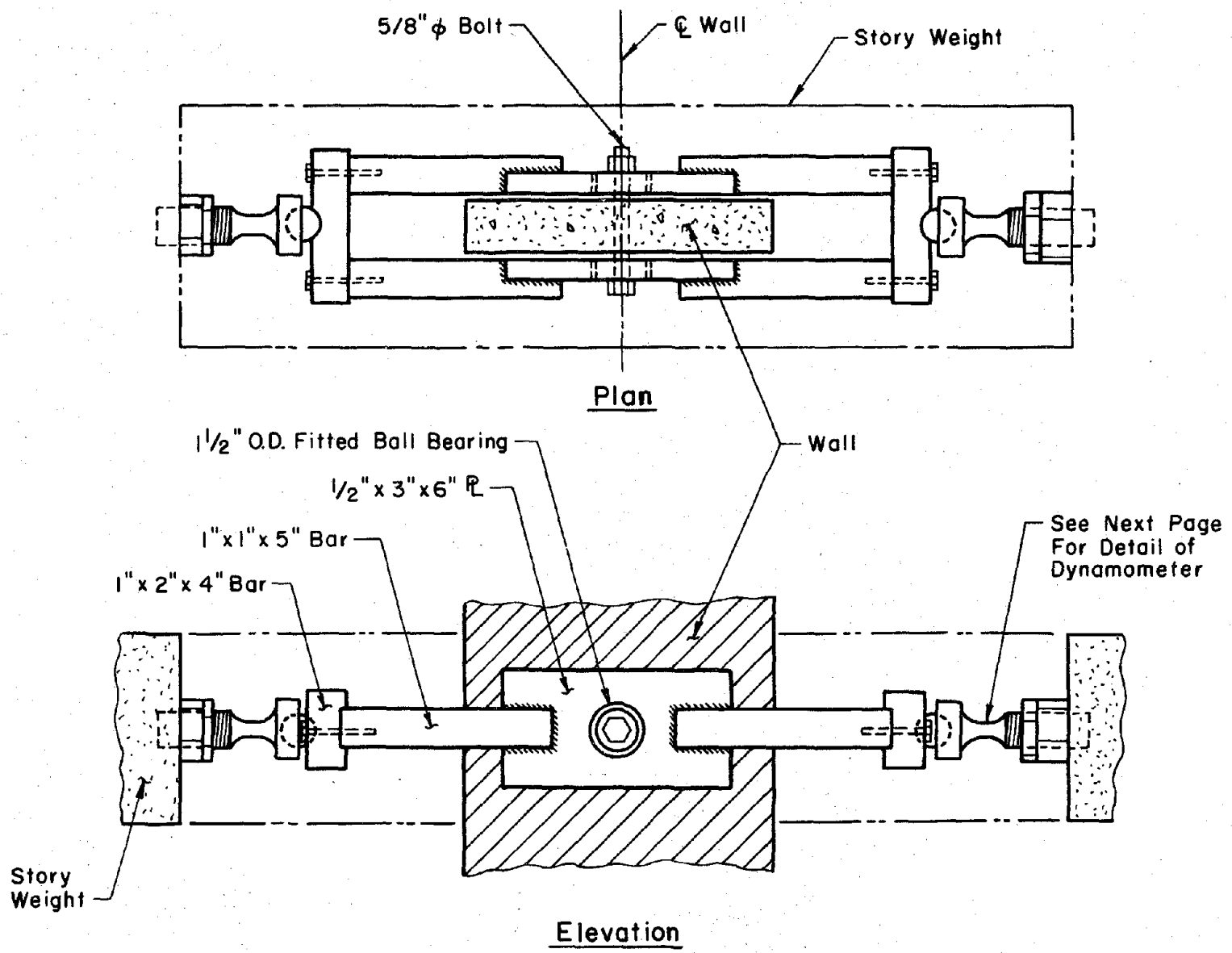
Fig. A.3 (contd.) Test-Structure Components



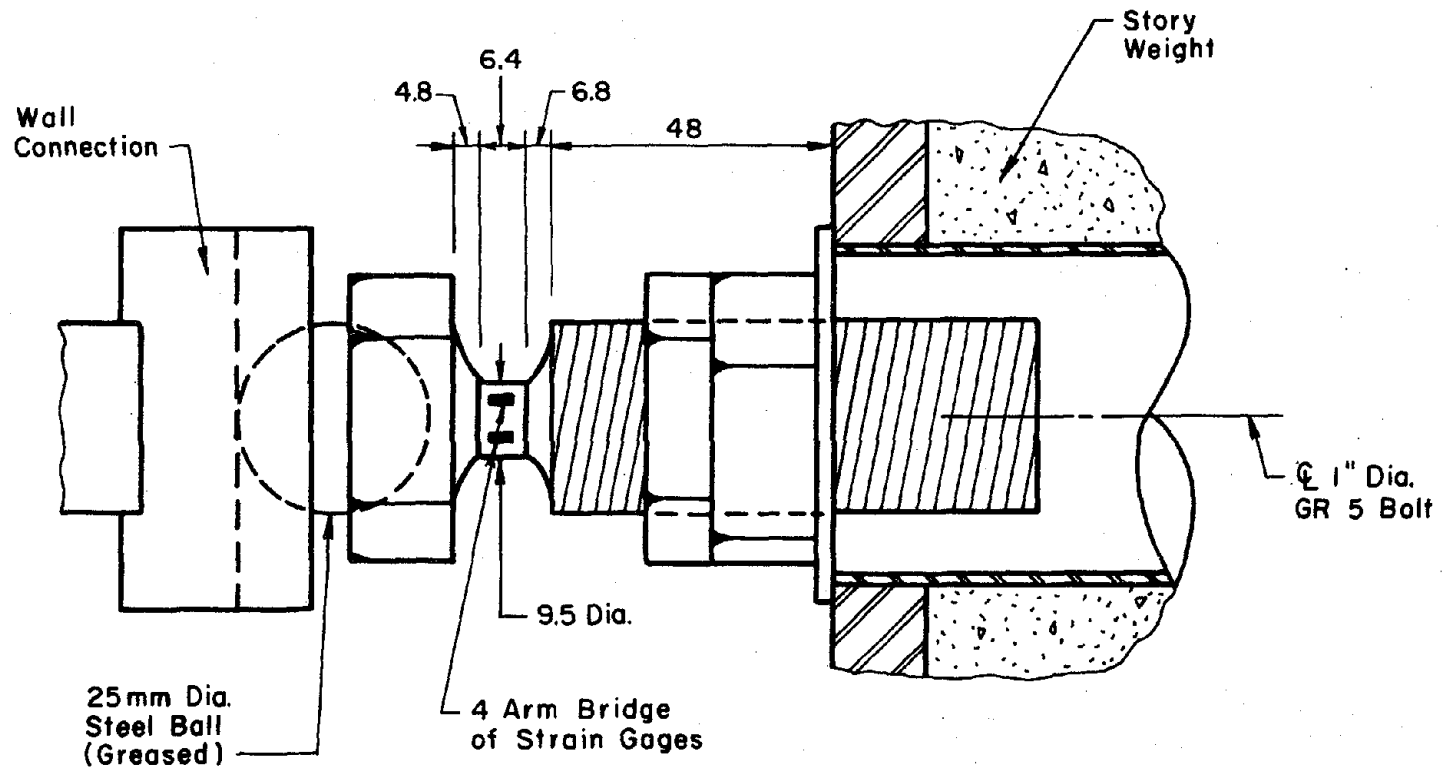
Sectional Plan A-A

375
Section B-B

(b) (contd.) Frame Connection
Fig. A.3 (contd.) Test-Structure Components

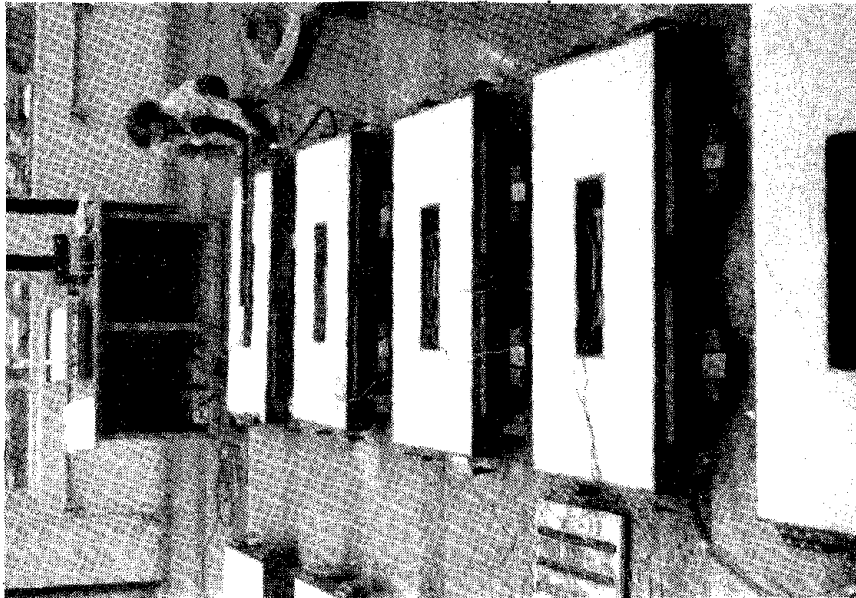
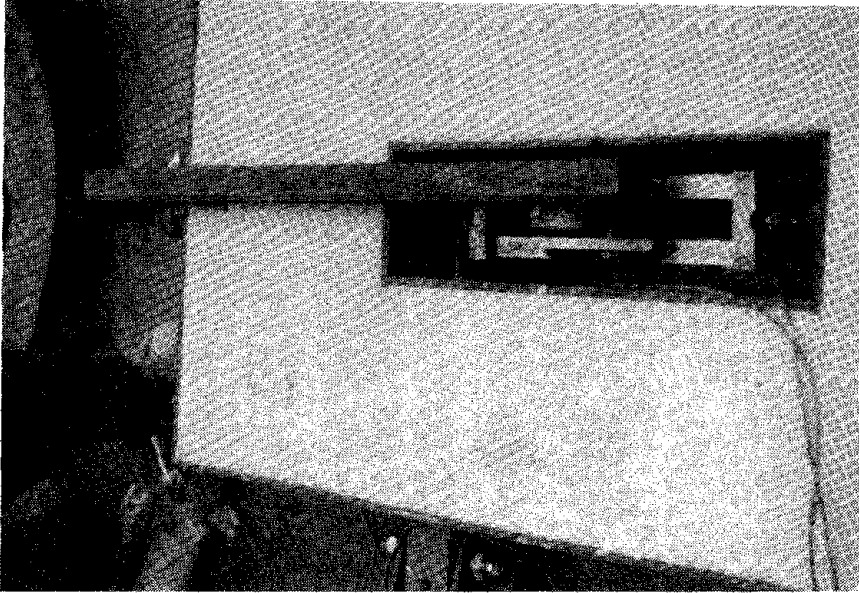


(c) (contd.) Wall Connection
 Fig. A.3 (contd.) Test-Structure Components



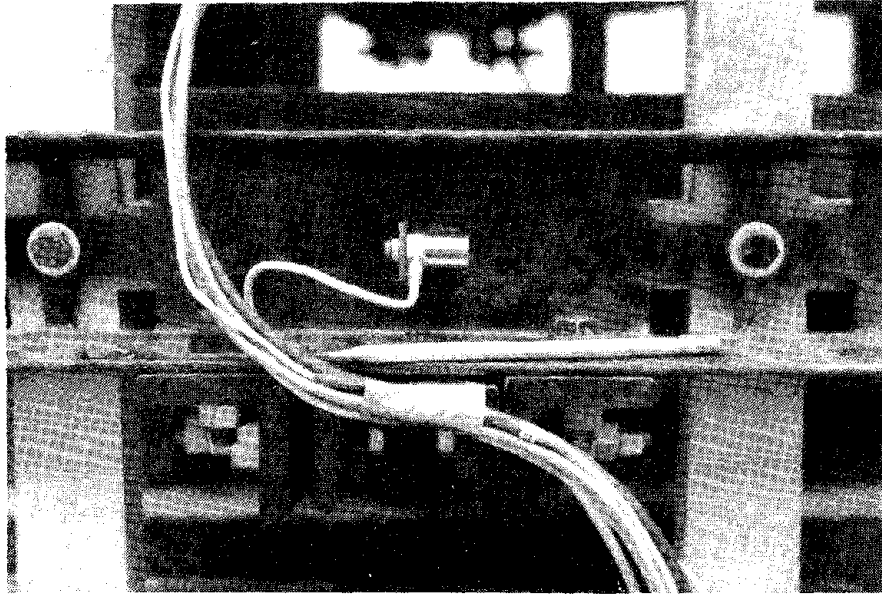
377

(a) Wall Dynamometer
 Fig. A.4 Instrumentation

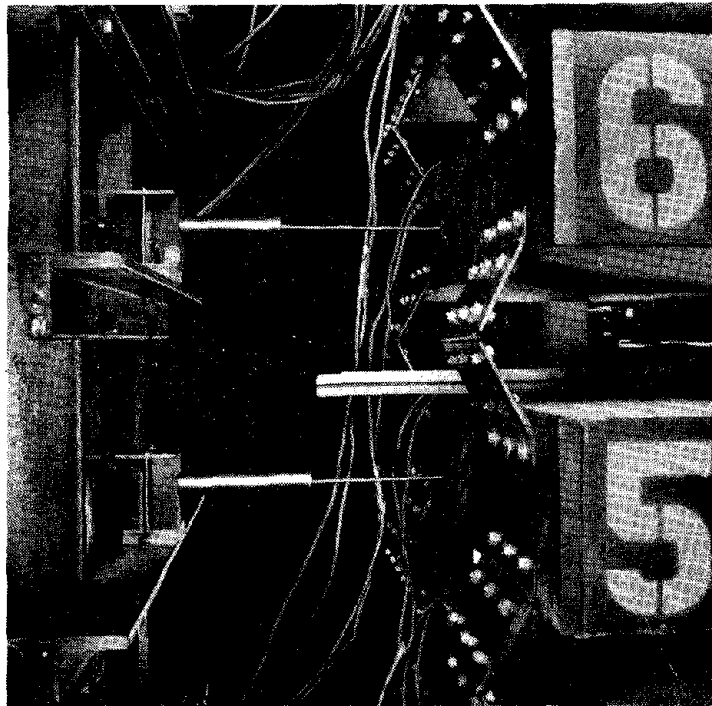


(b) Calibration of Wall Dynamometer

Fig. A.4 (contd.) Instrumentation

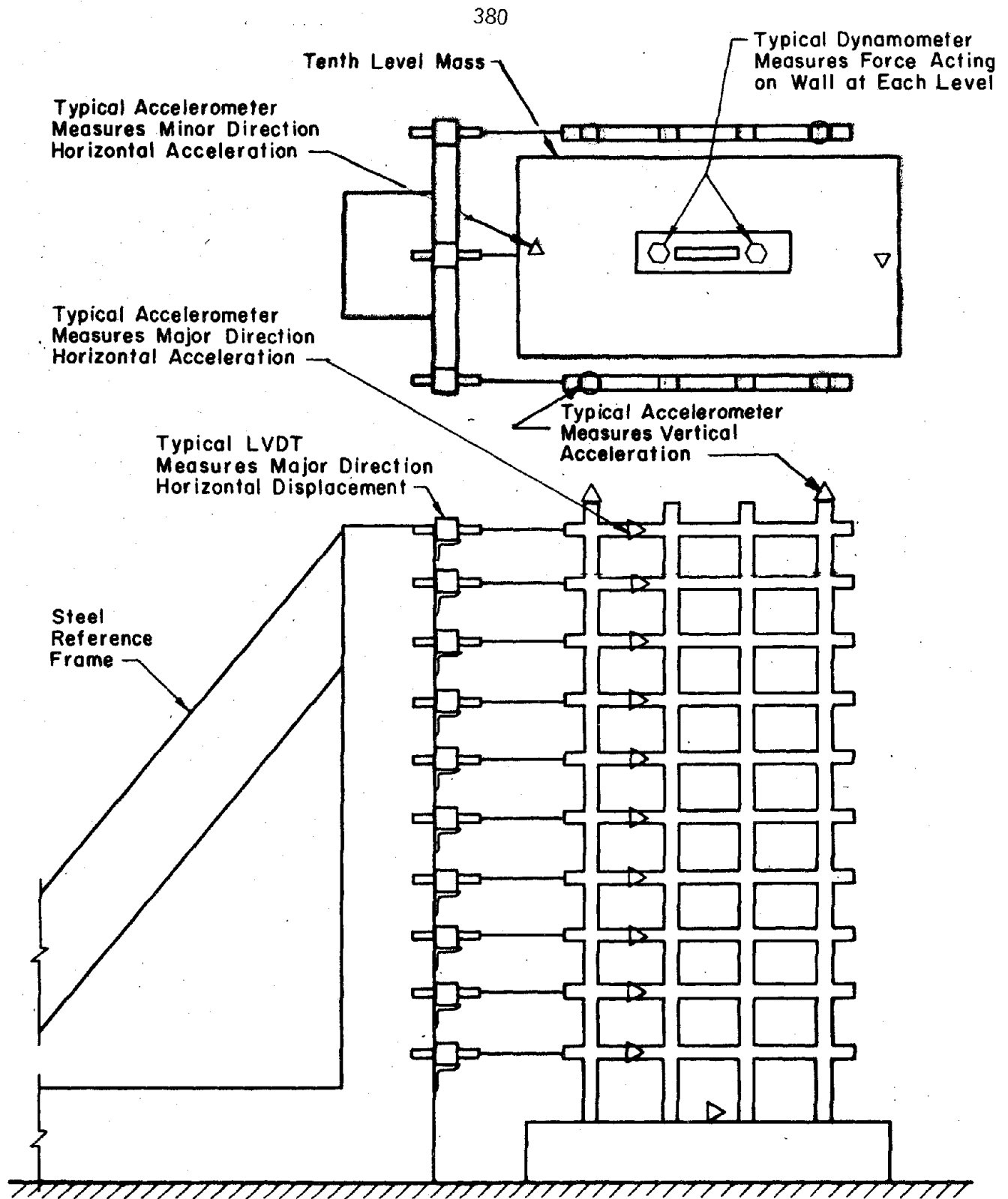


(c) Accelerometer



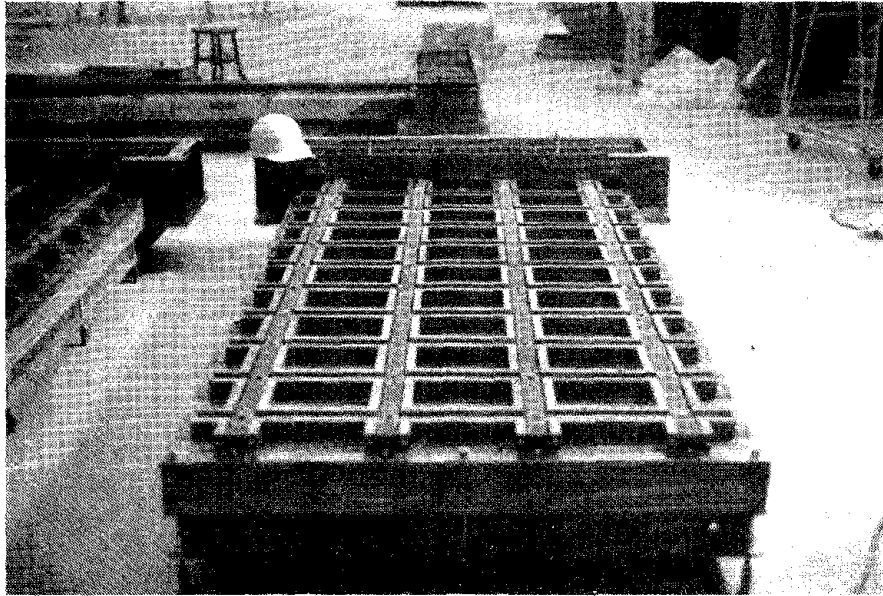
(d) LVDT's

Fig. A.4 (contd.) Instrumentation

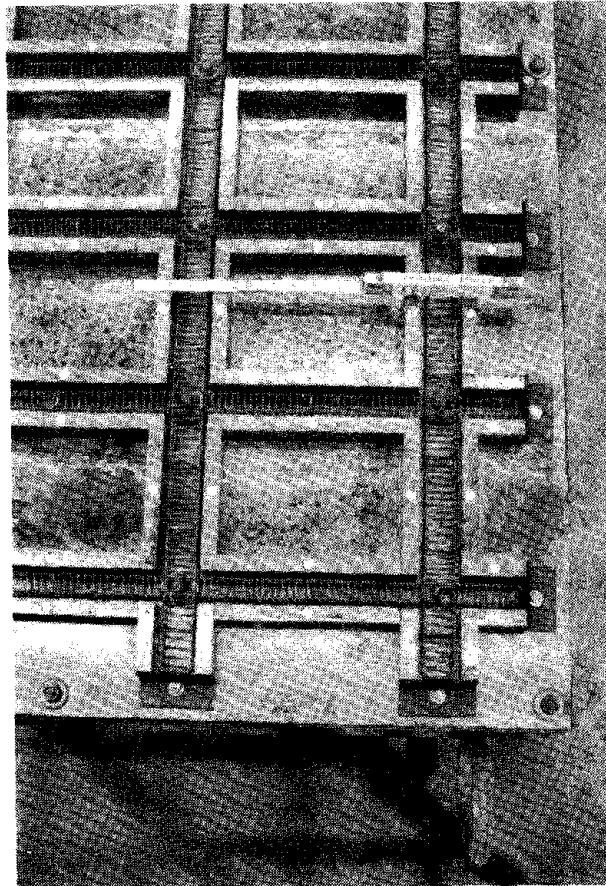


(e) Layout of Instrumentation

Fig. A.4 (contd.) Instrumentation

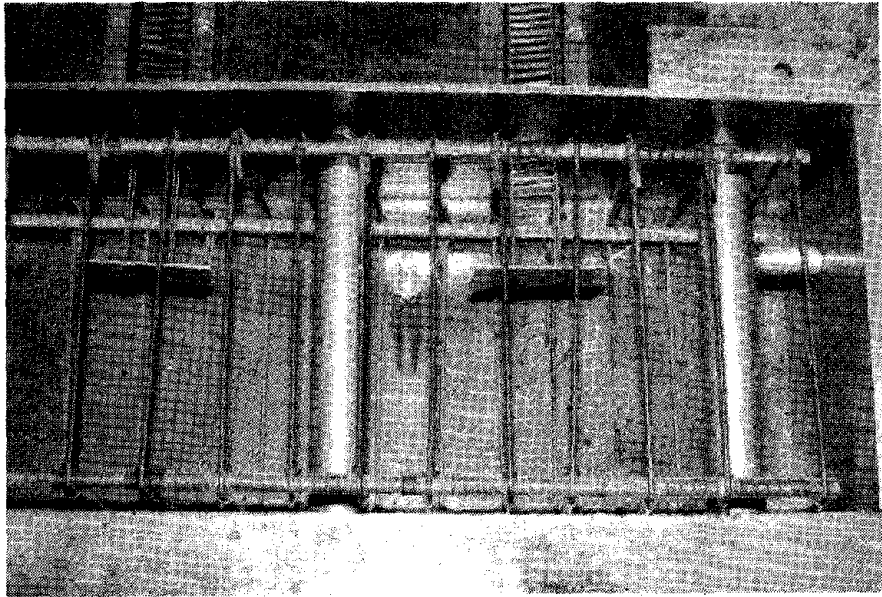


(a) Forms

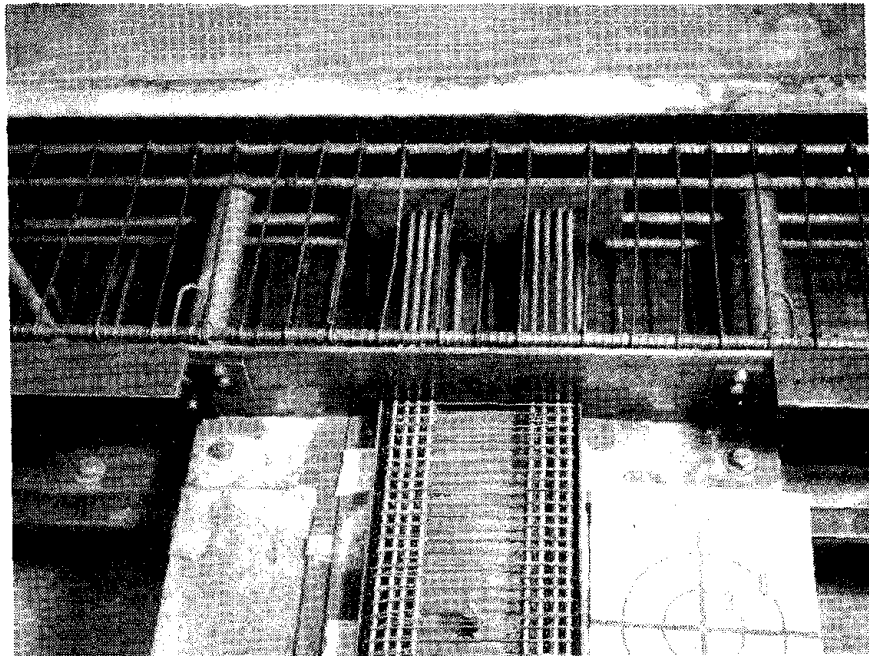


(b) Frame Reinforcement

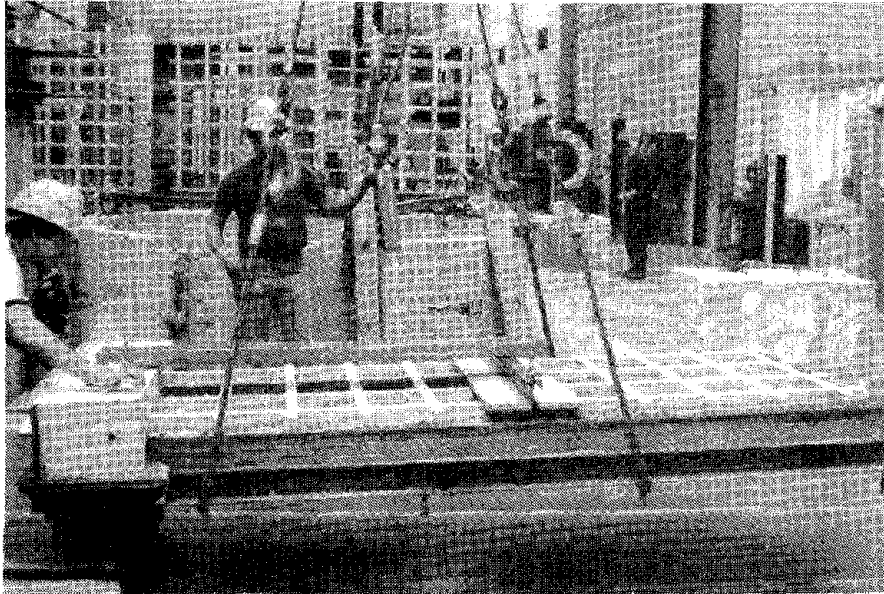
Fig. A.5 Fabrication of Specimens



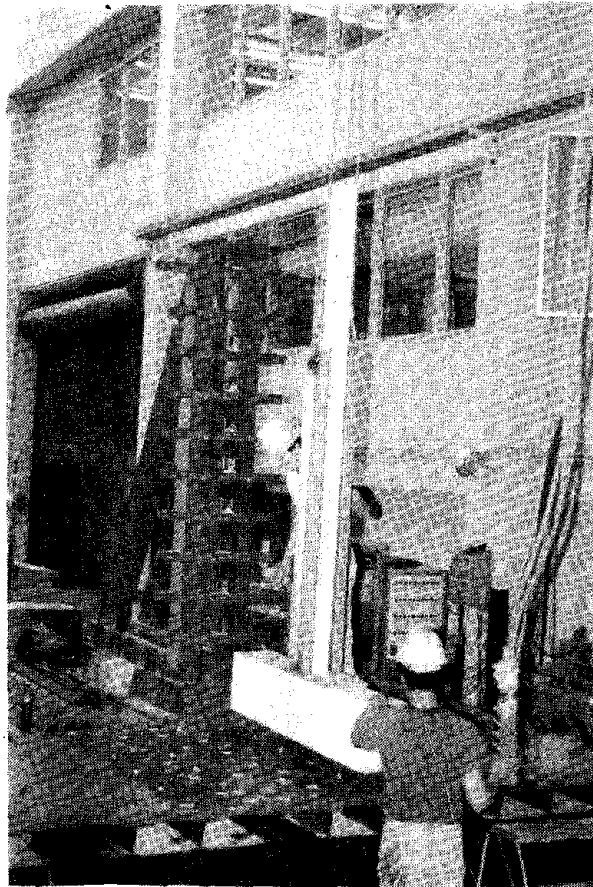
(c) Anchorage of Column Reinforcement at Base



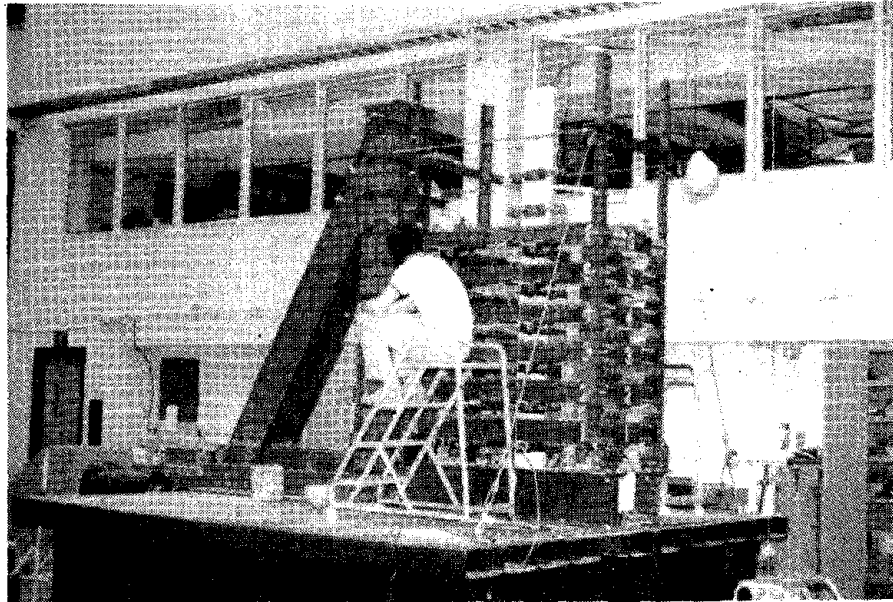
(d) Anchorage of Wall Reinforcement at Base



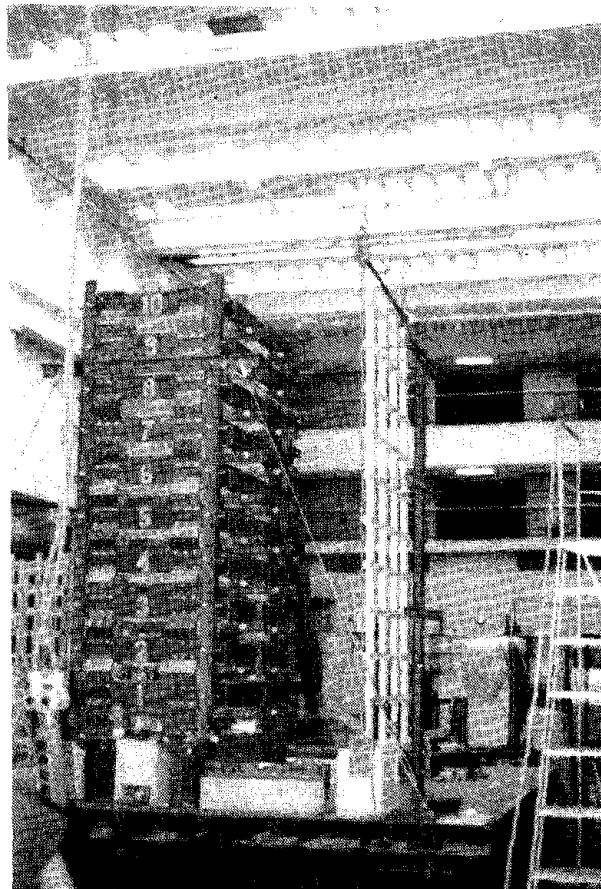
(a) Lifting Frames from Forms



(b) Placing Wall on Simulator Platform
Fig. A.6 Erection of Test Structures

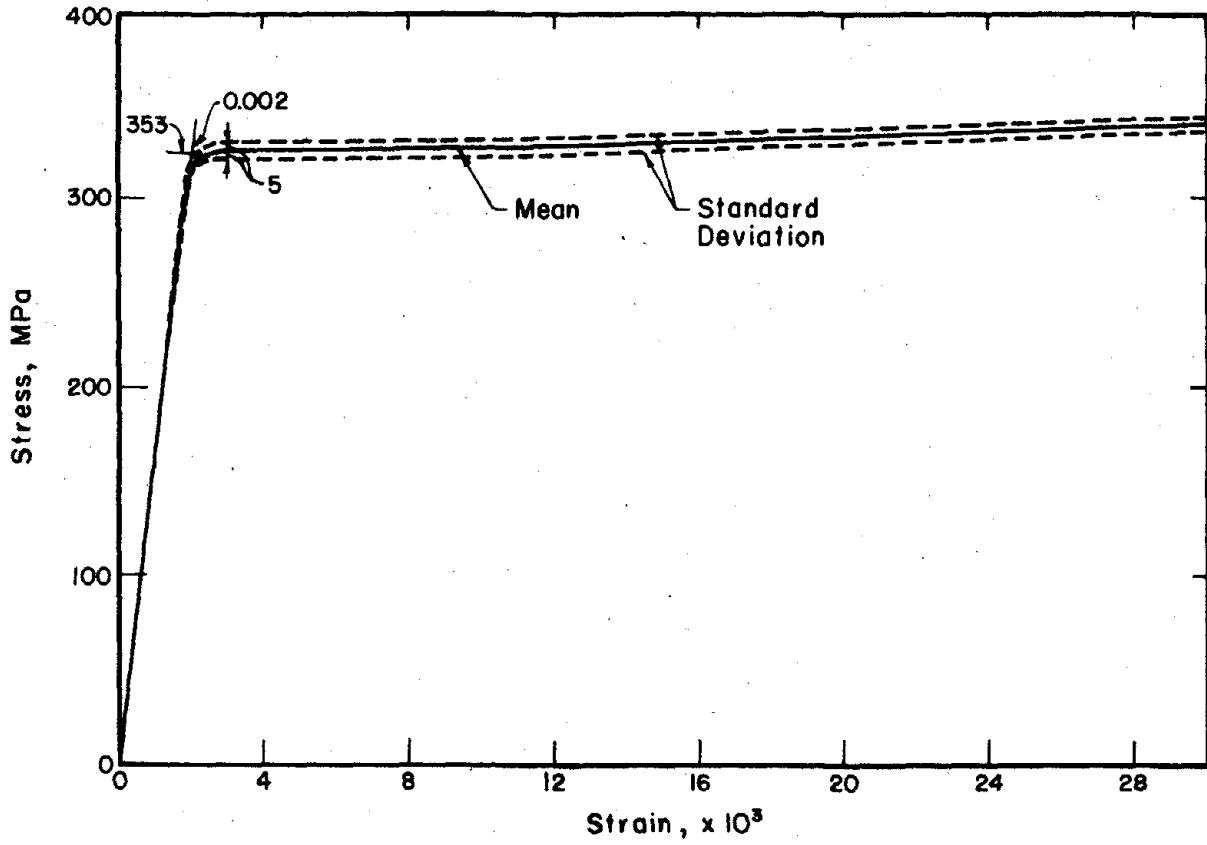


(c) Stacking Story Weights

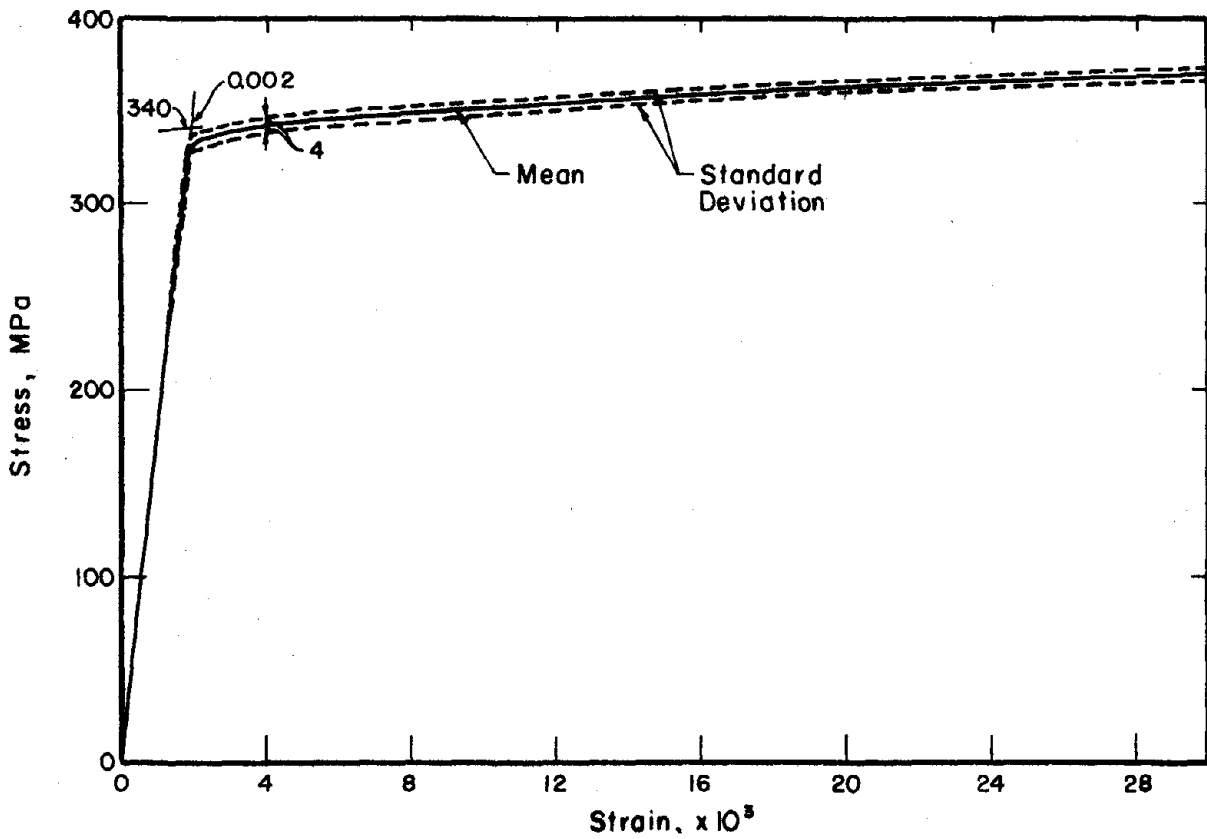


(d) Attaching Frames to Story Weights

Fig. A.6 (contd.) Erection of Test Structures

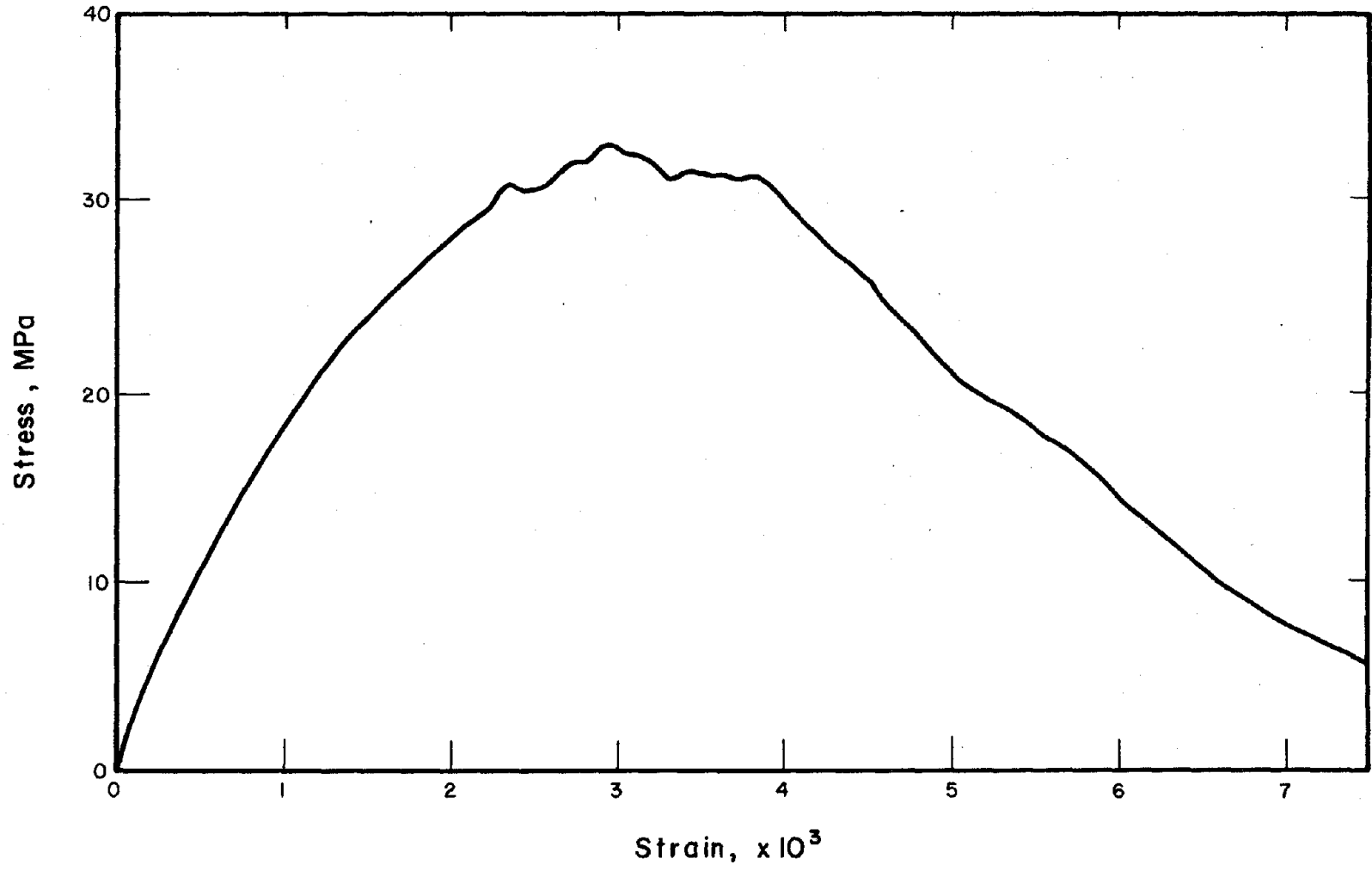


(a) No. 13 gage Wire



(b) No. 2 gage Wire

Fig. A.7 Measured Stress-Strain Diagrams



(c) Representative Curve for Concrete
Fig. A.7 (contd.) Measured Stress-Strain Diagrams